UNIVERSITAT POLITÈCNICA DE VALÈNCIA

Isirym
Instituto de Seguridad Industrial, Radiofísica y Medioambiental

Programa de Doctorado en Ingeniería y Producción Industrial

Recuperación de polifenoles de efluentes de almazara mediante procesos de membrana y tratamiento biológico de las corrientes de rechazo

TESIS DOCTORAL

Magdalena Soledad Cifuentes Cabezas

Dirigida por:

Dr. José Antonio Mendoza Roca

Dra. Silvia Álvarez Blanco

Valencia, 21 Noviembre 2022

AGRADECIMIENTOS

Esta tesis es el resultado de muchos años de trabajo, que no hubiera sido posible sin mis tutores, Silvia y José Antonio, a quienes agradezco mucho la confianza depositada en mí. Gracias por su apoyo, comprensión y por brindarme tanto conocimiento. Me siento muy afortunada de haber coincidido con ustedes.

También me gustaría agradecer a quienes han sido directa o indirectamente parte de esta tesis. A Cinta por confiarme junto a Silvia, a los alumnos de TFM y dejarme formar parte del proyecto al que pertenece mi tesis. A Louise, Alessio, Michael, José Luis y Sandra, quienes son parte importante del trabajo experimental desarrollado en esta tesis. A Bea y Alicia, gracias por su conocimiento, ayuda y por confiar en mí para formar parte del mundo contactor. A Sergio y Laura, siempre dispuestos a echarme una mano tanto con los montajes experimentales como con la petición de pedidos, son los mejores técnicos. A los chicos del laboratorio, a Carlos y Jose Luis por instruirme desde el principio de mi llegada al laboratorio, a Clara por ser mi primera compañera de doctorado, quien hoy es una excelente doctora y profesional. A Eva y MariaJo que me acompañaron a lo largo de toda mi tesis, enseñándome, ayudándome y asesorándome, moltes gràcies. A Mamen, compañera y amiga de aventuras en cada congreso, gracias por tu gran conocimiento y ayuda, tanto con la caracterización de los fenoles como por tu gran corazón fuera de la vida laboral. A Raúl quien siempre ha sido parte del laboratorio, ya sea estudiante, pasante y ahora doctorando, gracias por darme la oportunidad de conocerte, ya que eres una gran persona, organizada, inteligente y buen amigo. Todos ustedes son parte de mi familia de laboratorio, gracias por cada café, y por hacer del ambiente del labo algo único, todo gracias a cada uno de ustedes.

A mi familia, a quienes agradezco hoy y siempre, ya que fueron quienes me animaron a emprender camino fuera de mis tierras. A pesar de no estar físicamente presente en todo este proceso, siempre confiaron en mí y me alentaron a continuar. A mis padres Mariluz y Gerardo, mi hermana Malú y mi hermosa sobrina Elena, gracias a ellos he llegado a ser lo que soy hoy. Agradezco también a mis tíos, primos y abuelos, porque a pesar de la distancia, el aliento, el

apoyo y la alegría que me brindan en cada llamada y visita me da la fuerza necesaria para seguir adelante. A Ricardo por ser el mejor amigo que alguien pudiese desear, siempre con la palabra precisa. Llegaste a ser mi familia al otro lado del charco, gracias por las largas conversaciones, los consejos y celebraciones, simplemente gracias por ser incondicional. A Carlos, Adry y Lily por tantas alegrías, comidas deliciosas, consejos y momentos inolvidables. Finalmente quiero agradecer a Ernesto, quien me ha acompañado en este camino, gracias por tu cariño, por comprenderme y apoyarme.

ÍNDICE

Índice Figuras

Capítulo III

Capítulo IV

Índice Tablas

Capítulo III

Capítulo IV

Capítulo V

RESÚMENES

RESUMEN

Título: “Recuperación de polifenoles de efluentes de almazara mediante procesos de membrana y tratamiento biológico de las corrientes de rechazo”

Hoy en día, la recuperación de efluentes industriales se está convirtiendo en un enfoque prometedor en el contexto de la economía circular. La escasez de fuentes de agua dulce, junto con la protección del medio ambiente, hace necesarias tanto la reutilización del agua como la recuperación de compuestos valiosos. Millones de toneladas de aceite de oliva son producidos cada año en el sector mediterráneo, lo que conlleva gran cantidad de aguas residuales con elevada carga orgánica y polifenoles. Los polifenoles son compuestos de carácter fitotóxico, los cuales son dañinos para el medio ambiente. Sin embargo, poseen una alta actividad antioxidante, lo que los hace potencialmente valiosos para su comercialización. La presente Tesis Doctoral se ha llevado a cabo con el fin de implementar la economía circular (“zero waste”, cero desechos) para el tratamiento de estas aguas residuales. Para ello, diferentes combinaciones de procesos fueron utilizados para, por una parte, recuperar compuestos fenólicos, como también tratar estas aguas residuales para ser reincorporadas en el proceso productivo. El agua residual tratada corresponde a agua de lavado de aceite de oliva (OOWW, “olive oil washing wastewater”), obtenida a la salida de la centrifugación vertical, generada en la etapa de lavado de aceite del proceso de elaboración de aceite de oliva mediante centrifugación de dos fases. El estudio integral tiene como eje central la utilización de diferentes procesos de membrana, resinas de adsorción y aplicación de un tratamiento biológico para lograr el objetivo acometido.

En primera instancia se realizó un pretratamiento del OOWW que contempló flotación, sedimentación y filtración con cartucho, logrando eliminar el 89% de las grasas y aceites y un 40% de color, turbidez y sólidos en suspensión.

A continuación, el agua fue alimento del proceso de Ultrafiltración (UF). En esta etapa, diferentes membranas (diferentes materiales y cortes moleculares),

condiciones operacionales (variación de la presión transmembranal y de la velocidad tangencial, TMP y CFV, respectivamente) y protocolos de limpieza fueron estudiados con la finalidad de analizar cómo afectaban a la densidad de flujo de permeado y a la recuperación de estos compuestos fenólicos. En esta etapa, el objetivo era obtener un permeado rico en compuestos fenólicos, pero de baja carga orgánica. Se utilizaron modelos matemáticos semi-empíricos (modelos Hermia adaptados a filtración tangencial, modelo combinado y modelo de resistencias en serie), así como métodos estadísticos y de aprendizaje automático (superficies de respuesta (RSM) y redes neuronales artificiales (ANN)) para predecir el comportamiento de la densidad de flujo de permeado de cada membrana y, a su vez, para analizar el tipo de ensuciamiento predominante en cada una. La membrana UP005 de 5 kDa bajo las condiciones de TMP de 2 bar y CFV de 2.5 $m \cdot s^{-1}$ se consideró la mejor opción, obteniendo una densidad de flujo de permeado estable de 40 $L \cdot h^{-1} \cdot m^{-2}$, un bajo rechazo de compuestos fenólicos (8.01 %) y un alto rechazo de materia orgánica (61.18%). Los modelos matemáticos indicaron que más de un proceso de ensuciamiento (principalmente formación de torta y bloqueo de poros) contribuyeron al ensuciamiento de la membrana. El análisis estadístico ANOVA de RSM mostró que tanto la CFV como la TMP son variables significativas con respecto a la densidad de flujo de permeado para todas las membranas estudiadas. Con el modelo ANN fue posible predecir los datos experimentales de variación de densidad de flujo de permeado con el tiempo para las membranas de ultrafiltración consideradas.

Optimizada la etapa de UF, se estudiaron dos procesos para la concentración de los compuestos fenólicos presentes en el permeado de la UF, la nanofiltración (NF) y la ósmosis directa (FO). Al igual que con la UF, varias membranas fueron analizadas en la NF bajo diferentes condiciones operacionales, pero esta vez para obtener el mayor rechazo de compuestos fenólicos para ser concentrados. Con la membrana NF270 a CFV de $1 m \cdot s^{-1}$ de y TMP de 10 bar, se logró una densidad de flujo de permeado estable de 74.4 $L \cdot h^{-1} \cdot m^{-2}$, un rechazo de compuestos fenólicos totales del 94% y un rechazo de materia orgánica del 83%. Para el estudio del ensuciamiento de las membranas y la eficiencia del protocolo de limpieza utilizado, se utilizaron dos técnicas espectroscópicas, espectroscopía de fluorescencia 2D y espectroscopia infrarroja por transformada de Fourier (FTIR). Mediante estas técnicas fue posible obtener información sobre la adsorción de algunos compuestos en las superficies de las

membranas, así como evaluar la eficiencia del protocolo de limpieza. En cuanto a la FO, dos membranas diferentes fueron analizadas para la concentración de los compuestos fenólicos. En esta etapa se utilizaron aguas residuales procedentes de la etapa de fermentación en la elaboración de aceitunas de mesa (FTOP) como corriente de elevada presión osmótica (disolución de arrastre o extractora) debido a la alta salinidad. Esta etapa, con la membrana HFFO6 que proporcionó un caudal de 30 $L \cdot h^{-1}$, no solo permitió la concentración de compuestos fenólicos en un 79%, sino también la dilución de la FTOP.

Teniendo ya un concentrado de compuestos fenólicos proveniente de la FO o de la NF, cuatro resinas de adsorción fueron estudiadas para la adsorción de estos compuestos fenólicos presentes en los concentrados. Se estudiaron diferentes concentraciones de resina, tiempos de contacto y disolventes de desorción para la obtención de un concentrado puro, rico en compuestos fenólicos. En esta etapa los mejores resultados se obtuvieron con 40 $g \cdot L^{-1}$ de la resina MN200 y con una disolución 50% etanol/agua para la desorción. Una vez recuperados los compuestos mediante resinas, las aguas resultantes (concentrado de FO, rechazo de NF y rechazo del proceso de UF) fueron sometidas a tratamientos biológicos. Para ello, primero se realizaron estudios en "batch" para evaluar la concentración inicial a la cual se comenzaría el ensayo en los reactores biológicos. El tratamiento biológico mediante SBR permitió eliminar en gran medida la materia orgánica y los compuestos fenólicos (caso del rechazo de UF) presentes, logrando obtener efluentes con características aptas para ser utilizadas como agua de limpieza de maquinaria.

RESUM

Títol: “Recuperació de polifenols d'efluents de trull mitjançant processos de membrana i tractament biològic dels corrents de rebuig”

Avui dia, la recuperació d'efluents industrials esdevé un enfocament prometedor en el context de l'economia circular. L'escassetat de fonts d'aigua dolça juntament amb la protecció del medi ambient fa necessàries tant la reutilització de l'aigua com la recuperació de compostos valuosos. Milions de tones d'oli d'oliva són produïts cada any al sector mediterrani, cosa que comporta gran quantitat d'aigües residuals amb elevada càrrega orgànica i polifenols. Els polifenols són compostos de caràcter fitotòxic, els quals són perjudicials per al medi ambient. No obstant això, tenen una alta activitat antioxidant, cosa que els fa potencialment valuosos per a la seva comercialització. Aquesta Tesi Doctoral s'ha dut a terme per implementar l'economia circular (zero waste, zero deixalles) per al tractament d'aquestes aigües residuals. Per això, diferents combinacions de processos van ser utilitzats per, per una banda, recuperar compostos fenòlics, com també tractar aquestes aigües residuals per ser reincorporades al procés productiu. L'aigua residual tractada correspon a aigua de rentat d'oli d'oliva (OOWW, olive oil washing wastewater), obtinguda a la sortida de la centrifugació vertical, generada a l'etapa de rentat d'oli del procés d'elaboració d'oli d'oliva mitjançant centrifugació de dues fases. L'estudi integral té com a eix central la utilització de diferents processos de membrana, resines d'adsorció i aplicació d'un tractament biològic per assolir l'objectiu emprès.

En primera instància es va realitzar un pretractament de l'OOWW que va contemplar flotació, sedimentació i filtració amb cartutx, aconseguint eliminar el 89% dels greixos i olis i un 40% de color, terbolesa i sòlids en suspensió.

Tot seguit, l'aigua va ser aliment del procés d'Ultrafiltració (UF). En aquesta etapa, diferents membranes (diferents materials i talls moleculars), condicions operacionals (variació de la pressió transmembranal i de la velocitat tangencial, TMP i CFV, respectivament) i protocols de neteja van ser estudiats amb la finalitat d'analitzar com afectaven la densitat de flux de permeat i la recuperació d'aquests compostos fenòlics. En aquesta etapa, l'objectiu era

obtenir un ric permeat en compostos fenòlics, però de baixa càrrega orgànica. Es van utilitzar models matemàtics semi-empírics (models Hèrmia adaptats a filtració tangencial, model combinat i model de resistències en sèrie), així com mètodes estadístics i d'aprenentatge automàtic (superfícies de resposta (RSM) i xarxes neuronals artificials (ANN)) per predir el comportament de la densitat de flux de permeat de cada membrana i, alhora, per analitzar el tipus d'embrutament predominant en cadascuna. La membrana UP005 de 5 kDa sota les condicions de TMP de 2 bar i CFV de 2.5 $m \cdot s^{-1}$ es va considerar la millor opció, obtenint una densitat de flux de permeat estable de 40 $L \cdot h^{-1} \cdot m^{-2}$, un baix rebuig de compostos fenòlics (8.01%) i un alt rebuig de matèria orgànica (61.18%). Els models matemàtics van indicar que més d'un procés d'embrutament (principalment formació de coca i bloqueig de porus) van contribuir a embrutar la membrana. L'anàlisi estadística ANOVA de RSM va mostrar que tant la CFV com la TMP són variables significatives respecte a la densitat de flux de permeat per a totes les membranes estudiades. Amb el model ANN va ser possible predir les dades experimentals de variació de densitat de flux de permeat amb el temps per a les membranes d'ultrafiltració considerades.

Optimitzada l'etapa d'UF, es van estudiar dos processos per a la concentració dels compostos fenòlics presents al permeat de la UF, la nanofiltració (NF) i l'osmosi directa (FO). Igual que amb la UF, diverses membranes van ser analitzades a la NF sota diferents condicions operacionals, però aquesta vegada per obtenir el major rebuig de compostos fenòlics per ser concentrats. Amb la membrana NF270 a CFV de $1 m \cdot s^{-1}$ de i TMP de 10 bar, es va aconseguir una densitat de flux de permeat estable de 74.4 $L \cdot h^{-1} \cdot m^{-2}$, un rebuig de compostos fenòlics totals del 94% i un rebuig de matèria orgànica del 83%. Per estudiar l'embrutament de les membranes i l'eficiència del protocol de neteja utilitzat, es van utilitzar dues tècniques espectroscòpiques, espectroscòpia de fluorescència 2D i espectroscòpia infraroja per transformada de Fourier (FTIR). Mitjançant aquestes tècniques va ser possible obtenir informació sobre l'adsorció d'alguns compostos a les superfícies de les membranes, així com avaluar l'eficiència del protocol de neteja. Pel que fa a la FO, dues membranes diferents van ser analitzades per a la concentració dels compostos fenòlics. En aquesta etapa es van utilitzar aigües residuals procedents de l'etapa de fermentació en l'elaboració d'olives de taula (FTOP) com a corrent d'elevada pressió osmòtica (dissolució d'arrossegament o extractor) a causa de

l'alta salinitat. Aquesta etapa, amb la membrana HFFO6 que va proporcionar un cabal de 30 $L \cdot h^{-1}$, no només va permetre la concentració de compostos fenòlics en un 79%, sinó també la dilució de la FTOP.

Tenint ja un concentrat de compostos fenòlics provinent de la FO o de la NF, quatre resines d'adsorció van ser estudiades per a l'adsorció d'aquests compostos fenòlics presents als concentrats. Es van estudiar diferents concentracions de resina, temps de contacte i dissolvents de desorció per obtenir un concentrat pur, ric en compostos fenòlics. En aquesta etapa els millors resultats es van obtenir amb 40 $g \cdot L^{-1}$ de la resina MN200 i amb una dissolució 50% etanol/aigua per a la desorció. Un cop recuperats els compostos mitjançant resines, les aigües resultants (concentrat de FO, rebuig de NF i rebuig del procés d'UF) van ser sotmeses a tractaments biològics. Per això, primer es van realitzar estudis a batch per avaluar la concentració inicial a la qual es començaria l'assaig en els reactors biològics. El tractament biològic mitjançant SBR va permetre eliminar en gran mesura la matèria orgànica i els compostos fenòlics (cas del rebuig d'UF) presents, aconseguint obtenir efluents amb característiques aptes per ser utilitzades com a aigua de neteja de maquinària.

ABSTRACT

Title: “Recovery of polyphenols from oil mill effluents through membrane processes and biological treatment of reject streams”

Nowadays, the recovery of industrial effluents is becoming a promising approach in the context of the circular economy. The scarcity of fresh water sources, together with the protection of the environment, makes both the reuse of water and the recovery of valuable compounds necessary. Millions of tons of olive oil are produced each year in the Mediterranean sector, which leads to a large amount of wastewater with a high organic load and polyphenols. Polyphenols are phytotoxic compounds, which are harmful to the environment. However, they have high antioxidant activity, which makes them potentially valuable for marketing. This Doctoral Thesis has been carried out in order to implement the circular economy ("zero waste", zero waste) for the treatment of this wastewater. For this, different combinations of processes were used to, on the one hand, recover phenolic compounds, as well as treat this wastewater to be reincorporated into the production process. The treated wastewater corresponds to olive oil washing water (OOWW, "olive oil washing wastewater"), obtained at the outlet of the vertical centrifugation, generated in the oil washing stage of the olive oil production process by means of two-stage centrifugation. The central axis of the comprehensive study is the use of different membrane processes, adsorption resins and the application of a biological treatment to achieve the objective undertaken.

In the first instance, a pre-treatment of the OOWW was carried out that included flotation, sedimentation and cartridge filtration, managing to eliminate 89% of fats and oils and 40% of colour, turbidity and suspended solids.

Next, the water was fed into the Ultrafiltration (UF) process. In this stage, different membranes (different materials and molecular weight cut-off), operational conditions (variation of transmembrane pressure and cross flow velocity, TMP and CFV, respectively) and cleaning protocols were studied in order to analyse how they affected the density of permeate flux and the recovery of these phenolic compounds. In this stage, the objective was

to obtain a permeate rich in phenolic compounds, but with a low organic load. Semi-empirical mathematical models (Hermia models adapted to tangential filtration, combined model and series resistance model), as well as statistical and machine learning methods (response surfaces (RSM) and artificial neural networks (ANN)) were used to predict the behaviour of the permeate flux density of each membrane and, in turn, to analyse the type of fouling predominant in each one. The 5 kDa UP005 membrane under the conditions of TMP of 2 bar and CFV of 2.5 $m \cdot s^{-1}$ was considered the best option, obtaining a stable permeate flux density of 40 $L \cdot h^{-1} \cdot m^{-2}$, a low rejection of phenolic compounds (8.01%) and high rejection of organic matter (61.18%). Mathematical models indicated that more than one fouling process (primarily cake formation and pore blockage) contributed to membrane fouling. ANOVA statistical analysis of RSM showed that both CFV and TMP are significant variables with respect to permeate flux density for all membranes studied. With the ANN model it was possible to predict the experimental data of permeate flux density variation over time for the considered ultrafiltration membranes.

Once the UF stage was optimized, two processes were studied for the concentration of the phenolic compounds present in the UF permeate, nanofiltration (NF) and forward osmosis (FO). As with the UF, various membranes were tested at the NF under different operating conditions, but this time to obtain the highest rejection of phenolic compounds to be concentrated. With the NF270 membrane at CFV of $1 m \cdot s^{-1}$ and TMP of 10 bar, a stable permeate flux density of 74.4 $L \cdot h^{-1} \cdot m^{-2}$ was achieved, a rejection of total phenolic compounds of 94% and a rejection of organic matter of 83%. To study membrane fouling and the efficiency of the cleaning protocol used, two spectroscopic techniques were used: 2D fluorescence spectroscopy and Fourier transform infrared spectroscopy (FTIR). Through these techniques it was possible to obtain information on the adsorption of some compounds on the membrane surfaces, as well as to evaluate the efficiency of the cleaning protocol. Regarding FO, two different membranes were analysed for the concentration of phenolic compounds. In this stage, wastewater from the fermentation stage in the production of table olives (FTOP) was used as a current with high osmotic pressure (draw or extracting solution) due to the high salinity. This stage, with the HFFO6 membrane that provided a flow rate of 30 $L \cdot h^{-1}$, not only allowed the concentration of phenolic compounds by 79%, but also the dilution of the FTOP.

Already having a concentrate of phenolic compounds from FO or NF, four adsorption resins were studied for the adsorption of these phenolic compounds present in the concentrates. Different resin concentrations, contact times and desorption solvents were studied to obtain a pure concentrate, rich in phenolic compounds. In this stage, the best results were obtained with 40 $g \cdot L^{-1}$ of the MN200 resin and with a 50% ethanol/water solution for desorption. Once the compounds were recovered by means of resins, the resulting waters (FO concentrate, NF rejection and UF process rejection) were subjected to biological treatments. To do this, first batch studies were carried out to evaluate the initial concentration at which the test would begin in biological reactors. The biological treatment by means of SBR allowed to eliminate to a great extent the organic matter and the phenolic compounds (case of the rejection of UF) present, obtaining effluents with suitable characteristics to be used as cleaning water for machinery.

PREFACIO

PREFACIO

El presente trabajo de Tesis Doctoral se desarrolló dentro del Programa de Doctorado de Ingeniería y Producción Industrial de la Escuela de Doctorado de la Universitat Politècnica de València, gracias a la beca ligada a la subvención para la contratación de personal investigador de carácter predoctoral (referencia ACIF/2018/166), entregada por la Conselleria de Innovación, Universidades, Ciencia y Sociedad Digital de la Generalidad Valenciana, financiada por el Fondo Social Europeo 2014-2018. El trabajo ha formado parte de un proyecto de investigación con nombre "Implementación de tecnología de membranas para la valoración de los compuestos fenólicos presentes en las aguas residuales de la industria de producción de aceite de oliva" (referencia CTM2017-88645-R). El cual ha sido financiado por la Agencia estatal de investigación del Ministerio de Economía y Competitividad.

Por otra parte, agradecer al Laboratorio Asociado de Química Verde-LAQV de la Universidade Nova de Lisboa, el cual es financiado por fondos nacionales del FCT/MCTES (UIDB/50006/2020 y UIDP/50006/2020). Lugar donde la doctoranda realizó una estancia internacional, gracias a la beca de subvención para estancias de contratados predoctorales en centros de investigación fuera de la Comunitat Valenciana (referencia BEFPI/2021/018), entregada por la Conselleria de Innovación, Universidades, Ciencia y Sociedad Digital de la Generalidad Valenciana, financiada por el Fondo Social Europeo.

Los resultados se han presentado tanto de forma oral como mediante poster en diversos congresos de categoría internacional, obteniendo un premio al mejor póster en el congreso "9th International Water Association (IWA) membrane technology conference and exhibition for water and wastewater treatment and reuse" celebrado en junio de 2019 en Toulouse. Durante la tesis doctoral, se han publicado hasta la fecha cuatro artículos y tres se encuentran bajo revisión. Las revistas seleccionadas para publicar los resultados del trabajo son de ámbito internacional, con un índice de impacto situado en el primer cuartil, dentro de la categoría de Ingeniería Química e Ingeniería Ambiental.

Seis han sido los capítulos en los que se ha estructurado el trabajo de investigación, cuyo contenido se presenta a continuación. En el primero, Capítulo I, se presentan las

motivaciones y la justificación que han llevado al desarrollo de esta Tesis Doctoral. En este apartado también se presenta tanto el objetivo principal como los objetivos específicos a desarrollar. Le sigue el capítulo II, con un listado detallado de las contribuciones de esta Tesis, tanto en revistas como en congresos. En el siguiente, capítulo III, se presenta una revisión bibliográfica referente a todos los conceptos ligados a esta tesis doctoral. Se introducen los antecedentes de la producción de aceite de oliva, tanto a nivel nacional como internacional. En este capítulo también se detallan las características del efluente, así como las tecnologías disponibles actualmente para el tratamiento de estas aguas, destacando las tecnologías implementadas en este estudio, procesos de membrana, adsorción con resinas y tratamiento biológico. En el Capítulo IV se describen los materiales, reactivos y equipos de medición utilizados. De igual manera, se detallan los métodos analíticos empleados en la determinación de los diferentes parámetros. Por otra parte, se describe la metodología experimental seguida junto con las plantas piloto necesarias para cumplir con el desarrollo experimental. En el Capítulo V se presentan lo resultados en formato de artículo científico en versión autor. Por último, en el Capítulo VI se detallan las principales conclusiones obtenidas tras el análisis de todos los resultados aportados.

CAPÍTULO I
MOTIVACIÓN Y OBJETIVOS

I. MOTIVACIÓN Y OBJETIVOS

I.1 Motivación y Justificación

El crecimiento y desarrollo de la población mundial conlleva un aumento en las presiones sociales y la conciencia de la necesidad de mejorar y cuidar el medio ambiente. Esto genera una mayor presión a la hora de disponer y tratar los residuos generados por las industrias. Esto, unido a la escasez de fuentes de agua dulce, ha generado una preocupación mundial por la recuperación de efluentes de procesos industriales, ya que uno de los grandes problemas medioambientales es la gran cantidad de aguas residuales que generan cada año diversos sectores industriales.

Uno de estos sectores, que afecta principalmente a los países mediterráneos, es la industria del aceite de oliva, donde se produce una gran cantidad de aguas residuales de almazara (OMW, por siglas en inglés de olive mill wastewater). Estas aguas residuales tienen un alto contenido de materia orgánica, un perfil ácido y una gran cantidad de compuestos fitotóxicos. Estos compuestos fitotóxicos son los compuestos fenólicos, los cuales son dañinos para el medio ambiente, pero también tienen una excelente actividad antioxidante, lo que los hace comercialmente valiosos. Por otro lado, los alimentos funcionales de origen vegetal han ganado mucha atención en los últimos años, debido a su disponibilidad natural y potencial terapéutico, con un lugar destacado para los compuestos bioactivos que se encuentran en los vegetales. Entre ellos, los compuestos fenólicos son el grupo más abundante y extendido de moléculas bioactivas.

Si bien diversas técnicas se han implementado y estudiado para el tratamiento de estas aguas, la mayoría está basada en estudios con agua residual proveniente el proceso productivo de aceite de oliva mediante centrifugación de tres fases. Esto es debido a que la mayoría de los países que producen aceite de oliva utilizan aún este proceso. Sin embargo, se espera que esto cambie, ya que el proceso de centrifugado de dos fases es más eficiente y produce menos residuos. Esto es importante a la hora de buscar soluciones, ya que las características de las aguas residuales de almazara dependen directamente del proceso productivo utilizado. Por otra

parte, es importante destacar que España es el productor por excelencia del aceite de oliva, c siendo el proceso de centrifugación de dos fases el más utilizado en este país. Esto hace que se generen millones de metros cúbicos por año de OMW, con elevada concentración de compuestos fenólicos, ya que, aproximadamente, solo el 2% de estos compuestos son transferidos del fruto del olivo al aceite de oliva, mientras que el porcentaje restante se pierde en los residuos, especialmente en las corrientes líquidas, debido a que la mayoría de los polifenoles son hidrosolubles. Finalmente, la valorización de aguas y residuos del sector agroalimentario supone un reto a la vez que un factor clave para desarrollar nuevas estrategias para conseguir una economía circular.

El proceso propuesto para el tratamiento de OMW debe enfocarse en los principales problemas: alto consumo de energía, baja eficiencia y generación de contaminación secundaria. El tratamiento no solo debe reducir significativamente la materia orgánica, sino también asegurar la posibilidad de recuperar los compuestos fenólicos. Además, se deben cumplir muchos requisitos relacionados con la composición, la pureza y la calidad de los compuestos recuperados. Los tratamientos actuales para este tipo de aguas residuales (lagunas, evaporación natural, condensación térmica, compostaje, tratamiento con cal y arcilla, y procesos fisicoquímicos como coagulación, floculación y electrocoagulación), no entregan resultados del todo satisfactorios. Diversos estudios de investigación muestran que la verdadera gestión de OMW solo se puede lograr combinando diferentes tecnologías.

Esta tesis doctoral pretende, por tanto, encontrar una solución a este problema. Por un lado, se estudia la recuperación de los compuestos fenólicos contenidos en estas aguas residuales, y, por otro lado, la recuperación de agua corriente para su reintegración en el proceso productivo. De esta forma, se ayudaría a esta industria a lograr una economía circular en sus procesos productivos. Esto haría que, además de reducir el impacto ambiental causado por estas aguas residuales, se lograra obtener un producto de elevado valor añadido, además de la reutilización de esa agua para la limpieza de la maquinaria.

Con este fin, se han investigado varios métodos y se han propuesto dos opciones de tratamiento para tratar un OMW proveniente del proceso productivo de aceite de oliva de centrifugación en dos fases, ampliamente utilizado en España, denominado OOWW (por sus

siglas en inglés de olive oil washing wastewater). Se han considerado procesos de membrana combinados con adsorción de resina para la recuperación de compuestos fenólicos. A esto le sigue un tratamiento biológico para restaurar los cursos de agua. Es importante señalar que los estudios fueron realizados con disoluciones modelo y aguas residuales reales (Segorbe, Comunidad Valenciana, España).

I.2. OBJETIVOS

I.2.1. Objetivo General

El objetivo principal de esta tesis es establecer el pretratamiento y las condiciones óptimas de operación para recuperar, mediante procesos de membrana, compuestos fenólicos a partir de aguas residuales de almazara, así como efectuar un tratamiento biológico de las corrientes de rechazo, de modo que se propone una valorización y tratamiento integral de las aguas residuales.

I.2.2. Objetivos Específicos

Para conseguir el objetivo general planteado, fue necesario ir desarrollando una serie de objetivos más específicos, los cuales se presentan a continuación agrupados en etapas:

Etapa 1: Caracterización y Pretratamiento

- Caracterizar los efluentes de almazara provenientes del proceso de elaboración de aceite de oliva mediante centrifugación en dos fases.

- Proponer un pretratamiento para eliminar tanto la materia orgánica suspendida como aceites y grasas de los efluentes

Etapa 2: Procesos de membrana

- Estudiar el efecto de las condiciones de operación (velocidad tangencial y presión transmembranal) sobre la densidad de flujo de permeado y el rechazo a la materia orgánica y compuestos fenólicos para las diferentes membranas estudiadas.

- Seleccionar la membrana y las condiciones óptimas de operación en cada proceso de membrana para conseguir: en el proceso de UF: la mayor densidad de flujo de permeado y eliminación de materia orgánica, con baja eliminación de compuestos fenólicos. En el proceso

de NF: la mayor densidad de flujo de permeado y el mayor rechazo de compuestos fenólicos. En el proceso FO: la mayor densidad de flujo de permeado y el mayo rechazo de compuestos fenólicos, con bajo paso inverso de sales.

- Optimizar protocolos de limpieza de las membranas de UF y NF para recuperar la permeabilidad inicial de las membranas.

- Modelizar matemáticamente la variación de la densidad de flujo de permeado con el tiempo, e identificar el tipo de ensuciamiento para las membranas de UF.

- Evaluar las técnicas de espectroscopía de fluorescencia 2D y espectroscopía infrarroja por transformada de Fourier (FTIR) para estudiar el ensuciamiento de la membrana de NF.

Etapa 3: Proceso Adsorción/Desorción

- Estudiar el proceso de adsorción mediante resinas comerciales no iónicas con el fin de recuperar selectivamente los compuestos fenólicos presentes en las aguas residuales de las almazaras.

- Estudiar la desorción de los compuestos fenólicos de las resinas anteriormente estudiadas, encontrando el disolvente que recupere el mayor porcentaje de compuestos fenólicos.

- Determinar la mejor resina y evaluar su eficiencia en la recuperación de compuestos fenólicos a partir de las corrientes concentradas por medio de NF y FO, respectivamente.

Etapa 4: Tratamiento Biológico

- Determinar la concentración de cada tipo de corriente (rechazo de UF y NF, concentrado de FO) apropiada como alimentación inicial a un reactor biológico.

- Evaluar la eficacia del tratamiento biológico por medio de reactores biológicos secuenciales (SBR) de las corrientes para eliminar materia orgánica

CAPITULO II

CONTRIBUCIONES

II. CONTRIBUCIONES

Los resultados obtenidos durante el desarrollo de esta tesis doctoral se han divulgado tanto por medio de publicaciones en revistas de gran prestigio, como en congresos internacionales. A continuación, se presenta un listado de estas contribuciones.

II.1. Publicaciones en revistas

- M. Cifuentes-Cabezas, C. Carbonell-Alcaina, M.C. Vincent-Vela, J.A. Mendoza-Roca, S. Álvarez-Blanco, "Comparison of different ultrafiltration membranes as first step for the recovery of phenolic compounds from olive-oil washing wastewater", Process Safety and Environmental Protection 149 (2021) 724–734
  Doi: https://doi.org/10.1016/j.psep.2021.03.035
- M. Cifuentes-Cabezas, M.C. Vincent-Vela, J.A. Mendoza-Roca, S. Álvarez-Blanco, "Use of ultrafiltration ceramic membranes as a first step treatment for olive oil washing wastewater", Food and Bioproducts Processing 135 (2022) 60–73
  Doi: https://doi.org/10.1016/j.fbp.2022.07.002
- M. Cifuentes-Cabezas, C.M. Sanchez-Arévalo, J.A. Mendoza- Roca, M.C. Vincent-Vela, S. Álvarez-Blanco, "Recovery of phenolic compounds from olive oil washing wastewater by adsorption/desorption process", Separation and Purification Technology 298 (2022) 121562
  Doi: https://doi.org/10.1016/j.seppur.2022.121562
- M. Cifuentes-Cabezas, M.C. Vincent-Vela, J.A. Mendoza-Roca, S. Álvarez-Blanco, "Management of reject streams from hybrid membrane processes applied to phenolic compounds removal from olive mill wastewater by adsorption/desorption and biological processes", Journal of Water Process Engineering 50 (2022) 103208
  Doi: https://doi.org/10.1016/j.jwpe.2022.103208.
- M. Cifuentes-Cabezas, C.F. Galinha, J.G. Crespo, M.C. Vincent-Vela, J.A. Mendoza-Roca, S. Álvarez-Blanco, "Nanofiltration of wastewaters from olive oil production:

study of operating conditions and analysis of fouling by 2D fluorescence and FTIR spectroscopy", Chemical Engineering Journal 454 Part 1 (2023), 140025
Doi: https://doi.org/10.1016/j.cej.2022.140025

- M. Cifuentes-Cabezas, A. Pavani, M.C. Vincent-Vela, J.A. Mendoza-Roca, S. Álvarez-Blanco, "Concentration of phenolic compounds from olive washing wastewater by forward osmosis using table olive fermentation brine as draw solution". Environmental Technology & Innovation. (En revisión)
- M. Cifuentes-Cabezas, J.L. Bohórquez-Zurita, S. Gil-Herrero, M.C. Vincent-Vela, J.A. Mendoza-Roca, S. Álvarez-Blanco, "Deep study on fouling modelling of ultrafiltration membranes used for the treatment of OMW: comparison between semi-empirical models, response surface and artificial neural network". Food and Bioprocess Technology. (En revisión)

II.2. Presentaciones en congresos

II.2.1 Póster:

- M. Cifuentes-Cabezas, C.F. Galinha, J.G. Crespo, M.C. Vincent-Vela, J.A. Mendoza-Roca, S. Álvarez-Blanco, "Study of the use of 2D fluorescence spectroscopy and FTIR as a tool for analyzing membrane fouling after olive oil washing wastewater treatment", 37th EMS Summer School, 29 Mayo - 3 Junio 2022, Alentejo, Portugal
- M. Cifuentes-Cabezas, C. Carbonell-Alcaina, J.A. Mendoza-Roca, M.C. Vincent-Vela and S. Álvarez-Blanco, "Recovery of phenolic compounds from olive oil washing wastewater through membrane processes and resin adsorption", 18th Network Young Membrains Meeting (NYM), 25-27 Noviembre 2021, Lund, Suecia.
- M. Cifuentes-Cabezas, S. Álvarez-Blanco, J. A. Mendoza-Roca, L. Pastor-Alcañiz, "Effect of the operating conditions on the recovery of phenolic compounds from table olive wastewaters by nanofiltration", 9TH IWA-MTC, 23-27 Junio 2019, Toulouse, Francia. (Obteniendo el **Premio a mejor poster**)

- M. Cifuentes-Cabezas, C. Sempere-Vidal, C. Carbonell-Alcaina, M.C. Vincent-Vela, S. Álvarez-Blanco, J. A. Mendoza-Roca, “Treatment of olive oil production wastewater by means of coagulation/flocculation and nanofiltration”, 3RD ANQUE-ICCE, 19-21 Junio 2019, Santander, España.
- M. Cifuentes-Cabezas, S. Álvarez-Blanco, J. A. Mendoza-Roca, L. Pastor-Alcañiz. “Treatment of table olive wastewaters by means of a low fouling nanofiltration membrane”, Euromembrane, 9-13 Julio 2018, Valencia, España.

II.2.2 Oral:

- M. Cifuentes-Cabezas, J.L. Bohórquez, C. Carbonell-Alcaina, M.C. Vincent-Vela, J. A. Mendoza-Roca, S. Álvarez-Blanco "Evaluation of different ultrafiltration membranes as possible pre-treatment with a view to future recovery of phenolic compounds from olive oil washing wastewater", Euromembrane, 28 Noviembre - 02 Diciembre 2021, Copenhagen, Denmark
- M. Cifuentes-Cabezas, J.A. Mendoza-Roca, M.C. Vincent-Vela, S. Álvarez-Blanco, "Resins for the recovery of phenolic compounds from oil mill wastewater”, Flash communication, I Divulga NextGen Congress, 26-28 Mayo 2021, online modality.
- M. Cifuentes-Cabezas, J.A. Mendoza-Roca, M.C. Vincent-Vela, S. Álvarez-Blanco, "Evaluation of commercial resins to recover phenolic compounds", II Intl. Congress on Water and Sustainability, 24-26 Marzo 2021, online modality.
- M. Cifuentes-Cabezas, A. Pavani, M.-C. Vincent-Vela, J.A. Mendoza-Roca, S. Álvarez-Blanco, "Concentration of phenolic compounds from olive mill wastewater by forward osmosis using residual brines as draw solutions", **Keynote presentation**, 12th ICOM, 7-10 Diciembre 2020, online modality.
- M. Cifuentes-Cabezas, Carbonell-Alcaina, M.C. Vincent-Vela, J. A. Mendoza-Roca and S. Álvarez-Blanco, “Evaluation of permeate flux at different transmembrane pressures during the nanofiltration of table olive wastewaters”, 16th Network Young Membrains Meeting (NYM), 5-7 Julio 2018, Valencia, Spain.

CAPÍTULO III
INTRODUCCIÓN

III. INTRODUCCIÓN

III.1. PRODUCCIÓN DE ACEITE DE OLIVA Y ACEITUNA DE MESA

La producción de aceite de oliva y aceituna de mesa están relacionadas, ya que muchas veces el cultivo del olivar para ambos fines se realiza en instalaciones contiguas. Por ello, ambos serán analizados en este apartado.

III.1.1. Aceituna y Aceite de oliva; historia y antecedentes

La historia de la aceituna de mesa y del aceite de oliva se remonta hace unos 5000 años atrás con el inicio del cultivo de la aceituna. Si bien aún es un misterio su origen, una teoría nos sitúa en la región correspondiente a la antigua Persia y Mesopotamia, desde donde se extendió a Siria y Palestina. Las personas que vivían en estas áreas desarrollarían el cultivo del olivo, para luego llevarlo al norte de África. Otros creen que el árbol se originó en África, ya que los antiguos egipcios solían practicar el cultivo del olivo. Independiente del origen, hoy es el sector mediterráneo el productor mundial de aceitunas, concentrándose principalmente en España, Italia, Grecia, Turquía, Túnez y Marruecos. Todo esto gracias a los fenicios, quienes llevaron la oliva a las regiones occidentales, donde alrededor del siglo 28 a.c. llegó a los griegos, quienes fueron los que establecieron colonias en el mediterráneo [1,2].

Existen más de 35 especies de olivos de la familia *Olea*, siendo la *Olea europaea L.* la más conocida y cultivada debido a que su fruto (la aceituna) es comestible. La aceituna es una drupa de forma ovalada que pesa de 2 a 12 gramos, compuesto por un endocarpio (hueso) y un pericarpio (parte del fruto que recubre el endocarpio). Esta última está formada por el epicarpio (piel) y el mesocarpio (pulpa) y representa alrededor del 65-83% del peso total. El zumo oleoso denominado aceite de oliva, es un aceite vegetal obtenido de la aceituna y se concentra principalmente en el pericarpio (96-98%). La composición de la aceituna promedio

es principalmente agua, aceite y carbohidratos [3]. Su compleja composición química está compuesta principalmente por triglicéricos (99% del total), le siguen mono y diglicéricos, ácidos grasos, hidrocarburos, esteroles, alcoholes grasos, compuestos fenólicos, pigmentos y vitaminas liposolubles [4]. En España existen más de 260 variedades de aceitunas, si bien se utilizan principalmente 18 variedades para la producción tanto de aceite de oliva como de aceituna de mesa. De entre estas, destaca la variedad manzanilla como la más utilizada como aperitivo de mesa. Mientras que la variedad picual es la más popular para la producción de aceite de oliva virgen extra.

La calidad del aceite depende de la oliva y todo lo que le afecte como también de la tecnología de producción de este. Según el Consejo Oleico Internacional (IOC, por sus siglas en inglés) [5], el aceite obtenido exclusivamente por medios mecánicos o por otros medios físicos en condiciones, especialmente térmicas (que no provoquen alteraciones en el aceite), que no han tenido más tratamiento que el lavado, decantación, centrifugación y filtrado; es denominado aceite de *oliva virgen*, siendo el más cotizado a nivel mundial. También existe la denominación de aceite de *oliva virgen extra* que se entrega si la composición química del aceite es bastante buena y su evaluación organoléptica excelente [6].

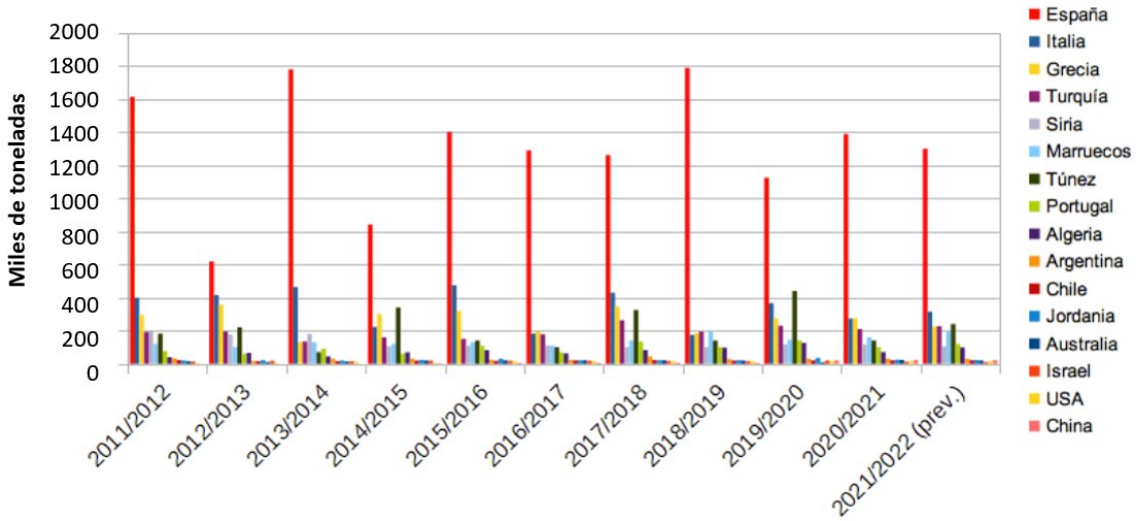

Figura 3.1. Crecimiento producción mundial aceite de oliva (modificación [7,8])

La demanda de aceite de oliva ha aumentado bebido a su reconocido alto valor nutricional y estabilidad oxidativa (debido al alto contenido en ácido oleico monoinsaturado y rica en compuestos bioactivos, entre los que destacan los compuestos fenólicos) [9],.y por ser la grasa de elección cuando se trata de salud humana y agronomía sostenible [10]. En los últimos años la producción mundial de aceite de oliva virgen se ha triplicado (ver figura 3.1) hasta alcanzar las 3.266.500 toneladas (t) en la campaña 2019/20, si bien esta cifra se redujo ligeramente en 2020/21 debido a la pandemia por Covid-19. Las estimaciones para la campaña 2021/22 proyectan un incremento del 2,9% situando la producción en 3.098.500 t. Del total de la campaña 2020/21, unas 2.051.200 t (+6,8% sobre la campaña anterior) procedían de la UE, con España siendo productor principal con 1.389.000 t (+23,4%), seguido de Italia 273.500 t (-25,4%), Grecia 275.000 t (estable) y Portugal 100.000 t (-28,8%) [11].

El sector del aceite de oliva es un pilar fundamental en la economía agroalimentaria española. El sector no solo tiene una indiscutible importancia económica, sino que también tiene un gran impacto social, ambiental y territorial. A la fecha, son 1837 las almazaras activas en España [12], 1.500 envasadoras y 22 refinerías, las que son parte fundamental de la economía de varias municipios, siendo una de las principales fuente de trabajo. España, aparte de ser líder mundial de producción de aceite de oliva, también es líder mundial en superficie y comercio exterior. El cultivo del olivo cuenta con la mayor superficie de Producción Integrada de España con 477.606 hectáreas (datos de 2019). El cultivo está presente en 15 de las 17 comunidades autónomas del país, con una distribución centro-sur y este peninsular, siendo Andalucía la mayor región productora con 1,67 millones de hectáreas. En cuanto a las exportaciones, es el tercer producto agroalimentario más exportado por España, con más de 150 países de destino [13]. Por otra parte, España cuenta con un amplio catálogo de aceites de oliva virgen, algunos poseedores de sello de calidad denominación de origen protegida (DOP), la cual identifica aquellos aceites en los que cada una de las etapas de elaboración se realiza en una zona geográfica definida. Según la última actualización (año 2016) realizada por el Ministerio de agricultura, pesca y alimentación, son 29 los aceites con este sello [14], sin embargo según la web *aceites de oliva de España* [15], son 32 los dotados con este sello.

En cuanto a la aceituna de mesa, presenta una tendencia similar a la del aceite de oliva. En los últimos años, debido al importante crecimiento de la demanda de este producto, como alimento de acompañamiento y celebración, el mercado de la aceituna de mesa ha registrado un importante crecimiento [16]. En cuanto a su producción, España también es líder mundial indiscutible en cuanto a producción y exportación, con el 62% de la producción de la UE y el 17% del mundo. Esto se debe a la gran variedad, calidad y versatilidad de la producción española. Al igual que el aceite de oliva, la industria de la aceituna de mesa aparte de ser parte esencial de la agricultura española, genera un gran impacto sociales, ambiental y territorial. Las olivas destinadas a consumo en mesa representan el 7% del total de la superficie olivarera, correspondiendo a 197.335 hectáreas (77.650 hectáreas de olivar de aceituna de mesa y 119.685 hectáreas de aptitud mixta). El 65% del total comercializado corresponde a exportaciones, exportando a más de 160 países. Si bien las cifras de la campaña 2020/21 presentaron una producción 10,1% menor con respecto a la campaña anterior (nuevamente debido a la pandemia Covid-19), España produjo el 20,5% de esta, superando en un 19,3% su volumen de producción en cuanto a la campaña anterior [17].

Estos antecedentes sitúan a la aceituna de mesa y al aceite de oliva como un producto en auge constante, siendo parte fundamental de la economía tanto de España como del sector mediterráneo debido a su importancia en la dieta del sector.

III.1.2. Procesos de extracción de Aceite de oliva

La producción de aceite de oliva es un proceso industrial que tiene como objetivo separar una de las fases líquidas (el aceite) del resto de constituyentes de la aceituna. El proceso comienza con el lavado de las aceitunas. A continuación, la estructura vegetal se rompe para hacer una pasta de aceituna, para posteriormente conseguir la formación de las fases sólida y líquida, para finalmente ser separadas. Finalmente, la fase líquida por decantación y/o centrifugación vertical se separa en aceite y agua de vegetación [18]. Esta separación da como subproducto una masa de sólidos con porcentajes variables de humedad y

contenido de aceite y residuos líquidos con porcentajes variables de materia sólida [19]. La producción de aceite de oliva se lleva a cabo en almazaras, dónde actualmente son tres son los métodos que se utilizan; prensa tradicional, centrifugación en tres fases y centrifugación en dos fases (proceso más nuevo, utilizado desde 1990) [20]. Los procesos de producción del aceite de oliva se resumen en la Figura 3.2; todos terminan con una etapa de filtrado y almacenado.

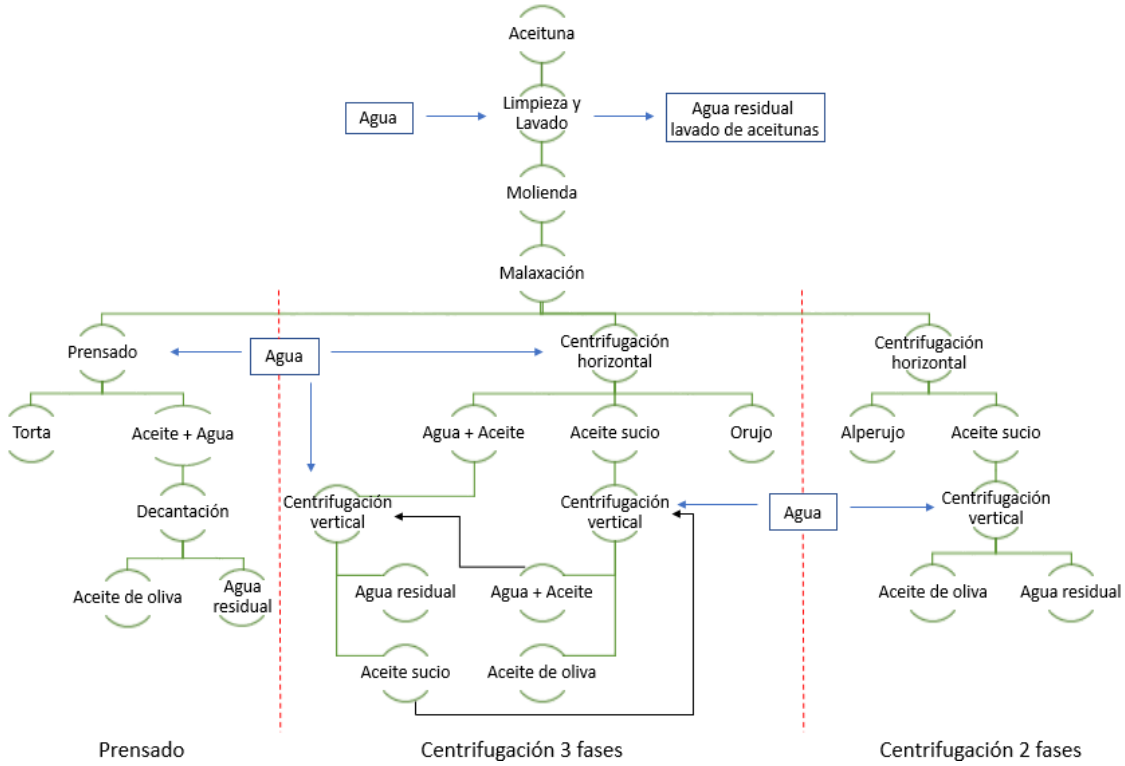

Figura 3.2. Diagrama de flujo de los diferentes procesos de extracción de aceite de oliva (modificación [21])

Es importante destacar que antes de someter la aceituna a algún proceso para la obtención de aceite de oliva, esta debe estar con un grado de maduración adecuada, ya que la maduración de la oliva afecta tanto a la acumulación de aceite en la aceituna como a la presencia y cantidad de compuestos activos presentes [19].

III.1.2.1. Proceso tradicional de prensado

Este proceso es uno de los más antiguos, por ello es denominado proceso tradicional. En este proceso de prensado, una vez lavadas, las aceitunas se trituran con agua (28 – 35 ºC) en molinos de piedra de forma cilíndrica. La pasta resultante pasa a una etapa de batido (malaxación) dónde es agitada para romper las emulsiones de aceite-agua y a la vez permitir que las gotas de aceite aumenten su tamaño. A continuación, con ayuda de una prensa, es sometida a presión, donde la fase líquida es drenada y así separada de la fase sólida. Finalmente, el aceite de oliva se separa del agua mediante centrifugación vertical o decantación. En este proceso productivo se generan dos tipos de residuos: un residuo líquido que consiste en una mezcla de zumo de aceituna y agua añadida, que contiene aceite residual; y una torta de sólidos prensados que pueden desgrasarse más mediante otros procesos [19,22]. Aunque su uso ha disminuido, este proceso tradicional de extracción del aceite de oliva se sigue utilizando en la actualidad. Un ejemplo es la región de Marrakech en Marruecos. Donde una de las técnicas de extracción del aceite de oliva es por prensado discontinuo en pequeñas unidades no motorizadas que utilizan tracción animal o unidades eléctricas semi-modernas de mayor tamaño [23]. Este proceso productivo se caracteriza por requerir poca agua, pero produce aguas residuales muy contaminadas.

III.1.2.2. Centrifugación continua de tres y dos fases

Las principales ventajas de los procesos de obtención de aceite de oliva mediante centrifugación continua frente a la tecnología de prensa tradicional son una mayor producción, un coste de mano de obra minimizado, un menor espacio requerido, una mejor calidad, un mejor control del proceso y una fácil automatización. Sin embargo, los costos de capital son altos en comparación con la tecnología de prensa. Estos métodos de separación se basan en el principio de separación de fases con diferentes densidades (agua y aceite), los cuáles gracias a la gravedad tenderán a dividirse espontáneamente. Si bien sin ayuda adicional este proceso de

separación es lento, gracias a la fuerza gravitacional artificial dada por la centrifuga, la velocidad de separación aumenta. Las centrífugas utilizadas en esta etapa son horizontales y operan con una velocidad angular logrando una aceleración entre 2.000- 3.600 veces mayor a la aceleración de la gravedad natural [19].

El proceso de obtención de aceite de oliva mediante centrifugación comienza con la molienda de las aceitunas mediante molinos metálicos, dentro de los cuales el más utilizado es el molino de martillo. Esto permite triturar las aceitunas y generar una pasta de un tamaño determinado, ya que poseen rejillas las cuales solo permiten la salida de un tamaño determinado de sólido. El proceso de molienda termina con molinos de disco, los cuales son utilizados para evitar la formación de emulsiones. A diferencia del proceso tradicional, el uso de molinos metálicos podría implicar el traspaso de trazas de metales a la pasta de la aceituna. Esto generaría cambios en el sabor y color del aceite debido a la reducción de su estabilidad oxidativa. Es por ello que los molinos deben ser fabricados con materiales inertes (tales como el acero inoxidable) para evitar dichos problemas [24]. El batido de la pasta posterior se realiza mediante batidoras que constan de entre dos y tres unidades de cubas horizontales por las cuales circula en su exterior agua a temperatura levemente superior a la ambiental (30 – 35ºC) [22]. Hasta esta etapa los procesos de centrifugación en continuo de tres y dos fases son similares. La siguiente etapa (centrifugación) es la que marca la diferencia entre ellos. La centrifugación se realiza con centrifugadoras horizontales, las cuales están formadas por un rotor cilíndrico y un rascador helicoidal, los cuales, al trabajar levemente a diferentes velocidades (diferencia de 10-20 rpm), generan que los sólidos de mayor peso se aparten al exterior, siendo arrastrados hacia un extremo del rotor, mientras que los líquidos se quedan en el centro para luego ser separados por el otro extremo [24]. En la figura 3.3 se observa un decantador centrífugo (centrífuga) utilizado en el proceso de dos y tres fases. Se puede observar que los procesos de centrifugación llevan el nombre de las fases a separar: El de tres fases, separación de aceite, fase acuosa y sólido (orujo); el de dos fases, separación de aceite del resto de componentes presentes en los frutos, tanto fase sólida como liquida (alperujo). Por otra parte, estos dos procesos de centrifugación difieren principalmente en los requerimientos de agua de proceso. En los sistemas de tres fases se añade agua al alimento antes de entrar a la centrífuga para obtener una mejor separación de los componentes, mientras que el proceso de

dos fases trabaja con el alimento directo del proceso de malaxación. Es por esto que este último proceso es denominado sistema ecológico. Otra diferencia es la fuerza (G) con la cual trabajan las centrífugas, ya que en los procesos de tres fases llegan a ser 2.000-2.600 rpm mientras que en la de dos entre 3.000-3.600 rpm [24].

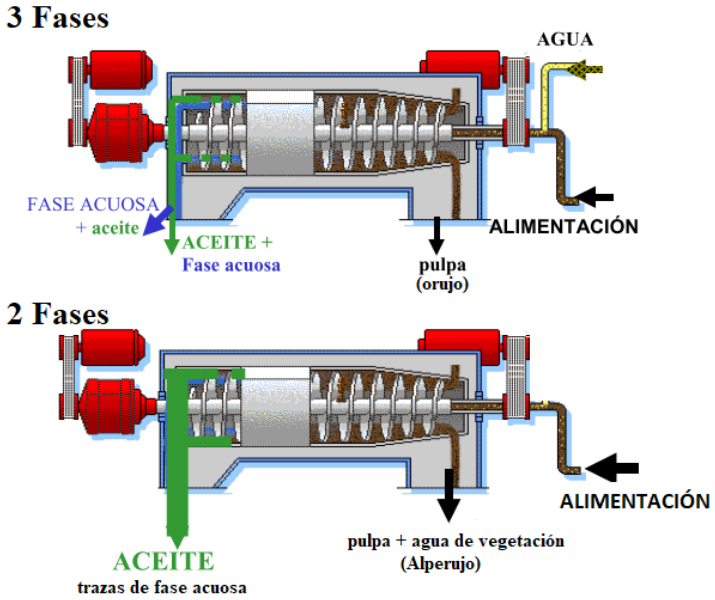

Figura 3.3. Diagrama de decantador utilizado en proceso de centrifugación continua de tres y dos fases (modificación [22])

Estos dos procesos productivos se denominan procesos *en continuo* debido a que tanto la etapa de molienda como la de centrifugación funcionan en continuo. Sin embargo, la batidora funciona por lotes, siendo el paso intermedio de los dos procesos continuos nombrados anteriormente. Por tanto, el proceso de malaxación es el cuello de botella del proceso, teniendo que trabajar en discontinuo las almazaras que no estén equipadas con varias batidoras [25].

Dependiendo del proceso de centrifugación, se generan diferentes cantidades de subproductos (residuos) (tabla 3.1). En el proceso de tres fases se generan aproximadamente tres veces más volúmenes de aguas residuales que el sistema de prensa. Al igual que el proceso

tradicional, esta técnica de centrifugado en tres fases genera un líquido denominado alpechín, formado por agua obtenida en la centrifugación y aguas de lavado, y un residuo sólido húmedo denominado orujo. Sin embargo, como se comentó anteriormente, el sistema tradicional da como resultado un agua residual más concentrada en contaminantes en comparación con los otros sistemas. Por otra parte, el proceso de dos fases, al utilizar menor cantidad de agua en su proceso, genera menos aguas residuales [21]. Esta tecnología por ende crea un desecho mixto sólido-líquido llamado alperujo (contiene alrededor de un 60% de agua y un 3% de aceite) proveniente de la centrifugación horizontal, y agua principalmente de lavado [26]. A día de hoy, en España, la tecnología de centrifugación continua de dos fases es la más utilizada. Sin embargo, varios países mediterráneos todavía utilizan el proceso de centrifugado de tres fases [27]. Se espera que en los próximos años más países adopten plenamente esta tecnología, principalmente para el ahorro de agua debido a la gran escasez de este recurso.

Tabla 3.1 Comparación de procesos productivos de aceite de oliva, [20,28,29]

Proceso		Entrada	Cantidad	Salida	Cantidad
Prensado		Aceitunas	1 ton	Aceite	200 - 230 kg
		Agua	0,1 – 0,2 m^3	Torta	400 - 500 kg
		Energía	40 – 63 kWh	Agua residual	0,4 – 0,6 m^3
Centrifugación	Tres fases	Olivas	1 ton	Aceite	200 - 260 kg
		Agua	0,8-1,1 m^3	Orujo	500 - 600 kg
		Energía	90 – 117 kWh	Agua residual	1 – 1,2 m^3
	Dos fases	Oliva	1 ton	Aceite	200 - 250 kg
		Agua	0,1 – 0,12 m^3	Alperujo	740 – 950 kg
		Energía	< 90 kWh	Agua residual	0,1 – 0,3 m^3

Independiente del proceso productivo, son tres los tipos de residuo generados. Por un parte se encentran las ramas y hojas con las que entran las olivas al proceso, un sólido húmedo (tortas, orujo o alperujo) obtenido en el proceso de extracción del aceite y alpechín o aguas residuales de almazara (OMW, por las siglas en ingles de *olive mill wastewater*), las cuales se pueden componen por agua de lavado de las aceitunas, aguas generadas en el proceso, aguas de lavado de aceite y aguas de limpieza de maquinaria [30]. Las hojas y ramas, aunque no tienen valor comercial, se utilizan en la alimentación animal, por lo que no requieren

tratamiento alguno. Diferente es lo que sucede con los otros dos residuos. El residuo semi-sólido, al todavía contener aceite, podría tener un valor comercial, pero esto depende de su contenido de aceite y agua. El orujo trifásico, con bajo contenido de humedad, tiene un mejor valor comercial que el obtenido en un sistema de proceso de dos fases. Sin embargo, gracias a las mejoras de los últimos años, este residuo pasó de tener un contenido de aceite superior al 15% a sólo el 3,5% [2]. Es por ello que hoy en día existen varias técnicas de tratamiento y valorización de estos residuos sólidos, tales como técnicas de recuperación de compuestos valiosos, uso como materia prima para manufacturar materiales cerámicos [31] y uso como piensos acuícolas [32]. Sin embargo, dado que no es objeto de esta tesis doctoral, no se profundizará en su explicación. Las características y tratamiento de las aguas residuales de almazara se describirán en la sección III.2 y III.3.

III.1.3. Proceso de elaboración de Aceituna de mesa

Según el IOC [33], se definen como "aceitunas de mesa" los productos que son elaborados a partir de frutos sanos de variedades cultivadas de olivo (*Olea europaea L.*), sometidos a tratamientos para eliminar el amargor natural y conservados mediante fermentación natural o tratamiento térmico, con o sin conservantes, envasadas con o sin líquido regulador. Existen varias técnicas de elaboración de aceitunas de mesa, siendo las más utilizadas a nivel mundial el estilo Aceitunas Naturales (las aceitunas se sumergen en salmuera y se someten a una fermentación espontánea), Estilo Californiano (aceitunas oscurecidas por oxidación en medio alcalino) y el denominado Estilo Español (aceitunas tras eliminación del amargor por tratamiento alcalino) [34]. Este último es el más utilizado en España y en los países que se dedican a la producción de aceitunas de mesa, por lo que se ahondará más en el proceso en el siguiente subapartado.

III.1.3.1. Aceitunas de mesa verdes al estilo español

En este proceso, denominado *Estilo Español*, las aceitunas verdes se procesan en 3 etapas como se observa en la figura 3.4. Primero las aceitunas son lavadas para luego pasar a la etapa de cocción, donde son remojadas durante unas 8 a 12 horas en medio alcalino (disolución de hidróxido de sodio, NaOH al 1 - 2% p/v). Durante este tiempo, la sosa penetra en la pulpa de la aceituna, produciendo la hidrólisis de la oleuropeína. En este paso se elimina el amargor del fruto, ya que éste se debe a la oleuropeína, compuesto fenólico más abundante en la fruta de la aceituna. La penetración en medio alcalino debe cubrir las tres cuartas partes de la pulpa de la aceituna. Esto se hace para que las aceitunas conserven un sabor ligeramente amargo y para que la pulpa aporte el azúcar necesario durante el periodo de fermentación. Esta etapa debe controlarse cuidadosamente ya que si la penetración de la disolución es insuficiente, las aceitunas quedarán demasiado amargas, y si es excesiva, puede desintegrar los frutos, y eliminar los hidratos de carbono necesarios para la etapa de fermentación. Debido a la elevada concentración de NaOH de la disolución generada (agua residual), esta puede ser reutilizada hasta en 14 ciclos, pero normalmente las industrias la reutilizan entre 5 y 7 ciclos. Finalmente en esta etapa se logra una reducción del volumen de agua residual y por ende una disminución del impacto ambiental [35,36].

Una vez cocida la aceituna se lava con agua para eliminar el NaOH restante. Esta fase consta de 2 a 3 lavados y dura entre 12 a 13 horas. En este caso, debido a que las aguas poseen baja concentración de NaOH, la recuperación de este compuesto no es rentable. Es por ello que como medida para mitigar el gran consumo de agua asociada a esta etapa, algunas industrias han decidido disminuir el número de lavados, dejándolo en un único lavado [37,38].

El último paso es la fermentación, el cual consiste en remojar las aceitunas en salmuera (4 a 8 % de cloruro de sodio, NaCl) durante 4 a 5 meses. La salmuera inicial puede incluir azúcar, ácido láctico, vinagre u otras sustancias aromatizantes. Es en este proceso donde se produce la descomposición del ácido elenólico del glucósido, liberando glucosa. Esta glucosa, junto con el azúcar que difunde de la pulpa de la aceituna, es utilizada como fuente de energía por los microorganismos fermentadores, los cuales las convierten en ácidos orgánicos

(principalmente ácido láctico), generando a su vez una disminución del pH a valores cercanos a 4 [39]. En este proceso se genera un agua residual de elevada carga orgánica y conductividad, la cual se denomina salmuera de fermentación del procesamiento de aceitunas de mesa (FTOP, por sus siglas en inglés de *fermentation brines from table olive processing*) [40].

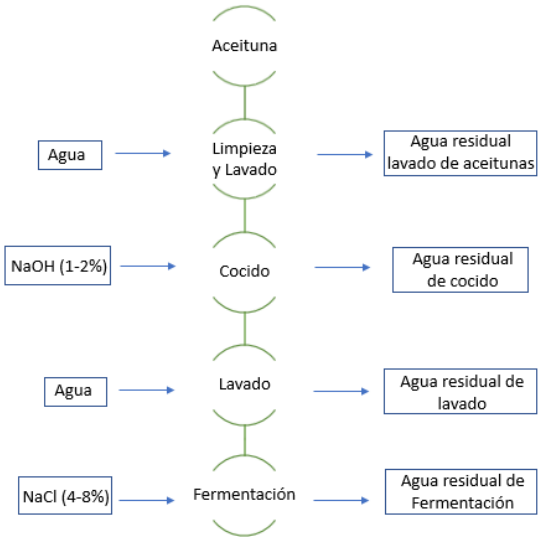

Figura 3.4. Proceso elaboración de aceituna de mesa mediante Estilo español (modificación [39])

Debido a sus características, su reutilización es difícil; es por ello que diversos estudios se han desarrollado para el tratamiento de la FTOP, ya sea para su eliminación o reutilización.

Finalmente, se ha demostrado que tanto en el proceso de elaboración de aceitunas de mesa estilo español, como en la elaboración de aceite de oliva se generan diversas aguas residuales. Estas debido a su gran volumen y elevada carga orgánica/contaminante deben ser tratadas antes de su vertido a la red [41,42]. Por otro lado, si es posible su valorización se podrían amortizar los gastos de tratamiento y transformarlo en un sistema de economía circular para la empresa.

III.2. AGUAS RESIDUALES DE ALMAZARA Y ACEITUNA DE MESA

Un punto importante a la hora de tratar y/o valorizar estos residuos, es saber su composición. En la tabla 3.2 se presentan las principales características de los residuos generados en ambos procesos productivos.

Tabla 3.2 Principales características de las aguas residuales generadas en proceso de producción de aceite de oliva y aceituna de mesa [23,38,44–51].

	Procesado						
	Aceite de oliva				Aceituna de mesa		
Parámetro	lavado aceitunas	Prensado	3 fases	2 fases*	Cocido	Lavado	FTOP
pH	5,5 – 6,6	4,5 – 5,1	3,5 – 6,0	3,5 – 6,0	9,5 – 11,5	7,2 – 12,9	3,6 – 4,5
CE (mS/cm)	2,5 – 3,0	2,0 – 5,0	2,0 – 7,9	1,5 – 3,8	10,2 – 13,0	10,0 –11,1	17 – 111
DQO (g/L)	0,8 – 2,2	30 – 190	30 – 200	4 – 24	9,4 – 35,0	4,5 – 35,0	4,5 – 61
SST (g/L)	8 – 18	10 – 12	5 – 35	2 – 7	0,1 – 3,4	0,03 – 0,2	0,09 – 2,5
TPC (g/L)	0,0– 0,1	1,0 – 11,5	0,3 – 9,8	0,1 – 1,2	0,2 – 2,5	0,5 – 2,5	0,1 – 6,0
NaOH (g/L)	–	–	–	–	11	1,5	–
Azúcares (g/L)	–		12 – 23	1,2 – 1,7	6 – 9	6 – 9	–

FTOP: aguas residuales de fermentación de la producción de aceituna de mesa; CE: conductividad eléctrica; DQO: demanda química de oxígeno; SS: sólidos suspendidos totales; TPH: compuestos fenólicos totales; *corresponde al agua residual obtenida en la centrifugación vertical (OOWW)

Las OMW, cuya producción anual en el Mediterráneo fluctúa entre 7×10^6 y 30×10^6 m^3, se caracterizan en general por una alta carga contaminante, un pH ligeramente ácido, baja alcalinidad y la presencia de fracciones lipídicas y compuestos fitotóxicos [43]. Es importante volver a recordar que el término OMW es general para las aguas residuales obtenidas en las almazaras. Cada proceso de elaboración de aceite produce aguas residuales de diferentes características dependiendo de la etapa en la cual son generadas. En cuanto a los datos presentados en la tabla correspondiente a las aguas residuales generadas en los procesos de

centrifugación, es importante señalar que para el proceso de tres fases la caracterización corresponde al agua generada en la centrifugación horizontal, mientras que para la de dos fases corresponde al agua generada en la centrifugación vertical en el proceso de lavado de aceite (OOWW, por siglas en inglés de *olive oil washing wastewater*).

Por otro lado, en cuanto a las aguas residuales del proceso de elaboración de aceituna de mesa, por cada kilo de aceituna procesada se generan 0,5 litros de agua residual en cada etapa del proceso (cocido, lavado y fermentado) [52]. Como se comentó anteriormente, la FTOP es el agua residual más problemática generada en este proceso, fluctuando su volumen entre 3,9 y 7,5 m^3 por tonelada de aceituna procesada. Este efluente, además de tener una alta carga orgánica, compuestos fenólicos y perfil ácido como el OMW, posee una elevada conductividad [47].

En el proceso de elaboración de aceite de oliva, el agua procedente del lavado de la aceituna posee alto contenido en materia inorgánica (tierra) y un contenido orgánico compuesto principalmente por piel, pulpa, triturados, ramas y restos de hojas, por lo que presenta una concentración relativamente baja de materia orgánica disuelta. Es un efluente variable en cuanto al caudal producido, ya que depende de la suciedad que contenga la aceituna y de la cantidad de aceituna lavada, para su frecuencia de renovación. Actualmente, según los artículos 4 y 5 de la Directiva de Aguas Residuales Urbanas 91/271/CEE, de la (legislación europea), se establece como valor máximo permitido de demanda química de oxígeno (DQO) para las aguas residuales urbanas una concentración de 125 mg/L [53]. Por tanto, esta agua de lavado de aceitunas se encuentra normalmente por debajo de los límites estándar para la descarga a terrenos superficiales adecuados. En cuanto a las aguas de lavado generadas en el proceso productivo de elaboración de aceitunas de mesa, algunos estudios han demostrado que es factible utilizarla como agua de riego durante el crecimiento de cuatro cultivos: pepino, pimiento, tomate y fresa. Esto demuestra que estas aguas libres de sales pueden ser utilizadas como fertilizantes y fungicidas naturales en sustitución de productos sintéticos [54].

Por el contrario, los efluentes que salen del prensado y centrifugado (horizontal y vertical) y el FTOP presentan una importante carga de orgánicos disueltos, en su mayoría

compuestos fitotóxicos que son recalcitrantes a la degradación biológica [44,55]. Los compuestos fenólicos son los responsables de los efectos fitotóxicos, a diferencia de otras sustancias como los nitrogenados, azúcares, ácidos orgánicos y polialcoholes, que en mayor o menor medida logran una degradación relativamente rápida en la naturaleza, siendo absorbidos por el medio ambiente. Sin embargo, los compuestos fenólicos poseen características antioxidantes, las cuales los hacen valiosos para diferentes industrias.

En resumen, el problema de estas aguas se debe a su fuerte olor desagradable, altísimo grado de contaminación orgánica (valores DQO de hasta 220 g/L) y una relación DQO/DBO5 entre 2,5 y 5 (difícilmente degradable), perfil ácido (pH entre 3 y 5,9), alto contenido de polifenoles (hasta 80 g/L) que no son fácilmente biodegradables y tóxicos para la mayoría de los microorganismos y alto contenido de materia sólida (sólidos totales hasta 20 g/L) [56]. En el apartado III.3 se ahondará más en las características de los compuestos y tratamientos propuestos para estas aguas.

III.2.1. Compuestos Fenólicos

Los compuestos fenólicos son metabolitos secundarios que están naturalmente presentes en varias plantas y frutas. Estos compuestos cumplen diferentes funciones, se encargan de proteger a las plantas contra patógenos o animales herbívoros, son inhibidores del crecimiento de plantas competidoras, siendo capaces también de atraer polinizadores [57]. Se caracterizan por poseer uno o más anillos aromáticos, uno o más grupos hidroxilo y varias cadenas funcionales. Se pueden clasificar según su peso molecular o estructura química, entre otras propiedades [58,59]. En la aceituna, estos compuestos representan el 1 - 3% de la masa total. En algunos trabajos de investigación se recoge que la fracción de contenido fenólico del aceite de oliva comprende sólo el 1-2% del total presente en la aceituna [60], quedando el restante en los subproductos generados en el proceso de extracción. Esto se debe a la naturaleza hidrofílica de los subproductos del aceite de oliva y la polaridad de los fenoles, por lo que son mayoritariamente más solubles en medios acuosos que en oleosos [58].

La concentración de compuestos fenólicos presentes en las aguas residuales generadas en la industria de la oliva (elaboración de aceituna de mesa y aceite) dependerá de varios factores, tanto de la solubilidad y de los coeficientes de reparto entre aceite y agua, como de todo lo que afecte al aceite (método de extracción, madurez y variedad de las aceitunas, su origen geográfico y condiciones climáticas). En general la fracción de compuestos fenólicos se encuentra compuesta por ácidos fenólicos, flavonoides, lignanos, secoiridoides y fenoles simples, entre otros [61]. En la figura 3.5 se presentan los principales grupos fenólicos, junto a su estructura química. Más de 50 compuestos fenólicos se han identificado en las OMW, siendo de entre todos los compuestos, la oleuropeína, el hidroxitirosol y el tirosol los más abundantes en los efluentes de almazara [62]. En la FTOP, la oleuropeína al hidrolizarse en el proceso de fermentación no será el compuesto mayoritario, pero sí sus productos, el tirosol y el hidroxitirosol [63].

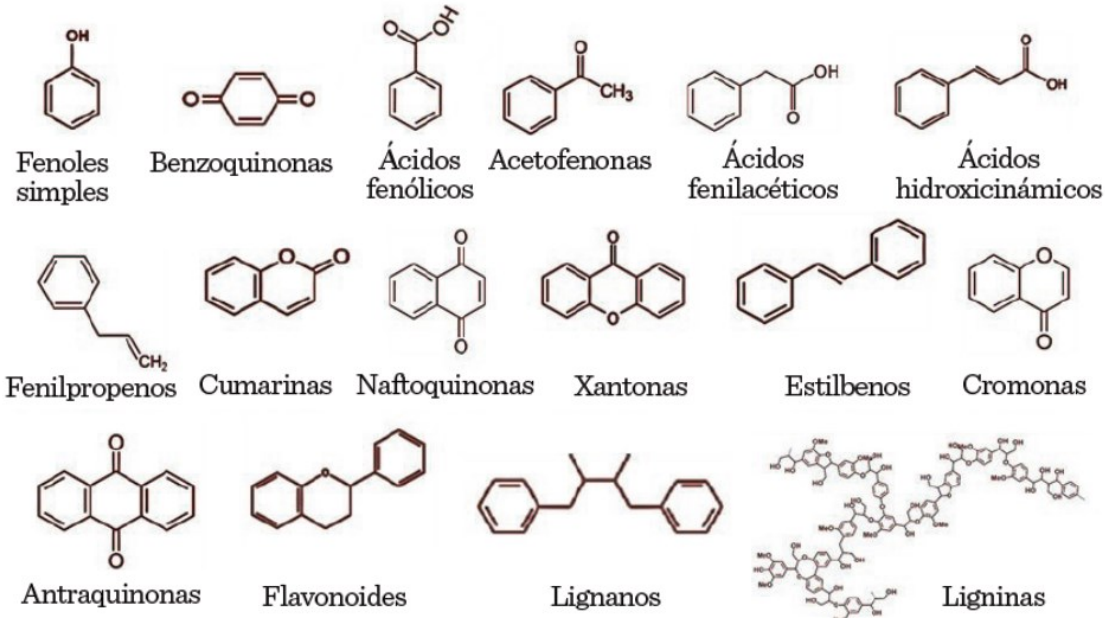

Figura 3.5. Principales clases de compuestos fenólicos [64]

Como se comentó anteriormente, debido a su carácter fitotóxico, los compuestos fenólicos presentan un gran riesgo para la vida acuática, los microorganismos y los mamíferos.

Esto hace que el tratamiento de las aguas residuales fenólicas antes de la descarga sea crucial [42]. Sin embargo, su fitotoxicidad se presenta como una dificultad a la hora de ser tratados en depuradoras con tratamientos biológicos convencionales. Durante los últimos años, han aparecido en la literatura una serie de trabajos informando sobre la gran oportunidad que implica la presencia de estos compuestos en las OMW y FTOP, y la opción de recuperar estos compuestos fenólicos. Su importancia radica en su gran poder antioxidante, el cual ataca a los radicales libres [65]. Estos radicales libres son estructuras que contienen electrones desapareados siendo altamente reactivos, los cuales pueden estar en forma libre o en cadena en el cuerpo humano. Estos radicales libres son los responsables de provocar el daño celular, ya que si bien su vida media es de microsegundos, tienen la capacidad de reaccionar con todo lo que esté a su alrededor. Estos antioxidantes son captadores de radicales libres y, por lo tanto, retrasan o inhiben la etapa de iniciación del proceso de oxidación, lo que disminuye la consiguiente formación de productos de descomposición [66]. Varios estudios confirman que los compuestos fenólicos provenientes de la aceituna son excelentes antioxidantes. Se presentan como protectores del estrés oxidativo en las células relacionadas con diferentes procesos fisiológicos y patológicos. Por lo tanto, tienen importantes beneficios para retrasar el envejecimiento, controlar los niveles de colesterol, ejercer propiedades antibacterianas, antipruriginosas, antiparasitarias y citotóxicas, así como propiedades quimio preventivas, cardioprotectoras y neuroprotectoras contra el cáncer, entre otras propiedades [51,67–70]. Esto ha generado un gran interés en estos antioxidantes por parte de la industria farmacéutica, cosmética y alimentaria [71]. Los hasta ahora denominados residuos, se consideran una fuente rica en antioxidantes naturales, por lo que se convierte en un sub-producto de la elaboración del aceite de oliva [57].

Estos antecedentes nos sitúan en dos escenarios; debido a la alta carga contaminante de estas aguas residuales, es importante encontrar tecnologías para tratar estas aguas y recuperar los cursos de agua; pero también al tener una alta concentración de compuestos fenólicos, existe la opción de recuperarlos y obtener un valioso subproducto de lo que hasta hace un tiempo era solo una corriente líquida desechada. A continuación, se presentan las normativas que rigen el tratamiento y vertido de estas aguas como también los tratamientos propuestos para su valorización.

III.3. GESTIÓN DE LAS AGUAS RESIDUALES, OMW y FTOP

Antiguamente las aguas residuales se vertían al medio ambiente o se utilizaban para la fertilización. Hoy por normativa ambiental la descarga de estas aguas residuales está prohibida, por lo que deben ser tratadas para reducir la cantidad de sustancias contaminantes a niveles aceptables [72]. A nivel europeo, la Dirección General de Medio Ambiente de la Comisión Europea, bajo la entrada en vigor de la Directiva 96/61/CE, relativa a la prevención y al control integrado de la contaminación, creó un departamento encargado de desarrollar y definir, para cada una de las actividades industriales un documento de referencia (BREF, siglas en inglés de *Best Available Technique* (BAT) *Reference Document*). Estos documentos si bien no son de carácter preceptivo, establecen medidas para evitar o, cuando ello no sea posible, reducir las emisiones de las citadas actividades a la atmósfera, agua y suelo mediante la aplicación de las mejores técnicas disponibles (MTD). En este documento, específicamente en el Anexo II, las aguas de la producción olivera figuran como una aguas residuales necesarias de gestionar [73]. En España es el Real Decreto 3499/1981 el que presenta la prohibición de contaminar cursos de aguas por los residuos de las almazaras [74]. Por otra parte, es el Real Decreto de 849/1986 [75], modificado y aprobado por el Real Decreto Legislativo 1/2001, de 20 de julio, el que fija los valores límites para la descarga de aguas residuales provenientes de las almazaras (pertenecientes al Grupo 3 de la Clase 1, Anexo IV) e instalaciones de elaboración de aceitunas de mesa (pertenecientes al Grupo 4 de la Clase 1, Anexo IV).

III.3.1. Técnicas de tratamiento OMW

Diversas son las técnicas de gestión de las OMW que se han estudiado y propuesto, entre ellas las balsas de inducción de evaporación en estanques de almacenamiento abiertos. Normalmente el agua debe ser neutralizada (ajuste del pH a 7), para lo cual se utilizan cal (óxido de calcio (CaO) y el hidróxido de calcio ($CaOH_2$)). Otros productos químicos también se utilizan a menudo para promover la sedimentación (sulfato de aluminio, cloruro férrico) o la

degradación (peróxido de hidrógeno en reactores de contacto). La problemática de este método es la extensa área necesaria junto con la producción de lodos los cuales son difíciles de eliminar [76]. Por otra parte, la infiltración de contaminantes en las aguas subterráneas y la proliferación de insectos también es un tema a tener en cuenta. Como se comentó anteriormente, estas aguas poseen un carácter fitotóxico, por lo que es muy importante prevenir su llegada a las aguas subterráneas. El riego de OMW directamente al suelo también es una práctica utilizada. Aunque se ha comprobado que tiene efectos beneficiosos por su alta concentración de nutrientes, especialmente potasio, los compuestos fenólicos, junto con su alto contenido en sales minerales y su bajo pH, hacen necesaria su dilución y tratamiento previo [30,77]. También se ha estudiado el posible uso de OMW como biopesticida. Esto es debido a los compuestos químicos naturales y compuestos fenólicos presentes, presentando un gran potencial para inhibir la germinación de bacterias, hongos fitopatógenos y especies de malezas sin afectar negativamente el crecimiento de las plantas. Esto podría evitar la aplicación de pesticidas sintéticos y reducir los problemas ambientales. Sin embargo, tanto la dosis como el tiempo de aplicación deben medirse cuidadosamente [78].

Otro proceso utilizado es la sedimentación, este proceso que se desarrolla en estanques de decantación, separa el OMW en 3 fases. Un sobrenadante que suele ser evaporado o utilizado para riego, fango el cuál se almacena para luego transformarse en compost; y una fracción aceitosa, la cual suele ser la más compleja de gestionar. Esta suele tratarse para recuperar su contenido de aceite o para pasar a compostaje junto con el fango. También se han estudiado métodos térmicos. Entre ellos la combustión parece ser un medio de recuperación de energía como combustible de la planta de extracción de aceite de oliva. Aunque esta técnica consigue reducir el volumen de residuos y ofrecer la posibilidad de valorización energética, requiere instalaciones costosas y conlleva la posible emisión de sustancias tóxicas a la atmósfera [79].

Otros estudios se han enfocado en la recuperación de la OMW mediante la eliminación de la materia orgánica presente. Este fue el caso del estudio realizado por Kiril Mert y otros [80], donde con procesos de oxidación avanzada mediante reactivo Fenton, lograron una eliminación del 80% de DQO y un 85% de eliminación total de fenoles. También se ha

estudiado la eliminación de materia orgánica por ozonización. Andreozzi et al. [81], lograron una reducción de polifenoles y DQO del 82,4% y 59,8%, respectivamente con un tiempo de contacto de 120 min. Estos autores también estudiaron la integración de ambas técnicas comentadas anteriormente, consiguiendo una reducción de polifenoles del 87,9% y una reducción de la DQO del 64,9% mediante foto-Fenton/ozonización. Los procesos biológicos también han sido estudiados. Chiavola et al. [82] investigaron la eficiencia de un reactor por lotes (SBR) en el tratamiento biológico de OMW. Estudiaron diferentes cargas orgánicas del afluente y la posibilidad de añadir un tratamiento con membranas previo o posterior. Con el fin de eliminar la DQO y los compuestos fenólicos, el SBR logra finalmente la eliminación en torno al 90% y 60%, respectivamente. Por otro lado, si bien la etapa de separación por membrana logró que la calidad del efluente del SBR cumpliera con los límites de DQO, pH y conductividad para descarga o reutilización de acuerdo con la legislación del país (Italia), los límites de compuestos fenólicos se encontraban por encima del límite de concentración requerido.

La recuperación de la fracción de compuestos fenólicos también es parte importante de los estudios realizados con OMW. La adsorción es una opción ampliamente estudiada, pudiendo utilizarse diversos materiales como adsorbentes. Un ejemplo son los materiales arcillosos. Chaari et al. [83] estudió este material para la adsorción de compuestos fenólicos que están contenidos en el OMW. Compararon arcilla cruda y otra previamente activada térmicamente (a 600ºC, para mejorar la capacidad de adsorción), consiguiendo una eficiencia de adsorción de compuestos fenólicos del 77,61% y 84,21%, respectivamente. Materiales como resinas también han mostrado buenos resultados en cuanto a adsorción/desorción de compuestos fenólicos. Frascari et al. [84] compararon 4 resinas neutras (Amberlite XAD16N, Optipore SD-2, Amberlite FPX66, Amberlite XAD761) y 1 resina de intercambio iónico (Amberlite IRA958 Cl) para la recuperación de compuestos fenólicos de OMW. Los resultados mostraron que la resina neutra (XAD16N) funcionó mejor gracias a su alta capacidad de sorción de los compuestos (81 mg/g de resina seca). Por otro lado, la resina de intercambio iónico (IRA958), aunque no mostró los mejores resultados, resulta ser la más económica. Finalmente, las dos resinas se compararon mediante pruebas de adsorción/desorción de flujo continuo realizadas en una columna de relleno. Los resultados indicaron que XAD16N genera

un producto más rico en fenoles (0,14 g/g de sólidos volátiles), logrando desorber entre un 87-95% de los compuestos fenólicos. También se ha estudiado la extracción líquido/líquido de compuestos fenólicos utilizando acetato de etilo (EA) como disolvente. Azzam y Hazaimeh [85] estudiaron varios parámetros, como el tiempo de extracción, el pH y la relación volumétrica EA/OMW. Estos autores consiguieron un porcentaje de recuperación de hidroxitirosol del 62% tras 2 h de extracción, a una relación EA/OMW de 2/1 (v/v) y un pH de 2.

Como queda en manifiesto, diversos estudios han sido propuestos e implementados para el tratamiento de OMW. Sin embargo, la mayoría ha sido estudiado con aguas residuales provenientes de los procesos productivos de aceite de oliva mediante prensado o centrifugación en tres fases, ya que como se comentó anteriormente, estos procesos son más antiguos y aún siguen siendo utilizados. La bibliografía anterior nos entrega un escenario, en dónde, debido a las características tan complejas de esta agua, se debe contemplar un proceso hibrido de diferentes etapas de tratamiento utilizando diversas técnicas. Con el fin, por un lado, de recuperar estos compuestos fenólicos, y tratar la elevada carga orgánica de estas.

Con respecto al agua residual proveniente del proceso de centrifugación de dos fases, son pocos los estudios que se encuentran, siendo la mayoría realizados por el grupo investigador del Departamento de Ingeniería Química de la Universidad de Granada. Si bien sus estudios utilizan diversas técnicas, los procesos de membranas han sido los más estudiados enfocados en la concentración y recuperación de compuestos fenólicos. Una de las propuestas que han publicado es la de un pretratamiento mediante centrifugación seguido del proceso de nanofiltración (NF) [86]. Con la centrifugación consiguieron una reducción de sólidos en suspensión, sin pérdida de compuestos fenólicos. Con NF obtuvieron un flujo de permeado de buena calidad, reduciendo la DQO en un 86,76% y prácticamente libre de contenido fenólico. Por otro lado, también consiguieron un concentrado de fenoles de alto valor añadido (hasta 1.318 mg/L). También estudiaron la combinación de dos procesos de membranas consecutivos, UF y NF, para el tratamiento de una mezcla 1:1 v/v de dos efluentes principales generados en almazaras que operan con tecnología de dos fases, siendo las aguas residuales de lavado de aceitunas (OWW) y las del lavado del aceite de oliva (OOWW) [87]. Como pretratamiento, estudiaron la floculación (optimizando pH y temperatura) de forma independiente o seguida de

fotocatálisis con nanopartículas de TiO_2 (activadas bajo irradiación UV). La mejor opción en términos de menor área total y módulos de membrana fue la UF precedida de floculación (bajo las mejores condiciones de pH y temperatura) y fotocatálisis UV/TiO_2, logrando un efluente compatible para riego (840 mg/L). Sin embargo, la mejor en cuanto a concentración final de DQO (130,2 mg/L) fue la del proceso NF precedido de UF, precedidos a su vez por los dos pretratamientos.

Finalmente, junto con toda la información recopilada, se decidió realizar en esta Tesis Doctoral un estudio de la gestión del agua residual de almazara OMW, en donde se pudiera realizar tanto el tratamiento de esta como la recuperación de los compuestos fenólicos. Para ello se propone la implementación de un pretratamiento de flotación, sedimentación y filtración, seguido de dos opciones de procesos de membrana; una UF seguida de NF; o tan solo una FO. Finalmente, mediante el proceso de adsorción y desorción con resinas se realiza la recuperación de los compuestos fenólicos. Por otro lado, las corrientes residuales seguirán un tratamiento biológico mediante SBR para recuperar los cursos de agua y potencialmente ser reincorporados al sistema como agua de lavado.

Si bien la FTOP no es el agua principal a tratar, dentro de la opción que contempla el proceso de membrana FO, se ha incorporado para su posible tratamiento en conjunto. Por ello se ha decidido presentar brevemente algunas opciones de tratamiento de la FTOP.

III.3.2. Técnicas de tratamiento FTOP

En cuanto a la FTOP, las balsas de evaporación son utilizadas igualmente, pero como se comentó anteriormente, esta práctica supone un alto riesgo de filtración a suelos y aguas subterráneas. La dilución de la FTOP con aguas urbanas para bajar su contenido en fenoles y poder ser tratadas en estaciones depuradoras de aguas residuales urbanas (EDARU) también se es utilizada. Sin embargo, su elevada salinidad y concentración de compuestos fitotóxicos

suponen un problema sobre los fangos activos. Por ello se requeriría trabajar con mucha dilución [39].

Diversos son los tratamientos en desarrollo y propuestos, los cuales principalmente se basan en la reducción o eliminación de la materia orgánica para reutilizarla en etapas posteriores del proceso, como por ejemplo en la etapa de envasado. Uno de ellos es el propuesto por García-Serrano et al. [41], quienes proponen cambiar la disolución de NaOH utilizada en la fase de fermentación por una a base de KOH. Esto serviría principalmente para luego de ser utilizada en la etapa de fermentación ser reutilizada como biofertilizantes. Los estudios realizados indicaron que con una concentración de KOH similar a la utilizada con NaOH (1,7 - 2%), se logra un producto fermentado con las mismas características que el método tradicional. Por otro lado, la disolución alcalina generada, tras ser sometida a una evaporación al vacío, logra una concentración rica en potasio (52 g/L). Esta disolución se aplicó en tomates junto a un fertilizante mineral (NH_4NO_3), resultando en un incremento de la calidad y rendimiento de estos en comparación al uso del fertilizante mineral solo. Tratamientos como la electrocoagulación también han sido propuestas. García-García et al. [79], estudiaron esta tecnología como pretratamiento (o depuración parcial) de las aguas residuales de la industria de la aceituna verde de mesa (FTOP y otras). Estos autores consiguieron con aluminio en el ánodo y hierro en el cátodo, una densidad de corriente de 25 mA/cm y una distancia entre electrodos de 0,6 cm, la eliminación del 40% de la DQO. También fueron capaces de neutralizar el pH, eliminar la mayor parte de los fenoles inicialmente presentes y el color. Finalmente, consiguieron generar una disolución de ácido láctico y acético, que podría ser reutilizada en envases o tratada por plantas depuradoras convencionales. Otras metodologías propuestas se basan en el tratamiento y recuperación de energía mediante sistemas bioelectroquímicos (BES, por sus siglas en inglés) acoplado a un digestor anaeróbico. En los estudios realizados por Marone, et al. [42], se logró una generación de metano (CH_4) cercana al 701 NmL/L de agua residual de fermentación tratada, en comparación a cero producción de metano sin incorporar el BES al sistema anaerobio. Por otra parte, lograron una eliminación de un 80% de compuestos fitotóxicos y del 32% de la demanda química de oxígeno (DQO), la cual está ligada a la materia orgánica presente. Otros estudios contemplan la ozonización como posible tratamiento. Segovia-Bravo et al. [88] mediante este

tratamiento lograron degradar los compuestos fenólicos más característicos presentes en la FTOP. Ello fue logrado con 15 mg/L de ozono en disoluciones ácidas (pH 4.0) y 7 mg/L en disoluciones alcalinas (pH 10). Las salmueras tratadas con ozono fueron previamente filtraron y diluidas (1:1) para ser reutilizadas como salmuera de cobertura para el envasado de aceitunas sin hueso y con hueso. Después de un equilibrio de 3 meses, observaron que las aceitunas sumergidas en la disolución de FTOP tratada y diluidas bajo condiciones alcalinas tuvieron mayor firmeza y características organolépticas similares a las que usaron salmuera fresca, mostrando esta tecnología como una alternativa económica y óptima para la regeneración parcial de la FTOP y posible reutilización.

Como se puede ver, diversos son los procesos que se han propuesto para gestionar estas aguas, teniendo como objetivo la mayoría de estos métodos reducir la fitotoxicidad de la OMW y FTOP para reutilizarla con fines agrícolas, adecuarla para su reincorporación al proceso, así como recuperar la fracción de compuestos fenólicos por sus interesantes propiedades antioxidantes. Aunque se pueden aplicar varios procesos, entre ellos se destacan los tratamientos biológicos, la extracción por disolventes, la adsorción-desorción y los procesos de extracción y separación por membrana [27,55,62,71,89]. A continuación, los procesos a ser utilizados en esta Tesis Doctoral pasarán a ser comentados en los siguientes apartados de forma más extensa.

III.4 PROCESOS DE MEMBRANAS

En la tabla 3.3 se presentan las contribuciones al desarrollo sostenible que estos procesos presentan. En comparación con las tecnologías convencionales, los procesos de separación por membrana presentan varias ventajas para el tratamiento de aguas residuales, tales como sus mejores eficiencias de eliminación de contaminantes, ahorro de espacio y consumo de energía reducido, entre otros [90].

Tabla 3.3 Sostenibilidad de los procesos de membranas (Modificación [90])

Propiedad	Sostenibilidad	Observaciones
Baja temperatura de funcionamiento	Económico-Ambiental	Bajo consumo de energía.
Uso reducido de productos químicos	Sostenible	Bajos costos, impacto ambiental y en la salud. Alta seguridad en el trabajo
Alta calidad del agua producida	Económico-Social	Logra cumplir con los requisitos legislativos. Preservación de la salud
Recuperación de productos valiosos en condiciones de funcionamiento moderadas	Sostenible	Conversión de flujos de residuos en un recurso. Conservación de las propiedades del producto.
Baja producción de lodos/salmuera	Económico-Ambiental	Bajos costos. Bajo impacto ambiental
Alta eficiencia de separación para un gran número de especies en la misma unidad	Sostenible	Reducido número de unidades necesarias para realizar la separación. Logra cumplir con los requisitos legislativos. Preservación de la salud
Sin partes móviles	Social	Alta seguridad en el trabajo
Tamaño pequeño	Económico-Ambiental	Reducción del espacio necesario
Alta flexibilidad	Económico	Permite utilizar la misma planta en diferentes condiciones
Alta modularidad	Económico	La alta modularidad ayuda en el diseño de la planta

Se puede definir una membrana como una película delgada que separa dos fases, la cual actúa como una barrera selectiva al transporte de materia, por lo que restringe el paso a algunas sustancias mientras que deja pasar a otras. Si bien la investigación del uso de las membranas comenzó su auge en el siglo pasado, fue en el año 1861 donde se documentaron los primeros ensayos de membranas para su uso en diálisis [91].

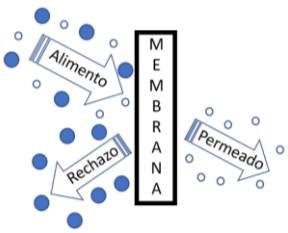

Figura 3.6. Mecanismo de separación membrana semipermeable

La corriente que se enfrenta a la membrana es denominada corriente de alimentación. Esta es separada en dos corrientes, permeado y rechazo (figura 3.6). El permeado se constituye por las sustancias que logran atravesar la membrana, mientras que el rechazo es la corriente retenida por esta barrera semipermeable. Esta separación se lleva a cabo gracias a la acción de una fuerza impulsora entre ambos lados de la membrana. Esta fuerza puede ser generada por diferencia de presión, diferencia de concentración o diferencia de potencial eléctrico. La Tabla 3.4 resume algunas tecnologías de membranas junto con su fuerza impulsora y tamaño de poro de las membranas utilizadas.

La separación por diferencia de presión es la técnica de membranas más aplicada en el tratamiento de aguas residuales. Existen cuatro procesos de separación de membranas basados en un gradiente de presión, los cuales utilizan la diferencia de presión entre el lado de alimentación y el permeado como fuerza impulsora para transportar el disolvente (generalmente agua) a través de la membrana [92].

Tabla 3.4 Procesos de separación de membranas (modificación [93])

Proceso de Membrana	Fuerza impulsora	Tamaño de poro (nm)
Microfiltración (MF)	Gradiente de presión (0,1 – 2 MPa)	100 – 10.000
Ultrafiltración (UF)	Gradiente de presión (1 – 10 MPa)	1 – 100
Nanofiltración (NF)	Gradiente de presión (10 – 30 MPa)	0,5 – 2
Osmosis inversa (OI)	Gradiente de presión (15 – 80 MPa)	< 0,5
Osmosis directa (OD)	Gradiente de presión osmótica (diferencia entre concentración)	< 5
Destilación por membranas (MD)	Gradiente de presión de vapor (diferencia entre temperatura)	10 – 1.000
Electrodiálisis (ED)	Gradiente de potencial eléctrico	< 1
Pervaporación (PV)	Gradiente de presión de vapor	< 0,5

Como se observa en la tabla 3.4, estos procesos se diferencian por el rango de presión transmembranal aplicada y el tamaño de poro de cada una de las membranas. Estos procesos también pueden diferenciarse por el corte molecular de las membranas (MWCO). Esta sigla

hace referencia a la frase en inglés *Molecular Weight CutOff*, el cual se define como el peso molecular equivalente de las especies más pequeñas que son rechazadas en un 90% por la membrana. Su unidad de medida es el Dalton (Da). Otra forma de caracterizarlos es a través de las sustancias rechazadas, estas se presentan en la figura 3.7.

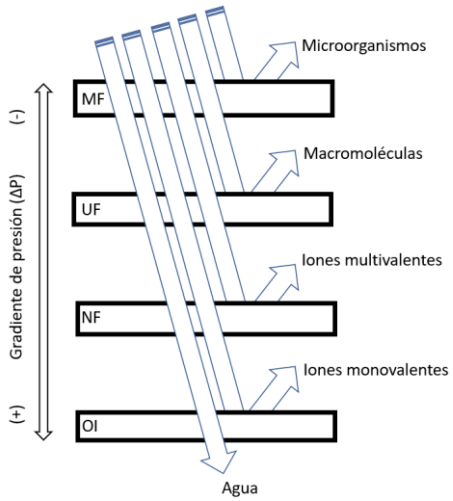

Figura 3.7. Selectividad de procesos de membranas basados en gradiente de presión.
MF: microfiltración, UF: ultrafiltración, NF: nanofiltración, OI: osmosis inversa

La MF se basa en el uso generalmente de membranas asimétricas capaces de separar partículas con diámetros mayores o iguales a los poros de su membrana, los cuales corresponden a sólidos en suspensión, coloides y bacterias. Sin embargo, los virus no se eliminan. Estas membranas presentan un MWCO mayor a 100 kDa. A continuación, sigue la UF, lo que implica el uso de membranas asimétricas con un tamaño de poro menor y de MWCO entre 1- 500 kDa. Este proceso de membranas proporciona una alta retención de macromoléculas y coloides de una disolución. La permeabilidad es considerablemente menor que en MF, por lo que se necesitan presiones más altas (normalmente se utilizan diferencias de presiones de 2 a 10 bar). El mecanismo de separación en los procesos de MF y UF se basa principalmente en un efecto de tamizado y las partículas se separan según sus dimensiones,

aunque existen otros factores, como la forma y la carga, así como las interacciones entre la propia membrana y las partículas que se filtran, que pueden desempeñar un papel clave en el mecanismo de separación [94,95].

En cuanto a la NF, este es un proceso de membrana intermedio entre UF y OI, el cual se utiliza normalmente para la separación de iones multivalentes, logrando también una eliminación de microcontaminantes orgánicos y colorantes de aguas superficiales. Las membranas de nanofiltración presentan un MWCO de entre 0,2 a 1 kDa con un tamaño de poro entre 0,5- 2 nm. Las membranas poliméricas de NF contienen grupos ionizables en su superficie (como grupos de ácido carboxílico o sulfónico), lo que da como resultado una carga superficial en presencia de algunas colusiones entre las partículas de la alimentación. El equilibrio entre la membrana cargada y la disolución se caracteriza por un potencial eléctrico, siendo el que retiene especies iónicas. Este mecanismo se denomina exclusión de Donnan y permite la eliminación de iones con un tamaño inferior al tamaño de poro de la membrana.

La OI se utiliza para separar compuestos de bajo peso molecular. Las membranas de OI generalmente tienen una estructura densa sin poros definidos. Debido a esto el rechazo no es resultado del tamizado, sino de un mecanismo de difusión de la solución. Normalmente se utilizan diferencias de presión de 10 a 100 bar para obtener un flujo transmembranal significativo, según la presión osmótica de la disolución de alimentación.

Otro proceso de membrana es la ósmosis directa, que como bien refleja el nombre, es directa y no necesita presión externa. Este proceso de membrana aprovecha el proceso natural de presión osmótica, es decir, se trata de la ósmosis, fenómeno natural que se conoce desde hace muchos años, pero que al resurgir para nuevas aplicaciones con membranas de mayor durabilidad y mejores características fue renombrado como ósmosis directa para distinguirlo claramente de la inversa. En cierta forma, el proceso de ósmosis inversa puede ser un poco más rápido debido a la presión suministrada. Al igual que las membranas MF y UF, las membranas NF y OD son membranas asimétricas, sin embargo, se denominan no porosas, debido a la densidad de la capa selectiva. [94,95].

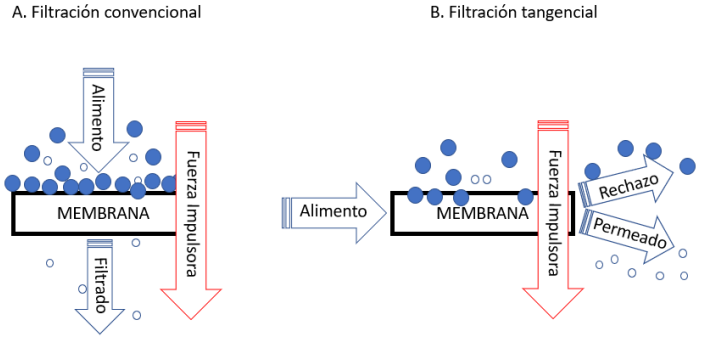

Figura 3.8. Tipo de flujo en procesos. A: flujo convencional (perpendicular), B: flujo tangencial

Por otra parte, según la orientación del flujo, los procesos de membrana se pueden clasificar en: filtración convencional (perpendicular) o filtración tangencial. Como se observa en la figura 3.8, en la filtración convencional, el flujo va en dirección perpendicular a la membrana. Esto hace que la acumulación de las partículas en la superficie de la membrana sea mayor. En la filtración tangencial la dirección del flujo va tangencial a la membrana, provocando un continuo arrastre de las partículas, disminuyendo así su retención en la superficie de la membrana. La modalidad de flujo perpendicular se utiliza principalmente para aplicaciones de laboratorio y de muy pequeña escala (poco volumen de solución a tratar), si bien esta configuración se ha adoptado en algunas aplicaciones industriales por su menor coste energético. La mayoría de los procesos de membrana de pequeña, mediana y gran escala se llevan a cabo en el modo de flujo cruzado (tangencial). La principal ventaja del flujo cruzado es la minimización de la acumulación de soluto y partículas cerca de la superficie de la membrana. La configuración de flujo tangencial también facilita la recirculación de la corriente de retenido al tanque de alimentación, lo que puede asociarse con la mezcla con alimentación fresca.

Las condiciones de operación de los procesos de membrana influirán tanto en el flujo de permeado como en la calidad de este. La presión transmembranal, la velocidad de flujo tangencial, temperatura y tiempo de operación son fundamentales en estos procesos.

A continuación, se desarrollarán más a fondo los tres procesos de membrana utilizados en esta Tesis Doctoral. Estos son los procesos de ultrafiltración, nanofiltración y osmosis directa.

III.4.1. Proceso de Ultrafiltración

Como se mencionó anteriormente, el proceso de UF utiliza membranas asimétricas. Estas están formadas por dos capas, una capa activa y un soporte. La capa activa es muy fina (entre 0,1 – 1 μm), y está formada por pequeños poros que entran en contacto con el alimento, por lo que el efecto de tamizado es la responsable de la separación. Por otro lado, el soporte es una estructura de mayor espesor y porosidad, proporcionando la resistencia mecánica a la membrana. Las membranas para ultrafiltración pueden eliminar bacterias y virus y también pueden separar macromoléculas como azúcares y proteínas, así como sílice coloidal y pirógenos (sustancias que inducen fiebre en humanos) [96].

Las membranas de UF abarcan un gran rango de MWCO, por ende, se utilizan para diferentes propósitos. Las de alto corte molecular, con MWCO entre 50 y 100 kDa, se utilizan fundamentalmente para recuperar diferentes tipos de macromoléculas (como sólidos en suspensión, carbohidratos, proteínas y pectinas). Las membranas de UF de 4 a 30 kDa son efectivas para concentrar componentes disueltos de alto peso molecular (como taninos, proteínas, hidrolizados y algunas fracciones fenólicas de alto peso molecular), mientras que las membranas de UF de menor MWCO, de 1 a 3 kDa, son altamente efectivas para concentrar compuestos de bajo peso molecular (tales como antocianinas, compuestos fenólicos de bajo peso molecular, azúcares de bajo peso molecular y péptidos); de hecho, estas membranas se encuentran en el límite molecular del proceso de NF [97].

La UF juega un papel importante en las industrias biotecnológica y farmacéutica, debido en gran parte a sus condiciones de operación "suaves" (temperaturas relativamente

bajas, bajas presiones, sin cambios de fase ni aditivos químicos), lo que minimiza la desnaturalización, desactivación y/o degradación de productos biológicos.

Estas membranas también pueden variar en materiales (pueden ser orgánicas o inorgánicos), como también en configuración (planas, tubulares, espiral). Esto no es algo específico de membranas de ultrafiltración, por lo que se comentará en un apartado diferente, después de comentar sobre los procesos de membranas.

III.4.2. Proceso de Nanofiltración

La nanofiltración (NF) ha sido bien establecida en las últimas décadas desde que se reconoció por primera vez a principios de la década de 1990. La NF es un proceso de membrana que se encuentra entre la UF que utiliza estructuras de membrana porosas y la OI que utiliza estructuras de membrana densas. Se requiere presiones mayores que en la UF, normalmente presiones de entre 3 bar a 60 bar.

Las membranas NF con un MWCO nominal más alto (en el rango de 350- 400 Da) pueden retener prácticamente las mismas moléculas que las recuperadas en las membranas UF de menor corte molecular (1-3 kDa). Sin embargo, se puede esperar una mayor eficiencia de separación con las membranas NF. Las membranas de menor corte molecular de NF (120-300 Da), por otro lado, son ideales para la recuperación selectiva y concentración de compuestos de bajo peso molecular. Por lo tanto, las membranas de NF son ideales para la recuperación de compuestos fenólicos [97].

Los métodos de separación de compuestos no se basan tan solo en mecanismos de "tamizado", basados en MWCO, sino también en otros fenómenos (por ejemplo, la polarización de la concentración, el ensuciamiento de la membrana, las interacciones entre membrana/sustancia e interacciones hidrofóbicas). Durante las últimas dos décadas, varios estudios han confirmado el mecanismo de separación de las membranas NF, que se compone principalmente de efectos estéricos, de Donnan y dieléctricos. El efecto estérico, que también

es el mecanismo de separación común para MF y UF, se debe esencialmente a la exclusión del tamaño molecular por los poros de la membrana. Los solutos con un tamaño molecular grande en comparación con el tamaño de los poros de la membrana son efectivamente excluidos por la membrana. Los solutos más pequeños que el tamaño de los poros de la membrana pueden penetrar a través de los poros de la membrana en respuesta a los fenómenos de transporte por difusión impedido. Por otra parte, es importante considerar que por el hecho de que sean membranas asimétricas, los poros de cada membrana no siempre reflejan rangos estrechos de MWCO [90].

III.4.3. Proceso de Osmosis Directa

La FO es un proceso de membrana diferente a los impulsados por presión, ya que es un proceso de concentración basado en el fenómeno natural de la ósmosis (Figura 3.9). Se basa en el transporte de agua a través de una membrana semipermeable, hacia una disolución con mayor potencial osmótico ($\Delta\pi$). Como resultado, se diluye la disolución con mayor potencial osmótico (DS, por siglas en ingles de *draw solution*), mientras que la disolución o suspensión de interés (FS, por siglas en ingles de *feed solution*) se concentra. El proceso de concentración continúa hasta que se establece el equilibrio del potencial químico.

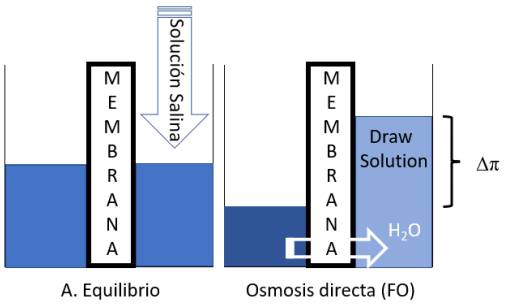

Figura 3.9. proceso de osmosis directa

Dado que el transporte de agua no está impulsado por la presión, la concentración se puede lograr con requisitos mínimos de energía. Además, la presión de operación más baja da como resultado un menor ensuciamiento (reversibilidad) de la membrana y menores costos de mantenimiento en comparación con los otros métodos mencionados anteriormente. Dado su ensuciamiento altamente reversible, el proceso de FO se puede aplicar directamente a una disolución compleja sin un tratamiento previo extenso. El alto rechazo de contaminantes disueltos es otra ventaja importante de la FO para el tratamiento de aguas residuales. Cuando la FO se combina con un proceso de extracción de solutos, se puede producir agua limpia a partir de la solución de extracción, lo que aumenta las oportunidades de reutilización del agua.

Estas características únicas de la FO han estimulado el desarrollo de varias configuraciones de sistemas para el tratamiento de aguas residuales y la recuperación de agua, por lo que ahora la FO se reconoce como una tecnología innovadora que se puede utilizar de manera efectiva para concentrar suspensiones y disoluciones cargadas de sustancias contaminantes. De hecho, se han investigado en la última década numerosas aplicaciones en el área del tratamiento de aguas residuales, incluidas las aplicaciones de concentración de aguas residuales municipales [98,99].

III.4.4. Materiales y Configuración de membranas

La morfología de las membranas poliméricas es compleja, diversa e irregular. Esta depende de la tecnología con la cual fueron preparadas. Básicamente, las membranas se dividen en orgánicas e inorgánicas.

III.4.4.1 Membranas Orgánicas

En la figura 3.10 se presenta La polisulfona (PSU), la polietersulfona (PES), el poliacrilonitrilo (PAN), el fluoruro de polivinilideno (PVDF) y el polipropileno (PP). Estos materiales son actualmente los más utilizados para la fabricación de membranas irgánicas.

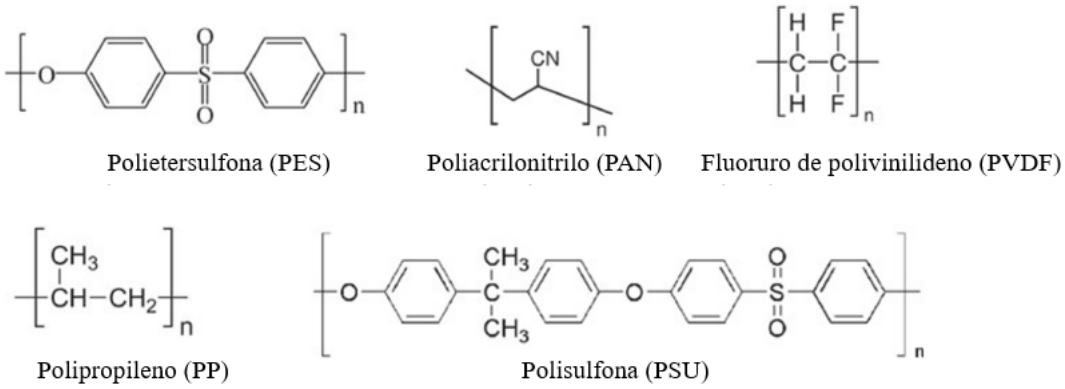

Figura 3.10. Estructuras químicas de los materiales poliméricas para membranas orgánicas más comunes (modificación [90])

Por otra parte, también se utiliza tanto la celulosa y sus derivados, sintetizados a partir de materias primas biológicas (azúcar, maíz, almidón, etc.), siendo el acetato de celulosa (CA) es el biopolímero más abundante disponible en la tierra. Es un polisacárido producido por las plantas y, con sus derivados, es muy apreciado para la producción de membranas hidrofílicas aplicadas principalmente en el tratamiento de aguas y en biomedicina. En los últimos años, se han desarrollado diversos polímeros naturales, entre ellos los biopolímeros producidos por bacterias, el poli (ácido láctico) (PLA) y los polihidroxialcanohatos (PHA), se encuentran entre los materiales más comunes utilizados para la preparación de membranas. [90].

III.4.4.2 Membranas Inorgánicas

Las membranas inorgánicas se pueden clasificar en 3 grupos, membranas porosas y amorfas, membranas porosas y cristalinas y membranas densas. Las membranas inorgánicas densas generalmente se fabrican a partir de metales como paladio, níquel, plata, circonio y sus aleaciones. Las membranas inorgánicas porosas dependiendo de su material y forma de preparación será amorfa o cristalina. Estas se producen a partir de óxidos metálicos (alúmina, titania, zirconia), carbono, sílice (vidrio), metales y zeolita. Dentro de las membranas inorgánicas las cerámicas son las más desarrolladas. Se pueden obtener membranas cerámicas con una amplia gama de tamaños de poros mediante el uso de diferentes técnicas de preparación, que incluyen moldeo por barbotina, moldeo por cinta, prensado, extrusión, proceso sol-gel, revestimiento por inmersión, deposición química de vapor y preparación. de membranas cerámicas de fibra hueca [90,100].

Las membranas inorgánicas son de gran interés debido a su mayor estabilidad química, térmica y mecánica en comparación con la mayoría de las membranas poliméricas. Con membranas inorgánicas, es posible el procesamiento a alta temperatura (hasta 500ºC) y valores de pH extremos (pH 1–14). Además, las membranas inorgánicas se pueden limpiar con productos químicos agresivos, disolventes orgánicos o chorro de agua caliente. Es por ello que su utilización para el tratamiento de aguas residuales complejas es cada vez mayor, obligando al mercado a fabricar membranas cerámicas con mayor eficiencia, resistencia a los medios y durabilidad.

III.4.4.3 Configuración de Membranas

Las membranas se pueden fabricar en forma de lámina plana, forma tubular, membranas capilares (diámetros simples o múltiples) o membranas de fibra hueca. Estos están organizados en elementos de membrana, constituyendo módulos en el siguiente paso. Estos

módulos pueden ser planos, tubulares, capilares o de fibras huecas. Para membranas planas, el módulo puede ser plano o tubular, si la membrana se arrolla en espiral. Las membranas cerámicas ofrecen la posibilidad de formar elementos de membrana multicanal. Un módulo es la unidad práctica más pequeña que contiene una o más membranas o elementos de membrana y estructuras de soporte como tapas de extremos y otros materiales necesarios que le permiten operar independientemente del resto de la planta cuando sea necesario. Uno de los criterios importantes para seleccionar un tipo de módulo para una aplicación particular es la densidad de empaquetamiento (m^2/m^3) de la membrana. Esto define el área de membrana efectiva instalada por volumen de módulo. La densidad de empaquetamiento es el principal indicador del grado de pretratamiento necesario para los diferentes módulos a fin de lograr una operación segura y sin problemas a largo plazo. Las aguas residuales generalmente requieren módulos de canales abiertos, caracterizados por valores bajos para la densidad de empaquetamiento de la membrana. Algunas de las razones de esto son los efectos de acumulación a largo plazo inducidos por partículas y el posible bloqueo del espaciador en el canal de agua de alimentación de los módulos con una alta densidad de empaquetamiento como resultado de incrustaciones y ensuciamiento (biológico e inorgánico) [96].

A continuación, se brindan algunas definiciones básicas para operar los procesos de membrana.

III.4.5. Definiciones de parámetros característicos

Hay parámetros que influyen en los procesos de membrana, así como parámetros a considerar para evaluar la eficiencia del proceso. Los más importantes se presentan a continuación:

- Densidad de flujo de permeado (flux): Se representa con la letra *J* (L/hm^2bar), se refiere a la densidad de flujo volumétrico que atraviesa la membrana, por ende sus

unidades son de volumen/(área de membrana·tiempo). Se describe por la Ley de Darcy bajo la siguiente ecuación:

$$J = \frac{\Delta P}{\mu \cdot R_t} = L_p \cdot \Delta P \qquad \text{(Eq.1)}$$

Donde ΔP es la presión transmembranal, μ la viscosidad del permeado, R_t la resistencia hidráulica total de la membrana y L_p el coeficiente de permeabilidad de la membrana.

- Rechazo (R): Este parámetro determina la eficiencia de la membrana en cuanto a retener un determinado compuesto. Entonces, representará el porcentaje de la sustancia retenida o rechazada bajo la siguiente ecuación:

$$R_j(\%) = \left(1 - \frac{C_{PJ}}{C_{FJ}}\right) \cdot 100 \qquad \text{(Eq.2)}$$

R_j es el rechazo del parámetro *j* (DQO, azúcares, compuestos fenólicos u otros) en %, C_{Pj} (ppm) es la concentración del parámetro *j* en la corriente de permeado y C_{Fj} (ppm) es la concentración del parámetro *j* en la solución de alimentación.

III.4.6 Ensuciamiento de membranas

El ensuciamiento de la membrana (*fouling*) es un fenómeno que ocurre debido a las interacciones de las moléculas con la superficie de la membrana. Esto genera que el flujo característico (inicial) de la membrana se reduzca por debajo del correspondiente flujo de agua pura. El ensuciamiento de la membrana se puede clasificar como ensuciamiento reversible e irreversible, cuya distinción depende completamente del contexto en el que se operan y limpian las membranas. El ensuciamiento reversible es aquel que puede eliminarse con agua, mientras que el irreversible necesitará de un agente químico para su eliminación.

Independiente del tipo de ensuciamiento, la membrana nunca logrará sus características iniciales. El ensuciamiento de las membranas es causado por complejas interacciones físicas y químicas entre los diversos componentes del ensuciamiento en la alimentación y entre estos componentes y la superficie de la membrana. El ensuciamiento de la membrana puede ocurrir por diferentes factores. Está determinado por la composición del agua de alimentación, la concentración de los componentes principales, las propiedades de la membrana (morfología de la superficie, hidrofobicidad, límite de carga y peso molecular), temperatura, modo de operación y condiciones hidrodinámicas (densidad de flujo de permeado inicial, CFV y TMP) [101,102].

En primer lugar, la polarización por concentración es una consecuencia natural de la selectividad de una membrana y es inevitable. Esto ocurre porque las moléculas disueltas en la disolución a tratar se acumulan en la superficie y reducen el paso de las partículas. Esto conduce a una acumulación continua de partículas en la capa límite de transferencia de masa adyacente a la superficie de la membrana, reduciendo por ende el flujo de permeado a través de la membrana. Esto se puede representar como una reducción en la fuerza impulsora de la TMP efectiva debido a una diferencia de presión osmótica entre el filtrado y la disolución de alimentación adyacente a la superficie de la membrana. El ensuciamiento de la membrana puede ocurrir durante un aumento en TMP para mantener un flujo particular o durante una disminución en el flujo cuando el sistema funciona a presión constante. Para controlar este fenómeno se deben estudiar tanto la TMP como la CFV de trabajo [103]. También pueden presentarse los siguientes tipos de ensuciamiento:

- Adsorción: La adsorción ocurre cuando existe una interacción atractiva entre la membrana y el soluto o las partículas. Una monocapa de partículas y solutos puede crecer incluso en ausencia de flujo de permeación, lo que genera una resistencia hidráulica adicional. Si el grado de adsorción depende de la concentración, la polarización de la concentración exacerba la cantidad de adsorción.
- Bloqueo de poros: al filtrar, puede ocurrir un bloqueo de poros de la membrana. Esto provoca una reducción del flujo debido al cierre (o cierre parcial) de los poros.

- Formación de torta: un depósito de partículas puede crecer capa por capa en la superficie de la membrana, lo que genera una resistencia hidráulica adicional. Esto a menudo se denomina resistencia a la torta.
- Formación capa gel: el nivel de polarización de la concentración puede conducir a la formación de gel para ciertas macromoléculas.

A la hora de implementar un proceso de membrana es importante saber el tipo de ensuciamiento que gobierna cada proceso, ya que para prevenir y mejorar es necesario saber la interacción entre membrana y soluto. Para ello, diversos modelos matemáticos se han desarrollado para el mejor entendimiento del ensuciamiento.

III.4.7. Modelación del ensuciamiento

Los modelos matemáticos ayudan a predecir el comportamiento del flujo de permeado dependiendo el tipo de ensuciamiento y las condiciones de operación. Una gran variedad de modelos, con mayor o menor precisión, se clasifican principalmente en modelos empíricos, teóricos, semi-empíricos. En los últimos años se han incorporado al estudio del comportamiento de procesos de membranas tanto métodos estadísticos como de aprendizaje automático. A continuación, se presentan los modelos de ensuciamiento de membranas estudiados en esta tesis para las membranas de UF.

III.4.7.1 Modelos de Hermia

Los modelos desarrollados por Hermia [104] se basan en el modelo clásico de Hermia para la filtración con flujo frontal a TMP constante. Consideran cuatro tipos principales de ensuciamiento de la membrana: bloqueo completo, bloqueo intermedio, bloqueo estándar y formación de capa de torta. Los modelos adaptados a la ultrafiltración de flujo tangencial

incorporan el flujo asociado con la transferencia de masa de retro-transporte, que se evalúa en el estado estacionario. La ecuación general para los modelos de Hermia adaptados a la ultrafiltración de flujo tangencial se muestra en la siguiente ecuación:

$$-\frac{dJ}{dt} = K(J - J_{ss}) \cdot J^{2-n} \quad \text{(Eq.3)}$$

Donde *K* es la constante del modelo de Hermia; *Jss* es el flujo de permeado en estado estacionario y *n* es el parámetro que indica el tipo de ensuciamiento. En este modelo se consideran cuatro tipos diferentes de mecanismos de ensuciamiento de la membrana. Cada mecanismo de ensuciamiento tiene una ecuación matemática para predecir el flujo de permeado en función del tiempo, que dependerá del valor de *n*: bloqueo completo de poros (n = 2), bloqueo intermedio (n = 1), bloqueo estándar (n = 1,5), y formación de capa de torta (n = 0) [101].

III.4.7.2 Modelo Combinado

Este modelo surge de la imposibilidad de explicar la evolución típica del flujo de permeado con un único mecanismo de ensuciamiento tal como lo representa Hermia. Fue desarrollado por Ho y Zydney [105], pero luego fue simplificado y modificado por otros autores [106–108]. Este modelo señala que el ensuciamiento es la combinación de dos etapas. Una primera bajada abrupta en los primeros minutos de la densidad de flujo de permeado, debido a fenómenos de bloqueo de poros, seguida de una lenta disminución causada principalmente por la acumulación de moléculas en la superficie de la membrana que da como resultado una capa de torta. El modelo muestra una transición suave entre dos mecanismos de ensuciamiento propuestos por Hermia, el modelo de bloqueo completo y el modelo de formación de capa de torta. El modelo combinado representa un modelo más realista para explicar el ensuciamiento de la membrana que los modelos que consideran solo un mecanismo de ensuciamiento. Se representa bajo la siguiente fórmula:

$$J_{modelo\ combinado} = \alpha \cdot J_{bloqueo\ completo\ de\ poros} + (1-\alpha) \cdot J_{formación\ de\ torta} \quad \text{(Eq.4)}$$

Como es la combinación de los modelos propuestos por Hermia, cada *J* es el obtenido mediante la ecuación presentada en la sección anterior con su valor de n correspondiente. En este modelo, solo una fracción de los poros de la membrana está completamente bloqueada, representada por el parámetro *α*.

III.4.7.3 Modelo de Resistencia en serie

Este modelo considera que la disminución del flujo de permeado es causada por diferentes resistencias. Estas son, la resistencia de la propia membrana (R_m), la resistencia debida a la polarización de adsorción y concentración (R_a) y la resistencia debida a la formación de la capa de torta (R_{cf}). El parámetro denominado resistencia hidráulica total (R) es la suma de las resistencias individuales. La ecuación general sigue la Ley de Darcy y se presenta por la siguiente ecuación, con Ra ajustada a una ecuación exponencial:

$$J = \frac{\Delta P}{\mu\left(R_m + R_a'\left(1-e^{-b\cdot t}\right) + R_{cf}\right)} \quad \text{(Eq.5)}$$

Donde R'_a representa la adsorción en estado estacionario y la resistencia a la polarización por concentración y *b* la tasa de ensuciamiento debido a la adsorción.

III.4.7.4 Metodología de superficie de respuesta (RSM)

Esta metodología con siglas RSM (siglas en inglés de *Response Surface Methodology*) predice la relación entre las variables de entrada y salida mediante un proceso complejo donde

se considera la interacción de diferentes variables entre sí, y así poder determinar las condiciones óptimas de funcionamiento. Muchas veces, para obtener un análisis fiable, se realiza en conjunto con un análisis estadístico multivariante de los datos experimentales. En el análisis estadístico multifactorial de datos experimentales, todos los factores varían simultáneamente [109]. Para el caso de esta Tesis Doctoral, se estudió la influencia de TMP y CFV en la densidad de flujo de permeado promedio (J_a) y la disminución del flujo acumulado (*SFD*), utilizando las ecuaciones 6 y 7.

$$J_a = \frac{1}{t_N} \cdot \int_0^t J(t) \cdot dt \qquad \text{(Eq.6)}$$

$$\text{SFD} = \sum_{i=1}^{N} \frac{J(0)-J(i)}{J(0)} \qquad \text{(Eq.7)}$$

Con *J(t)* representando la evolución de la densidad de flujo de permeado en el tiempo obtenida a partir de datos experimentales, t es el tiempo y t_N es el tiempo correspondiente al último valor de flujo de permeado considerado. En este caso, la técnica empleada para lograr los modelos deseados fue la eliminación hacia atrás, comenzando con todas las variables del modelo y eliminando una a una hasta que solo quedan las variables significativas en el modelo. Una vez obtenidos los coeficientes de regresión, se obtiene también la ecuación que define el modelo como resultado del análisis de la significancia de cada una de las variables consideradas, obtenida tras el análisis de varianza (ANOVA).

III.4.7.5 Modelos de Redes neuronales (ANN)

Las redes neuronales artificiales (ANN) son denominadas modelo de caja negra. Por lo tanto, las predicciones de las ANN son completamente empíricas y pueden considerarse no fenomenológicas. Las ANN predice valores de salida a partir de datos de entrada, pero no proporcionan información sobre el proceso. Una red neuronal tiene dos componentes: el nodo, que consiste en una neurona con información de posicionamiento, y una conexión, que consiste en un peso con información de direccionamiento del nodo. Las neuronas (elementos

únicos de procesamiento) están interconectadas a través de un conjunto de sinapsis o enlaces de conexión, cada uno de los cuales se caracteriza por un peso escalar (*w*). Para cada neurona que recibe "*n*" entradas de varias fuentes, las señales de entrada se ponderan de acuerdo con los pesos sinápticos respectivos de la neurona, y a continuación se agregan a otro escalar aplicado externamente, llamado sesgo (*b*), de acuerdo con la siguiente ecuación:

$$Sum = \sum_{i=1}^{n} x_i \cdot w_i + b \qquad \text{(Eq.8)}$$

Con, x_i representando la i-ésima variable de entrada. En este trabajo se trabajó con una ANN de tipo *feed-forward* no recurrente con aprendizaje supervisado correctivo, en el que se conocen las entradas y los objetivos [110]. El tipo de red se conoce como perceptrón multicapa (MLP) y son denominadas como aproximadores de funciones universales, donde con una sola capa oculta y una capa de salida, predicen casi cualquier relación entre las variables de entrada y salida. La red neuronal *feed-forward* suele tener una o más capas ocultas, que permiten a la red modelar funciones complejas y no lineales. En esta tesis se decidió trabajar con una o dos capas ocultas, aumentando el número de neuronas hasta comprobar que la mejora en la medida de ajuste con una neurona más no era significativa. La selección de la partición de datos para el entrenamiento y la validación de la red es otro factor importante a considerar. Generalmente, el grupo de entrenamiento es el que tiene mayor cantidad de datos, con alrededor del 70% u 80% de todos los datos utilizados en este grupo, mientras que los datos restantes se utilizan para validación y predicción.

III.5. PROCESO DE ADSORCIÓN/DESORCIÓN

III.5.1 Adsorción

La adsorción es un proceso de separación en el que uno o más componentes son atraídos (atrapados o retenidos) a la superficie de un material sólido al entrar en contacto (Figura 3. 11).

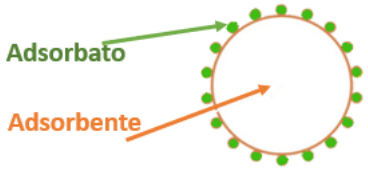

Figura 3.11. Diagrama del proceso de adsorción

La sustancia adsorbida se llama adsorbato o soluto, y la sustancia que retiene se llama adsorbente. Esta técnica tiene muchas ventajas sobre las otras técnicas mencionadas anteriormente, tal como simplicidad de diseño y operación, debido a sus simples pasos a seguir en la operación del proceso. Por otra parte, los costes de funcionamiento y requerimientos de energía son más bajos [39]. El proceso de adsorción consta de una serie de interacciones. Primero ocurre la transferencia de masa desde la fase líquida a la superficie exterior de las partículas. Tras ello ocurre la difusión del soluto por los poros del adsorbente, para llegar a continuación a la adsorción del soluto debido a las interacciones entre ellos como la atracción hidrófoba y electrostática y los enlaces de hidrógeno [111].

La naturaleza de la interacción adsorbato/adsorbente depende de las propiedades de los compuestos involucrados. Esto se verá afectado entonces, por el área superficial específica y la porosidad del adsorbente, así como por el tipo y la concentración del adsorbente. La química de la superficie del adsorbente, como los grupos funcionales, también afecta la selectividad y la cantidad de solutos adsorbidos, pero también la velocidad a la que se produce la adsorción. En cuanto al soluto adsorbido, su concentración y solubilidad en disolución también afectan el proceso. Cuanto mayor sea su concentración en la disolución a tratar, mayor será la cantidad de adsorción, mientras que a mayor solubilidad menor será la adsorción. Los grupos funcionales de su estructura química juegan un papel importante, ya que pueden promover la adsorción específica entre solutos y adsorbentes. La disolución donde está presente el soluto a ser adsorbido y sus propiedades también afectan el proceso. El pH de una disolución determina el grado de disociación del soluto y afecta su solubilidad. Dado que la adsorción es un fenómeno exotérmico, la temperatura también es un factor para considerar, ya que el aumento de la temperatura disminuye la adsorción. Y finalmente la competencia entre solutos puede

afectar la capacidad de adsorción de un soluto en particular compitiendo por los sitios del adsorbente [39,112,113].

La adsorción se puede categoriza en 3 tipos, según el tipo de atracción entre soluto y adsorbente:

- Fisisorción: Interacciones físicas, es la más débil de las interacciones y no son específicas. Principalmente son interacciones de tipo Van der Waals, dipolo-dipolo o puentes de hidrógeno. Estas son interacciones reversibles de baja entalpía ((1-10 kcal/mol) y permiten la formación de mono y multi capas de adsorbato.
- Químisorción: Interacciones químicas especificas generalmente irreversibles. Son enlaces fuertes (covalentes), de alta entalpía (50-100 kcal/mol), que permiten la formación de solo mono capas de adsorbato.
- Intercambio iónico: Esta interacción es especifica de un tipo de adsorbentes (resinas de intercambio iónico) y ocurre cuando los iones del adsorbato son atraídos (se concentran) en la superficie del adsorbente como resultado de la atracción electrostática.

La adsorción es una de las técnicas a escala industrial más utilizadas para la eliminación de compuestos tóxicos y/o no biodegradables de corrientes líquidas. Por lo tanto, los compuestos fenólicos en corrientes líquidas han sido ampliamente estudiados.

III.5.2. Materiales Adsorbentes

Varios materiales han sido estudiados como adsorbentes selectivos de compuestos fenólicos, siendo el carbón activo el más utilizado. Sin embargo, el uso de este material presenta dificultades cuando los compuestos adsorbidos deben ser desorbidos (separados de la matriz adsorbente), ya que el proceso de adsorción es muchas veces irreversible [114]. Entre los adsorbentes sintéticos, las resinas son las más estudiadas y utilizadas debido a su estabilidad química, selectividad, capacidad de adsorción y baja toxicidad, lo que las hace de

gran interés para la recuperación de compuestos. Estas resinas tienen varias propiedades que las distinguen, como polaridad, material, tamaño de partícula, área de superficie específica y tamaño de poro. En general, son relativamente económicas, fáciles de preparar y recuperar, y adecuadas para la producción a gran escala [115–117].

Tabla 3.5. Adsorbentes utilizados para la recuperación de compuestos fenólicos de OMW

Adsorbente	Tipo de solución	Eficiencia	Referencia
Arcilla/arcilla calcinada	OMW[1], Túnez	77,6% / 84,2%	[83]
Resinas (XAD4, XAD16, FPX66)	OMW[1], Grecia	75% con 20% resina FPX66	[118]
Semillas de Granada	OMW*, Grecia	92,8%	[119]
Toba (roca) volcánica, carbón activo de arcilla natural y combinaciones	OMW[1], Jordania	21 - 80% (carbón activo de arcilla mayor eficiencia)	[120]
Zeolitas/Nanopartículas de zeolita	OMW*, Arabia Saudita	97,8% / 98,2%	[121]
Resinas (Dowex 21KXLT y Dowex66)	OMW[2], Spain	60,8% / 83,3%	[46]
Resinas (XAD7, XAD16, IRA96, ENV+)	OMW[1], Italy	53-88% (ENV+, mayor eficiencia)	[122]

[1]: proveniente proceso centrifugación de tres fases; [2]: proveniente proceso centrifugación de dos fases; *: no especifica proceso de procedencia

Específicamente en la adsorción de compuestos fenólicos del OMW, se han estudiado tanto la adsorción simple en resinas no iónicas neutras como la adsorción en resinas iónicas de intercambio iónico. Ambos tipos de adsorbentes se han utilizado con éxito en varios campos. Si bien la mayoría se centran en disoluciones sintéticas [123,124], en los últimos años el uso de OMW reales se ha intensificado. En la tabla 3.5 se presentan algunos estudios realizados con agua residual de almazara real. Es importante el estudio con aguas reales, ya que existe competencia entre compuestos fenólicos y también con otras sustancias presentes en las muestras [125]. Esto es determinante a la hora de seleccionar el tipo de resina. Yangui et al. [126], investigaron la adsorción competitiva y la selectividad de fenoles tóxicos e hidroxitirosol presentes en OMW en dos resinas (FPX66 y MN202). Observaron que a bajas concentraciones de FPX66, el fenol exhibió una tasa de adsorción mucho más alta que el hidroxitirosol, lo que indica una interacción más fuerte con la resina. En cuanto al hidroxitirosol, debido a la alta afinidad por la resina MN202, la adsorción y su recuperación

superó el 90 %. Por lo tanto, en condiciones de operación adecuadas, el fenol se eliminó selectivamente en FPX66 y el hidroxitirosol se recuperó en gran medida del OMW por adsorción en MN202.

La información de equilibrio de adsorción es la información más importante requerida para una correcta comprensión del proceso de adsorción. Una comprensión e interpretación adecuadas de las isotermas de adsorción es fundamental para la mejora general de las vías del mecanismo de adsorción y el diseño eficaz de los sistemas de adsorción. A continuación, se presentarán las Isotermas y Cinéticas de adsorción estudiadas en esta Tesis Doctoral.

III.5.3. Isotermas de Adsorción

Las isotermas de adsorción se definen por interacciones adsorbato-adsorbente, y su conocimiento es esencial para la operación práctica. Se han definido cuatro clases de isotermas de adsorción (S, L, H, C) y subgrupos según su configuración. IUPAC (*International Union of Pure and Applied Chemistry*) considera seis tipos de isotermas de adsorción para describir la adsorción en adsorbentes microporosos y macroporosos. Se han publicado varios estudios sobre la utilidad de las diferentes isotermas y revisión de los fundamentos, modelos y ecuaciones de adsorción. Las ecuaciones de isoterma de dos parámetros de Langmuir y Freundlich se utilizan comúnmente para evaluar la adsorción de compuestos fenólicos [127]. Estas fueron las estudiadas en esta Tesis Doctoral y se presentan a continuación.

III.5.3.1 Isotermas de Langmuir y Freundlich

La adsorción de Langmuir, que se diseñó principalmente para describir la adsorción en fase gas-sólida, también se utiliza para cuantificar y contrastar la capacidad de adsorción de varios adsorbentes. La isoterma de Langmuir explica la cobertura de la superficie equilibrando

las tasas relativas de adsorción y desorción (equilibrio dinámico). La adsorción es proporcional a la fracción de la superficie del adsorbente que está abierta, mientras que la desorción es proporcional a la fracción de la superficie del adsorbente que está cubierta. Este modelo de Langmuir considera una adsorción monocapa con sitios de sorción energéticamente idénticos, donde no ocurre interacción entre las moléculas adsorbidas [128]. La ecuación de Langmuir se puede escribir en la siguiente forma lineal:

$$\frac{C_e}{q_e} = \frac{1}{K_L \cdot q_0} + \frac{1}{q_0} C_e \qquad \text{(Eq.9)}$$

donde C_e (ppm) es la concentración de equilibrio de compuestos fenólicos en la solución, q_e (mg·g^{-1}) es la cantidad de soluto adsorbido por gramo de adsorbente en equilibrio respectivamente, q_0 (mg·g^{-1}) es la capacidad máxima de adsorción y K_L es la constante de Langmuir, que se obtiene por extrapolación de los datos analíticos. K_L puede correlacionar con la variación del área adecuada y la porosidad del adsorbente, lo que implica que un área de superficie y un volumen de poro grandes darán como resultado una mayor adsorción capacidad.

La isoterma de Langmuir se puede expresar mediante una constante de equilibrio adimensional llamada factor de separación R_L. Este parámetro está relacionado con el parámetro K_L y se obtiene mediante la siguiente ecuación:

$$R_L = \frac{1}{1 + K_L + C_0} \qquad \text{(Eq.10)}$$

Con Co (ppm) como la concentración inicial de adsorbato. En cuanto a los valores del parámetro, si $RL>1$, indica que la adsorción es desfavorable, favorable cuando $0<RL<1$, e irreversible cuando $RL=0$.

Por otro lado, el modelo de isoterma de Freundlich da una expresión que define la heterogeneidad de la superficie y asume una superficie de adsorción heterogénea que se caracteriza por sitios de sorción a diferentes energías. La forma lineal de la isoterma de Freundlich es la siguiente [129].

$$\log q_e = \log K_f + \frac{1}{n}\log C_e \qquad \text{(Eq.11)}$$

donde K_f es la capacidad de adsorción ($L \cdot mg^{-1}$) y $1/n$ es la intensidad de adsorción; también indica la distribución relativa de energía y la heterogeneidad de los sitios de adsorbato, siendo favorable la adsorción si su valor es inferiores a 1[111].

III.5.4. Cinéticas de Adsorción

El estudio de las cinéticas es de interés para la química de superficies, proporcionando información valiosa para la comprensión de mecanismos de adsorción/desorción. Los parámetros cinéticos son útiles para la predicción de la tasa de adsorción y brindan información importante para el diseño y modelado de procesos. Se han propuesto varios modelos cinéticos para evaluar la adsorción de solutos aromáticos. Los mecanismos involucrados en la adsorción de fenoles son el complejo donador-aceptor de electrones, las interacciones de dispersión π-π, los efectos del disolvente, las fuerzas de dispersión e inducción, las interacciones hidrofóbicas y de intercambio iónico y el acoplamiento oxidativo.

En general, el transporte del adsorbato ocurre en cuatro pasos secuenciales: transporte del adsorbato desde el seno de la disolución hasta la capa límite que rodea las partículas del adsorbente; transporte de solutos a través de la capa límite; difusión intra-partícula de solutos en los poros; adsorción y desorción de adsorbatos. El proceso global se puede controlar mediante cualquiera de los pasos anteriores o mediante una combinación de los mismos [127].

A continuación, se presentan los modelos de pseudo-primer y segundo orden e intra-partícula, los cuales fueron utilizados en este estudio.

III.5.4.1. Cinética de Pseudo primer orden y Pseudo segundo orden

La ecuación de Lagergren [130], mejor conocida como ecuación cinética de pseudo-primer orden, fue el primer modelo propuesto para describir la adsorción en un sistema sólido-líquido, donde la tasa de adsorción se basa en la capacidad de sorción de los adsorbentes. Se obtiene mediante la fórmula descrita por la ecuación 12.

$$\ln(q_e - q_t) = \ln q_e - k_1 \cdot t \qquad \text{(Eq.12)}$$

El modelo de pseudo-segundo orden (ecuación 13) indica que la tasa de adsorción es proporcional a los sitios disponibles en la superficie adsorbente [131].

$$\frac{1}{q_t} = \frac{1}{k_2 \cdot q_e^2} + \frac{1}{q_e} \cdot t \qquad \text{(Eq.13)}$$

q_t (mg·g^{-1}) es la capacidad de adsorción de cada adsorbente, k_1 (min^{-1}) es la constante de velocidad de pseudo-primer orden y k_2 (g·mg^{-1}· min^{-1}) es la constante de velocidad de pseudo-segundo orden. Para la determinación de las constantes se trazaron dos gráficas, una correspondía a *Ln* (q_e-q_t) versus tiempo (t) y la otra a t/q_t versus tiempo (t). Luego, realizando una regresión lineal, fue posible obtener q_e de cada modelo, así como los parámetros del modelo.

Estas dos ecuaciones se han utilizado ampliamente para estudiar la adsorción de disoluciones líquidas.

III.5.4.2 Modelo Intra-partícula

El modelo de difusión intra-partícula, también conocido como modelo de difusión de Weber, se utilizó para identificar el mecanismo involucrado en el proceso de adsorción. La adsorción de compuestos fenólicos está controlada por diferentes pasos, que pueden estar

relacionados con la película o la difusión en la superficie externa, la difusión en los poros, la difusión en la superficie y la adsorción en la superficie de los poros, o una combinación de ellos [111]. El modelo de difusión intra-partícula se puede derivar de la segunda ley de Fick y se representa mediante la ecuación 14.

$$q_t = k_d^{\frac{1}{2}} + I \qquad \text{(Eq.14)}$$

Donde k_d (mg·g^{-1} ·min$^{-½}$) es la constante de velocidad de difusión intra- partícula e I representa el espesor de la capa límite en la superficie del adsorbente. Ambos parámetros se obtuvieron mediante un gráfico lineal de q_t frente a t ½.

III.5.5. Desorción

La disolución utilizada para extraer los compuestos fenólicos (Figura 3.12) de las resinas es otro tema importante en el proceso de adsorción/desorción. Se han estudiado diversas disoluciones para la desorción de compuestos fenólicos, siendo los más utilizados el etanol, el etanol acidificado, el metanol y el agua [115,132]. Esto también dependerá de la resina utilizada, así como de los compuestos fenólicos presentes en la disolución.

Figura 3.12. Diagrama del proceso de desorción

Algunos estudios presentan al etanol como mejor extractante, como el realizado por Bertin et al. [122], donde estudiaron cuatro resinas (Amberlite XAD7, XAD16, IRA96 e Isolute ENV+) frente a la adsorción y desorción de compuestos fenólicos presentes en muestras de OMW de un almazara en Italia. Observaron altas proporciones de desorción de fenoles totales con etanol acidificado, sin embargo, la mayor recuperación específica de hidroxitirosol se produjo cuando se utilizó etanol no acidificado como desorbente. Varios estudios han concluido que el etanol es uno de los mejores disolventes para la desorción de compuestos fenólicos de aguas residuales de almazara adsorbidos en resinas [133]. Sin embargo, el utilizar el compuesto puro conlleva un alto coste. Un estudio realizado por Frascari et al. [84] demostró que la mezcla al 50% v/v de agua desionizada y etanol, acidificada con HCl hasta alcanzar una concentración de 2 mol/L (pH = 0.3), era la mejor opción para la desorción de compuestos fenólicos a partir de una resina de intercambio utilizando permeado de microfiltración OMW como alimentación.

III.6 TRATAMIENTO BIOLÓGICO

Los procesos biológicos son uno de los tratamientos de aguas residuales más utilizados, ya que es un método económico, simple de diseñar y mantener, para transformar compuestos orgánicos en productos finales simples [134]. El tratamiento biológico es capaz de eliminar la materia orgánica y los nutrientes inorgánicos. Si bien este proceso para el tratamiento de OMW ha sido estudiado, la presencia de compuestos fenólicos y lípidos hacen que la OMW sea difícil de tratar [135]. Los métodos biológicos pueden implicar tratamientos de digestión aeróbica o anaeróbica. La mayoría de los estudios de tratamiento biológico de OMW se centran en la digestión anaeróbica, pero independientemente de trabajar en presencia o en ausencia de oxígeno se recalca que se requiere una eliminación suficiente de polifenoles o diluciones sustanciales para una degradación más efectiva en el tratamiento biológico [136,137]. En este trabajo de tesis solo se ahondará en el proceso biológico aeróbico, ya que fue el proceso utilizado.

III.6.1. Tratamiento aeróbico

En estos procesos, aquellas bacterias que prosperan en condiciones donde hay suficiente oxígeno y contaminantes descomponen la materia orgánica del agua residual oxidándola con oxígeno suministrado desde una fuente externa (ya sea aire u oxígeno inyectado). En condiciones aeróbicas, los compuestos orgánicos son oxidados por microorganismos a CO_2, agua y formas oxidadas de nitrógeno y azufre [2].

Como se comentó anteriormente, la alta concentración de compuestos fenólicos en el OMW hace inadecuado este efluente para su tratamiento aeróbico biológico directo. Dicho de otro modo, es difícil usar procesos aeróbicos para lograr la eficiencia de eliminación requerida para ciertas clases de contaminantes, como por ejemplo los polifenoles en el caso del OMW y los colorantes en el caso de aguas residuales textiles [79].

Los procesos aeróbicos más conocidos para el tratamiento de las aguas residuales son los fangos activos, que incluye la variante SBR (reactores biológicos secuenciales). Se ha de tener en cuenta que estos procesos solo pueden trabajar con cargas orgánicas altas si la planta opera con un tiempo de retención hidráulico prolongado y/o altas tasas de recirculación (es decir, altas tasas de flujo de efluentes tratados se devuelven a la entrada de la planta) [2].

Estudios como los realizados por El Hajjouji et al. [138] han evaluado la eficiencia del tratamiento en términos de viabilidad del proceso, concentración a tratar y reducción de compuestos fitotóxicos. Para ello, relacionaron la concentración de compuestos fenólicos con el efecto fitotóxico en la germinación de semillas y el análisis de crecimiento de Vicia faba en un suelo arcilloso. Durante 45 días probaron diferentes concentraciones de OMW tratado como sin tratar. Sus resultados mostraron una disminución den la genotoxicidad y toxicidad con OMW diluido al 10 y 20%, lo que relacionaron con la biodegradación del 76% del total de compuestos fenólicos. Estudios como este demuestran la alta toxicidad de estas aguas, logrando solo la degradación de compuestos fenólicos una vez las bacterias se aclimaten.

Por ello, a menudo se realiza una dilución o pretratamiento del OMW antes del tratamiento biológico, con el fin de reducir la toxicidad de los microorganismos responsables de la descomposición de la materia orgánica. Algunos estudios recomiendan diluciones de entre 70 a 100 veces para reducir el nivel de DQO del alimento (al menos hasta 1 g/L) antes de ser sometido a tratamiento biológico [137,139].

El trabajo de investigación titulado "Tratamiento SBR de OMW: ¿dilución o pretratamiento?" [82] evalúa el rendimiento del SBR alimentado con OMW pretratado (craqueo ácido y adsorción de carbón activo granular) y lo compara con un SBR idéntico alimentado solo con aguas residuales sin diluir. Los resultados mostraron que los mejores rendimientos de SBR se obtuvieron cuando se alimentó con OMW diluido (1:25), con una eficiencia de eliminación del 90 y 76 % en promedio para la DQO y los compuestos fenólicos, respectivamente. Por otra parte, la comparación del SBR alimentado con 1:50 pretratado o 1:50 crudo (sin pretratamiento) produjo valores de reducción de DQO muy similares (7% mayor con OMW pretratado). En cuanto a la eliminación de compuestos fenólicos, fue mayor con el alimento pretratado. Por otra parte, como bien comenta este autor, el potencial de algunos sistemas innovadores aún no se ha explotado por completo, siendo pocos los estudios sobre la aplicación de SBR, aunque se ha demostrado ampliamente su capacidad para biodegradar varios compuestos fenólicos. Por ello se ha considerado el SBR la mejor opción de tratamiento biológico aerobio de la OMW, siendo el proceso empleado en esta Tesis Doctoral.

Recientemente, Rifi et al. [140] también investigaron la capacidad de un reactor SBR para tratar OMW diluido, esta vez con aguas residuales domésticas. Se probaron dos diluciones diferentes, 50% OMW 50% aguas residuales domésticas y 75% OMW 25% aguas residuales domésticas. La primera opción mostró una tasa de reducción de 69% y 67% para DQO y compuestos fenólicos, respectivamente, mientras que la segunda alternativa eliminó el 40% de DQO y el 47% de compuestos fenólicos. Esto nuevamente recalca la importancia de una dilución y/o un pretratamiento al SBR.

III.7 PROCESOS HIBRIDOS

El estudio del estado del arte sobre el tratamiento de OMW, llevó a la conclusión de que había que seleccionar un sistema hibrido compuesto por procesos de diferente naturaleza para tanto la recuperación de compuestos fenólicos como para el tratamiento final del OMW. Si bien durante toda la introducción se han presentado procesos híbridos, se ha decidido agregar otros para su conocimiento.

Vuppala et al. [141] buscaron optimizar el proceso de coagulación y floculación para ser utilizado como pretratamiento del OMW, consiguiendo una reducción de turbidez, COT, DQO y compuestos fenólicos del orden del 99% 17%, 57% y 63% respectivamente con una concentración de 800 mg/L de alumbre. El agua clarificada fue luego sometida a un tratamiento de oxidación biológica donde se logró una disminución adicional del 83%, 72% y 99.6% en los niveles de DQO, COT y fenoles, respectivamente. Ciggin et al. [142] estudiaron las condiciones experimentales de un sistema híbrido compuesto por un pretratamiento de oxidación Fenton, seguido de un reactor biológico secuencial (SBR). Uno de los factores a estudiar fue el grado de dilución que se podría lograr sin alterar el desempeño del proceso biológico, bajo las condiciones de 105 días con cuatro ciclos por día, con una edad del lodo de 8 días, una DQO constante (400 mg/L) y la adición de OMW gradualmente creciente en cuatro fases consecutivas con aumentos de DQO entre 40 y 100 mg/ L y sin adición de OMW en la última fase. Estos autores consiguieron una eliminación completa de DQO biodegradable en OMW mantenido en condiciones de estado estacionario cíclico de cada fase.

Chiavola et al. [143] investigaron el proceso biológico y químico-físico combinado para el tratamiento de OMW. Estos autores emplearon tres coagulantes como pretratamiento (sales de cal, aluminio y cloruro de hierro). Los resultados mostraron que, con sales de aluminio y cloruro de hierro, la eliminación de DQO fue del 20% (dosis de 4 g/l) y del 19% (dosis de 3 g/l), respectivamente. En cuanto a los rendimientos tras añadir cal, la eliminación de DQO alcanzó el 51% (pH óptimo alrededor de 12), siendo este compuesto el seleccionado. A continuación, con un SBR (alimentado con OMW pretratado diluido) se logró una eficiencia de eliminación final de alrededor del 60% de DQO.

Ochando-Pulido et al. [144], estudiaron a escala piloto la regeneración de OMW. El procedimiento contempló un proceso de oxidación avanzada basado en el reactivo de Fenton junto con una etapa final de ósmosis inversa (OI) (etapa de purificación). Modelaron también la hidrodinámica y la selectividad de la membrana. El modelado ayudó a la optimización de las condiciones hidrodinámicas. Esto les permitió obtener un rendimiento estable y amortiguar los problemas de ensuciamiento. Finalmente lograron valores paramétricos por debajo de los límites estándar para la reutilización del efluente regenerado, lo que se consiguió con rechazos en la membrana de hasta 99% y 98% de los contaminantes orgánicos y de conductividad, respectivamente.

III.8 REFERENCIAS

[1] V. Zampounis, Olive Oil in the World Market, Second Edi, AOCS Press, 2006. https://doi.org/10.1016/B978-1-893997-88-2.50007-9.

[2] I.E. Kapellakis, K.P. Tsagarakis, J.C. Crowther, Olive oil history, production and by-product management, Rev. Environ. Sci. Biotechnol. 7 (2008) 1–26. https://doi.org/10.1007/s11157-007-9120-9.

[3] D. Boskou, G. Blekas, M. Tsimidou, Olive Oil Composition, Second Edi, AOCS Press, 2006. https://doi.org/10.1016/B978-1-893997-88-2.50008-0.

[4] D. Boskou, Characteristics of the Olive Tree and Olive Fruit, Second Edi, AOCS Press, 2006. https://doi.org/10.1016/B978-1-893997-88-2.50006-7.

[5] International Olive Council, Olive oil, Des. Defin. Olive Oils. https://www.internationaloliveoil.org/olive-world/olive-oil/ (accessed April 24, 2022).

[6] A. Boudebouz, A. Romero, J.F. Hermoso, R. Boqué, M. Mestres, Processing factors that affect the balance of alcohols and alkyl esters during 'Arbequina' olive oil production: Separation and clarification steps, Lwt. 149 (2021). https://doi.org/10.1016/j.lwt.2021.111842.

[7] Directo del Olivar, Mercado del aceite de oliva y su consumo en el mundo, (2022). www.directodelolivar.com (accessed May 21, 2022).

[8] International Olive Oil Council, Olive oil world production, (2021). http://www.internationaloliveoil.org. (accessed May 15, 2022)

[9] L.J. Stolp, D.R. Kodali, Naturally occurring high-oleic oils: Avocado, macadamia, and

olive oils, Elsevier Inc., 2022. https://doi.org/10.1016/b978-0-12-822912-5.00003-4.

[10] D. Klisović, A. Novoselić, I. Lukić, K. Brkić Bubola, Extra virgin olive oil under simulated consumption conditions: Evaluation of quality, health, and flavour properties, J. Food Compos. Anal. 110 (2022) 104570. https://doi.org/10.1016/j.jfca.2022.104570.

[11] International Olive Council, The world of olive oil, (2022). https://www.internationaloliveoil.org/the-world-of-olive-oil/ (accessed May 15, 2022).

[12] M. Parras Rosa, Informe anual de coyuntura del sector oleícola, (2020). https://doi.org/10.17561/ree.n1.2022.6814.

[13] Ministerio de Agricultura Pesca y Alimentación, Aceite de oliva y aceituna de mesa, (2021). https://www.mapa.gob.es/es/agricultura/temas/producciones-agricolas/aceite-oliva-y-aceituna-mesa/aceite.aspx (accessed May 15, 2022).

[14] Ministerio de Agricultura Pesca y Alimentación, Mapa de los aceites con denominación de origen protegida, (2015). https://www.mapa.gob.es/es/cartografia-y-sig/publicaciones/alimentacion/mapa_dop_aceites.aspx (accessed May 17, 2022)

[15] Aceites de Oliva de España, Entidades relacionadas con el sector. https://www.aceitesdeolivadeespana.com/universo-aceites-de-oliva/ (accessed May 21, 2022).

[16] J. Rangel Preciado, F. Parejo-Moruno, J. Rangel Preciado, El Mercado Mundial De Aceituna De Mesa (1990-2015), Reg. Sect. Econ. Stud. 16 (2016) 127–146.

[17] Ministerio de Agricultura Pesca y Alimentación, avance de la situación de mercado del sector del aceite de oliva, aceituna de mesa y aceite de orujo de oliva, (2021), https://www.mapa.gob.es/es/agricultura/temas/producciones-agricolas/aceite-oliva-y-aceituna-mesa/aceite.aspx (accessed May 21, 2022).

[18] S.A. Vekiari, P. Papadopoulou, A. Koutsaftakis, Comparison of different olive oil extraction systems and the effect of storage conditions on the quality of the virgin olive oil, Grasas y Aceites. 53 (2002) 324–329. https://doi.org/10.3989/gya.2002.v53.i3.324.

[19] C. Petrakis, Olive Oil Extraction, Second Edi, AOCS Press, 2006. https://doi.org/10.1016/B978-1-893997-88-2.50013-4.

[20] A. Khdair, G. Abu-Rumman, Sustainable environmental management and valorization options for olive mill byproducts in the Middle East and North Africa (MENA) region, Processes. 8 (2020) 1–22. https://doi.org/10.3390/PR8060671.

[21] S. Souilem, A. El-Abbassi, H. Kiai, A. Hafidi, S. Sayadi, C.M. Galanakis, Olive oil production sector: Environmental effects and sustainability challenges, in: Olive Mill Waste Recent Adv. Sustain. Manag., (2017). https://doi.org/10.1016/B978-0-12-805314-0.00001-7.

[22] A. Fernández Garrido, P. García García, A. López López, F.N. López Arroyo, Tecnología de la elaboración de aceite de oliva y aceitunas de mesa Índice, Technol. Dissem. Centres, TDC-OLIVE. (2006) 25.

[23] A. Ben Sassi, A. Boularbah, A. Jaouad, G. Walker, A. Boussaid, A comparison of Olive oil Mill Wastewaters (OMW) from three different processes in Morocco, Process Biochem. 41 (2006) 74–78. https://doi.org/10.1016/j.procbio.2005.03.074.

[24] M. Uceda, A. Jiménez, G. Beltrán, Olive oil extraction and quality, Grasas y Aceites. 57 (2006) 25–31. https://doi.org/10.3989/gya.2006.v57.i1.19.

[25] M.L. Clodoveo, An overview of emerging techniques in virgin olive oil extraction process: strategies in the development of innovative plants, J. Agric. Eng. XLIV (2s): (2013) 297–305. https://doi.org/10.4081/jae.2013.s2.e60.

[26] N. Azbar, A. Bayram, A. Filibeli, A. Muezzinoglu, F. Sengul, A. Ozer, A review of waste management options in olive oil production, Crit. Rev. Environ. Sci. Technol. 34 (2004) 209–247. https://doi.org/10.1080/10643380490279932.

[27] C.J. McNamara, C.C. Anastasiou, V. O'Flaherty, R. Mitchell, Bioremediation of olive mill wastewater, Int. Biodeterior. Biodegrad. 61 (2008) 127–134. https://doi.org/10.1016/j.ibiod.2007.11.003.

[28] J.M. Ochando-Pulido, R. González-Hernández, A. Martinez-Ferez, On the effect of the operating parameters for two-phase olive-oil washing wastewater combined phenolic compounds recovery and reclamation by novel ion exchange resins, Sep. Purif. Technol. 195 (2018) 50–59. https://doi.org/10.1016/j.seppur.2017.11.075.

[29] P. Mohammadnejad, K. Haghbeen, H. Rasouli, Treatment and valorization of olive mill wastewater, INC, 2021. https://doi.org/10.1016/b978-0-12-819528-4.00058-4.

[30] A.Y. Gebreyohannes, R. Mazzei, L. Giorno, Trends and current practices of olive mill wastewater treatment: Application of integrated membrane process and its future perspective, Sep. Purif. Technol. 162 (2016) 45–60. https://doi.org/10.1016/j.seppur.2016.02.001.

[31] J.A. de la Casa, J.S. Bueno, E. Castro, Recycling of residues from the olive cultivation and olive oil production process for manufacturing of ceramic materials. A comprehensive review, J. Clean. Prod. 296 (2021). https://doi.org/10.1016/j.jclepro.2021.126436.

[32] M.K. Hazreen-Nita, Z. Abdul Kari, K. Mat, N.D. Rusli, S.A. Mohamad Sukri, H. Che Harun, S.W. Lee, M.M. Rahman, N.H. Norazmi-Lokman, M. Nur-Nazifah, M. Firdaus-Nawi, M.A.O. Dawood, Olive oil by-products in aquafeeds: Opportunities and challenges, Aquac. Reports. 22 (2022) 100998. https://doi.org/10.1016/j.aqrep.2021.100998.

[33] Consejo Oleíco Internacional, Normal comercial aplicable a las aceitunas de mesa, (2004), https://www.internationaloliveoil.org/wp-content/uploads/2019/11/COI-OT-NC1-2004-Esp.pdf (accessed May 21, 2022)

[34] M. Campus, N. Degirmencioglu, R. Comunian, Technologies and trends to improve table olive quality and safety, Front. Microbiol. 9 (2018). https://doi.org/10.3389/fmicb.2018.00617.

[35] O. Syed Haris, Oleuropein in Olive and its Pharmacological Effects, Sci. Pharm. 78 (2010) 133–154. https://doi.org/10.3797/scipharm.0912-18.

[36] A.H.S. Gómez, P. García, L.R. Navarro, Elaboration of table olives, Grasas y Aceites. 57 (2006) 86–94.

[37] F.J. Santos, Las nuevas tecnologías aplicadas al sector de la aceituna manzanilla fina sevillana, Grasas y Aceites. 50 (1999) 131–140. https://doi.org/10.3989/gya.1999.v50.i2.648.

[38] C.S. Parinos, C.D. Stalikas, T.S. Giannopoulos, G.A. Pilidis, Chemical and physicochemical profile of wastewaters produced from the different stages of Spanish-style green olives processing, J. Hazard. Mater. 145 (2007) 339–343. https://doi.org/10.1016/j.jhazmat.2006.12.061.

[39] E. Ferrer-Polonio, tratamiento biológico aerobio para aguas residuales con elevada conductividad y concentración de fenoles, tesis doctoral (2017).

[40] Junta de Andalucía Consejería de Agricultura y Pesca Servicio de Publicación y Divulgación, Potencial Energético de los Subproductos de la Industria Olivarera en Andalucía, (2010) https://www.juntadeandalucia.es/export/drupaljda/Potencial%20energ%C3%A9tico.pdf (accessed May 7, 2022).

[41] B. Rincón-Llorente, D. De la Lama-Calvente, M.J. Fernández-Rodríguez, R. Borja-Padilla, Table olive wastewater: Problem, treatments and future strategy. A review, Front. Microbiol. 9 (2018). https://doi.org/10.3389/FMICB.2018.01641/FULL.

[42] X. Sun, C. Wang, Y. Li, W. Wang, J. Wei, Treatment of phenolic wastewater by combined UF and NF/RO processes, Desalination. 355 (2015) 68–74. https://doi.org/10.1016/j.desal.2014.10.018.

[43] T. Chatzistathis, T. Koutsos, Olive mill wastewater as a source of organic matter, water and nutrients for restoration of degraded soils and for crops managed with sustainable systems, Agric. Water Manag. 190 (2017) 55–64. https://doi.org/10.1016/j.agwat.2017.05.008.

[44] M.S. Cifuentes Cabezas, Recuperación de polifenoles de aguas residuales del procesado de aceituna de mesa mediante membranas, 2017. https://riunet.upv.es:443/handle/10251/89644.

[45] E. Ferrer-Polonio, C. Carbonell-Alcaina, J.A. Mendoza-Roca, A. Iborra-Clar, S. Álvarez-Blanco, A. Bes-Piá, L. Pastor-Alcañiz, Brine recovery from hypersaline wastewaters from table olive processing by combination of biological treatment and membrane technologies, J. Clean. Prod. 142 (2017) 1377–1386. https://doi.org/10.1016/j.jclepro.2016.11.169.

[46] J.M. Ochando-Pulido, S. Pimentel-Moral, V. Verardo, A. Martinez-Ferez, A focus on advanced physico-chemical processes for olive mill wastewater treatment, Sep. Purif. Technol. 179 (2017) 161–174. https://doi.org/10.1016/j.seppur.2017.02.004.

[47] M. Maaitah, G. Hodaifa, A. Malvis, S. Sánchez, Kinetic growth and biochemical composition variability of Chlorella pyrenoidosa in olive oil washing wastewater cultures enriched with urban wastewater, J. Water Process Eng. 35 (2020) 101197. https://doi.org/10.1016/j.jwpe.2020.101197.

[48] M. Alexandra Núñez Camacho, A. Isabel García López, A. Martinez-Ferez, J.M. Ochando-Pulido, Two-Phase Olive-Oil Washing Wastewater Treatment Plus Phenolic Fraction Recovery By Novel Ion Exchange Resins Process Modelling And Optimization, Sep. Purif. Technol. 269 (2021) 118755. https://doi.org/10.1016/j.seppur.2021.118755.

[49] M.J. Luján-Facundo, J.A. Mendoza-Roca, J.L. Soler-Cabezas, A. Bes-Piá, M.C. Vincent-Vela, B. Cuartas-Uribe, L. Pastor-Alcañiz, Management of table olive processing wastewater by an osmotic membrane bioreactor process, Sep. Purif. Technol. 248 (2020) 117075. https://doi.org/10.1016/j.seppur.2020.117075.

[50] A.K. Benekos, C. Zampeta, R. Argyriou, C.N. Economou, I.E. Triantaphyllidou, T.I. Tatoulis, A.G. Tekerlekopoulou, D. V. Vayenas, Treatment of table olive processing wastewaters using electrocoagulation in laboratory and pilot-scale reactors, Process Saf. Environ. Prot. 131 (2019) 38–47. https://doi.org/10.1016/j.psep.2019.08.036.

[51] M. Cifuentes-Cabezas, C. Carbonell-Alcaina, M.C. Vincent-Vela, J.A. Mendoza-Roca, S. Álvarez-Blanco, Comparison of different ultrafiltration membranes as first step for the recovery of phenolic compounds from olive-oil washing wastewater, Process Saf. Environ. Prot. 149 (2021) 724–734. https://doi.org/10.1016/j.psep.2021.03.035.

[52] A. El-Abbassi, H. Kiai, A. Hafidi, Phenolic profile and antioxidant activities of olive mill wastewater, Food Chem. 132 (2012) 406–412. https://doi.org/10.1016/j.foodchem.2011.11.013.

[53] Consejo Europeo, Directiva 91/271/CEE del Consejo sobre el tratamiento de las aguas residuales urbanas, (1991). http://data.europa.eu/eli/dir/1991/271/oj. (accessed May 1, 2022)

[54] B. de los Santos, M. Brenes, P. García, A. Aguado, E. Medina, C. Romero, Effect of table olive wastewaters on growth and yield of cucumber, pepper, tomato and strawberry, Sci. Hortic. 256 (2019) 108644. https://doi.org/10.1016/J.SCIENTA.2019.108644.

[55] E. Ferrer-Polonio, J.A. Mendoza-Roca, A. Iborra-Clar, J.L. Alonso-Molina, L. Pastor-Alcañiz, Biological treatment performance of hypersaline wastewaters with high phenols concentration from table olive packaging industry using sequencing batch reactors, J. Ind. Eng. Chem. 43 (2016) 44–52. https://doi.org/10.1016/j.jiec.2016.07.046.

[56] O.M. Wastewater, E. Tsagaraki, H.N. Lazarides, K.B. Petrotos, Olive Mill Wastewater Treatment, 8 (2004) 133–157.

[57] M.F. Ramadan, S. Ercisli, I. Sifaoui, C. Benincasa, E. Perri, M. Pellegrino, E. Romano,

S. Claps, C. Fallara, Qualitative and Quantitative Analysis of Phenolic Compounds in Spray-Dried Olive Mill Wastewater The processing of olives for oil production generates the most abundant agro-industrial by-products in the, Front. Nutr. 8 (2022) 782693. https://doi.org/10.3389/fnut.2021.782693.

[58] J.S. Torrecilla, J.C. Cancilla, Phenolic compounds in olive oil mill wastewater, Olives Olive Oil Heal. Dis. Prev. (2021) 693–700. https://doi.org/10.1016/b978-0-12-819528-4.00051-1.

[59] L. Deflaoui, W. Setyaningsih, M. Palma, A. Mekhoukhe, A. Tamendjari, Phenolic compounds in olive oil by solid phase extraction – Ultra performance liquid chromatography – Photodiode array detection for varietal characterization, Arab. J. Chem. 14 (2021) 103102. https://doi.org/10.1016/j.arabjc.2021.103102.

[60] H.K. Obied, M.S. Allen, D.R. Bedgood, P.D. Prenzler, K. Robards, Investigation of Australian olive mill waste for recovery of biophenols, J. Agric. Food Chem. 53 (2005) 9911–9920. https://doi.org/10.1021/jf0518352.

[61] E. Tripoli, M. Giammanco, G. Tabacchi, D. Di Majo, S. Giammanco, M. La Guardia, The phenolic compounds of olive oil: structure, biological activity and beneficial effects on human health, Nutr. Res. Rev. 18 (2005) 98–112. https://doi.org/10.1079/nrr200495.

[62] G. Çelik, Ö. Saygın, I. Balcıoğlu Akmehmet, Multistage recovery process of phenolic antioxidants with a focus on hydroxytyrosol from olive mill wastewater concentrates, Sep. Purif. Technol. (2020) 117757. https://doi.org/10.1016/j.seppur.2020.117757.

[63] C. Carbonell Alcaina, Recuperación de compuestos fenólicos contenidos en la salmuera residual del proceso de fermentación de las aceitunas de mesa mediante procesos de membrana: Combinación de la ultrafiltración y la nanofiltración. Tesis doctoral., 2017.

[64] C.E. Lizárraga-Velázquez, C. Hernández, G.A. González-Aguilar, J. Basilio-Heredia, Propiedades antioxidantes e inmunoestimulantes de polifenoles en peces carnívoros de cultivo, CienciaUAT. 12 (2018) 127. https://doi.org/10.29059/cienciauat.v12i2.904.

[65] N. Balasundram, K. Sundram, S. Samman, Phenolic compounds in plants and agri-industrial by-products: Antioxidant activity, occurrence, and potential uses, Food Chem. (2006). https://doi.org/10.1016/j.foodchem.2005.07.042.

[66] M. Coronado H., S. Vega Y León, R. Gutiérrez T., V.F. Marcela, C. Radilla V., Antioxidants: Present perspective for the human health, Rev. Chil. Nutr. 42 (2015) 206–212. https://doi.org/10.4067/S0717-75182015000200014.

[67] D.G. Carvalho, L. Ranzan, L.F. Trierweiler, J.O. Trierweiler, Determination of the concentration of total phenolic compounds in aged cachaça using two-dimensional fluorescence and mid-infrared spectroscopy, Food Chem. 329 (2020) 127142. https://doi.org/10.1016/j.foodchem.2020.127142.

[68] A. Romani, F. Ieri, S. Urciuoli, A. Noce, G. Marrone, C. Nediani, R. Bernini, Health effects of phenolic compounds found in extra-virgin olive oil, by-products, and leaf of

olea europaea L., Nutrients. 11 (2019). https://doi.org/10.3390/nu11081776.

[69] M. Araújo, F.B. Pimentel, R.C. Alves, M.B.P.P. Oliveira, Phenolic compounds from olive mill wastes: Health effects, analytical approach and application as food antioxidants, Trends Food Sci. Technol. 45 (2015) 200–211. https://doi.org/10.1016/j.tifs.2015.06.010.

[70] S. Bulotta, M. Celano, S.M. Lepore, T. Montalcini, A. Pujia, D. Russo, Beneficial effects of the olive oil phenolic components oleuropein and hydroxytyrosol: Focus on protection against cardiovascular and metabolic diseases, J. Transl. Med. 12 (2014) 1–9. https://doi.org/10.1186/s12967-014-0219-9.

[71] Z. Kaleh, S.U. Geißen, Selective isolation of valuable biophenols from olive mill wastewater, J. Environ. Chem. Eng. 4 (2016) 373–384. https://doi.org/10.1016/j.jece.2015.11.010.

[72] International Olive Oil Council, World Olive Encyclopaedia, 1996. 17-467, ISBN: 84-01-61881-9

[73] Consejo de la Unión Europea, Directiva 96/61/CE del Consejo, relativa a la prevención y al control integrados de la contaminación, (1996), 26-40.

[74] Presidencia del Gobierno, Orden por la que se dictan normas complementarias para la aplicación del Real Decreto 3499/1981BOE-A-1982-14154, (1981) 16046–16047.

[75] Ministerio de Obras Públicas y Urbanismo, Por el que se aprueba el Reglamento del Dominio Público Hidráulico, que desarrolla los títulos preliminar I, IV, V, VI y VII de la Ley 29/1985 de Aguas, BOE-A-1986-10638, (1986).

[76] E. Lagoudianaki, T. Manios, M. Geniatakis, N. Frantzeskaki, V. Manios, Odor control in evaporation ponds treating olive mill wastewater through the use of Ca(OH)2, J. Environ. Sci. Heal. - Part A Toxic/Hazardous Subst. Environ. Eng. 38 (2003) 2537–2547. https://doi.org/10.1081/ESE-120024445.

[77] B. de los Santos, P. García-Serrano, C. Romero, A. Aguado, P. García-García, D. Hornero-Méndez, M. Brenes, Effect of fertilisation with black table olive wastewater solutions on production and quality of tomatoes cultivated under open field conditions, Sci. Total Environ. 790 (2021) 148053. https://doi.org/10.1016/j.scitotenv.2021.148053.

[78] A. El-Abbassi, N. Saadaoui, H. Kiai, J. Raiti, A. Hafidi, Potential applications of olive mill wastewater as biopesticide for crops protection, Sci. Total Environ. 576 (2017) 10–21. https://doi.org/10.1016/J.SCITOTENV.2016.10.032.

[79] P. Paraskeva, E. Diamadopoulos, Technologies for olive mill wastewater (OMW) treatment: A review, J. Chem. Technol. Biotechnol. 81 (2006) 1475–1485. https://doi.org/10.1002/jctb.1553.

[80] B. Kiril Mert, T. Yonar, M. Yalili Kiliç, K. Kestioğlu, Pre-treatment studies on olive oil mill effluent using physicochemical, Fenton and Fenton-like oxidations processes, J.

Hazard. Mater. 174 (2010) 122–128. https://doi.org/10.1016/j.jhazmat.2009.09.025.

[81] R. Andreozzi, M. Canterino, I. Di Somma, R. Lo Giudice, R. Marotta, G. Pinto, A. Pollio, Effect of combined physico-chemical processes on the phytotoxicity of olive mill wastewaters, Water Res. 42 (2008) 1684–1692. https://doi.org/10.1016/j.watres.2007.10.018.

[82] G. Farabegoli, A. Chiavola, E. Rolle, SBR treatment of olive mill wastewaters: Dilution or pre-treatment?, Water Sci. Technol. 65 (2012) 1684–1691. https://doi.org/10.2166/wst.2012.068.

[83] I. Chaari, A. Touil, M. Medhioub, Adsorption-desorption of phenolic compounds from olive mills wastewater using Tunisian natural clay, Chinese J. Chem. Eng. 40 (2021) 287–292. https://doi.org/10.1016/j.cjche.2020.12.020.

[84] D. Frascari, G. Rubertelli, F. Arous, A. Ragini, L. Bresciani, A. Arzu, D. Pinelli, Valorisation of olive mill wastewater by phenolic compounds adsorption: Development and application of a procedure for adsorbent selection, Chem. Eng. J. 360 (2019) 124–138. https://doi.org/10.1016/j.cej.2018.11.188.

[85] M.O.J. Azzam, S.A. Hazaimeh, Olive mill wastewater treatment and valorization by extraction/concentration of hydroxytyrosol and other natural phenols, Process Saf. Environ. Prot. 148 (2021) 495–523. https://doi.org/10.1016/j.psep.2020.10.030.

[86] J.M. Ochando-Pulido, J.R. Corpas-Martínez, A. Martinez-Ferez, About two-phase olive oil washing wastewater simultaneous phenols recovery and treatment by nanofiltration, Process Saf. Environ. Prot. 114 (2018) 159–168. https://doi.org/10.1016/j.psep.2017.12.005.

[87] J.M. Ochando-Pulido, V. Verardo, A. Segura-Carretero, A. Martinez-Ferez, Technical optimization of an integrated UF/NF pilot plant for conjoint batch treatment of two-phase olives and olive oil washing wastewaters, Desalination. 364 (2015) 82–89. https://doi.org/10.1016/j.desal.2014.10.040.

[88] K.A. Segovia-Bravo, P. Garcia-Garcia, F.N. Arroyo-López, A. López-López, A. Garrido-Fernández, Ozonation process for the regeneration and recycling of Spanish green table olive fermentation brines, Eur. Food Res. Technol. 227 (2008) 463–472. https://doi.org/10.1007/S00217-007-0742-5.

[89] D.P. Zagklis, A.I. Vavouraki, M.E. Kornaros, C.A. Paraskeva, Purification of olive mill wastewater phenols through membrane filtration and resin adsorption/desorption, J. Hazard. Mater. 285 (2015) 69–76. https://doi.org/10.1016/j.jhazmat.2014.11.038.

[90] A. Figoli, A. Criscuoli, Sustainable Membrane Technology for Water and Wastewater Treatment, 2017. https://doi.org/10.1007/978-981-10-5623-9.

[91] L. Palacio, P. Prádanos, A. Hernández, Procesos de separación: membranas en el día a día, Rev. Ciencias. (2014) 5–10. https://dialnet.unirioja.es/descarga/articulo/4674758.pdf.

[92] J. Contreras Martínez, Development of dual-layer membranes and recycling of reverse osmosis membrane modules for water treatment, tesis doctoral, (2021).

[93] E.O. Ezugbe, S. Rathilal, Membrane technologies in wastewater treatment: A review, Membranes (Basel). 10 (2020). https://doi.org/10.3390/membranes10050089.

[94] B. Van Der Bruggen, C. Vandecasteele, T. Van Gestel, W. Doyenb, R. Leysenb, Review of Pressure-Driven Membrane Processes, Environ. Prog. 22 (2003) 46–56.

[95] C. Conidi, E. Drioli, A. Cassano, Membrane-based agro-food production processes for polyphenol separation, purification and concentration, Curr. Opin. Food Sci. (2018) 149–164. https://doi.org/10.1016/j.cofs.2017.10.009.

[96] T. Peters, Membrane technology for water treatment, Chem. Eng. Technol. 33 (2010) 1233–1240. https://doi.org/10.1002/ceat.201000139.

[97] A. Cassano, C. Conidi, R. Ruby-Figueroa, R. Castro-Muñoz, Nanofiltration and tight ultrafiltration membranes for the recovery of polyphenols from agro-food by-products, Int. J. Mol. Sci. 19 (2018) 351. https://doi.org/10.3390/ijms19020351.

[98] J.C. Ortega-Bravo, G. Ruiz-Filippi, A. Donoso-Bravo, I.E. Reyes-Caniupán, D. Jeison, Forward osmosis: Evaluation thin-film-composite membrane for municipal sewage concentration, Chem. Eng. J. 306 (2016) 531–537. https://doi.org/10.1016/j.cej.2016.07.085.

[99] A.J. Ansari, F.I. Hai, W.E. Price, J.E. Drewes, L.D. Nghiem, Forward osmosis as a platform for resource recovery from municipal wastewater - A critical assessment of the literature, J. Memb. Sci. 529 (2017) 195–206. https://doi.org/10.1016/j.memsci.2017.01.054.

[100] C. Charcosset, 1. Principles on membrane and membrane processes, 2012. https://doi.org/10.1016/b978-0-444-56334-7.00001-0.

[101] M. osé Corbatón-Báguena, S. Álvarez-Blanco, M.C. Vincent-Vela, Fouling mechanisms of ultrafiltration membranes fouled with whey model solutions, Desalination. 360 (2015) 87–96. https://doi.org/10.1016/j.desal.2015.01.019.

[102] W. Guo, H.H. Ngo, J. Li, A mini-review on membrane fouling, Bioresour. Technol. 122 (2012) 27–34. https://doi.org/10.1016/j.biortech.2012.04.089.

[103] P. Bacchin, P. Aimar, R.W. Field, Critical and sustainable fluxes: Theory, experiments and applications, J. Memb. Sci. 281 (2006) 42–69. https://doi.org/10.1016/j.memsci.2006.04.014.

[104] J. Hermia, Constant pressure blocking filtration laws – application to power-law non-newtonian fluids., Inst. Chem. Enginners. 60 (1982) 183–187.

[105] C.C. Ho, A.L. Zydney, A combined pore blockage and cake filtration model for protein fouling during microfiltration, J. Colloid Interface Sci. 232 (2000) 389–399. https://doi.org/10.1006/jcis.2000.7231.

[106] E.J. de la Casa, A. Guadix, R. Ibáñez, F. Camacho, E.M. Guadix, A combined fouling model to describe the influence of the electrostatic environment on the cross-flow microfiltration of BSA, J. Memb. Sci. 318 (2008) 247–254. https://doi.org/10.1016/j.memsci.2008.02.047.

[107] M. Taniguchi, james E. Kilduff, G. Belfort, Modes of natural organic matter fouling durign ultrafiltration, Environ. Sci. Technol. 37 (2003) 1676–1683. http://busick-portfolio.wikispaces.com/file/view/ADHD+and+academic+performance.pdf.

[108] J. Huang, X. Wu, H. Zha, B. Yuan, S. Deng, A hypercrosslinked poly(styrene-co-divinylbenzene) PS resin as a specific polymeric adsorbent for adsorption of 2-naphthol from aqueous solutions, Chem. Eng. J. 218 (2013) 267–275. https://doi.org/10.1016/j.cej.2012.12.032.

[109] M.C. Martí-Calatayud, M.C. Vincent-Vela, S. Álvarez-Blanco, J. Lora-García, E. Bergantiños-Rodríguez, Analysis and optimization of the influence of operating conditions in the ultrafiltration of macromolecules using a response surface methodological approach, Chem. Eng. J. 156 (2010) 337–346. https://doi.org/10.1016/j.cej.2009.10.031.

[110] J. Dasgupta, J. Sikder, D. Mandal, Modeling and optimization of polymer enhanced ultrafiltration using hybrid neural-genetic algorithm based evolutionary approach, Appl. Soft Comput. J. 55 (2017) 108–126. https://doi.org/10.1016/j.asoc.2017.02.002.

[111] P. Barkakati, A. Begum, M.L. Das, P.G. Rao, Adsorptive separation of Ginsenoside from aqueous solution by polymeric resins: Equilibrium, kinetic and thermodynamic studies, Chem. Eng. J. 161 (2010) 34–45. https://doi.org/10.1016/j.cej.2010.04.018.

[112] S.D. Faust, O.M. Aly, Elements of Surface Chemistry, in: Adsorpt. Process. Water Treat., 1987: pp. 1–23. https://doi.org/10.1016/b978-0-409-90000-2.50004-2.

[113] W. John Thomas, Barry Crittenden, 2 - Adsorbents, Adsorption Technology & Design, Butterworth-Heinemann, (1998), 8-30, ISBN 9780750619592, https://doi.org/10.1016/B978-075061959-2/50003-3.

[114] F. Elayadi, W. Boumya, M. Achak, Y. Chhiti, F.E.M. Alaoui, N. Barka, C. El Adlouni, Experimental and modeling studies of the removal of phenolic compounds from olive mill wastewater by adsorption on sugarcane bagasse, Environ. Challenges. 4 (2021) 100184. https://doi.org/10.1016/j.envc.2021.100184.

[115] P. Pérez-Larrán, B. Díaz-Reinoso, A. Moure, J.L. Alonso, H. Domínguez, Adsorption technologies to recover and concentrate food polyphenols, Curr. Opin. Food Sci. 23 (2018) 165–172. https://doi.org/10.1016/j.cofs.2017.10.005.

[116] J.J. Park, W.Y. Lee, Adsorption and desorption characteristics of a phenolic compound from Ecklonia cava on macroporous resin, Food Chem. 338 (2021) 128150. https://doi.org/10.1016/j.foodchem.2020.128150.

[117] N. Solomakou, A.M. Goula, Treatment of olive mill wastewater by adsorption of phenolic compounds, Rev. Environ. Sci. Biotechnol. 20 (2021) 839–863.

https://doi.org/10.1007/s11157-021-09585-x.

[118] A.I. Vavouraki, M.A. Dareioti, M. Kornaros, Olive Mill Wastewater (OMW) Polyphenols Adsorption onto Polymeric Resins: Part I—Batch Anaerobic Digestion of OMW, Waste and Biomass Valorization. 12 (2021) 2271–2281. https://doi.org/10.1007/s12649-020-01168-1.

[119] L. Papaoikonomou, K. Labanaris, K. Kaderides, A.M. Goula, Adsorption–desorption of phenolic compounds from olive mill wastewater using a novel low-cost biosorbent, Environ. Sci. Pollut. Res. 28 (2021) 24230–24244. https://doi.org/10.1007/s11356-019-07277-2.

[120] M.O.J. Azzam, Olive mills wastewater treatment using mixed adsorbents of volcanic tuff, natural clay and charcoal, J. Environ. Chem. Eng. 6 (2018) 2126–2136. https://doi.org/10.1016/j.jece.2018.03.009.

[121] A.A. Aly, K.N.S. Alashgar, A.S. Al-Farraj, H.M. Ibrahim, Contaminants and salinity removal of olive mill wastewater using zeolite nanoparticles, Sep. Sci. Technol. 53 (2018) 1638–1653. https://doi.org/10.1080/01496395.2018.1425301.

[122] L. Bertin, F. Ferri, A. Scoma, L. Marchetti, F. Fava, Recovery of high added value natural polyphenols from actual olive mill wastewater through solid phase extraction, Chem. Eng. J. 171 (2011) 1287–1293. https://doi.org/10.1016/j.cej.2011.05.056.

[123] J.R. Njimou, M. Stoller, A. Cicci, A. Chianese, C.P. Nanseu-Njiki, E. Ngameni, M. Bravi, Adsorption of phenol/tyrosol from aqueous solutions on macro-reticular aromatic and macro-porous polystyrene cross-linked with divinylbenzene polymeric resins, Chem. Eng. Trans. 57 (2017) 757–762. https://doi.org/10.3303/CET1757127.

[124] D. Pinelli, A. Esther, M. Bacca, A. Kaushik, S. Basu, M. Nocentini, L. Bertin, D. Frascari, Batch and Continuous Flow Adsorption of Phenolic Compounds from Olive Mill Wastewater : A Comparison between Nonionic and Ion Exchange Resins, Int. J. Chem. Eng. 2016 (2016) 1–13. https://doi.org/10.1155/2016/9349627.

[125] J. Kammerer, D.R. Kammerer, R. Carle, Impact of saccharides and amino acids on the interaction of apple polyphenols with ion exchange and adsorbent resins, J. Food Eng. 98 (2010) 230–239. https://doi.org/10.1016/j.jfoodeng.2010.01.001.

[126] A. Yangui, J.R. Njimou, A. Cicci, M. Bravi, M. Abderrabba, A. Chianese, Competitive adsorption, selectivity and separation of valuable hydroxytyrosol and toxic phenol from olive mill wastewater, J. Environ. Chem. Eng. 5 (2017) 3581–3589. https://doi.org/10.1016/j.jece.2017.06.037.

[127] M.L. Soto, A. Moure, H. Domínguez, J.C. Parajó, Recovery, concentration and purification of phenolic compounds by adsorption: A review, J. Food Eng. 105 (2011) 1–27. https://doi.org/10.1016/j.jfoodeng.2011.02.010.

[128] N. Ayawei, A.N. Ebelegi, D. Wankasi, Modelling and Interpretation of Adsorption Isotherms, J. Chem. (2017) 3039817. https://doi.org/10.1155/2017/3039817.

[129] D.R. Kammerer, Z.S. Saleh, R. Carle, R.A. Stanley, Adsorptive recovery of phenolic compounds from apple juice, Eur. Food Res. Technol. 224 (2007) 605–613. https://doi.org/10.1007/s00217-006-0346-5.

[130] S. Lagergren, Lagergren, S., About the Theory of so Called Adsorption of Soluble Substances, Kungliga Svenska Vetenskapsakademiens Handlingar, 24, 1-39, 1898., K. Sven. Vetenskapsakademiens Handl. (1898) 1–39. http://www.sciepub.com/reference/163936.

[131] Y.S. Ho, G. McKay, Pseudo-second order model for sorption processes, Process Biochem. 34 (1999) 451–465. https://doi.org/10.1016/S0032-9592(98)00112-5.

[132] M. Ahmaruzzaman, Adsorption of phenolic compounds on low-cost adsorbents: A review, Adv. Colloid Interface Sci. 143 (2008) 48–67. https://doi.org/10.1016/j.cis.2008.07.002.

[133] M. Savarese, E. De Marco, S. Falco, I. D'Antuoni, R. Sacchi, Biophenol extracts from olive oil mill wastewaters by membrane separation and adsorption resin, Int. J. Food Sci. Technol. 51 (2016) 2386–2395. https://doi.org/10.1111/ijfs.13219.

[134] L.G.C. Villegas, N. Mashhadi, M. Chen, D. Mukherjee, K.E. Taylor, N. Biswas, A Short Review of Techniques for Phenol Removal from Wastewater, Curr. Pollut. Reports. 2 (2016) 157–167. https://doi.org/10.1007/s40726-016-0035-3.

[135] C.I.L. Justino, R. Pereira, A.C. Freitas, T.A.P. Rocha-Santos, T.S.L. Panteleitchouk, A.C. Duarte, Olive oil mill wastewaters before and after treatment: A critical review from the ecotoxicological point of view, Ecotoxicology. 21 (2012) 615–629. https://doi.org/10.1007/s10646-011-0806-y.

[136] A. Speltini, M. Sturini, F. Maraschi, D. Dondi, G. Fisogni, E. Annovazzi, A. Profumo, A. Buttafava, Evaluation of UV-A and solar light photocatalytic hydrogen gas evolution from olive mill wastewater, Int. J. Hydrogen Energy. 40 (2015) 4303–4310. https://doi.org/10.1016/j.ijhydene.2015.01.182.

[137] Z.S. Lee, S.Y. Chin, J.W. Lim, T. Witoon, C.K. Cheng, Treatment technologies of palm oil mill effluent (POME)and olive mill wastewater (OMW): A brief review, Environ. Technol. Innov. 15 (2019) 100377. https://doi.org/10.1016/j.eti.2019.100377.

[138] H. El Hajjouji, L. El Fels, E. Pinelli, F. Barje, A. El Asli, G. Merlina, M. Hafidi, Evaluation of an aerobic treatment for olive mill wastewater detoxification, Environ. Technol. (United Kingdom). 35 (2014) 3052–3059. https://doi.org/10.1080/09593330.2014.930514.

[139] A. Rozzi, F. Malpei, Treatment and Disposal of Olive Mill Effluents, Int. Biodeterior. Biodegrad. 38 (1996) 135–144. https://doi.org/10.1016/s0964-8305(96)00042-x.

[140] S.K. Rifi, L.E. Fels, A. Driouich, M. Hafidi, Z. Ettaloui, S. Souabi, Sequencing batch reactor efficiency to reduce pollutant in olive oil mill wastewater mixed with urban wastewater, Int. J. Environ. Sci. Technol. (2022). https://doi.org/10.1007/s13762-021-03866-2.

[141] S. Vuppala, I. Bavasso, M. Stoller, L. Di Palma, G. Vilardi, Olive mill wastewater integrated purification through pre-treatments using coagulants and biological methods: Experimental, modelling and scale-up, J. Clean. Prod. 236 (2019) 117622. https://doi.org/10.1016/j.jclepro.2019.117622.

[142] A.S. Ciggin, A. Iravanian, S. Doğruel, D. Orhon, Co-metabolism of olive mill wastewater in sequencing batch reactor under aerobic conditions after Fenton-based oxidation, J. Water Process Eng. 43 (2021). https://doi.org/10.1016/J.JWPE.2021.102277.

[143] A. Chiavola, G. Farabegoli, E. Rolle, Combined biological and chemical-physical process for olive mill wastewater treatment, Desalin. Water Treat. 23 (2010) 135–140. https://doi.org/10.5004/dwt.2010.1987.

[144] J.M. Ochando-Pulido, G. Hodaifa, M.D. Victor-Ortega, S. Rodriguez-Vives, A. Martinez-Ferez, Reuse of olive mill effluents from two-phase extraction process by integrated advanced oxidation and reverse osmosis treatment, J. Hazard. Mater. 263P (2013) 158–167. https://doi.org/10.1016/j.jhazmat.2013.07.015.

CAPÍTULO IV

METODOLOGÍA

IV.1. PROCESOS PROPUESTOS

A partir de la exhaustiva revisión bibliográfica que respecta tanto a la recuperación de compuestos fenólicos presentes en aguas residuales de almazara, como a la recuperación de los cursos de agua, se ha decidido proponer dos procesos alternativos para alcanzar los objetivos de la Tesis Doctoral. Como se puede observar en la figura 4.1, ambos procesos contemplan un pretratamiento, seguido de procesos de membrana y adsorción/desorción con resinas, finalizando con un tratamiento biológico del agua residual resultante.

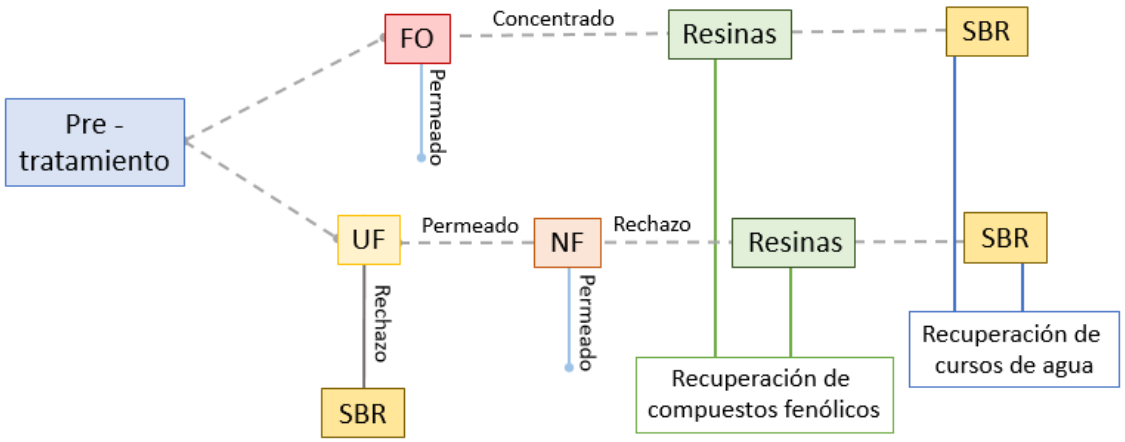

Figura 4.1 Esquema propuesto para la recuperación de compuestos fenólicos y cursos de agua a partir de agua de lavado de aceite de oliva (OOWW) proveniente de almazara operada con proceso de centrifugación continua de dos fases. UF: Ultrafiltración; FO: Osmosis directa NF: Nanofiltración; SBR: Reactor biológico secuencial

Las líneas propuestas se diferencian principalmente en los procesos de membrana utilizados. La primera alternativa contempla solo la osmosis directa (FO), mientras que la otra considera dos procesos de membranas, ultrafiltración (UF), seguida de una nanofiltración (NF).

Las diferentes líneas propuestas fueron seleccionadas para evaluar diferentes objetivos. Por un lado, se decidió evaluar la ultrafiltración como segunda etapa de pretratamiento para

eliminar materia orgánica de mayor tamaño. Por otra parte, la nanofiltración y la osmosis directa se evaluaron como posibles procesos para la concentración de compuestos fenólicos. La adsorción con resinas se evaluó para la recuperación de estos compuestos fenólicos a partir de las corrientes concentradas. Y, finalmente, el tratamiento biológico se estudió para eliminar la materia orgánica restante, ya sea para reutilizar las corrientes como riego o como aguas de limpieza de maquinaria del mismo proceso productivo de aceite de oliva.

A continuación, se procede a explicar en detalle cada proceso considerado, desde las muestras de agua residual utilizadas hasta los equipos empleados y las condiciones de operación ensayadas.

IV.2. MUESTRAS DE AGUAS RESIDUALES UTILIZADAS

Las muestras fueron proporcionadas por una almazara de aceite de oliva ubicada en la Comunidad Valenciana (España), donde se utiliza el proceso de centrifugación continua de dos fases. Las muestras correspondieron a las aguas residuales del lavado de aceite de oliva, obtenidas a la salida de la centrífuga vertical. Las muestras fueron recogidas en bidones de 25 litros entre octubre y noviembre (campaña de aceite de aceite de oliva) entre los años 2018-2020. Una vez llegadas a la universidad, estas se almacenaron inmediatamente a -20 °C para evitar la degradación.

Figura 4.2. Muestras de agua residual de lavado de aceite de oliva empleadas en esta Tesis Doctoral

Como se puede observar en la figura 4.2, el OOWW se caracteriza por tener un color marrón oscuro, una ligera capa oleosa, aparte de su elevado contenido en materia orgánica. Como se comentó anteriormente, las características del agua residual de almazara dependen de todos los factores que afecten a las propiedades de la aceituna, como también del proceso productivo. Es por ello que las muestras utilizadas durante la tesis doctoral presentaron algunas variaciones en cuanto a concentración de materia orgánica y compuestos fenólicos. Se decidió no descartar ninguna muestra, ya que la idea es encontrar un proceso que se acople a la variabilidad de las características de las aguas residuales de lavado de aceite de oliva.

Durante la pasantía realizada en la Universidade Nova de Lisboa (UNV), se utilizó OMW diferente. La muestra fue proporcionada por Zeyton Nutraceuticals, (Portugal) y provenía de un proceso de centrifugación continua de tres fases. Esta muestra solo se utilizó en estudios ligados a la NF.

IV.3. PRETRATAMIENTO

La primera etapa del proceso propuesto contempló un pretratamiento con el objetivo principal de eliminar las partículas de gran tamaño, así como también la capa oleosa formada por grasas y aceites presentes en la muestra (ver figura 4.2). Por otra parte, este pretratamiento permite tanto cuidar de las membranas como de las plantas de membranas a utilizar. El pretratamiento contempló tres etapas: una etapa de flotación, seguida de una sedimentación y, finalmente, una filtración.

El proceso de flotación se realizó en recipientes de 8 litros (figura 4.3A), dejando las muestras entre 2 y 3 horas sin agitación alguna. La duración se determinó a partir de pruebas anteriores realizadas en el laboratorio (datos no incluidos en esta tesis). Transcurrido el tiempo, se observa cómo la muestra se separa en dos fases (figura 4.3B). El sobrenadante, que contenía principalmente aceites y grasas, se retiró con una pipeta graduada. Posteriormente, se realizó un proceso de sedimentación en las mismas vasijas para eliminar los sólidos en suspensión.

Para ello, se dejó la muestra en el recipiente hasta cumplir las 24 horas. Nuevamente se observan dos fases, pero esta vez fue el sedimentado la fase a retirar. Los sólidos sedimentados se eliminaron a través de una pequeña válvula ubicada en el fondo del recipiente (figura 4.3C). Finalmente, en la tercera etapa (figura 4.3D) se realizó una filtración por gravedad. La muestra se filtró a través de un cartucho de poliéster de 60 μm de tamaño de poro (CA-0202-00, modelo GT, HidroWater, España). La unidad de filtración está formada por un vaso transparente de estireno acrilonitrilo y una tuerca de polipropileno (BWF, Alemania).

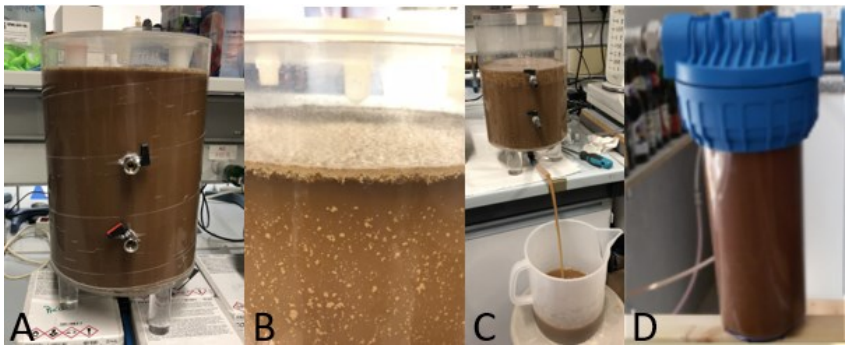

Figura 4.3. Pretratamiento de la muestra de agua de lavado de aceite de oliva. A: recipiente para flotación y sedimentación; B: eliminación de sobrenadante (flotación); C: eliminación de sedimentado; D: filtración por cartucho

Terminado el pretratamiento, al igual que en el caso de la muestra cruda, la muestra pretratada se almacenó a −20 ◦C, para evitar su degradación. Es importante destacar que el pretratamiento no contempló fuerza externa, tan solo la diferencia de densidades como de alturas. Por otro lado, también es importante resaltar que mientras se realizó el pretratamiento la temperatura del laboratorio se mantuvo lo más controlada posible por debajo de los 18 ◦C para no afectar a la muestra. Esto fue posible ya que se realizó durante el invierno, controlando, además, la temperatura del laboratorio mediante aire acondicionado.

La muestra de OMW utilizada en UNL fue tratada siguiendo el mismo protocolo que se aplicó para la OOWW, con la diferencia de los filtros utilizados (Hytrex II, OSMONIC,

EE.UU). Luego del pretratamiento, el OMW se diluyó para obtener una composición similar a la presentada por OOWW.

Antes y después del tratamiento, es decir las muestras de OOWW y OMW crudas y pretratadas fueron caracterizadas en términos de pH, conductividad, color, turbidez, solidos suspendidos totales, concentración de azúcares, grasas y aceites, DOQ y concentración de compuestos fenólicos.

IV.4. ULTRAFILTRACIÓN

IV.4.1. Planta y membranas de Ultrafiltración

Como se comentó anteriormente, la etapa de ultrafiltración actúa como un segundo pretratamiento, para la completa eliminación de las partículas en suspensión contenidas en la muestra. El objetivo es conseguir la mayor eliminación de materia orgánica (medida mediante el parámetro DQO), sin afectar la concentración de compuestos fenólicos en la muestra. En la figura 4.4 se muestra el esquema de la planta de ultrafiltración utilizada en los ensayos.

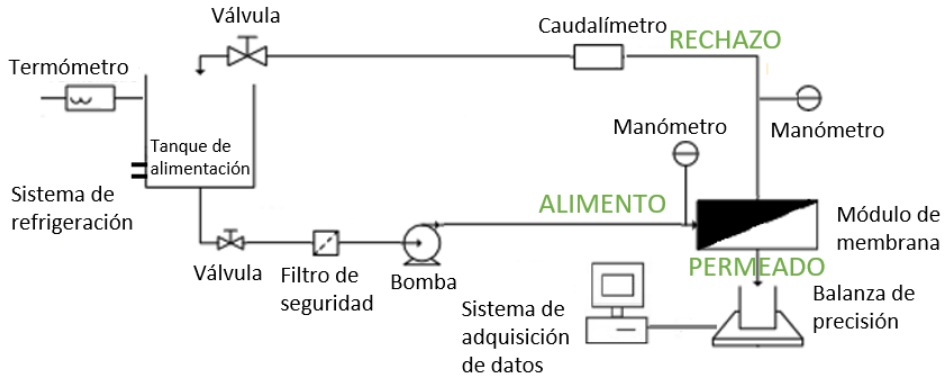

Figura 4.4. Diagrama de la planta de ultrafiltración

La planta es de escala de laboratorio, correspondiendo al modelo VF-S11 UF de Orelis (Francia). Tiene un depósito que permite trabajar con hasta 10 litros de muestra (A, figura 4.5). Este depósito tiene doble carcasa, permitiendo controlar la temperatura mediante circulación de agua muestra través del encamisado. La temperatura fue registrada con un termómetro digital (H en la figura 4.5). La CFV y la TMP se controlaron mediante la regulación de la frecuencia de la bomba (B, en figura 4.5) y mediante una válvula situada en la corriente de rechazo (C, en figura 4.5). La CFV se midió mediante el caudal de rechazo registrado en un rotámetro (D, en la figura 4.5) y la presión a la entrada y salida del módulo se midieron por medio de manómetros (E y F en la figura 4.5). El permeado obtenido se recoge en un vaso, el cual está situado sobre una balanza (G, en la figura 4.5) con precisión de 0,001 g (Kern, Alemania), permitiendo el registro de su masa (I, en la figura 4.5) para luego ser transformado en volumen y finalmente en densidad de flujo de permeado.

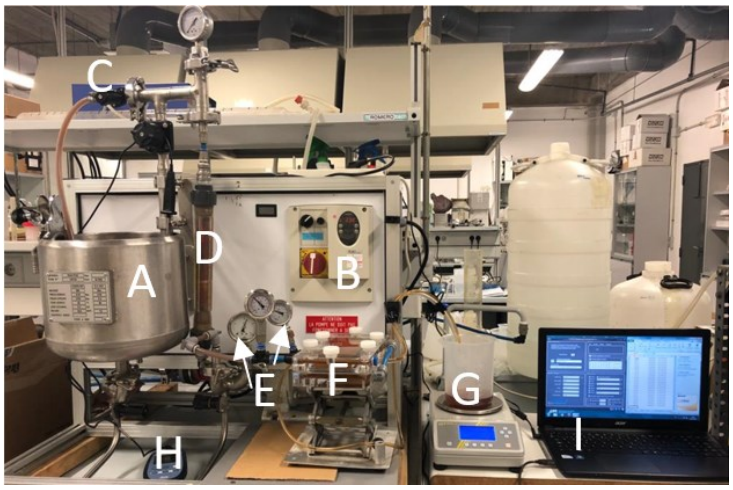

Figura 4.5. Fotografía de la planta de ultrafiltración (UPV, Valencia, España)
A: tanque de alimentación; B: panel regulación frecuencia bomba; C: válvula corriente rechazo; D: caudalímetro; E: manómetros; F: módulo de membrana; G: recolección de permeado con registro balanza; H: termómetro; I: computadora para registro de datos

La planta de UF está configurada para trabajar en un rango de presiones de entre 1 y 3,5 bar, ya sea con un módulo plano (A, figura 4.6) o tubular (B, figura 4.6), dependiendo la membrana utilizada. El módulo plano es el modelo Rayflow (Orelis, Francia), permitiendo trabajar con uno o dos recortes de membrana, cada uno con una superficie activa total de 0,0125 m^2. En este caso se decidió trabajar con dos recortes de membrana, por lo que el área total fue de 0.025 m^2. El módulo tubular es de la casa comercial Tami Idustries (Francia) de 20 cm de largo.

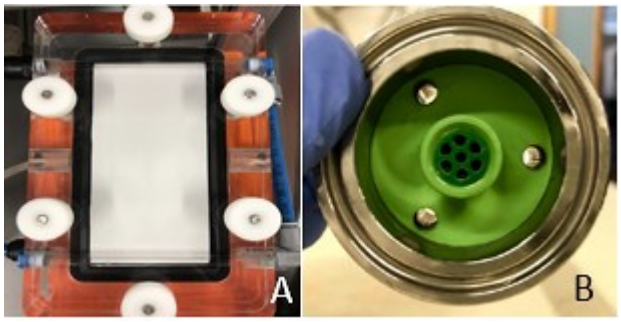

Figura 4.6. Módulos de membrana de ultrafiltración utilizados (UPV, Valencia, España)
A: módulo de membrana plana; B: módulo de membrana tubular

Siete fueron las membranas de UF estudiadas, de diferente material, configuración y umbral de corte molecular. Sus especificaciones se encuentran en la tabla 4.1. Cuatro de ellas son de material orgánico y configuración plana, mientras que las otras 3 son de cerámica con configuración tubular. Las tres membranas cerámicas poseían 7 canales circulares y una superficie activa total de 0,0132 m^2.

Tabla 4.1. Especificaciones de las membranas de ultrafiltración ensayadas en este trabajo

Membrana	UH004	UP005	Inside Céram 5	RC70PP	Inside Céram 15	UH050	Inside Céram 50
Fabricante	Microdyn Nadir	Microdyn Nadir	Tami Industries	Alfa Laval	Tami Industries	Microdyn Nadir	Tami Industries
Material	PESH[b]	PES[c]	TiO_2/TiO_2[d]	ACR[e]	TiO_2/ ZrO_2[f]	PESH[b]	TiO_2/ ZrO_2[f]
Configuración	plana	plana	Tubular	plana	Tubular	plana	Tubular
MWCO[a] (kDa)	4	5	5	10	15	50	50
T max (˚C)	95	95	300	60	300	95	300
pH	0 - 14	0 - 14	0 - 14	0 – 10	0 - 14	0 - 14	0 - 14
Permeabilidad hidráulica* ($L \cdot h^{-1} \cdot m^{-2} \cdot bar^{-1}$)	>27[g] 32,67[h]	>30[g] 44,07[h]	>80[g] 94,99[h]	>40[g] 78,50[h]	>80[g] 100,26[h]	>200[g] 191,75[h]	>210[g] 223,33[h]

[a]MWCO: umbral de corte molecular; [b]PESH: polietersulfona permanentemente hidrófila; [c]PES: polietersulfona; [d]TiO_2/TiO_2: soporte y capa activa de dióxido de titanio; [e]ACR: acetato de celulosa regenerada; [f]TiO_2/ ZrO_2: capa de soporte de dióxido de titanio y capa activa de dióxido de circonio; [g]Datos del fabricante; [h]Determinado experimentalmente en esta tesis; * Agua, a 25℃.

IV.4.2. Ensayo de adsorción con membranas de Ultrafiltración

Para evaluar la interacción entre las membranas y los compuestos fenólicos se decidió realizar pruebas de adsorción. Las pruebas consistieron en sumergir piezas de membrana de 10 cm^2 durante 24 h en 500 mL de una disolución de compuestos fenólicos manteniendo agitación continua, siguiendo el procedimiento descrito por Sotto et al., 2013 [1]. La disolución fue preparada con agua y contenía una concentración de 1 $g \cdot L^{-1}$ de dos compuestos fenólicos de diferente peso molecular: 0,98 $g \cdot L^{-1}$ de tirosol (138,16 $g \cdot mol^{-1}$) y 0.02 $g \cdot L^{-1}$ de catequina (290,26 $g \cdot mol^{-1}$).

IV.4.3. Ensayos de Ultrafiltración

Primero, las membranas planas fueron cortadas al tamaño adecuado para el módulo utilizado e hidratadas en agua osmotizada (conductividad <40 µS/cm) durante 24 horas para eliminar cualquier sustancia conservante. Luego estas fueron compactadas durante 3 h a una TMP de 3 bar. Las condiciones fueron seleccionadas en base a las condiciones máximas de trabajo de la planta. La presión es la máxima soportada por el sistema (por ende, la máxima de trabajo de los ensayos) y el tiempo es el necesario para obtener un flujo de permeado estable. Estos pasos solo se realizaron con las membranas orgánicas, pues las inorgánicas no sufren compactación.

Antes de comenzar los ensayos, las membranas fueron caracterizadas, determinando su permeabilidad hidráulica. Como se comentó en el apartado de introducción, este parámetro es específico para cada membrana y relaciona el flujo de permeado con la TMP. A una CFV fija (2,2 $m \cdot s^{-1}$ para las membranas orgánicas y 2 $m \cdot s^{-1}$ para las membranas inorgánicas) se midió el flujo de permeado a diferentes TMP (0,5; 1; 2; 3 bar). Finalmente, al representar la densidad de flujo de permeado ($L \cdot h^{-1} \cdot m^{-2}$) frente a la TMP (bar), la relación lineal existente entre ambos permite obtener el coeficiente de permeabilidad de la membrana o permeabilidad hidráulica en unidades de ($L \cdot h^{-1} \cdot m^{-2} \cdot bar^{-1}$), correspondiendo a la pendiente de la recta obtenida.

Para evaluar el comportamiento de las membranas frente al agua residual a tratar (OOWW), diferentes condiciones de operación fueron analizadas, las cuales se presentan en la tabla 4.2. Las condiciones de trabajo utilizadas fueron combinación de cinco CFV diferentes entre 1,5 y 3,4 $m \cdot s^{-1}$, cuatro TMP entre 1 y 3 bar y una duración de 3 h de ensayo, manteniendo la temperatura constante a 25 ± 1ºC. Todos los ensayos se realizaron con recirculación completa de las corrientes de permeado y rechazo.

Tabla 4.2 Condiciones de operación ensayadas con las diferentes membranas de UF: combinación de TMP y CFV

Presión transmembranal (TMP) (bar)	Velocidad de flujo tangencial (CFV) ($m \cdot s^{-1}$)					
	1,5	2	2,5	3	3,4	4
1	X	O X	X	O X	X	
1,5	X	O X	X	O X	X	O
2	X	O X	X	O X	X	O
2,5	X	O X	X	O X	X	O
3	X*	O X*	X*	O X*	X*	O

X: ensayada con membrana orgánica; O: ensayada con membrana inorgánica; * solo con la membrana UH050

La evolución de la densidad de flujo de permeado con el tiempo fue un parámetro a evaluar junto con los rechazos a la DQO y compuestos fenólicos. El permeado obtenido fue el alimento utilizado en la siguiente etapa de nanofiltración, mientras que el rechazo se guardó para su futuro tratamiento mediante SBR. En todos los ensayos se recogieron cada 30 min 50 mL de muestra de la corriente de permeado para su posterior análisis. El análisis contempló medida de pH, conductividad, color, turbidez, SST, DQO y concentración de compuestos fenólicos.

IV.4.4. Limpieza de las membranas de Ultrafiltración

Las membranas fueron limpiadas después de cada experimento de ultrafiltración. Se propusieron cuatro protocolos de limpieza basados en estudios previos (datos no mostrados pero extraídos de la referencia [2]). El procedimiento de limpieza uno (C1) consistió en enjuagar las membranas con agua osmotizada a 25 °C durante 40 min. El procedimiento de limpieza dos (C2) se realizó en las mismas condiciones que C1 excepto por la temperatura (35 °C). El procedimiento de limpieza tres (C3) incluyó limpieza química con P3 Ultrasil 115 (1% v/v) (Ecolab, España) a 25 °C. Finalmente, el último procedimiento (C4) fue en las mismas condiciones que el C3, pero aumentando la temperatura a 35°C. Los tres primeros protocolos de limpieza se utilizaron con las membranas orgánicas, empleando una velocidad tangencial de

2,2 $m \cdot s^{-1}$ y una TMP de 0,25 bar durante 30 minutos. Sin embargo, los cuatro protocolos se probaron con las membranas inorgánicas a una velocidad tangencial de 2 $m \cdot s^{-1}$ y una TMP de 0,5 bar durante 40 minutos. La diferencia en las condiciones de limpieza de las membranas se debe principalmente a la optimización basada en ensayos anteriores.

La eficiencia de la limpieza de las membranas se determinó analizando la permeabilidad hidráulica antes y después de cada experimento. Después de cada ensayo, se aclaró la membrana durante 5 minutos con agua de red, para luego comenzar primero con el protocolo de limpieza C1. El siguiente protocolo de limpieza (C2) solo se realizaba si la recuperación de la membrana no era igual o superior al porcentaje mencionado anteriormente. Lo mismo ocurre con el protocolo C2. Por lo tanto, el protocolo de limpieza C3 solo se realizaba si no se recuperaba la permeabilidad después de haber considerado ambos protocolos, C1 y C2, y el C4, si C1, C2 y C3 no lograban los porcentajes de recuperación propuestos. Después de cada limpieza química y antes de la determinación de la permeabilidad, las membranas fueron aclaradas con agua osmotizada (conductividad <40 µS/cm) a la misma CFV y TMP (2 $m \cdot s^{-1}$ y 0,5 bar, respectivamente) de las limpiezas.

IV.5. NANOFILTRACIÓN

IV.5.1. Planta y membranas de Nanofiltración

La etapa de NF tiene como objetivo lograr una corriente concentrada en compuestos fenólicos, por lo que, a diferencia del proceso de UF, la corriente deseada es el rechazo. La finalidad será, entonces, encontrar una membrana que logre el mayor rechazo de compuestos fenólicos. Por otra parte, el permeado obtenido será apto para ser utilizado como agua de limpieza de maquinaria en el proceso productivo de aceite de oliva. En la figura 4.7 se presenta el diagrama de la planta de nanofiltración.

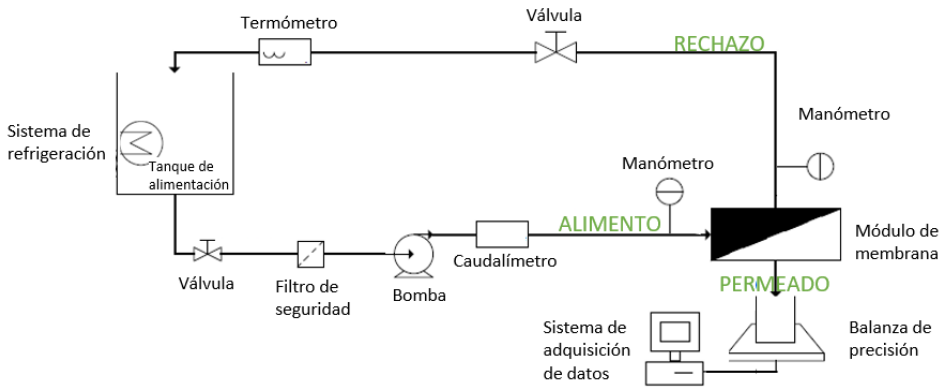

Figura 4.7. Diagrama de la planta de nanofiltración

En la figura 4.8 se presenta una fotografía de la planta, la cual funciona con una bomba de desplazamiento positivo 3CP1231 (Catpumps, EE.UU) y tiene un depósito que permite trabajar con hasta 10 litros de muestra (A, figura 4.8). En este caso, también se utilizó agua para controlar la temperatura, pero esta vez con un serpentín de vidrio, el cual se introdujo dentro del depósito de alimentación. La CFV se controla desde una interfaz (panel de control, B Figura 4.8), donde se presenta el diagrama de la planta y los parámetros de operación, tales como presiones (de entrada, salida y transmembranal), temperatura y caudal de permeado. La planta también tiene un equipo de emergencia que permite parar el sistema en caso de fallo o error. La TMP también se controla mediante una válvula (C, en figura 4.8) situada en la corriente de rechazo, teniendo en cuenta la presión a la entrada y salida del módulo (F, en la figura 4.8), medida por medio de manómetros (E, en la figura 4.8). Nuevamente, el volumen de permeado se determina mediante el registro de la masa de permeado con una balanza (G, en la figura 4.8) con precisión de 0,001 g (Kern, Alemania), de modo que los datos se registran directamente en un ordenador portátil (H, en la figura 4.8).

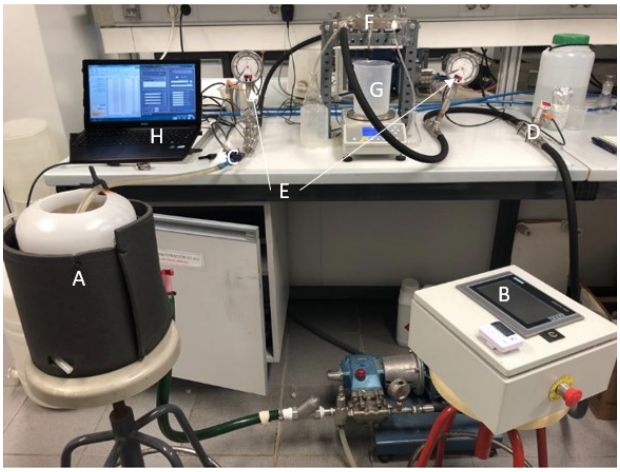

Figura 4.8. Fotografía de la planta de nanofiltración (UPV, Valencia, España) A: tanque de alimentación; B: panel de control proceso; C: válvula corriente rechazo; D: caudalímetro; E: manómetros; F: módulo de membrana; G: recolección de permeado con registro balanza; H: computadora para registro de datos

El módulo de membrana utilizado fue diseñado [3] en el Instituto Universitario de Seguridad Industrial, Radiofísica y Medioambiental (ISIRYM), perteneciente a la Universitat politécnica de València (España). Este módulo (Figura 4.9) permite trabajar con membranas planas de superficie activa de membrana de 0,0072 m^2, soportando presiones superiores a 20 bares.

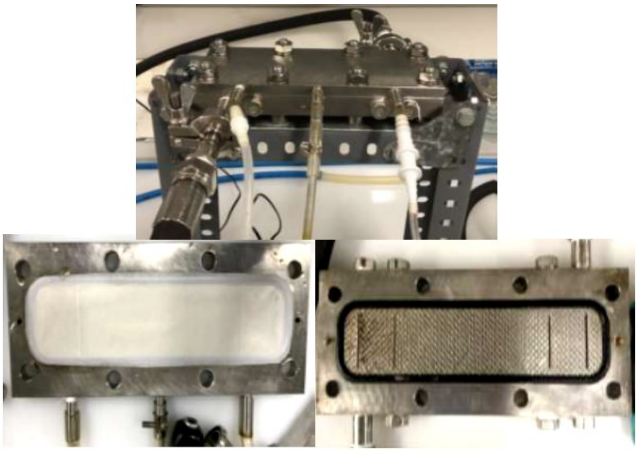

Figura 4.9. Módulo de membrana de nanofiltración utilizado (UPV, Valencia, España)

Durante la estancia realizada en la Universidade Nova de Lisboa (UNL) en Portugal, otra planta de nanofiltración escala laboratorio fue utilizada. Esta planta se presenta en la figura 4.10 y está formada por una bomba de modelo Hydra-cell G13 (Wanner Engineering Inc., EE.UU) y un módulo de membrana (F, en la figura 4.10) plana Sepa CFII (GE, EE.UU), que permite trabajar con un recorte de membrana de superficie activa de 0,014 m^2. El tanque de alimentación (A, en la figura 4.10) permite trabajar con un volumen de hasta 25 litros. Al igual que la otra planta de nanofiltración, se puede trabajar a presiones de hasta 20 bares, las cuales se registran con un manómetro (D, en la figura 4.10). La TMP y la CFV se controlan manualmente con una válvula situada en la corriente de rechazo (C, en la figura 4.10), y mediante la variación de la frecuencia de la bomba (B, en la figura 4.10). El caudal de trabajo fue medido por un caudalímetro modelo SK72, (Georg Fischer, Switzerland). El volumen de permeado fue determinado manualmente con una probeta y un cronómetro. La temperatura fue registrada con un termómetro y se controló mediante compresas de hielo sumergidas en la muestra dentro del recipiente.

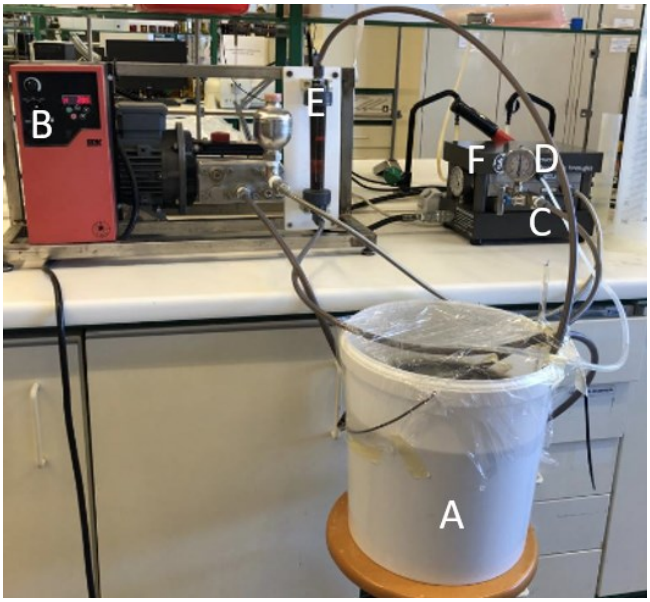

Figura 4.10. Fotografía de la planta de nanofiltración utilizada en la estancia (Universidade Nova de Lisboa, UNL, Lisboa, Portugal) A: tanque de alimentación; B: panel regulación frecuencia bomba; C: válvula corriente rechazo; D: manómetros; E: caudalímetro; F: módulo de membrana

Tabla 4.3 Especificaciones de las membranas de nanofiltración ensayadas en este trabajo

Membrana	Fabricante	Material	MWCO[1] (Da)	T max (°C)	P max (bar)	Rango pH	Permeabilidad* ($L \cdot h^{-1} \cdot m^{-2} \cdot bar^{-1}$)
NF90	Dow Filmtech	TFC[a]PA[b]	90-180	40	41	2–11	3,80
NF245	DuPont	TFC[a]PP[c]	300	50	54,8	3–10	4,87
NF270	Dow Filmtech	TFC[a]PA[b]	150-340	45	41	3–10	12,45
DuraMem900	Evonik	ISA[d] Modified PI[e]	900[f]	50	20	0 -7	6,32

[1] MWCO: sigla inglés de Molecular Weight CutOff (corte molecular de las membranas); [a]TFC: compuesto de película delgada; [b]PA: Poliamida; [c]PP: Polipropileno; [d]ISA: asimétrico de piel integral; [e]PI: poliimida; [f]Umbral de peso molecular medido con oligómeros de estireno disueltos en acetona; * Agua, a 25 °C, determinada experimentalmente en este trabajo

Cuatro fueron las membranas estudiadas y sus especificaciones se muestran en la Tabla 4.3. Las cuatro membranas fueron utilizadas con ambas plantas de nanofiltración.

IV.5.2. Ensayo de adsorción con membranas de Nanofiltración

Al igual que con las membranas de UF, se realizó un ensayo de adsorción para evaluar la posible interacción entre los compuestos fenólicos y las membranas estudiadas. Las cuatro membranas se evaluaron de la misma manera bajo el siguiente protocolo: se sumergió un trozo de membrana (3x3 cm) en diferentes disoluciones durante 24 horas para después analizar la superficie de las membranas por fluorescencia 2D y espectroscopía FTIR, con el fin de averiguar si algunos compuestos fueron adsorbidos por la membrana. Basado en la composición del OOWW real, se seleccionó un compuesto de cada familia (clase química): ácido cítrico correspondiente a los ácidos orgánicos, ácido cafeico correspondiente a los ácidos fenólicos, hidroxitirosol, que representa a los fenoles simples, luteolina a los flavonoides y una mezcla de glucosa, fructosa y sacarosa a los azúcares. Con excepción de los azúcares, la concentración de cada compuesto en las disoluciones de agua destilada fue de 20 ppm (conductividad <70 µS/cm). La disolución de azúcar tenía una concentración de 30 ppm, con 10 ppm de cada compuesto. Como control, se decidió dejar un trozo de membrana en agua destilada.

IV.5.3. Ensayos de Nanofiltración

Al igual que con las membranas de UF, todas las membranas fueron acondicionadas previamente bajo el mismo protocolo. Las membranas se sumergieron para su hidratación durante 24 horas en agua pura (conductividad <40 µS/cm) y luego se compactaron durante 3 horas, a una TMP de 16 bar y una CFV de 1 $m \cdot s^{-1}$.

Terminada la compactación, se procedió a caracterizar las membranas de NF bajo una CFV fija de 1 $m \cdot s^{-1}$ a diferentes TMP de 5, 10 y 15 bar. Cuatro diferentes CFV (0,5-1,5 $m \cdot s^{-1}$) y TMP (5 - 15 bar), respectivamente, fueron utilizadas para evaluar el comportamiento de cada membrana frente a OOWW. La combinación de condiciones de operación consideradas se

presenta en la tabla 4.4. Cada 30 minutos se recogieron 50 mL de muestra de permeado para su posterior análisis de pH, conductividad, color, turbidez, SST, DQO y concentración de compuestos fenólicos y azúcares.

Tabla 4.4 Condiciones de operación ensayadas con las diferentes membranas de NF: combinación de TMP y CFV

Presión transmembranal (TMP) (bar)	Velocidad de flujo tangencial (CFV) ($m \cdot s^{-1}$)		
	0.5	1.0	1.5
5	X	X	X
10	X	X	X
15	X	X	X

X: combinación ensayada con las membrana de NF

El comportamiento de las cuatro membranas presentadas en la tabla 4.3 se estudió con OOWW en la planta de la figura 4.8 bajo todas las condiciones presentadas en la tabla 4.4. Por otra parte, con la planta presentada en la figura 4.10, todas las membranas fueron estudiadas con una disolución modelo (SM), mientras que solo la membrana NF270 fue estudiada con OMW. Las condiciones de operación utilizadas en la planta de la figura 4.10 fueron solamente las óptimas obtenidas en el estudio con la planta de la figura 4.8 y siempre fueron las mismas condiciones, tanto con SM como con OMW. Estas condiciones de operación fueron $1 m \cdot s^{-1}$ de CFV y 10 bar de TMP. Los compuestos utilizados en la SM, así como su concentración se presentan en la tabla 4.5.

La concentración de cada compuesto en la SM fue consistente con la concentración obtenida de la caracterización por cromatografía líquida-espectrometría de masas del OOWW [4]. Se utilizó una nueva solución modelo para cada prueba.

Tabla 4.5. Caracterización de la disolución modelo utilizada como alimentación en los ensayos de nanofiltración

Compuesto	Familia (Clase)	Concentración (ppm)
Ácido cítrico	Acido orgánico	207,10 ± 1,06
Ácido Cafeico	Anido fenólico	4,22 ± 0,05
Hidroxitirosol	Fenol simple	3,43 ± 0,16
Luteolina	Flavonoides	3,33 ± 0,02
Glucosa	Azúcar	700,02 ± 0,02
Fructosa	Azúcar	100,35 ± 0,01
Sacarosa	Azúcar	100,67 ± 0,02

IV.5.4. Limpieza de las membranas de Nanofiltración

El proceso de limpieza propuesto para las membranas NF es similar al propuesto para las membranas UF. En primer lugar, se hizo pasar agua del grifo por el sistema durante 5 minutos. Luego, cuatro protocolos sucesivos fueron analizados, realizándose únicamente los necesarios para recuperar la permeabilidad inicial de la membrana en al menos un 95%. La duración de cada paso fue de 30 minutos y la condición de TMP fue de 1 bar, sin ajustar el CFV (CFV del sistema igual a 0,14 m s^{-1}). Los pasos del protocolo fueron los mismos: C1: agua osmotizada a 25°C, C2: agua osmotizada a 35°C, C3: disolución de Ultrasil al 1% v/v a 25°C y C4: disolución de Ultrasil al 1% v/v a 35°C. °C Las dos últimas disoluciones para limpieza química se prepararon con P3 Ultrasil 115 (Ecolab, Barcelona, España).

IV.6. OSMOSIS DIRECTA

IV.6.1. Planta y membranas de Osmosis directa

La osmosis directa (FO, por sus siglas en ingles de forward osmosis) también fue estudiada como potencial proceso para concentrar compuestos fenólicos. Dos membranas fueron estudiadas, una de configuración plana (área 0,0042 m^2) y otra de fibras huecas (área 0,6 m^2). Debido a la diferencia entre sus áreas de superficie activa, la planta tuvo que ser modificada dependiendo la membrana a emplear, pero la configuración es la misma y se muestra en la Fig. 4.11.

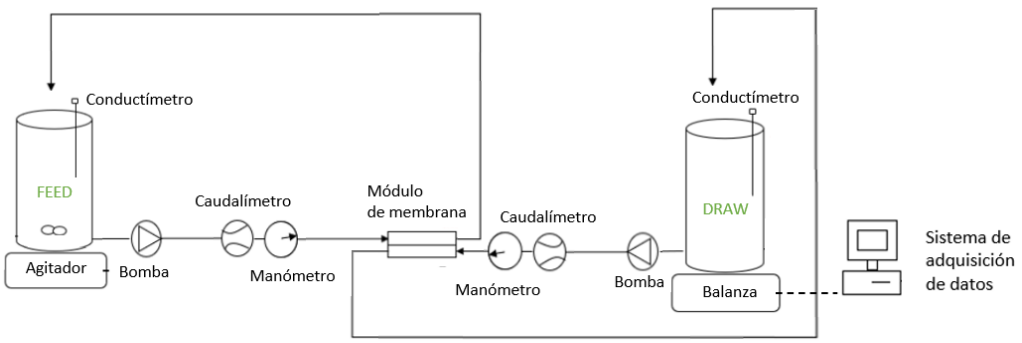

Figura 4.11. Diagrama de la planta de osmosis directa

En la Figura 4.12 se presentan las fotografías del montaje experimental (montaje propio) de ambas plantas.

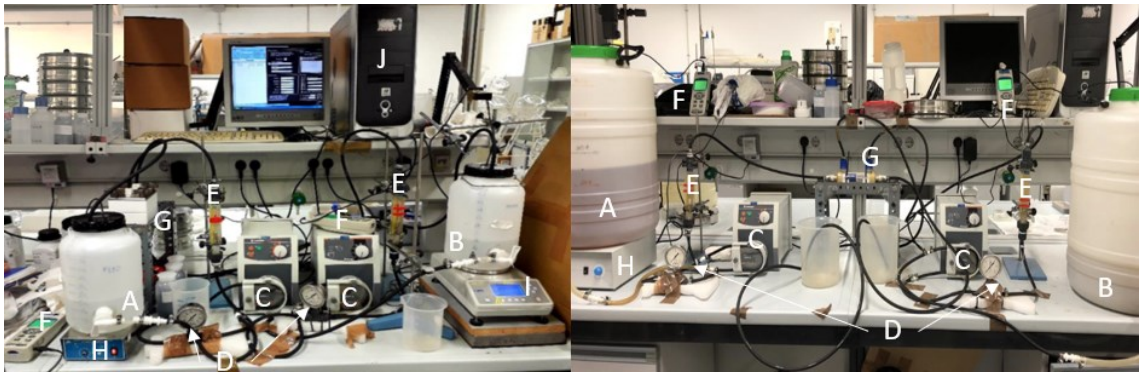

Figura 4.12. Fotografía de la planta de osmosis directa. Izquierda: planta de módulo plano, Derecha: planta de módulo de fibras huecas (UPV, Valencia, España) A: tanque de solución de alimento (FS); B: tanque solución de arrastre (DS); C: bombas; D: manómetros; E: caudalímetros; F; conductímetros; G: módulo de membrana; H: agitador; I: balanza; J: computadora para registrar datos balanza

Se utilizaron tanques de plástico, con un volumen de 5 L para la membrana plana y de 50 L para la membrana de fibras huecas, como contenedores para las disoluciones de arrastre (B, en figura 4.12) y alimentación (A, en figura 4.12), respectivamente. El tanque de la disolución de arrastre (DS, por siglas en ingles de draw solution) se montó en una balanza digital (PKP 4200-2, Kern, Alemania) que se utilizó para la medición continua de su masa (I, en figura 4.12). Los datos de la báscula se transfirieron a un software de registro de datos en una computadora (J, en figura 4.12) para luego ser transformados a volumen. La balanza, y por ende la computadora, solo se utilizaron con el tanque de 5 L, ya que, debido a la escala, no se pudo medir masa del tanque de 50 litros, por lo que el incremento de volumen se midió por medio de la altura del tanque. El tanque de alimentación (FS, por sus siglas en inglés de feed solution) se colocó en un agitador magnético (H, en figura 4.12) (SBS, España) para evitar la deposición de partículas. Los tanques estaban conectados a tubos de goma, a través de los cuales se alimentaban las disoluciones al módulo, donde las corrientes interactuaban a través de la membrana. Entre los tanques y el módulo, cada circuito disponía de manómetro (D, en figura 4.12) de casa comercial Nuova Fima, Italia, caudalímetro (E, en figura 4.12) del proveedor Tecfluid, España (modelo Psm-21) y bomba peristáltica (C, en figura 4.12) de

Heidolph, Alemania (modelo Pumpdrive 5106). La planta también fue equipada con dos medidores de conductividad eléctrica (CDH-SD1, Omega Engineering), uno para cada disolución (F, en figura 4.12). El módulo CFO42 (G izquierda, en figura 4.12.) fabricado por Sterlitech Corporation (EE.UU.) se utilizó para alojar la membrana de plana FTSH2O™ (Fluid Technology Solutions, EE.UU.) hecha de triacetato de celulosa (CTA, por sus siglas en inglés de cellulose triacetate). La otra membrana ensayada correspondió a la membrana HFFO.6 (G derecha, en figura 4.12.) de fibras huecas (Aquaporin Inside, Dinamarca), con una capa activa de compuesto de película fina de poliamida (TFC) con proteínas de acuaporina integrada, la cual viene en su propio módulo. Se decidió trabajar en modo contracorriente, ya que, al trabajar con FS con una gran concentración de solutos, la presión osmótica puede elevarse en gran medida. La posición de la membrana fue FS frente a la capa activa para todos los experimentos.

IV.6.2. Ensayos de Osmosis directa

Como se comentó anteriormente, lo primero fue, para el caso de la membrana plana, hidratarla en agua osmotizada (conductividad <40 μS/cm) durante 24 horas. Por otra parte, la membrana de fibras huecas se instaló en el sistema y se le paso agua osmotizada durante 10 minutos, tanto para hidratarla como para retirar posibles sustancias conservantes. Luego se procedió a caracterizar ambas membranas. Para la caracterización de membranas se prepararon diferentes concentraciones de DS utilizando NaCl a 25, 50, 75, 100, 125, 150 y 200 $g \cdot L^{-1}$ (0,43; 0,85; 1,3; 1,7; 2,1; 2,6; 3,5 M, respectivamente). Las condiciones de operación de las pruebas de caracterización fueron las mismas para las dos membranas: caudales de 25 $L \cdot h^{-1}$ para la FS y de 15 $L \cdot h^{-1}$ para la DS.

Debido a la diferencia de área superficial de cada membrana, los ensayos realizados con la membrana FTSHO2, de menor área superficial, duraron 4300 minutos (71,6 h), mientras que los ensayos con la membrana HFFO.6 duraron unos 120 minutos (2 h). Después de cada

experimento, las membranas se limpiaron durante 30 minutos con agua del grifo y luego 10 minutos con agua osmotizada a través de los lados de alimentación y extracción.

Se realizaron diferentes ensayos con estas membranas, tanto con agua modelo como con aguas residuales. En la tabla 4.6 se presentan los ensayos realizados.

El agua residual sintética utilizada como FS se preparó con 1 $g \cdot L^{-1}$ de tirosol (Maybridge, Reino Unido). Esta concentración fue seleccionada debido a la concentración de compuestos fenólicos totales obtenidos en la caracterización de las muestras de OOWW (1161,80 ± 13,43 mgTirosol $eq \cdot L^{-1}$ [5]). Para la DS sintética se utilizó una disolución de 30 $g \cdot L^{-1}$ de cloruro de sodio (NaCl) proporcionada por VWR Chemicals (Bélgica), ya que este valor se aproximaba a la concentración de NaCl registrada en la caracterización de la FTOP (33,41 ± 0.13g $Cl^{-} \cdot L^{-1}$[6])

Tabla 4.6 Disolución de alimento (FS, por sus siglas en inglés de feed solution) y disolución de arrastre (DS, por siglas en ingles de draw solution) empleadas en cada ensayo de ósmosis directa

Ensaayos	Membrana utilizada	FS	DS
E1	FTSH20 y HFFO.6	Diolución modelo (1$g \cdot L^{-1}$ tirosol)	Diolución modelo (30 $g \cdot L^{-1}$ NaCl)
E2	FTSH20 y HFFO.6	5F- OOWW	Diolución modelo (30 $g \cdot L^{-1}$ NaCl)
E3	HFFO.6	5F- OOWW	60F- FTOP
E4	HFFO.6	UF- OOWW	60F- FTOP

OOWW: agua residual de lavado de aceite de oliva; FTOP: agua residual del proceso de fermentación de las aceitunas de mesa; 5F-OOWW: OOWW filtrada a 5 µm; UF-OOWW: permeado de la ultrafiltración de OOWW; 60F-FTOP: FTOP filtrada a 60 µm

IV.6.3. Limpieza de las membranas de Osmosis directa

Después de cada experimento, las membranas se limpiaron durante 30 minutos con agua del grifo y luego durante 10 minutos con agua osmotizada (conductividad <40 µS/cm) a través de los lados de alimentación y extracción. Antes (con la membrana nueva) y después de la limpieza, se realizó un ensayo de un solo paso (sin recirculación) para verificar la recuperación de la permeabilidad de la membrana. Se utilizó una disolución de NaCl 0.5 M como DS y agua osmotizada como FS. Los caudales fueron de 25 $L \cdot h^{-1}$ y 15 $L \cdot h^{-1}$ para las FS y DS, respectivamente.

IV.7. ADSORCIÓN/DESORCIÓN CON RESINAS

IV.7.1. Adsorción

El objetivo de los ensayos de adsorción fue evaluar la influencia de la dosificación de resina en la adsorción de compuestos fenólicos. Los ensayos de adsorción contemplaron dos etapas. La primera fue el estudio de diferentes resinas bajo condiciones ideales (con disoluciones modelo) y con agua real (OOWW pretratada). Para ello, se evaluaron dos resinas MacronetTM, MN200 y MN202, y dos resinas PurosorbTM, PAD900 y PAD950, todas suministradas por Purolite, a diferentes concentraciones (10, 20, 30, 40, 50 y 60 $g \cdot L^{-1}$). Las principales propiedades físicas de las resinas se muestran en la Tabla 4.7.

Antes de su uso, las resinas se acondicionaron en una disolución de hidróxido de sodio (2% p/v) durante 60 min a 140 rpm. Luego, se lavaron dos veces con agua osmotizada durante 5 min a la misma velocidad. Las diferentes dosis de resina estudiadas, indicadas anteriormente, se mezclaron con 200 mL de disolución modelo durante 180 min en agitación constante de 140 rpm a temperatura ambiente (21 ± 2 °C). Después de la adsorción, la fase líquida, que contenía la fracción de compuestos fenólicos no adsorbidos, se separó de la matriz sólida mediante filtración a través de un filtro de membrana de 0,2 µm.

Tabla 4.7. Principales propiedades físicas de las resinas empleadas (datos del proveedor).

Resina	Matriz	*área superficial ($m^2\ g^{-1}$)	*diámetro de poro (Å)	*volumen de poro ($mL\ g^{-1}$)	Gravedad específica	Tamaño partícula (mm)	Hidrofobicidad
MN200	PS/DVB[1]	1100	700/15[#]	0,4	1,04	0,5-0,7	Moderada
MN202	PS/DVB[1]	950	220/15[#]	0,3	1,04	0,3-1,2	Moderada
PAD900	PDVB[2]	850	220	1,9	1,02	0,35-1,2	Moderada
PAD950	Polimetacrílico	450	120	0,6	1,1		baja

[1]PS/DVB: poliestireno reticulado con divinilbenceno; [2]PDVB: Polidivinilbenceno
* medido por adsorción de nitrógeno; [#] macroporos/microporos

Todos los experimentos de adsorción se llevaron a cabo en un floculador Jar test "FLOC-6" (Figura 4.14), suministrado por RAYPA. En los ensayos se midió la concentración de compuestos fenólicos, azúcares y DQO en el sobrenadante.

Figura 4.14. Fotografía de los ensayos de adsorción/desorción (UPV, Valencia, España)

La segunda etapa contempló solo la mejor resina (MN200) y las mejores condiciones (dosis de 40 $g{\cdot}L^{-1}$ durante 180 min a una velocidad constante de 140 rpm) obtenidas en la primera etapa. En ella se recuperaron los compuestos fenólicos a partir de las corrientes

concentradas obtenidas en los procesos de Nanofiltración y osmosis directa previamente mencionados. En este caso, el análisis del sobrenadante contempló la determinación individual de compuestos fenólicos, azúcares y DQO.

IV.7.2. Desorción

La etapa de desorción también contempló dos etapas. La primera se realizó después del primer estudio de adsorción con el objetivo de encontrar la mejor opción para extraer los compuestos fenólicos de las resinas. Para ello, después de los ensayos de adsorción, las resinas se lavaron 3 veces con agua osmotizada durante 5 min a 150 rpm, luego las resinas se secaron a 50 °C durante 3 h en contenedores de vidrio (Figura 4.15).

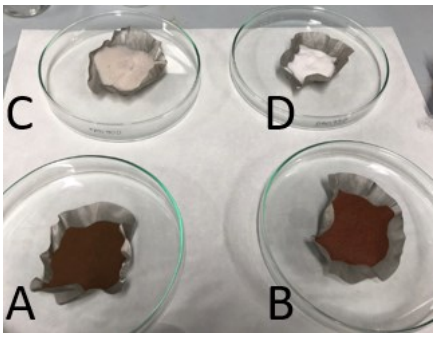

Figura 4.15. Resinas antes de entrar a la etapa de secado
A: resina MN200, B: resina MN202, C: resina PAD900, D: resina PAD950

Se probaron dos disolventes, etanol y una mezcla de etanol-agua al 50% v/v, para recuperar la mayor cantidad de compuestos fenólicos. El etanol absoluto (H3CCH2OH, ≥ 99,5 %) se adquirió de VWR International (EE.UU). Las resinas se pusieron en contacto con 100 mL de cada disolvente durante 180 min a una velocidad constante de 140 rpm y temperatura

ambiente (21 ± 2 °C). Después de la desorción, las resinas se lavaron nuevamente bajo el mismo protocolo mencionado anteriormente y se reutilizaron para la siguiente prueba. Además de la determinación individual de compuestos fenólicos y azúcares, se realizó una caracterización completa de cada compuesto fenólico mediante cromatografía líquida acoplada a espectrometría de masas (LC-MS).

Al igual que con la adsorción, la segunda etapa de la desorción se llevó a cabo solamente bajo las mejores condiciones, con la finalidad de extraer los compuestos fenólicos de las resinas puestas en contacto con los concentrados de NF y FO, respectivamente. El disolvente utilizado fue mezcla de etanol-agua al 50% v/v durante 180 min a una velocidad constante de 140 rpm y temperatura ambiente (21 ± 2 °C). En este caso, el análisis del extracto solo contempló la determinación individual de compuestos fenólicos, azúcares y DQO.

IV.8. TRATAMIENTO BIOLÓGICO

Debido a la alta carga orgánica presente en las muestras de aguas residuales, se realizó un estudio preliminar al SBR, con el objetivo de encontrar una concentración en la que las bacterias no se vieran afectadas.

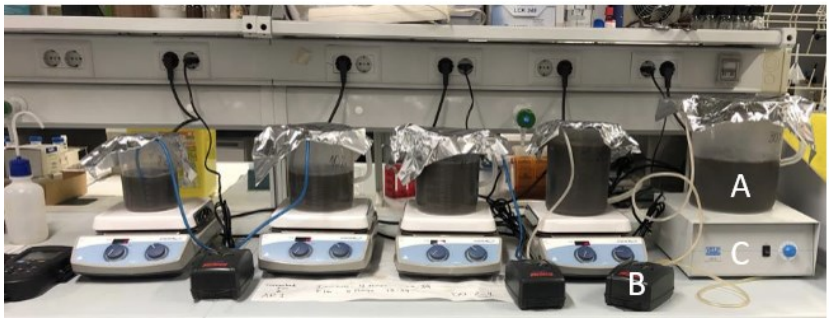

Figura 4.16. Montaje experimental del estudio biológico preliminar. A: reactor; B: oxigenación; C: agitación (UPV, Valencia, España)

Para ello, diferentes concentraciones de cada muestra en agua del grifo (5%, 10%, 15%, 20% y 30% v/v) se pusieron en contacto en vasos de precipitados con biomasa extraída de un reactor de lodos activos de una planta de tratamiento de aguas residuales municipales. El montaje se presenta en la figura 4.16. El tiempo de operación fue de 24 h y la agitación y aireación fueron continuas (B, en la figura 4.16). Las condiciones de operación fueron las mismas para todas las pruebas, manteniendo los sólidos suspendidos en licor mixto (MLSS) de 3,5 $g \cdot L^{-1}$, un volumen de alimentación de 0,25 L y una relación alimento-microorganismos (F/M) de 0,15 $gDQO \cdot gMLSS^{-1} \cdot d^{-1}$.

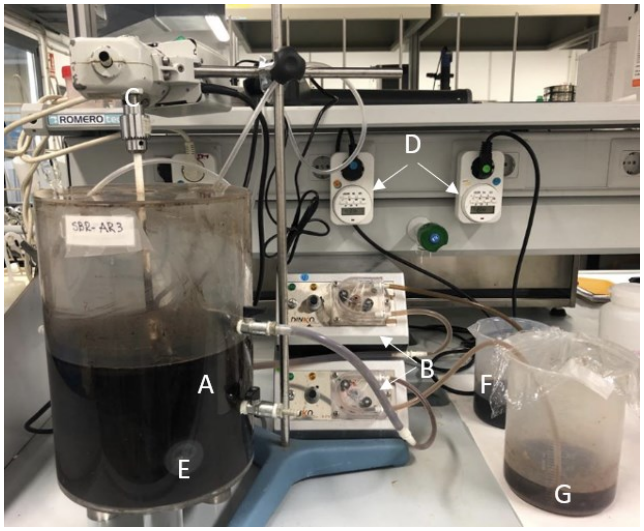

Figura 4.17. Montaje experimental del tratamiento biológico en reactor biológico secuencial. A: reactor, B: bombas; C: sistema de agitación; D: controladores de tiempo; E: aireación; F: efluente; G: Influente (UPV, Valencia, España)

Una vez seleccionada la concentración inicial, se operaron durante 65 días tres reactores discontinuos (SBR) a escala de laboratorio, con diferentes corrientes a tratar (rechazos de UF y NF; y concentrado de FO). Los reactores de 6 litros se sembraron con lodos activos de una estación depuradora de aguas residuales municipales (Valencia, España), manteniendo controlada relación DQO:N:P de 100:5:1, añadiendo fosfato dipotásico y urea.

Los SBR se operaron configurando 1 ciclo por día, con cinco fases por ciclo, llenado (10 min), reacción (1h/21h anaeróbico/aeróbico), sedimentación (1,5 h), extracción (10 min) y reposo (10 min). El volumen de alimentación inicial fue de 900 mL/día para el SBR alimentado con muestras de FO-C y NF-R y de 600 mL/día para el SBR/UF-R. El volumen de alimentación (y, en consecuencia, el volumen extraído de aguas residuales tratadas) se incrementó gradualmente durante el experimento, aumentando un 5% cada 10 o 15 días (dependiendo del reactor).

IV.9. CARACTERIZACIÓN DE LAS MUESTRAS

Se caracterizaron tanto las aguas residuales sin tratar como las diferentes corrientes obtenidas en cada proceso. Cada parámetro se midió por triplicado y el valor del error experimental se calculó como la desviación estándar. En la figura 4.18 se presenta el conductímetro digital calibrado (EC-Meter GLP 31+) y el pH-metro (GLP 21+), utilizados para determinar la conductividad eléctrica (CE) y el pH, respectivamente (ambos suministrados por Crison, Spain). También se muestra la fotografía del turbidímetro D-112 (DINKO, España) utilizado para medir la turbidez siguiendo el método estándar UNE-EN ISO 7027.

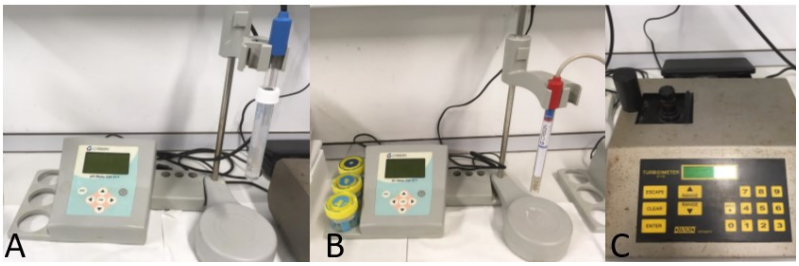

Figura 4.18. Fotografía de algunos equipos utilizados para la caracterización de las corrientes A: pH-metro; B: conductímetro; C turbidímetros.

El protocolo de medida de los tres parámetros (pH, conductiviad y turbidez) fue similar. Se escogieron tres muestras diferentes para su análisis, hasta que el valor entregado por el equipo fuese estable. Esta caracterización se realizó nuevamente al inicio de cada ensayo para prevenir variación debido a degradación de la muestra (congelación/descongelación).

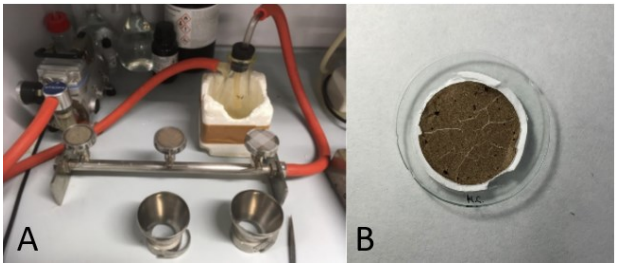

Figura 4.19. Análisis de sólidos en suspensión. A: montaje experimental; B: filtro con muestra

La medición de sólidos en suspensión totales (TSS) se realizó siguiendo el método estándar UNE 77034 (APHA, 2005). En la figura 4.19 se observa el montaje de filtración a vacío dotado de bomba de vacío de membrana Vakuumsystem modelo ME2 (Vacuubrand GMBH + CO, Alemania), una trampa de vacío y dos soportes de filtro. La cantidad de TSS correspondió a la diferencia entre el peso inicial de un filtro de microfibra de vidrio (tamaño de poro de 1.2 µm) y su peso después de la filtración de 25 mL de muestra y posterior secado utilizando un horno a 105 °C durante 2 h.

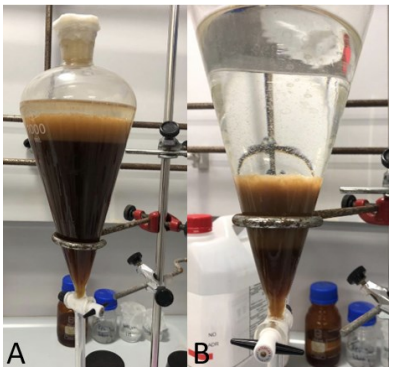

Figura 4.20. Extracción con Hexano para la determinación de grasas y aceites
A: inicio del ensayo; B: final del ensayo

Para la determinación de la concentración de grasas y aceites se empleó un proceso de extracción con hexano que se presenta en la figura 4.20. Para ello, 500 mL de muestra se pusieron en contacto mediante agitación con 250 mL de hexano (25 °C), para luego dejar reposar la mezcla en un embudo de decantación durante 30 min. El sobrenadante (que contiene disolvente + aceites y grasas, B en figura 4.20) se extrajo con la ayuda de una pipeta. A continuación, se agregaron 250 mL de hexano al resto, repitiendo el proceso de extracción. Este paso se repitió 3 veces. Todos los sobrenadantes (extractos) se filtraron con un filtro de celulosa (45 µm de diámetro de poro). A continuación, se pesaron antes y después de la evaporación del disolvente (a 50 °C en un evaporador rotatorio). La diferencia de masa correspondió a la cantidad de aceites y grasas y el resultado se expresó en $mg \cdot L^{-1}$.

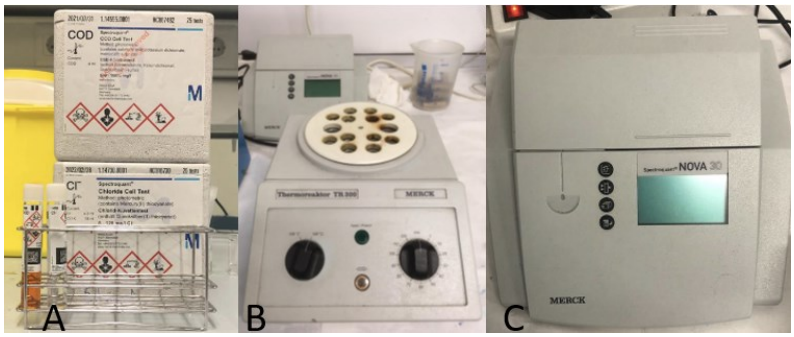

Figura 4.21. Determinación de DQO y de cloruros mediante Kits. A: cubetas para análisis; B: termoreactor para cubetas de DQO; C: espectrofotómetro para análisis de resultados.

La determinación de DQO y ion cloruro se realizó mediante kits de la casa comercial Merck (Alemania). En la figura 4.21 A, se observan los Kits de DQO, los cuales se basan en la oxidación de la materia orgánica con una disolución de ácido sulfúrico y dicromato de potasio en presencia de sulfato de plata como catalizador. Mientras que para la determinación de cloruros el método analítico se basa en la reacción de los iones cloruro con tiocianato de mercurio (II), los cuales al interactuar forman cloruro de mercurio (II) e iones tiocianato, que en presencia de sales de hierro (III) reaccionan nuevamente pasando a formar tiocianato de hierro (III). En la figura 4.21 B se presenta el termoreactor de la misma casa comercial (modelo TR300, Merk, Alemania) necesario para activar la reacción y de oxidación de la materia orgánica. Para ello, el vial debe dejarse por 2 horas a una temperatura de 148 grados, luego debe estar en reposo durante 30 minutos a temperatura ambiente. Trascurrido 20 minutos del tiempo total de reposo, las muestras son agitadas, luego se espera a que cumpla el tiempo para ser medidas. En la figura 21 C se presenta el espectrofotómetro NOVA 30 (Merck, Alemania) utilizado para la determinación de ambos parámetros.

Otro parámetro analizado fue el color, para lo que fue necesario diluir la muestra, debido a su fuerte coloración. Se determinó que una dilución de 1:50 era necesaria para el análisis de las muestras crudas, variando de 1:1 a 1:25 para las muestras tratadas. Para ello, se midió la absorbancia a las longitudes de onda (λ) de 436 nm, 525 nm y 620 nm en el

espectrofotómetro UV-VIS DR 6000 [7]. Las cubetas utilizadas fueron de poliestireno óptico (PS) de 1,5 mL de volumen. El color se calculó mediante la siguiente fórmula:

$$Color = \frac{(A_{436\lambda})^2+(A_{A525\lambda})^2+(A_{A620\lambda})^2}{A_{436\lambda}+A_{A525\lambda}+A_{A620\lambda}} \quad \text{Eq. 15}$$

Donde $A436\lambda$ es la absorbancia a 436 nm, $A525\lambda$ es la absorbancia a 525nm y $A620\lambda$ es la absorbancia a 620nm.

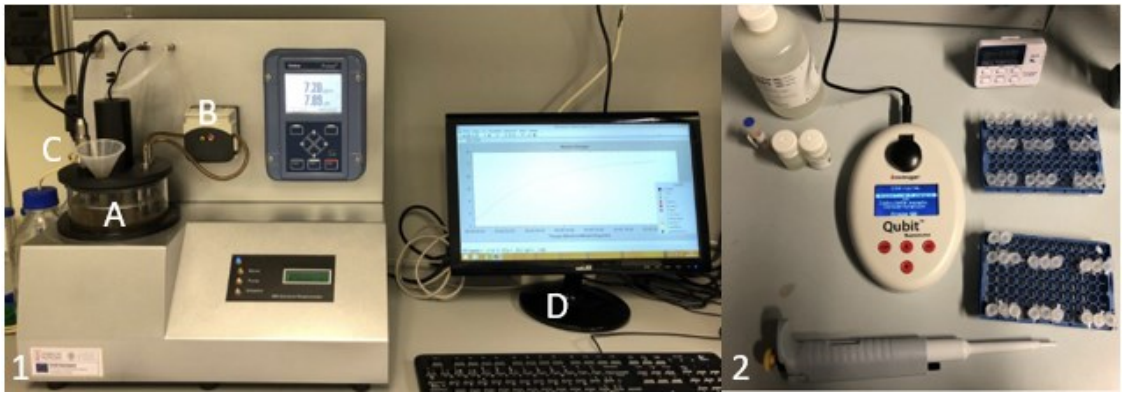

Figura 4.22. 1: montaje experimental análisis respirometría; 2: montaje para la determinación de ADN. A: licor de mezcla; B: bomba; C: embudo para adición de muestra; D: sistema computacional

También se decidió realizar un análisis de biodegradabilidad mediante ensayo respirométrico para determinar la toxicidad de cada muestra. La prueba se realizó siguiendo el protocolo presentado por Zuriaga-Agustí et al., 2016 [8]. La respirometría se basa en el consumo de oxígeno por parte de los microorganismos del lodo activo. El montaje experimental se presenta en la figura 4.22(1). Los análisis se realizaron en un analizador BM-Advance de SURCIS (España) y se llevaron a cabo mediante la adición de diferentes dosis (10 mL como primera dosis y 5 mL para el resto de las dosis) de agua residual a una muestra inicial de 500 mL de licor de mezcla (A en la figura 4.22(1), con el fin de medir mediante sistema computacional (D, en figura 4.22(1)) la influencia de la adición de la muestra en la tasa

de consumo de oxígeno estándar. La muestra inicial de licor de mezcla fue previamente aireada durante 24h para asegurar condiciones endógenas en la biomasa. El ensayo fue dinámico con agitación continua, aireación y recirculación entre ambos lados del recipiente por medio de una bomba peristáltica (B, en figura 4.22(1)), donde se midió continuamente el oxígeno disuelto. En la Figura 4.22(2) se observa el montaje y los reactivos utilizados para el análisis de ADN, el cual fue extraído mediante el kit FastDNA® SPIN (MP Biomedicals, EE.UU) siguiendo el protocolo del fabricante, también presentado en Ferrer-Polonio et al., 2019 [9]. Los productos finales de ADN obtenidos por el kit se eluyeron en un volumen final de 50 µL, añadiendo inhibidores de PCR OneStep™ (Zymo Research, CA, EE.UU) para eliminar posibles inhibidores que podrían afectar las reacciones enzimáticas. Finalmente las muestras se midieron mediante el kit de ensayo Qubit® dsDNA BR y el espectrofotómetro NanoDrop ND-1000 UV/Vis, ambos de Thermo Fisher Scientific (EE.UU)

La concentración de azúcares totales en las muestras se midió mediante dos metodologías. En primer lugar, se utilizó el método de Antrona [10], el cual determina la concentración total de carbohidratos (azúcares libres o formando un polisacárido). Este método se basa en la deshidratación e hidrólisis de los azúcares que reaccionan con Antrona en un medio ácido, bajo la acción de la temperatura, para formar un derivado del furano de color verde azulado. Para ello, se pusieron en contacto 1 mL de muestra y 2 mL de reactivo de Antrona en un tubo cuidadosamente cerrado y se agitaron durante 15 segundos en un vortex. Luego, se sumergieron en un baño de agua a 100°C durante 14 minutos. A continuación, se enfriaron en un recipiente con hielo durante 5 minutos para detener la reacción y, finalmente, se realizó la lectura de la absorbancia a una longitud de onda de 625nm.

También se determinó la concentración de azucares mediante el kit colorimétrico (Figura 4.22) Sucrose/D-Glucose/D-Fructose de r-biopharm (Alemania), utilizando glucosa (Panreac, España) como patrón. Esta técnica se basa en la hidrólisis enzimática de la sacarosa mediante diferentes reacciones, los cuales permiten obtener absorbancias las cuales luego son trasformadas en concentración.

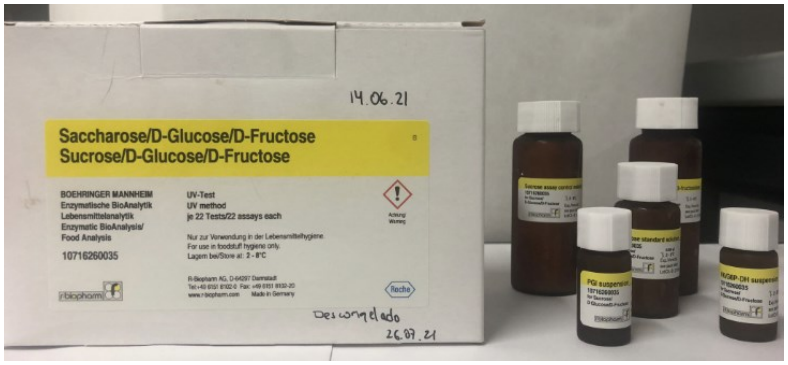

Figura 4.23. Kit colorimétrico para la determinación de azucares

Como se puede observar en la figura 4.23, el kit viene con diferentes botes, cada bote está señalado con un número. Para la medición se debe preparar diferentes cubetas a las cuales se les añadirá diferentes soluciones.

Preparación de soluciones:

- Disolución 1: Disolver el contenido del frasco 1 con 10 ml de agua destilada
- Disolución 2: Disolver el contenido del frasco 2 con 45 ml de agua destilada
- Disolución 3: Usar el contenido de la botella 3 sin diluir.
- Disolución 4: Usar el contenido de la botella 4 sin diluir.

La Tabla 4.8 resume el procedimiento experimental. El procedimiento contempla la adición de las diferentes soluciones (mencionadas anteriormente) a cubetas (denominadas A, B, C y D) para luego de sucedida la reacción medir su absorbancia.

Tabla 4.8 Protocolo para la determinación de Azúcares mediante el Kit Sucrose/D-Glucose/D-Fructose de r-biopharm

	Cubetas			
	A Blanco[1]	B Muestra[1]	C Blanco[2]	D Muestra[2]
Soluciones a pipetear en cubetas				
Disolución 1*	0.2 mL	0.2 mL	-	-
Muestra*	-	0.1 mL	-	0.1 mL
Mezclar** e incubar por 15 minutos a 20-25ºC o por 5 minutos a 37ºC. Antes de pasar a siguiente paso, calentar la disolución 1 a 37ºC.				
Disolución 2	1.0 mL	1.0 mL	1.0 mL	1.0 mL
Agua destilada	1.8 mL	1.7 mL	2.0 mL	1.9 mL
Mezclar*** y leer las absorbancias de las disoluciones (A1***) después de aproximadamente 3 min e iniciar la reacción mediante la adición de:				
Disolución 3	0.02 mL	0.02 mL	0.02 mL	0.02 mL
Mezclar** y esperar aprox. 10-15 min (tiempo para reacción completa), y leer las absorbancias de las disoluciones (A2***). Si la reacción no se ha detenido después de 15 min, continuar leyendo las absorbancias a intervalos de 2 min hasta que las absorbancias aumenten constantemente durante 2 min.				
Disolución 4	-	-	0.02 mL	0.02 mL
Mezclar** y leer las absorbancias de las disoluciones después de 10-15 min (A3***)				

* Pipetear la solución 1 y la solución de muestra cada una en el fondo de la cubeta y mezcle agitando suavemente. ** Si se mezcla con una espátula de plástico, retirarla de la cubeta solo directamente antes de medir la absorbancia *** Todas las absorbancias se miden a la misma longitud de onda (340 nm). [1]: sacarosa; [2]: D-glucosa/D- fructosa

A partir del protocolo detallado en la tabla 4.8 se determinan las diferencias de absorbancia (A2-A1) tanto para el blanco como para la muestra. Restando la diferencia de absorbancia del blanco a la diferencia de absorbancia de la muestra siguiendo la Eq. 16

$$\Delta A = (A_2 - A_1)_{muestra} - (A_2 - A_1)_{blanco} \qquad \text{Eq. 16}$$

La diferencia de las cubetas 1 (A y B) corresponde a $\Delta A_{\text{total D-Glucosa}}$, las diferencias de las cubetas 2 (C y D) se obtiene $\Delta A_{\text{D-glucosa}}$. La diferencia entre ellas entrega el valor de $\Delta A_{\text{sacarosa}}$. Para la determinación de $\Delta A_{\text{D-fructosa}}$ se debe determinar las diferencias de

absorbancia (A3-A2) tanto para el blanco como para la muestra de las cubetas 2 (C y D). Luego restando la diferencia de absorbancia del blanco a la diferencia de absorbancia de la muestra entrega el valor. Como se comentó anteriormente, todas las absorbancias se miden a 340 nm y, mediante la ecuación 17, se obtiene el valor de cada concentración.

$$c = \frac{V \cdot MW}{\varepsilon \cdot d \cdot v \cdot 1000} \cdot \Delta A \qquad \text{Eq. 17}$$

Donde "V" es el volumen final (mL), "v" el volumen de muestra (mL), "MW" el peso molecular de la sustancia a ensayar (g/mol), "d" el paso de luz (cm), "ε" el coeficiente de extinción nicotinamida adenina dinucleótida (NADPH, por sus siglas en inglés de nicotinamide-adenine dinucleotide phosphate) el cual a 340 nm es de 6.3 (L/mmol·cm). Finalmente ΔA corresponderá al valor de la adsorbancia de D- glucosa o D-fructosa.

Dos técnicas fueron utilizadas, Fluorescencia 2D y FTIR para analizar las muestras y las membranas tras los ensayos detallados en las secciones IV.5.2. y IV5.3. Los espectros de fluorescencia de las membranas y las muestras se obtuvieron con un espectrofotómetro de fluorescencia Varian Cary Eclipse (EE.UU) equipado con monocromadores de excitación y emisión y acoplado a una sonda de fibra óptica (A, Figura 4.24). Las mediciones de espectroscopía de fluorescencia de emisión de excitación (EEM) se obtuvieron a una velocidad de barrido de 12000 nm·min^{-1}, y rendijas de excitación y emisión de 5 y 10 nm, respectivamente. Los espectros de fluorescencia se determinaron en un rango de longitud de onda de excitación entre 245 y 745 nm y un rango de longitud de onda de emisión entre 250 y 750 nm con un paso de 5 nm. Los espectros FTIR de las membranas se obtuvieron utilizando el equipo Shimadzu IRAffinity-1S, Japón) (B, Figura 4.24) en modo de absorción de 400 a 4000 cm^{-1} con 4 barridos de acumulación y una resolución de 10 cm^{-1}.

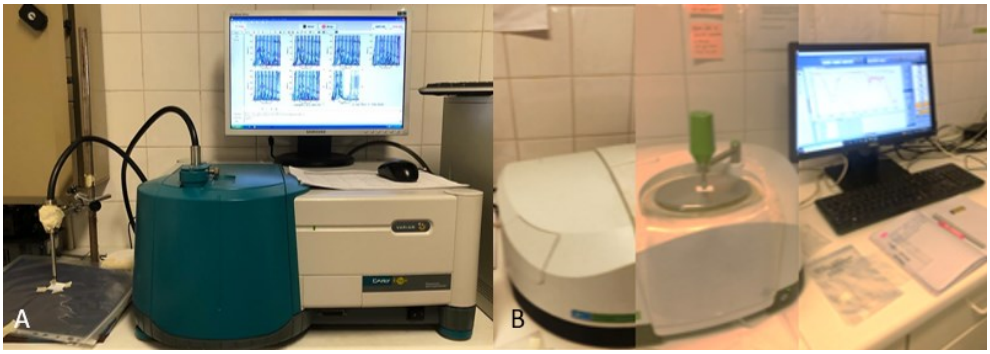

Figura 4.24. Equipos de espectroscopía de fluorescencia (A) y de espectroscopia infrarroja por transformada de Fourier (FTIR, por siglas en inglés de Fourier-transform infrared spectroscopy) (B) (UNL, Lisboa, Portugal)

Para las muestras de membranas, se realizaron 6 mediciones por cada membrana en diferentes partes de su superficie. Las muestras líquidas solo fueron analizadas mediante fluorescencia 2D y se realizaron tres mediciones por muestra.

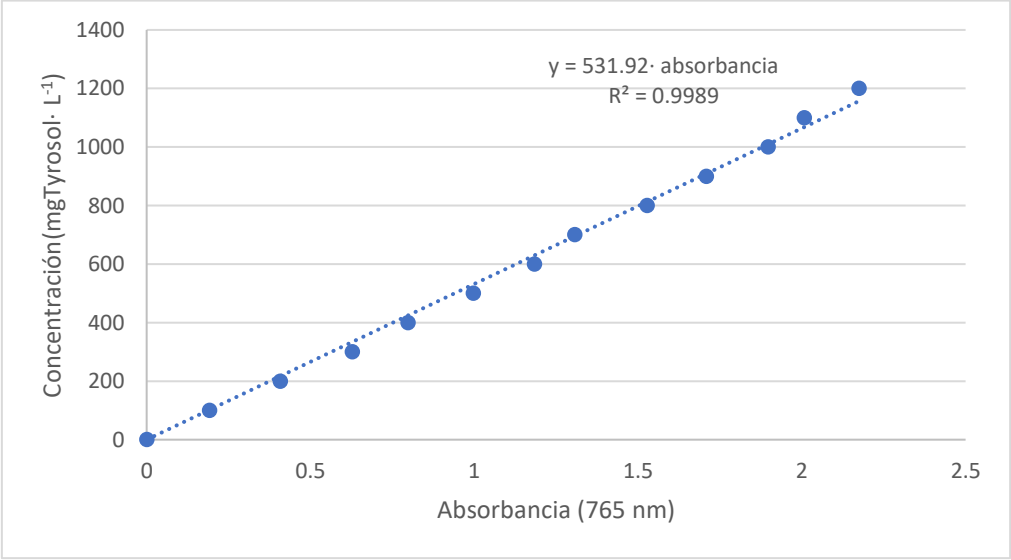

Figura 4.25. Recta de calibrado para la determinación de compuestos fenólicos totales mediante el método de Folin-Ciocalteau utilizando Tirosol como patrón

La determinación de la concentración de compuestos fenólicos totales se realizó siguiendo el método colorimétrico de Folin-Ciocalteau [11]. Este método se basa en la reducción en medio alcalino de una mezcla de ácidos fosfomolíbdico y fosfowolfrámico (reactivo de Folin-Ciocalteau) por los compuestos fenólicos, formando una mezcla de óxidos con un característico color azul. Estos óxidos formados por wolframio y molibdeno absorben la luz entre 620 – 765 nm, siendo la medida de la absorbancia proporcional a la concentración de compuestos fenólicos a una longitud de onda 765 nm. El procedimiento contempla diferentes pasos: el primero consiste en mezclar 6.8 mL de agua osmotizada y 0.2 mL de la muestra a analizar; tras agitar, se añadieron 0.5 mL, del reactivo de folin, para luego agitar la disolución con la ayuda de un sonicador (ultrasonido) modelo Elmasonic P (ELMA, Alemania) durante 3 minutos; seguidamene se añadió 1 mL de una disolución de Na_2CO_3 (20% p/p) y se guardó evitando la luz durante 1 hora; transcurrido el tiempo se determinó la absorbancia de cada muestra a una longitud de onda de 765 nm en el espectrofotómetro DR 6000. Se preparó además un blanco sin muestra (7 mL de agua osmotizada) para su correcta medida en el espectrofotómetro. Para relacionar la lectura de la absorbancia con la concentración de compuestos fenólicos se prepararon disoluciones patrón de tirosol. En la figura 4.25 se presenta la recta de calibrado utilizada para la determinación de compuestos fenólicos.

La determinación de ATPc (Trifosfato de adenosina de células vivas), AVSS (solidos viables activos) y BSI% (estrés bacterial), incluidos en el capítulo V.7 de resultados, así como los análisis de compuestos fenólicos mediante cromatografía líquida acoplada a espectrometría de masas (LC-MS), presentados en los apartados de resultados V. 5 y 6 no se detallan en esta sección ya que no fueron realizados por la doctoranda.

IV. 10 REFERENCIAS

[1] A. Sotto, J.M. Arsuaga, B. Van der Bruggen, Sorption of phenolic compounds on NF/RO membrane surfaces: Influence on membrane performance, Desal. 309 (2013) 64–73. http://dx.doi.org/10.1016/j.desal.2012.09.023

[2] M. Cifuentes-Cabezas, C.M. Sanchez-Arévalo, J.A. Mendoza-Roca, M.C. Vincent-Vela, S. Álvarez-Blanco, Recovery of Phenolic Compounds from Olive Oil Washing Wastewater by Adsorption/Desorption Process, Sep. Purif. Technol. 298 (2022) 121562. https://doi.org/10.1016/j.seppur.2022.121562

[3] M.J. Luján-Facundo, J.A. Mendoza-Roca, B. Cuartas-Uribe, S. Álvarez-Blanco, Evaluation of cleaning efficiency of ultrafiltration membranes fouled by BSA using FTIR-ATR as a tool, J. Food Eng. 163 (2015) 1–8. http://dx.doi.org/10.1016/j. jfoodeng.2015.04.015

[4] A. Santafé-Moros, J.M. Gonzálvez-Zafrilla, D. Valencia, Design of a Flat Membrane Module for Fouling and Permselectivity Studies, In Proceedings of the COMSOL Conference, Paris, France, (29–30 October 2010) 1–7.

[5] M. Cifuentes-Cabezas, C. Carbonell-Alcaina, M.C. Vincent-Vela, J.A. Mendoza- Roca, S. Alvarez-Blanco, Comparison of different ultrafiltration membranes as first step for the recovery of phenolic compounds from olive-oil washing wastewater, Process Saf. Environ. Prot. 149 (2021) 724–734. https://doi.org/10.1016/j. psep.2021.03.035.

[6] E. Ferrer-Polonio, C. Carbonell-Alcaina, J.A. Mendoza-Roca, A. Iborra-Clar, S. Álvarez-Blanco, A. Bes-Piá, L. Pastor-Alcañiz, Brine recovery from hypersaline wastewaters from table olive processing by combination of biological treatment and membrane technologies, J. Clean. Prod, 142(4), (2017) 1377-1386. https://doi.org/10.1016/j.jclepro.2016.11.169.

[7] E. Döepkens, R. Jonas, T. Jung, R. Krull, Rückführung von Abwasserteilströ- men der Textilveredlung in den Produktionsprozess. In: GVC (Ed.), Prepr. Colloq. Produktionsintegrieter Wasser Abwasserechnik. “Nachhaltige Prod. der Textil-veredlung” und “Membrantechnik”, Bremen, (2001) B143eB15.

[8] E. Zuriaga-Agustí, G. Garrido-Mauri, J.A. Mendoza-Roca, A. Bes-Piá, J.L. Alonso-Molina, Reduction of the sludge production in a sequencing batch reactor by addition of chlorine dioxide: Influence on the process performance, Chem. Eng. J. 209 (2012) 318–324. https://doi.org/10.1016/j.cej.2012.08.004.

[9] E. Ferrer-Polonio, J. Fernández-Navarro, J.L. Alonso-Molina, J.A. Mendoza-Roca, A. Bes-

Piá, I. Amorós, Towards a cleaner wastewater treatment: influence of folic acid addition on sludge reduction and biomass characteristics, J. Clean. Prod. 232 (2019) 858-866. https://doi.org/10.1016/j.jclepro.2019.06.021

[10] B. Frolund, P. Rikke, K. Keiding, P.H. Nielsen, Extraction of extracellular polymers from activated sludge using a cation exchange resin. Water Res. 30 (1996) 1749–1758

[11] V.L. Singleton, R. Orthofer, R.M. Lamuela-Raventós, Analysis of total phenols and other oxidation substrates and antioxidants by means of folin-ciocalteu reagent, Methods Enzymol. 299 (1999) 152–178. https://doi.org/10.1016/S0076-6879(99)99017-1.

CAPÍTULO V
RESULTADOS

V. RESULTADOS

A continuación, se presentan los resultados en formato artículos en versión autor. Los primeros tres artículos se refieren al proceso de ultrafiltración, el cuarto al proceso de nanofiltración, el siguiente corresponde a la etapa de ósmosis directa, para luego presentar el estudio de adsorción/desorción con resinas y, finalmente, el tratamiento biológico.

V.1. Comparison of different ultrafiltration membranes as first step for the recovery of phenolic compounds from olive-oil washing wastewater

ELSEVIER

Process Safety and Environmental Protection

Volume 149, May 2021, Pages 724-734

Comparison of different ultrafiltration membranes as first step for the recovery of phenolic compounds from olive-oil washing wastewater

Magdalena Cifuentes-Cabezas [a], Carlos Carbonell-Alcaina [a], María Cinta Vincent-Vela [a, b], José Antonio Mendoza-Roca [a, b], Silvia Álvarez-Blanco [a, b]

Show more

+ Add to Mendeley Share Cite

https://doi.org/10.1016/j.psep.2021.03.035

Get rights and content

Abstract

The production of olive oil generates wastewater with a high organic load and toxicity due to the high concentration of phenolic compounds. In recent years, the treatment of these waters has been intensified together with the search for a process to recover these phenolic compounds due to their great antioxidant potential. All this with the aim of implementing the concept of circular economy. In this study, four different organic ultrafiltration membranes were evaluated in order to recover the phenolic compounds present in olive oil washing wastewater (OOWW) from an oil mill in the Valencian Community (Spain). The tested

membranes differ in materials and molecular weight cut-off (MWCO): two permanently hydrophilic polyethersulfone (PESH) membranes with MWCO of 4 and 50 kDa, respectively, one polyethersulfone (PES) membrane with a MWCO of 5 kDa and a regenerated cellulose acetate (RCA) membrane with a MWCO of 10 kDa. Transmembrane pressure (TMP) and crossflow velocity (CFV) were varied from 1 to 3 bar and from 1.5 to 3.4 $m \cdot s^{-1}$, respectively. The effectiveness of the different membranes and operating conditions were evaluated comparing the permeate flux and the rejection of chemical oxygen demand (COD) and total phenolic compounds (TPhs). The membranes with lower MWCO showed stable permeate fluxes without significant changes over time, while the UHO50 membrane showed a gradual decrease, without achieving a stable flux. Low rejection of phenolic compounds was observed in all cases, while the rejection of COD varied between 19.5% to 62.9% depending on the membrane and operating conditions tested. Except for the 50 kDa PESH membrane, initial permeability recovery greater than 95% was achieved with a 35 °C water rinse, indicating that membrane fouling was not severe. Since the aim was to recover the TPhs in the permeate stream and separate them from the organic matter, the 5 kDa PES membrane at 2 bar and 2.5 $m \cdot s^{-1}$ was noticed to be the best option. At those conditions a stable permeate flux of 40 $L \cdot h^{-1} \cdot m^{-2}$ was obtained, while the lowest TPhs rejection was observed (8.01%) with a high COD rejection (61.18%).

Keywords Ultrafiltration; Olive Oil washing wastewater; Phenolic compounds; Separation

1. Introduction

The worldwide concern for the recovery of effluents from industrial processes is becoming increasingly powerful due to the shortage of freshwater sources and the environmental protection initiatives. The large volumes of wastewater generated, together with their inadequate disposal, lead to the contamination of water sources from the sea to rivers [1]. In this context, the recovery of waste and water from the food and agriculture industry is

presented as a challenge and, at the same time, is the key factor in the development of new strategies to achieve a circular economy [2,3].

In the Mediterranean countries, the production of olive oil is one of the most important industrial sectors, generating, in the last years, an estimated amount of 30 million m^3 per year of an acidic and dark liquid, called olive mill wastewater (OMWW) [4]. This wastewater is a mixture of different effluents generated in the production process of olive oil. Its composition depends on the olive oil extraction method (conventional press process, three-phase centrifugal continuous process or two-phase centrifugal continuous process). Most of the countries where olive oil is produced use the three-phase centrifugal process, although the more recent two-phase centrifugal process shows greater efficiency and produces lower amount of wastes. However, in Spain about 90% of the olive oil is produced by the two-phase centrifugal process [5]. Olive mill effluents can include the following streams: olive washing water (OWW), olive vegetation water mixed with the water added in the horizontal centrifugation (OVW), olive oil washing wastewater (OOWW) generated in the vertical centrifugation and water used for process machinery washing [6]. Apart from having high loads of organic matter, these wastewaters are characterized by high levels of phenolic compounds. These phenolic compounds are highly phytotoxic and recalcitrant substances, presenting a great risk to aquatic life, microorganisms and vegetables. That is the reason why biological treatment plants result inadequate, since wastewater toxicity may inhibit the microbial population. Therefore, the efficient treatment of phenolic wastewater before discharge is crucial for sustainable development [7]. Due to this, OMW has been considered as a problematic wastewater until now. However, the natural antioxidant character of the polyphenols, converts this effluent into a potential low-cost material for food, pharmaceutical and cosmetic industries [8-9]. Several studies point to phenolic compounds as great natural antioxidants, presenting them as beneficial for the prevention of heart, microbial, diabetes and cancer diseases [10].

Approximately, only 2% of the phenolic compounds of the olive fruit are transferred to the oil phase, while the remaining percentage is lost in the wastes, especially in the liquid streams, since most phenols are water soluble [11].

Many physical and chemical methods have been proposed for phenolic compounds recovery and for the treatment of these wastewaters [12], focusing on the main problems, which are high energy consumption, low efficiency and generation of secondary pollution. The treatments should guarantee not only a significant reduction of the organic matter, but also the possibility of the phenolic compounds recovery. In addition, it is necessary to meet a series of requirements, related to the composition, purity and quality of the recovered compounds [3].

Research studies have shown that the actual management of OMW cannot be achieved without the combination of different technologies [13]. In this regard, several published articles suggest the combination of membrane processes (e.g. microfiltration (MF), ultrafiltration (UF), nanofiltration (NF), reverse osmosis (RO)), as a good option. This is also an environmentally friendly alternative due to the no need for chemicals addition [14-18].

Although the reported works have shown good results in eliminating the organic load and concentrating the phenolic compounds, the process bottleneck is the fouling of the membranes. Several studies have focused on preventing fouling of UF membranes. A statistical review carried out by Al Aani et al. [19] reported that 27% of all publications on ultrafiltration membranes applied for wastewater and water processing focused on this topic (fouling). Among the possible strategies to control the fouling of the membranes, pretreatment is presented as a fundamental step. These pretreatments must be adapted to the specific feed and the type of membrane [20]. It should be noted that the characteristics of the wastewater from olive oil production are affected both by the variety of the olives and the production process used.

In the present work, different ultrafiltration membranes have been evaluated as a possible pretreatment in view of a further recovery of the phenolic compounds from the two-phase OOWW by nanofiltration. Membranes with different molecular weight cut-offs (MWCO) and made of different materials were tested in order to achieve the highest permeate flux and organic matter rejection and the lowest rejection of phenolic compounds. All the membranes were evaluated under the same parameters (temperature, cross flow velocity (CFV) and transmembrane pressure (TMP)). Previous to ultrafiltration, a pretreatment was also carried out, consisting of flotation, sedimentation and filtration. Since most of the countries

that produce olive oil use the three-phase centrifugal process, there are very few studies on the treatment of this wastewater (olive oil washing water from the two-phase process). Based on its higher efficiency, it is expected that most of the olive oil producers will adopt the two-phase process in the next future.

2. Material and Methods

2.1 Feed samples

The samples were provided by an olive oil milling plant located in the Valencian Community (Spain), where the two-phase continuous centrifugal process is used. The collection was carried out in November 2018. The samples correspond to the olive oil washing water (OOWW) obtained during the olive oil production, at the exit of the vertical centrifuge after the olive oil washing. Samples were immediately stored at -20 °C, to prevent degradation.

2.2 Pretreatment

Before starting the ultrafiltration process, a pretreatment was carried out to avoid the rapid fouling of the membrane due to the large particles present in the wastewater and for the care of the ultrafiltration plant. A three-stage pretreatment was planned. The first stage consisted of natural flotation. The flotation process was carried out in 8-liter vessels, leaving the samples between 2 and 3 hours without any stirring. The duration was determined from previous tests (data not shown). Then, the supernatant, which mainly contained oils and fats, was withdrawn using a graduated pipet. Afterwards, a sedimentation process was performed in the same vessels to remove suspended solids (settling time = 24 h). The settled solids were removed through a small valve located at the bottom of the vessel. Finally, in the third stage, the sample was filtered through a 60 μm pore size polyester cartridge (CA-0202-00, model GT, HidroWater, Spain). As in the case of the raw sample, the pretreated wastewater was stored at -20 °C, to avoid degradation.

2.3 Adsorption tests

To evaluate the interaction between the membranes and phenolic compounds, adsorption tests were performed. The tests consisted of immersing membrane pieces 24 hours

in a stirred water solution that contained phenolic compounds following the procedure as previously described [21]. The solution contained 1 $g \cdot L^{-1}$ of two phenolic compounds of different molecular weight, 0.98 $g \cdot L^{-1}$ of tyrosol (138.164 $g \cdot mol^{-1}$) and 0.02 $g \cdot L^{-1}$ of catechin (290.26 $g \cdot mol^{-1}$). The amount of phenolic compounds adsorbed ($mg \cdot m^{-2}$) was calculated as the concentration difference of the total phenolic compounds in the solution before (C_{Before}) and after adsorption (C_{After}) [22], as Eq. 1 shows.

$$M_p = \left(C_{before} - C_{after}\right) * \frac{V}{A} \quad (1)$$

where M_p is the mass (g) of the phenolic compound adsorbed on the membrane, V corresponds to the volume of the solution (500 mL) and A to the effective membrane area (10 cm^2).

2.4 Ultrafiltration experiments

Ultrafiltration experiments were carried out in a laboratory-scale membrane plant. The feed stream was pumped from the feed vessel (8 L) to a Rayflow membrane module (Orelis, France), which contained two flat sheet membranes (0.025 m^2 of total active surface). The permeate and concentrate streams were returned to the feed container. From the permeate stream, samples of 50 mL were collected every 30 minutes for further analysis. A precision balance (Kern, Germany) was used to monitor the permeate flux and the collected data were recorded by a data acquisition system. A schematic flow diagram of the ultrafiltration system used is shown in Fig. 5.1.

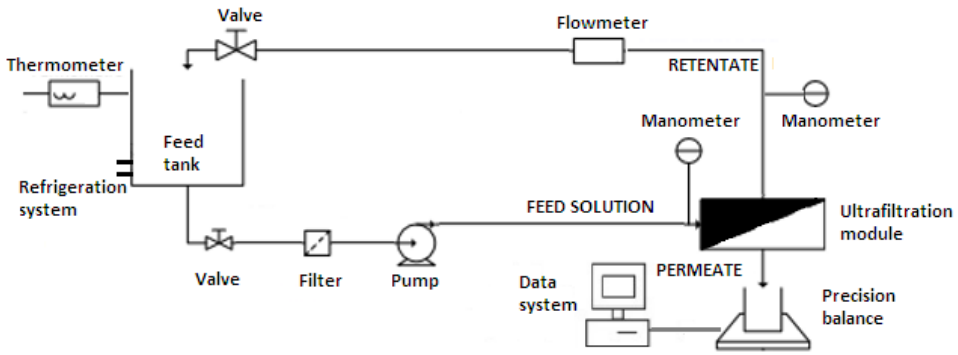

Fig. 5.1 Schematic diagram of the ultrafiltration plant.

The feed tank was provided with a cooling system to keep the temperature at 25°C. The working conditions used were five different CFVs between 1.5 and 3.4 $m \cdot s^{-1}$, four TMPs between 1 and 3 bar and a duration of 3 hours, which was enough time to reach the steady state permeate flux. The performance of the membrane was evaluated by calculating the rejection of chemical oxygen demand (COD) and phenolic compounds (Eq. 2).

$$R_j(\%) = \left(1 - \frac{C_{Pj}}{C_{Fj}}\right) \times 100 \quad (2)$$

Where R_j is the rejection of parameter j (COD or phenolic compounds) in %, C_{Pj} is the concentration of parameter j in the permeate stream and C_{Fj} is the concentration of parameter j in the feed solution. The characteristic of the selected membranes according to manufacturers as well as the permeability experimentally determined in this work are presented in Table 5.1.

Table 5.1 Characteristic of the UF membranes used in this work (data obtained from the manufacturer and experimentally)

Membrane	UH004	UP005	RC70PP	UH050
Manufacturer	Microdyn Nadir	Microdyn Nadir	Alfa Laval	Microdyn Nadir
Material	PESH[b]	PES[c]	RCA[d]	PESH[b]
MWCO[a] (kDa)	4	5	10	50
T max (˚C)	95	95	60	95
pH operating range	0 - 14	0 - 14	0 - 10	0 - 14
Permeability* ($L \cdot h^{-1} \cdot m^{-2} \cdot bar^{-1}$)	>27[e] 32.67[f]	>30[e] 44.07[f]	>40[e] 78.50[f]	>200[e] 191.75[f]

[a]MWCO: molecular weight cut-off; [b]PESH: Permanently hydrophilic polyethersulfone; [c]PES: Polyethersulfone; [d]RCA: Regenerated cellulose acetate; * water, at 25ºC; [e]: Manufacturer data; [f]: Experimentally determined in this work

All membranes were initially compacted for 3 hours at a transmembrane pressure of 3 bar. Then, the hydraulic permeability (K) of all the membranes was determined from experiments performed with osmotized water (conductivity <40 µS/cm) and it was calculated as the slope of the straight line obtained by plotting the water flux values measured at 25 °C, versus the applied TMP, following the Darcy's equation (Eq. 3):

$$J = K \cdot \Delta P = \frac{\Delta P}{\mu \cdot R_m} \quad (3)$$

Where J represents the water permeate flux at a specific TMP (ΔP), μ the viscosity of the permeate and R_m the intrinsic membrane resistance.

2.5 Cleaning protocol

The membranes were cleaned after each ultrafiltration experiment. Four cleaning protocols were proposed. Cleaning procedure one (C1) consisted of rinsing the membranes with osmotized water at 25°C for 40 min. Cleaning procedure two (C2) was performed under the same conditions as C1 except for the temperature (35°C). Cleaning procedure three (C3) included chemical cleaning with P3 Ultrasil 115 (1% v/v) (Ecolab, España) at 25°C for 30 min. Finally, cleaning procedure four (C4) was identical to C3 but varying the temperature (35°C). All of the cleaning methods were carried out at 2.2 $m \cdot s^{-1}$, with a TMP of 0.25 bar. The efficiency of the cleaning protocol was obtained by comparing the hydraulic permeability of the membrane before and after each experiment. The membrane was considered to be clean if the method led to recover more than 95% of the initial water permeability (P_0).

2.6 Analytical methods

The raw wastewater and the feed and permeate samples from the UF process were characterized, each parameter was measured in triplicate and the average value was calculated. Electrical conductivity (EC) and pH were determined by digital calibrated conductivity meter (EC-Meter GLP 31+) and pH-meter (GLP 21+), respectively, both from Crison, Spain. A D-112 turbidimeter (DINKO, Spain) was used to measure the turbidity following the UNE-EN ISO 7027 standard method. For colour determination (FZ, Farb-Zahl in German), the procedure proposed by Döepkens et al. (Döepkens et al., 2001) was followed. A DR600 spectrophotometer (Hach Lange, Germany) was utilized for the measurement of the absorbances at different wavelengths.

$$FZ = \frac{A_{436}^2 + A_{525}^2 + A_{620}^2}{A_{436} + A_{525} + A_{629}} \quad (4)$$

The FZ was calculated according to Eq. 4, where A_{436}, A_{525} and A_{620} are the absorbance values measured at 436, 525 and 620 nm, respectively.

Sugar concentration was determined by the Anthrone colorimetric method [23], where glucose (Panreac, Spain) was used as standard. The sugars present in the sample react with anthrone (Panreac, Spain) under acidic conditions, presenting a greenish blue colour. The total concentration of phenolic compounds was determined by means of the Folin-Ciocalteau method [24]. Tyrosol (VWR Chemicals, EE.UU) was used as standard and the results were expressed as milligrams of tyrosol equivalents per litter (mg ty eq·L^{-1}).

Oils and fats were measured using a modified Soxhlet protocol. The extraction process consisted of shaking 500 mL of sample with 250 mL of hexane (25°C) and letting it rest in a separating funnel for 30 min. The supernatant (which contains solvent + oils and fats) was extracted with the help of a pipette, then 250 mL of hexane were added to the rest, repeating the extraction process. This step was repeated 3 times. All supernatants (extracts) were filtered with a cellulose filter (45 μm pore diameter). They were then weighed before and after evaporation of the solvent (at 50 °C using a rotary evaporator). The difference in mass corresponded to the amount of oils and fats and the result was expressed in mg·L^{-1}.

The measurement of total suspended solids (TSS) was performed following the UNE 77034 standard method. The amount of TSS corresponded to the difference between the initial weight of a glass microfiber filter (1.2 μm pore size) and its weight after the filtration of 25 mL of sample and subsequent drying in an oven at 105˚C for 2 hours. The COD was measured using commercial kits supplied by Merck (Germany).

3 Results and discussion

3.1 Characterization of the feed samples

OOWW sample presented a dark green-brown colour due to the natural pigments of the olives. Two layers with different density were visibly distinguished. A large amount of fats and oils were clearly observed in the surface layer. The main physicochemical characteristics

of the OOWW before (raw OOWW) and after (PR-OOWW) the pretreatment are presented in Table 5.2.

Table 5.2. Characteristics of the raw and pretreated (PR) olive oil washing wastewater (OOWW).

Parameter	Raw OOWW	PR-OOWW	Reduction %
pH	5.09 ± 0.01	4.82 ± 0.01	5.3
Conductivity ($mS \cdot cm^{-1}$)	3.77 ± 0.25	3.44 ± 0.03	8.7
FZ[a] (colour index)	4.30 ± 0.11	2.58 ± 0.01	40.0
Turbidity (NTU[b])	364.2 ± 7.90	211.6 ± 1.25	41.9
TSS[c] ($mg \cdot L^{-1}$)	986.67 ± 15.92	397.20 ± 9.09	40.3
Sugars (mg glucose $\cdot L^{-1}$)	1645.32 ± 17.24	1334.75 ± 8.14	18.9
Oils and fats ($mg \cdot L^{-1}$)	308.15 ± 3.08	33.55 ± 0.81	89.1
COD[d] ($mgO_2 \cdot L^{-1}$)	23775 ± 238.17	17545 ± 220.61	26.2
TPhs[e] (mg tyrosol eq.$\cdot L^{-1}$)	1161.8 ± 13.43	1103.8 ± 9.32	5.0

[a] FZ: Farb-Zahl, colour index; [b] NTU: Nephelometric Turbidity Units; [c] TSS: Total suspended solids; [d] COD: chemical oxygen demand; [e] TPhs: Total phenolic compounds

The presence of a large amount of organic matter (COD around 24 $gO_2 \cdot L^{-1}$) as well as an acidic pH value (pH 5.09) in the raw wastewater can be highlighted from the results shown in Table 5.2. In addition, a high concentration of total phenolic compounds (more than 1 g of tyrosol-eq.$\cdot L^{-1}$) was found; among them hydroxytyrosol, tyrosol, succinic acid, oleuropein derivatives and other phenolic compounds [25]. A similar acidic profile was reported by Ochando-Pulido et al. [26], who characterized the OOWW from a two-phase centrifugal process. However, these authors reported lower values of COD (around 14 $gO_2 \cdot L^{-1}$) and total phenolic compounds (758.6 $mg \cdot L^{-1}$). This variation may be attributed to the different olive cultivars, since the composition qualitatively and quantitatively varies with the olive variety and with all the factors that affect olive growth and olive oil production (climate conditions, soil composition, cultivation practices, olives storage time and the extraction process [27]).

The presence of a high sugar content (around 1.6 g glucose$\cdot L^{-1}$) was expected, since, apart from phenolic compounds and organic acids, one of the main components of these

wastewaters are sugars [28]. The oil and fat content is within the range observed in other raw OMWs (200- 10000 $mg \cdot L^{-1}$) [1].

The samples also showed a high concentration of TSS (986.67 $mg \cdot L^{-1}$) and turbidity (364.2 NTU). These two parameters together with the colour (FZ), presented a decrease of around 40% after the pretreatment process. The reduction in the content of fats and oils was large, reaching an efficiency of 89.1%. This is important for the care of the membranes, as reported by Bolto, et al. [29]. These authors indicated that organic membranes, although they have advantages in oily wastewater treatment, such as low manufacturing cost, ease of processing and low energy requirements, show a relatively high tendency to fouling compared to inorganic membranes. This is due to the oil droplets, which adhere to the surface of the membrane. It leads to flux decay, due to heavy fouling, which implies a diminution of the membrane lifetime. According to organic matter values, the pretreatment managed to reduce the COD by 26% without affecting the total concentration of phenolic compounds (only 5% reduction).

An important point to note is that blockage of the filter was observed after filtering 50 litres of sample. However, the particles attached to the filter were easily removed with water. In industrial-scale applications, it is important to consider the life of the filter and also to choose the specific pore size after determining the particle size distribution of the solids in the sample [30].

3.2 Adsorption of phenolic compounds on the membranes

Since polyphenols can interact with the membranes [31], an adsorption test was made to find out whether the phenolic compounds were adsorbed on the different membranes considered in this work. Table 5.3 shows the amount of phenolic compounds adsorbed on each membrane.

Table 5.3. Adsorption of phenolic compounds on the surface of each membrane

Membrane	UH004	UP005	RC70PP	UH050
Amount adsorbed ($mg \cdot m^{-2}$)	0.331 ± 0.045	0.349 ± 0.014	0.195 ± 0.019	0.465 ± 0.037

Adsorption experiments demonstrated a higher affinity of phenolic compounds for the PES membranes compared to the RCA membrane. The measured values were of the same order of magnitude, although slightly lower, as those observed by Ulbricht et al. [32]. These authors reported a higher adsorption of wine polyphenols (tannic acid) on PES MF membranes (~0.7 $mg \cdot m^{-2}$) compared to polypropylene (PP) membranes (< 0.1 $mg \cdot m^{-2}$). According to Cassano et al. [33], the polar character of the PESH membranes would result in strong adsorption of polyphenols on the membrane, probably due to specific interactions between these compounds and the membrane itself (electron donor-receptor interactions, hydrogen bonds).

Although it was expected that the RCA membrane (RC70PP) had the highest adsorption due to its higher hydrophilicity (contact angle between 8°- 20° [34-35]), the lowest phenols adsorption was measured for this membrane. This may be due to specific characteristics of the membrane surface. Damar et al [35], observed that the hydraulic permeability values of the RC70PP membrane did not correlate with its hydrophilicity in comparison with the other membranes tested (ETNA10PP and GR73PP). These authors reported that this membrane yielded the lowest hydraulic permeability and, at the same time, the highest hydrophilicity. They concluded that this might be due to a reorientation of the active groups of the membrane upon contact with water or due to the effect of other surface characteristics such as pore size distribution, porosity, morphology, thickness and roughness. In this case, a rearrangement in the membrane matrix might generate a lower affinity of the membrane towards phenolic compounds. These authors also pointed out that the spongy pore morphology presented by the active layer of the RC70PP membrane caused greater resistance to water permeation. It should also be noted that these authors remarked that this membrane

had a high resistance to fouling. As adsorption is one of the causes of membrane fouling, it agrees with the low adsorption data observed.

The UH050 membrane presented the highest adsorption of phenolic compounds, 2.39 times the value of the membrane that produced the lowest adsorption (RC70PP). This was expected, as it is the most hydrophilic membrane (35 ° contact angle) compared to the other PES tested membranes. This can be explained due to the pore size, as the larger the pore size the more water is absorbed, which is reasonable, as there is more pore volume available to be filled with water. Furthermore, compared to membranes made of the same polymeric material (UH004), but with a smaller pore size, it retains more water than membranes with a smaller pore size due to capillarity [36].

UH004 and UP005 membranes presented similar phenolic compounds adsorption (0.327 and 0.365 $mg \cdot m^2$). Although the UH004 membrane has been modified to improve its hydrophilicity, the manufacturer reports both membranes as hydrophilic. This is confirmed by their contact angle values, which are practically the same (53° and 54° for the UH004 and UP005 membranes, respectively, according to [37-38]).

Li et al [31], analysed the effects of phenolic moieties present in dissolved organic matter (DOM) solutions on membrane fouling. These authors observed that the greater the presence of species with aromatic structures, the greater the adsorption on the surface of the membrane. This would explain the adsorption values of phenolic compounds observed for the membranes. The simulated water prepared for the adsorption tests had a similar concentration of phenolic compounds (1 $g \cdot L^{-1}$ phenolic compounds) to that of the OOWW (1.1 $gTyeq \cdot L^{-1}$). According to the results obtained, it was expected that the UH050 membrane presented greater fouling than the other membranes.

3.3 Hydraulic permeability of the membranes

The permeate fluxes obtained at different transmembrane pressures for all the tested membranes in the water permeability tests are shown in figure 5.2.

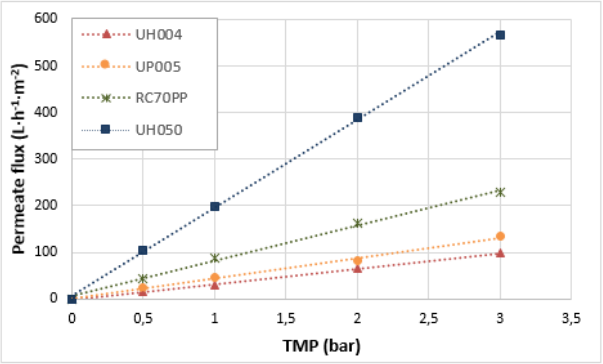

Fig. 5.2 Variation of permeate flux with transmembrane pressure (TMP) in the permeability tests for the different ultrafiltration membranes (osmotic water, 25°C)

With the Darcy equation (Equation 3), it was possible to estimate the hydraulic permeability for the UH004, UP005, RC70PP and UH050 membranes, which was 32.67, 44.07, 78.49 and 191.75 $L \cdot h^{-1} \cdot m^{-2} \cdot bar^{-1}$, respectively (with a regression coefficient (R^2) between 0.990 and 0.999). It was observed that the permeability value was directly related to the pore size, as expected. When water permeabilities were compared with those specified by the manufacturers (table 5.1), it was observed that all the experimental values were within the ranges provided (except for the UH050 membrane, whose measured permeability was slightly lower). The variability observed for the hydraulic permeability, which has been reported by different authors [39-40], may be due to several factors, such as the total number of TMP values considered for the permeability calculation, the compaction time, the different TMP values used in the experiments, the size of the membrane pieces used for the test and the configuration of the membrane module used.

3.4 Permeate fluxes in the ultrafiltration of pretreated OOWW

Fig. 5.3 shows the permeate flux obtained at different operating conditions when OOWW was ultrafiltered. As it can be observed, the UH004, UP005 and RC70PP membranes exhibited a similar variation of flux with TMP, since the increase in TMP produced an increment in the permeate flux within the range considered. The UP005 membrane exhibited the most remarkable growth of flux with TMP for all the CFVs tested. Thus, at the highest

TMP tested (2.5 bar) this membrane showed higher values of permeate flux than the other two, despite of having smaller pore size than the RC70PP membrane.

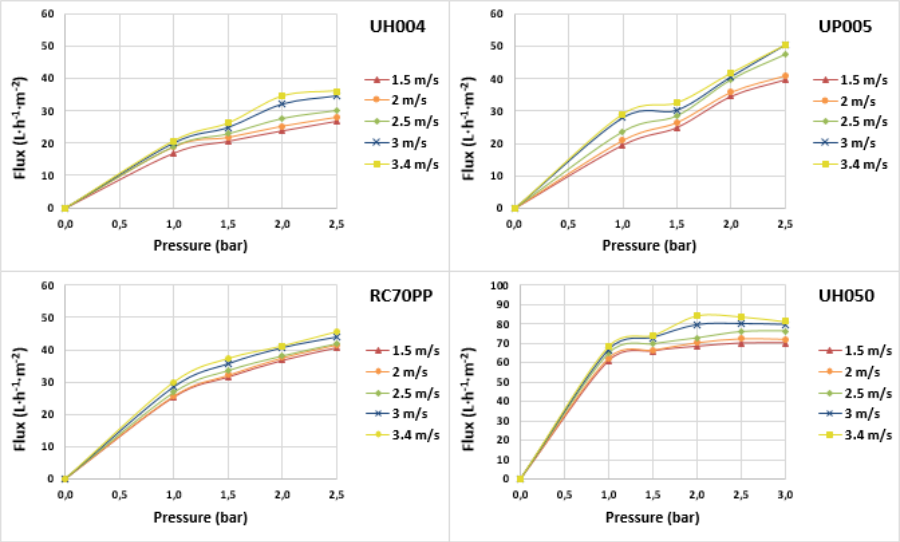

Fig. 5.3 Steady state permeate fluxes for the membranes tested when the pretreated wastewater was ultrafiltered at different operating conditions

On the other hand, for this three membranes, permeate flux was observed to increase with CFV too. For the UH004 and UP005 membranes the increment in flux with CFV was less noticeable when the values of CFV were high (variation from 3 to 3.4 $m \cdot s^{-1}$). The RC70PP membrane showed a small influence of CFV on permeate flux. Similar results were reported in a study performed by Sun, X. et al. [39]. These authors tested different membranes to ultrafilter a microalgae medium, observing that when CFV increased from 3.86 $m \cdot s^{-1}$ to 7.72 $m \cdot s^{-1}$ under a constant TMP of 2.3 bar, the RC70PP membrane showed a less pronounced increment in flux than the other membranes tested (polysulfone membrane GR40PP and fluoro polymer membrane FS40PP, both with a MWCO of 100 kDa). These authors attributed this observation to a relatively weaker binding of the cake layer to the membrane surface and a high intrinsic resistance of the membrane ($Rm > 6 \cdot 10^{12}$ m^{-1}).

For the UH050 membrane a different performance was observed, as the variation of flux with TMP was much smaller. This may be explained by the fact that the critical transmembrane pressure was reached and therefore the linear relationship between TMP and flux was lost [41]. At TMPs higher than 2 bar a stable flux was achieved at the lowest CFVs tested, while for the 2 highest CFVs, a slight decrease in flux was observed with increasing TMP. Thus, the limiting flux was reached. Therefore, it can be considered that a gel layer was formed on the surface of the membrane. Once a gel layer is formed, an increase in the TMP does not lead to an increase in the flux, but it increases the gel layer thickness. The reduction in permeate flux when TMP increases was also observed by other authors that ultrafiltered different feed streams [42]. The reduction in permeate flux with TMP can be due to the compaction of the gel layer. Moreover, this membrane presented the highest adsorption of phenolic compounds, as commented in section 2.2. This adsorption results in the formation of a monolayer of solutes on the surface of the membrane, representing an additional resistance for permeation [43]. For this membrane, the increase in flux with CFV was observed too.

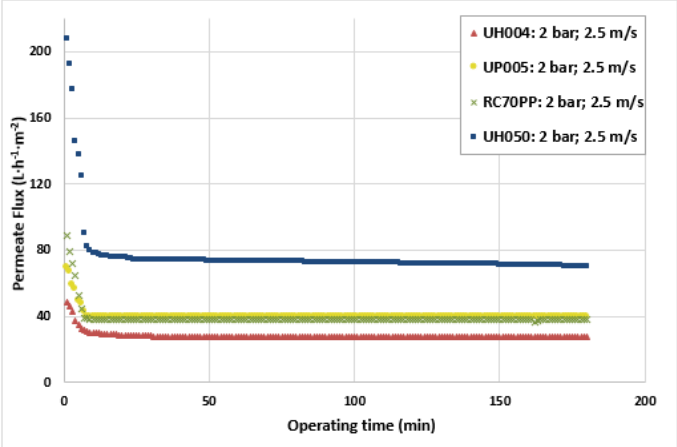

Fig. 5.4 Evolution of permeate flux with time for the different ultrafiltration membranes at a cross flow velocity of 2.5 m·s^{-1} and a transmembrane pressure of 2 bar (25°C)

The evolution of permeate flux with time at 2 bar and 2.5 $m \cdot s^{-1}$ is presented in Fig. 5.4. All the membranes exhibited a fast drop in the permeate flux at the beginning of the run, reaching stable values after the first minutes. The same trend was observed in all the tests carried out at the other operating conditions. The values of all of the stationary permeate fluxes were far from the permeate fluxes obtained with osmotized water (Fig. 5.2), indicating severe fouling. This variation of permeate flux with time, which is typical of UF processes, is due to two important effects: concentration polarization and membrane fouling. In the first minutes, a high amount of rejected particles is deposited on the membrane surface in a short time, which results in a rapid accumulation and compaction of foulants at the membrane surface. This accumulation of particles form a mass transfer boundary layer on the surface of the membrane, increasing the filtration resistance [44]. This is a particular problem in UF process, due to the presence of low and high molecular-weight solutes in the feed stream [45], appearing both of them in the OOWW too.

As expected, the UH050 membrane yielded the highest permeate flux at the beginning of the run (208.07 $L \cdot h^{-1} \cdot m^{-2}$), followed by the RC70PP membrane (82.59 $L \cdot h^{-1} \cdot m^{-2}$), which agreed with the corresponding molecular weight cut offs of the membranes. However, the UH050 membrane showed the greatest decrease in the permeate flux compared to the initial flux (60% - 65% reduction), presenting a slow and continuous flux decline as the operating time increased. Penha et al. [40] observed similar results when they tested five Microdyn-Nadir membranes (including UH004, UP005 and UH050) to pretreat mixtures of macauba oil and n-hexane before solvent separation. The UH050 membrane showed the greatest decrease in flux over time (50% - 70%). This indicates that the membrane presented severe fouling. As mentioned above, this can be attributed to the larger pore size of the membrane, which favours the passage of the solutes through the pores, blocking them partially. Moreover, this membrane showed the greater affinity for the phenolic compounds according to the adsorption tests performed. It is important to note that this behaviour was observed in all the tests performed at different operating conditions and it was more noticeable at the highest TMPs. As TMP increases, the convective transport of solute molecules towards the membrane surface is greater due to the increase in the driven force. Therefore, the amount of solute molecules that reach the membrane surface is higher and membrane fouling increases, observing a greater

decrease in the permeate flux. The UH004 membrane showed the smallest decrease in permeate flux during the test (42.1%), but the steady permeate flux was the lowest (27.96 $L \cdot h^{-1} \cdot m^{-2}$).

The RCA membrane presented lower fouling than the UH050 membrane, but higher than that observed for the UP005 and UH004 membranes. Although the RCA membrane initially showed higher flux than the UP005 membrane (82.59 $L \cdot h^{-1} \cdot m^{-2}$ vs 69.59 $L \cdot h^{-1} \cdot m^{-2}$), the steady flux was slightly higher for the UP005 (39.65 $L \cdot h^{-1} \cdot m^{-2}$ vs 38.16 $L \cdot h^{-1} \cdot m^{-2}$), which indicates that fouling was less severe for the UP005 membrane. This could be explained by the larger pore size of the RC70PP membrane in comparison with the UP005 membrane. More particle paths are observed in membranes with higher MWCO, favouring pore blocking, which generates greater resistance to the passage of fluid. Another aspect to take into account is the hydrophilicity of this membrane, which is the highest among the tested membranes. as it shows the lowest contact angle, as commented in section 2.2. As it was also indicated in that section, several authors concluded that the affinity of phenolic compounds for membrane materials increases when the hydrophilicity is greater [32-33]. Therefore, a higher irreversible fouling could be expected for this membrane compared to the UP005 and UH004 membranes.

For all the tested membranes, the highest permeate fluxes were observed at the highest TMP and CFV tested. For the selection of the best working conditions, not only a high permeate flux should be considered, but also if this increase is significant enough to make up for the increment of the energy costs caused by increasing TMP and/or CFV. All this, together with the rejection of both COD and phenolic compounds, will provide the best operating conditions for the process.

3.5 COD and Phenolic compound rejection

First of all, it is important to mention that, in all the performed UF tests, suspended solids were completely removed for all the tested membranes, as expected. Concerning permeate colour, UF permeates presented a slight yellowish pigmentation, despite having reduced the colour between 60% and 80%, depending on the membrane and operating

conditions. Fig. 5.5 shows the rejection of soluble COD and total phenolic compounds at the different operating conditions.

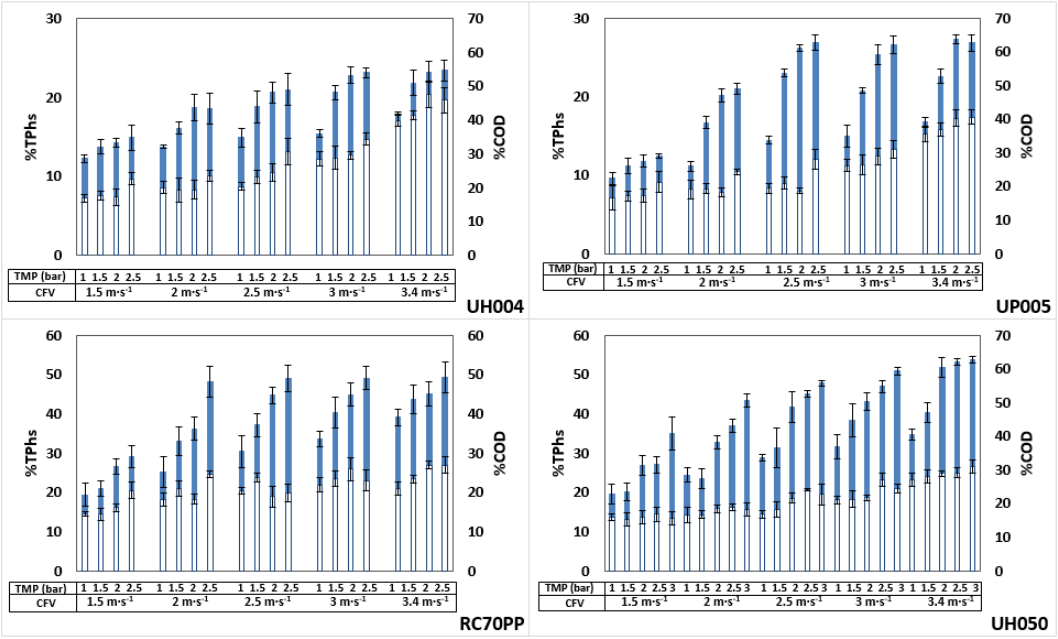

Fig 5.5 Steady state rejection of total phenolic compounds (white) and COD (blue), for all the ultrafiltration membranes tested at different operating conditions

In general terms, at low values of TMP and CFV, the greatest rejection of COD was observed for the UP005 and UH004 membranes, which was expected, as these membranes are the ones with the lowest MWCO. However, as TMP increased, the differences in COD removal efficiencies decreased, presenting all the membranes high percentages of COD rejection (greater than 50% in some cases). The behaviour of the UH004 and UP005 membranes was very similar, increasing COD rejection when TMP increased. Nevertheless, the influence of TMP on COD rejection became almost negligible at the highest values of CFV and TMP. In this case, the values of COD rejection at 2 and 2.5 bar were similar. The UH050 membrane presented the highest COD rejection (62.87% ± 1.68; at 3.4 $m \cdot s^{-1}$ and 3 bar), which

was very similar to the highest rejection yielded by the UP005 membrane (62.83% ± 1.20; at 3.4 $m \cdot s^{-1}$ and 2 bar). The high rejection of the membrane with the highest molecular weight cut-off (UH050) is again attributed to the severe membrane fouling observed for this membrane. The high concentration of solutes in the wastewater promoted the formation of a gel layer. This layer generated an extra resistance to the passage of solutes, thus increasing the rejection of COD. The increase in COD rejection with TMP can be attributed to the increase in solvent flux with TMP, but also to the increase in membrane fouling with this parameter, as the fouling layer creates an additional filtration layer.

COD rejection was observed to increase when CFV was raised. This can be attributed to the reduction in solute concentration on the membrane surface when CFV is raised, thus increasing the observed rejection. For all the membranes, the greatest influence of CFV on COD rejection was observed when this parameter increased from 1.5 to 2 $m \cdot s^{-1}$.

Regarding the rejection of phenolic compounds, for the UH004 and UP005 membranes, it increased significantly at CFVs higher than 2.5 $m \cdot s^{-1}$. The greatest change in phenolic compounds rejection was observed by increasing the CFV from 3 to 3.4 $m \cdot s^{-1}$ for the UH004 membrane (12.69% vs 20.44% at a fixed 2 bar) and from 2.5 to 3 $m \cdot s^{-1}$ for the UP005 membrane (8.01% vs 12.46% at a fixed 2 bar). For these two membranes, the increase in TMP generated as well an increase in the rejection of phenolic compounds, as expeted due to the increment in the permeate flux. The greatest increase in phenolic compounds rejection was observed when TMP was raised from 2 to 2.5 bar (8.01% vs 12.05% for the UP005 membrane and 10.54% vs 13.20% for the UH004 membrane, at a CFV of 2.5 $m \cdot s^{-1}$). However, for the RC70PP membrane, the effect of TMP and CFV on the rejection of phenolic compounds did not follow a regular trend. In addition, the influence of TMP on phenolic compounds rejection was not significant for the UH050 membrane, which is due to the fact that water permeate flux did not change with the TMP as explained in section 3.4.

Giacobbo, et al. [46], also observed an increase in polyphenols rejection with increasing TMP using wine lees from the second racking as feed solution. They explained that this behaviour is attributed to the fact that the higher the TMP, the more severe the phenomena of concentration polarization and fouling is, giving rise to an additional formation of selective

layers on the surface of the membrane, thus increasing the rejection coefficients. Other authors [47] also reported increases in the retention of phenolic compounds from oil mill wastewater with the increase in TMP. In this work, despite the variations with TMP and CFV, phenolic compounds were poorly retained by the tested membranes, which indicates that most of these compounds have molecular weights lower than the MWCO of the membranes. However, the increase in TMP led to a much less marked increase in the rejection of phenolic compounds compared to the increase in CFV.

The lowest rejections of phenolic compounds occurred at the lowest values of TMP and CFV (1.5 $m \cdot s^{-1}$ and 1 bar), being 7.11%, 7.27%, 13.83% and 14.47%, for the UP005, UH004, UH050 and RC70PP membranes, respectively. Phenolic compounds rejection for the first three membranes is in agreement with the adsorption values commented in section 3.2. The UP005 and UH004 membranes showed similar and small adsorption of phenolic compounds on the membrane surface, while it was greater for the UH050 membrane. The adsorption of phenolic compounds on the membrane could affect the values of rejection measured for these membranes. However, the RC70PP membrane presented the lowest adsorption of phenolic compounds and their rejection was the largest.

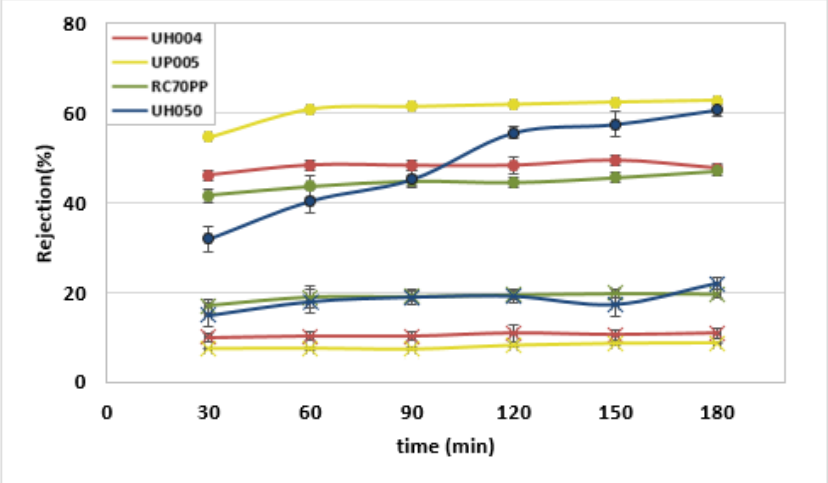

Fig. 5.6. Evolution of COD (•) and Total phenolic compounds (x) rejection with time for all the membranes tested at a cross flow velocity of 2.5 $m \cdot s^{-1}$ and transmembrane pressure of 2 bar (25°C)

It is important to note that the values shown in fig. 5.5 are average values. The evolution of the rejection of both COD and phenolic compounds over time was also studied. Fig. 5.6 shows the evolution of COD and phenolic compounds rejection during the operating time for all the tested membranes at the same operating conditions (2.5 $m \cdot s^{-1}$, 2 bar and 25°C). It can be seen that the UH004 and RC70PP membranes showed a quite stable rejection of COD over time, with a mean value of 48.05% and 44.63%, respectively. In the case of the rejection of phenolic compounds, the UH004 membrane presented a similar stable rejection with an average value of 10.50%. However, the RC70PP membrane presented a slight rejection increase of 9% in the first minutes, stabilizing after the first half hour of work with an average of value 19.01%. This could be attributed to the adsorption of phenolic compounds on this membrane as it is the more hydrophilic one [32-33]. In general, this behaviour was observed at all the operating conditions tested for these membranes. For the UP005 membrane, at high TMP and CFV values, rejection increased in the first minutes and then reached a stable value. The increase in rejection can be attributed to a rapid fouling of the membrane in the first minutes of work. For the operating conditions considered in Fig. 6, the membrane showed an increase in COD rejection from 54.6% to 60.9% in the first hour, and then it stabilized at 62%. The rejection of phenolic compounds was more stable and varied between 7.4 to 8.7% throughout the test.

However, in the case of the membrane with the largest MWCO (UH050), both rejections increased during the experiment and reached the highest value at the end (rejection of 60.8% and 22.1% for COD and phenolic compounds, respectively). The increase in rejection was much greater for COD, which increased by 28.8% in 150 minutes, while the rejection of phenolic compounds increased by 7.1% in the same time period. This can be attributed to a severe fouling of the UH050 membrane. From figure 5.3, the formation of a gel layer on the UH050 can be assumed, as previously commented. Moreover, as this membrane has large pores, pore blocking at the beginning of the UF process could also occur. Pore blocking could be due to compounds with adequate molar mass (size similar to that of the membrane pores) or to compounds with high affinity for the membrane, as this membrane showed the greatest adsorption of phenolic compounds in the adsorption tests. As a consequence, the size of the pores could be reduced, increasing the retention. After solute

adsorption, the formation of a gel layer would occur, which would further increase rejection, thereby generating an upward curve of rejection versus time. This is supported by the evolution of permeate flux versus time, which steadily decreased. As it will be commented in section 3.6, intensive cleaning protocols were necessary to recover the initial permeability of this membrane, which also indicates severe fouling.

The best operating conditions for each membrane were selected taking into account high permeate flux, high COD rejection and low rejection of phenolic compounds. These conditions are shown in table 5. 4.

Table 5.4. Best operating conditions for each membrane to obtain high permeate flux, high chemical oxygen demand rejection and low phenolic compounds rejection

Parameter	UH004	UP005	RC70PP	UH050
CFV[a] ($m \cdot s^{-1}$)	3.0	2.5	2.5	2.0
TMP[b] (bar)	2.0	2.0	2.5	3.0
Permeate Flux ($L \cdot h^{-1} \cdot m^{-2}$)	32.11	39.70	42.02	72.14
%COD[c] rejection	53.28 ± 2.50	61.18 ± 0.92	49.02 ± 3.98	50.58 ± 1.98
%TPhs[d] rejection	12.69 ± 0.50	8.01 ± 0.36	19.82 ± 0.90	15.59 ± 1.68

[a] CFV: cross flow velocity; [b] TMP: transmembrane pressure; [c] COD: chemical oxygen demand; [d] TPhs: Total phenolic compounds

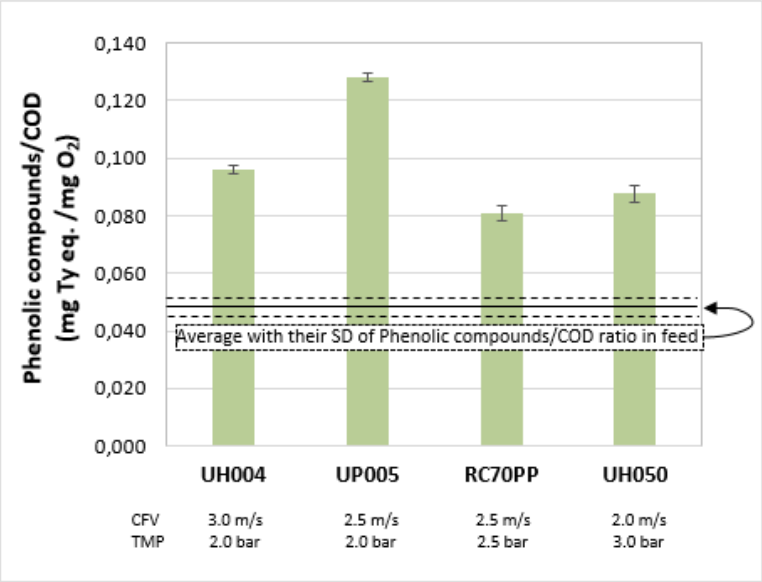

Fig 5.7. Phenolic compounds/chemical oxygen demand (COD) ratio in the permeate streams at the best operating conditions for each membrane

All the membranes showed good results in terms of low phenolic compounds retention with a significant decrease in the amount of organic matter in the permeate in comparison with the feed stream. Fig. 5.7 shows the phenolic compounds/COD ratio in the permeate streams at the best operating conditions for each membrane. In all the cases the ratio was greater than that in the feed, which indicates that the permeate was enriched in phenolic compounds. The UP005 membrane presented much higher permeate ratio (0.128 mgTyeq/mgO_2) than the rest of the membranes. In previous works [48] the UP005 membrane was compared to the UH030 membrane (Mycrodin nadir, Germany) to recover phenolic compounds from a residual brine from table olive production. The authors also obtained the best results with the UP005 membrane, but the ratio phenolic compounds/COD in permeate was lower (0.105 mgTyeq/mgO_2). The difference may be due to the different wastewater used. The phenolic compounds/COD ratios reached in the permeate are also higher than those reported by Casano et al. [33]. In their study, they tested four different membranes (two from PESH and two from RC) in the treatment of OMW. They observed that the RC, C010F membrane (Microdyn-Nadir, Germany) presented the greatest increase (approximately 1.2 times) in the ratio

compared to the feed (permeate ratio 0.142 vs feed ratio 0.118, approximate data). In our case, all the membranes achieved greater increases in the phenolic compounds/COD ratio, achieving 2.14 times the feed ratio with the best membrane (UP005). It is important to highlight that the results obtained with the UP005 membrane are very good and promising in view of the recovery of the phenolic compounds, since a great separation of them with respect to other organic compounds present in the wastewater was achieved, making the permeate highly enriched in phenolic compounds with small rejection of these compounds.

3.6 Cleaning results

After each test, the membranes were cleaned following the procedures previously described in section 2.4. Fig. 5.8 shows the average recovery of the hydraulic permeability of the membranes with regard to the permeability measured for the pristine membrane.

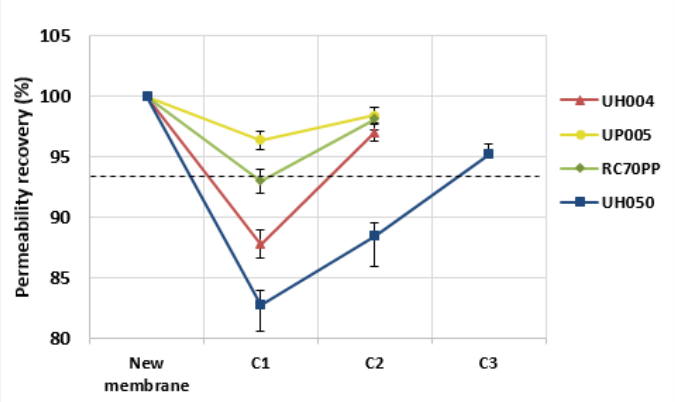

Fig 5.8. Average recovery of initial pure water permeability after the different cleaning protocols for the different tested membranes. C1: water at 25°C, C2: water at 35°C and C3: chemical cleaning with P3 Ultrasil 115 (1%) at 25°C

Except for the UH050, all the membranes were cleaned efficiently by means of a simple water rinsing, recovering at least 95% of the initial permeability (minimum value assigned to consider a membrane to be clean). The UP005 membrane only needed the first

cleaning method (water rinsing at room temperature) to achieve a permeability recovery of 96 ± 0.85% for all the ultrafiltration tests performed at the different operating conditions tested. The cleaning protocol C2 was also tested to evaluate if greater recovery was achieved, reaching a 98.4 ± 0.64% average permeability recovery. These results confirmed the low fouling observed for this membrane, since a linear increase in flux with increasing PTM was observed for all the CFVs tested (Fig.5.3). It also presented a stable permeate flux over time without a great difference compared to the initial flux (Fig. 5.4).

The RC70PP and UH004 membranes achieved a permeability recovery greater than 95% when they were cleaned with water at 35°C. This indicates that fouling was not severe. However, the UH050 membrane required the third cleaning method (C3), which involves chemical cleaning, to recover the permeability. The result was expected as this membrane presented the greatest adsorption towards phenolic compounds, the greatest decline in permeate flux with time (Fig. 5.4) and a progressive increase in rejection with time (Fig. 5.6). All this implies a severe fouling of the membrane and a greater difficulty to recover the membrane permeability.

Taking into account all the results commented, it can be established that the UP005 membrane was the one that presented the best results. This membrane exhibited the lowest rejection towards phenolic compounds (8%), a high rejection of COD (61%), a stable value of permeate flux (40 $L \cdot h^{-1} \cdot m^{-2}$) and it was easily cleaned.

4. Conclusions

In the present work, four UF membranes (UH004, UP005, RC70PP and UH050) were compared to ultrafilter pre-treated wastewater from olive oil production with the aim of obtaining a permeate enriched in phenolic compounds. Permeate flux decreased rapidly over time during the first few minutes of operation for all the membranes and operating conditions tested, which is indicative of membrane fouling. The UH050 membrane showed the greatest decrease in flux with time (60% -65%) due to the larger pore size and also to the highest adsorption of phenolic compounds observed onto the membrane material (0.463 ± 0.004 $mg \cdot m^{-2}$). The lowest flux decline (42%) was observed for the UH004 membrane. This

membrane also presented the lowest value of steady-state permeate flux (27.96 $L \cdot h^{-1} \cdot m^{-2}$), as it has the lowest pore size.

The UH004, UP005 and RC70PP membranes exhibited a similar influence of TMP on the flux, presenting a linear increase in the permeate flux with increasing TMP. The UP005 membrane exhibited the most remarkable flux growth with TMP for all CFVs tested. The permeate flux for the UH050 membrane was more influenced by CFV than by TMP, since the limiting flux was reached at 2 bar.

All the membranes were able to effectively remove suspended solids, colour, and COD, while the rejection of phenolic compounds was low. The highest rejection of COD (62.87% ± 1.09) was obtained with the UH050 membrane at a CFV of 3.4 $m \cdot s^{-1}$and 3 bar of TMP, and the lowest rejection of phenolic compounds (7.1% ± 1.55) was obtained with the UP005 membrane at a TMP of 1 bar and a CFV of 1.5 $m \cdot s^{-1}$. This last membrane presented the best performance, with a COD rejection of 61.18% and a phenolic compounds rejection of 8.01% (2.5 $m \cdot s^{-1}$CFV and TMP of 2 bar). It should be noted that all the membranes were able to enrich the permeate in phenolic compounds; obtaining ratios of phenolic compounds/COD between 1.5 to 2.1 times greater than the ratio in the feed.

The greater fouling of the UH050 membrane was confirmed by the cleaning protocol, since this membrane required a chemical cleaning with P3 Ultrasil 115 (1% v/v) to restore the initial water permeability, while the rest of the membranes were cleaned with a simple water rinsing. The UP005 membrane managed to recover its permeability by more than 95% just by cleaning with water at 25°C, confirming that this membrane suffered the less severe fouling, which can be related to the lowest hydrophilicity of the membrane material.

As the objective of this work was to select the membrane that presented the highest removal of organic matter without affecting the concentration of phenolic compounds (minimum rejection of phenolic compounds) with a high value of permeate flux and easy to clean, the UP005 membrane was observed to be the best option as a pretreatment for the recovery of phenolic compounds from this type of wastewater.

Acknowledgements

The authors acknowledge the financial support from the Spanish Ministry of Economy, Industry and Competitiveness through the project CTM2017-88645-R and The European Union through the Operational Program of the Social Fund (FSE).

References

[1] Z.S. Lee, S.Y. Chin, J.W. Lim, T. Witoon, C.K. Cheng, Treatment technologies of palm oil mill effluent (POME) and olive mill wastewater (OMW): A brief review, Environ. Technol. Innov. 15 (2019) 100377. https://doi.org/10.1016/j.eti.2019.100377.

[2] M. Volpe, D. Wüst, F. Merzari, M. Lucian, G. Andreottola, A. Kruse, L. Fiori, One stage olive mill waste streams valorisation via hydrothermal carbonisation, Waste Manag. 80 (2018) 224–234. https://doi.org/10.1016/j.wasman.2018.09.021.

[3] A. El-Abbassi, H. Kiai, J. Raiti, A. Hafidi, Application of ultrafiltration for olive processing wastewaters treatment, J. Clean. Prod. 65 (2014) 432–438. https://doi.org/10.1016/j.jclepro.2013.08.016.

[4] L. Ioannou-Ttofa, I. Michael-Kordatou, S.C. Fattas, A. Eusebio, B. Ribeiro, M. Rusan, A.R.B. Amer, S. Zuraiqi, M. Waismand, C. Linder, Z. Wiesman, J. Gilron, D. Fatta-Kassinos, Treatment efficiency and economic feasibility of biological oxidation, membrane filtration and separation processes, and advanced oxidation for the purification and valorization of olive mill wastewater., Water Res. 114 (2017) 1–13. https://doi.org/10.1016/j.watres.2017.02.020.

[5] R. Borja, F. Raposo, B. Rincón, Treatment technologies of liquid and solid wastes from two-phase olive oil mills, Grasas y Aceites. 57 (2006) 32–46. https://doi.org/10.3989/gya.2006.v57.i1.20.

[6] A.Y. Gebreyohannes, R. Mazzei, L. Giorno, Trends and current practices of olive mill wastewater treatment: Application of integrated membrane process and its future perspective, Sep. Purif. Technol. 162 (2016) 45–60.

https://doi.org/10.1016/j.seppur.2016.02.001.

[7] X. Sun, C. Wang, Y. Li, W. Wang, J. Wei, Treatment of phenolic wastewater by combined UF and NF/RO processes, Desalination. 355 (2015) 68–74. https://doi.org/10.1016/j.desal.2014.10.018.

[8] Z. Kaleh, S.U. Geißen, Selective isolation of valuable biophenols from olive mill wastewater, J. Environ. Chem. Eng. 4 (2016) 373–384. https://doi.org/10.1016/j.jece.2015.11.010.

[9] H.K. Obied, M.S. Allen, D.R. Bedgood, P.D. Prenzler, K. Robards, R. Stockmann, Bioactivity and analysis of biophenols recovered from olive mill waste, J. Agric. Food Chem. 53 (2005) 823–837. https://doi.org/10.1021/jf048569x.

[10] M. Abbas, F. Saeed, F.M. Anjum, M. Afzaal, T. Tufail, M.S. Bashir, A. Ishtiaq, S. Hussain, H.A.R. Suleria, Natural polyphenols: An overview, Int. J. Food Prop. 20 (2017) 1689–1699. https://doi.org/10.1080/10942912.2016.1220393.

[11] H.K. Obied, M.S. Allen, D.R. Bedgood, P.D. Prenzler, K. Robards, Investigation of Australian olive mill waste for recovery of biophenols, J. Agric. Food Chem. 53 (2005) 9911–9920. https://doi.org/10.1021/jf0518352.

[12] A. El-Abbassi, M. Khayet, A. Hafidi, Micellar enhanced ultrafiltration process for the treatment of olive mill wastewater, Water Res. 45 (2011) 4522–4530. https://doi.org/10.1016/j.watres.2011.05.044.

[13] A. Yangui, J.R. Njimou, A. Cicci, M. Bravi, M. Abderrabba, A. Chianese, Competitive adsorption, selectivity and separation of valuable hydroxytyrosol and toxic phenol from olive mill wastewater, J. Environ. Chem. Eng. 5 (2017) 3581–3589. https://doi.org/10.1016/j.jece.2017.06.037.

[14] F. Bazzarelli, E. Piacentini, T. Poerio, R. Mazzei, A. Cassano, L. Giorno, Advances in membrane operations for water purification and biophenols recovery/valorization from OMWWs, J. Memb. Sci. 497 (2016) 402–409.

https://doi.org/10.1016/j.memsci.2015.09.049.

[15] A. Nazir, K. Khan, A. Maan, R. Zia, L. Giorno, K. Schroën, Membrane separation technology for the recovery of nutraceuticals from food industrial streams, Trends Food Sci. Technol. (2019) 426–438. https://doi.org/10.1016/j.tifs.2019.02.049.

[16] M. Stoller, J.M. Ochando-Pulido, Going from a critical flux concept to a threshold flux concept on membrane processes treating olive mill wastewater streams, Procedia Eng. 44 (2012) 607–608. https://doi.org/10.1016/j.proeng.2012.08.500.

[17] J.M. Ochando-Pulido, G. Hodaifa, M.D. Victor-Ortega, S. Rodriguez-Vives, A. Martinez-Ferez, Reuse of olive mill effluents from two-phase extraction process by integrated advanced oxidation and reverse osmosis treatment, J. Hazard. Mater. 263P (2013) 158–167. https://doi.org/10.1016/j.jhazmat.2013.07.015.

[18] D.P. Zagklis, A.I. Vavouraki, M.E. Kornaros, C.A. Paraskeva, Purification of olive mill wastewater phenols through membrane filtration and resin adsorption/desorption, J. Hazard. Mater. 285 (2015) 69–76. https://doi.org/10.1016/j.jhazmat.2014.11.038.

[19] S. Al Aani, T.N. Mustafa, N. Hilal, Ultrafiltration membranes for wastewater and water process engineering: A comprehensive statistical review over the past decade, J. Water Process Eng. 35 (2020) 101241. https://doi.org/10.1016/j.jwpe.2020.101241.

[20] J.M. Ochando-Pulido, J.R. Corpas-Martínez, A. Martinez-Ferez, About two-phase olive oil washing wastewater simultaneous phenols recovery and treatment by nanofiltration, Process Saf. Environ. Prot. 114 (2018) 159–168. https://doi.org/10.1016/j.psep.2017.12.005.

[21] A. Sotto, J.M. Arsuaga, B. Van der Bruggen, Sorption of phenolic compounds on NF/RO membrane surfaces: Influence on membrane performance, Desalination. 309 (2013) 64–73. https://doi.org/10.1016/j.desal.2012.09.023.

[22] M. Ji, J. Luo, J. Wei, J. Woodley, A. Egede, Commercial polysulfone membranes pretreated with ethanol and NaOH : Effects on permeability, selectivity and antifouling

properties Separation and Puri fi cation Technology Commercial polysulfone membranes pretreated with ethanol and NaOH : E ff ects on , Sep. Purif. Technol. 219 (2019) 82–89. https://doi.org/10.1016/j.seppur.2019.03.020.

[23] B. Frolund, P. Rikke, K. Keiding, P.H. Nielsen, Extraction of extracellular polymers from activated sludge using a cation exchange resin, Water Res. 30 (1996) 1749–1758.

[24] V.L. Singleton, R. Orthofer, R.M. Lamuela-Raventós, Analysis of total phenols and other oxidation substrates and antioxidants by means of folin-ciocalteu reagent, Methods Enzymol. 299 (1999) 152–178. https://doi.org/10.1016/S0076-6879(99)99017-1.

[25] A. Jiménez-Herrera, Silvia; Ochando-Pulido, J.M.; Martínez-Ferez, Comparison between different liquid-liquid and solid phase methods of extraction prior to the identification of the phenolic fraction present in olive oil washing wastewater from the two-phase olive oil extraction system, Grasas y Aceites. 68 (2017) 1–13. http://dx.doi.org/10.3989/gya.0225171.

[26] J.M. Ochando-Pulido, J.R. Corpas-Martínez, J.A. Vellido-Perez, A. Martinez-Ferez, Optimization of polymeric nanofiltration performance for olive-oil-washing wastewater phenols recovery and reclamation, Sep. Purif. Technol. 236 (2020) 116261. https://doi.org/10.1016/j.seppur.2019.116261.

[27] C.I.L. Justino, R. Pereira, A.C. Freitas, T.A.P. Rocha-Santos, T.S.L. Panteleitchouk, A.C. Duarte, Olive oil mill wastewaters before and after treatment: A critical review from the ecotoxicological point of view, Ecotoxicology. 21 (2012) 615–629. https://doi.org/10.1007/s10646-011-0806-y.

[28] S. Dermeche, M. Nadour, C. Larroche, F. Moulti-Mati, P. Michaud, Olive mill wastes: Biochemical characterizations and valorization strategies, Process Biochem. (2013) 1532–1552. https://doi.org/10.1016/j.procbio.2013.07.010.

[29] B. Bolto, J. Zhang, X. Wu, Z. Xie, A review on current development of membranes for

oil removal from wastewaters, Membranes (Basel). 10 (2020) 1–18. https://doi.org/10.3390/membranes10040065.

[30] E.O. Akdemir, A. Ozer, Investigation of two ultrafiltration membranes for treatment of olive oil mill wastewater, Desalination. 249 (2009) 660–666. https://doi.org/10.1016/j.desal.2008.06.035.

[31] D. Li, X. Yang, Z. Zhou, B. Jiang, A. Tawfik, S. Zhao, Molecular traits of phenolic moieties in dissolved organic matter : Linkages with membrane fouling development, Environ. Int. 133 (2019) 105202. https://doi.org/10.1016/j.envint.2019.105202.

[32] M. Ulbricht, W. Ansorge, I. Danielzik, M. König, O. Schuster, Fouling in microfiltration of wine: The influence of the membrane polymer on adsorption of polyphenols and polysaccharides, Sep. Purif. Technol. (2009). https://doi.org/10.1016/j.seppur.2009.06.004.

[33] A. Cassano, C. Conidi, E. Drioli, Comparison of the performance of UF membranes in olive mill wastewaters treatment, Water Res. 45 (2011) 3197–3204. https://doi.org/10.1016/j.watres.2011.03.041.

[34] N.H. Abd-Razak, Y.M.J. Chew, M.R. Bird, Membrane fouling during the fractionation of phytosterols isolated from orange juice, Food Bioprod. Process. 113 (2019) 10–21. https://doi.org/10.1016/j.fbp.2018.09.005.

[35] I. Damar, K. Cinar, H.A. Gulec, Concentration of whey proteins by ultrafiltration: Comparative evaluation of process effectiveness based on physicochemical properties of membranes, Int. Dairy J. 111 (2020) 104823. https://doi.org/10.1016/j.idairyj.2020.104823.

[36] M.C. Proner, I.R. Marques, A. Ambrosi, K. Rezzadori, C. da Costa, G. Zin, M.V. Tres, M. Di Luccio, Impact of MWCO and dopamine/polyethyleneimine concentrations on surface properties and filtration performance of modified membranes, Membranes (Basel). 10 (2020) 1–18. https://doi.org/10.3390/membranes10090239.

[37] F.M. Penha, K. Rezzadori, M.C. Proner, V. Zanatta, G. Zin, D.W. Tondo, J. Vladimir De Oliveira, J.C.C. Petrus, M. Di Luccio, Influence of different solvent and time of pre-treatment on commercial polymeric ultrafiltration membranes applied to non-aqueous solvent permeation, Eur. Polym. J. 66 (2015) 492–501. https://doi.org/10.1016/j.eurpolymj.2015.03.010.

[38] M.J. Luján-Facundo, J.A. Mendoza-Roca, B. Cuartas-Uribe, S. Álvarez-Blanco, Evaluation of cleaning efficiency of ultrafiltration membranes fouled by BSA using FTIR-ATR as a tool, J. Food Eng. 163 (2015) 1–8. https://doi.org/10.1016/j.jfoodeng.2015.04.015.

[39] X. Sun, C. Wang, Y. Tong, W. Wang, J. Wei, Microalgae filtration by UF membranes: Influence of three membrane materials, Desalin. Water Treat. 52 (2013) 5229–5236. https://doi.org/10.1080/19443994.2013.813103.

[40] F.M. Penha, K. Rezzadori, M.C. Proner, G. Zin, L.A. Fogaça, J.C.C. Petrus, J.V. De Oliveira, M. Di Luccio, Evaluation of permeation of macauba oil and n-hexane mixtures through polymeric commercial membranes subjected to different pre-treatments, J. Food Eng. 155 (2015) 79–86. https://doi.org/10.1016/j.jfoodeng.2015.01.020.

[41] A. Cassano, C. Conidi, R. Ruby-Figueroa, R. Castro-Muñoz, Nanofiltration and tight ultrafiltration membranes for the recovery of polyphenols from agro-food by-products, Int. J. Mol. Sci. 19 (2018) 351. https://doi.org/10.3390/ijms19020351.

[42] M. Minhalma, M.N. De Pinho, Tannic-membrane interactions on ultrafiltration of cork processing wastewaters, Sep. Purif. Technol. 22–23 (2001) 479–488. https://doi.org/10.1016/S1383-5866(00)00169-6.

[43] P. Bacchin, P. Aimar, R.W. Field, Critical and sustainable fluxes: Theory, experiments and applications, J. Memb. Sci. 281 (2006) 42–69. https://doi.org/10.1016/j.memsci.2006.04.014.

[44] J.M. Ochando-Pulido, A review on the use of membrane technology and fouling control for olive mill wastewater treatment, Sci. Total Environ. 563–564 (2016) 664–675. https://doi.org/10.1016/j.scitotenv.2015.09.151.

[45] X. Shi, G. Tal, N.P. Hankins, V. Gitis, Fouling and cleaning of ultrafiltration membranes : A review, J. Water Process Eng. 1 (2014) 121–138. https://doi.org/10.1016/j.jwpe.2014.04.003.

[46] A. Giacobbo, A.M. Bernardes, M.N. de Pinho, Sequential pressure-driven membrane operations to recover and fractionate polyphenols and polysaccharides from second racking wine lees, Sep. Purif. Technol. 173 (2017) 49–54. https://doi.org/10.1016/j.seppur.2016.09.007.

[47] S. Sanches, M.C. Fraga, N.A. Silva, P. Nunes, J. Crespo, V.J. Pereira, Pilot scale nanofiltration treatment of olive mill wastewater: a technical and economical evaluation, Environ. Sci. Pollut. Res. 24 (2017) 3506–3518. https://doi.org/10.1007/s11356-016-8083-1.

[48] C. Carbonell-Alcaina, S. Álvarez-Blanco, M.A. Bes-Piá, J.A. Mendoza-Roca, L. Pastor-Alcañiz, Ultrafiltration of residual fermentation brines from the production of table olives at different operating conditions, J. Clean. Prod. 189 (2018) 662–672. https://doi.org/10.1016/j.jclepro.2018.04.127.

V.2. Use of ultrafiltration ceramic membranes as a first step treatment for olive oil washing wastewater

ELSEVIER

Food and Bioproducts Processing

Volume 135, September 2022, Pages 60-73

Use of ultrafiltration ceramic membranes as a first step treatment for olive oil washing wastewater

Magdalena Cifuentes-Cabezas [a, 1], María Cinta Vincent-Vela [a, b], José Antonio Mendoza-Roca [a, b], Silvia Álvarez-Blanco [a, b]

Show more

+ Add to Mendeley Share Cite

https://doi.org/10.1016/j.fbp.2022.07.002

Abstract

Olive oil is a food product in great demand throughout the world, its production generating large volumes of wastewater with a high organic load, where phenolic compounds are present. These compounds have outstanding antioxidant characteristics, so their recovery is of great interest. In this way, the treatment of these wastewaters should be based on reusing water and, at the same time, on recovering valuable compounds. Ultrafiltration with ceramic membranes (5, 15 and 50 kDa) is proposed as a first treatment step for olive oil washing wastewater (OOWW) from the continuous two-phase centrifugation process. The effect of cross flow velocity and transmembrane pressure was evaluated against permeate flux values and the removal of turbidity, colour, chemical oxygen demand (COD), sugars and the phenolic

compounds recovery. The CFV had a great influence on the removal of colour and turbidity. COD rejection increased with increasing TMP, being the highest rejection obtained under the most extreme conditions. The rejection of phenolic compounds and sugars did not show great variation between conditions. The 50 kDa membrane was the one that presented the largest permeate flux decline and the lowest permeability recovery after the cleaning, confirming the great fouling that this membrane suffered. The 15 kDa membrane at the operating conditions of 3 $m.s^{-1}$ and 3 bar was observed as a good option to eliminate much of the colour (72%) and turbidity (99%) and to reduce considerably the organic load (54%) without greatly affecting the concentration of phenolic compounds (rejection of 21%) for future recovery.

Keywords Ultrafiltration, ceramic membranes, olive oil washing wastewater, phenolic compounds, Industrial wastewater, Wastewater reuse

1. Introduction

Nowadays generation of wastewater is inevitable. The increasing demand for water, caused by the increase in economic activity, and the subsequent rapid industrial growth, has caused an abundant production of wastewater every year. Therefore, to face the threat of water scarcity, the purification or treatment of industrial wastewater is an essential factor to be considered [1].

These industrial activities generate wastewaters that vary significantly, with each industrial sector generating its own mix of pollutants. In the Mediterranean countries, one of the main sources of contamination is wastewater from olive oil mills (OMW), seasonally generated during the olive oil extraction process in the October-December season. Depending on the olive oil extraction methodology used, different wastewaters are generated. Of the three extraction processes (mechanical pressing, two-phase centrifugation and three-phase centrifugation), the centrifugation processes are the most widely used. These processes receive their name from the different phases that are obtained after the centrifugation of the olive paste to obtain olive oil. A horizontal decanter is used for this purpose. The three-phase centrifugation generates a solid waste, a raw olive oil and a wastewater; while the two-phase centrifugation process releases a wet solid phase and a raw olive oil. These two processes

differ mainly in water consumption. Water is added in the three-phase process in the horizontal decanter unlike in the two-phase process [2]. The less amount of water used is the reason why two-phase centrifugation is considered a more ecological process than the three-phase centrifugation [3]. In both processes, after the horizontal centrifugation, the raw oil is processed with a vertical centrifuge to remove residual water and solid particles, obtaining a clear virgin olive oil. Currently in Spain, the world's largest producer of olive oil in the world, the continuous two-phase centrifugation process is used in practically all the oil mills. Two types of wastewaters are generated in this centrifugation process: wastewater from olive washing (WOW) and wastewater from olive oil washing (OOWW) [4].

Some studies have reported that WOW does not present an environmental problem (chemical oxygen demand (COD) <1 g $O_2 \cdot L^{-1}$) and can be used directly for irrigation or reused after a simple physical-chemical treatment. The case of OOWW is different, since it constitutes a serious environmental problem due to its high content of organic matter (COD between 3 $gO_2 \cdot L^{-1}$ and 15 $gO_2 \cdot L^{-1}$) [5]. Apart from a high COD, another problem comes from the presence of phenolic compounds, which have a negative effect on the biological treatment of OOWW. However, these compounds are widely known for their outstanding properties, such as anti-inflammatory, antimicrobial and antioxidant activity, inhibition of oxidative damage and elimination of free radicals, being highly valued by the pharmaceutical, cosmetic and food sectors [6-7].

Several alternatives have been considered for the treatment of OMW, such as physical, chemical and biological (aerobic and anaerobic) treatments and membrane processes [8]. Membrane processes can be classified according to the driving force of separation. Among them, there are four processes where the driving force is provided by pressure. These can be classified according to the pore size distribution of the membrane and to the size of the retained substances. These processes are microfiltration (MF), ultrafiltration (UF), nanofiltration (NF), and reverse osmosis (RO). Membranes can also be grouped according to the materials used in their preparation (polymeric or ceramic membranes) [9]. Polymeric membranes have been widely studied and they are mainly used in industrial water filtration processes. On the other hand, ceramic membranes have been studied in a limited way, due to

several factors, one of the most important being the high manufacturing cost. However, in recent years, research on the applications of ceramic membranes in water treatment has attracted increased attention. This is due to the existing development, giving them greater mechanical, thermal and chemical stability, greater resistance to fouling and greater longevity of the membrane, favouring themselves to challenge water purification processes, such as textile wastewater treatment, oil-water separations and pharmaceutical wastewater treatment [10-12]. Although the use of ceramic membranes for the treatment of olive mill wastewater has already been studied [13], most of the published works are focused on the use of these membranes in membrane bioreactor (MBR) systems [14-15]. In addition, in olive mills, unlike the wastewater produced in the three-phase centrifugation process, the effluent from the two-phase centrifugation process has been hardly studied. Of the three extraction processes (mechanical pressing, two-phase centrifugation and three-phase centrifugation), the centrifugation processes are the most widely used. These processes receive their name from the different phases that are obtained after the centrifugation of the olive paste to obtain olive oil. A horizontal decanter is used for this purpose. The three-phase centrifugation generates a solid waste, a raw olive oil and a wastewater; while the two-phase centrifugation process releases a wet solid phase and a raw olive oil. These two processes differ mainly in water consumption. Water is added in the three-phase process in the horizontal decanter unlike in the two-phase process [2]. The less amount of water used is the reason why two-phase centrifugation is considered a more ecological process than the three-phase centrifugation [3]. In both processes, after the horizontal centrifugation, the raw oil is processed with a vertical centrifuge to remove residual water and solid particles, obtaining a clear virgin olive oil. Although the three-face process is the most widely used today, because the two-face process is more environmentally friendly, it is expected that the olive oil industry will adopt this production process in the future.

The main objective of this work was to evaluate the efficacy of ultrafiltration with ceramic membranes as a possible pre-treatment for a two-phase OOWW. For this, three Tami ceramic membranes with different molecular weights were tested in order to reduce the colour, turbidity, sugars and organic load of the wastewater, without significantly affecting the concentration of phenolic compounds in view of a future recovery of these compounds from

the UF permeate. All membranes were tested under the same parameters, varying the cross flow velocity (CFV) and transmembrane pressure (TMP). There are very few studies carried out with ceramic membranes for the treatment of olive mill wastewater, the majority being with microfiltration membranes. On the other hand, almost all of the phenolic compound recovery works focus on wastewater from the three-phase process, with very few contemplating the two-phase process and none using ultrafiltration with ceramic membranes for this purpose. In addition, due to the numerous advantages of the two-phase process, especially from the environmental point of view, it will gain importance, which reinforces the interest of this work. Therefore, this study aims to expand the use of ceramic ultrafiltration membranes to remove the organic load from this type of wastewater.

2. Material and Methods

2.1 Wastewater samples

The wastewater samples correspond to olive oil washing wastewater (OOWW) obtained at the outlet of the vertical centrifuge in the continuous two-phase centrifugation process. The samples were provides by a Cooperative located in the Valencian Community in Spain. The sample were taken the same day and stored at -20°C, to avoid degradation.

2.2 Ultrafiltration procedure

Before the ultrafiltration stage, the effluents were pre-treated by flotation, sedimentation and filtration with a cartridge filter (60 μm), following the procedure explained in [16]. This treatment removes most of the larger particles, suspended solids and oils and fats from the effluent, which can cause severe fouling of the membrane or damage to the ultrafiltration module and the plant.

The ultrafiltration experiments were carried out a laboratory-scale membrane plant (Orelis, France) (Fig. 5.9), where a tubular membrane module (Carbosep, Oreli Industriess, France) was installed. The experiments were carried out in full recycling filtration mode. Thus, the concentrate and permeate streams were continuously recirculated to the feed tank. Every 30 minutes, approximately 50 mL of permeate was collected for further analysis. A precision

balance (Kern, Germany) was used to gravimetrically determine the permeate flux through the weight of the permeate. The measurements were recorded by a data acquisition system. During all the tests the temperature was kept constant around 25 °C (± 1) by means of a cooling jacket surrounding the feed vessel and a heat exchanger.

Three seven channel INSIDE CéRAM^{TM} tubular ceramic membranes (Tami Industries, France) of different MWCO with an effective area of 132 cm^2 and 20 cm length were tested. The characteristics of these commercial membranes are shown in Table 5.5.

Table 5.5 Characteristic properties of the UF ceramic membranes tested in the experiments, manufacturer, literature and experimental data

	INSIDE-CéRAM^{TM} ultrafiltration membranes		
Support layer	TiO_2	TiO_2	TiO_2
Active layer	TiO_2 thin layer	ZrO_2	ZrO_2
MWCO[a] (kDa)	5	15	50
Pore size (nm)	2 – 4[b]	-	8.6[c]
T max (°C)	300	300	300
pH range	0 - 14	0 - 14	0 - 14
Contact angle (°)	40[d]	43.8[e]	42.4[e]
Roughness (nm)	42[b]	17.90[f]	27.13[f]
Permeability	>80[a]	>80[a]	>210[a]
($Lh^{-1}m^{-2}bar^{-1}$)	97.38[h]	100.37[h]	220.77[h]

[a]: manufacturer data [17]; [b]: [18]; [c]: [19]; [d]: [20]; [e]: [21]; [f]: [22]; [g]: Water at 25°C; [h]: Experimentally determined in this study

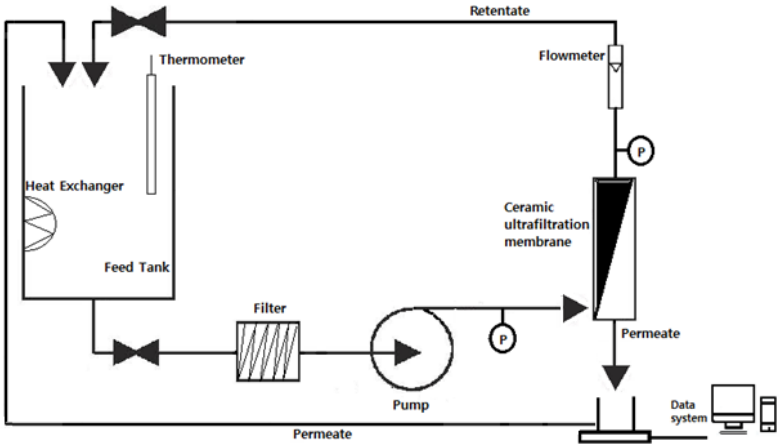

Fig. 5.9 Diagram of the ultrafiltration laboratory scale plant.

The aim was to study the evolution of the permeate flux over time as well as the rejection of colour, turbidity, COD, sugars and phenolic compounds, varying the crossflow velocity (CFV) and the transmembrane pressure (TMP). The CFV was varied between 2 and 4 $m \cdot s^{-1}$ and the TMP between 1 and 3 bar. The duration of each test was 3 hours, which was enough time to reach the steady permeate flux. These operating conditions were selected to be comparable with other studies carried out with ultrafiltration membranes. Working ranges between 0.8 - 2.8 TPM and CFV of 3.9 - 5 ms^{-1} have been reported for the treatment of olive mill wastewater with ceramic microfiltration and ultrafiltration membranes [13,14,23,24]. On the other hand, similar ranges of operating conditions have been studied by other authors using the same membranes as in this study for the treatment of different wastewaters [25,26].

The efficiency of the membrane was evaluated by calculating the removal efficiency of colour and turbidity (Eq. 1) and the rejection of COD, sugars or phenolic compounds (Eq. 2).

$$E_i(\%) = \left(1 - \frac{V_{Pi}}{V_{Fi}}\right) \times 100 \quad (1)$$

$$R_j(\%) = \left(1 - \frac{C_{Pj}}{C_{Fj}}\right) \times 100 \quad (2)$$

Where E_i is the removal efficiency of parameter *i* (colour or turbidity) in %, V_{Pi} is the value of parameter *i* in the permeate stream, V_{Fi} is the value of parameter *i* in the feed solution, R_j is the rejection of parameter *j* (COD, sugars or phenolic compounds) in %, C_{Pj} is the concentration of parameter *j* in the permeate stream and C_{Fj} is the concentration of parameter *j* in the feed solution.

After each experiment, the membranes were rinsed with tap water for 30 minutes. Then four cleaning protocols were proposed. Two of them were carried out with osmotic water varying the temperature (C_1 at 25 °C and C_2 at 35 °C). The other two protocols consisted of chemical cleaning using P3 Ultrasil 115 (Ecolab, Spain) at 1% v/v at different temperatures (C_3 at 25 °C and C_4 at 35 °C). This chemical was selected since its testified effect to reduce organic fouling [25]. All cleaning methods were carried out at 2 $m \cdot s^{-1}$, with a TMP of 0.5 bar for 40 minutes. Before and the cleaning, the membranes were rinsed with osmotic water and then the hydraulic permeability and verify the cleaning effectiveness. The hydraulic permeability (K) of all the membranes was calculated following the Darcy's equation (Eq. 3). Hydraulic permeability was determined with osmotized water at 25 °C, at TMPs of 0.5, 1, 2 and 3 bar.

$$J = K \cdot \Delta P = \frac{\Delta P}{\mu \cdot R_m} \quad (3)$$

With *J* representing the osmotic water permeate flux at a specific TMP (ΔP), μ the viscosity of the permeate and *Rm* the intrinsic membrane resistance. The membranes were considered to be clean if after the cleaning at least 90% of the initial osmotic water permeability was reached.

2.3 Analytical methods

A GLP 31+ conductivity-meter and a GLP 21+ pH-meter (Crison, Spain) were used for the conductivity and pH measurement, respectively. For the turbidity, the D-112 (DINKO, Spain) device was used following the UNE-EN ISO 7027 standard method. Colour (FZ) was calculated by spectral absorption coefficient [27], measuring the absorbances at 436, 525 and 620 nm with a DR600 spectrophotometer (Hach Lange, Germany). Anthrone colorimetric method [28] was used for sugar content determination and Folin-Ciocalteau method [29] for

the measurement of total phenolic compounds concentration. Total suspended solids (TSS) were assessed following the UNE 77034 standard method [30]. Oils and fats ($mg \cdot L^{-1}$) were measured by mass difference before and after an extraction process (modified Soxhlet protocol), and finally commercial kits (Merck, Germany) were used for COD measurement.

2.4 Particle size distribution

To evaluate the possible fragmentation of the particles present due to the turbulence generated on the membrane surface, it was decided to analyse the particle size distribution. For this, the feed samples were analysed before and after the experimental tests. The particle size distribution was determined by Dynamic Light Scattering using the Zetasizer Nano ZS90 equipment (Malvern Instruments Ltd., UK).

3. Results and discussion

3.1 Characterization of OOWW samples

The main physicochemical characteristics of the raw and pre-treated OOWW (PR-OOWW) are shown in Table 5.6. In general, OMWs are slightly acidic, red to black coloured with high conductivity and organic matter concentration [31]. In this case, the acidic profile (pH 5.09) and the high organic content (around 22 $gO_2 \cdot L^{-1}$) were also observed. However, a yellow-green colour was predominant in the samples. Furthermore, their conductivity was not very high ($3.77 \pm 0.25\ mS \cdot cm^{-1}$). The samples presented a high concentration of total phenolic compounds (around 1.2 g Tyrosol $eq \cdot L^{-1}$). This was expected since OMWs are a good source of phenolic antioxidants (1–1.8% w/v), and according to Çelik et al. [32] around 90% of the phenolic compounds presented in the olives are transferred to the wastewaters, obtained during the production process. This is due to the polar nature of oil mill wastewater compared to the non-polar nature of olive oil [33].

Table 5.6 Characterization results of raw (OOWW) and pre-treated (PR-OOWW) olive oil washing wastewater

Parameter	Raw OOWW	PR-OOWW
pH	5.09 ± 0.01	4.82 ± 0.01
Conductivity ($mS \cdot cm^{-1}$)	3.77 ± 0.25	3.44 ± 0.03
FZ[a] (colour)	4.30 ± 0.01	2.58 ± 0.01
Turbidity (NTU)	364.2 ± 7.9	211.6 ± 1.2
TSS[b] ($mg \cdot L^{-1}$)	986.67 ± 15.92	397.20 ± 9.09
Sugars ($mgGlucose \cdot L^{-1}$)	1645.32 ± 17.24	1334.75 ± 8.14
Oils and fats ($mg \cdot L^{-1}$)	308.15 ± 3.08	33.55 ± 0.81
Dissolved COD[c] ($mgO_2 \cdot L^{-1}$)	23775.3 ± 238.2	17544.8 ± 220.6
TPhC[d] ($mgTyrosol\ eq \cdot L^{-1}$)	1161.80 ± 13.43	1103.80 ± 9.32

[a] FZ: Farb-Zahl, colour measure; [b] TSS: Total suspended solids; [c] COD: chemical oxygen demand; [d] TPhC: Total phenolic compounds

The high concentration of TSS (986.67 ± 15.92$mg \cdot L^{-1}$) and turbidity (354 ± 7.9 NTU) emphasizes the importance of a pre-treatment before the UF process for the removal of large particles that can severely damage both the membranes and the plant. Similar physicochemical characteristics were observed in other studies carried out by Ochando-Pulido et al. [34-35] It is important to highlight that the composition of the OMWs not only depends on the olive oil extraction process, but it also changes with the variety of olive, the climatic conditions and the cultivation practices [36].

Although the pre-treatment only decreased the content of organic matter (COD) by 26%, turbidity, colour and suspended solids concentration were reduced to a higher extent (around 40%). Regarding fats and oils, their elimination was very high, close to 90%. Their removal was very important as they have been demonstrated to have a great potential to foul the membranes [37]. The other parameters did not show great change, which is positive for the objective of the process, since the pre-treatment aimed to eliminate the largest organic particles, without affecting the concentration of phenolic compounds for their subsequent recovery.

3.2 Ultrafiltration: Hydraulic permeability of the membranes and permeate fluxes of the different conditions tested

The variation of permeate flux with TMP using osmotic water as feed for each membrane is shown in Fig. 5.10. By fitting osmotic water permeate flux against TMP, it was possible to calculate the hydraulic permeability for the membranes tested, according to Eq. 3. This parameter is characteristic of each membrane and was used to analyse the fouling produced when working with OOWW.

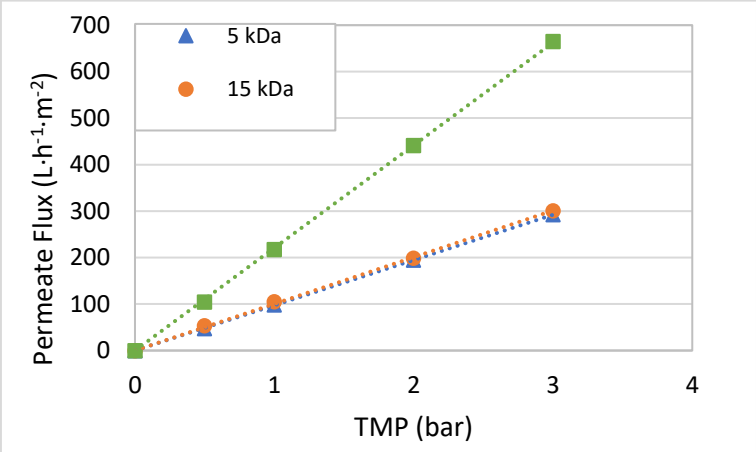

Fig. 5.10 Variation of permeate flux with transmembrane pressure for the different ultrafiltration membranes when osmotic water was used as feed (25 °C)

For the 5, 15 and 50 kDa MWCO membranes the hydraulic permeabilities were 97.38, 100.37 and 220.77 $L \cdot m^{-2} \cdot h^{-1} \cdot bar^{-1}$, respectively, with regression coefficients being higher than 0.998. According to the Hagen-Poiseuille equation, the value of the permeate flux must be proportional to the pore size of the membrane [38]. However, in this case, the hydraulic permeability of the 15 kDa membrane was practically the same as that of 5 kDa one. This was not expected, but it is consistent with the information provided by the manufacturer (section 2.2). On the other hand, a similar phenomenon was also observed by other authors. Majewska-

Nowak [39] studied four ceramic membranes (also supplied by TAMI Industries) of different MWCO (1, 5, 8, and 15 kDa) for the separation of dyes. They pointed out that the permeability of these membranes did not show significant differences despite of their different MWCO, being the hydraulic permeability of the 1 kDa membrane greater than that of the 5 and 8 kDa membranes. This may mean that for, these Tami Inside ceramic membranes, pore size was not a key factor in the permeate flux value; and there are other factors that also influence the permeability of the membranes, such as surface porosity and the tortuosity of the pores.

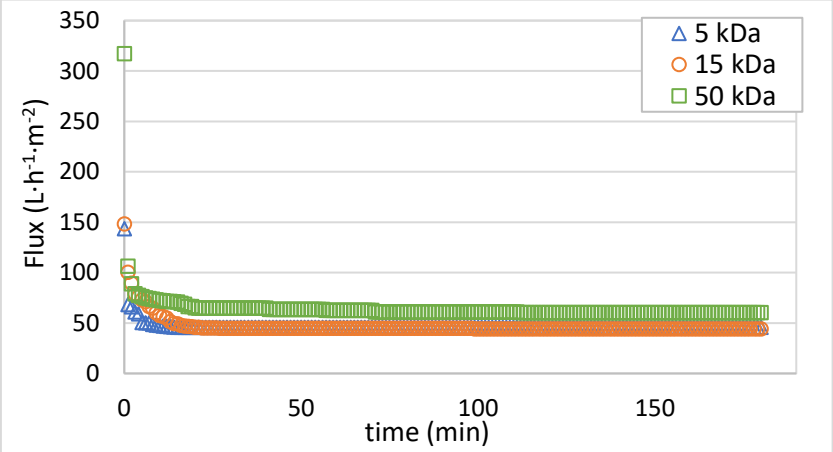

Fig. 5.11 Evolution of permeate flux with time for the tested ceramic membranes at a cross flow velocity of 3 $m \cdot s^{-1}$ and a transmembrane pressure of 1.5 bar (25°C) during pre-treated olive oil washing wastewater (PR-OOWW) ultrafiltration

Regarding the tests with OOWW, Fig. 5.11 shows permeate flux decline over time for the tests performed at 3 $m \cdot s^{-1}$ and 1.5 bar using PR-OOWW as feed. A sharp decrease in permeate flux was observed in the first minutes. After that sharp drop, there was a gradual but slow decrease in permeate flux, reaching afterwards almost constant values. The same trend was observed for all the operating conditions considered. The decrease in permeate flux with time is mainly due to two phenomena: the accumulation and adsorption of molecules, gels and particles (fouling) on the surface of the membrane and inside the membrane pores and also an

increase in the concentration of particles and solutes in a layer adjacent to the membrane surface due to convective transport, which causes concentration polarization phenomena, affecting the performance of the membrane [40]. The 50 kDa membrane was the one that presented the greatest decrease in permeate flux in the first minutes (from 320 to 106 $L \cdot h^{-1} \cdot m^{-2}$ at the conditions considered in Fig. 5.11). This was observed in all the tests carried out, being more pronounced at the most extreme conditions (highest CFV and TMP). This can be related to the size of the membrane pores. As previously mentioned, the 50 kDa membrane presented the highest hydraulic permeability. Thus, the convective transport towards this membrane was expected to be the highest, generating a high concentration of solutes on the surface of the membrane. Moreover, this concentration polarization phenomenon favours fouling and gel layer formation, which also cause a flux drop over time. On the other hand, fouling is more severe when there difference between the MWCO of the membrane and the molecular weight of the solute molecules is small, as observed by several authors [22-25]. Therefore, the large flux decay for the 50 kDa membrane may also be due to a blockage of the pores by substances with similar size to that of the membrane pores, which directly affects the selectivity of the membrane. This will be discussed again in section 3.3.

As in the case of the hydraulic permeability (Fig. 5.10), the 5 and 15 kDa membranes showed similar permeate flux values. This was observed for almost all tested operating conditions. Only under the operating conditions of 2 bar and 4 $m \cdot s^{-1}$ the 5 kDa membrane presented higher but less stable fluxes compared to the 15 kDa membrane. The similar fluxes were also observed when steady permeate flux was plotted against TMP (Fig. 5.12). Then again, the 50 kDa membrane presented higher values of steady permeate flux due to its larger pore size and hydraulic permeability.

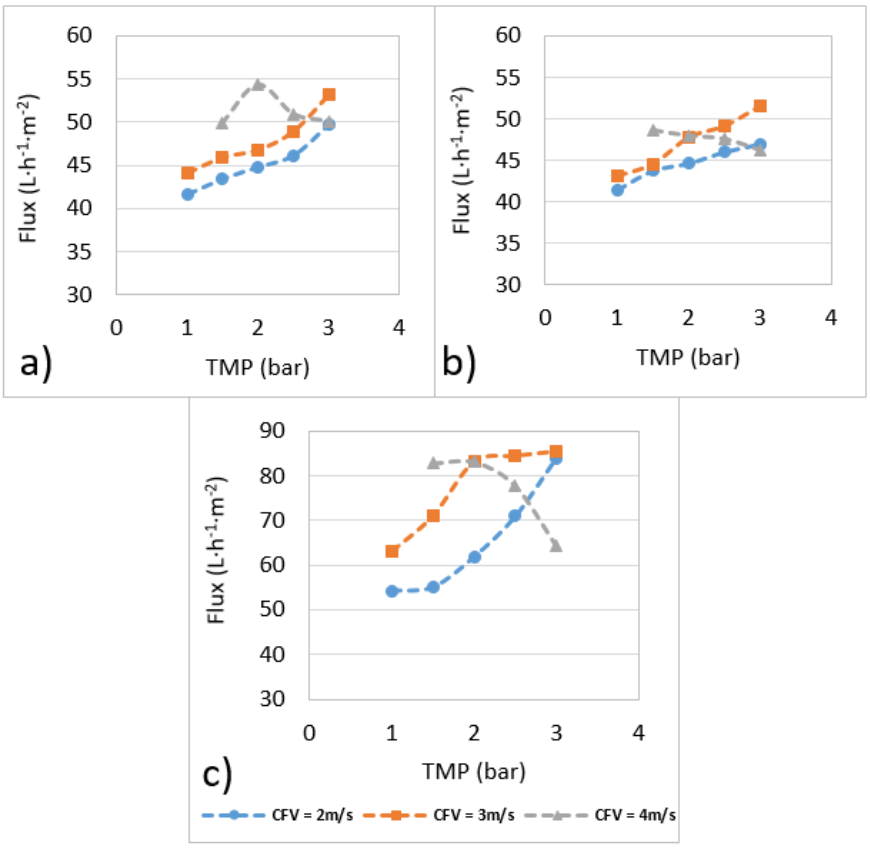

Fig. 5.12 Steady state permeate fluxes for the membranes tested at different operating conditions (a) 5 kDa; b) 15 kDa; c) 50 kDa)

According to the parameters evaluated, permeate flux increased slightly with TMP and CFV, the variation with CFV being greater for the membrane with the largest pore size. However, it can be seen in Fig. 5.12 that the variations with pressure are very small, sometimes even insignificant. This is because the limiting flux zone has been reached and therefore a gel layer has been formed on the surface of the membranes. For the highest CFV permeate flux showed a decrease with increasing TMP, especially in the case of the 50 kDa membrane. Ren et al. [41] observed similar results when studying the best operating conditions for treating cattle wastewater with multichannel ceramic ultrafiltration membranes. They observed that the increase in both TMP and CFV generated an increase in the permeate flux until it reached the

critical point. For TMP values above the critical point, permeate fluxes remained constant and even decreased. For the case of TMP, they stated that the decrease in flux might be due to the thickening and compression of the cake on the surface of the membrane, as well as to the distortion of the deposited particles. Concerning CFV, according to Foley et al. and Jepsen et al. [42-43] as the CFV increases a reduction in the thickness of the cake is observed, however, smaller particles are present in the layer. Therefore, the porosity of the cake decreases, which could generate a reduction in the flux. Jepsen et al. [43] concluded that it is the ratio between the specific cake resistance and its thickness what can cause CFV to decrease the permeate flux. Therefore, higher rejections at the highest CFV were expected for the three membranes as a result of the compaction of the gel layer (This was confirmed from the experimental results shown in section 3.3). On the other hand, Tonova et al. [44] also observed that permeate flux decreased with CFV under the presence of particles (flocs). These authors explained that the increase in CFV could cause a degradation of the particle size, which led to an improvement of the membrane fouling negatively affecting the flux. This can also be related to the fact that the suspended particles can break due to greater turbulence causing pore blocking, which is favoured by the increase in pressure. This implies an increase in the irreversible fouling.

To support this hypothesis, the particle size distribution of the feed samples used in the tests with the 50 kDa membrane were analysed. Samples before (initial) and after each test were characterized. It can be seen in Fig. 5.13 that the tests at 2 and 3 $m \cdot s^{-1}$ do not present a great variation in the particle size distribution when increasing the TMP from 1 to 3 bar. However, at 4 $m \cdot s^{-1}$ the pressure increase generated a notable decrease in particle size, reaching a mean particle size of 695.7 nm at the highest TMP tested when the initial average size was 1183 nm. It has to be mentioned that the measure of the particle size distribution was performed by dynamic light scattering. The measurement values are higher than the real values when particles of a wide range of sizes are found in a sample. This is due to fact that the equipment measures intensities of scattered light and larger particles hide the intensity scattered by the smaller ones. However, it is clear the diminution of the particle size in the feed for the highest cross-flow velocity.

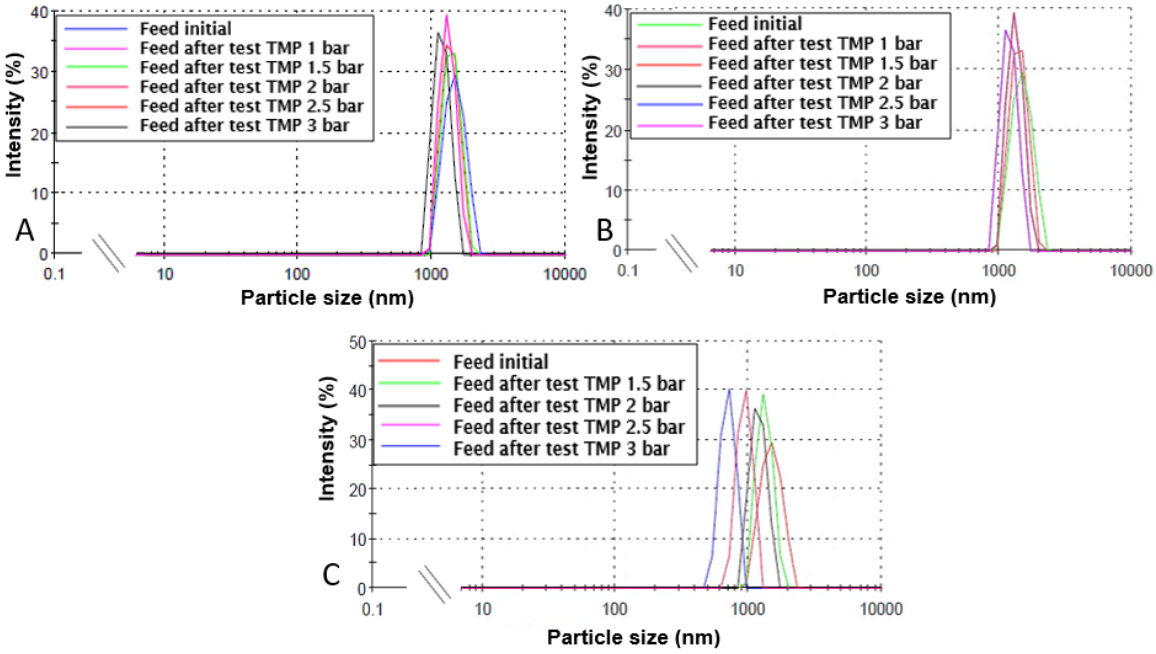

Fig.5.13 Feed particle size distribution for the ultrafiltration tests performed with the 50 kDa membrane A: CFV of 2m·s^{-1}; B: CFV of 3 m·s^{-1}; C: CFV of 4 m·s^{-1}

A reduction in the particle size of the feed with CFV was also observed by Ho and Sung [45] in their work on the effect of solids concentration and CFV on anaerobic sludge microfiltration. They observed a decrease in the mean particle size of the anaerobic sludge from 56 µm (CFV of 0.1 m·s^{-1}) to 44 µm after 6 h of filtration at 0.7 m·s^{-1}. These authors explained that the particles in MBR broke down into finer particles due to the high shear stress, to later form a denser cake layer. The shear stress generated by the CFV showed a linear trend. Moreover, Du et al. [46] reported that high CFV induced a higher shear stress by increasing the lifting force exerted on the particles, which could help large particles to move away from the membrane surface, causing small particles to settle on the membrane surface and cause severe fouling. That reason why this behaviour was observed for this membrane and not for the others may be due to the fact that pores with a larger diameter are more susceptible to internal obstruction by smaller particles [47].

Finally, the trend observed in Fig. 5.12c, that is, the loss of the linear correlation of the permeate flux with the TMP, is due to the fact that this increase in pressure generates a compaction of the membrane or enhances the polarization of the concentration. This in turn produces an increase in transfer resistance; then the dependence of flow against pressure deviates significantly from the linear trend and can exhibit a null trend (Fig.5.12c, test at 3 $m \cdot s^{-1}$) or even negative trend (Fig. 5.12c, test at 4 $m \cdot s^{-1}$).

It is also important to note that flux values were considerably lower than those measured for osmotic water. This was observed for all the tested operating conditions and the difference was even more relevant for the membrane with the highest MWCO. This indicates a strong fouling of the membrane, which is generally attributed to solute adsorption, pore blocking and to the formation of a gel layer. The "fouling potential" of each membrane depends on the characteristics of the membrane surface and the wastewater (solute present) [48]. In this way, the fouling tendency of a membrane is related to the roughness of the active layer. The higher its roughness, the more susceptible the membrane is to fouling [49]. This is explained because a rougher surface could favour the entrapment of solute molecules, forming a fouling layer which acts as a second barrier to separation [50]. According to studies carried out by Corbatón-Báguena et al. [22], the 50 kDa membrane has higher surface roughness than the 15 kDa membrane (root mean square roughness of 27.33 nm vs 17.90 nm, respectively). On the other hand, the pore size of the membrane and the molecular weight of the solute molecules present in the wastewater play an important role in fouling. If the sizes are similar, the membrane is more susceptible to pore blockage [51].

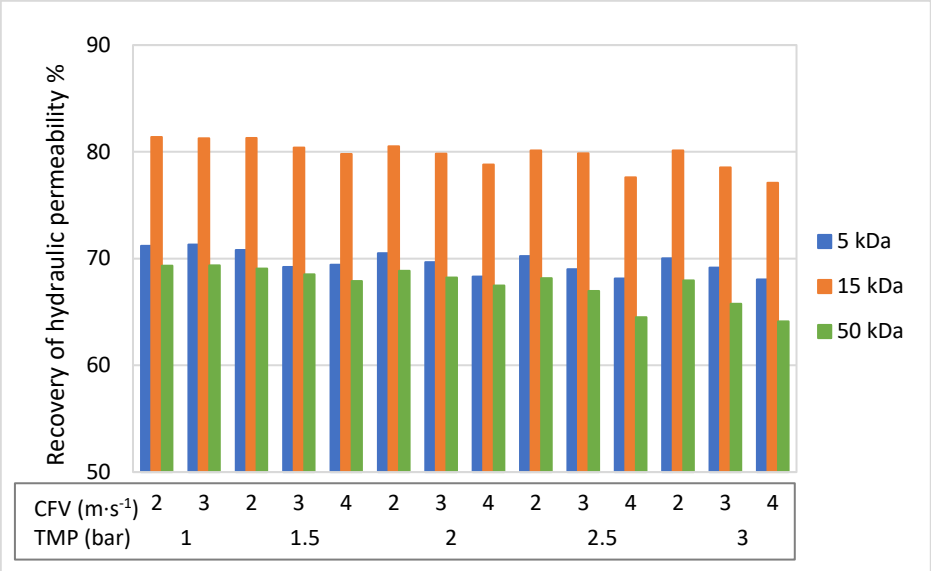

Fig. 5.14 Recovery of the hydraulic permeability of the ceramic ultrafiltration membranes by rinsing with osmotic water (25°C) after the tests performed at the different operating conditions

Fig. 5.14 corroborates what has been commented above. It shows the recovery of the hydraulic permeability of the membranes after rinsing with tap water followed by rinsing with osmotic water. It is observed that the higher the CFV and the TMP, the lower the recovery of the permeate flux, being more noticeable for the membrane with the highest MWCO. Therefore, irreversible fouling increases with increasing CFV and TMP above 1 bar. In addition, it can be also observed that the 50 kDa membrane exhibited the most severe fouling.

On the other hand, the 15 kDa membrane was the one that showed the highest percentage of permeability recovery (around 80%), corresponding therefore to the lowest irreversible fouling. This was observed in all the tests carried out at the different operating conditions. Interestingly, it can be noted that the membranes with higher and lower MWCO presented greater irreversible fouling.

Water rinsing removes the reversible membrane fouling, while the remaining fouling corresponds to the irreversible fouling of each membrane. To eliminate it, it would be necessary to use a chemical agent, as will be discussed in section 3.4.

3.3 Ultrafiltration: solute rejection

Fig. 5.15 shows turbidity (white) and colour (green) removal efficiencies, calculated according to equation (2). For the three membranes, the removal of turbidity increased with CFV and TMP. This was expected since the higher the CFV, the lower the concentration of solutes on the membrane surface. The percentages of turbidity removal were high, reaching in some cases values close to 99%. These high percentages are due to the fact that most of the solids that contributed to turbidity are larger than the pores of the membranes. In this way, UF membranes are able to almost completely eliminate turbidity regardless of the type of wastewater [52-53]. Moreover, as expected, the 5 kDa membrane (the one with the lowest MWCO) achieved the greatest turbidity removal.

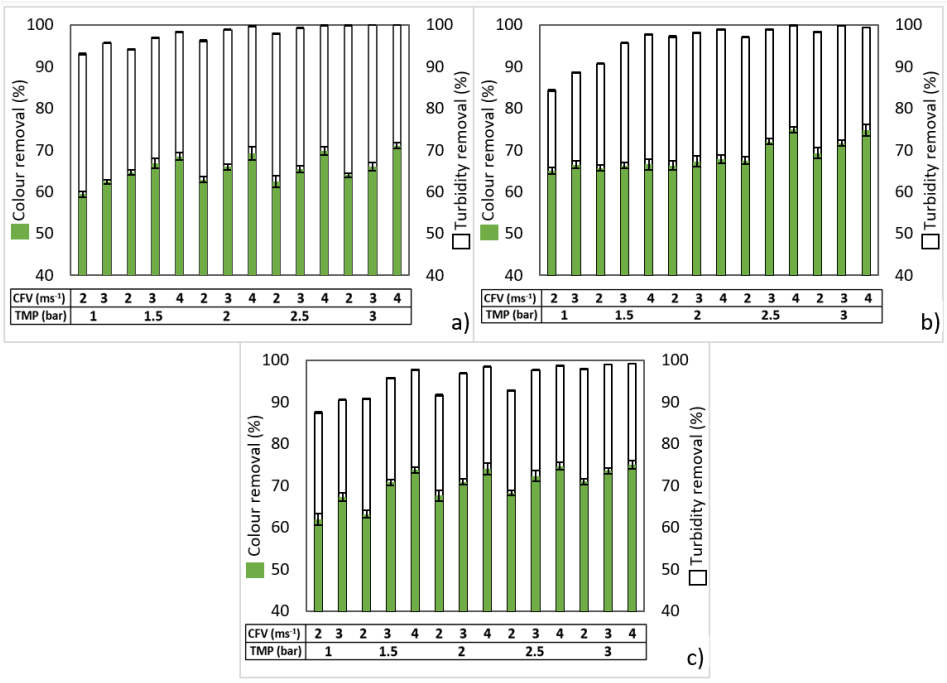

Fig. 5.15 Removal of Colour (green) and turbidity (white) for the different membranes and operating conditions; a) 5 kDa; b) 15 kDa; c) 50kDa

Colour reduction was lower than turbidity removal, being in the range of 59-75%. In this case, it was the 50 kDa membrane the one that presented the highest elimination values (average value of 70.3%). However, it was not very different from that observed for the other membranes (average colour elimination of 68.72%). Although the lowest MWCO membrane was expected to show the highest colour removal, the slightly higher retention exhibited by the 50 kDa membrane can be explained due to its more severe fouling during the tests.

Similar results were observed by Carbonell-Alcaina et al. [54], who tested two organic UF membranes (5 kDa and 30 kDa) for the treatment of residual fermentation brine from the processing of table olives. These authors reported that the membrane with the highest MWCO showed the highest colour removal (around 80%), attributing it to the severe fouling exhibited by the 30 kDa membrane. Following the same analysis as for turbidity, the high removal values may also be due to the fact that most of the compounds that contributed to the colour presented higher molecular weight than the MWCO of the membranes. However, part of the coloured substances did manage to cross the membrane. They are low molecular weight solutes such as phenolic compounds. The compounds present in oil mill wastewater (including OOWW) that give the characteristic dark colour are related to polyphenols, lignin, tannin and other high amount of minor organic compounds [55-56]. Therefore, coloured substances have different molecular weights and cannot be completely retained by the membrane.

For the 5 and 50 kDa membranes, colour removal was affected by both CFV and TMP, the latter variable being the one that had the greatest influence. The increase in TMP at a fixed CFV generated an increase in membrane fouling that directly influenced the percentage of colour rejection, increasing it. For the 15 kDa membrane, colour rejection was not significantly influenced by changes in TMP and CFV, being almost constant (around 66% rejection), which can be due to the lower fouling observed for this membrane as previously commented. However, for the highest TMPs tested, the increase in CFV did generate an increase in rejection.

All the three membranes showed the highest colour removal at the most extreme condition (a CFV of 4 $m \cdot s^{-1}$ and a TMP of 3 bar). This result confirms what was commented in section 3.2. Under these conditions, the membranes work above the critical flux and presented

the highest fouling. The deposited particles (gel layer or cake) act as an additional layer that affects the permeation, observing a decreasing permeate flux and causing a change in selectivity (higher rejections) [57]. In addition, as could be observed from Fig. 5.14, under these conditions the three membranes presented the lowest recovery of the permeate flux after rinsing; corresponding to the most severe fouling.

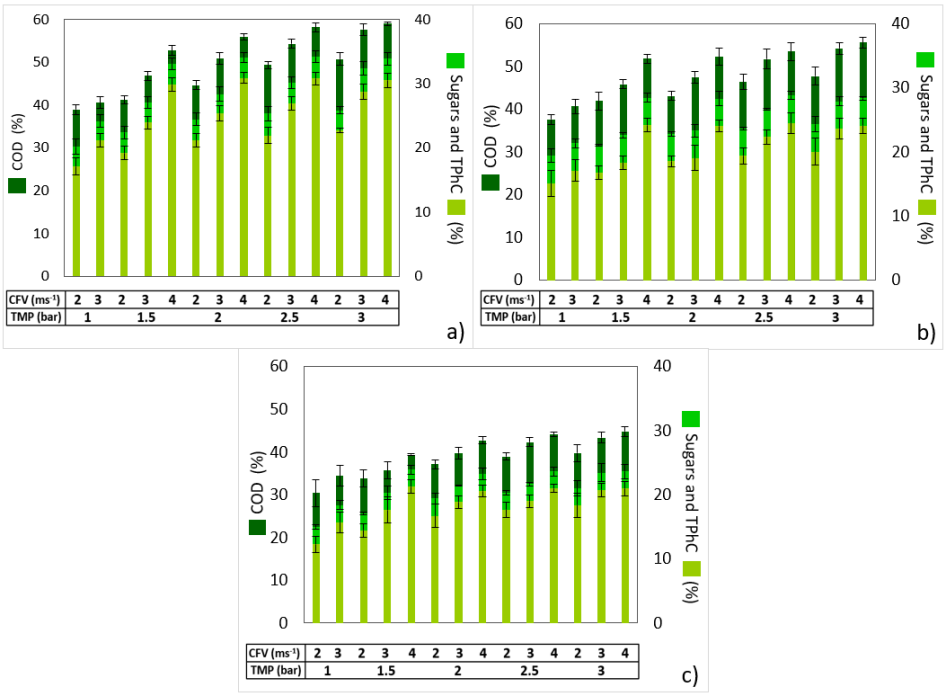

Fig. 5.16 COD (dark green), sugars (medium green) and Phenolic compounds (light green) rejection for the different membranes (a) 5 kDa; b) 15 kDa; c) 50kDa) and operating conditions

The membranes presented rejections between 30% and 59% of COD (Fig. 5.16), being the membrane with the lowest MWCO the one that presented the highest values. At 2 and 3 $m \cdot s^{-1}$, a linear dependence of COD rejection with TMP was observed, achieving COD rejections between 40.9 and 57.7% for the 5kDa membrane, and between 37.6% and 54.2% for the 15 kDa one. Similar results were reported by Dafinov et al [58], achieving COD retentions in the range of 40-60 % when three Tami Inside ceramic membranes (including the 5 kDa and 15 kDa ones used in this study) were tested for the treatment of black liquor from wood

pulping. De Almeida et al. [59] also observed an increase in the rejection of COD with increasing TMP by different UF ceramic membranes (50 kDa and 150 kDa) in the treatment of OMW. As commented in section 3.2, it can be explained by the formation of a layer on the surface of the membrane mainly consisting of high molecular weight solutes that offer additional resistance to permeation [60]. An increase in the TMP causes an increase in the gel layer thickness, thus increasing solute rejection [61]. The highest COD rejections occurred at the highest CFV tested, as a result of the reduction of the concentration of solutes at the membrane surface as CFV increases. Moreover, as CFV increases the specific cake resistance increases, which affects solute rejection, as it was explained in section 3.2 and observed by several authors [42-43]. In all the analysed tests, the 50 kDa membrane was the one that presented the least influence of the operating parameters (CFV and TMP) on COD rejection. Unlike what was observed for the removal of turbidity and colour, in this case, the pore size of the membrane did influence COD rejections, being higher when the MWCO of the membrane decreased.

Rejection of phenolic compounds showed a similar trend as COD rejection, being the highest for the lowest MWCO membrane (30.9% at 4 $m \cdot s^{-1}$ and 2 bar). However, in this case the difference between the tested membranes was not so noticeable, presenting average rejections of 20% and 18% for the 15 and 50 kDa membranes, respectively. As the 50 kDa membrane has a much larger pore size than the other two membranes, a greater passage of phenols to the permeate side was expected. It is important to note that the presence of more than 30 different types of biophenols and related compounds (including tyrosol, hydroxytyrosol and oleuropein) has been found in the wastewaters from oil mills [62]. This is due to the fact that only 2% of the phenolic compounds of the olives are found in the oily phase, leaving 98% of the remaining phenols in the wastewater [63-64]. Concerning their size, it has been reported that the molecular weight of the phenolic compounds present in the olives ranges between 138 - 624 $g \cdot mol^{-1}$ [65]; the molecular weight of the phenolic compounds present in the studied OOWW can cover a wide range.

Several factors govern the interaction between the membrane and the phenolic compounds, influencing rejection, fouling, and permeate flux. These factors include

hydrophobic and hydrophilic interactions and competition between the solvent and polyphenols for the interaction sites on the membrane surface [66]. The Interaction depend on both the characteristics of the membrane and the phenolic compounds present in the sample, such as the pore size of the membrane, the molecular weight of the phenolic compounds and the electrical charge of the membrane and phenolic compounds [67].

The rejection is similar for all membranes due to the small size of the compounds in comparison with the MWCO of the membranes. Thus, the rejection of phenolic compounds is very low. This rejection is not 0% because of the phenolic compounds adsorption on the membrane. Although phenolic compounds could also be adsorbed by the cake layer generated during the filtration stage [68], sorption on the membrane structure itself cannot be ruled out. This adsorption is due to van der Waals interactions and hydrogen bonds with the hydroxyl groups of polyphenolic structures. The hydroxyl groups of phenolic compounds can form cooperative hydrogen bonds with the hydroxyl groups on the alumina surface, resulting in more frequent and longer lasting hydrogen bonding interactions [69].

El Rayess et al. [70] observed a decrease in permeate flux (slight fouling) during the filtration of tannin-laden filtered wine with a 15 kDa ceramic membrane. They attributed this mainly to adsorption phenomena on the membrane, since the wine, when filtered, did not contain large particles that could form a deposit on the membrane surface. The adsorption of these components is lower on hydrophobic membranes than on hydrophilic ones. Ceramic membranes have a marked hydrophilic character and therefore the electrostatic interaction can have a significant impact on the adsorption of the phenolic compounds on the surface [71].

In this work, the membrane was positively charged (isoelectric point 6-6.9) [67-72], while the phenolic compounds in the sample (pH 4.8) had neutral charge as their pKa value is greater than 9.0. Thus, there is no attraction between the membrane and the phenolic compounds, which facilitated their passage through the membrane and justified the low rejection presented. Similar results were observed by Harman et al. [73] in their study of the rejection of phenol through ceramic ultrafiltration membranes at three different pH values (7.0, 10.5 and 11.5). Poor phenol rejections (3–7%) were achieved at a solution pH of 7.0. On the other hand, with increasing pH, a significant increase in phenol rejections was observed (63

and 77% of rejection at pH 10.5 and 11.5, respectively). These authors finally pointed out that these results were mainly due to electrostatic repulsion mechanisms. Since phenol is an aromatic compound with a pKa value of 9.98, at neutral or acidic pH values phenol is mainly in the neutral/undissociated form.

Considering all these comments, it can be inferred that the rejection of phenolic compounds is due to their adsorption on the surface of the membranes. On the other hand, the molecular weight of the phenolic compounds in the feed samples is lower than 15 kDa. This justifies the similar percentage of rejection obtained by 15 kDa and 50 kDa membranes, explaining, at the same time, that phenolic compounds rejection did not increase in spite of the severe fouling of the 50 kDa membrane at a CFV of 4 $m \cdot s^{-1}$. It is important to highlight that the 50 kDa membrane was the one with the highest fouling. Therefor the phenolic compounds rejection could be also explained by membrane fouling, which led to the formation of an additional barrier to the passage of some phenolic compounds [74].

Although both operating parameters, CFV and TPM, were observed to affect the rejection of phenolic compounds, in this case rejection was influenced more significantly by the CFV, increasing as this variable augmented. Phenolic compounds rejection increased linearly with the rise in TMP. However, for the highest CFV, the rejection of phenolic compounds for all the tested membranes did not show a great variation with increasing TMP. This could be explained as a result of the greatest fouling observed at these conditions, as commented in section 3.2. Again, the 50 kDa membrane was the one that presented the least variability in the rejection values when the operating conditions varied, being the highest rejection only 2% higher than the average rejection. This membrane was the one that presented the lowest rejection of phenolic compounds (12.3% at 1 bar and 2 $m \cdot s^{-1}$). Nevertheless, this low rejection was only observed under these operating conditions, then the rejection fluctuated between 17.6% and 20.9%. The 5 kDa membrane was the one with the greatest variability, presenting rejections of phenolic compounds between 17.1% and 30.8%.

On the other hand, the behaviour of the membranes against the rejection of sugars was very similar to that described for the rejection of phenolic compounds, presenting an increase in rejection with increasing both TMP and CFV. This is due to the fact that the sugars present

in this water (mainly fructose, glucose, mannose and sucrose [64,75]) have molecular weights similar to those of some phenolic compounds. Therefore a large percentage of sugars managed to cross the membrane appearing in the permeate, which makes difficult to properly separate them from the phenolic compounds [76]. The 5 kDa membrane, under the conditions of 4 $m \cdot s^{-1}$ and 2.5 bar, presented the highest rejection of sugars (34.2%), followed by the 15 kDa membrane, whose highest rejection (28.8%) was observed at the same conditions.

The best operating conditions were selected taking into account the permeate flux values, colour and turbidity removal and also the rejection of sugars, COD and phenolic compounds. A stable and high value of permeate flux is desirable, with the greatest elimination of organic matter, but without affecting the presence of phenolic compounds. These conditions were, for the 5 kDa membrane 2 $m \cdot s^{-1}$ and 2 bar, for the 15 kDa 3 $m \cdot s^{-1}$ and 3 bar, and for the 50 kDa membrane 4 $m \cdot s^{-1}$ and 2.5 bar. The phenolic compounds/COD ratio in the permeate streams at the best operating conditions selected for each membrane is presented in Fig. 5.17.

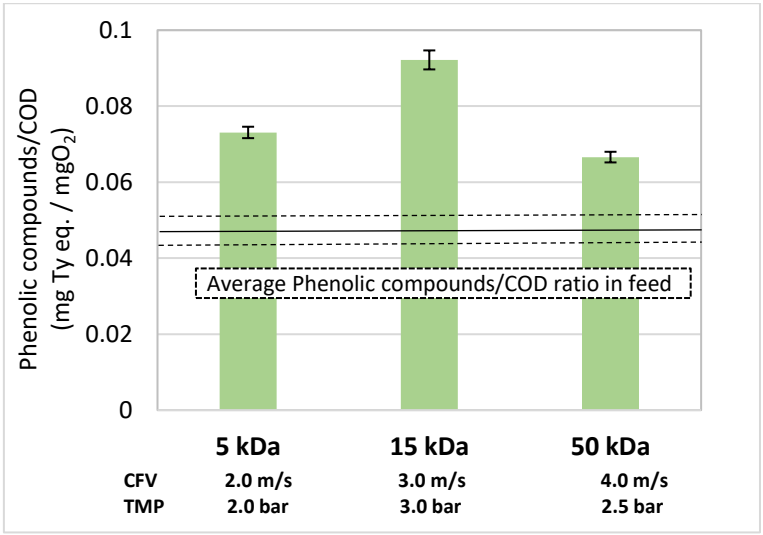

Fig. 5.17 Phenolic compounds/chemical oxygen demand (COD) ratio in the permeate streams for the best operating conditions for each membrane

Although the three membranes achieved an increase in the phenolic compounds/COD ratio (comparing feed and permeate streams), it was the 15 kDa membrane the one that yielded the highest increase in the ratio of phenolic compounds to COD (from 0.05 in the feed to 0.09 in the permeate), showing the greatest separation of phenolic compounds from other organic substances present in the OOWW. Cassano et al. [77] tested different organic UF membranes with MWCOs between 4-10 kDa to treat OMW. However, they obtained similar polyphenols/total organic carbon (TOC) ratios in the feed and permeate steams. Therefore, a larger separation of phenolic compounds from other organic compounds was reached with the inorganic membranes considered in this work.

The results obtained present the 15 kDa membrane as the best option for the treatment of OOWW, achieving a partial elimination of the organic matter present in the wastewater, without significantly affecting the concentration of phenolic compounds.

3.4 Cleaning results

As previously commented, membrane fouling was observed in all the tests, being more severe for the membrane with the highest MWCO.

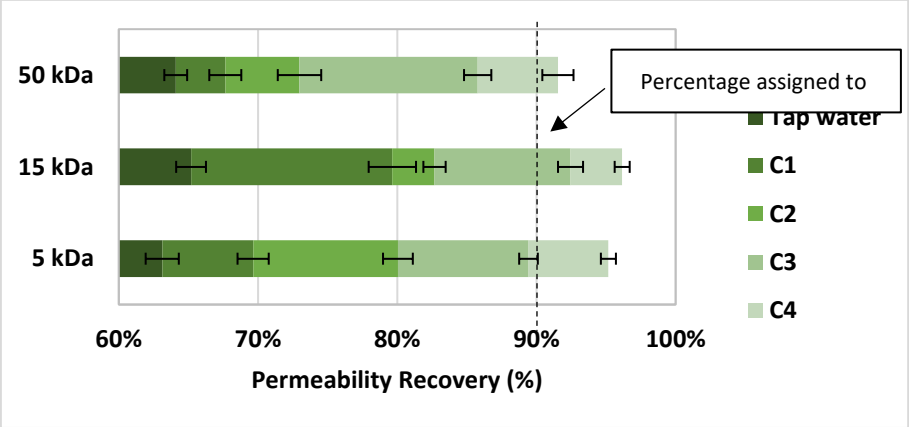

Fig. 5.18 Average recovery of initial pure water permeability after the different cleaning methods (rinsing with tap water; cleaning with osmotic water: C1 at 25°C and C2 at 35°C; chemical cleaning with Ultrasil 115 1%v/v: C3 at 25°C and C4 at 35°C)

Fig. 5.18 shows the permeability recovery of the membranes using different cleaning methods. As explained in section 2.3, firstly the membranes were rinsed with tap water and the permeability was measured immediately. Then, the different cleaning methods were successively performed, and the permeability was measured in between until all the proposed methods were completed. It was observed that the three membranes presented severe fouling, which was partially irreversible (Fig. 5.14). Rinsing with tap water achieved membrane permeability recoveries of around 65%. The lowest MWCO membranes showed the highest flux recovery after rinsing with tap water. Treatment C1 showed good results for the 15 kDa membrane, achieving an average permeability recovery close to 80%. However, the other two membranes reached recovery percentages below 70%. The permeability recovery after cleaning by means of C1 method for each tested operating condition can be seen in Fig. 5.14.

The C2 cleaning procedure improved the permeability recovery for the membrane with the lowest MWCO, which achieved 80% recovery. However, it did not represent a great change for the 15 kDa membrane, in comparison with C1 treatment. Although C2 treatment improved the permeability recovery for the 50 kDa membrane, it did not exceed 75%. In this way, cleaning with water independently of the applied temperature was not enough to recover the permeability of the membranes.

The first treatment with the chemical agent (C3) showed a great improvement in the permeability recovery for the 3 membranes. The 15 kDa membrane achieved the highest permeability recovery (93%), while the 50 kDa membrane showed the lowest recovery (86%). The increase in temperature to 35 °C (C4) implied that all the membranes could exceed the percentage assigned to consider the membrane to be clean (90%). Nevertheless, it is important to note that the 50 kDa membrane achieved the lowest recovery percentage (92%). These results were expected, since this membrane was the one that presented the greatest permeate flux decay over time in all the tests carried out, which indicates severe fouling. The nominal pore size of the membranes affects the extent and the type of fouling. It has to be highlighted that the membrane with the lowest MWCO did not yield the highest permeability recovery after cleaning, which may be due to the type of fouling that the membrane presents, which depends on the relationship between the pore size of the membranes and the size of the solutes.

Corbatón-Báguena et al. [22] studied the cleaning of several ultrafiltration membranes (including the 50 kDa Tami inside ceramic one used in this work) fouled with BSA using saline solutions. Despite the high temperatures tested, they were unable to fully recover the permeability of the 50 kDa membrane. They attributed the results to severe fouling presented by the membrane, mainly due to the penetration of BSA molecules into the porous structure of this membrane compared to smaller MWCO membranes. They explained this assumption due to the similar size of BSA and the pores of the 50 kDa membrane. Finally, it has to be pointed out that the results showed that the 15 kDa membrane was the one that presented the least irreversible fouling when the OOWW was treated under the operating conditions tested.

Nowadays, fouling remains one of the bottlenecks in the application of ceramic membranes in water treatment [12]. Therefore, it is essential to develop fouling prevention and control strategies to improve the hydraulic performance of the membrane. These strategies will vary depending on the wastewater. But, in general, in order to obtain higher recovery percentages, both the operational parameters of the CIP (cross flow rate, transmembrane pressure, time), as well as the pH, temperature and concentration of the chemical agent must be evaluated [78].

4 Conclusions

Ultrafiltration with ceramic membranes of olive oil washing wastewater has been demonstrated to be an interesting alternative as a previous step for the recovery of phenolic compounds. In order to get the best membrane performance, different CFVs and TMPs have been tested. The 50 kDa membrane, although achieved the highest permeate flux, as expected, showed a decrease in flux as the TMP increased at a CFV of 4 $m \cdot s^{-1}$. This behaviour indicated that operation at this CFV is above the limiting conditions, presenting severe fouling. On the other hand, the other two membranes did not show significant differences in terms of rejection and permeate flux when CFV increased from 3 to 4 $m \cdot s^{-1}$. In this way, this increase is not profitable from an economic point of view.

All the three ceramic membranes tested achieved high removal of turbidity (average over 95%) and colour (average over 65%). As expected, the highest rejections were obtained

for the lowest MWCO membranes, with the highest COD rejection values for the 5 kDa, 15 kDa and 50 kDa membranes being 59%, 56% and 45%, respectively. The total phenolic compounds and sugars rejection presented a similar behaviour, with the 5 kDa membrane presenting the highest rejection values for both compounds (rejection between 17.1% and 30.8% for phenolic compounds, and between 20.1% and 34.2% for sugars).

The 15 kDa membrane at the operating conditions of 3 $m \cdot s^{-1}$ and 3 bar was observed to be the best option, achieving high elimination of colour (72%), turbidity (99%) and COD (54%), without greatly affecting the concentration of phenolic compounds (rejection of 21%). A stable permeate flux of 51.4 $L \cdot h^{-1} \cdot m^{-2}$ was obtained. This membrane had the best permeability recovery under the cleaning procedures tested.

The results demonstrated that the membrane performance is conditioned by the working conditions, being affected by the interaction between the substances present in the feed and by the membrane material. This shows the importance of the selection of the appropriate membrane and operating conditions depending on the characteristics of the sample to be treated. To sum up, the ultrafiltration of OOWW using ceramic membranes seems to be a technically feasible way to remove organic matter without greatly affecting the phenolic compounds content.

Acknowledgements

The authors acknowledge the financial support from the Spanish Ministry of Economy, Industry and Competitiveness through the project CTM2017-88645-R and The European Union through the Operational Program of the Social Fund (FSE) of the Comunitat Valenciana 2014-2020.

References

[1] G. Mustafa, K. Wyns, A. Buekenhoudt, V. Meynen, Antifouling grafting of ceramic membranes validated in a variety of challenging wastewaters, Water Res. 104 (2016) 242–253. https://doi.org/10.1016/j.watres.2016.07.057.

[2] M.A. Núñez Camacho, A.I. García López, A. Martinez-ferez, J.M. Ochando-Pulido, Increasing large-scale feasibility of two-phase olive-oil washing wastewater treatment and phenolic fraction recovery with novel ion exchange resins, Chem. Eng. Process. - Process Intensif. 164 (2021) 108416. https://doi.org/10.1016/j.cep.2021.108416.

[3] A. Khdair, G. Abu-Rumman, Sustainable environmental management and valorization options for olive mill byproducts in the Middle East and North Africa (MENA) region, Processes. 8 (2020) 1–22. https://doi.org/10.3390/PR8060671.

[4] A.Y. Gebreyohannes, R. Mazzei, L. Giorno, Trends and current practices of olive mill wastewater treatment: Application of integrated membrane process and its future perspective, Sep. Purif. Technol. 162 (2016) 45–60. https://doi.org/10.1016/j.seppur.2016.02.001.

[5] M. Maaitah, G. Hodaifa, A. Malvis, S. Sánchez, Kinetic growth and biochemical composition variability of Chlorella pyrenoidosa in olive oil washing wastewater cultures enriched with urban wastewater, J. Water Process Eng. 35 (2020) 101197. https://doi.org/10.1016/j.jwpe.2020.101197.

[6] E. Garcia-Castello, A. Cassano, A. Criscuoli, C. Conidi, E. Drioli, Recovery and concentration of polyphenols from olive mill wastewaters by integrated membrane system., Water Res. (2010). https://doi.org/10.1016/j.watres.2010.05.005.

[7] Z. Kaleh, S.U. Geißen, Selective isolation of valuable biophenols from olive mill wastewater, J. Environ. Chem. Eng. 4 (2016) 373–384. https://doi.org/10.1016/j.jece.2015.11.010.

[8] A. El-Abbassi, M. Khayet, A. Hafidi, Micellar enhanced ultrafiltration process for the treatment of olive mill wastewater, Water Res. 45 (2011) 4522–4530. https://doi.org/10.1016/j.watres.2011.05.044.

[9] Z. He, Z. Lyu, Q. Gu, L. Zhang, J. Wang, Ceramic-based membranes for water and wastewater treatment, Colloids Surfaces A Physicochem. Eng. Asp. 578 (2019)

123513. https://doi.org/10.1016/j.colsurfa.2019.05.074.

[10] S.M. Samaei, S. Gato-Trinidad, A. Altaee, The application of pressure-driven ceramic membrane technology for the treatment of industrial wastewaters – A review, Sep. Purif. Technol. 200 (2018) 198–220. https://doi.org/10.1016/j.seppur.2018.02.041.

[11] C. Li, W. Sun, Z. Lu, X. Ao, S. Li, Ceramic nanocomposite membranes and membrane fouling : A review, Water Res. 175 (2020) 115674. https://doi.org/10.1016/j.watres.2020.115674.

[12] M.B. Asif, Z. Zhang, Ceramic membrane technology for water and wastewater treatment: A critical review of performance, full-scale applications, membrane fouling and prospects, Chem. Eng. J. 418 (2021) 129481. https://doi.org/10.1016/j.cej.2021.129481.

[13] C.A. Paraskeva, V.G. Papadakis, E. Tsarouchi, D.G. Kanellopoulou, P.G. Koutsoukos, Membrane processing for olive mill wastewater fractionation, Desalination. 213 (2007) 218–229. https://doi.org/10.1016/j.desal.2006.04.087.

[14] N. Değermenci, İ. Cengiz, E. Yildiz, A. Nuhoglu, Performance investigation of a jet loop membrane bioreactor for the treatment of an actual olive mill wastewater, J. Environ. Manage. 184 (2016) 441–447. https://doi.org/10.1016/j.jenvman.2016.10.014.

[15] H. Dhaouadi, B. Marrot, Olive mill wastewater treatment in a membrane bioreactor: Process feasibility and performances, Chem. Eng. J. 145 (2008) 225–231. https://doi.org/10.1016/j.cej.2008.04.017.

[16] M. Cifuentes-Cabezas, C. Carbonell-Alcaina, M.C. Vincent-Vela, J.A. Mendoza-Roca, S. Álvarez-Blanco, Comparison of different ultrafiltration membranes as first step for the recovery of phenolic compounds from olive-oil washing wastewater, Process Saf. Environ. Prot. 149 (2021) 724–734. https://doi.org/10.1016/j.psep.2021.03.035.

[17] Tami Industries, INSIDE CéRAM, (2016) 1–2. ⟨https://www.tami-in- dustries.com/⟩

[18] J. Kujawa, S. Cerneaux, W. Kujawski, M. Bryjak, J. Kujawski, How to Functionalize Ceramics by Perfluoroalkylsilanes for Membrane Separation Process? Properties and Application of Hydrophobized Ceramic Membranes, ACS Appl. Mater. Interfaces. 8 (2016) 7564–7577. https://doi.org/10.1021/acsami.6b00140.

[19] D. Lu, T. Zhang, J. Ma, Ceramic membrane fouling during ultrafiltration of oil/water emulsions: Roles played by stabilization surfactants of oil droplets, Environ. Sci. Technol. 49 (2015) 4235–4244. https://doi.org/10.1021/es505572y.

[20] J. Kujawa, W. Kujawski, S. Cerneaux, G. Li, S. Al-Gharabli, Zirconium dioxide membranes decorated by silanes based-modifiers for membrane distillation – Material chemistry approach, J. Memb. Sci. 596 (2020) 117597. https://doi.org/10.1016/j.memsci.2019.117597.

[21] A. Urbanowska, M. Kabsch-Korbutowicz, The use of flat ceramic membranes for purification of the liquid fraction of the digestate from municipal waste biogas plants, Energies. 14 (2021). https://doi.org/10.3390/en14133947.

[22] M.-J. Corbatón-Báguena, S. Álvarez-blanco, M.C. Vincent-Vela, Cleaning of ultrafiltration membranes fouled with BSA by means of saline solutions, Sep. Purif. Technol. 125 (2014) 1–10. https://doi.org/10.1016/j.seppur.2014.01.035.

[23] A. Bottino, G. Capannelli, A. Comite, A. Jezowska, M. Pagliero, C. Costa, R. Firpo, Treatment of olive mill wastewater through integrated pressure-driven membrane processes, Membranes (Basel). 10 (2020) 1–16. https://doi.org/10.3390/membranes10110334.

[24] C. Saf, M. Villain-Gambier, M. Belaqziz, I. Ziegler-Devin, D. Trebouet, N. Ouazzani, Fouling control investigation by pH optimization during olive mill wastewater ultrafiltration, Process Saf. Environ. Prot. 164 (2022) 119–128. https://doi.org/10.1016/j.psep.2022.06.010.

[25] M.J. Luján-Facundo, J.A. Mendoza-Roca, B. Cuartas-Uribe, S. Álvarez-Blanco,

Cleaning efficiency enhancement by ultrasounds for membranes used in dairy industries, Ultrason. Sonochem. 33 (2016) 18–25. https://doi.org/10.1016/j.ultsonch.2016.04.018.

[26] M.J. Corbatón-Báguena, S. Álvarez-Blanco, M.C. Vincent-Vela, Evaluation of fouling resistances during the ultrafiltration of whey model solutions, J. Clean. Prod. 172 (2018) 358–367. https://doi.org/10.1016/j.jclepro.2017.10.149.

[27] E. Döpkens, R. Jonas, T. Jung, R. Krull, Rückführung von Abwasserteilströmen der Textilveredlung in den Produktionsprozess, "Prepr. Colloq. Produktionsintegrieter Wasser Abwasserechnik,"Nachhaltige Prod. Der Textilveredlung" Und "Membrantechnik" Bremen. (2001) B143–B15.

[28] B. Frolund, P. Rikke, K. Keiding, P.H. Nielsen, Extraction of extracellular polymers from activated sludge using a cation exchange resin, Water Res. 30 (1996) 1749–1758.

[29] V.L. Singleton, R. Orthofer, R.M. Lamuela-Raventós, Analysis of total phenols and other oxidation substrates and antioxidants by means of folin-ciocalteu reagent, Methods Enzymol. 299 (1999) 152–178. https://doi.org/10.1016/S0076-6879(99)99017-1.

[30] APHA, Standard Methods for the Examination of Water and Wastewater, in: Am. Public Heal. Assoc. Washington, DC, 2005: p. 21 st. ed.

[31] S. Dermeche, M. Nadour, C. Larroche, F. Moulti-Mati, P. Michaud, Olive mill wastes: Biochemical characterizations and valorization strategies, Process Biochem. (2013) 1532–1552. https://doi.org/10.1016/j.procbio.2013.07.010.

[32] G. Çelik, Ö. Saygın, I. Balcıoğlu Akmehmet, Multistage recovery process of phenolic antioxidants with a focus on hydroxytyrosol from olive mill wastewater concentrates, Sep. Purif. Technol. (2020) 117757. https://doi.org/10.1016/j.seppur.2020.117757.

[33] E. Roselló-Soto, M. Koubaa, A. Moubarik, R.P. Lopes, J.A. Saraiva, N. Boussetta, N. Grimi, F.J. Barba, Emerging opportunities for the effective valorization of wastes and

by-products generated during olive oil production process: Non-conventional methods for the recovery of high-added value compounds, Trends Food Sci. Technol. 45 (2015) 296–310. https://doi.org/10.1016/j.tifs.2015.07.003.

[34] J.M. Ochando-Pulido, A. Martínez-Férez, About the recovery of the phenolic fraction from olive mill wastewater by micro and ultracentrifugation membranes, Chem. Eng. Trans. 60 (2017) 271–276. https://doi.org/10.3303/CET1760046.

[35] J.M. Ochando-Pulido, G. Hodaifa, M.D. Victor-Ortega, S. Rodriguez-Vives, A. Martinez-Ferez, Reuse of olive mill effluents from two-phase extraction process by integrated advanced oxidation and reverse osmosis treatment, J. Hazard. Mater. 263P (2013) 158–167. https://doi.org/10.1016/j.jhazmat.2013.07.015.

[36] A. Roig, M.L. Cayuela, M.A. Sánchez-Monedero, An overview on olive mill wastes and their valorisation methods, Waste Manag. 26 (2006) 960–969. https://doi.org/10.1016/j.wasman.2005.07.024.

[37] W. Tomczak, M. Gryta, Application of ultrafiltration ceramic membrane for separation of oily wastewater generated by maritime transportation, Sep. Purif. Technol. 261 (2020) 118259. https://doi.org/10.1016/j.seppur.2020.118259.

[38] I. Ahmed, K.S. Balkhair, A. Ahmed, J. Shaiban, Desalination. Chapter 10. Importance and Significance of UF / MF Membrane Systems in Desalination Water Treatment, 2017. 10.5772/intechopen.68694.

[39] K.M. Majewska-Nowak, Application of ceramic membranes for the separation of dye particles, Desalination. 254 (2010) 185–191. https://doi.org/10.1016/j.desal.2009.11.026.

[40] W. Tomczak, Determination of critical flux for ultrafiltration used for separation of glycerol fermentation broths, in: M. Jozef (Ed.), Proc. 40th Int. Conf. Slovak Soc. Chem. Eng., 2013: pp. 707–714.

[41] Q. Ren, X. Chen, Y. Yumminaga, N. Wang, W. Yan, Y. Li, L. Liu, J. Shi, Effect of

operating conditions on the performance of multichannel ceramic ultrafiltration membranes for cattle wastewater treatment, J. Water Process Eng. 41 (2021) 102102. https://doi.org/10.1016/j.jwpe.2021.102102.

[42] G. Foley, D.M. Malone, F. MacLoughlin, Modelling the effects of particle polydispersity in crossflow filtration, J. Memb. Sci. 99 (1995) 77–88. https://doi.org/10.1016/0376-7388(94)00207-F.

[43] K.L. Jepsen, M.V. Bram, S. Pedersen, Z. Yang, Membrane fouling for produced water treatment: A review study from a process control perspective, Water (Switzerland). 10 (2018). https://doi.org/10.3390/w10070847.

[44] K. Tonova, M. Lazarova, M. Dencheva-Zarkova, S. Paniovska, I. Tsibranska, V. Stanoev, D. Dzhonova, J. Genova, Separation of glucose, other reducing sugars and phenolics from natural extract by nanofiltration: Effect of pressure and cross-flow velocity, Chem. Eng. Res. Des. 162 (2020) 107–116. https://doi.org/10.1016/j.cherd.2020.07.030.

[45] J. Ho, S. Sung, Effects of solid concentrations and cross-flow hydrodynamics on microfiltration of anaerobic sludge, J. Memb. Sci. 345 (2009) 142–147. https://doi.org/10.1016/j.memsci.2009.08.047.

[46] X. Du, K. Zhang, H. Yang, K. Li, X. Liu, Z. Wang, Q. Zhou, G. Li, H. Liang, The relationship between size-segregated particles migration phenomenon and combined membrane fouling in ultrafiltration processes: The significance of shear stress, J. Taiwan Inst. Chem. Eng. 96 (2019) 45–52. https://doi.org/10.1016/j.jtice.2018.11.016.

[47] F. Waeger, T. Delhaye, W. Fuchs, The use of ceramic microfiltration and ultrafiltration membranes for particle removal from anaerobic digester effluents, Sep. Purif. Technol. 73 (2010) 271–278. https://doi.org/10.1016/j.seppur.2010.04.013.

[48] M. Žabková, E.A.B. da Silva, A.E. Rodrigues, Recovery of vanillin from lignin/vanillin mixture by using tubular ceramic ultrafiltration membranes, J. Memb. Sci. 301 (2007)

221–237. https://doi.org/10.1016/j.memsci.2007.06.025.

[49] A.I. Schäfer, A.G. Fane, T.D. Waite, Fouling effects on rejection in the membrane filtration of natural waters, Desalination. 131 (2000) 215–224. https://doi.org/10.1016/S0011-9164(00)90020-1.

[50] J. Garcia-Ivars, J. Durá-María, C. Moscardó-Carreño, C. Carbonell-Alcaina, M.I. Alcaina-Miranda, M.I. Iborra-Clar, Rejection of trace pharmaceutically active compounds present in municipal wastewaters using ceramic fine ultrafiltration membranes: Effect of feed solution pH and fouling phenomena, Sep. Purif. Technol. 175 (2017) 58–71. https://doi.org/10.1016/j.seppur.2016.11.027.

[51] J. Liu, K. Chen, K. Zou, L. He, D. Zhao, Z. Wang, Y. Qiu, Y. Chen, Insights into the roles of membrane pore size and feed foulant concentration in ultrafiltration membrane fouling based on collision-attachment theory, Water Environ. Res. (2020) 1–8. https://doi.org/10.1002/wer.1453.

[52] S. Hube, M. Eskafi, K.F. Hrafnkelsdóttir, B. Bjarnadóttir, M.Á. Bjarnadóttir, S. Axelsdóttir, B. Wu, Direct membrane filtration for wastewater treatment and resource recovery: A review, Sci. Total Environ. (2020). https://doi.org/10.1016/j.scitotenv.2019.136375.

[53] W. Gao, H. Liang, J. Ma, M. Han, Z. lin Chen, Z. shuang Han, G. bai Li, Membrane fouling control in ultrafiltration technology for drinking water production: A review, Desalination. 272 (2011) 1–8. https://doi.org/10.1016/j.desal.2011.01.051.

[54] C. Carbonell-Alcaina, S. Álvarez-Blanco, M.A. Bes-Piá, J.A. Mendoza-Roca, L. Pastor-Alcañiz, Ultrafiltration of residual fermentation brines from the production of table olives at different operating conditions, J. Clean. Prod. 189 (2018) 662–672. https://doi.org/10.1016/j.jclepro.2018.04.127.

[55] Z.S. Lee, S.Y. Chin, J.W. Lim, T. Witoon, C.K. Cheng, Treatment technologies of palm oil mill effluent (POME)and olive mill wastewater (OMW): A brief review, Environ.

Technol. Innov. 15 (2019) 100377. https://doi.org/10.1016/j.eti.2019.100377.

[56] M. UĞurlu, S. İlteriş Yilmaz, A. VaizoĞullar, Removal of Color and COD from Olive Wastewater by Using Three-Phase Three-Dimensional (3D) Electrode Reactor, Mater. Today Proc. 18 (2019) 1986–1995. https://doi.org/10.1016/j.matpr.2019.06.690.

[57] P. Bacchin, P. Aimar, R.W. Field, Critical and sustainable fluxes: Theory, experiments and applications, J. Memb. Sci. 281 (2006) 42–69. https://doi.org/10.1016/j.memsci.2006.04.014.

[58] A. Dafinov, J. Font, R. Garcia-Valls, Processing of black liquors by UF/NF ceramic membranes, Desalination. 173 (2005) 83–90. https://doi.org/10.1016/j.desal.2004.07.044.

[59] M.S. De Almeida, R.C. Martins, R.M. Quinta-Ferreira, L.M. Gando-Ferreira, Optimization of operating conditions for the valorization of olive mill wastewater using membrane processes, Environ. Sci. Pollut. Res. 25 (2018) 21968–21981. https://doi.org/10.1007/s11356-018-2323-5.

[60] E. Turano, S. Curcio, M.G. De Paola, V. Calabrò, G. Iorio, An integrated centrifugation-ultrafiltration system in the treatment of olive mill wastewater, J. Memb. Sci. 209 (2002) 519–531. https://doi.org/10.1016/S0376-7388(02)00369-1.

[61] R.W. Baker, Membrane Technology and Applications, third edit, John Wiley and Sons Ltd., Newark, California, 1986.

[62] R. Castro-Muñoz, C. Conidi, A. Cassano, Recovery of Phenolic-Based Compounds From Agro-Food Wastewaters Through Pressure-Driven Membrane Technologies, 2019. https://doi.org/10.1016/b978-0-12-815056-6.00006-1.

[63] H.K. Obied, M.S. Allen, D.R. Bedgood, P.D. Prenzler, K. Robards, R. Stockmann, Bioactivity and analysis of biophenols recovered from olive mill waste, J. Agric. Food Chem. 53 (2005) 823–837. https://doi.org/10.1021/jf048569x.

[64] N. Rahmanian, S.M. Jafari, C.M. Galanakis, Recovery and removal of phenolic compounds from olive mill wastewater, J. Am. Oil Chem. Soc. 91 (2014) 1–18. https://doi.org/10.1007/s11746-013-2350-9.

[65] D. Ryan, K. Robards, Phenolic compounds in olives, Analyst. 123 (1998) 31–44. https://doi.org/10.1039/a708920a.

[66] A. Cassano, G. De Luca, C. Conidi, E. Drioli, Effect of polyphenols-membrane interactions on the performance of membrane-based processes. A review, Coord. Chem. Rev. 351 (2017) 45–75. https://doi.org/10.1016/j.ccr.2017.06.013.

[67] J. Sabaté, M. Pujolà, J. Llorens, Comparison of polysulfone and ceramic membranes for the separation of phenol in micellar-enhanced ultrafiltration, J. Colloid Interface Sci. 246 (2002) 157–163. https://doi.org/10.1006/jcis.2001.8057.

[68] P. Tapia-Quirós, M.F. Montenegro-Landívar, M. Reig, X. Vecino, J. Saurina, M. Granados, J.L. Cortina, Integration of membrane processes for the recovery and separation of polyphenols from winery and olive mill wastes using green solvent-based processing, J. Environ. Manage. 307 (2022). https://doi.org/10.1016/j.jenvman.2022.114555.

[69] I.-C. Yeh, J.L. Lenhart, B.C. Rinderspacher, Molecular Dynamics Simulations of Adsorption of Catechol and Related Phenolic Compounds to Alumina Surfaces, J. Phys. Chem. 2015 (n.d.) 7721–7731. https://doi.org/10.1021/jp512780s.

[70] Y. El Rayess, C. Albasi, P. Bacchin, P. Taillandier, M. Mietton-Peuchot, A. Devatine, Analysis of membrane fouling during cross-flow microfiltration of wine, Innov. Food Sci. Emerg. Technol. 16 (2012) 398–408. https://doi.org/10.1016/j.ifset.2012.09.002.

[71] X. Shi, L. Zhu, B. Li, J. Liang, X. yan Li, Surfactant-assisted thermal hydrolysis off waste activated sludge for improved dewaterability, organic release, and volatile fatty acid production, Waste Manag. 124 (2021) 339–347. https://doi.org/10.1016/j.wasman.2021.02.024.

[72] G.S. Live Lozada, A.I. García López, A. Martínez-Férez, J.M. Ochando-Pulido, Boundary flux modelling of ceramic tubular microfiltration towards fouling control and performance maximization for olive-oil washing wastewater treatment and revalorization, J. Environ. Chem. Eng. 10 (2022). https://doi.org/10.1016/j.jece.2022.107323.

[73] B.I. Harman, H. Koseoglu, N.O. Yigit, M. Beyhan, M. Kitis, The use of iron oxide-coated ceramic membranes in removing natural organic matter and phenol from waters, Desalination. 261 (2010) 27–33. https://doi.org/10.1016/j.desal.2010.05.052.

[74] R. Navarro-Lisboa, C. Herrera, R.N. Zúñiga, J. Enrione, F. Guzmán, S. Matiacevich, C. Astudillo-Castro, Quinoa proteins (Chenopodium quinoa Willd.) fractionated by ultrafiltration using ceramic membranes: The role of pH on physicochemical and conformational properties, Food Bioprod. Process. 102 (2017) 20–30. https://doi.org/10.1016/j.fbp.2016.11.005.

[75] M.D. Di Mauro, B. Tomasello, R.C. Giardina, S. Dattilo, V. Mazzei, F. Sinatra, M. Caruso, N. D'Antona, M. Renis, Sugars and minerals enriched fraction from olive mill wastewater for promising cosmeceutical application: Characterization, in vitro and in vivo studies, Food Funct. 8 (2017). https://doi.org/10.1039/C7FO01363A.

[76] C.M. Sánchez-Arévalo, Á. Jimeno-Jiménez, C. Carbonell-Alcaina, M.C. Vincent-Vela, S. Álvarez-Blanco, Effect of the operating conditions on a nanofiltration process to separate low-molecular-weight phenolic compounds from the sugars present in olive mill wastewaters, Process Saf. Environ. Prot. 148 (2021) 428–436. https://doi.org/10.1016/j.psep.2020.10.002.

[77] A. Cassano, C. Conidi, E. Drioli, Comparison of the performance of UF membranes in olive mill wastewaters treatment, Water Res. 45 (2011) 3197–3204. https://doi.org/10.1016/j.watres.2011.03.041.

[78] P. Blanpain-Avet, J.F. Migdal, T. Bénézech, Chemical cleaning of a tubular ceramic microfiltration membrane fouled with a whey protein concentrate suspension-

Characterization of hydraulic and chemical cleanliness, J. Memb. Sci. 337 (2009) 153–174. https://doi.org/10.1016/j.memsci.2009.03.033.

V.3 Deep study on fouling modelling of ultrafiltration membranes used for OMW treatment: comparison between semi-empirical models, response surface and artificial neural networks

Presentado en Food and Bioprocess Technology, Noviembre 2022
(Estado: En revisión)

Magdalena Cifuentes-Cabezas[a*], José Luis Bohórquez-Zurita[b], Sandra Gil-Herrero[b], María Cinta Vincent-Vela[a,b], José Antonio Mendoza-Roca[a,b], Silvia Álvarez-Blanco[a,b]

[a] Research Institute for Industrial, Radiophysical and Environmental Safety (ISIRYM), Universitat Politècnica de València, C/Camino de Vera s/n, 46022, Valencia, Spain

[b] Department of Chemical and Nuclear Engineering, Universitat Politècnica de València, C/Camino de Vera s/n, 46022, Valencia, Spain

*magcica@posgrado.upv.es

Abstract

Olive oil production generates a large amount of wastewater, called olive mill wastewater (OMW). This paper presents the study of the effect of transmembrane pressure (TMP) and cross flow velocity (CFV) on the decrease in permeate flux of different ultrafiltration membranes (material and pore size) when treating a two-phase olive mill wastewater (olive oil washing wastewater, OOWW). Both semi-empirical models (Hermia models adapted to tangential filtration, combined model and series resistance model), as well as statistical and machine learning methods (response surfaces (RSM) and artificial neural networks (ANN)), were studied. Regarding the Hermia model, despite the good fit, the main drawback is that it does not consider the possibility that these mechanisms occur simultaneously in the same process. According to the accuracy of the fit of the models, in

terms of R^2 and SD, both the series resistance model and the combined model were able to represent the experimental data well. This indicates that both cake layer formation and pore blockage contributed to membrane fouling. The inorganic membranes showed a greater tendency to irreversible fouling, with higher values of the Ra/RT (adsorption/total resistance) ratio. RSM ANOVA showed that both CFV and TMP are significant variables with respect to permeate flux for all membranes studied. Using the ANN model, all data provided high R^2, ranging from 0.96 to 0.99. However, the comparison of all the analyzed models showed that depending on the membrane, one model fits better than the others. Finally, through this work it was possible to provide a better understanding of the data modeling of different ultrafiltration membranes used for the treatment of OMW.

Keywords Ultrafiltration; Fouling mechanisms; Semi-empirical models; Response surface; Artificial neural networks

1. Introduction

Olive oil is one of the fundamental pillars on which the Mediterranean diet is built. The relevance of this product is based, among other reasons, on the versatility of olive oil. The antioxidant nature, derived from the presence of phenolic compounds, and the prevention of diseases such as diabetes, obesity and cancer make olive oil an essential product in people's diet. Currently, there are three different methods for the production of olive oil, traditional or pressed process, three-phase continuous centrifugation and two-phase continuous centrifugation. The latter is the most widely used in Spain, and due to its lower water consumption, more countries are expected to adopt this production methodology [1]. Olive Oil Washing Wastewater (OOWW) is, together with two-phase olive pomace (alperujo in Spanish), the characteristic residue of the two-phase centrifugation process [2].

Membrane processes have become a widely used technique in the food industry, either for the treatment of food products or by-products. Membrane processes provide gentle treatment of product at low (to moderate) temperature, they produce no chemical damage, can be highly automated and easy operated, and they have low energy consumption compared to other processes and achieve high separation and selectivity. Although there are many

experimental studies with pressure-driven membranes for olive mill wastewater (OMW) treatment, few are focused on analysis modelling studies of fouling membranes [3-5], few refer to UF [6,7]. Specifically regarding OOWW, there are few experimental studies with UF membranes [8-10], and narrowing down even more when it comes to UF modelling [11]. On the other hand, to the best of our knowledge, there is no study that compares theoretical models with statistical and machine learning methods to predict the permeate flux of the OMW ultrafiltration. The importance of the study through mathematical models of the behavior of the membranes in a specific process, not only allows to identify the predominant type of fouling, but also to know what the optimal conditions are to carry out the separation process in the most efficient way.

Ultrafiltration (UF), either as a previous or final stage (pretreatment to post-treatment), has been studied experimentally, analyzing different membranes and operational conditions; as well as through mathematical models [12]. Membrane modeling helps to understand and mitigate the main bottleneck of membrane processes, membrane fouling [13]. The constant interaction between the feed particles and the membrane surface leads to fouling, which causes a partial or severe restriction of permeate passage. Fouling is caused by several complex kinetic processes that result in the continuous deposition of molecules on the membrane surface, leading to eventual substance adsorption and/or blockage of the membrane pores. This fouling depends on multiple factors such as the characteristics of the stream to be treated, type of membrane (material, configuration and pore size) and operating conditions. Fouling is the main cause for the lack of large-scale implementation of these membrane separation processes. Severe membrane fouling not only increases operating time and cost (energy, cleaning, and maintenance), it reduces membrane life and deteriorates permeate quality. Therefore, understanding the mechanisms of membrane fouling and providing effective fouling control is crucial in membrane filtration research [12,14,15].

To this end, wide varieties of models have been developed to study fouling, which can be classified into empirical, theoretical or semi-empirical models. Among all the existing models in the literature, the semi-empirical ones proposed by Hermia [16] are the most used to fit experimental data in UF processes. These models were developed for conventional filtration

processes, but their adaptation to tangential flow is, at the same time, widely used in the scientific community. The main drawback of the models proposed by Hermia lies in the fact that they do not take into account the possibility that these mechanisms occur simultaneously in the same process [17]. Various authors point out that the decrease in permeate flux is not only explained by one of these mechanisms but may be due to the action of various types of fouling. This is the case of Bowen et al. [18] and Jonsson et al. [19], who studied the fouling of microfiltration membranes during protein filtration (BSA). They concluded that membrane fouling consists of (complete or intermediate) pore blockage followed by cake formation. Finally, hence the need to propose a new mathematical model, which combines the phenomena of complete pore obstruction and cake formation, in an attempt to adjust more closely to reality [20-22]. On the other hand, the most widely used empirical model is based on Darcy's law and considers that the permeate flux decline is due to different hydraulic resistances [23].

In recent years, statistical and machine learning methods have been used in various areas [24-27], as well as for the modeling of membrane processes [28-29]. One of the widely used statistical approaches is the Response Surface Methodology (RSM) which can analyze complex multi-component processes by approximating the relationship between the independent variables and response variables in terms of a polynomial regression equation. RSM is a statistical method of data analysis that allows a better understanding of a process than conventional experimental methods [30]. Machine learning relates to intelligent systems that can adapt their behavior during the system training stage to newly provided information. Modeling through intelligent methods such as Artificial Neural Networks (ANN) has proven to be a predominant option that is made up of a generic structure that has the ability to learn and memorize data trends and accurately predict response variables [31]. ANN has proven to be an effective predictive tool for modeling the behavior of nonlinear dynamic systems in engineering applications. They have been used successfully to model the permeate flux decline of ultrafiltration and other membrane processes as a function of process operating variables [32].

The aim of this work is to study the effect of transmembrane pressure (TMP) and cross flow velocity (CFV) on the decrease in permeate flux of different ultrafiltration membranes

when treating OOWW. For this purpose, the Hermia adapted to cross flow filtration models, combined model and series resistance model were studied to identify the main fouling mechanism. Then response surface (RSM) and artificial neural networks (ANN) were used to obtain the best operational conditions for each membrane. Finally, the models were compared with each other. As far as we are concerned, there are no works on mathematical models implemented to understand the fouling of ultrafiltration membranes of different pore sizes, both inorganic and organic, when treating OOWW. On the other hand, no studies were found on the use of non-phenomenological models for the study of OMW (including OOWW).

2. Theory: Modeling of ultrafiltration membranes

The models used in this study are presented in this section.

2.1 Hermia model adapted to cross flow filtration

The model is based on the one formulated by Hermia [16] for dead-end filtration at constant pressure. The model adapted to cross flow ultrafiltration incorporates the flow associated with mass transfer by reverse transport. Eq. (1) presents the general equation for the Hermia model adapted to crossflow filtration:

$$-\frac{dJ}{dt} = K(J - J_{ss}) \cdot J^{2-n} \quad (1)$$

Where K is the constant of the Hermia model; J is the permeate flux; J_{ss} is the steady-state permeate flux and n is the parameter indicating the type of fouling. Four different types of membrane fouling mechanisms are considered in this model. Each fouling mechanism has a mathematical equation to predict the permeate flux as a function of time, which will depend on the value of n: complete pore blocking (n = 2), intermediate blocking (n = 1), standard blocking (n = 1.5), and cake layer formation (n = 0) [33].

2.2 Combined model

This model arises from the impossibility of explaining the typical evolution of permeate flux with a single fouling mechanism. It was developed by Ho and Zydney [21] and then simplified and modified by different authors [22,34,35]. This model combines two stages, a first abrupt decline in the first minutes, due to pore blocking phenomena, followed by a slow decrease in permeate flow caused mainly by the accumulation of molecules on the membrane surface resulting in a cake layer. The model shows a smooth transition between the two fouling mechanisms proposed by Hermia, the complete blocking model and the cake layer formation model. The combined model represents a more realistic model to explains membrane fouling than models considering only one fouling mechanism [22].

$$J_{combined\ model} = \alpha \cdot J_{complete\ blocking\ model} + (1-\alpha) \cdot J_{cake\ layer\ formation\ model} \quad (2)$$

Each model has a constant; K_{cb} for the complete pore blocking model and K_{cf} for the cake formation model. In this model, only a fraction of the membrane pores is completely blocked, represented by the parameter α. Finally, the equation for the combined model is the one presented in Eq.2.

2.3 Resistance in series model

This model considers that decline in permeate flux is caused by different hydraulic resistances. These are, the resistance of the membrane itself (R_m), the resistance due to adsorption and concentration polarization (R_a) and resistance due to cake layer formation (R_{cf}). The parameter called total hydraulic resistance (R) is the sum of individual resistances. The general equation follows the Darcy`s Law and is presented in Eq. 3:

$$J = \frac{\Delta P}{\mu \cdot R} \quad (3)$$

Where ΔP is the transmembrane pressure and μ is the feed solution viscosity. Furthermore, Ra can be adjusted using an exponential equation. Finally, the general equation for the resistance in series model is the following:

$$J = \frac{\Delta P}{\mu\left(R_m + R_a'\left(1 - e^{-b \cdot t}\right) + R_{cf}\right)} \quad (4)$$

With R'_a representing the steady-state adsorption and concentration polarization resistance and b the fouling rate due to adsorption [15].

2.4 Response surface methodology

Response surface methodology (RSM) predicts the relation between input and output variables by means of a complex process where the interaction of different variables with each other is considered. And thus, be able to determine the optimal operating conditions [36]. To obtain a reliable analysis, a multivariate statistical analysis of the experimental data was performed. In multifactorial statistical analysis of experimental data, all factors vary simultaneously. The influence of TMP and CFV on the average permeate flux (J_a) and cumulative flux decline (SFD) were studied, using Equation 5 and 6:

$$J_a = \frac{1}{t_N} \cdot \int_0^t J(t) \cdot dt \quad (5)$$

$$\text{SFD} = \sum_{i=1}^{N} \frac{J(0) - J(i)}{J(0)} \quad (6)$$

Where *J(t)* is the evolution of the permeate flux over time obtained from experimental data, t is time and t_N is the time corresponding to the last permeate flux value considered. The technique to achieve the desired models was *Backwards* elimination, it starts with all the variables in the model and eliminates them one at a time until only the significant variables are left in the model. Once the regression coefficients are obtained, the equation that defines the model is also obtained as a result of analysis of the significance of each of the variables considered, obtained after the analysis of variance (ANOVA).

2.5 Artificial neural networks

Artificial Neural Networks (ANN) use a black box model. Therefore, ANN predictions are completely empirical and can be considered not phenomenological. ANN predict output

values from input data but do not provide information about the process. A neural network has two components: the node, which consists of a neuron with positioning information, and a connection, which consists of a weight with node addressing information. Neurons (single processing elements) are interconnected through a set of synapses or connecting links, each of which is characterized by a scalar weight (w). For each neuron receiving n inputs from various sources, the input signals are weighted according to the neuron's respective synaptic weights, then added to another externally applied scalar, called bias (b), according to the following equation:

$$Sum = \sum_{i=1}^{n} x_i \cdot w_i + b \tag{7}$$

With, x_i representing the i^{th} input variable. In this work, a type of non-recurrent feed-forward ANN with corrective supervised learning is used, in which the inputs and targets are known [37]. The type of network is known as a multilayer perceptron (MLP). MLP ANNs (Fig. 5.19) are known as universal function approximators and, with a single hidden layer and an output layer, the predict nearly any relationship between input and output variables. The feed-forward neural network usually has one or more hidden layers, which allow the network to model complex and non-linear functions [38]. There are studies that indicate that working with two or more hidden layers is better than working with one [39], others comment that more hidden layers generate an excessive focus of the network on the idiosyncrasies of the individual samples, making it difficult for the model to adapt to the new inputs [40]. Regarding the number of neurons, as Sarkar et al. [41] well explained, there is no concrete rule for the selection of the number of hidden neurons, rather than it is mainly determined by experience and trial and error. However, it is important to note that the number of neurons is a critical point for network performance. In this way, too few neurons can waste a large amount of training time to find the optimal representation, while too many neurons can lead the system to memorize the pattern in the data or to overtraining [42]. Finally, each neural network will be specific to a given system, always keeping in mind that the neural network must be as simple as possible to make good predictions, otherwise overfitting problems may occur [43]. Therefore, it was decided to evaluate working with one or two hidden layers, increasing the number of neurons until verifying that the improvement in the measure of fit with one more

neuron was not significant. In this work only the results with a hidden layer of 5 and 6 neurons and two hidden layers of 5 neurons are presented. The selection of the data partition for network training and validation is another important factor to consider. Generally, the training group is the one with the higher amount of data, with around 70% or 80% of all the data used in this group, whereas the remaining data are used for validation and prediction [44].

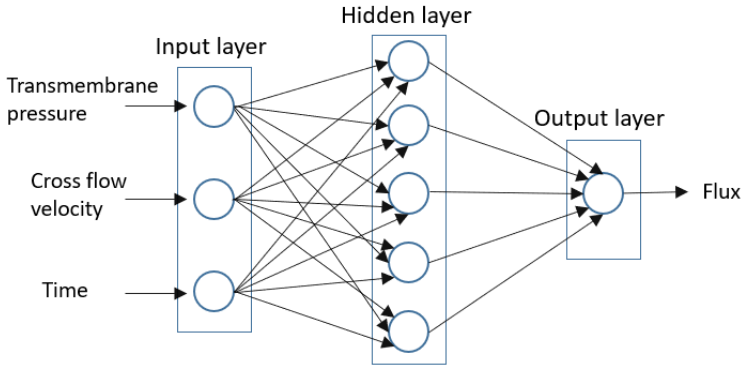

Fig. 5.19 Diagram of multilayer layer perceptron (MLP) neural network structure, example for 1 hidden layer with 5 neurons

Therefore, the experimental data were randomly divided into three groups, but with the higher weight of number for the training group (70% data for training group, 15% data for validation group, and 15% for test group). Once the neural network is trained, the analysis of the regression results for the 3 groups of data mentioned above is of special importance because it provides information about the accuracy of the ANN. It is also important to check whether the error histogram fits a narrow normal distribution around zero error.

3. Experimental Methodology

Seven membranes were tested for the OOWW treatment. The feed samples were obtained at the outlet of the vertical centrifuge after washing the olive oil, where the two-phase continuous centrifuge process is used. Prior to the ultrafiltration stage, the samples were

pretreated by sedimentation, flotation, and cartridge filtration (60 microns). The experimental data, as well as the analysis of the results, were presented in previous studies [9,10]. The operational conditions were CFVs between 1.5 and 3.4 $m \cdot s^{-1}$ and TMPs between 1 - 3 bar for the organic membranes, and CFVs between 2 and 4 $m \cdot s^{-1}$ and TMPs between 1 - 3 bar for inorganic membranes. In table 1 are presented the characteristics of the membranes used. It can be seen that they differ in their molecular weight cut-off (MWCO) as well as in material and configuration.

Table 5.7 Characteristics of the UF membranes analyzed in this work (manufacturer data)

Membrane	UH004	UP005	Inside Céram 5	RC70PP	Inside Céram 15	UH050	Inside Céram 50
Manufacturer	Microdyn Nadir	Microdyn Nadir	Tami Industries	Alfa Laval	Tami Industries	Microdyn Nadir	Tami Industries
Material	PESH[b]	PES[c]	TiO_2/TiO_2[d]	RCA[e]	TiO_2/ ZrO_2[f]	PESH[b]	TiO_2/ ZrO_2[f]
Configuration	Flat	Flat	Tubular	Flat	Tubular	Flat	Tubular
MWCO[a] (kDa)	4	5	5	10	15	50	50
T max (˚C)	95	95	300	60	300	95	300
pH	0 - 14	0 - 14	0 - 14	0 – 10	0 - 14	0 - 14	0 - 14
Hydraulic permeability*	>27[g]	>30[g]	>80[g]	>40[g]	>80[g]	>200[g]	>210[g]
$(L \cdot h^{-1} \cdot m^{-2} \cdot bar^{-1})$	32.67[h]	44.07[h]	94.99[h]	78.50[h]	100.26[h]	191.75[h]	223.33[h]

[a]MWCO: molecular weight cut-off; [b]PESH: Permanently hydrophilic polyethersulfone; [c]PES: Polyethersulfone; [d] TiO_2/TiO_2: support and active layer of titanium dioxide; [e]RCA: Regenerated cellulose acetate; [f]TiO_2/ ZrO_2: support layer of titanium dioxide and active layer of zirconium dioxide; [g]Manufacturer data; [h]Experimentally determined in previous works; * Water, at 25 ℃.

3.1 Software

Hermia models and the combined model were fitted to the experimental data using MathCad®15 software (PTC Needham, EE.UU), for fouling mechanism analysis. The fitting was carried out with the Genfit algorithm, which uses an optimized version of the Levenberg-Marquadt curve-fitting method. The fitting accuracy for each operating condition tested was

evaluated in terms of the regression coefficient (R^2) and the standard deviation (SD). Statgraphics Centurion 18 software was used for RSM analysis. For ANN, MATLAB® R2021b (MathWorks, EE.UU) was used. The transfer function used for t the hidden layer was the sigmoidal function called transig, whereas a linear function (purelin) was used in the output layer. The training algorithm used is trainlm, which uses the Levenberg-Marquardt algorithm, which offers the fastest convergence capacity among the available training methods. The statistical study (ANOVA) was carried out with the Statgraphics Centurion 18 software.

4 Results

4.1 Analysis of membrane fouling mechanisms by means of Hermia's, model

When analyzing the results obtained with the Hermia model (supplementary material, tables S1-S2), it was observed that in most of the cases studied, the models fit the experimental data with almost the same precision (acceptable values of R^2 and SD). However, the standard pore blockage model (n=1.5) did not accurately fit the experimental data and was therefore not considered in this analysis. Fig. 5.20 shows the fit obtained using the Hermia model for organic membranes at fixed conditions (TMP of 2 bar and CFV of 2 $m \cdot s^{-1}$). It can be seen how the difference between the Hermia models for organic membranes was minimal; this was observed in most of the operating conditions tested (Table 5.S1-S4). This was also reflected in the values of R^2, obtaining very similar mean values for the different models. The mean R^2 values from complete pore blocking, intermediate pore blocking, and cake formation were between 0.87 – 0.95, 0.89 – 0.94, 0.82 – 0.95 and 0.81 – 0.91 from UH004, UP005, RC70PP and UH050, respectively. Considering all the experiments, for the UP005, UH004 and RC70PP membranes the model that best fits the experimental results was complete pore blocking (n=2), followed by intermediate pore blockage (n=1) and cake formation (n=0). Similar results were obtained by Luján-Facundo et al. [45] in their study on ultrafiltration membrane fouling in whey processing. They observed similar R^2 values for the UP005. The models that fitted the best in their case were the intermediate blocking model and the complete blocking model. They related it to the fact that both fouling mechanisms occurred simultaneously since both models consider external fouling to occur on the membrane surface. This could also be explained by the MWCO, since external membrane fouling is directly

related to the size difference between the solute molecule and the membrane pores [46]. The complete pore blockage model assumes that the molecules in the feed are much larger than the pore size of the membranes [47]. Therefore, larger particles can be deposited on the surface of membranes with low MWCO. Regarding the RC70PP membrane, Wang et al. [48] also obtained similar results when studying the mechanism of membrane fouling in broth succinic acid fermentation ultrafiltration. They found that the full pore-blocking model fitted the best, however, they also obtained high fitting accuracy using standard and intermediate blocking models.

Comparing the results obtained for intermediate pore blockage and cake formation from the RC70PP with those of the UP005 and UH004 membranes, a slight increase in the value of R^2 is observed for both fouling mechanisms. This may be due to the type of material (regenerated cellulose acetate) and the specific characteristics of the RC70PP membrane surface, which give them different properties from PES membranes (UP005 and UH004) [49]. Also, the fact that the RC70PP membrane has a higher MWCO (10 kDa) than the UP005 (5 kDa) and UH004 (4 KDa) membranes, favors the passage of larger particles and therefore and it also influences the fouling mechanism. This can also be related with the result obtained with the UH050 membrane, although once again the three models delivered acceptable values of accuracy (mean R^2 value of 0.88), the cake layer formation fouling mechanism was the predominant one (mean R^2 above 0.91). High MWCOs reduce the prevalence of fouling due to pore obstruction, giving greater weight to the formation of a cake layer. This was also observed by Yang et al. [50] in his study of tanning wastewater treatment by ultrafiltration. When analyzing two membranes of the same MWCO (50 kDa) but different material (PES and PVDF), they observed that the cake filtration was the main fouling mechanism (R^2 over 0.92) in the process and was independent of membrane material. This fact can be explained by Fick's law and the boundary layer theory, since the higher the permeate flux is, the greater the backflow and, therefore, there will be a higher concentration of particles near the membrane surface, causing cake formation [51].

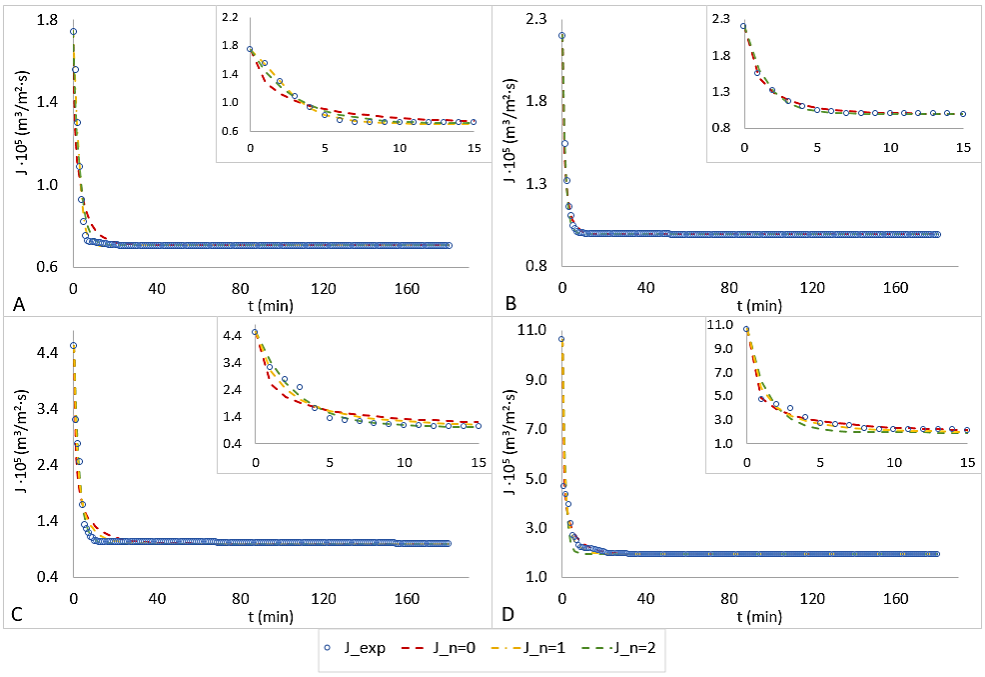

Fig.5.20 Hermia model fitting for the organic membranes at a transmembrane pressure of 2 bar and cross flow velocity of 2 $m \cdot s^{-1}$. A: UH004; B: UP005; C: RC70PP; D: UH050

On the other hand, if the results are analyzed based on the operating conditions of the experiment, an increase in TMP resulted in a better accuracy for the cake layer formation model. This was more significant for the membrane with higher MWCO. This is because higher TMPs lead to a higher concentration of substances on the membrane surface for a specific filtration time, which leads to a higher cake layer build up and thus an increase in the membrane resistance [52]. Only the UH050 membrane showed a significant influence of CFV in the accuracy of the model, presenting the worst fits for complete pore blockage at higher CFVs. This was also noted by Alborzi et al. [53] in their analysis of fouling in ultrafiltration of producer water (the largest waste byproduct of oil and gas production), noting that more studies also reported this trend. Although the operating conditions influence the accuracy of each model, they do not change the predominant fouling mechanism for each membrane. For low MWCO membranes (UH004, UP005 and RC70PP) the fouling mechanisms is complete

pore blockage, whereas for high MWCO membranes such as the UH050 membrane the cake layer formation model fitted the best.

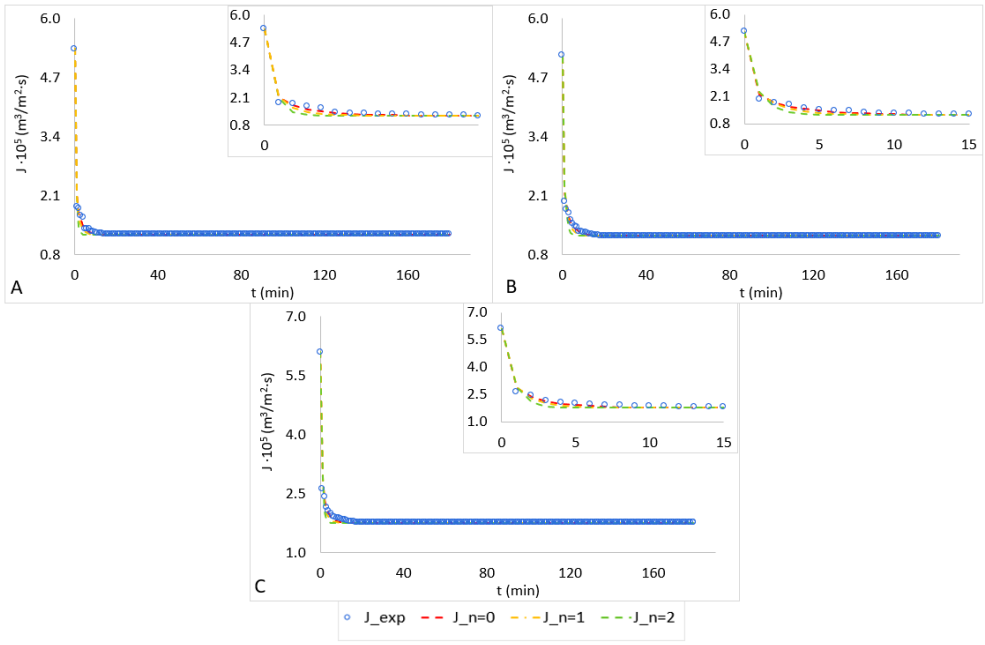

Fig.5.21 Hermia model fitting for the inorganic membranes at a transmembrane pressure of 2 bar and cross flow velocity of 2 m/s. A: Inside Céram 5; B: Inside Céram 15; C: Inside Céram 50

The inorganic membranes presented a very different behavior from the organic ones. The difference in the fitting accuracy between models was significantly larger than that observed for organic membranes, with the cake formation model having the highest R^2 (Table 5.S3). These results are similar to those observed by Corbatón-Báguena et al. [20]. In their study of the fouling mechanism of ultrafiltration membranes fouled with whey model solution, they also observed better results with the cake layer formation model for the 15 kDa inorganic membrane than in the case of two organic membranes (5 and 30 kDa). As can be seen in Fig. 5.21, the sharp flux decline obtained in the first few minutes is responsible for the low accuracy of the other models to predict the experimental data. Both R^2 and standard deviation

values worsened as TMP increased at a fixed CFV or viceversa. The complete pore blocking model showed at the extreme operating conditions (TMP 3 bar and CFV 4m·s^{-1}) fit values well below those for cake layer formation. On the other hand, at a fixed TMP and intermediate values of CFV, the models fit better than in the case of high or low values of CFV. Likewise, if the variable that changes is the TMP, it can be observed that for the same CFV, the values of R^2 are higher at low TMP. In the ultrafiltration fouling studies with Huanggi (Radix astragalus, root of Astragalus) extracts carried out by Cai et al. [54], also observed a strong influence of TMP on cake formation in a hollow fiber membrane of 10 kDa (Microza, USA). Indicating that TMP is an important driving force for cake formation and the most important factor in UF membrane fouling. As with the other inorganic membranes, the cake layer formation model fits the experimental data of the Inside Céram 50 membrane better than the other models. In this case, as with the UH050 membrane, the high permeate flux due to its high MWCO causes an increase in solute concentration at the membrane surface due to convective transport. The boundary layer will continue to grow until the permeate flux and the back-diffusion flux away from the membrane surface reach equilibrium. Therefore, the higher the permeate flux density is, the higher the concentration at the membrane surface, which favors the cake layer formation fouling mechanism.

Finally, the Hermia model was not able to accurately predict membrane fouling exclusively with one of the proposed mechanisms for the most extreme operating conditions tested. Very low R^2 values of the three fouling models (sometimes 0.4) were obtained, especially for the higher MWCO membranes tested. The fact that the model cannot differentiate one mechanism from another may be because all the fouling mechanisms occur at the same time.

4.2 Analysis of membrane fouling mechanisms by means of the resistance in series and Combined model

Continuing with the resistance in series and combined model (Tables 5.S4-S7), both models achieved a higher R^2 (over 0.9) than Hermia models. Similar results were observed by Carbonell-Alcaina et al. [55] in the study of the UP005 membrane for the treatment of brine from the table olive production process. The combined model, which considers the

intermediate pore blocking and the cake formation mechanisms proposed by Hermia, presented a better fit than the Hermia models separately. On the other hand, as in this study, they observed that the higher the CFV, the better the fit of both models. They also observed a direct relationship of model accuracy with the TMP. Higher accuracy was achieved as TMP increased. A high fitting accuracy of the combined and resistance in series models was observed (Fig 5.S1), which implies that the predominant fouling mechanisms for this case are the combination of different types of fouling. Therefore, both models are capable of predicting the behavior of the flux both in the first minutes of the experiment, where the permeate flux falls sharply, and in the remaining minutes when the permeate flux becomes practically constant. However, taking into account the R^2 values, the combined model presented a better fit than the resistances in series model for all organic membranes. Similar results were obtained by Corbatón-Báguena et al. [20]. They observed that the combined model had the highest fitting accuracy for the polymeric membranes (UP005 and UH030) when treating a whey model solution. This is due to the fact that the two fouling mechanisms that this model takes into account manage to represent the real scenario. In this case, the fouling mechanism that represents the total obstruction of the pores is responsible for the pronounced decrease in permeate flux in the first minutes, giving way to a cake formation that induces stabilization and reaches a steady state.

Again, due to the good fits presented by both models (Fig. 5.S2), it was difficult to select one, but again it is the combined model that presents the best fitting accuracy. As for the organic membrane, it could be inferred that both fouling mechanisms, cake filtration and pore blocking contribute to the fouling of the membrane. Huang et al. [56] presented similar conclusions on 20 kDa ceramic membranes used for cold rolling emulsion wastewater treatment. They observed that for a CFV between 4 and 4.3 $m \cdot s^{-1}$, both models offered similar precision. It is important to highlight that they worked with a plant made up of 6 modules, each of which contains 36 tubular ceramic membranes with a filtration area of 0.47m^2 each, which allows them to work with a capacity of 24 $m^3 \cdot h^{-1}$ of wastewater. Therefore, the fouling mechanism observed in this study with a laboratory scale plant can be extrapolated to industrial size plants.

Table 5.8. Combined model and Resistance in series model parameters for organic membranes (boundary conditions)

			Combined			Resistance in series		
Membrane	CFV ($m \cdot s^{-1}$)	TMP (bar)	K_{cb} (s^{-1})	$K_{cf} \cdot 10^7$ ($s \cdot m^{-2}$)	α	R_a/R_t (%)	R_{cf}/R_t (%)	Rm/Rt (%)
	1.5	1	278.127	12.298	0.973	27.64	64.37	7.99
UH004	1.5	2.5	216.509	10.142	0.655	31.11	61.49	7.41
	3.4	2.5	449.533	0.216	0.960	39.47	53.16	7.36
	1.5	1	397.941	5.680	0.611	3.01	77.31	13.68
UP005	1.5	2.5	214.995	6.531	0.257	12.89	79.15	7.96
	3.4	2.5	159.583	1.115	0.963	28.78	62.49	8.73
	1.5	1	120.257	3.149	0.767	12.22	80.88	6.90
RC70PP	1.5	2.5	214.995	6.531	0.257	23.34	72.45	4.21
	3.4	2.5	110.448	2.275	0.254	29.02	66.23	4.75
	1.5	1	70.175	0.8286	0.963	33.96	62.24	3.80
UH050	1.5	2.5	166.403	10.66	0.687	30.45	66.02	3.52
	3.4	2.5	226.229	3.411	0.676	45.92	48.78	5.29

Ra/Rt: adsorption/total resistance ratio; Rcf/Rt: cake layer formation/total resistance ratio; Rm/Rt: membrane/total resistance ratio

Table 5.8 shows the parameters referring to the combined model, for the boundary conditions (lowest and highest CFV and TMP tested) of the organic membranes (full table in supplementary material). Although the Hermia model predicted that complete pore blockage was the most appropriate fouling mechanism, the cake formation mechanism is also an important part of fouling of low MWCO membranes. In the same way, when using the Hermia model, it was difficult to select the model that reflected the experimental data well. This can be explained with the combined model or the resistance in series model. As it was mentioned before, more than one process is responsible for fouling. It can be seen how, as the CFV increases the parameters α and K_{cb} increase, while K_{cf} decreases. On the other hand, at a fixed CFV, the increase in TMP generates an increase in the K_{cf} values (only for low CFV values). The parameter K_{cb} is related to complete pore blocking while K_{cf} is related to cake formation. On the other hand, the higher the value of α is, the greater the relevance of pore blockage in membrane fouling. Similar results were observed for the RC70PP membrane, this observed trend could be explained by the accumulation of molecules on the membrane surface. The higher the pressure at low CFV, the higher the concentration of molecules on the membrane

surface, which will tend to form cake layer. Whereas an increase in CFV will generate greater turbulence at the membrane surface, thus minimizing the concentration polarization at the membrane surface, which significantly inhibits the formation of a cake layer. Regarding UH050, the values of α confirm that for low TMP the predominant fouling mechanism is the complete blockage of the pores. On the other hand, observing the constants K_{cb} and K_{cf}, it can be concluded that at the same TMP an increase in CFV generates less cake formation and greater pore obstruction. The highest value of K_{cb} in UH050 membrane was expected since the blocking resistance increases with membrane pore size [57].

The great influence of cake layer formation in low MWCO membranes could also be observed when analyzing the parameters of the resistance in series model, where the R_{cf}/R_t ratio was greater than the R_a/R_t. Elevated R_{cf} values, linked mainly to reversible fouling, were also observed in the study of the fractionation of the by-product of lignin processing by membranes processes to obtain phenolic compounds performed by Knapp [58]. The observed that cake layer formation was responsible for almost 90% of the fouling of UH004 and UH030 membranes. It is important to note that for membranes with a lower MWCO, the influence of R_m is higher. This is due to the fact that the lower the pore size of the membrane is, the higher the value of R_m [59]. In addition, the highest percentage of R_m/R_t presented by the UP005 could be related with the characteristics of the membrane. Gulec et al. [60] observed that the R_m of the UC030 represented the 61% of the total resistance. They attributed it to the greater the hydrophobicity of the membrane. Although the influence of R_m is low in the total membrane resistance, the R_m/R_t ratio slightly increases when the CFV increases at a fixed TMP. This could be due to the fact that a higher CFV reduces membrane fouling, improving the permeation flux through the membrane, which leads to a reduction of the retention coefficients that are external to the membrane [61].

Although all the membranes show a greater influence of R_{cf} than Ra in membrane performance, the UH050 membrane was the one that showed the greatest influence of R_a, presenting values close to 90% of the total resistance. This, together with the high influence of R_{cf} on the total resistance of the UP005 and RC70PP membranes, makes sense when analyzing the flux recovery percentages obtained after the experimental tests. As discussed in the

methodology section, the data analyzed in this work were analyzed in another study [9], where different cleaning protocols were also analyzed to recover the membranes. These two membranes were found to achieve a higher recovery (over 90%) of the initial hydraulic permeability after rinsing with osmosis water at 25°C. Since fouling due to cake layer formation is reversible [47,58], these values correspond to the high recovery observed. On the other hand, the UH050 membrane was the one that presented the highest irreversible fouling, especially at the boundary operating conditions tested, which also agrees with the highest percentages of R_a.

Table 5.9 Combined model and Resistance in series model parameters for inorganic membranes (boundary conditions)

			Combined			Resistance in series		
Membrane	CFV ($m \cdot s^{-1}$)	TMP (bar)	K_{cb} (s^{-1})	$K_{cf} \cdot 10^8$ ($s \cdot m^{-2}$)	α	R_a/R_t (%)	R_{cf}/R_t (%)	Rm/Rt (%)
Ins. Céram 5	2	1	187.126	2.467	0.630	38.28	48.47	13.25
	2	3	47.005	0.094	0.093	34.80	51.63	13.57
	4	3	60.478	1.701	0.128	36.56	49.82	13.62
Ins. Céram 15	2	1	54.013	2.467	0.388	40.32	40.85	8.83
	2	3	4.140	3.304	0.097	39.96	48.85	11.19
	4	3	47.241	19.890	0.290	34.03	54.99	10.98
Ins. Céram 50	2	1	33.961	3.391	0.220	53.65	41.17	5.18
	2	3	18.267	5.658	0.080	52.99	41.53	5.47
	4	3	15.786	5.133	0.440	54.07	40.95	4.98

Ra/Rt: adsorption/total resistance ratio; Rcf/Rt: cake layer formation/total resistance ratio; Rm/Rt: membrane/total resistance ratio

Table 5.9 presents information similar to the previous table but for inorganic membranes. For the Inside Céram 5 membrane, the values of α for low TMPs indicate that there is no clear predominance of a fouling mechanism for that operating pressure, regardless of CFV, that is, that the complete pore blockage mechanism would have, approximately the same weight in membrane fouling as the cake layer formation mechanism. It is necessary to increase TMP above 2.5 bar to observe a predominant fouling mechanism, that in this case it is cake formation. These results are consistent with those obtained for the Hermia model. Similar results were obtained for the 15 kDa membrane, the predominant fouling mechanism for high TMP was cake formation. For the membrane inside Céram 50, the low values of α present in

all the conditions analyzed, affirm that the predominant fouling mechanism in this membrane is the formation of cake layer.

Several previous studies concluded that high MWCOs are more susceptible to irreversible fouling (due to blockage and clogging of the pores) [62]. This justifies the higher percentage of R_a over R_t. It is important to highlight that the Ra parameter refers to both adsorption and concentration polarization resistance. The latter being an immovable resistance, that is, it can be removed by chemical cleaning, while that related to adsorption and pore blockage is an irreversible resistance, which is a permanent fouling that cannot be removed by any method [7]. On the other hand, the high R_{cf} values presented by low MWCO organic membranes are linked to removable fouling, which can be removed with water rinsing. These results agree with what was observed after the cleaning protocol implemented for both organic and inorganic membranes (presented in previous studies [9,10]). In general, low MWCO membranes presented the greatest recovery of the hydraulic permeability after rinsing with water, according to the following classification UP005>RC70PP>UH004> Inside Céram 15> Inside Céram 5> UH050>Inside Céram 50. The same trend was observed for the parameters R_{cf} and K_{cf}. While the parameter related to pore blocking and adsorption (K_{cb}, α and R_a) showed an inverse trend.

Within the medium-low MWCO range, the greater irreversible fouling that inorganic membranes present respect to organic membranes could be explained by the characteristics of the membrane itself and of the feed solution. Membranes with a more hydrophobic character are less resistant to fouling [63]. On the other hand, the roughness of the membrane contributes to the potential for irreversible fouling [64]. Inorganic membranes are characterized by greater roughness. In the case of the ceramic membranes the roughness parameters were 20 and 50 nm for the Inside Céram 5 and 15 membranes, respectively. For the organic membranes UP005, UH004 and RC70PP the roughness parameters were 30, 40 and 60 nm, respectively.

4.3 Statistical analysis ANOVA

To analyze which operating conditions and interactions between variables are more significant with respect to the response variable, an analysis of variance, ANOVA, was carried

out. Two independent variables were chosen to perform the statistical analysis, TMP and CFV, while average permeate flux (*Ja*) and cumulative flux decline (SFD) were chosen as the response variable. All the statistical estimators (R^2, F-ratio, T-statistic and p-value) revealed that the response model was reliable from the statistical point of view for the prediction of the response variable in the range of values considered for the dependent variables. The graphs of the contour surface of the parameter *Ja* (Fig. 5.S3 and 5.S4), showed that for the case of organic membranes, the highest values of permeate flux were achieved for the maximum values of CFV and TMP tested, this was not observed for inorganics membranes. However, it should be noted that higher values of those parameters represent higher costs and may result in a greater decrease in permeate flux. It can be seen in table 5.10, that *Ja* for most membranes seemed to be influenced by at least two independent variables or factors. All the membranes showed influence of both the CFV and TMP parameters, either by one of them alone or by their coupled influence. For organic membranes, it was observed that as the MWCO increased, more factors were significant in the prediction of with *Ja*. The *Ja* for membranes UH004 and UP005 was influenced by two factors: TMP and CFV·TMP in the case of the UH004 membrane and CFV and TMP^2 in the case of the UP005) membrane; whereas the *Ja* for the RC70PP and UH050 membranes was influenced by three factors. The R^2 value for the average permeate flux was between (90.78 – 97.28%), close to 100%, which is desirable. For the UH004 and UP005 membranes, the effects of CFV and TMP as standardized for both factors are positive, which implies that the average flux rate increases as CFV and TMP increase. The influence of the interaction between both factors was the most significant due to its higher T-statistical value. Regarding RC70PP and UH050, the influence of TMP alone and CFV^2, present a positive influence, while the influence of is TMP^2 negative on *Ja*. On the other hand, the *Ja* for the inorganic membranes was influenced by CFV and TMP^2, with the Ja for the Inside Céram 50 also influenced by TMP. The variable TMP^2 was the most significant one due to its lower p-value (between 0 – 0.007) and its higher value of the parameter T-statistic. The 50 kDa membranes, both organic and inorganic and the RC70PP membrane responded to negative influences for the *Ja* parameter. The membranes were constrained by the effect of TMP^2, which is related to pore blockage and gel layer formation [36]. This is in agreement with the results obtained when modeling fouling with theoretical models in the previous section (4.1).

Table 5.10 Model Equations obtained with ANOVA for all the membranes tested

Membrane	Model Equation
UH004	Ja = 11.8644 + 2.48071·TMP + 2.4381·CFV·TMP
	SFD = 25.7359-12.6961·CFV + 83.7588·TMP – 15.604·TMP^2
UP005	Ja = 8.73705 + 4.69545·CFV + 4.37459·TMP^2
	SFD = 109.508-2.24186·CFV·TMP
RC70PP	Ja = 6.4518 + 20.862·TMP – 2.996·TMP^2 + 0.583212·CFV^2
	SFD = 112.026 + 19.46·TMP – 3.486·TMP^2 – 1.46967·CFV^2 + 1.89379·TMP·CFV
UH050	Ja = 39.5799 + 23.2215·TMP – 4.07657·TMP^2 + 1.14624·CFV^2
	SFD = - 15.1328 + 122.313·TMP – 22.3806·TMP^2
Ins. Céram 5	Ja = 35.7028 + 2.664·CFV + 1.01538·TMP^2
	SFD = 47.014 – 3.704·CFV + 76.6129·TMP – 13.5257·TMP^2
Ins. Céram 15	Ja = 38.0768 + 2.02·CFV + 0.906483·TMP^2
	SFD = 52.326 – 4.348CFV + 73.2234·TMP – 12.6629·TMP^2
Ins. Céram 50	Ja = 16.7443 + 15.7302·TMP – 10.8953·CFV – 0.632316·TMP^2
	SFD = 163.12 – 16.3768·CFV + 5.38967·TMP·CFV – 0.427848·TMP^2

Ja: permeate flux average, SFD: cumulative flux decline

A different behavior was observed for SFD. All the membranes presented at least one factor that negatively affects the SFD. In organic membranes, MWCOs have no influence on the number of factors that have an influence on SFD. In terms of SFD, the membrane UH050 was only affected by TMP (alone and squared value), while UP005 was only affected by the coupled effect of TMP·CFV (p-value 0.0021). Regarding the low MWCO membranes (UP005, UH004 and Inside Céram, 5), it should be noted that the regression coefficient of the model predicted by ANOVA was the lowest, indicating that only 53.7% (mean value) of the variability in SFD is explained by the analysis (with the UP005 presenting the lowest percentage, 40.3%). Similar results were observed by Martí-Calatayud et al. [36] in the study of the ultrafiltration of macromolecules. Obtaining low precision for SFD with the Inside céram 5 kDa membrane, attributing it to the fact that the permeate flux decline was more noticeable in the other membrane tested (Carbosep M2 membrane). Therefore, it is possible that the use of the SDF parameter is more representative in the case of the other membranes (higher MWCO) than in the case of these ones (UP005, UH004 and Inside Céram, 5). The

UH050 membrane (R^2 of 77.84%) also presented an R^2 outside the average (R^2 average 94.33%), but it was higher than that of the UP005.

Again, the Inside Céram membranes of 5 and 15 MWCO presented a similar behavior between them for SFD, being more influenced by TMP (positively). For Inside Céram 50, the combined effect of CFV·TMP had the most significant (positive) influence on SFD. The high CFV creates a turbulence that breaks up larger molecules allowing smaller particles to come closer to the membrane surface. This phenomenon favors both the blocking of some pores and the formation of a more compact cake layer, which translates into a greater resistance to filtration and, therefore, in a decrease in the permeate flow rate. The counterproductive effect of CFV occurs at a high TMP when the tangential forces caused by CFV are lower than the driving force of TMP bringing solute molecules closer to the membrane surface [65]. This agrees with the experimental data obtained for the Inside Céram 50 membrane [10], and it is reflected in the contour surface of the parameter (Fig5. S5 and 5.S6).

Once the most suitable equations for each membrane have been obtained through multifactorial statistical analysis, the process is optimized using RSM. Second order models were applied to select the optimal operating conditions.

4.4 Response Surface Methodology (RSM)

The RSM was carried out in order to obtain the optimal operating conditions, with the idea of achieving the highest average permeate flow and the minimum SFD. It is important not to forget that the permeate flux decline with time is included in the SFD parameter, the largest values of SFD indicate that a greater permeate flux decline has been obtained, so the smallest possible SFD value is of interest. Since for a CFV 4 $m \cdot s^{-1}$ it is considered that the membrane has reached the critical point, the data corresponding to these values will not be modelled. On the other hand, as a good fit for the model of the SFD response variable for the UP005 membrane was not achieved, the representation of the contour surface plot was not carried out. The model fails to explain the behavior of the UP005 membrane for the SFD variable. For this reason, the graph of two superimposed response variables was not obtained for this membrane. For all membranes, an increase in the CFV produces an increase in the average permeate flux

and a decrease in SFD (Fig. 5.S7). The influence variable studied with respect to the response variable is also observed in the main effects of each of the variables obtained in the ANOVA analysis (section 4.3), when the effect is positive it means that by increasing the study variable (TMP, CFV) the response variable increases (*Ja*, SFD). All organic membranes showed an increase in Ja when increasing CFV, due to the greater turbulence within the membrane module, which contributes to the back diffusion of the solute from the membrane surface, reducing the phenomenon of concentration polarization [66].

Table 5.11 Summary of the minimum, maximum and optimum of the study and response variables.

Membrane		TMP (bar)	CFV ($m \cdot s^{-1}$)	$J_a(L \cdot h^{-1} \cdot m^{-2})$	SFD
UH004	Min.	1.0	1.5	17.85	49.74
	Max.	2.5	3.4	37.94	112.32
	Opt.	2.45	3.4	37.84	88.21
UP005	Min.	1.0	1.5	20.16	-
	Max.	2.5	3.4	52.05	-
	Opt.	2.5	3.4	52.04	-
RC70PP	Min.	1.0	1.5	25.63	116.3
	Max.	2.5	3.4	46.62	141.82
	Opt.	2.02	3.4	43.07	127.31
UH050	Min.	1.0	1.5	61.30	84.79
	Max.	2.5	3.4	85.41	150.77
	Opt.	1.07	3.4	73.07	90.40
Ins. Céram 5	Min.	1.0	2.0	42.05	98.99
	Max.	3.0	3.0	52.83	147.71
	Opt.	1.02	3.0	44.71	98.99
Ins. Céram 15	Min.	1.0	2.0	43.38	98.99
	Max.	3.0	3.0	52.83	147.71
	Opt.	1.39	3.0	45.65	116.22
Ins. Céram 50	Min.	1.0	2.0	53.63	128.73
	Max.	3.0	3.0	90.93	158.85
	Opt.	1.57	3.0	72.61	138.37

Ja: permeate flux average, SFD: cumulative flux decline

Table 5.11 shows the minimum (min.) (experimental conditions that achieve the lowest value of SFD), maximum (max.) (experimental conditions that achieve the highest value of *Ja*) and optimal conditions of each membrane to obtain simultaneously the highest values of *Ja* and lowest values of SFD.

It can be seen in table 5.11 how all the membranes, regardless of MWCO and material, presented the highest CFV as the optimum. Within organic membranes, it can be observed that the larger the pore size, the lower the optimal transmembrane pressure. The opposite occurs in the case of inorganic membranes, where the larger the pore size, the higher transmembrane pressure is needed to achieve an optimal performance of the membrane process. This may be due to the fact that inorganic membranes present greater fouling compared to organic ones, which is why they need higher TMPs. This is observed with the highest values of SFD, which indicates a decrease in cumulative permeate flux decline throughout the process. Therefore, higher TMP are needed for a better permeate flux. It has also been observed that organic membranes need higher transmembrane pressures than inorganic membranes, with the inorganic membranes presenting an optimal TMP between 1 - 1.57 bar. This may be because the latter membranes have higher permeabilities.

The UP005 membrane achieved a higher *Ja* value compared to the RC70PP membrane despite having a smaller pore size. This can be explained considering that the RC70PP membrane is made of RCA, with a spongy pore morphology of the active layer that causes a higher resistance to water penetration [67]. UH004 showed the least cumulative flux decline for optimal conditions. Higher values of SFD correspond to a faster and more evident the decrease in permeate flux, so that the fouling of the membrane will be more severe. Although the range of SFD values corresponding to the UH050 membrane are higher than those of RC70PP membrane, the optimal values for the RC70PP membrane present the highest fouling within the organic membranes, followed by the UH050 membrane and the UH004 membrane. This means that, although the UH050 membrane achieves the highest level of fouling under the operating conditions tested, it is reduced when selecting the optimal conditions by reducing it below the values for the RC70PP membrane.

As in the case of inorganic membranes, Inside Céram 15, despite having a higher MWCO, reached average permeate flux values practically equal to Inside Céram 5. These values were of the same order of magnitude as the values obtained for the smaller MWCO organic membranes. This could explain why pore size is not always a key factor, sometimes other membrane factors such as porosity and membrane material also affect it. The membrane that shows the greatest fouling is the Inside Céram 50 membrane (higher MWCO), followed by the organic membrane with the smallest pore size, the RC70PP membrane. In the same way, membranes with higher MWCO reach higher permeate flux values with low transmembrane pressures. Comparing membranes of the same MWCO (UP005 and Inside Céram 5), it can be seen how both achieve similar values of *Ja*, with the highest optimal value corresponding to the organic membrane. It is important to highlight that the regression coefficient of the model goes from the minimum of 0.9 to the maximum reached in the UP005 membrane with a value of 0.97.

4.5 Artificial Neural network (ANN)

As it was commented in section 2.5, several network architectures were considered but only two are presented in this work: two hidden layers each with 5 neurons and a single hidden layer varying with neurons 5 and 6. Table S8 shows the total regression coefficients for each of the tested architectures. It is important to highlight that the R^2 obtained in the training, validation and test sets are a reflection of the total R^2 presented, since the total R^2 was obtained for the three sets of values (training, validation and test sets) altogether and the values were all close. For organic membranes, the highest R^2 values were obtained in the case of the training and test sets, which were similar for each membrane. While in the case of the three ceramic membranes the values of the R^2 presented the following trend: R^2 validation > R^2 test > R^2 training. It was observed that when working with a hidden layer with 5 to 6 neurons, in general the ANN R^2 (complete data) does not present great changes (Table 5.S8). The UH050 membrane and Inside Céram 15 are the ones that are the most positively influenced. However, working with two hidden layers improves R^2 for all membranes compared to working with one hidden layer with either 5 or 6 neurons, although in most cases this improvement is not significant and a simplest network architecture with one layer is preferred. Inside Céram 15

membrane was the one with the lowest R^2 (1 hidden layer, 5 neurons). The ANN model was the only one that showed differences in the measure of fit between the Inside Céram 5 membrane and the Inside Céram 15 membrane, adjusting better to the membrane with lower MWCO. Regardless of the neurons or hidden layers used, the trend in the fitting accuracy of the different network architectures for the membranes did not change, with Inside Céram 5, UP005 and Inside Céram 50 membranes always obtaining the best fits.

All error histograms showed low error when comparing experimental target values and neural network output values, while the number of times large errors occur is low (narrow zero-centered normal distribution with small amplitude). Despite the differences between neurons and hidden layers, the regression percentages are acceptable ($R^2 > 0.9$). As it was mentioned before in section 2.5, several authors [68-69] reported that MLP with two hidden layers can often produce a better approximation with fewer weights than an MLP with one hidden layer. However, it has also been reported that a hidden layer is sufficient to approximate any continuous nonlinear function [70]. In this case, it was found that either one or two hidden layers provided good fits (Fig.5.22), and that the number of neurons has a greater impact in R^2 than the number of hidden layers. However, a larger difference in ANN fitting accuracy was expected when changing the number of neurons. Ghandehari et al. [71] observed something similar when they studied cross-flow microfiltration using ANN, where no significant improvement occurred with an additional increase from 7 to 10 neurons. Finally, the optimal neuronal architecture for the membranes was not the same for all of them. Considering a good adjustment without overly complicating the neural network, the following neuronal architectures were selected. For the UH004, UP005, RC70PP, Inside Céram 5 and Inside Céram 50 membranes, it was selected to work with 1 hidden layer and 5 neurons, whereas in the case of the Inside Céram 15 and UH0050 membranes a network architecture with 1 hidden layer and 6 neurons was selected.

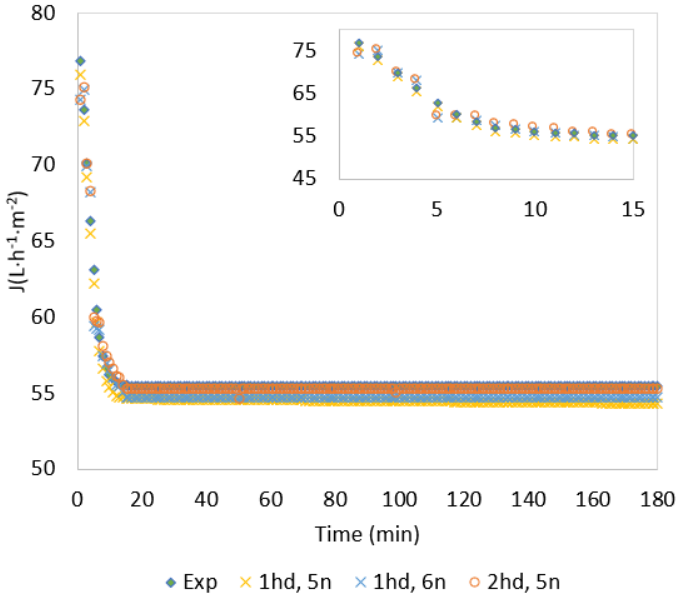

Fig. 5.22 Comparison between different ANN architectures and experimental results, Example for Inside Céram 5, CFV 4m·s^{-1}, TMP 1bar. Exp: Experimental flux; 1hd, 5n: one hidden layer with 5 neurons flux; 1hd, 6n: one hidden layer 6 neurons flux; 2hd, 5n: two hidden layers with 5 neurons each flux

Regarding the results presented in Fig. 5.22, the ANN model was able to accurately predict the non-linear evolution of the permeate flux at any time during ultrafiltration. However, in some cases, there were some deviations. It can be observed that these deviations were independent of the ANN architecture. For the UH004 membrane at a CFV 2 m·s^{-1} at low TMPs, the values experimental data and ANN predictions for short time scales present a slight deviation. A similar trend was observed with the UP005 membrane at CFVs of 1.5 and 2 m·s^{-1} and low TMPs, but the difference was small. At the same CFV conditions but at higher TMP for the RC70PP membrane, the ANN predictions vary slightly with respect to the experimental data except near steady-state conditions. Regarding the UH050 membrane, it is observed that in the first minutes the ANN predictions vary slightly with respect to the experimental data for all the experimental conditions tested. This is observed to a greater extent for a CFV 2.5 m·s^{-1} and high TMPs. For inorganic membranes at low time scales, the model predictions and

experimental values do not show exactly the same trend. This was observed at CFV of 2 $m \cdot s^{-1}$ for all inorganic membranes.

The validity of ANN models has been tested with good results, since they offer a fairly accurate description of the evolution of the experimental flux, achieving a better approach to process optimization. In addition to a precise description of the global process, the models manage to adapt to very different operating conditions. Therefore, the number of experimental tests was sufficient for the training procedure. An advantage of these models is that since flux is a constantly monitored parameter in all ultrafiltration systems, whether operated in cross flow or dead-end flow mode, the application of ANN models can be extrapolated to large-scale treatment plants [72].

4.6 Comparison between Models

Once all the models were analyzed separately, they were compared with each other. The Hermia models were not included in the analysis because it was shown that it cannot give an accurate permeate flux prediction because more than one fouling mechanisms is involved in the ultrafiltration of OOWW. As Corbatón-Báguena et al. [73] well commented, the regression coefficient R^2 sometimes exceeds its maximum value ($R^2 > 1$) or has a negative value in some cases. Although this was not observed in our case, for a possible future comparison with other works, it was decided to use [-log10(1 - R^2)], a normal distribution of R^2 to compare between models. The study was performed with a 95% confidence level. As was commented above, for the comparison of the models, for the ANN the data obtained with one hidden layer and 5 neurons were used for UH004, UP005, RC70PP, Inside Céram 5 and Inside Céram 50 membranes in ANN, and in the case of the other two membranes one hidden layer with 6 neurons was selected. The results shown in figure 5 correspond to the mean values for the fitting accuracy obtained for each model for all the combinations of TMP and CFV analyzed.

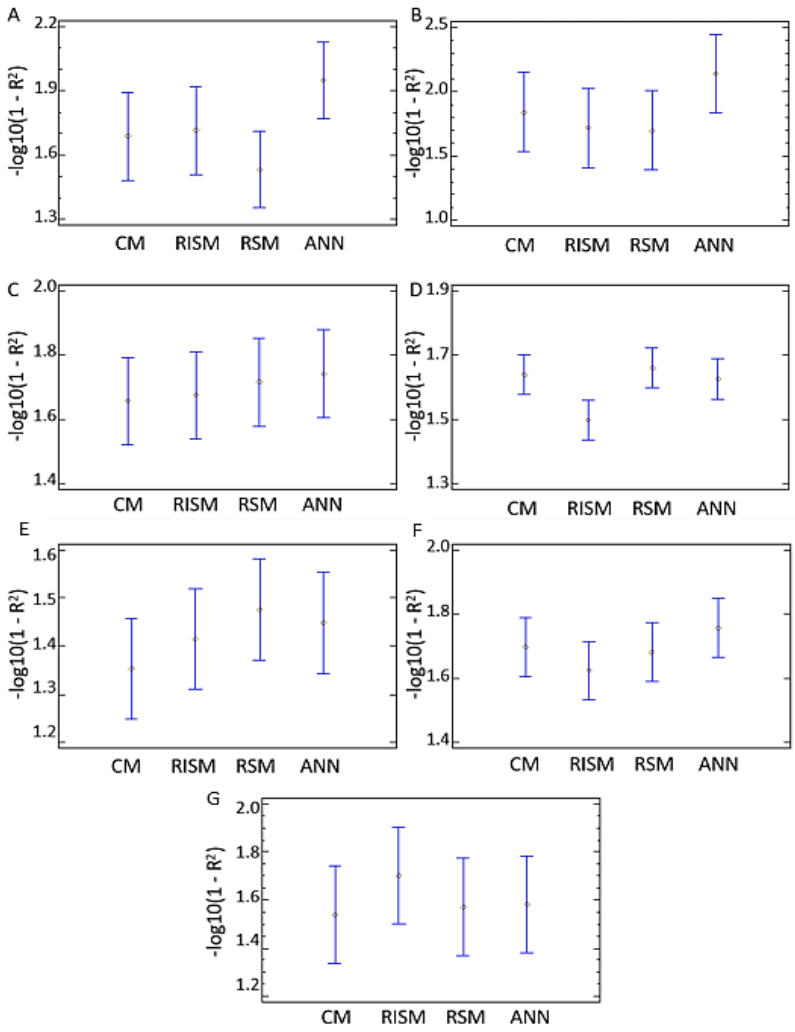

Fig. 5.23 Comparison between models fitting accuracy, means and LSD value of all membranes for all combination of TMP and CFV tested. CM: Combined Model; RISM: Resistance in series Model. A: UH004; B: UP005; C: RC70PP; D: UH050, E: Inside Céram 5; F: Inside Céram 15; G: Inside Céram 50

Fig. 5.23 show the means and LSD values for the fitting accuracy achieved for models tested for organic and inorganic membranes, respectively. When comparing the models, it was observed that there is no single model that best represents all the membranes under the operating conditions tested. Low MWCO organic membranes showed similar results in terms of fitting accuracy for the four models considered. The best predictions were obtained by the

ANN model flowed by the CM, RSM and RISM models. Although the RC70PP membrane also shows this trend, the accuracy of the models is much similar between ANN and CM models. The main differences were observed with UH050 membrane. In that case the ANN model achieved the worst accuracy and the CM and RSM models showed a similar and better accuracy.

Regarding the inorganic membranes, the ANN model is classified in second and first place in terms of fitting accuracy for the membrane Inside Céram 5 and 15, respectively. For Inside Céram 50, ANN fitting accuracy it is well below that of RSM, which is the model with the highest accuracy. Interestingly, a different trend is again observed between Inside Céram 5 and 15, with RSM having better accuracy for the first one but the worse for the latter membrane. It is important to note that the RSM model does not consider the CFV 4m·s^{-1} condition in inorganic membranes. That may justify its greater accuracy.

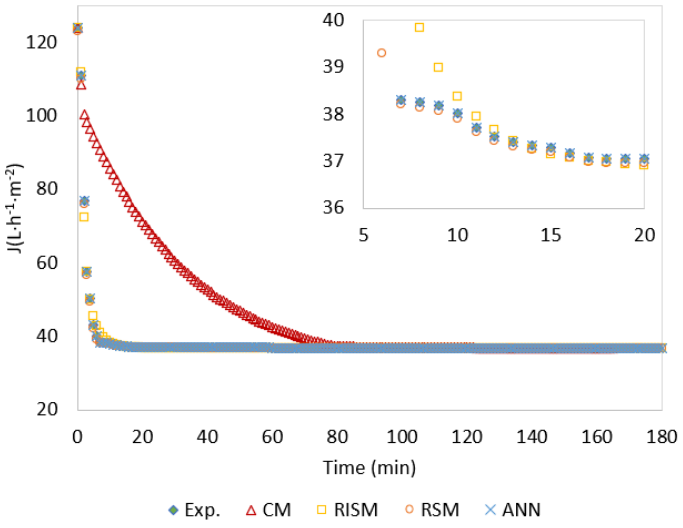

Fig. 5.24 Flux prediction comparison between models, example for RC70PP, CFV 3.4m·s^{-1}, TMP 1.5bar. Exp: Experimental; CM: Combined Model; RISM: Resistance in series Model; RSM: Response surface methodology; ANN: Artificial neural networks

Although it could not be said that a particular model better predicts the flux of all the membranes, in general ANN presented good accuracy for all the membranes. As an example,

fig 5.24 present the result obtained for RC70PP membrane under a fixed condition of CFV 3.4m·s^{-1}, TMP 1.5 bar. It can be clearly seen that the CM model presents difficulties in the first minutes, without achieving a real representation of the experimental data until minute 80. In the zoom it is possible to see how the RSM and ANN models are the ones that best fit the data, the last being the best. Other authors have also demonstrated the modeling capacity of ANN and RSM for other studies related to membranes, specifically fouling. Khan et al. [30] evaluated SBM (empirical slot-pore blocking model), RSM and ANN modeling techniques for accurate mapping of TMP by oscillating slotted pore membrane to treat deformable oil droplets, varying permeate fluxes. Noting that while both RSM and ANN delivered good results, ANN achieved better data modeling.

5 Conclusions

Theoretical models showed that more than one fouling mechanism occurs simultaneously in the same process, achieving both the series resistance model and the combined model, a good representation of the experimental data. This indicates that both cake layer formation and pore blockage contributed to membrane fouling. The ANOVA performed by fitting the response surface models shows that both CFV and TMP are significant variables with respect to permeate flux.

RSM made it possible to study the best operating conditions for membrane processes. Using ANN, the model fits all provided data with high regression coefficients R^2. When comparing all the models, it was shown that depending on the membrane, one model fits better than the others; however, the ANN model is the one that best fits all the experimental data of low/medium MWCO ultrafiltration membranes. The work carried out provides extensive knowledge of the data modeling of ultrafiltration membranes used for the treatment of OMW.

Acknowledgements

The authors acknowledge the financial support from the Ministry of Economy, Industry and Competitiveness of Spain through the project CTM2017-88645-R and The European Union through the Operational Program of the Social Fund (FSE).

References

[1] M. Maaitah, G. Hodaifa, A. Malvis, S. Sánchez, Kinetic growth and biochemical composition variability of Chlorella pyrenoidosa in olive oil washing wastewater cultures enriched with urban wastewater, J. Water Process Eng. 35 (2020) 101197. https://doi.org/10.1016/j.jwpe.2020.101197.

[2] R. Borja, F. Raposo, B. Rincón, Treatment technologies of liquid and solid wastes from two-phase olive oil mills, Grasas y Aceites. 57 (2006) 32–46. https://doi.org/10.3989/gya.2006.v57.i1.20.

[3] J.M. Ochando-Pulido, A. Martínez-Ferez, Fouling modelling on a reverse osmosis membrane in the purification of pretreated olive mill wastewater by adapted crossflow blocking mechanisms, J. Memb. Sci. 544 (2017) 108–118. https://doi.org/10.1016/j.memsci.2017.09.018.

[4] M. Stoller, J.M.O. Pulido, L. Di Palma, Study on fouling behaviour of ultrafiltration and nanofiltration during purification of different organic matter polluted wastewaters, Chem. Eng. Trans. 60 (2017) 295–300. https://doi.org/10.3303/CET1760050.

[5] M. Stoller, M. Bravi, Critical flux analyses on differently pretreated olive vegetation waste water streams: Some case studies, Desalination. 250 (2010) 578–582. https://doi.org/10.1016/j.desal.2009.09.027.

[6] E. Turano, S. Curcio, M.G. De Paola, V. Calabrò, G. Iorio, An integrated centrifugation-ultrafiltration system in the treatment of olive mill wastewater, J. Memb. Sci. 209 (2002) 519–531. https://doi.org/10.1016/S0376-7388(02)00369-1.

[7] C. Saf, M. Villain-Gambier, M. Belaqziz, I. Ziegler-Devin, D. Trebouet, N. Ouazzani, Fouling control investigation by pH optimization during olive mill wastewater ultrafiltration, Process Saf. Environ. Prot. 164 (2022) 119–128. https://doi.org/10.1016/j.psep.2022.06.010.

[8] J.M. Ochando-Pulido, V. Verardo, A. Segura-Carretero, A. Martinez-Ferez, Technical optimization of an integrated UF/NF pilot plant for conjoint batch treatment of two-phase olives and olive oil washing wastewaters, Desalination. 364 (2015) 82–89. https://doi.org/10.1016/j.desal.2014.10.040.

[9] M. Cifuentes-Cabezas, C. Carbonell-Alcaina, M.C. Vincent-Vela, J.A. Mendoza-Roca, S. Álvarez-Blanco, Comparison of different ultrafiltration membranes as first step for the recovery of phenolic compounds from olive-oil washing wastewater, Process Saf. Environ. Prot. 149 (2021) 724–734. https://doi.org/10.1016/j.psep.2021.03.035.

[10] M. Cifuentes-Cabezas, M.C. Vincent-Vela, J.A. Mendoza-Roca, S. Álvarez-Blanco, Use of ultrafiltration ceramic membranes as a first step treatment for olive oil washing wastewater, Food Bioprod. Process. 135 (2022) 60–73.

https://doi.org/10.1016/j.fbp.2022.07.002.

[11] J.M. Ochando-Pulido, M.D. Victor-Ortega, A. Martínez-Ferez, On the cleaning procedure of a hydrophilic reverse osmosis membrane fouled by secondary-treated olive mill wastewater, Chem. Eng. J. 260 (2015) 142–151. https://doi.org/10.1016/j.cej.2014.08.094.

[12] J.M. Ochando-Pulido, A review on the use of membrane technology and fouling control for olive mill wastewater treatment, Sci. Total Environ. 563–564 (2016) 664–675. https://doi.org/10.1016/j.scitotenv.2015.09.151.

[13] C. Niu, X. Li, R. Dai, Z. Wang, Artificial intelligence-incorporated membrane fouling prediction for membrane-based processes in the past 20 years: A critical review, Water Res. 216 (2022) 118299. https://doi.org/10.1016/j.watres.2022.118299.

[14] S.F. Ahmed, F. Mehejabin, A. Momtahin, N. Tasannum, N.T. Faria, M. Mofijur, A.T. Hoang, D.N. Vo, T.M.. Mahlia, Strategies to improve membrane performance in wastewater treatment, Chemosphere. 306 (2022) 135527. https://doi.org/10.1016/j.chemosphere.2022.135527.

[15] M.J. Corbatón-Báguena, S. Álvarez-Blanco, M.C. Vincent-Vela, Evaluation of fouling resistances during the ultrafiltration of whey model solutions, J. Clean. Prod. 172 (2018) 358–367. https://doi.org/10.1016/j.jclepro.2017.10.149.

[16] J. Hermia, Constant pressure blocking filtration laws – application to power-law non-newtonian fluids., Inst. Chem. Enginners. 60 (1982) 183–187.

[17] S. Mondal, S. De, Generalized criteria for identification of fouling mechanism under steady state membrane filtration, J. Memb. Sci. 344 (2009) 6–13. https://doi.org/10.1016/j.memsci.2009.08.015.

[18] W.R. Bowen, J.I. Calvo, A. Hernández, Steps of membrane blocking in flux decline during protein microfiltration, J. Memb. Sci. 101 (1995) 153–165. https://doi.org/10.1016/0376-7388(94)00295-A.

[19] G. Jonsson, P. Prádanos, A. Hernández, Fouling phenomena in microporous membranes. Flux decline kinetics and structural modifications, J. Memb. Sci. 112 (1996) 171–183. https://doi.org/10.1016/0376-7388(95)00286-3.

[20] M.-J. Corbatón-Báguena, S. Álvarez-Blanco, M.C. Vincent-Vela, Fouling mechanisms of ultrafiltration membranes fouled with whey model solutions, Desalination. 360 (2015) 87–96. https://doi.org/10.1016/j.desal.2015.01.019.

[21] C.C. Ho, A.L. Zydney, A combined pore blockage and cake filtration model for protein fouling during microfiltration, J. Colloid Interface Sci. 232 (2000) 389–399. https://doi.org/10.1006/jcis.2000.7231.

[22] E.J. de la Casa, A. Guadix, R. Ibáñez, F. Camacho, E.M. Guadix, A combined fouling model to describe the influence of the electrostatic environment on the cross-flow microfiltration of BSA, J. Memb. Sci. 318 (2008) 247–254. https://doi.org/10.1016/j.memsci.2008.02.047.

[23] S.W. Choi, J.Y. Yoon, S. Haam, J.K. Jung, J.H. Kim, W.S. Kim, Modeling of the permeate flux during microfiltration of BSA-adsorbed microspheres in a stirred cell, J. Colloid Interface Sci. 228 (2000) 270–278. https://doi.org/10.1006/jcis.2000.6940.

[24] B. Ibrahim, A. Ewusi, I. Ahenkorah, Y.Y. Ziggah, Modelling of arsenic concentration in multiple water sources: A comparison of different machine learning methods, Groundw. Sustain. Dev. 17 (2022) 100745. https://doi.org/10.1016/j.gsd.2022.100745.

[25] J.A. Okolie, S. Savage, C.C. Ogbaga, B. Gunes, Assessing the potential of machine learning methods to study the removal of pharmaceuticals from wastewater using biochar or activated carbon, Total Environ. Res. Themes. 1–2 (2022) 100001. https://doi.org/10.1016/j.totert.2022.100001.

[26] Q.V. Ly, V.H. Truong, B. Ji, X.C. Nguyen, K.H. Cho, H.H. Ngo, Z. Zhang, Exploring potential machine learning application based on big data for prediction of wastewater quality from different full-scale wastewater treatment plants, Sci. Total Environ. 832 (2022) 154930. https://doi.org/10.1016/j.scitotenv.2022.154930.

[27] N.P. Sibiya, G. Amo-duodu, Model prediction of coagulation by magnetised rice starch for wastewater treatment using response surface methodology (RSM) with artificial neural network (ANN), Sci. African. (2022) e01282. https://doi.org/10.1016/j.sciaf.2022.e01282.

[28] D.J. Kovacs, Z. Li, B.W. Baetz, Y. Hong, S. Donnaz, X. Zhao, P. Zhou, H. Ding, Q. Dong, Membrane fouling prediction and uncertainty analysis using machine learning : A wastewater treatment plant case study, J. Memb. Sci. 660 (2022) 120817. https://doi.org/10.1016/j.memsci.2022.120817.

[29] M. Kamali, L. Appels, X. Yu, T.M. Aminabhavi, R. Dewil, Artificial intelligence as a sustainable tool in wastewater treatment using membrane bioreactors, Chem. Eng. J. 417 (2021) 128070. https://doi.org/10.1016/j.cej.2020.128070.

[30] H. Khan, S.U. Khan, S. Hussain, A. Ullah, Modelling of transmembrane pressure using slot/pore blocking model, response surface and artificial intelligence approach, Chemosphere. 290 (2022) 133313. https://doi.org/10.1016/j.chemosphere.2021.133313.

[31] M. Lowe, R. Qin, X. Mao, A Review on Machine Learning, Artificial Intelligence, and Smart Technology in Water Treatment and Monitoring, Water (Switzerland). 14 (2022). https://doi.org/10.3390/w14091384.

[32] S. Curcio, V. Calabrò, G. Iorio, Reduction and control of flux decline in cross-flow

membrane processes modeled by artificial neural networks, J. Memb. Sci. 286 (2006) 125–132. https://doi.org/10.1016/j.memsci.2006.09.024.

[33] F. Lipnizki, L. Fortunato, S. Arabia Jingwei Wang, P. Czermak, R. Fan, O. Birrenbach, F. Faust, M. Ebrahimi, Recovery and Purification of Protein Aggregates From Cell Lysates Using Ceramic Membranes: Fouling Analysis and Modeling of Ultrafiltration, Front. Chem. Eng. |. 3 (2021) 656345. https://doi.org/10.3389/fceng.2021.656345.

[34] M. Taniguchi, james E. Kilduff, G. Belfort, Modes of natural organic matter fouling durign ultrafiltration, Environ. Sci. Technol. 37 (2003) 1676–1683. http://busick-portfolio.wikispaces.com/file/view/ADHD+and+academic+performance.pdf.

[35] W. Yuan, A. Kocic, A.L. Zydney, Analysis of humic acid fouling during microfiltration using a pore blockage-cake filtration model, J. Memb. Sci. 198 (2002) 51–62. https://doi.org/10.1016/S0376-7388(01)00622-6.

[36] M.C. Martí-Calatayud, M.C. Vincent-Vela, S. Álvarez-Blanco, J. Lora-García, E. Bergantiños-Rodríguez, Analysis and optimization of the influence of operating conditions in the ultrafiltration of macromolecules using a response surface methodological approach, Chem. Eng. J. 156 (2010) 337–346. https://doi.org/10.1016/j.cej.2009.10.031.

[37] J. Dasgupta, J. Sikder, D. Mandal, Modeling and optimization of polymer enhanced ultrafiltration using hybrid neural-genetic algorithm based evolutionary approach, Appl. Soft Comput. J. 55 (2017) 108–126. https://doi.org/10.1016/j.asoc.2017.02.002.

[38] B. Rahmanian, M. Pakizeh, S.A.A. Mansoori, R. Abedini, Application of experimental design approach and artificial neural network (ANN) for the determination of potential micellar-enhanced ultrafiltration process, J. Hazard. Mater. 187 (2011) 67–74. https://doi.org/10.1016/j.jhazmat.2010.11.135.

[39] V. Gökmen, Ö.E. Aar, A. Serpen, I. Süüt, Modeling dead-end ultrafiltration of apple juice using artificial neural network, J. Food Process Eng. 32 (2009) 248–264. https://doi.org/10.1111/j.1745-4530.2007.00214.x.

[40] J.S. Torrecilla, L. Otero, P.D. Sanz, A neural network approach for thermal/pressure food processing, J. Food Eng. 62 (2004) 89–95. https://doi.org/10.1016/S0260-8774(03)00174-2.

[41] B. Sarkar, A. Sengupta, S. De, S. DasGupta, Prediction of permeate flux during electric field enhanced cross-flow ultrafiltration-A neural network approach, Sep. Purif. Technol. 65 (2009) 260–268. https://doi.org/10.1016/j.seppur.2008.10.032.

[42] H. Nourbakhsh, Z. Emam-Djomeh, M. Omid, H. Mirsaeedghazi, S. Moini, Prediction of red plum juice permeate flux during membrane processing with ANN optimized using RSM, Comput. Electron. Agric. 102 (2014) 1–9.

https://doi.org/10.1016/j.compag.2013.12.017.

[43] M.A. Razavi, A. Mortazavi, M. Mousavi, Dynamic modelling of milk ultrafiltration by artificial neural network, J. Memb. Sci. 220 (2003) 47–58. https://doi.org/10.1016/S0376-7388(03)00211-4.

[44] J. Jawad, A.H. Hawari, S. Javaid Zaidi, Artificial neural network modeling of wastewater treatment and desalination using membrane processes: A review, Chem. Eng. J. 419 (2021) 129540. https://doi.org/10.1016/j.cej.2021.129540.

[45] M.J. Luján-Facundo, J.A. Mendoza-Roca, B. Cuartas-Uribe, S. Álvarez-Blanco, Membrane fouling in whey processing and subsequent cleaning with ultrasounds for a more sustainable process, J. Clean. Prod. 143 (2017) 804–813. https://doi.org/10.1016/j.jclepro.2016.12.043.

[46] V.B. Brião, C.R.G. Tavares, Pore blocking mechanism for the recovery of milk solids from dairy wastewater by ultrafiltration, Brazilian J. Chem. Eng. 29 (2012) 393–407. https://doi.org/10.1590/S0104-66322012000200019.

[47] M.K. Amosa, M.S. Jami, M.F. Alkhatib, T. Majozi, A.G. Adeniyi, F.A. Aderibigbe, S.A. Abdulkareem, Modeling of Pore-Blocking Behaviors of Low-Pressure Membranes during Constant-Pressure Filtration of an Agro-Industrial Wastewater, Water Manag. (2019) 137–167. https://doi.org/10.1201/b22241-9.

[48] C. Wang, Q. Li, H. Tang, D. Yan, W. Zhou, J. Xing, Y. Wan, Membrane fouling mechanism in ultrafiltration of succinic acid fermentation broth, Bioresour. Technol. 116 (2012) 366–371. https://doi.org/10.1016/j.biortech.2012.03.099.

[49] P.J. Evans, M.R. Bird, A. Pihlajamäki, M. Nyström, The influence of hydrophobicity, roughness and charge upon ultrafiltration membranes for black tea liquor clarification, J. Memb. Sci. 313 (2008) 250–262. https://doi.org/10.1016/j.memsci.2008.01.010.

[50] F. Yang, Z. Huang, J. Huang, C. Wu, R. Zhou, Y. Jin, Tanning wastewater treatment by ultrafiltration: Process efficiency and fouling behavior, Membranes (Basel). 11 (2021). https://doi.org/10.3390/membranes11070461.

[51] S.S.L. Peppin, Diffusion and permeation in binary solutions: Application to protein ultrafiltratio, Oxford centre for collaborative applied mathematics, 2019.

[52] H. Sari Erkan, N. Bakaraki Turan, G. Önkal Engin, Membrane Bioreactors for Wastewater Treatment, Compr. Anal. Chem. 81 (2018) 151–200. https://doi.org/10.1016/bs.coac.2018.02.002.

[53] A. Alborzi, I.-M. Hsieh, D. Reible, M. Malmali, Analysis of Fouling Mechanism in Ultrafiltration of Produced Water, SSRN Electron. J. (2022) 1–19. https://doi.org/10.2139/ssrn.4041300.

[54] M. Cai, S. Wang, H. Liang, Modeling and fouling mechanisms for ultrafiltration of Huanggi (Radix astragalus) extracts, Food Sci. Biotechnol. 22 (2013) 407–412. https://doi.org/10.1007/s10068-013-0094-9.

[55] C. Carbonell-Alcaina, M.J. Corbatón-Báguena, S. Álvarez-Blanco, M.A. Bes-Piá, J.A. Mendoza-Roca, L. Pastor-Alcañiz, Determination of fouling mechanisms in polymeric ultrafiltration membranes using residual brines from table olive storage wastewaters as feed, J. Food Eng. 187 (2016) 14–23. https://doi.org/10.1016/j.jfoodeng.2016.04.016.

[56] Y. Huang, H. Liu, Y. Wang, G. Song, L. Zhang, Industrial application of ceramic ultrafiltration membrane in cold-rolling emulsion wastewater treatment, Sep. Purif. Technol. 289 (2022) 120724. https://doi.org/10.1016/j.seppur.2022.120724.

[57] S. Mondal, S. De, A fouling model for steady state crossflow membrane filtration considering sequential intermediate pore blocking and cake formation, Sep. Purif. Technol. 75 (2010) 222–228. https://doi.org/10.1016/j.seppur.2010.07.016.

[58] M.A. Knapp, Fracionamento de subproduto do processamento de lignina por processos com membranas para obtencao de compostos fenólicos, 2020.

[59] V. Gökmen, Ö. Çetinkaya, Effect of pretreatment with gelatin and bentonite on permeate flux and fouling layer resistance during apple juice ultrafiltration, J. Food Eng. 80 (2007) 300–305. https://doi.org/10.1016/j.jfoodeng.2006.04.060.

[60] H.A. Gulec, P.O. Bagci, U. Bagci, Clarification of Apple Juice Using Polymeric Ultrafiltration Membranes: a Comparative Evaluation of Membrane Fouling and Juice Quality, Food Bioprocess Technol. 10 (2017) 875–885. https://doi.org/10.1007/s11947-017-1871-x.

[61] S. Barredo-Damas, M.I. Alcaina-Miranda, A. Bes-Piá, M.I. Iborra-Clar, A. Iborra-Clar, J.A. Mendoza-Roca, Ceramic membrane behavior in textile wastewater ultrafiltration, Desalination. 250 (2010) 623–628. https://doi.org/10.1016/j.desal.2009.09.037.

[62] S. Mondal, C. Rai, S. De, Identification of Fouling Mechanism During Ultrafiltration of Stevia Extract, Food Bioprocess Technol. 6 (2013) 931–940. https://doi.org/10.1007/s11947-011-0754-9.

[63] P. van der Marel, A. Zwijnenburg, A. Kemperman, M. Wessling, H. Temmink, W. van der Meer, Influence of membrane properties on fouling in submerged membrane bioreactors, J. Memb. Sci. 348 (2010) 66–74. https://doi.org/10.1016/j.memsci.2009.10.054.

[64] F. Galiano, I. Friha, S.A. Deowan, J. Hoinkis, Y. Xiaoyun, D. Johnson, R. Mancuso, N. Hilal, B. Gabriele, S. Sayadi, A. Figoli, Novel low-fouling membranes from lab to pilot application in textile wastewater treatment, J. Colloid Interface Sci. 515 (2018) 208–220. https://doi.org/10.1016/j.jcis.2018.01.009.

[65] E. Alventosa-deLara, S. Barredo-Damas, M.I. Alcaina-Miranda, M.I. Iborra-Clar, Ultrafiltration technology with a ceramic membrane for reactive dye removal: Optimization of membrane performance, J. Hazard. Mater. 209–210 (2012) 492–500. https://doi.org/10.1016/j.jhazmat.2012.01.065.

[66] C.M. Sánchez-Arévalo, Á. Jimeno-Jiménez, C. Carbonell-Alcaina, M.C. Vincent-Vela, S. Álvarez-Blanco, Effect of the operating conditions on a nanofiltration process to separate low-molecular-weight phenolic compounds from the sugars present in olive mill wastewaters, Process Saf. Environ. Prot. 148 (2021) 428–436. https://doi.org/10.1016/j.psep.2020.10.002.

[67] I. Damar, K. Cinar, H.A. Gulec, Concentration of whey proteins by ultrafiltration: Comparative evaluation of process effectiveness based on physicochemical properties of membranes, Int. Dairy J. 111 (2020) 104823. https://doi.org/10.1016/j.idairyj.2020.104823.

[68] B.K. Nandi, A. Moparthi, R. Uppaluri, M.K. Purkait, Treatment of oily wastewater using low cost ceramic membrane: Comparative assessment of pore blocking and artificial neural network models, Chem. Eng. Res. Des. 88 (2010) 881–892. https://doi.org/10.1016/j.cherd.2009.12.005.

[69] M.K. Purkait, V.D. Kumar, D. Maity, Treatment of leather plant effluent using NF followed by RO and permeate flux prediction using artificial neural network, Chem. Eng. J. 151 (2009) 275–285. https://doi.org/10.1016/j.cej.2009.03.023.

[70] P. Rai, G.C. Majumdar, S. DasGupta, S. De, Modeling the performance of batch ultrafiltration of synthetic fruit juice and mosambi juice using artificial neural network, J. Food Eng. 71 (2005) 273–281. https://doi.org/10.1016/j.jfoodeng.2005.02.003.

[71] S. Ghandehari, M.M. Montazer-Rahmati, M. Asghari, A comparison between semi-theoretical and empirical modeling of cross-flow microfiltration using ANN, Desalination. 277 (2011) 348–355. https://doi.org/10.1016/j.desal.2011.04.057.

[72] C. Teodosiu, O. Pastravanu, M. Macoveanu, Neural network models for ultrafiltration and backwashing, Water Res. 34 (2000) 4371–4380. https://doi.org/10.1016/S0043-1354(00)00217-7.

[73] M.J. Corbatón-Báguena, M.C. Vincent-Vela, J.M. Gozálvez-Zafrilla, S. Álvarez-Blanco, J. Lora-García, D. Catalán-Martínez, Comparison between artificial neural networks and Hermia's models to assess ultrafiltration performance, Sep. Purif. Technol. 170 (2016) 434–444. https://doi.org/10.1016/j.seppur.2016.07.007.

Supplementary Material

1. Analysis of membrane fouling mechanism

Fig. 5.S1 and 5.S2 shows Permeate flux vs. TMP for organic and inorganic membranes at the operating conditions in which both models (resistance in series and combined resistance) have the best fitting accuracy.

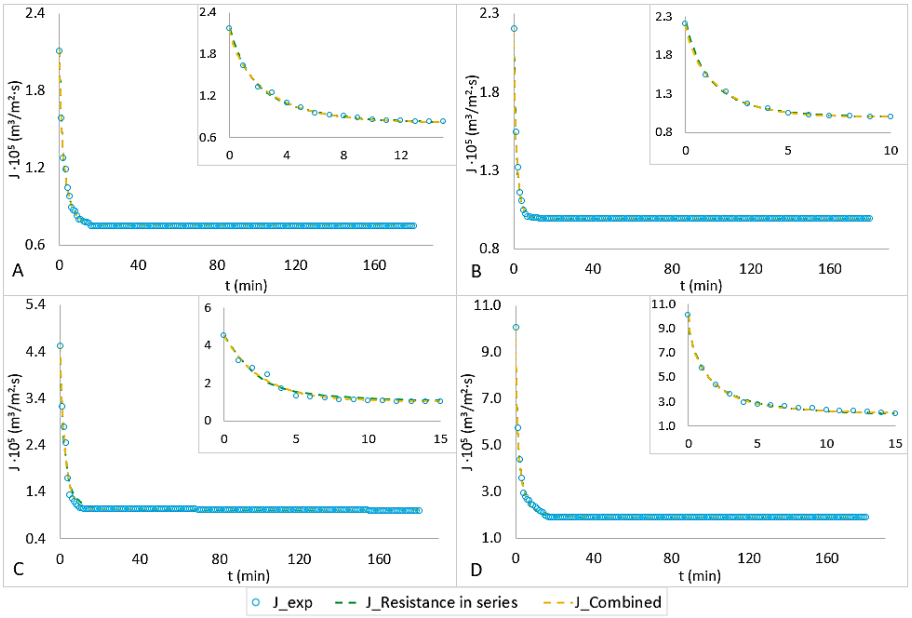

Fig.5.S1 Predictions of permeate flux vs. time from resistance in series and combined models at best-fit experimental conditions for different organic membranes. A: UH004, TMP 2.5 bar and CFV 2 m/s; B: UP005, TMP 2 bar and CFV 2 m/s; C: RC70PP, TMP 2 bar and CFV 2 m/s; D: UH050, TMP 2 bar and CFV 1.5 m/s

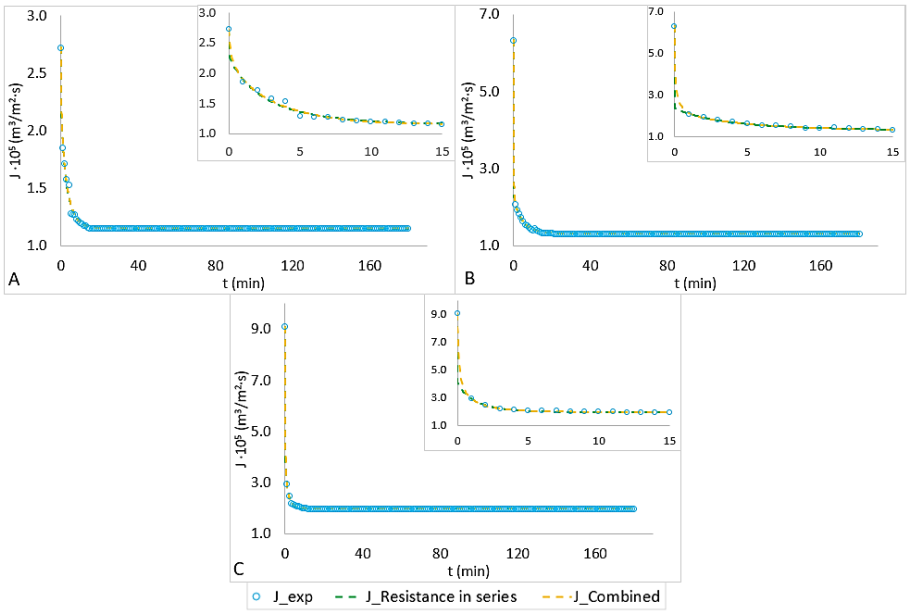

Fig.5.S2 Predictions of permeate flux vs. time from resistance in series and combined models at best-fit experimental conditions for different inorganic membranes. A: Inside céram 5, TMP 2.5 bar and CFV 2 m/s; B: Inside Céram 15, TMP 2 bar and CFV 2 m/s; C: Inside Céram 50, TMP 2 bar and CFV 2 m/s

In the following tables of Theoretical Models, R^2 is presented in different colors to favor its differentiation, from green (best fit) to red (worst accuracy). It is important to note that the colors are only for comparison within the same table, not among different tables.

Table 5.S1 Measures of fit, as per standard deviation SD and regression coefficient R^2, for Hermia model for UH004 and UP005 organic membranes

		UH004						UP005					
TMP (bar)	CFV (m/s)	Complete pore blocking		Intermediate pore blocking		Cake layer formation		Complete pore blocking		Intermediate pore blocking		Cake layer formation	
		R^2	SD	R^2	SD	R^2	SD	R^2	SD	R^2	SD	R^2	SD
1	1.5	0.931	0.018	0.923	0.018	0.854	0.026	0.968	0.025	0.935	0.036	0.891	0.041
	2	0.9	0.020	0.89	0.020	0.81	0.028	0.908	0.051	0.865	0.061	0.807	0.064
	2.5	0.976	0.009	0.966	0.011	0.92	0.017	0.843	0.049	0.814	0.055	0.767	0.06
	3	0.953	0.007	0.951	0.007	0.939	0.007	0.971	0.02	0.931	0.032	0.859	0.046
	3.4	0.94	0.009	0.949	0.008	0.951	0.008	0.952	0.033	0.91	0.045	0.843	0.057
1.5	1.5	0.921	0.031	0.872	0.040	0.768	0.057	0.963	0.019	0.928	0.027	0.873	0.032
	2	0.95	0.019	0.914	0.027	0.843	0.039	0.96	0.02	0.956	0.023	0.928	0.03
	2.5	0.957	0.025	0.923	0.034	0.865	0.044	0.944	0.042	0.906	0.053	0.843	0.063
	3	0.894	0.025	0.856	0.028	0.788	0.031	0.971	0.026	0.931	0.039	0.864	0.05
	3.4	0.984	0.009	0.968	0.013	0.937	0.017	0.82	0.057	0.809	0.057	0.769	0.06
2	1.5	0.982	0.014	0.944	0.028	0.874	0.037	0.947	0.012	0.982	0.006983	0.981	0.06641
	2	0.967	0.016	0.922	0.025	0.843	0.037	0.98	0.005374	0.997	0.002287	0.984	0.005317
	2.5	0.95	0.019	0.906	0.026	0.84	0.032	0.959	0.018	0.925	0.025	0.871	0.031
	3	0.958	0.018	0.928	0.023	0.885	0.028	0.989	0.007043	0.985	0.009547	0.955	0.014
	3.4	0.921	0.016	0.89	0.019	0.842	0.023	0.972	0.015	0.949	0.021	0.909	0.026
2.5	1.5	0.965	0.022	0.935	0.034	0.865	0.050	0.806	0.018	0.921	0.012	0.961	0.009258
	2	0.961	0.016	0.995	0.005	0.975	0.014	0.856	0.017	0.928	0.012	0.975	0.006841
	2.5	0.973	0.014	0.953	0.021	0.901	0.031	0.996	0.005491	0.978	0.012	0.934	0.019
	3	0.912	0.026	0.875	0.030	0.812	0.035	0.99	0.007009	0.975	0.012	0.941	0.017
	3.4	0.923	0.024	0.892	0.027	0.836	0.032	0.996	0.005509	0.981	0.011	0.942	0.017

Table 5.S2: Measures of fit, as per standard deviation SD and regression coefficient R^2, for Hermia model for RC70PP and UH050 organic membranes

		RC70PP						UH050					
		Complete pore blocking		Intermediate pore blocking		Cake layer formation		Complete pore blocking		Intermediate pore blocking		Cake layer formation	
TMP (bar)	CFV (m/s)	R^2	SD	R^2	SD	R^2	SD	R^2	SD	R^2	SD	R^2	SD
1	1.5	0.973	0.015	0.931	0.027	0.846	0.037	0.978	0.012	0.969	0.015	0.954	0.019
	2	0.983	0.014	0.935	0.028	0.84	0.041	0.976	0.008861	0.972	0.00996	0.964	0.012
	2.5	0.953	0.019	0.896	0.031	0.793	0.043	0.978	0.019	0.957	0.026	0.9	0.037
	3	0.958	0.019	0.994	0.018	0.878	0.027	0.971	0.022	0.947	0.027	0.891	0.037
	3.4	0.922	0.035	0.901	0.036	0.835	0.041	0.535	0.056	0.527	0.057	0.513	0.058
1.5	1.5	0.994	0.008	0.962	0.018	0.868	0.031	0.992	0.01	0.98	0.022	0.927	0.037
	2	0.993	0.009	0.981	0.020	0.898	0.039	0.972	0.015	0.926	0.024	0.843	0.033
	2.5	0.94	0.028	0.875	0.042	0.758	0.056	0.939	0.024	0.914	0.026	0.855	0.031
	3	0.945	0.028	0.888	0.043	0.784	0.058	0.89	0.038	0.922	0.033	0.902	0.033
	3.4	0.953	0.019	0.892	0.033	0.785	0.046	0.933	0.027	0.978	0.018	0.952	0.027
2	1.5	0.921	0.026	0.966	0.025	0.914	0.040	0.757	0.041	0.992	0.014	0.944	0.026
	2	0.966	0.031	0.925	0.046	0.818	0.065	0.732	0.5	0.92	0.025	0.96	0.021
	2.5	0.831	0.046	0.75	0.053	0.618	0.061	0.855	0.048	0.925	0.043	0.886	0.06
	3	0.955	0.028	0.884	0.046	0.761	0.061	0.879	0.031	0.947	0.024	0.927	0.026
	3.4	0.952	0.032	0.891	0.049	0.771	0.068	0.801	0.039	0.942	0.021	0.974	0.018
2.5	1.5	0.807	0.037	0.944	0.019	0.951	0.025	0.812	0.046	0.954	0.034	0.892	0.059
	2	0.976	0.019	0.977	0.027	0.886	0.053	0.833	0.057	0.947	0.035	0.939	0.037
	2.5	0.977	0.032	0.908	0.061	0.771	0.086	0.801	0.064	0.918	0.043	0.948	0.033
	3	0.975	0.031	0.913	0.061	0.791	0.084	0.71	0.053	0.85	0.042	0.887	0.037
	3.4	0.971	0.070	0.914	0.048	0.796	0.070	0.644	0.053	0.894	0.029	0.975	0.017

Continuation Table 5.S2: Measures of fit, as per standard deviation SD and regression coefficient R^2, for Hermia model for RC70PP and UH050 organic membranes

		RC70PP						UH050					
		Complete pore blocking		Intermediate pore blocking		Cake layer formation		Complete pore blocking		Intermediate pore blocking		Cake layer formation	
TMP (bar)	CFV (m/s)	R^2	SD	R^2	SD	R^2	SD	R^2	SD	R^2	SD	R^2	SD
3	1.5							0.52	0.069	0.921	0.035	0.909	0.055
	2							0.742	0.067	0.927	0.038	0.946	0.036
	2.5							0.55	0.086	0.804	0.059	0.946	0.034
	3							0.652	0.058	0.83	0.045	0.88	0.039
	3.4							0.735	0.048	0.927	0.027	0.979	0.015

Table 5.S3: Measures of fit, as per standard deviation SD and regression coefficient R^2, for Hermia model for Inside Cèram 5, 15 and 50 inorganic membranes

TMP (bar)	CFV (m/s)	Inside Cèram 5						Inside Cèram 15						Inside Cèram 50					
		Complete pore blocking		Intermediate pore blocking		Cake layer formation		Complete pore blocking		Intermediate pore blocking		Cake layer formation		Complete pore blocking		Intermediate pore blocking		Cake layer formation	
		R^2	SD	R^2	SD	R^2	SD	R^2	SD	R^2	SD	R^2	SD	R^2	SD	R^2	SD	R^2	SD
1	2	0.904	0.015	0.955	0.01	0.974	0.009	0.351	0.054	0.533	0.045	0.744	0.033	0.689	0.05	0.878	0.032	0.977	0.014
	3	0.856	0.017	0.915	0.013	0.95	0.01	0.987	0.017	0.968	0.024	0.925	0.035	0.631	0.026	0.813	0.018	0.921	0.012
1.5	2	0.612	0.03	0.813	0.02	0.927	0.012	0.623	0.033	0.826	0.022	0.947	0.012	0.52	0.061	0.797	0.04	0.957	0.018
	3	0.597	0.029	0.794	0.02	0.911	0.013	0.834	0.04	0.933	0.024	0.972	0.021	0.817	0.016	0.939	0.009	0.979	0.006
	4	0.547	0.028	0.737	0.021	0.862	0.015	0.945	0.016	0.966	0.015	0.945	0.022	0.265	0.022	0.384	0.02	0.47	0.019
2	2	0.46	0.034	0.705	0.025	0.865	0.016	0.316	0.071	0.6	0.053	0.845	0.032	0.508	0.048	0.802	0.03	0.945	0.016
	3	0.461	0.033	0.701	0.024	0.858	0.016	0.556	0.063	0.802	0.041	0.944	0.022	0.602	0.016	0.786	0.012	0.873	0.010
	4	0.406	0.029	0.624	0.023	0.781	0.017	0.279	0.054	0.519	0.045	0.733	0.033	0.288	0.022	0.406	0.02	0.485	0.019
2.5	2	0.437	0.034	0.686	0.025	0.852	0.017	0.475	0.06	0.767	0.039	0.931	0.021	0.439	0.044	0.693	0.032	0.88	0.02
	3	0.359	0.033	0.597	0.026	0.775	0.019	0.662	0.044	0.873	0.026	0.932	0.024	0.559	0.018	0.741	0.013	0.836	0.011
	4	0.306	0.034	0.551	0.028	0.737	0.021	0.439	0.041	0.683	0.031	0.865	0.02	0.256	0.026	0.38	0.023	0.469	0.022
3	2	0.248	0.034	0.47	0.029	0.658	0.023	0.347	0.097	0.7	0.07	0.905	0.046	0.351	0.04	0.578	0.032	0.772	0.023
	3	0.313	0.029	0.496	0.025	0.651	0.021	0.562	0.047	0.827	0.03	0.956	0.016	0.503	0.016	0.653	0.013	0.733	0.012
	4	0.339	0.033	0.575	0.027	0.754	0.02	0.411	0.04	0.658	0.031	0.847	0.02	0.383	0.044	0.666	0.033	0.864	0.021

Table 5.S4: Measures of fit, as per standard deviation SD and regression coefficient R^2, for Resistance in series and Combined model for UH004 and UP005 organic membranes

		UH004										UP005									
TMP (bar)	CFV (m/s)	Combined Model					Resistance in series Model					Combined Model					Resistance in series Model				
		K_{cb} (s^{-1})	$K_{cf}\cdot10^7$ ($s\cdot m^{-2}$)	α	R^2	DS	R_a	R_{cf}	R_t	R^2	DS	K_{cb} (s^{-1})	$K_{cf}\cdot10^7$ ($s\cdot m^{-2}$)	α	R^2	DS	R_a	R_{cf}	R_t	R^2	DS
1	1.5	269.892	1.725	1.153	0.959	0.012	42.67	99.37	154.37	0.975	0.010	182.934	2.626	1.443	0.98	0.018	6.02	51.65	66.81	0.963	0.024
	2	259.501	1.622	1.225	0.957	0.012	49.8	99.65	161.78	0.943	0.013	158.985	2.951	2.702	0.973	0.032	6.8	51.91	67.85	0.94	0.038
	2.5	271.853	1.113	1.248	0.984	0.007	50.71	97.45	160.49	0.984	0.007	307.993	10.44	3.454	0.972	0.022	10.3	47.48	66.92	0.973	0.026
	3	730.58	1.109	2.091	0.954	0.007	56.48	95.27	164.08	0.972	0.006	224.44	4.189	1.719	0.992	0.011	14.24	46	69.38	0.979	0.02
	3.4	796.596	0.235	2.247	0.953	0.008	61.6	93.89	167.82	0.949	0.008	141.339	2.172	1.971	0.984	0.021	16.6	45.47	71.21	0.953	0.034
1.5	1.5	273.148	3.406	1.584	0.984	0.012	44.34	100.255	156.925	0.947	0.023	267.699	4.041	1.693	0.982	0.013	8.8	56.45	74.39	0.964	0.018
	2	264.047	3.115	1.421	0.987	0.009	47.44	99.684	159.454	0.978	0.012	168.713	5.722	0.669	0.967	0.02	10.54	53.2	72.88	0.959	0.021
	2.5	209.258	3.994	2.285	0.998	0.005	52.32	96.6962	161.3462	0.975	0.018	165.189	7.275	1.576	0.973	0.032	12.73	54.12	75.99	0.951	0.04
	3	289.695	2.474	1.448	0.969	0.012	60.93	94.698	167.958	0.929	0.018	162.383	2.585	1.73	0.992	0.014	12.18	46.432	67.752	0.972	0.027
	3.4	303.903	5.196	1.637	0.993	0.006	66.41	86.042	164.782	0.988	0.008	180.873	0.017	0.95	0.93	0.034	18.67	46.645	74.455	0.942	0.034
2	1.5	261.201	4.843	1.469	0.994	0.008	44.69	101.81	158.83	0.978	0.016	501.664	4.109	0.32	0.985	0.006	12.12	101.13	122.39	0.984	0.006
	2	392.723	8.088	1.916	0.998	0.005	54.03	103.727	170.087	0.986	0.011	377.077	11.2	0.518	0.998	0.002	14.5	84.69	108.33	0.997	0.002
	2.5	352.231	5.893	2.23	0.995	0.006	60.37	97.507	170.207	0.981	0.014	191.192	2.481	2.146	0.992	0.010	25.07	62.93	97.14	0.97	0.017
	3	205.79	2.517	2.11	0.988	0.010	63.68	92.964	168.974	0.965	0.017	158.691	4.166	0.893	0.991	0.007	31.265	56.34	96.745	0.989	0.008
	3.4	367.051	5.458	2.918	0.975	0.009	64.61	87.514	164.454	0.959	0.011	141.495	1.478	1.715	0.985	0.01	33.07	54.847	97.057	0.973	0.016
2.5	1.5	216.468	1.306	1.059	0.966	0.022	51.77	102.332	166.432	0.941	0.030	216.509	12.67	0.973	0.962	0.009	14.8	90.86	114.8	0.966	0.009
	2	271.092	5.739	0.394	0.996	0.005	59.44	96.923	168.693	0.996	0.005	422.965	3.107	-0.865	0.995	0.004	30.7	81.08	120.92	0.993	0.004
	2.5	208.857	4.192	0.819	0.973	0.014	58.32	92.771	163.421	0.976	0.016	197.932	1.762	1.067	0.996	0.005	27	67.76	103.9	0.988	0.009
	3	334.707	6.461	2.261	0.961	0.019	67.23	91.299	170.859	0.951	0.018	13.304	0.135	-2.556	0.991	0.006	31.261	66.91	107.311	0.989	0.008
	3.4	249.533	0.206	0.963	0.969	0.019	66.09	89.003	167.423	0.967	0.018	159.583	1.115	0.963	0.996	0.005	30.12	65.4	104.66	0.988	0.009

K_{cb}: complete pore blocking model constant; K_{cf}: cake formation model constant; α: fraction of blocked pores in the membrane; R_a: adsorption resistance; R_{cf}: cake layer formation resistance; R_t: total resistance

Table 5.S5: Measures of fit, as per standard deviation SD and regression coefficient R^2, for Resistance in series and Combined model for RC70PP and UH050 organic membranes

TMP (bar)	CFV (m/s)	RC70PP										UH050									
		Combined Model					Resistance in series Model					Combined Model					Resistance in series Model				
		K_{cb} (s^{-1})	$K_{cf}\cdot10^7$ ($s\cdot m^{-2}$)	α	R^2	DS	R_a	R_{cf}	R_t	R^2	DS	K_{cb} (s^{-1})	$K_{cf}\cdot10^7$ ($s\cdot m^{-2}$)	α	R^2	DS	R_a	R_{cf}	R_t	R^2	DS
1	1.5	343.649	13.720	0.982	0.973	0.016	9.090	60.177	74.399	0.951	0.021	70.175	8.286	0.963	0.978	0.012	18.768	34.398	55.267	0.972	0.014
	2	321.381	33.040	1.084	0.991	0.011	10.430	59.213	74.775	0.983	0.015	94.880	13.430	0.848	0.978	0.009	17.995	20.927	41.023	0.974	0.010
	2.5	357.382	33.040	1.346	0.995	0.009	12.010	61.663	78.805	0.994	0.010	84.763	22.078	0.966	0.979	0.017	18.221	16.840	37.162	0.964	0.023
	3	278.372	0.553	0.958	0.963	0.016	16.550	58.364	80.046	0.990	0.012	87.868	14.820	0.905	0.974	0.019	18.131	18.980	39.212	0.964	0.022
	3.4	277.976	0.143	0.953	0.958	0.020	16.120	56.043	77.295	0.976	0.021	75.984	9.219	0.667	0.983	0.019	18.870	14.160	35.131	0.965	0.022
1.5	1.5	280.192	1.044	0.983	0.994	0.008	15.730	62.041	82.903	0.997	0.006	70.982	11.042	0.999	0.995	0.010	18.136	20.550	40.787	0.984	0.019
	2	186.617	4.328	0.827	0.997	0.007	19.310	61.142	85.584	0.993	0.013	101.029	15.840	0.932	0.993	0.009	18.780	31.460	52.341	0.985	0.012
	2.5	313.474	33.040	1.495	0.990	0.017	26.620	58.173	89.925	0.985	0.019	144.879	12.514	0.868	0.948	0.020	18.605	15.122	35.828	0.973	0.018
	3	191.789	4.281	1.730	0.978	0.020	23.090	59.584	87.806	0.955	0.026	194.044	6.101	0.699	0.988	0.011	18.458	19.748	40.307	0.940	0.029
	3.4	287.257	7.989	1.879	0.999	0.006	24.110	58.376	87.618	0.994	0.010	105.680	3.152	0.650	0.985	0.017	18.608	22.150	42.859	0.983	0.017
2	1.5	131.729	31.650	0.687	0.982	0.019	24.440	74.896	104.468	0.968	0.025	86.998	12.830	0.821	0.993	0.014	18.290	33.360	53.751	0.994	0.012
	2	152.221	0.029	0.982	0.976	0.021	26.560	73.864	105.556	0.947	0.034	97.284	1.452	0.690	0.978	0.016	18.198	20.520	40.819	0.976	0.016
	2.5	330.403	33.040	1.739	0.972	0.030	30.140	70.430	105.702	0.983	0.023	82.815	1.742	0.722	0.958	0.040	18.180	19.110	39.391	0.942	0.041
	3	203.115	4.768	1.708	0.992	0.015	32.120	65.565	102.817	0.974	0.023	193.569	2.284	0.736	0.973	0.012	18.538	17.680	38.319	0.962	0.020
	3.4	131.352	0.083	0.988	0.952	0.031	32.340	62.404	99.876	0.980	0.025	107.489	3.189	0.643	0.984	0.015	18.741	19.880	40.722	0.984	0.015

K_{cb}: complete pore blocking model constant; K_{cf}: cake formation model constant; α: fraction of blocked pores in the membrane; Ra: adsorption resistance; Rcf: cake layer formation resistance; Rt: total resistance

Continuation Table 5.S5: Measures of fit, as per standard deviation SD and regression coefficient R^2, for Resistance in series and Combined model for RC70PP and UH050 organic membranes

		RC70PP										UH050									
TMP (bar)	CFV (m/s)	Combined Model					Resistance in series Model					Combined Model					Resistance in series Model				
		K_{cb} (s^{-1})	$K_{cf}\cdot10^7$ ($s\cdot m^{-2}$)	α	R^2	DS	R_a	R_{cf}	R_t	R^2	DS	K_{cb} (s^{-1})	$K_{cf}\cdot10^7$ ($s\cdot m^{-2}$)	α	R^2	DS	R_a	R_{cf}	R_t	R^2	DS
	1.5	158.845	2.447	0.282	0.978	0.016	28.420	88.222	121.774	0.971	0.018	166.403	10.066	0.887	0.978	0.031	20.134	34.430	56.665	0.962	0.034
	2	125.884	0.134	0.980	0.992	0.014	30.570	80.702	116.404	0.980	0.023	73.884	0.980	0.943	0.970	0.028	18.143	25.702	45.946	0.969	0.029
2.5	2.5	125.770	0.107	0.979	0.983	0.026	32.430	73.842	111.404	0.949	0.043	159.470	3.876	0.054	0.956	0.033	18.025	23.580	43.706	0.951	0.300
	3	101.880	0.155	1.006	0.981	0.025	29.780	71.508	106.420	0.940	0.048	245.948	1.722	0.666	0.966	0.016	18.281	19.960	40.342	0.911	0.034
	3.4	110.448	2.275	1.254	0.979	0.021	31.370	71.601	108.103	0.949	0.033	126.229	3.411	0.676	0.987	0.015	18.460	16.990	37.551	0.984	0.015
	1.5											71.387	1.025	0.919	0.978	0.031	18.169	39.390	59.660	0.962	0.034
	2											78.317	2.308	0.549	0.967	0.030	18.174	33.150	53.425	0.969	0.029
3	2.5											120.857	1.833	0.644	0.956	0.031	18.014	23.510	43.625	0.950	0.030
	3											250.485	1.698	0.670	0.959	0.018	18.275	20.290	40.666	0.907	0.035
	3.4											142.487	3.71	0.681	0.984	0.013	18.224	19.36	39.685	0.979	0.016

Table 5.S6: Measures of fit, as per standard deviation SD and regression coefficient R^2, for Resistance in series and Combined model for Inside Cèram 5 and 15 inorganic membranes

		Inside Cèram 5										Inside Cèram 15									
TMP (bar)	CFV (m/s)	Combined Model					Resistance in series Model					Combined Model					Resistance in series Model				
		K_{cb} (s^{-1})	$K_{cf}\cdot10^7$ ($s\cdot m^{-2}$)	α	R^2	DS	R_a	R_{cf}	R_t	R^2	DS	K_{cb} (s^{-1})	$K_{cf}\cdot10^7$ ($s\cdot m^{-2}$)	α	R^2	DS	R_a	R_{cf}	R_t	R^2	DS
1	2	187.126	2.467	0.630	0.982	0.007	12.250	15.509	32.000	0.979	0.008	54.013	2.467	0.388	0.970	0.013	18.688	14.338	34.830	0.969	0.014
	3	177.696	2.195	0.626	0.966	0.009	13.000	16.098	33.339	0.963	0.009	94.323	1.701	1.233	0.989	0.014	19.098	15.623	36.525	0.982	0.019
1.5	2	120.697	2.265	0.317	0.972	0.009	13.720	15.666	33.627	0.973	0.009	94.812	2.214	0.315	0.995	0.004	18.812	14.185	34.801	0.994	0.004
	3	123.165	2.024	0.332	0.966	0.009	12.785	15.580	32.606	0.970	0.008	92.306	2.172	0.589	0.991	0.013	15.817	13.705	31.326	0.984	0.017
	4	133.647	1.714	0.378	0.945	0.010	11.352	15.614	31.207	0.954	0.009	112.274	1.375	0.593	0.980	0.012	16.201	15.784	33.789	0.970	0.015
2	2	58.340	2.128	0.206	0.957	0.010	10.561	15.905	30.707	0.966	0.009	94.793	2.128	0.298	0.969	0.017	20.066	13.475	35.345	0.961	0.021
	3	89.791	1.950	0.212	0.958	0.009	12.440	15.601	32.282	0.966	0.009	25.039	0.179	0.310	0.988	0.013	19.443	14.388	35.635	0.981	0.017
	4	86.152	1.440	0.247	0.985	0.005	10.396	15.214	29.851	0.957	0.008	38.115	1.841	0.398	0.970	0.011	16.328	15.660	33.792	0.976	0.011
2.5	2	31.434	2.376	0.258	0.961	0.009	10.623	15.536	30.400	0.970	0.008	32.567	2.675	0.279	0.980	0.018	18.605	13.853	34.262	0.971	0.018
	3	73.142	1.779	0.263	0.935	0.011	11.567	15.701	31.509	0.954	0.009	86.708	2.445	0.228	0.964	0.017	18.527	14.562	34.893	0.948	0.022
	4	61.302	1.666	0.256	0.919	0.013	11.128	15.494	30.863	0.951	0.010	159.110	1.870	0.219	0.993	0.005	16.338	16.025	34.167	0.994	0.005
3	2	47.005	0.094	0.093	0.899	0.013	10.877	16.136	31.254	0.931	0.011	4.140	3.304	0.027	0.962	0.025	17.464	13.688	32.956	0.969	0.030
	3	54.133	1.504	0.104	0.920	0.010	10.051	15.887	30.179	0.949	0.008	11.633	0.261	0.028	0.976	0.011	18.284	14.801	34.889	0.981	0.012
	4	60.478	1.701	0.128	0.934	0.011	11.380	15.510	31.131	0.954	0.009	47.241	19.890	0.129	0.980	0.008	19.598	14.841	36.243	0.982	0.008

K_{cb}: complete pore blocking model constant; K_{cf}: cake formation model constant; α: fraction of blocked pores in the membrane; Ra: adsorption resistance; Rcf: cake layer formation resistance; Rt: total resistance

Table 5.S7: Measures of fit, as per standard deviation SD and regression coefficient R^2, for Resistance in series and Combined model for Inside Cèram 50 inorganic membranes

		Inside Cèram 50									
TMP (bar)	CFV (m/s)	Combined Model					Resistance in series Model				
		K_{cb} (s^{-1})	$K_{cf}\cdot10^7$ ($s\cdot m^{-2}$)	α	R^2	DS	R_a	R_{cf}	R_t	R^2	DS
1	2	33.961	3.391	0.220	0.988	0.011	18.688	14.338	34.830	0.986	0.012
	3	66.976	9.176	0.203	0.990	0.004	19.098	15.623	36.525	0.992	0.004
1.5	2	43.335	13.980	0.307	0.985	0.012	18.812	14.185	34.801	0.985	0.012
	3	54.839	4.575	0.082	0.996	0.002	15.817	13.705	31.326	0.988	0.004
	4	32.770	6.189	0.079	0.984	0.003	16.201	15.784	33.789	0.989	0.003
2	2	63.283	8.201	0.265	0.974	0.013	20.066	13.475	35.345	0.968	0.015
	3	33.468	5.201	0.048	0.942	0.006	19.443	14.388	35.635	0.963	0.005
	4	21.524	5.282	0.044	0.931	0.007	16.328	15.660	33.792	0.982	0.004
2.5	2	33.559	3.658	0.099	0.970	0.010	18.605	13.853	34.262	0.978	0.010
	3	40.725	5.102	0.054	0.934	0.007	18.527	14.562	34.893	0.958	0.006
	4	22.416	7.016	0.049	0.945	0.007	16.338	16.025	34.167	0.988	0.003
3	2	18.267	5.658	0.080	0.968	0.010	17.464	13.688	32.956	0.974	0.009
	3	27.071	5.350	0.028	0.909	0.007	18.284	14.801	34.889	0.953	0.005
	4	15.786	5.133	0.044	0.939	0.015	19.598	14.841	36.243	0.982	0.008

K_{cb}: complete pore blocking model constant; K_{cf}: cake formation model constant; α: fraction of blocked pores in the membrane; Ra: adsorption resistance; Rcf: cake layer formation resistance; Rt: total resistance

2. Statistical and Machine learning methods

The contour surface plot of permeate flux average (Ja) and cumulated flux decline (SDF) for organic and inorganic membranes are presented. Due to the low R^2 of the results obtained for SDF with the UP005 membrane, its plot is not shown. Similarly, the graph for the UH050 membrane is not shown because only one factor (TMP) affects the parameter.

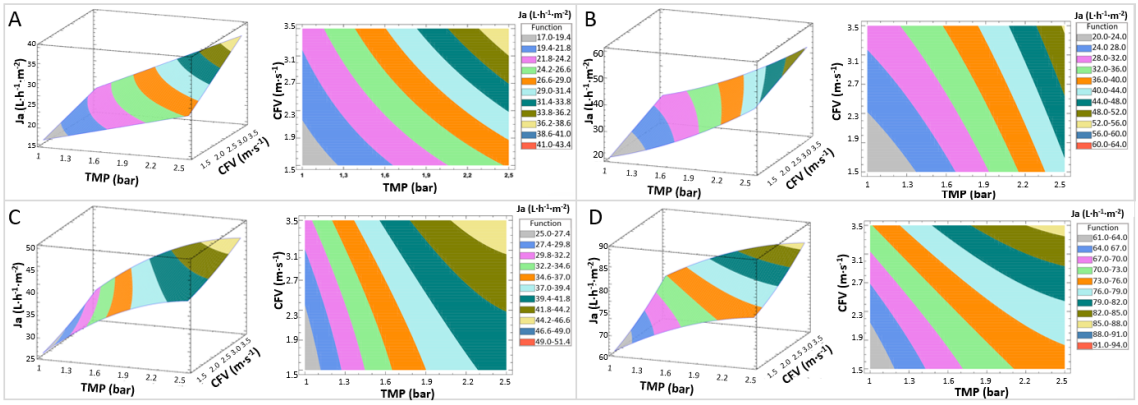

Fig. 5.S.3 Contour surface of the average permeate flux response variable (Ja) vs. TMP and CFV for organic membranes A: UH004; B: UP005; C: RC70PP; D: UH050.

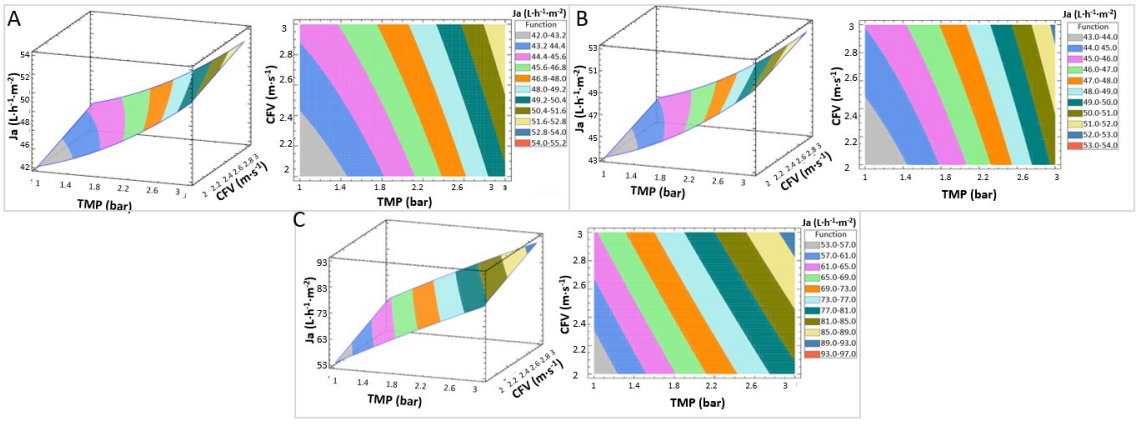

Fig. 5.S.4 Contour surface of the average permeate flux response variable (Ja) vs. TMP and CFV for inorganic membranes A: Inside Céram 5; B: Inside Céram 15; C: Inside Céram 50

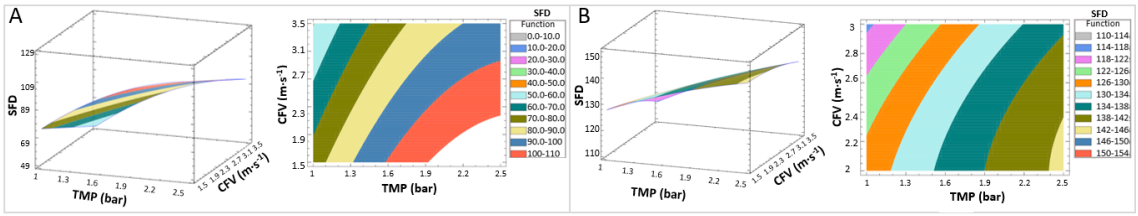

Fig. 5.S.5 Contour surface of the cumulated flux decline (SFD) for organic membranes A: UH004; B: RC70PP.

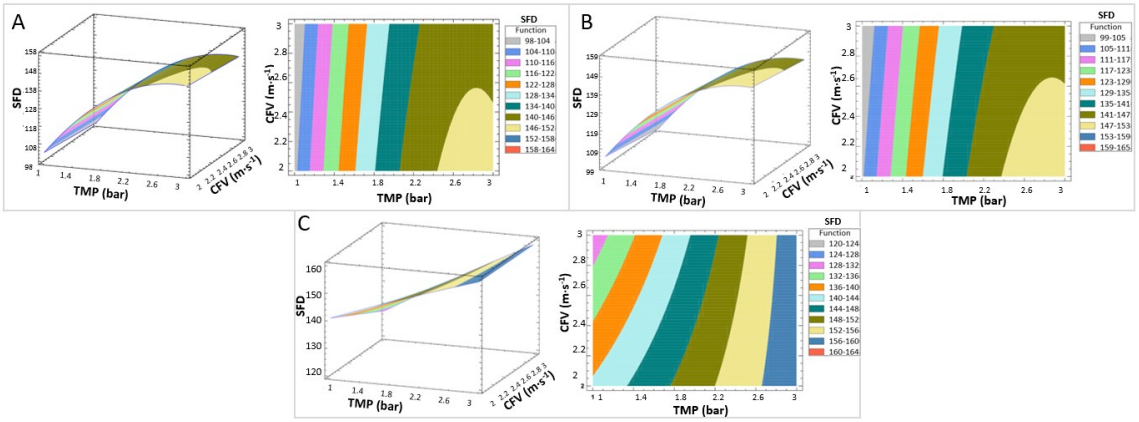

Fig. 5.S.6 Contour surface of the cumulated flux decline (SFD) for inorganic membranes A: Inside Céram 5; B: Inside Céram 15; C: Inside Céram 50

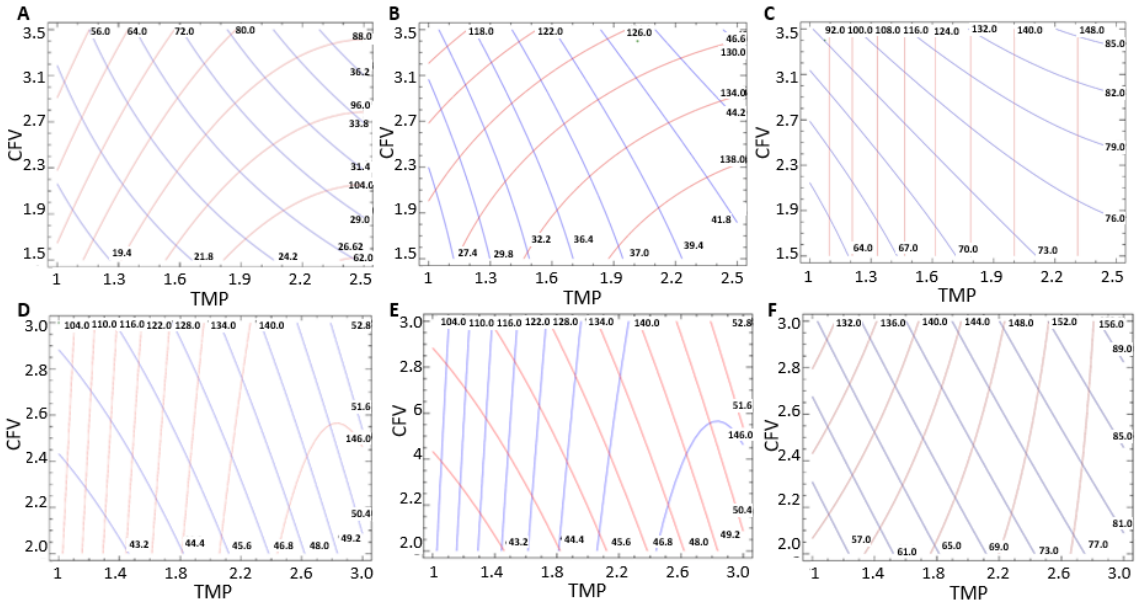

Fig. 5.S7 Superimposed contour plots of response variables Ja (blue) and SFD (red), as a function of TMP and CFV. A: UH004; B: RC70PP; C: UH050; D: Inside Céram 5; E: Inside Céram 15; F: Inside Céram 50.

Table 5.S8 Comparison of the regression coefficient (R^2 for the complete data) of the different ANN architectures for all membranes

Membrane	Nº Hidden layer	Nº neuron	R^2 (complete data)
UH004	1	5	0.9919
	1	6	0.9925
	2	5	0.9960
UP005	1	5	0.9948
	1	6	0.9950
	2	5	0.9990
RC70PP	1	5	0.9837
	1	6	0.9884
	2	5	0.9903
UH050	1	5	0.9635
	1	6	0.9814
	2	5	0.9792
Inside Céram 5	1	5	0.9955
	1	6	0.9962
	2	5	0.9987
Inside Céram 15	1	5	0.8970
	1	6	0.9736
	2	5	0.9752
Inside Céram 50	1	5	0.9946
	1	6	0.9957
	2	5	0.996

V.4 Nanofiltration of wastewaters from olive oil production: study of operating conditions and analysis of fouling by 2D fluorescence and FTIR spectroscopy

ELSEVIER

Chemical Engineering Journal

Volume 454, Part 1, 15 February 2023, 140025

Nanofiltration of wastewaters from olive oil production: Study of operating conditions and analysis of fouling by 2D fluorescence and FTIR spectroscopy

Magdalena Cifuentes-Cabezas [a], Claudia F. Galinha [b], João G. Crespo [b], María Cinta Vincent-Vela [a, c], José Antonio Mendoza-Roca [a, c], Silvia Álvarez-Blanco [a, c]

Show more

+ Add to Mendeley Share Cite

https://doi.org/10.1016/j.cej.2022.140025

Get rights and content

Abstract

The presented work tries to solve the problem of the large volumes of oil mill wastewater (OMW). For this, nanofiltration is presented as a possible second stage of treatment. Different membranes were tested under different operating conditions, varying cross flow velocity (CFV) and transmembrane pressure (TMP), in order to obtain a concentrate rich in phenolic compounds and also an adequate permeate able to be returned to the process as machinery cleaning water. The NF270 membrane under the conditions of 1 ms^{-1} CFV and 10 bar of TMP was observed to be the best to concentrate the phenolic compounds, with high permeate flux and low fouling. Different types of tests were performed: membrane adsorption tests with different compounds, nanofiltration tests with a model solution (MS) to analyse fouling and check the effectiveness of the cleaning protocol and, finally, the selected NF270 membrane was tested with OMW. Also, for the first time, 2D fluorescence spectroscopy and Fourier-transform infrared spectroscopy (FTIR) were used together as tools to study membrane

fouling. From the adsorption tests it was observed that all the considered compounds had an effect on the membrane surfaces, which was also confirmed from the nanofiltration tests (with the DM900 membrane the most affected). After cleaning, the membranes fouled with MS and OMW did not recover the spectra of the pristine membranes but, instead, matched the spectra presented by the new membranes subjected to the cleaning protocol. Finally, the following a suitable membrane for this purpose is selected In addition, it has been proved that the used spectroscopic techniques are a feasible option for the study of both fouling and efficiency of cleaning protocols.

Keywords Olive mill wastewater; Phenolic compounds; Nanofiltration (NF); 2D fluorescence spectroscopy; Fourier-transform infrared spectroscopy (FTIR)

1. Introduction

As the world's population continues to grow and social pressures and awareness of the need for environmental improvement increase, solutions to environmental issues of industry must be found. One of the greatest problems is the large amount of wastewater generated each year by various industrial sectors. One of these sectors, which mainly affects Mediterranean countries, is the olive oil industry, where olive mill wastewater (OMW) is enormously produced. This wastewater has a high content of organic matter, an acidic profile and a large quantity of phytotoxic compounds. These phytotoxic compounds in OMW are phenolic compounds, which are, at the same time, harmful to the environment, but they also show an outstanding antioxidant activity, making them potentially valuable for commercialization [1]. Different processes have been proposed and developed for the treatment of OMW, including membrane processes. These processes are basically a separation generated by a membrane. This membrane acts as a semi-permeable barrier that separates two phases by selectively restricting the movement of components through it. This separation occurs through different driving forces, being pressure-driven separation the most widely applied in wastewater treatment [2]. The advantages of membrane technologies, such as modularity, compactness, easy scalability and adaptability to different capacities make them a promising alternative in situations where wastewater treatment is combined with the recovery of useful components [3]. Within these membrane processes, nanofiltration (NF) is a widely used process for the

treatment of OMW. Due to its high capacity to retain a large amount of organic content as well as monovalent (partially) and divalent ions, it produces a high quality final permeate (with low organic matter concentration and ionic content) suitable for reuse in irrigation, and a concentrate enriched in phenolic compounds [4].

Today there are still some problems in upscaling some membrane process to treat industrial wastewaters due to fouling. The complexity of fouling is due to the presence of multiple species that can interact with each other to form dense and compact fouling layers through pore blockage, adsorption and/or cake formation [5]. This fouling shortens the life of the membranes due to the increase frequency of cleaning procedures. Membrane fouling increases wastewater treatment costs and energy consumption, which affects the industrial application of membranes [6]. Therefore, it is recommended to integrate pre-treatment processes to mitigate fouling phenomena. The combination of different techniques and sequential membrane processes has proven to be a good approach to prevent membranes from fouling [7-8]. Paraskeva et al. [9] and Coskun et al. [10] investigated different membrane techniques for the treatment of OMW. These authors were able to reduce total chemical oxygen demand (COD) with the combination of ultrafiltration (UF), NF and reverse osmosis (RO). Sanches et al. [11] studied the treatment of OMW by a sequence of dissolved air flotation pre-treatment and NF at pilot plant scale, reaching a reduction between 83 to >99% of suspended solids and 53 to 77% of COD. Furthermore, in previous studies by the authors of this work [12] a permeate highly enriched in phenolic compounds was obtained by means of UF with organic membranes. However, this stream was very diluted. Therefore, this permeate could be later concentrated by techniques such as NF. The utilization integrated membrane processes to obtain a concentrated stream enriched in phenolic compounds has also been proposed by other authors [13]. On the other hand, establishing appropriate operating conditions and studying the interaction between the membrane and the compounds present in the influent allows a better understanding of the system, control fouling and thus improve membrane performance [14]. Therefore, understanding the fouling mechanism of individual foulants is crucial for fouling prevention and control in order to find hindrance strategies and optimise cleaning treatments. The lack of papers about characterization of fouling components in NF membranes after the treatment of OMW, has generated the need to search for techniques that deliver fast and complete results. To date, various methods have been proposed and/or

applied to characterise fouling, such as scanning electron microscopy with energy dispersive X-ray spectroscopy, atomic force microscopy, three-dimensional (3D) optical coherence tomography, molecular spectroscopic methods and others [15-16]. Spectroscopic techniques rely on the interaction of electromagnetic radiation with the sample, where the radiation can be absorbed, transmitted or scattered. These techniques have several advantages, such as low sample consumption, rapid analysis that does not require pre-treatment of the samples, as well as ease of use, reduction in the use of solvents, minimising potential environmental impact and providing a wealth of information in a short time [15-17].

In 2D fluorescence spectroscopy, the natural fluorescence of a variety of compounds is used for their detection. When a fluorophore compound is excited, it emits light that can be recorded by fluorescence spectroscopy. The spectra generated can provide quick and useful information about the composition of the samples, with the help of mathematical tools. This technique has been used in various fields such as reverse electrodialysis [18], membrane bioreactors [19] and in the food industry [20,21]. An outstanding advantage of 2D fluorescence spectroscopy is that it can be used for in in situ monitoring of fouling. Although the number of papers on this matter is very limited, the results obtained were promising. Therefore, this work could provide the first indications to check if this technique is appropriate to characterize OMW-fouled NF membranes prior to further studies to implement this technique for in situ characterization. Fourier transform infrared spectroscopy (FTIR) is another method often used to characterise membrane materials and impurities. In this case, the spectra profiles comprise specific bond stretchs and allow the identification of the chemical species in the sample [22].

The results are also readily available and can provide valuable information on the composition. Principal component analysis (PCA) and partial least squares (PLS) are some of the multivariate techniques commonly used to deconvolute and interpret spectroscopic data [23].

In this paper, NF was analysed as a possible second stage treatment after UF, for the recovery of phenolic compounds from an olive oil washing wastewater (OOWW). The NF process was fed with the permeate obtained from a previous UF step that demonstrated to be efficient to remove a large amount of the organic matter and obtain a permeate rich in phenolic compounds [12]. Different NF membranes and operating conditions were tested to obtain a

concentrated stream containing phenolic compounds and a permeate stream suitable to be recycled to the process as machinery wash water. The membranes used in this study are commercial. Although good results have been reported with modified membranes, most membrane manufacturing and modification strategies are not yet implemented at industrial scale due to cost and repeatability problems [24]. Moreover, the utilization of 2D fluorescence spectroscopy and FTIR as tools to investigate membrane fouling was considered. Finally, a PCA data analysis was employed to evaluate the efficiency of the cleaning protocols using the data obtained from these techniques. The purpose of this study was, firstly, to find the best membrane and operating conditions for the recovery of these antioxidants with NF and, secondly, to investigate the potential of these spectroscopic techniques to study the fouling phenomenon and cleaning protocols of the membranes.

2. Materials and Methods

2.1 Nanofiltration experiments for process optimization

2.1.1 Nanofiltration process

Four polymeric membranes with different properties were analysed as a second stage of treatment of an OOWW. All the membranes were first conditioned under the same protocol. The membranes were submerged for hydration for 24 hours in pure water (conductivity <40 µS/cm) and then compacted for three hours. The operating conditions were: transmembrane pressure (TMP) of 16 bar and a cross-flow velocity (CFV) of 1 $m \cdot s^{-1}$. The conditions used were based on studies carried out by Sanchez-Arévalo et al. [25] and following the standard procedures for membrane compaction [26]. Once the compaction was finished, the hydraulic permeability (K) was measured and obtained using the following equation:

$$J = K \cdot \Delta P \quad (1)$$

Where J ($L \cdot h^{-1} \cdot m^{-2}$) is the permeate flux and ΔP (bar) the TMP. Previously, a UF process was carried out as first membrane process stage to eliminate the major organic matter. It was performed with an UP005 Microdyn-Nadir membrane, under the operating conditions of 2 bar of TMP and CFV of 2.5 $m \cdot s^{-1}$. The UF process feed was an OOWW pre-treated (PR-OOWW) following the protocol presented in other studies [12]. The raw OOWW was collected during the production of olive oil in October 2019 in the Valencian Community (Spain). It was taken at the outlet of the vertical centrifuge after the olive oil washing in the

two-phase continuous centrifugation process. The characterization of the PR-OOWW and UF permeate is shown in Table 5.12.

Table 5.12 Characterization of samples from pre-treatment stages

	PR-OOWW*	UF Permeate
pH	5.14 ± 0.01	5.19 ± 0.02
Conductivity ($mS \cdot cm^{-1}$)	4.54 ± 0.03	5.35 ± 0.01
Turbidity (NTU[a])	22.80 ± 0.57	0.04 ± 0.00
Suspended solids ($mg \cdot L^{-1}$)	1400 ± 11.02	0.12 ± 0.00
COD[b] ($mg \cdot O_2 \cdot L^{-1}$)	42950 ± 198.12	14580 ± 12.37
TPhC[c] ($mgTyeq \cdot L^{-1}$)	1101.16 ± 16.12	954.78 ± 12.70
SUG[d] ($mg \cdot GluL^{-1}$)	4484 ± 57.37	3730 ± 325.10

[a] NTU: Nephelometric Turbidity Units; [b] COD: chemical oxygen demand; [c] TPhC: Total phenolic compounds; SUG: sugars; *PR-OOWW: pre-treated olive oil washing wastewater (OOWW)

Table 5.13: Specifications of the nanofiltration membranes used

	NF90	NF245	NF270	DM900
Supplier	Dow Filmtech	DuPont	Dow Filmtech	Evonik
Material	TFC[a]PA[b]	TFC[a]PP[c]	TFC[a]PA[b]	ISA[d] Modified PI[e]
Contact angle	66.45[1]	11.0[2]	25.4[3]	69.7[4]
MWCO (Da)	90 – 180	300	150 - 340	900F
Pore size (nm)	0.38[5]	-	0.44[5]	-
Zeta potential at neutral pH (mV)	-17.5[5]	-	-21.6[5]	-
T max (°C)	40	50	45	50
P max (bar)	41	54.8	41	20
pH range	2 - 11	3 - 10	3 - 10	0 - 7
Permeability* ($L \cdot h^{-1} \cdot m^{-2} \cdot bar^{-1}$)	3.80	4.87	12.45	6.32

[a]TFC: thin film composite; [b]PA: Polyamide; [c]PP: Polypropylene; [d]ISA: integrally skinned asymmetric; [e]PI: polyimide; [f]Molecular weight cut-off of styrene oligomers dissolved in acetone; * Water, at 25 °C, experimentally determined in this work. [1]: [27]; [2] [28] [3] [29]; 4: [30] ; [5] [31]; 6 [32]

Once the necessary volume of UF permeate was reached, it was fed to the NF process, which was carried out in a laboratory-scale plant. This plant operated in full recycling mode

and was equipped with a feed tank of 40L and a plunger pump. The membrane module was designed by the research institute ISIRYM [33]. This module allows the use of one flat sheet membrane with an active area of 0.0072 m^2. Four different membranes were tested under different CFV (0.5-1.5 $m \cdot s^{-1}$) and TMP (5 - 15 bar). The specifications of the membranes are presented in table 5.13.

Every 30 minutes 50 mL of permeate sample was collected for further analysis. The experiments were performed at a constant temperature of 21 ± 1°C, controlled by an electrical resistance and a cooling coil. The performance of the membranes was evaluated by calculating the rejection of the chemical oxygen demand (COD), total phenolic compounds (TPhC) and sugars (SUG), under the following equation (Eq. 2)

$$\%R_J = \left(1 - \frac{C_{pj}}{C_{fj}}\right) \cdot 100 \quad (2)$$

Where *Rj* corresponds to the apparent rejection of the different parameters *j* (COD, TPhC or SUG) expressed in %; *Cpj* and *Cfj* are the concentration of parameter *j* in the permeate stream and in the feed solution, respectively.

2.1.2 Samples analysis

All the samples were characterized for the same parameters. Electrical conductivity was determined by means of a digital calibrated conductivity meter (EC-Meter GLP 31+) and pH by using a pH-meter (GLP 21+), both from Crison (Barcelona, Spain). For turbidity, a D-112 turbidimeter (DINKO, Barcelona, Spain) was used following the UNE-EN ISO 7027 standard method. COD was measured with Merck kits (Darmstadt, Germany) in a range of 500-10.000 $mg \cdot L^{-1}$ and the measurement of suspended solids was performed following the UNE 77034 standard method from APHA [34]. Total phenolic compounds concentration was determined by means of the Folin-Ciocalteau method [35] with tyrosol (VWR Chemicals, USA) as standard. Sugar concentration was determined by the Anthrone colorimetric method [36], whit glucose (Panreac, Barcelona, Spain) as standard.

2.1.3 Cleaning protocol

The membranes were cleaned after each test to remove fouling. Firstly, tap water was flushed through the system for 5 minutes. The cleaning procedure consisted of four successive steps, only performing the steps needed to recover the initial permeability of the membrane by at least 95%. The duration of each step was 30 minutes. The protocol steps were the following: C1: pure water at 25°C, C2: pure water at 35°C, C3: 1%v/v Ultrasil solution at 25°C and C4: 1%v/v Ultrasil solution at 35°C. The last two solutions for the chemical cleaning were prepared with P3 Ultrasil 115 (Ecolab, Barcelona, Spain).

2.2 Analysis with 2D fluorescence spectroscopy and FTIR

The diagram plotted in fig. 5.25 shows the methodology followed for the analysis of the effect of fouling and cleaning of the membrane surface with 2D fluorescence spectroscopy and FTIR. Each stage is explained separately below.

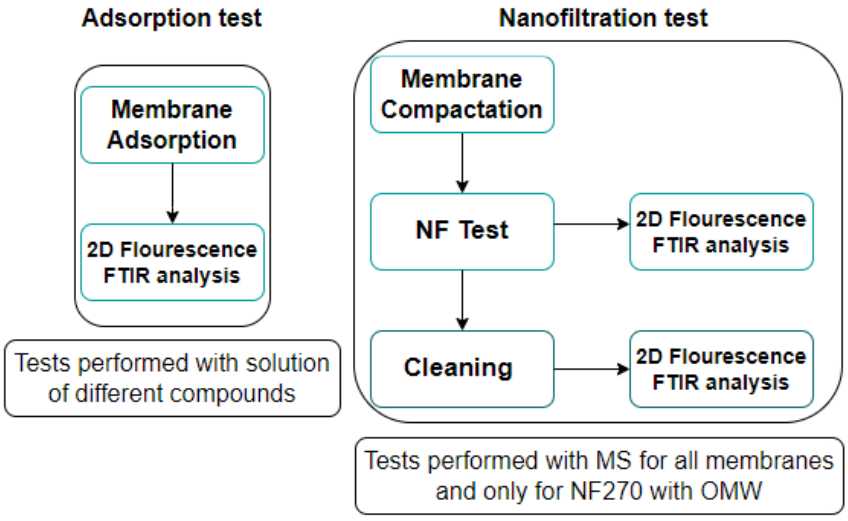

Fig. 5.25 Methodology to evaluate the effect fouling and cleaning of the membranes with 2D fluorescence spectroscopy and FTIR. NF: nanofiltration; MS: model solution; OMW: olive mill wastewater

2.2.1 Adsorption tests

First, adsorption tests were performed with all the membranes. The four membranes were evaluated in the same way under the following protocol: a piece of membrane (3x3 cm) was immersed in different solutions for 24 hours to further analyse the surface of the membranes by 2D fluorescence and FTIR spectroscopy, in order to find out whether some compounds were adsorbed by the membrane. The compounds (supplier by BioNova Científica (Spain) and PanReac Applichem (Spain)) selected for the adsorption tests were based on the composition of the real OOWW used [37]. One compound of each family (chemical class) was selected: citric acid (CI) corresponding to organic acids, caffeic acid (CA) corresponding to phenolic acids, hydroxytyrosol (HT) representing simple phenols, luteolin (LUT) to flavonoids and a mixture of glucose, fructose and sucrose to sugars (SUG). It is important to emphasize that the adsorption assay did not consider the actual concentrations of each compound present in the OOWW, but the aim was to use the same concentration for each compound. With the exception of sugars, the concentration of each compound in distilled water solutions was 20 ppm (conductivity <70 µS/cm). The sugar solution had a concentration of 30 ppm, with 10 ppm of each compound. As a control, it was decided to leave a piece of membrane in distilled water. On the other hand, other pieces of membrane were also immersed in a solution with the chemical reagent used in chemical cleaning (P3 Ultrasil 115, 1% v/v). This followed the same adsorption protocol as the membrane pieces in the different solutions. This is done to analyze if there were changes in the membrane surface after cleaning (also acts as a control).

2.2.2 Nanofiltration tests for membrane fouling analysis

For these NF tests, a model solution (Table 5.14) made with the same reagents used for adsorption analysis was used as feed stream. In this case, the concentration of each compound was consistent with the concentration obtained from the liquid chromatography–mass spectrometry characterization of the real OOWW, which can be found elsewhere [37]. A new model solution was used for each test. The tests were carried out under the best operating conditions ($1 m \cdot s^{-1}$ of CFV and 10 bar of TMP) that were selected after a previous study with OOWW (section 2.1). These tests were carried out in another nanofiltration plant. In this case, the plant was assembled with a GE-Sepa CF module (GE OSmonic, Minnetonka, USA) and a Hydra-cell G13 model pressure pump (Wanner Engineering Inc., Minneapolis, USA). The NF

active membrane area was 0.014 m^2. Permeate and concentrate samples were collected after half an hour and at the end of the test and stored for future analysis.

Table 5.14. Characterization of model solution used as feed in the nanofiltration tests

Compound	Family (Chemical class)	Concentration (ppm)
Citric acid	Organic acids	207.10 ± 1.06
Caffeic acid	Phenolic acids	4.22 ± 0.05
Hydroxytyrosol	Simple phenols	3.43 ± 0.16
Luteolin	Flavonoids	3.33 ± 0.02
Glucose	Sugars	700.02 ± 0.02
Fructose	Sugars	100.35 ± 0.01
Sucrose	Sugars	100.67 ± 0.02

Upon completion of the assay, the membrane was removed from the module and 2D fluorescence was measured immediately to avoid drying out of the membrane. The FTIR spectra of the membrane was also determined after the test. The membranes were stored in a refrigerator (5°C) to avoid their degradation.

To analyse the effectiveness of the cleaning protocol, the test explained above was repeated, but, this time, followed by a chemical cleaning. For this, the cleaning protocol that presented the best results at the time of recovering the initial permeate flux in the OOWW test was used (C4: 1%v/v Ultrasil solution at 35°C). First, the membrane was rinsed with tap water for 5 minutes, before circulating the cleaning solution for 30 minutes under a TMP of 1 bar at 35°C (same protocol presented in 2.1.3.). The membrane was then rinsed with distilled water to remove all chemical residues and afterwards the 2D fluorescence of the membrane surface was immediately measured. As mentioned above, the membrane was later analysed with FTIR spectroscopy, keeping it refrigerated to avoid degradation.

Finally, a NF test was performed with OMW using only the membrane that showed the best results in the study with OOWW. The OMW sample was provided by Zeyton Nutraceuticals, Portugal from a three-phase continuous centrifugation process. The sample was treated following the same protocol as that applied for the OOWW. Then, it was diluted to

obtain a composition similar to that presented by OOWW. The operating conditions for both the NF test and the cleaning protocol were the same ones describe above. The membrane was also evaluated under 2D fluorescence and FTIR spectroscopy after the NF test. Finally, a chemical cleaning was performed.

2.2.3 2D fluorescence and FTIR spectroscopy

The fluorescence spectra of the membranes and samples were acquired with a Varian Cary Eclipse fluorescence spectrophotometer equipped with excitation and emission monochromators and coupled to an optical fibre bundle probe. The excitation-emission fluorescence spectroscopy measurements (EEMs) were obtained at a scan speed of 12000 $nm \cdot min^{-1}$, and excitation and emission slits of 5 and 10 nm, respectively. Fluorescence spectra were determined in a wavelength range of 245 and 745 nm of excitation and an emission wavelength range between 250 and 750 nm with an incrementing step of 5 nm. FTIR spectra of the membranes were obtained utilizing Shimadzu IRAffinity-1S in absorption mode from 400 to 4000 cm^{-1} with 4 accumulations scans and a resolution of 10 cm^{-1}. Furthermore, the data obtained by these techniques was deconvoluted and compressed into some major PCA components (Supplementary material, section 1) for better analysis.

3. Results

3.1 Membrane characterization and permeate fluxes in nanofiltration tests for process optimization

The measured hydraulic permeability values agree with the data obtained by other authors [25,38,39], with the NF270 membrane exhibiting the highest permeability (12.45 $L \cdot h^{-1} \cdot m^{-2} \cdot bar^{-1}$) and the NF90 membrane the lowest one (3.80 $L \cdot h^{-1} \cdot m^{-2} \cdot bar^{-1}$). No record of the water permeability of the DuraMem900 (DM900) membrane was found in the literature. The hydraulic permeability for the other membranes were 6.32 $L \cdot h^{-1} \cdot m^{-2} \cdot bar^{-1}$ and 4.87 $L \cdot h^{-1} \cdot m^{-2} \cdot bar^{-1}$ for DM900 and NF245, respectively.

Fig. 5.26 shows the mean permeate flux values for the different operating conditions tested in the NF experiments with OOWW. The error is not presented, but in all cases it was less than 9%. In general, it is observed that permeate flux was more affected by TMP, showing a linear increase with TMP for all the CFVs tested. However, this behaviour was not observed in all tests. For the NF90 and DM900 membranes, the permeate flux presented a deviation

from linearity at high TMPs (above 10 bar). This may be explained because the critical flux is being reached, which is evidence of membrane fouling [40]. In the case of the DM900 membrane, similar flux values were obtained at 10 and 15 bar, which was more noticeable at low CFV. This may be due to the fact that high TMP values could contribute to concentration polarization [41], which would result in a greater flux decrease (in this case from 10 bar). Higher flux values were obtained at higher CFV conditions. The decrease in flux is mainly due to the formation of a gel layer or cake. Thus, increasing CFV allows improving the transfer of solids present on the membrane surface back into the bulk stream [42]. Therefore, a reduction in the thickness of the fouling layer occurs, with the subsequent increase of the permeate flux. It also allows working at higher TMP values. On the other hand, in nanofiltration, especially at high TMP, the effect of the osmotic pressure gradient may be relevant. The accumulation of inorganic or organic solutes generates an increase in the osmotic pressure difference between the two sides of the membrane and will lead to the reduction of the effective TMP and the permeate flux [11,43]. Mohammad et al. [43] pointed out that while studies of fouling mechanisms have been conducted, it remains difficult so far to predict which mechanism is involved.

The lower hydraulic resistance to water transport exhibited by the NF270 membrane due to its relatively loose semi-aromatic skin rejection layer may explain the high permeate fluxes [44]. The DM900 was the membrane that presented the greatest hydraulic resistance, due to the more hydrophobic properties of the modified polyimide [30] in comparison to the other membranes materials. Also, when comparing the hydraulic permeability and the permeate flux with the OOWW, this membrane (DM900) was the one that presented the greatest difference, showing a flux decrease between 56-65% (depending on the TMP), which could infer that this membrane was the most affected by fouling. Similar results were observed by Böcking [45] when using a membrane of the same material (DuraMem500). They observed that the addition of PEG as a solute generated a significant decrease in permeate flux (close to 45%). They attributed it primarily to concentration polarization effects.

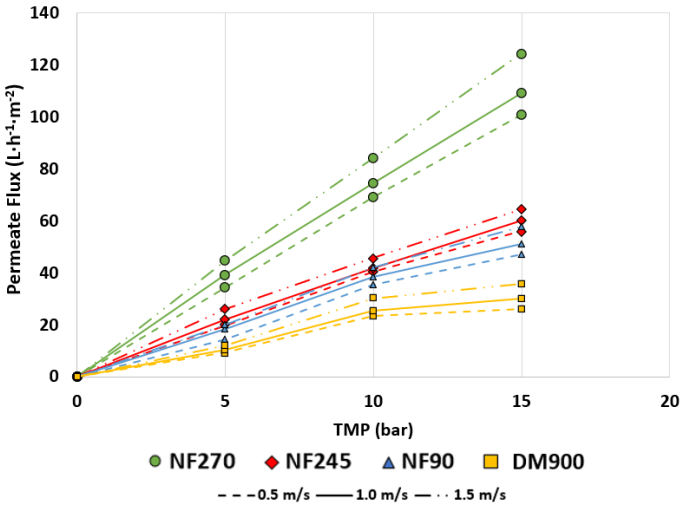

Fig. 5.26 Stationary permeate flux obtained at the different TMP and CFV during the nanofiltration of olive oil washing wastewater

It has been usually reported that permeate flux affects permeability reduction because the higher the flux, the faster the accumulation of solutes on the membrane surface [46,47]. However, a linear relationship between higher permeate flux values and higher fouling was not observed (Fig. 5.27). The membrane with the highest permeate flux (NF270) was found to exhibit relatively similar fouling to those of the NF245 and DM900 membranes in terms of permeate flux decline over time. This could indicate a non-severe fouling in the NF270 membrane. Once again, it can be seen how the DM900 membrane was the most affected by fouling, due to its constant flux decrease, being the last to reach a steady state. On the other hand, the membrane with the lowest MWCO reached faster the stationary permeate flux, which could be due to rapid fouling. Nunes et al. [44], in their study on the extraction and concentration of bioactive compounds from olive pomace using membranes, observed a similar performance of the NF90 membrane, attributing it to the polymeric structure of the membrane. This membrane is open enough to let the foulants penetrate through the membrane, but, at the same time, it is closed enough to generate a close/block in one step, generating a rapid decrease in flux prior to a flux stabilization. Similarly, as in this study, these authors observed an opposite behaviour with the NF270 membrane, which suffered from progressive

fouling. As the intra-polymeric voids in its active layer are too large to block them all at once, flux decay is not so abrupt as in the case of NF90 membrane.

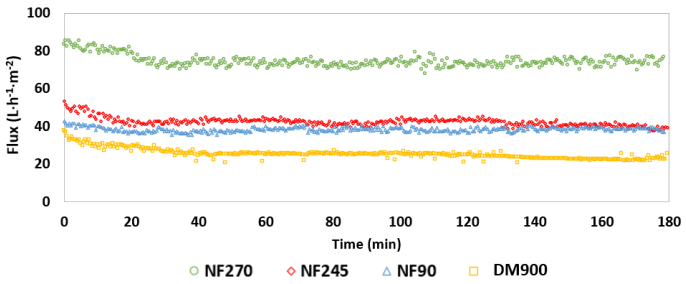

Fig. 5.27 Variation of permeate flux over time in OOWW nanofiltration at a TMP of 10 bar and CFV of 1 $m \cdot s^{-1}$

3.2 Membrane rejections

Fig. 5.28 shows the percentages of rejection obtained in the NF tests performed. In all tests, an increase in rejection percentages can be seen with increasing TMP as expected. Regarding the CFV, rejection seemed to increase at increased CFV values. However, this behaviour did not repeat for all the membranes. At a fixed TMP of 10 bar, the NF245 membrane had the highest rejections for all the compounds at 1 $m \cdot s^{-1}$. Therefore, the increase in CFV generated a decrease in the rejection efficiency for this membrane. This could be due to the aforementioned effect of fouling layer diminution by increasing CFV, and better external mass transfer conditions (lower concentration polarization). This fouling layer could act as an additional layer, generating additional resistance to the pass of the solute through the membrane [48].

The NF90 membrane was the one that presented the highest COD retention percentages, while the DM900 had the lowest. This agrees with the retentive properties of these membranes, with the NF90 being the one with the lowest MWCO. On the other hand, although according to the manufacturer, both NF245 and NF270 membranes exhibit similar MWCO, the higher retention exhibited by the NF270 suggested a tighter top layer structure than that of the NF245.

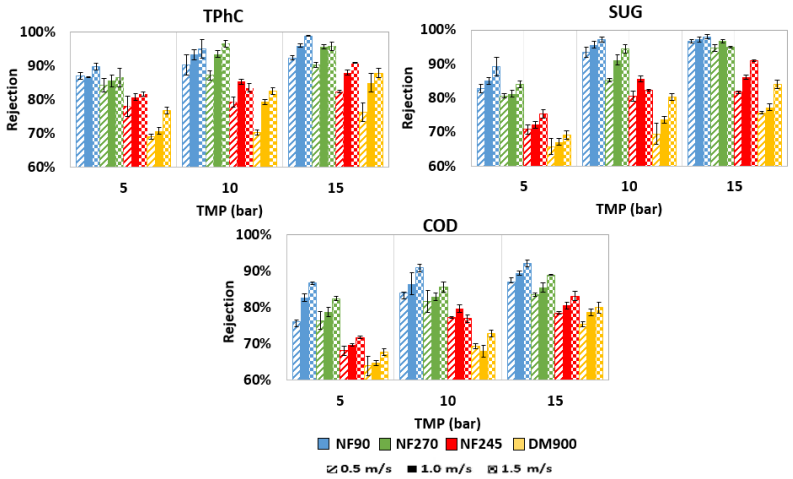

Fig. 5.28 Steady state rejection of TPhC (total phenolic compounds), SUG (sugars) and COD in the nanofiltration of olive oil washing wastewater

Interesting results were obtained with the DM900 membrane. Although low permeate fluxes were obtained, the percentages of phenolic compounds rejection are within the range of the other membranes. Although this membrane was manufactured for use with organic solvents, the cross-linking reaction that occurs in its manufacture generates an increase in hydrophilicity, with a contact angle indicating a polar active layer [45], therefore it is suitable for use in aqueous solutions. Other studies have shown great rejection of total phenolic compounds in organic solvent solutions (near 80%) using this membrane [30]. In this case, the rejections were similar and in some cases higher; this may be due to the fact that for hydrophilic membranes the rejections in water will be higher than in organic solvents [49]. Although, the NF90, NF245 and NF270 membranes presented similar rejection ranges for phenolic compounds, the NF270 was by far the one that presented the highest permeate flux in all tests carried out. Thus, this membrane was found to be the most appropriate for the concentration of phenolic compounds from OOWW. Similar results were observed by López-Borrell et al. [50] in the recovery of phenolic compounds from wine lees. Although the rejection of the phenolic compounds that presented the NF90 and NF245 membranes was high, they showed very low permeate flux values. Also, the zeta potential (table 5.13), can be related with the higher rejections presented by NF90 and NF270 membrane. It can be due to higher cross-linking of the aromatic polyamide (as deduced from zeta potential measurements), which

corresponds to higher polymer density and hindered diffusion of the solute [51]. Therefore, the NF270 membrane was selected as the optimal one because it presented the highest values of permeate flux with a rejection of phenolic compounds above 93%. It is important to highlight that no interactions between the membranes and the phenolic compounds are expected. Due to the pH of the OMW, the membranes are negatively charged (isoelectric point, 4.0 - 5.0 [160–163]), and the phenolic compounds are found in their deprotonated form at basic pHs, which is not the case.

The rejection of sugars showed a similar trend to the rejection of phenolic compounds, with all membranes presenting high percentages of sugar rejection. The increase of TMP from 5 to 10 led to a significant increase in rejection. This was also observed by Nguyen et al. [55], who studied the use of NF and RO for the detoxification of lignocellulosic hydrolysates. They observed that when TMP was raised at values higher than 10 bar glucose rejection increased (>94%), regardless of the membrane analysed. Although only glucose was considered, about 60% of the sugars present in OOWW correspond to glucose, so the trend can be extrapolated to the sugars analysed in this study. On the other hand, the permeate obtained by all membranes was adequate to be reincorporated into the process as machinery cleaning water, with low COD and TPhC. Ochando-Pulido et al. [56] also obtained high COD rejection (86.76%) with the 300Da DK membrane (GE Water & Process Tech) when working with OOWW. These authors used the permeate (practically without phenolic compounds) for irrigation.

3.3 Membrane cleaning

The recovery of the hydraulic permeability of the membranes after each test and the cleaning protocols performed are shown in Fig. 5.29 (A and B). It can be seen that from the 4th use of the membranes there was a decrease in the permeability recovery percentage for most of them (Fig. 5.29A). This was more significant for the NF90 and DM900 membranes. This could be explained because these tests were performed above sustainable flux conditions, as they were performed at high values of TMP. This term is related to the permeate flux value that corresponds to non-severe fouling an to a profitable balance between investment and operating costs [57-59]. Therefore, the operating conditions generated high fouling, which made cleaning difficult, hindering the recovery of the hydraulic permeability. In this case, working with the NF90 and DM900 membranes under the conditions of tests 4-9 would imply the need for a

more aggressive cleaning, as high TMP and low CFV values were considered for these tests, thus increasing membrane fouling. This could result in higher spending of chemical reagents for cleaning or more energy to raise the temperature. On the other hand, the NF245 and NF270 membranes were the only ones capable of recovering permeability in all tests by at least 95%. It is important to note that these two membranes mostly present reversible fouling, managing to recover an average of 86.7 ± 3.8% and 82.3 ± 4.1% after C1, which was performed with water at room temperature. Membrane materials and feed solution also play an important role in the reversibility/irreversibility of the fouling process. In this case, the interaction between the membrane material and foulants was higher for the NF90 and DM900 membranes than for the others, making fouling removal more difficult. Although the NF270 and NF90 membranes are made of the same material, the NF90 exhibited high fouling. Similar results were obtained by Arboleda Mejia et al. [39], who only recovered 60% of the initial water permeability of this membrane when it was used to recover phenolic compounds from red grape pomace. They attributed it to the possible adsorption of phenolic compounds, which tends to irreversible. This will be discussed in the next section, where the results of the adsorption tests will be commented.

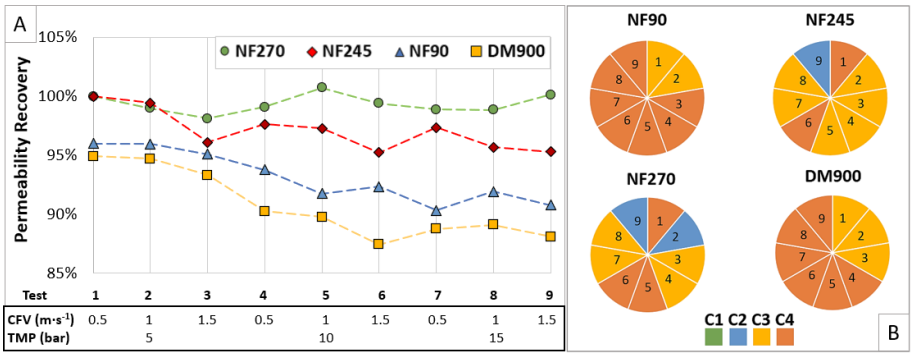

Fig 5.29 A: recovery of the initial hydraulic permeability after cleaning. B: cleaning protocol necessary to achieve the hydraulic permeability recovery in each test (1-9) indicated in figure A; C1: water at 25°C, C2: water at 35°C, C3: chemical cleaning with P3 Ultrasil 115 (1% v/v) at 25°C and C4: P3 Ultrasil 115 (1% v/v) at 35°C.

In fig.5.29B, it can be seen that almost all the tests required chemical cleaning (protocol C3 and C4) to recover the initial hydraulic permeability, which means that fouling was mainly irreversible. For the NF245 and NF270 membranes, the cleaning protocol proposed was successful. However, the NF90 and DM900 membranes would require a more exhaustive cleaning for a higher permeability recovery.

As a general conclusion for sections 3.1, 3.2 and 3.3, it can be stated that the NF270 membrane showed the best performance for the studied application. Under the operating conditions of $1 m \cdot s^{-1}$ of CFV and 10 bar of TMP, it yielded a stable permeate flux of 74.4 $L \cdot h^{-1} \cdot m^{-2}$, a rejection of total phenolic compounds of 94% and a COD rejection of 83%.

3.4 Adsorption tests

Figures 5.30-5.33 present the contour spectra obtained with 2D fluorescence spectroscopy for the adsorption experiments. In all the figures, the emission (Em) wavelength (in nm) is plotted on the "x" axis and the excitation (Ex) wavelength (in nm) on the "y" axis. The fluorescence intensity is also shown through colours, with the yellow colour representing the highest intensity.

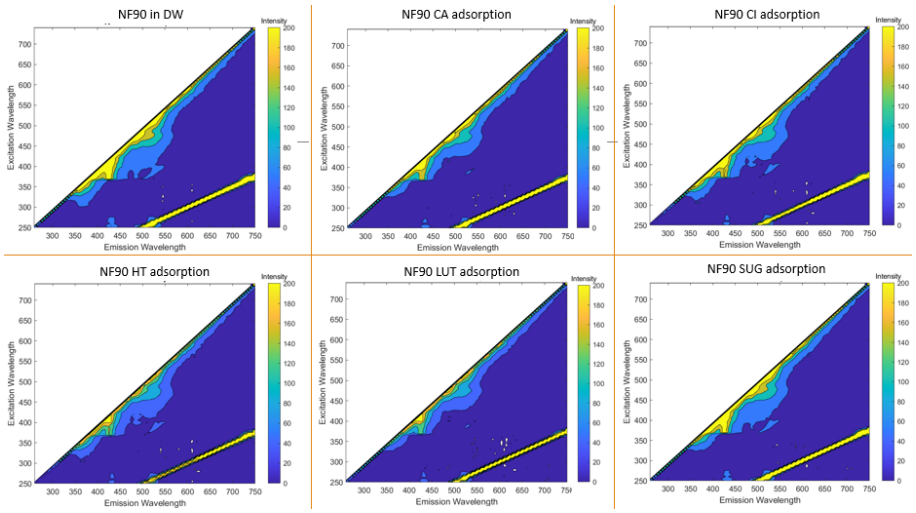

Fig.5.30 2D fluorescence spectra for the adsorption test performed with the NF90 membrane. DW: deionized water; CA: caffeic acid; CI: citric acid; HT: hydroxytyrosol; LUT: luteolin; SUG: sugars

Fig. 5.30 shows the spectra obtained for the NF90 membrane. The membrane Ex/Em characteristic region (NF90 in deionized water (DW)) was between 325-525/350-575 nm. With the exception of SUG, the contact with the different compounds during adsorption studies slightly affect the characteristic signal of the membrane between the Ex/Em lengths of 400/450 nm. However, due to the low fluorescence signal of the membrane it is difficult to see differences between the compounds tested. The DM900 membrane (Fig. 5.31) showed similar results as the NF90 membrane. A fluorescence signal characteristic of the membrane was observed in all DM900 adsorption experiments. The low intensity of the signals may be due to the nature of the membrane, specifically the material from which it is made. In this particular case, the DM900 membrane has an intense brown colour, indicating light absorption, contributing to the low signal intensity. Nevertheless, CA clearly affected the signal of the membrane, followed by LUT.

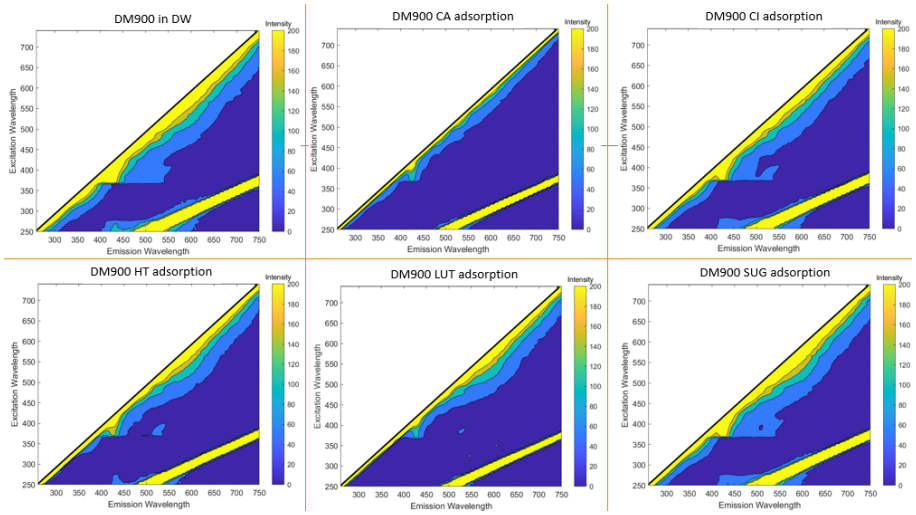

Fig. 5.31 2D fluorescence spectra for the adsorption test performed with the DuraMem900 (DM900) membrane. DW: deionized water; CA: caffeic acid; CI: citric acid; HT: hydroxytyrosol; LUT: luteolin; SUG: sugars

A very different result was obtained with the NF245 and NF270 membranes (Fig. 5.32 and 5.33, respectively). A strong characteristic Ex/Em signal between 300-450/325-475 nm was observed for both membranes. Clearly, a great influence of LUT and CA was observed on

the signal, completely overshadowing the NF245 membrane signal. This means that these compounds have being adsorbed by the surface of the membrane, hiding the characteristic signal of the membrane. Although CI did not completely eliminate the signal of the NF245 membrane, it did affect it, reducing its intensity. For the NF270 membrane no changes in the signal were observed with CI. Moreover, HT and SUG did not cause clear changes in the characteristic signal of both membranes. These results show that either these compounds are little or no adsorbed by the membrane surface or that they do not induce visible changes in the fluorescence spectra. In fact, besides the natural fluorescence ability, the natural colour of some compounds can affect the signals emitted by the membrane surface and may alter the membrane surface colour [18]. Therefore, the coloured compounds can be easily detected, more than the non-coloured compounds (HT - CI - SUG). Nevertheless, the effect of CI on the NF245 membrane signal points out a higher impact of CI on this membrane than on the other 3 membranes tested.

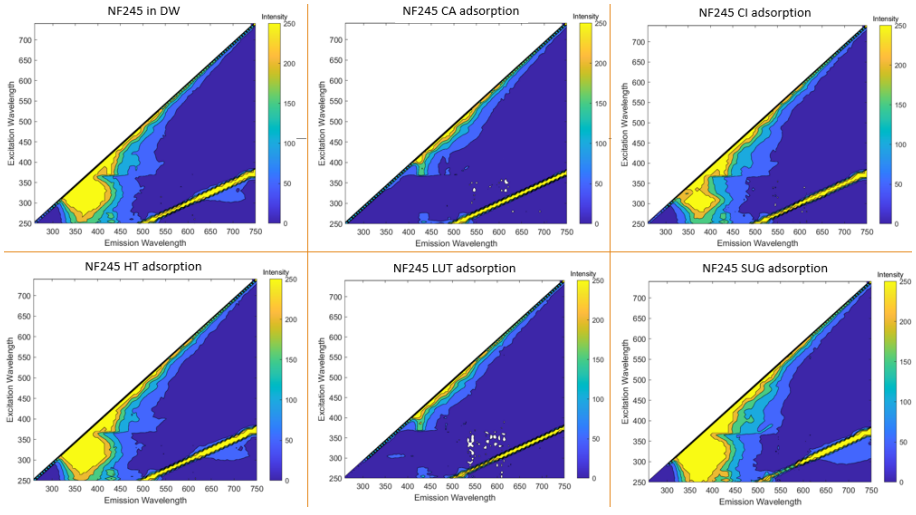

Fig. 5.32 2D fluorescence spectra for the adsorption test performed with the NF245 membrane. DW: deionized water; CA: caffeic acid; CI: citric acid; HT: hydroxytyrosol; LUT: luteolin; SUG: sugars

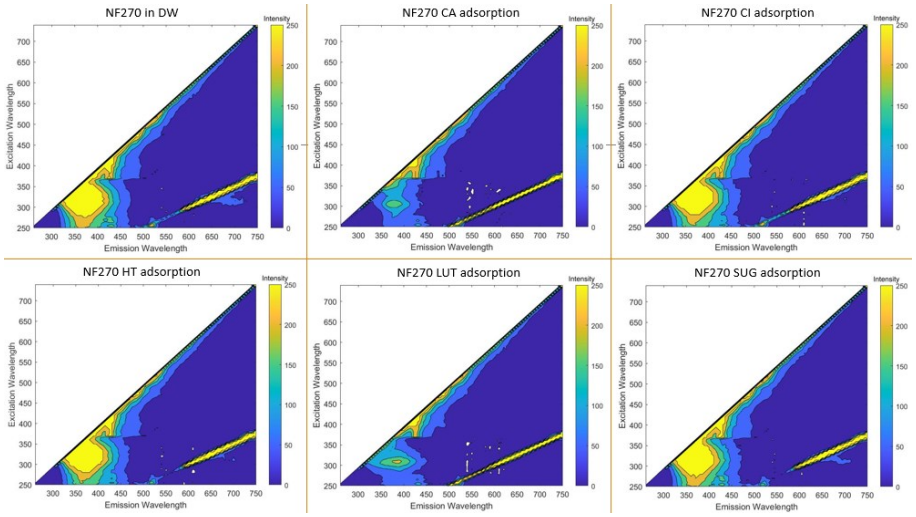

Fig. 5.33 2D fluorescence spectra for the adsorption test performed with the NF270 membrane. DW: deionized water; CA: caffeic acid; CI: citric acid; HT: hydroxytyrosol; LUT: luteolin; SUG: sugars

To better understand the effect of the compounds tested on the membrane surface, the results will be analysed together with the FTIR spectra.

The FTIR spectra acquired for the membrane surfaces exposed to the different compounds can be compared with the spectra of the original membrane (only exposed to deionized water). The impact of each compound is reflected not only by changes on the spectrum profile (different peaks), but also through the effect on the characteristic peaks from the original membrane. In all graphs, the "x" axis represents the intensity of the infrared spectra (cm^{-1}); and the "y" axis represents the amount of infrared light transmitted by the material being analysed (% Transmittance (T)), which is inversely related to absorbance.

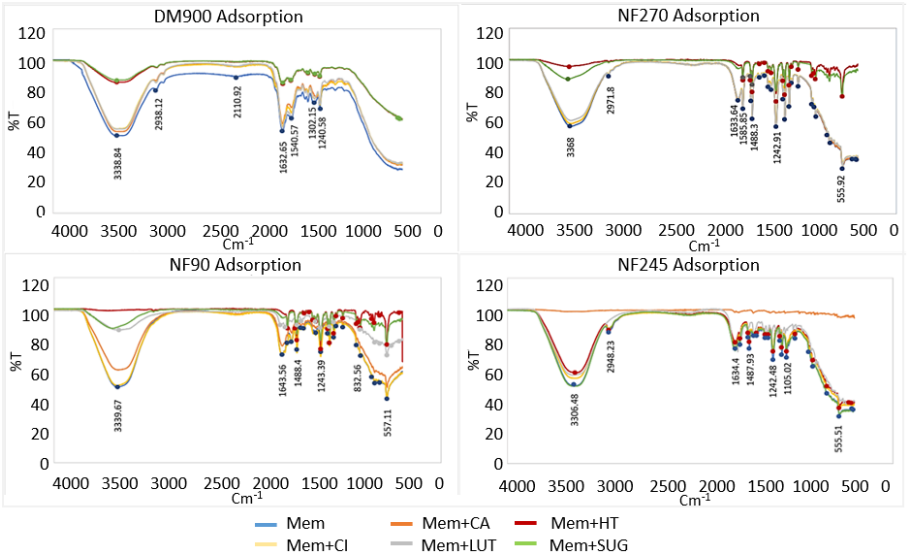

Fig. 5.34 FTIR spectra for all the membrane tested. Mem: Pristine membrane; CA: caffeic acid; CI: citric acid; HT: hydroxytyrosol; LUT: luteolin; SUG: sugars

It can be seen in Fig. 5.34 that the NF90 and NF270 membranes have similar specific peaks due to the material, three of them being the most characteristic, around 555-557 cm^{-1}, 1643-1633 cm^{-1} and 3368-3339 cm^{-1}, respectively. The range between 500 and 900 cm^{-1} is attributed to aromatic rings, the peak around 1600 cm^{-1} can be due to aromatic C=C stretching, while the peaks around 3300-3400 cm^{-1} can be attributed, besides the -COH group, to stretching vibration between the carboxyl group (-COOH) of polyamide (PA) layer and N-H [60]. The N270 membrane presents also a characteristic peak at 2971.8 cm^{-1}, that can be due to CH_2 asymmetric stretching [29]. Both membranes present a complete elimination of the signal in the presence of HT, followed by SUG, indicating that both compounds have been adsorbed. This could be explained by the membrane material, as both membranes are made of polyamide, being more susceptible to the adsorption of these compounds. Cassano et al. [61-62], when artichoke brine was nanofiltered with a PA membrane (Desal DK, from GE Osmonics), observed that when the volume reduction factor (VRF) increased the concentration of chlorogenic acid and caffeoylquinic acid derivatives did not proportionally augmented. They pointed out that it was due to different factors, one of which was the adhesion of these compounds to the membrane. Our observation could be explained taking into account that HT

is more hydrophobic than another non-adsorbed compound such as citric acid (octanol-water partition coefficient (Log P) of 0.96 [63] and −1.99 [64] for HT and citric acid, respectively). Lopez-Muñoz, et al. [31] reported that this is the main parameter to describe the adsorption of phenolic compounds on nanofiltration membranes. When analysing the NF90 membrane, they observed that the hydrophobicity (log P) of the phenolic compounds was directly related to the adsorption of the solute on the membrane surface.

The NF90 membrane also showed an adsorption of LUT similar to that of SUG and a slight CA adsorption. This could also be explained trough the hydrophobicity character, since LUT and CA present a Log P similar to HT (0.7 [65] and 1.3 ± 0.240 [66] for LUT and CA, respectively). However, this was not observed for the NF270 membrane. Although both are made of polyamide, it has been reported that the NF90 membrane material is an aromatic polyamide, while the NF270 is a mixed aliphatic-aromatic polyamide membrane. This indicates that the NF90 membrane surface is rough, while the NF270 membrane shows a smooth surface [67]. The "peak-valley" morphology at the surface of the roughened membranes results in a higher specific surface area. Thus, the adsorption capacity would be larger for membranes with rougher surfaces [47]. This could also explain the difficulties encountered when cleaning this membrane (section 3.3). Corbatón-Báguena et al. [68] also reported in their study of saline solutions for cleaning ultrafiltration membranes fouled with BSA, that the greater the roughness, the greater the difficulty in cleaning the membranes. On the other hand, the NF245 membrane shows the characteristic signals of the material (PP). Vibrations of the –CH, $–CH_2$ and $–CH_3$ groups were observed, such as the methyl absorption band between 1242 and 1487 cm^{-1}. C-H bonds were detected at around 2948 cm^{-1} and the characteristic peak of hydroxyl groups at around 3000 – 3600 cm^{-1} [69]. The FTIR spectrum of the NF245 membrane submerged in CA showed a transmittance higher than 95%T for all the wavelengths, being the only compound that caused changes in the characteristic signal of the membrane. Except for the SUG, the other compounds show a slightly increase in %T. LUT, on the other hand, overshadows the characteristic signal of C-H at 2948 cm^{-1}.

The most characteristic peaks of the DM900 membrane corresponded to the imide (1720 and 1237 cm^{-1}) and also amide group (1632 and 1530 cm^{-1}) due to crosslinking [70]. As in the case of the NF90 membrane, by means of FTIR, it was possible to corroborate that there

is adsorption of some compounds on this membrane, being the SUG and the HT the ones that presented the highest impact. On the other hand, the other compounds, although they had less impact on the membrane surface, all of them caused a slight increase in transmittance in the range of 3000 - 1600 cm^{-1}, demonstrating that there was adsorption.

It can be concluded that the fluorescence spectra acquired on NF90 and DM900 membrane surfaces had low signal intensity and changes caused by possible adsorption of foulants were not clearly visible by direct visual inspection. The PCA of the obtained fluorescence response (supplementary material, Fig. 5.S8) showed that the DM900 membrane was affected by both CA and LUT. This is because the presence of such compounds can be detected not only due to a shadow effect (possible quenching effects), but also by spectral changes due to their natural fluorescence (even if these differences are not clearly seen on the spectra) [71].

Regarding NF90, it presented a significant fluorescence difference from the other membranes, and besides, the differences with the membranes exposed to the compounds were not so evident (most probably due to low fluorescence signal captured for this membrane). All measurements clustered differently in the PCA plot, showing clear differences for membrane surfaces exposed to the compounds. NF270 and NF245 surfaces have similar spectra and the effect of the compounds was similar on both, with CA and LUT being the compounds that most affected the membranes. These conclusions were confirmed with PCA analysis.

With FTIR it was possible to observe that the NF90, NF270 and DM900 membranes were the most affected by HT and SUG, while the NF245 membrane was mostly affected by CA. In FTIR PCA analysis (Supplementary material, Fig. 5.S9), the similarity between the composition of all membranes is clear and the differences in the membrane surfaces were not captured (such as the brown colour of DM900). However, the DM900 membrane shows a different behaviour when exposed to the selected compounds, being clearly affected by all the compounds. While fluorescence analysis showed a more pronounced response for CA and LUT, from FTIR it was possible to see more clearly the effect of the other compounds tested. Based on both methods, it can be determined that all the compounds had an effect on the membrane surfaces, meaning that all were adsorbed on the 4 membranes. However, the DM900 membrane was clearly the membrane most affected by all compounds studied.

It was shown that using these techniques it is possible to determine changes on the membrane surface due to fouling caused by adsorption. The 2D fluorescence spectroscopy was useful to determine the adsorption of coloured compounds, while FTIR was able to evaluate the adsorption of colourless compounds and demonstrated that there was adsorption on the NF90 and DM900 membranes. Finally, it can be concluded that both techniques together are a powerful tool when analysing possible changes on membrane surfaces, induced by fouling.

To analyse the membranes with FTIR it is necessary to remove them from the module. However 2D fluorescence spectroscopy is very sensitive and non-invasive, being suitable for in situ monitoring [72]. 2D fluorescence spectroscopy can be assessed using an optical probe directly from membrane surface using a membrane module with a window. This will be explored in future studies.

3.5 Nanofiltration study: 2D Fluorescence spectroscopy and FTIR

Fig. 5.35 shows the fluorescence spectra of all membranes after the NF test with MS (fouled membranes with model solution) and after cleaning. As was indicated in section 2.2.2, the operating conditions of all the nanofiltration tests carried out to evaluate the spectroscopic techniques were the same, 3 hours of test at CFV of 1 ms^{-1} and TMP of 10 bar. Due to fouling, the membranes reduced their fluorescence emission compared to pristine membranes (fluorescence of pristine membranes is shown in section 3.4). This is because the compounds present at the fouling layer can partially absorb the light emitted by the surface of the membrane, attenuating its signal [73]. Regarding the initial spectra of the membranes, the NF245 membrane was the one that presented the highest attenuation. Avram et al. [38] observed in their study on the concentration of polyphenols from blueberry pomace extract using NF245 and NF270 membranes, that the application of mechanical agitation can interrupt the agglomeration or adsorption of polyphenols. When comparing the two membranes, the effect was more pronounced for the NF270 membrane than for the NF245 one. They attributed it to the more compact polymeric structure of the active separation layer of the latter membrane, inducing a larger interaction surface between the polyaromatic membrane moieties and the polyphenols, which could generate a greater adsorption of these compounds.

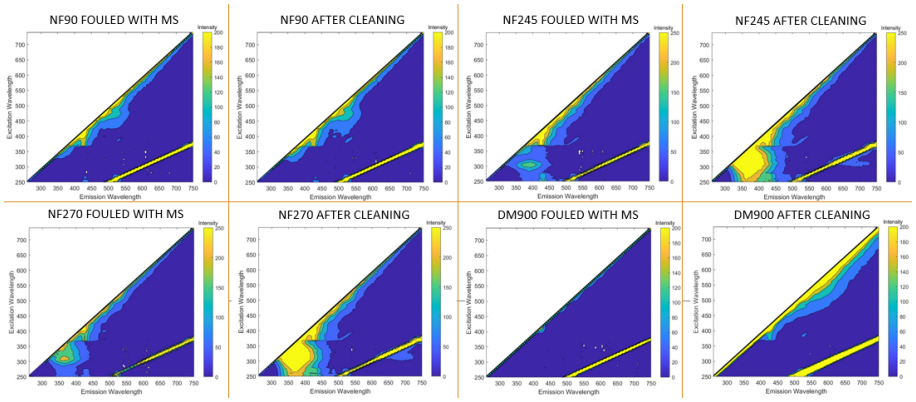

Fig. 5.35 2D fluorescence data of the membranes after nanofiltration test with the model solution (MS) and after chemical cleaning. Operating conditions of nanofiltration test, 3 hours at CFV of 1 ms^{-1} and TMP of 10 bar.

Although at a first glance analysis of the data obtained, all membranes managed to recover their initial fluorescence after applying the cleaning protocol, they did not manage to emit the same signal as the pristine membranes. This can be seen through the analysis of PCA (Fig. 5.36), where it is also observed that they are more similar to the samples of the new membranes after being subjected to the cleaning protocol. This may be due to the removal of chemicals used to preserve the membranes after the initial membrane cleaning, thus changing the characteristic signal. Simon et al. [74], in a study on the impact of chemical cleanings (acid and basic) on the NF270 membrane surface, presented the hypothesis that cleanings might alter the tightness of the polymeric matrix and even the hydrophilicity of the active layer of the membrane.

These results can be related to those obtained in section 3.3 on membrane cleaning (Fig 5.29). It can be observed that those membranes that show a greater proximity between the pristine cleaned membrane and the membrane cleaned after the NF test in the PCA, correspond to the membranes with the highest permeability recovery ratio in Fig. 5.29A, following the order NF270>NF245>NF90>DM900.

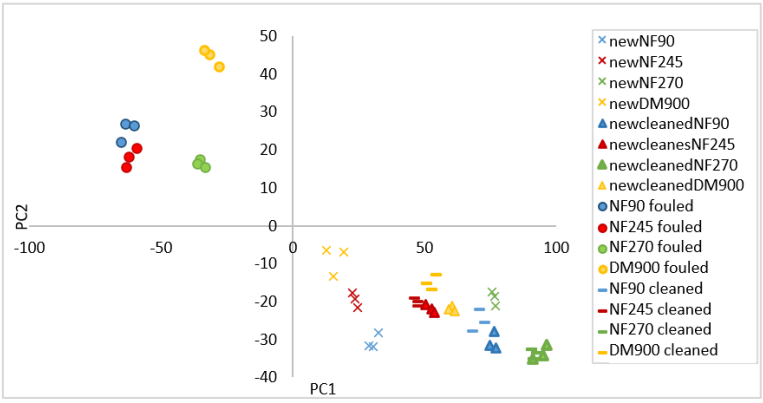

Fig. 5.36 Principal components (PCA) PC1 (71.24%var) and PC2 (16.41%var) of 2D fluorescence data for the nanofiltration tests with the model solution and after chemical cleaning. Operating conditions of nanofiltration test, 3 hours at CFV of 1 ms^{-1} and TMP of 10 bar

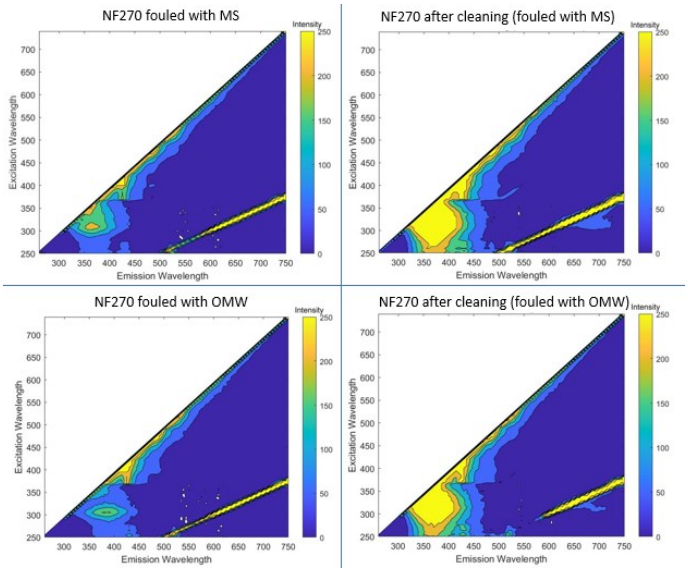

Fig. 5.37 2D fluorescence data of the NF270 membrane after nanofiltration tests with the model solution (MS) and olive mill wastewater (OMW). Operating conditions, 3 hours at CFV of 1 ms^{-1} and TMP of 10 bar.

In Fig. 5.37 the spectra of the NF270 membrane after the tests performed with MS and OMW are compared. It can be seen that the membrane fouled with OMW shows a greater

signal reduction than the one fouled with MS. In the same way, both managed to recover the characteristic Ex/Em signal after cleaning, but, as mentioned above, the signal was closer to that of a new membrane after cleaning than to that of the pristine membrane.

Fig. 5.38 shows the FTIR results for the tests performed with the NF270 membrane. The great difference between the new membrane and the membrane after cleaning is clearly seen. The large peak at around 3300 cm^{-1} could be attributed to preservation compounds such as glycerol [60]. On the other hand, the elimination of this peak for the membranes fouled by OMW and MS is associated with the adsorption of the phenolic compounds present in the samples [75]. Both membranes, fouled with MS and OMW, have lower signals at 1637.7 cm^{-1} and 900-1200 cm^{-1} than the pristine one, as HT and SUG were shown (Fig. 5.34) to attenuate these regions. However, the stronger effect was observed for the membrane fouled with OMW, which can be due to the adsorption of other compounds, such as proteins (at 1637.7 cm^{-1}) [76], polysaccharides and nucleic acids (at 900-1200 cm^{-1}) [77].

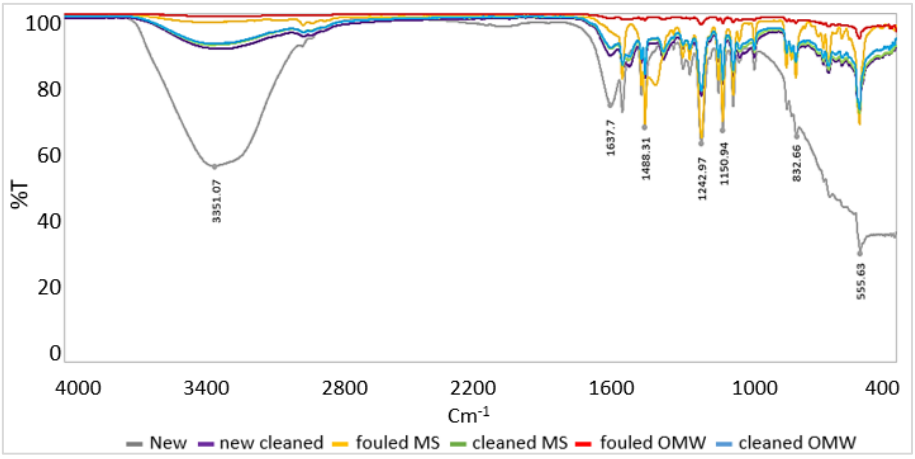

Fig. 5.38 FTIR spectra for the new and cleaned NF270 membrane and after the tests performed with the model solution (MS) and olive mill wastewater (OMW). Operating conditions, 3 hours at CFV of 1 ms^{-1} and TMP of 10 bar

Finally, after cleaning the membranes fouled with MS and OMW, the spectra obtained were found to be similar to that observed for the new membrane after cleaning. For a better

evaluation of the results, it was decided to perform the PCA analysis (Fig. 5.39). The PCA was used to compare the performance of the cleaning protocol, as well as to evaluate the similarity between the MS and the OMW. It can be seen in Fig. 5.39 that both membranes, fouled with MS and OMW, are close to each other, which implies a similarity between them. These results are inverse to those obtained after chemical cleaning, which are similar to those for the new cleaned membranes. It can be observed that the membrane fouled by the MS achieved a greater proximity to the new membrane after cleaning, which infers a greater cleaning efficiency. The differences between the membranes used with MS and OMW are probably due to the larger number of foulants present in the OMW, which led to higher fouling, making cleaning more difficult. Nevertheless, both membranes achieved optimal cleaning after undergoing the optimized cleaning protocol.

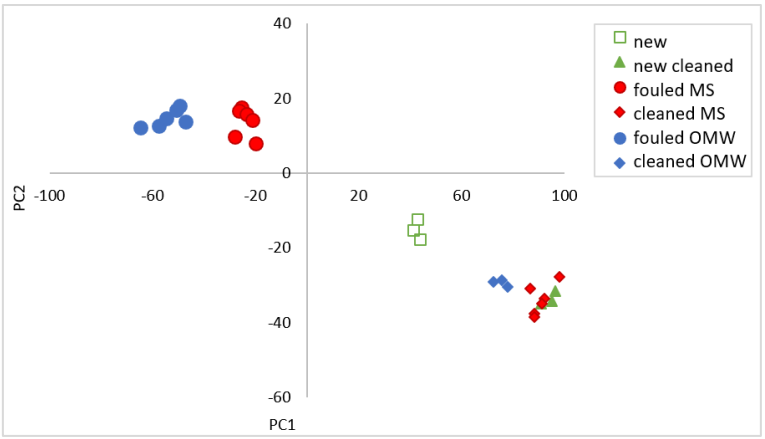

Fig. 5.39 PCA of 2D fluorescence data (62.52% and 14.89% of PC1 and PC2 variance, respectively) for the new and cleaned NF270 membrane and after the test with the model solution (MS) and olive mill wastewater (OMW). Operating conditions, 3 hours at CFV of 1 ms^{-1} and TMP of 10 bar

Both feeds (MS and OOWW), as well as permeates and concentrates, were also analysed by 2D fluorescence spectroscopy. Through PCA (supplementary material, Fig 5.S.10), a similarity between the two feed samples was observed, which implies that the fluorescence of the MS is representative of the real OMW. On the other hand, the quality of the

permeates obtained was also verified, being similar after 5 and 180 minutes of operation for both types of feed streams.

4. Conclusions

Nanofiltration was studied as a possible second stage for an olive mill wastewater treatment, after a previous ultrafiltration step. Within the operating condition tested, the permeate flux was found to be more affected by transmembrane pressure than by crossflow velocity. All membranes were capable of concentrating phenolic compounds with a rejection greater than 70%. The membrane with the lowest molecular weight cut-off was the one that presented the highest percentage of rejection, but it did not achieve the established recovery (95%) of hydraulic permeability through the proposed cleaning protocols. The NF270 membrane under a cross flow velocity of 1 ms^{-1} and a transmembrane pressure of 10 bar was found to be the most suitable. After the analysis of different membranes and operating conditions, the effectiveness of nanofiltration to concentrate polyphenols from olive oil washing wastewaters, as well as to obtain a permeate suitable for reuse, was demonstrated.

Additionally, a study employing 2D Fluorescence and FTIR spectroscopy allowed to obtain valuable information about membrane fouling. Fluorescence analysis presented a more pronounced response to coloured compounds, while by means of FTIR it is possible to see more clearly the effect of the other tested foulant compounds. The main advantage of 2D Fluorescence spectroscopy is the possibility to use it for *in-situ* monitoring. According to both analyses, all tested compounds have an effect on the membrane surfaces. These techniques together represent a promising approach to analyse the efficiency of cleaning protocols.

Acknowledgements

The authors acknowledge the financial support of the Ministry of Economy, Industry and Competitiveness of Spain through the project CTM2017-88645-R, the European Union through the Operational Program of the Social Fund (FSE) financing ACIF-2018 and BEFPI-2021, and the Associate Laboratory for Green Chemistry-LAQV which is financed by national funds from FCT/MCTES (UIDB/50006/2020 and UIDP/50006/2020).

References

[1] J.M. Ochando-Pulido, A review on the use of membrane technology and fouling control for olive mill wastewater treatment, Sci. Total Environ. 563–564 (2016) 664–675.

https://doi.org/10.1016/j.scitotenv.2015.09.151.

[2] E.O. Ezugbe, S. Rathilal, Membrane technologies in wastewater treatment: A review, Membranes (Basel). 10 (2020). https://doi.org/10.3390/membranes10050089.

[3] E. Kavitha, E. Poonguzhali, D. Nanditha, A. Kapoor, G. Arthanareeswaran, S. Prabhakar, Current status and future prospects of membrane separation processes for value recovery from wastewater, Chemosphere. 291 (2022) 132690. https://doi.org/https://doi.org/10.1016/j.chemosphere.2021.132690.

[4] N.N.R. Ahmad, W.L. Ang, Y.H. Teow, A.W. Mohammad, N. Hilal, Nanofiltration membrane processes for water recycling, reuse and product recovery within various industries: A review, J. Water Process Eng. 45 (2022) 102478. https://doi.org/10.1016/j.jwpe.2021.102478.

[5] Z. Su, T. Liu, X. Li, N.J.D. Graham, W. Yu, Tracking metal ion-induced organic membrane fouling in nanofiltration by adopting spectroscopic methods: Observations and predictions, Sci. Total Environ. 708 (2020) 135051. https://doi.org/10.1016/j.scitotenv.2019.135051.

[6] H.-P. Ma, H.-L. Wang, Y.-H. Qi, Z.-L. Chao, L. Tian, W. Yuan, L. Dai, W.-J. Lv, Reducing fouling of an industrial multi-stage nanofiltration membrane based on process control: A novel shutdown system, J. Memb. Sci. 644 (2022) 120141. https://doi.org/10.1016/j.memsci.2021.120141.

[7] S. Zainith, L.F.R. Ferreira, G.D. Saratale, S.I. Mulla, R.N. Bharagava, Membrane-based hybrid processes in industrial waste effluent treatment, INC, 2021. https://doi.org/10.1016/B978-0-12-823804-2.00008-2.

[8] R. Castro-Muñoz, J. Yáñez-Fernández, V. Fíla, Phenolic compounds recovered from agro-food by-products using membrane technologies: An overview, Food Chem. 213 (2016) 753–762. https://doi.org/10.1016/j.foodchem.2016.07.030.

[9] B.M. Esteves, R. Fernandes, S. Morales-Torres, F.J. Maldonado–Hódar, A.M.T. Silva, L.M. Madeira, Integration of catalytic wet peroxidation and membrane distillation processes for olive mill wastewater treatment and water recovery, Chem. Eng. J. 448 (2022). https://doi.org/10.1016/j.cej.2022.137586.

[10] C.A. Paraskeva, V.G. Papadakis, E. Tsarouchi, D.G. Kanellopoulou, P.G. Koutsoukos, Membrane processing for olive mill wastewater fractionation, Desalination. 213 (2007)

218–229. https://doi.org/10.1016/j.desal.2006.04.087.

[11] T. Coskun, E. Debik, N.M. Demir, Treatment of olive mill wastewaters by nanofiltration and reverse osmosis membranes, Desalination. 259 (2010) 65–70. https://doi.org/10.1016/j.desal.2010.04.034.

[12] S. Sanches, M.C. Fraga, N.A. Silva, P. Nunes, J. Crespo, V.J. Pereira, Pilot scale nanofiltration treatment of olive mill wastewater: a technical and economical evaluation, Environ. Sci. Pollut. Res. 24 (2017) 3506–3518. https://doi.org/10.1007/s11356-016-8083-1.

[13] M. Cifuentes-Cabezas, C. Carbonell-Alcaina, M.C. Vincent-Vela, J.A. Mendoza-Roca, S. Álvarez-Blanco, Comparison of different ultrafiltration membranes as first step for the recovery of phenolic compounds from olive-oil washing wastewater, Process Saf. Environ. Prot. 149 (2021) 724–734. https://doi.org/10.1016/j.psep.2021.03.035.

[14] P. Tapia-Quirós, M.F. Montenegro-Landívar, M. Reig, X. Vecino, J. Saurina, M. Granados, J.L. Cortina, Integration of membrane processes for the recovery and separation of polyphenols from winery and olive mill wastes using green solvent-based processing, J. Environ. Manage. 307 (2022). https://doi.org/10.1016/j.jenvman.2022.114555.

[15] H. Li, V. Chen, Chapter 10. Membrane Fouling and Cleaning in Food and Bioprocessing, Membr. Technol. (2010) 213–254. https://doi.org/10.1016/B978-1-85617-632-3.00010-0.

[16] W. Chen, C. Qian, K.G. Zhou, H.Q. Yu, Molecular Spectroscopic Characterization of Membrane Fouling: A Critical Review, Chem. 4 (2018) 1492–1509. https://doi.org/10.1016/j.chempr.2018.03.011.

[17] G. Rudolph, T. Virtanen, M. Ferrando, C. Güell, F. Lipnizki, M. Kallioinen, A review of in situ real-time monitoring techniques for membrane fouling in the biotechnology, biorefinery and food sectors, J. Memb. Sci. 588 (2019) 117221. https://doi.org/10.1016/j.memsci.2019.117221.

[18] O. Abbas, A. Pissard, V. Baeten, 3 - Near-infrared, mid-infrared, and Raman spectroscopy, Second Edi, Elsevier Inc., 2020. https://doi.org/10.1016/B978-0-12-813266-1/00003-6.

[19] S. Pawlowski, C.F. Galinha, J.G. Crespo, S. Velizarov, 2D fluorescence spectroscopy

for monitoring ion-exchange membrane based technologies - Reverse electrodialysis (RED), Water Res. 88 (2016) 184–198. https://doi.org/10.1016/j.watres.2015.10.010.

[20] C.F. Galinha, G. Carvalho, C.A.M. Portugal, G. Guglielmi, M.A.M. Reis, J.G. Crespo, Multivariate statistically-based modelling of a membrane bioreactor for wastewater treatment using 2D fluorescence monitoring data, Water Res. 46 (2012) 3623–3636. https://doi.org/10.1016/j.watres.2012.04.010.

[21] L. Lenhardt, R. Bro, I. Zeković, T. Dramićanin, M.D. Dramićanin, Fluorescence spectroscopy coupled with PARAFAC and PLS DA for characterization and classification of honey, Food Chem. 175 (2015) 284–291. https://doi.org/10.1016/j.foodchem.2014.11.162.

[22] M. Cabrera-Bañegil, M. del C. Hurtado-Sánchez, T. Galeano-Díaz, I. Durán-Merás, Front-face fluorescence spectroscopy combined with second-order multivariate algorithms for the quantification of polyphenols in red wine samples, Food Chem. 220 (2017) 168–176. https://doi.org/10.1016/j.foodchem.2016.09.152.

[23] L. Benavente, C. Coetsier, A. Venault, Y. Chang, C. Causserand, P. Bacchin, P. Aimar, FTIR mapping as a simple and powerful approach to study membrane coating and fouling, J. Memb. Sci. 520 (2016) 477–489. https://doi.org/10.1016/j.memsci.2016.07.061.

[24] M.N. Pons, S. Le Bonté, O. Potier, Spectral analysis and fingerprinting for biomedia characterisation, J. Biotechnol. 113 (2004) 211–230. https://doi.org/10.1016/j.jbiotec.2004.03.028.

[25] Z. Chen, J. Luo, X. Hang, Y. Wan, Physicochemical characterization of tight nanofiltration membranes for dairy wastewater treatment, J. Memb. Sci. 547 (2018) 51–63. https://doi.org/10.1016/j.memsci.2017.10.037.

[26] C.M. Sánchez-Arévalo, Á. Jimeno-Jiménez, C. Carbonell-Alcaina, M.C. Vincent-Vela, S. Álvarez-Blanco, Effect of the operating conditions on a nanofiltration process to separate low-molecular-weight phenolic compounds from the sugars present in olive mill wastewaters, Process Saf. Environ. Prot. 148 (2021) 428–436. https://doi.org/10.1016/j.psep.2020.10.002.

[27] A. Volkov, Membrane Compaction, in: E. Drioli, L. Giorno (Eds.), Encycl. Membr., Springer, Berlin, Heidelberg, 2014. https://doi.org/10.1007/978-3-642-40872- 4_1404-

2.

[28] N. Tanne, R. Xu, M. Zhou, P. Zhang, X. Wang, X. Wen, Influence of pore size and membrane surface properties onarsenic removal by nanofiltration membranes, Front. Environ. Sci. Eng. Vol. 13 (2019) 19. https://doi.org/10.1007/s11783-019-1105-8.

[29] Y. Suo, Y. Ren, Research on the mechanism of nanofiltration membrane fouling in zero discharge process of high salty wastewater from coal chemical industry, Chem. Eng. Sci. 245 (2021) 116810. https://doi.org/10.1016/j.ces.2021.116810.

[30] C.P. Leo, M.Z. Yahya, S.N.M. Kamal, A.L. Ahmad, A.W. Mohammad, Potential of nanofiltration and low pressure reverse osmosis in the removal of phosphorus for aquaculture, Water Sci. Technol. 67 (2013) 831–837. https://doi.org/10.2166/wst.2012.625.

[31] L. Gao, H. Wang, Y. Zhang, M. Wang, Nanofiltration membrane characterization and application: Extracting lithium in lepidolite leaching solution, Membranes (Basel). 10 (2020) 1–18. https://doi.org/10.3390/membranes10080178.

[32] U.T. Syed, C. Brazinha, J.G. Crespo, J.M. Ricardo-da-Silva, Valorisation of grape pomace: Fractionation of bioactive flavan-3-ols by membrane processing, Sep. Purif. Technol. 172 (2017) 404–414. https://doi.org/10.1016/j.seppur.2016.07.039.

[33] M.J. López-Muñoz, A. Sotto, J.M. Arsuaga, B. Van der Bruggen, Influence of membrane, solute and solution properties on the retention of phenolic compounds in aqueous solution by nanofiltration membranes, Sep. Purif. Technol. 66 (2009) 194–201. https://doi.org/10.1016/j.seppur.2008.11.001.

[34] A. Santafé-Moros, J.M. Gonzálvez-Zafrilla, D. Valencia, Design of a Flat Membrane Module for Fouling and Permselectivity Studies, in: COMSOL Conf. Paris, 2010. http://www.comsol.asia/papers/8300/download/gozalvez-zafrilla_paper.pdf.

[35] APHA, Standard Methods for the Examination of Water and Wastewater, in: Am. Public Heal. Assoc. Washington, DC, 2005: p. 21 st. ed.

[36] V.L. Singleton, R. Orthofer, R.M. Lamuela-Raventós, Analysis of total phenols and other oxidation substrates and antioxidants by means of folin-ciocalteu reagent, Methods Enzymol. 299 (1999) 152–178. https://doi.org/10.1016/S0076-6879(99)99017-1.

[37] B. Frolund, P. Rikke, K. Keiding, P.H. Nielsen, Extraction of extracellular polymers

from activated sludge using a cation exchange resin, Water Res. 30 (1996) 1749–1758.

[38] M. Cifuentes-Cabezas, C.M. Sanchez-Arévalo, J.A. Mendoza-Roca, M.C. Vincent-Vela, S. Álvarez-Blanco, Recovery of Phenolic Compounds from Olive Oil Washing Wastewater by Adsorption/Desorption Process, Sep. Purif. Technol. 298 (2022) 121562. https://doi.org/10.1016/j.seppur.2022.121562.

[39] A.M. Avram, P. Morin, C. Brownmiller, L.R. Howard, A. Sengupta, S.R. Wickramasinghe, Concentrations of polyphenols from blueberry pomace extract using nanofiltration, Food Bioprod. Process. 106 (2017) 91–101. https://doi.org/10.1016/j.fbp.2017.07.006.

[40] J.A. Arboleda Mejia, A. Ricci, A.S. Figueiredo, A. Versari, A. Cassano, G.P. Parpinello, M.N. de Pinho, Recovery of phenolic compounds from red grape pomace extract through nanofiltration membranes, Foods. 9 (2020). https://doi.org/10.3390/foods9111649.

[41] P. Bacchin, P. Aimar, R.W. Field, Critical and sustainable fluxes: Theory, experiments and applications, J. Memb. Sci. 281 (2006) 42–69. https://doi.org/10.1016/j.memsci.2006.04.014.

[42] A.I. Schäfer, A.G. Fane, T.D. Waite, Nanofiltration of natural organic matter: Removal, fouling and the influence of multivalent ions, Desalination. 118 (1998) 191–204.

[43] M. Mänttäri, M. Nyström, Critical flux in NF of high molar mass polysaccharides and effluents from the paper industry, J. Memb. Sci. 170 (2000) 257–273. https://doi.org/10.1016/S0376-7388(99)00373-7.

[44] A.W. Mohammad, Y.H. Teow, W.L. Ang, Y.T. Chung, D.L. Oatley-Radcliffe, N. Hilal, Nanofiltration membranes review: Recent advances and future prospects, Desalination. 356 (2015) 226–254. https://doi.org/10.1016/j.desal.2014.10.043.

[45] M.A. Nunes, S. Pawlowski, A.S.G. Costa, R.C. Alves, M.B.P.P. Oliveira, S. Velizarov, Valorization of olive pomace by a green integrated approach applying sustainable extraction and membrane-assisted concentration, Sci. Total Environ. 652 (2019) 40–47. https://doi.org/10.1016/j.scitotenv.2018.10.204.

[46] A. Böcking, Membrane Transport Properties and Process Design in Nanofiltration with Organic Solvents and Aqueous Solvent Mixtures, 2020.

[47] A.R. Costa, M.N. De Pinho, Effect of membrane pore size and solution chemistry on

the ultrafiltration of humic substances solutions, J. Memb. Sci. 255 (2005) 49–56. https://doi.org/10.1016/j.memsci.2005.01.016.

[48] G.S. Vieira, F.K.V. Moreira, R.L.S. Matsumoto, M. Michelon, F.M. Filho, M.D. Hubinger, Influence of nanofiltration membrane features on enrichment of jussara ethanolic extract (Euterpe edulis) in anthocyanins, J. Food Eng. (2018). https://doi.org/10.1016/j.jfoodeng.2018.01.013.

[49] A. Giacobbo, A.M. Bernardes, M.N. de Pinho, Sequential pressure-driven membrane operations to recover and fractionate polyphenols and polysaccharides from second racking wine lees, Sep. Purif. Technol. 173 (2017) 49–54. https://doi.org/10.1016/j.seppur.2016.09.007.

[50] J. Geens, K. Peeters, B. Van Der Bruggen, C. Vandecasteele, Polymeric nanofiltration of binary water-alcohol mixtures: Influence of feed composition and membrane properties on permeability and rejection, J. Memb. Sci. 255 (2005) 255–264. https://doi.org/10.1016/j.memsci.2005.01.039.

[51] A. López-borrell, M.F. López-Pérez, S.C. Cardona, J. Lora-garcía, Experimental Study and Mathematical Modeling of a Nanofiltration Membrane System for the Recovery of Polyphenols from Wine Lees, Membranes (Basel). 12 (2022) 240. https://doi.org/10.3390/membranes12020240.

[52] N. Nguyen, C. Fargues, W. Guiga, M.L. Lameloise, Assessing nanofiltration and reverse osmosis for the detoxification of lignocellulosic hydrolysates, J. Memb. Sci. 487 (2015) 40–50. https://doi.org/10.1016/j.memsci.2015.03.072.

[53] M. Mänttäri, A. Pihlajamäki, M. Nyström, Effect of pH on hydrophilicity and charge and their effect on the filtration efficiency of NF membranes at different pH, J. Memb. Sci. 280 (2006) 311–320. https://doi.org/10.1016/j.memsci.2006.01.034.

[54] M. Bédas, G. Tanguy, A. Dolivet, S. Méjean, F. Gaucheron, G. Garric, G. Senard, R. Jeantet, P. Schuck, Nanofiltration of lactic acid whey prior to spray drying: Scaling up to a semi-industrial scale, LWT - Food Sci. Technol. 79 (2017) 355–360. https://doi.org/10.1016/j.lwt.2017.01.061.

[55] C.P. Leo, W.K. Chai, A.W. Mohammad, Y. Qi, A.F.A. Hoedley, S.P. Chai, Phosphorus removal using nanofiltration membranes, Water Sci. Technol. 64 (2011) 199–205. https://doi.org/10.2166/wst.2011.598.

[56] N. Nguyen, C. Fargues, R. Lewandowski, W. Guiga, M.L. Lameloise, Assessing nanofiltration and reverse osmosis for the detoxification of fermentable solutions, Procedia Eng. 44 (2012) 1476–1478. https://doi.org/10.1016/j.proeng.2012.08.834.

[57] J.M. Ochando-Pulido, J.R. Corpas-Martínez, A. Martinez-Ferez, About two-phase olive oil washing wastewater simultaneous phenols recovery and treatment by nanofiltration, Process Saf. Environ. Prot. 114 (2018) 159–168. https://doi.org/10.1016/j.psep.2017.12.005.

[58] M.C. Martí-Calatayud, S. Schneider, M. Wessling, On the rejection and reversibility of fouling in ultrafiltration as assessed by hydraulic impedance spectroscopy, J. Memb. Sci. 564 (2018) 532–542. https://doi.org/10.1016/j.memsci.2018.07.021.

[59] R.W. Field, G.K. Pearce, Critical, sustainable and threshold fluxes for membrane filtration with water industry applications, Adv. Colloid Interface Sci. 164 (2011) 38–44. https://doi.org/10.1016/j.cis.2010.12.008.

[60] B. Van der Bruggen, M. Mänttäri, M. Nyström, Drawbacks of applying nanofiltration and how to avoid them: A review, Sep. Purif. Technol. 63 (2008) 251–263. https://doi.org/10.1016/j.seppur.2008.05.010.

[61] M. Gryta, J. Bastrzyk, D. Lech, Evaluation of fouling potential of nanofiltration membranes based on the dynamic contact angle measurements, Polish J. Chem. Technol. 14 (2012) 97–104. https://doi.org/10.2478/v10026-012-0091-4.

[62] A. Cassano, C. Conidi, R. Ruby-Figueroa, R. Castro-Muñoz, Nanofiltration and tight ultrafiltration membranes for the recovery of polyphenols from agro-food by-products, Int. J. Mol. Sci. 19 (2018) 351. https://doi.org/10.3390/ijms19020351.

[63] A. Cassano, W. Cabri, G. Mombelli, F. Peterlongo, L. Giorno, Recovery of bioactive compounds from artichoke brines by nanofiltration, Food Bioprod. Process. 98 (2016) 257–265. https://doi.org/10.1016/j.fbp.2016.02.004.

[64] T.M. Olajide, T. Liu, H. Liu, X. Weng, Antioxidant properties of two novel lipophilic derivatives of hydroxytyrosol, Food Chem. 315 (2020) 126197. https://doi.org/10.1016/j.foodchem.2020.126197.

[65] H. Fu, Y. Sun, H. Teng, D. Zhang, Z. Xiu, Salting-out extraction of carboxylic acids, Sep. Purif. Technol. 139 (2015) 36–42. https://doi.org/10.1016/j.seppur.2014.11.001.

[66] L. Quintieri, P. Palatini, A. Nassi, P. Ruzza, M. Floreani, Flavonoids diosmetin and

luteolin inhibit midazolam metabolism by human liver microsomes and recombinant CYP 3A4 and CYP3A5 enzymes, Biochem. Pharmacol. 75 (2008) 1426–1437. https://doi.org/10.1016/j.bcp.2007.11.012.

[67] S. Son, B.A. Lewis, Free radical scavenging and antioxidative activity of caffeic acid amide and ester analogues: Structure-activity relationship, J. Agric. Food Chem. 50 (2002) 468–472. https://doi.org/10.1021/jf010830b.

[68] J.F. Fernández, B. Jastorff, R. Störmann, S. Stolte, J. Thöming, Thinking in terms of structure-activity-relationships (T-SAR): A tool to better understand nanofiltration membranes, Membranes (Basel). 1 (2011) 162–183. https://doi.org/10.3390/membranes1030162.

[69] M.-J. Corbatón-Báguena, S. Álvarez-blanco, M.C. Vincent-Vela, Cleaning of ultrafiltration membranes fouled with BSA by means of saline solutions, Sep. Purif. Technol. 125 (2014) 1–10. https://doi.org/10.1016/j.seppur.2014.01.035.

[70] M. Gryta, Resistance of polypropylene membrane to oil fouling during membrane distillation, Membranes (Basel). 11 (2021). https://doi.org/10.3390/membranes11080552.

[71] H. Siddique, E. Rundquist, Y. Bhole, L.G. Peeva, A.G. Livingston, Mixed matrix membranes for organic solvent nanofiltration, J. Memb. Sci. 452 (2014) 354–366. https://doi.org/10.1016/j.memsci.2013.10.012.

[72] C.F. Galinha, G. Carvalho, C.A.M. Portugal, G. Guglielmi, M.A.M. Reis, J.G. Crespo, Two-dimensional fluorescence as a fingerprinting tool for monitoring wastewater treatment systems, J. Chem. Technol. Biotechnol. 86 (2011) 985–992. https://doi.org/10.1002/jctb.2613.

[73] M. Sá, J. Monte, C. Brazinha, C.F. Galinha, J.G. Crespo, 2D Fluorescence spectroscopy for monitoring Dunaliella salina concentration and integrity during membrane harvesting, Algal Res. 24 (2017) 325–332. https://doi.org/10.1016/j.algal.2017.04.013.

[74] S. Pawlowski, C.F. Galinha, J.G. Crespo, S. Velizarov, Prediction of reverse electrodialysis performance by inclusion of 2D fluorescence spectroscopy data into multivariate statistical models, Sep. Purif. Technol. 150 (2015) 159–169. https://doi.org/10.1016/j.seppur.2015.06.032.

[75] A. Simon, W.E. Price, L.D. Nghiem, Effects of chemical cleaning on the nanofiltration

of pharmaceutically active compounds (PhACs), Sep. Purif. Technol. 88 (2012) 208–215. https://doi.org/10.1016/j.seppur.2011.12.009.

[76] B.H. Gursoy-Haksevenler, I. Arslan-Alaton, UV fluorescence, FTIR, and GC–MS analyses and resin fractionation procedures as indicators of the chemical treatability of olive mill wastewater, Desalin. Water Treat. 57 (2016) 2372–2382. https://doi.org/10.1080/19443994.2014.992979.

[77] J. Bastrzyk, M. Gryta, K. Karakulski, Fouling of nanofiltration membranes used for separation of fermented glycerol solutions, Chem. Pap. 68 (2014) 757–765. https://doi.org/10.2478/s11696-013-0520-8.

[78] A. Houari, D. Seyer, K. Kecili, V. Heim, P. Di Martino, Kinetic development of biofilm on NF membranes at the Méry-sur-Oise plant, France, Biofouling. 29 (2013) 109–118. https://doi.org/10.1080/08927014.2012.752464.

Supplementary material

1. Principal component analysis (PCA)

For a better understanding of the results obtained, the data captured by EEMs and FTIR spectroscopy could be deconvoluted and compressed into few principal components. For that, the parallel factor analysis (PARAFAC) function [1] was used in MATLAB (R2021b) programme. The models were developed using ten Principal Components (PCs) resulting from the PCA applied to both techniques separately. The data did not need to be standardized.

A. Adsorption test

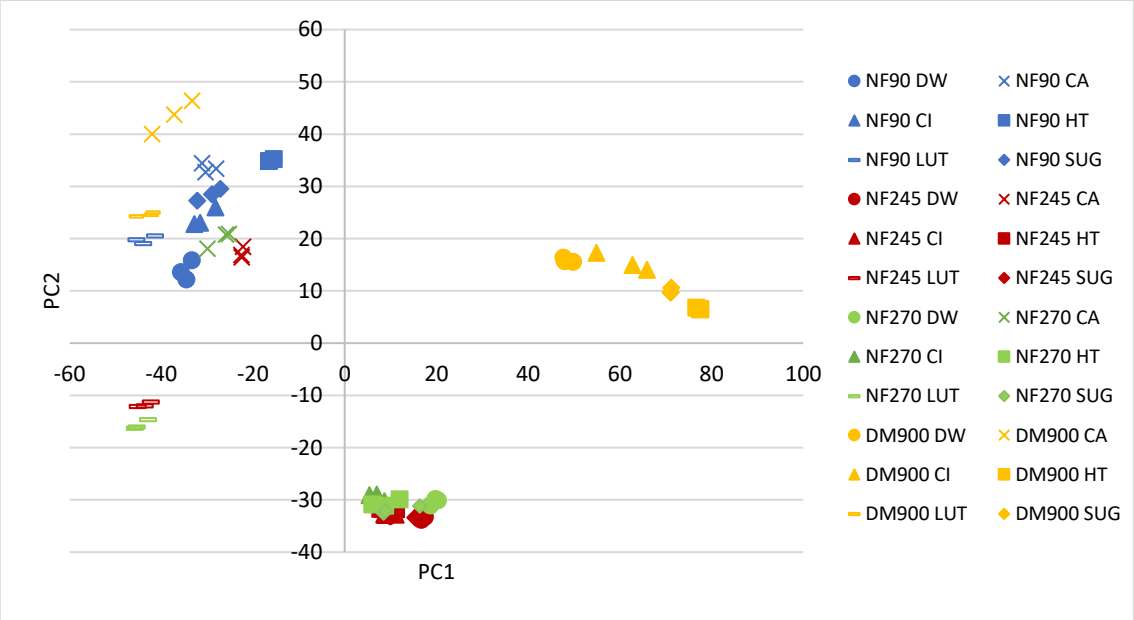

Fig. 5.S8. Principal components (PC) 1 and 2 (86.24% of the total variance captured) from PCA of 2D fluoresce data obtained in the adsorption test performed

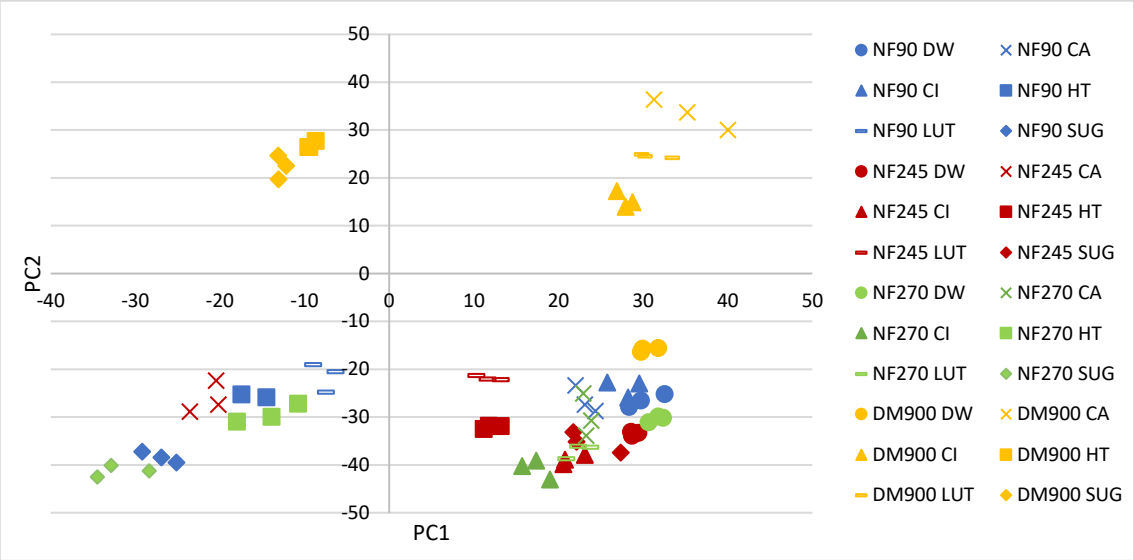

Fig. 5.S9. Principal components (PC) 1 and 2 (87.64% of the total variance captured) from PCA of FTIR data obtained in the adsorption test performed

B. Nanofiltration test

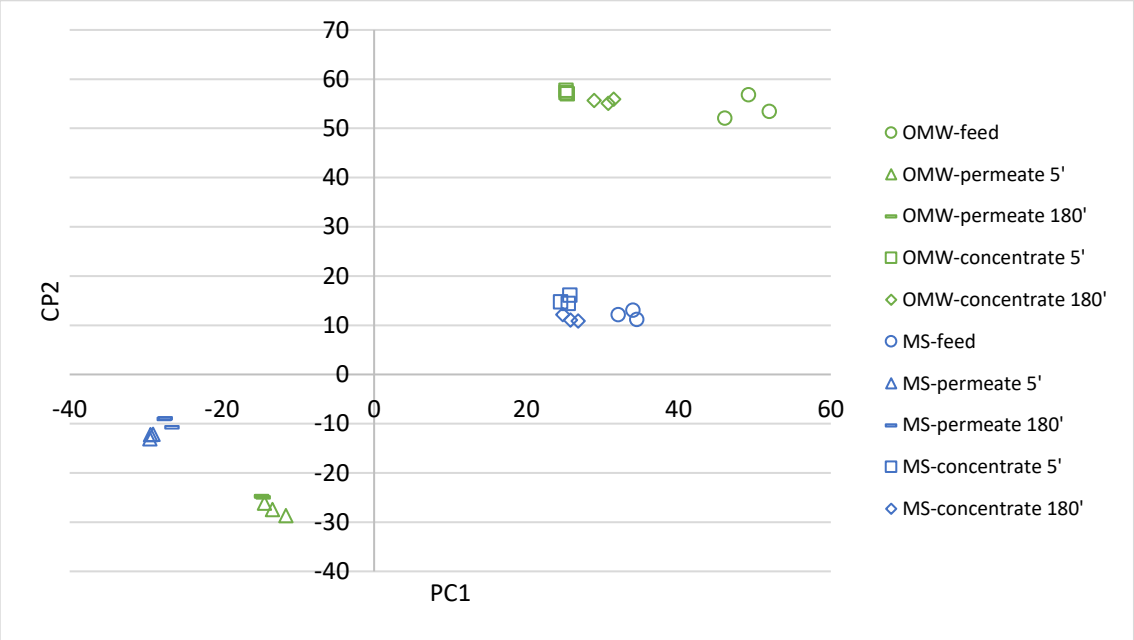

Fig. 5.S10 Principal components (PC) 1 and 2 (89.92% of variance captured) from PCA of 2D fluorescence data obtained from the NF process with model solution (MS) and olive oil washing wastewater (OMW). Feed, permeate and concentrate

References

[1] C.A. Andersson, R. Bro, The N-way Toolbox for MATLAB, Chemom.Intell., (2000) Labor 52. 1-4.

V.5 Concentration of phenolic compounds from olive washing wastewater by forward osmosis using table olive fermentation brine as draw solution

Presentado en Environmental Technology & Innovation, Noviembre 2022
(Estado: En Revisión)

Magdalena Cifuentes-Cabezas[a*], Alessio Pavani[a], María Cinta Vincent-Vela[a,b], José Antonio Mendoza-Roca[a,b], Silvia Álvarez-Blanco[a,b]

[a] Research Institute for Industrial, Radiophysical and Environmental Safety (ISIRYM), Universitat Politècnica de València, C/Camino de Vera s/n, 46022, Valencia, Spain

[b] Department of Chemical and Nuclear Engineering, Universitat Politècnica de València, C/Camino de Vera s/n, 46022, Valencia, Spain

*magcica@posgrado.upv.es

Abstract

The proper management of the large volumes of wastewater generated by the olive industry (olive oil and table olives) is of utmost importance due to its toxic impacts on the environment. The forward osmosis (FO) process is presented as an option to concentrate phenolic compounds (TPhC) for their further recovery. Two membranes, OsmoF2OTM (FTS, USA) and HFFO.6 (Aquaporin, Denmark) were evaluated with NaCl as draw solution (DS) and olive oil washing wastewater (OOWW) filtered at 5 microns (5F) as feed solution (FS). Both membranes were able to concentrate TPhC with acceptable volume reduction (VR) values. The HFFO.6 membrane, which presented the lowest passage of TPhC to the DS, was tested with fermentation brine from table olive processing (FTOP) as DS. As FS apart from 5F-OOWW, an OOWW ultrafiltration permeate (UF-OOWW) was also considered. Interestingly, greater percentages of TPhC concentration were observed compared to the tests with NaCl as DS (74.13-76.93% versus 62.6%, respectively). Although the tests with UF-OOWW presented greater flux, the recovery percentages of TPhC were similar, even slightly lower than those obtained with 5F-OOWW. FO appears as a promising option to treat

wastewater from the olive industry at the same time; concentrating TPhC from OOWW and diluting FTOP.

Keywords Olive oil washing wastewater; Fermentation brines from table olive processing; Phenolic compounds; Forward Osmosis

1. Introduction

Due to the great industrial development that exists today, millions of liters of industrial wastewater are generated each year, becoming an environmental pressure. Most of the industrial effluents are collected by a local sewage system after their conditioning at the industries, treated in an urban wastewater treatment plant and subsequently discharged into the environment. However, there are cases in which these wastewaters are discharged into a water body either directly or after an insufficient treatment in the industrial facility. Therefore, wastewater treatment is a key element for the care and control of the environment [1]. Wastewaters generated in industrial plants are characterized by containing substances that, due to their nature or concentration (toxicity or long-term biological effects), cannot always be eliminated by conventional urban wastewater treatments [2]. In processes related to olives, such as the production of olive oil and table olives, a large amount of wastewater containing high levels of organic matter and phenolic compounds is generated. Due to their phytotoxic nature, phenolic compounds pose an environmental threat and therefore any discharge of phenolic effluents into the environment should be prohibited or at least controlled and reduced [3-5]. On the other hand, from some time ago, phenolic compounds have been targets for the food and pharmaceutical industries [6]. Several phenolic compounds such as tyrosol, hydroxytyrosol, oleuropein and catechin, among others, are being studied for the treatment of various diseases, including prevention of neurodegenerative diseases and cancer [7], improvement of type 2 diabetes [8] and for prevention of heart diseases [9]. Therefore, oil mill wastewater (OMW) and table olive process wastewater (TOPW) are a potential source of phenolic compounds whose concentration and isolation could have two great benefits: obtaining valuable substances and the solution of possible environmental problems, avoiding damaging soil and watercourses.

Different treatment processes have been proposed for the recovery of phenolic compounds from OMW [10]. Among them, pressure-driven membrane technologies provide some environmentally friendly advantages, such as no need for chemical reagents such as solvents, simplicity of industrial scaling given its modular configuration, and easy operation [11]. Nevertheless, fouling is the bottleneck that affects pressure-driven membrane processes, restricting the scaling of conventional membrane technologies. Severe fouling directly affects the investment costs as a result of the reduction of the membrane useful life and the increase in chemical costs, necessary to clean the membranes [12]. Due to this, it has been necessary to incorporate different techniques (hybrid processes) to care for the membranes and reduce fouling. The combination of different membrane processes is a solution too. In this field Cassano et al. [13] proposed a process for the recovery of phenolic compounds from OMW, which includes a combination of micro/ultrafiltration (UF), followed by tight UF or nanofiltration (NF), and finally a reverse osmosis (RO) concentration. It has to be pointed out that a pretreatment with more open membranes is very often necessary, to provide an adequate solution to the following in processes based on the use of NF or RO membranes for the recovery of phenolic compounds from OMW. However, adding more steps to the treatment process implies higher investment and maintenance costs. Forward osmosis (FO) is resurfacing as a membrane operation that requires little energy for the concentration of aqueous solutions, with a membrane fouling that is mainly reversible due to the low compaction of the fouling layer as a result of the insignificant hydraulic pressure. This technique is based on the phenomenon of osmosis, where the driving force for water transport across a semi-permeable membrane is the osmotic pressure difference between both sides of the membrane [14]. A selectively permeable membrane allows passage of water but rejects solute molecules or ions. FO requires two solutions that, due to their different chemical potential, promote solvent flow through the membrane. These two solutions are a feed solution (FS), generally the solution to be concentrated, with low chemical potential, and an extraction/draw solution (DS) that, due to its high chemical potential, promotes the passage of water through the membrane, diluting itself at the same time as the FS is concentrated. Among the available commercial FO membranes, cellulose triacetate (CTA) and thin-film composite (TFC) ones stand out, in two configurations, flat sheet and hollow fiber [15].

Few studies have been conducted about the application of FO to the treatment of OMW. One of them is the work carried out by Gebreyohannes et al. [12], who investigated cellulose acetate FO membranes for the treatment of OMW from a three-phase centrifuge located in Italy. These authors studied two options. The first one consisted of a FO step with 3.7 M $MgCl_2$ as DS and a crossflow velocity of 6 $cm \cdot s^{-1}$, achieving a volume reduction of 71% with a rejection greater than 98% of the OMW components, including biophenols and ions. The second option included a biological membrane reactor (MBR) prior to the FO step, achieving a permeate flux improvement of 30%. These authors observed a strong decrease in permeate flow (23%) one hour after the start of the operation, followed by a continuous decrease until matching the values obtained in the tests without MBR. It was attributed to a reduction in the osmotic driving force, due to an increase in the osmotic pressure of the feed solution. This was due to the hydrolysis of the pectins by the enzymes immobilized on the membrane surface, generating an MBR permeate rich in galacturonic acid (low molecular weight). Another study was carried out by Sponza and Biyink [16], who reported an increase in the concentration of phenolic compounds of 74% from raw OMW from an olive mill in Turkey with FO. These authors proposed a hybrid FO-CMD (contact membrane distillation) process, successfully achieving a high removal of COD and TSS and total phenols removal yield of 99.98%. However, before the FO process, a pretreatment with Polyethylene (PE) hollow fiber membranes with a pore size of 0.42 mm was performed, where 24% of the phenolic compounds present in the raw OMW were lost.

Unlike for OMW, many studies have been carried out with urban wastewater, highlighting the FO process as a promising process for the removal of emerging pollutants. These works report high volume reduction factors and rejection of specific compounds, being the process economically and technically feasible [17-18]. The large number of studies carried out with these wastewaters has allowed to test different membranes and operating conditions, being a key point the DS used. Salamanca et al. [19] pointed out that, with a hollow fiber aquaporin membrane, NaCl solution appeared as the most appropriate DS to be used because it led to higher permeate flux and lower reverse salt flux. Other studies carried out by Valladares Linares et al. [20] presented the use of sea water as DS to integrate the purification of municipal wastewater and the desalination of seawater for the production of drinking water.

With nutrients retention (N and P) between 56% and 99%, and almost complete retention of trace metals, the study provides a possible energy-saving strategy to combine municipal wastewater treatment and desalination of seawater, promoting sustainable urban water management and water reuse in coastal cities. Summarizing, both salt solutions and residual brines could be used as DS. The use of residual brines can be an appropriate option, since they do not have to be regenerated and their dilution is a crucial step for their further discharge or treatment. In the table olive production process, different TOPWs are generated depending on the process step. The first step is debittering with sodium hydroxide solution (1-2% w/v), followed by rinsing cycles to remove excess alkali. It ends with the fermentation of the olives in a brine (4-8% w/v) of sodium chloride for several months, generating the fermentation brine wastewater from the processing of table olives (FTOP). Although it represents only 20% of the total volume of TOPW (3.9 to 7.5 m^3/t of green olives), it contributes to 80-85% of the global wastewater pollution generated in these types of agro-food industries [21].

In this work, the main objective is to use the characteristics of the FO process to treat simultaneously two wastewaters of the olive industry: olive oil washing wastewater (OOWW) and table olive fermentation brine wastewater (FTOP). The large difference in chemical potential (due to the difference in salt content) between the feed solution (OOWW) and the extraction solution (FTOP), will not only allow the concentration of phenolic compounds, but will also dilute the fermentation brine, whose treatment is extremely difficult due to its hypersalinity. For this, two different membranes were tested to analyse their performance in terms of concentration of phenolic compounds and transmembrane flux. This work is presented as a novelty since there are no studies carried out with the aim of treating simultaneously two different wastewaters from the olive production processes, both of them with a high contaminant load.

2. Materials and methods

2.1 Feed solution, draw solution and performed tests

Both synthetic and actual wastewaters have been used as FS and DS in the experiments. The synthetic wastewater used as FS was prepared with 1 $g \cdot L^{-1}$ of tyrosol (Ty) (Maybridge, United Kingdom). This concentration was selected due to the total phenolic

compound concentration measured in the characterization of an OOWW sample (1115.72 mgTy eq·L^{-1}). For the synthetic DS, a solution of 30 g·L^{-1} of sodium chloride (NaCl) provided by VWR chemicals (Belgium) was used, since this value was close to the concentration of NaCl registered in the characterization of the FTOP.

Table 5.15 Feed solutions (FS) and draw solutions (DS) used for each test performed

Test	Membrane tested	FD	DS
E1	FTSH20 and HFFO.6	Synthetic (tyrosol 1g·L^{-1})	Synthetic (30 g·L^{-1} NaCl)
E2	FTSH20 and HFFO.6	5F- OOWW	Synthetic (30 g·L^{-1} NaCl)
E3	HFFO.6	5F- OOWW	60F- FTOP
E4	HFFO.6	UF- OOWW	60F- FTOP

OOWW: olive oil washing wastewater; FTOP: table olive fermentation brine wastewater; 5F-OOWW: 5 μm filtered OOWW; UF-OOWW: UF permeate from OOWW; 60F-FTOP: 60 μm filtered FTOP

OOWW samples were provided by a cooperative located in the Valencian Community (Spain), meanwhile FTOP samples were taken from a table olive packaging industry located in the same area. The performed experiments are summarized in Table 5.15. This table shows the FS and DS considered for each experiment and the membrane used. The wastewater samples were filtered through cartridges (CA-0202- 00, model GT, HydroWater, Spain), one of 5 μm and another of 60 μm for OOWW and FTOP, respectively. Regarding the UF permeate, this was obtained with the UP005 membrane (Microdyn Nadir, Germany), under the operating conditions of 2.5 m s^{-1} CFV and 2 bar TMP. The operating conditions were selected from the results obtained in a previous work [22].

2.2 Plant setup

The experiments were carried out in two plants, which were very similar, changing the type of the module and the volume of the tanks for the FS and DS, since the membranes used had different configuration and active surface. The configuration of the plants is shown in Fig. 5.40.

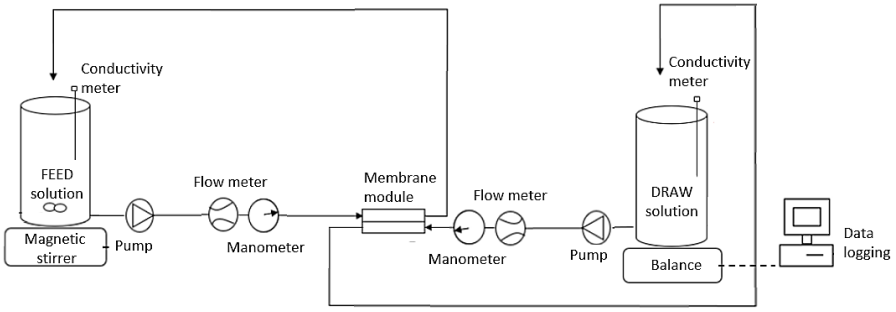

Fig. 5.40 Scheme diagram of the forward osmosis pilot plant

As mentioned above, due to the differences in membrane area, different tanks were used. Plastic tanks, with a volume of 5 L (for flat sheet membrane) and 50 L (for hollow fiber membrane), were used as containers for draw and feed solutions. DS tank was mounted on a digital balance (PKP 4200-2, Kern, Germany) which was used for continuous measuring of its mass. The data from scale were transferred to data logging software on personal computer. FS tank was placed on a magnetic stirrer (SBS, Spain) to prevent particle deposition. The tanks were connected to rubber tubes, through which the solutions were fed to the FO module, where the streams interacted through the membrane. Between the tanks and module, each circuit had a manometer (Nuova Fima, Italy), flowmeter (Psm-21, Tecfluid, Spain) and peristaltic pump (Pumpdrive 5106, Heidolph, Germany). The plant was also equipped with two electrical conductivity meters (CDH-SD1, Omega Engineering), one for each solution. The CFO42 module manufactured by Sterlitech Corporation (USA) was used to host the FTSH2O^{TM} flat sheet membrane (Fluid Technology Solutions, USA) made from cellulose triacetate (CTA), with an active area of 0.0042 m^2. The other membrane tested corresponded to the hollow fiber membrane HFFO.6 (Aquaporin Inside, Denmark), with an active layer of polyamide thin film composite (TFC) with integrated aquaporin proteins and an active surface of 0.6 m^2. It was decided to work in counter-current mode since it has been reported that, when working with FS with a high amount of solutes, the osmotic pressure can rise to a large extent. Thus, the counter-current operation increases de driving force compared to co-current operation [23]. The membrane position was FS facing the active layer for all the experiments. For membrane

characterization, different concentrations of DS were prepared, using NaCl at 25, 50, 75, 100, 125, 150 and 200 $g \cdot L^{-1}$ (0.43, 0.85, 1.3, 1.7, 2.1, 2.6, 3.5 M, respectively). The operating conditions of the characterization tests were flow rates of 25 $L \cdot h^{-1}$ for FS and of 15 $L \cdot h^{-1}$ for DS. For the experiments with wastewater, in the case of the FTSH2O membrane, both FS and DS pumps were adjusted to a flow rate of 30 $L \cdot h^{-1}$, whereas for the HFFO.6 the experiments were performed at 60 $L \cdot h^{-1}$ for the FS and 25 $L \cdot h^{-1}$ for the DS. The performance of the membrane was evaluated by the ability to increase the phenolic compounds concentration in the feed solution [*% TPhC*], through Equation 1:

$$[\%\, TPhC] = \left(\frac{C_f}{C_i} - 1\right) \cdot 100 \quad (1)$$

where C_f (ppm) and C_i (ppm) are the total phenolic compounds concentration in the feed solution at the end of the experiment and at the beginning, respectively. In order to characterize the membranes, water and reverse salt fluxes were measured. Water flux (Jw, $L \cdot m^{-2} \cdot h^{-1}$) was measured by the variation in weight of the DS as described in equation 2.

$$Jw = \frac{\Delta_m}{A_m \cdot \Delta t} \quad (2)$$

where Δ_m correspond to the mass change of the draw solution (g), A_m (m^2) is the membrane active surface and Δ_t (h) is the time between mass measures.

The reverse salt flux (*Js*, $g \cdot m^{-2} \cdot h^{-1}$) represents the salt passing through the membrane from the DS to the FS and it is experimentally valued considering the mass salt variation in the FS, through the following expression:

$$Js = \frac{V_t \cdot C_t - V_{t-1} \cdot C_{t-1}}{A_m \cdot \Delta_t} \quad (3)$$

where C_t (ppm) and V_t (L) are the salt concentration and the volume of the feed solution, respectively, at time t. The volume reduction (VR) of the FS was also evaluated for each experiment and it was determined based on the volume of permeate (volume transferred to the draw in relation to the initial volume of the feed [24]) (eq. 4):

$$\%VR = (\frac{V_p}{V_i}) \cdot 100 \quad (4)$$

Where Vp (L) and Vi (L) are the volume of the permeate and the initial feed solution, respectively. The tests carried out with the flat sheet membrane were carried out with 4.5 L of initial FS and 2.5 L of initial DS, while 25 L of FS and 15 L of DS were used for the tests with the hollow fiber membrane. Due to the volume involved in each test, the tests performed with the FTSHO2, with the smallest surface area, lasted 4300 minutes (71.6 h), while the test with the HFFO.6 lasted about 120 minutes (2 h). After each experiment, the membranes were cleaned for 30 min with tap water and then 10 minutes with osmotized water through both the feed and draw sides. Before (with the pristine membrane) and after cleaning, a single pass test (without recirculation) was carried out to verify the membrane permeability recovery. A 0.5 M NaCl solution was used as DS and osmotized water as FS. The flow rates were 25 $L \cdot h^{-1}$ and 15 $L \cdot h^{-1}$ for FS and DS, respectively. Jw and Js average values were measured and used for comparison.

2.3 Analytical methods

The characterization of the draw and feed solutions consisted of determining the concentration of total phenolic compounds (TPhC), chemical oxygen demand (COD), chloride ions (Cl^-), pH and conductivity. COD and Cl^- concentration were measured with Merck kits (Germany) and a photometer (Nova 30, Merck, Germany). For the phenolic compounds content determination, the Folin-Ciocalteau (F-C) spectrophotometric method [25], with tyrosol as a standard, was used. F-C reagent was acquired from Panreac (Spain) and absorbance (765 nm) of samples was measured with a UV VIS spectrophotometer DR 6000 provided by Hach Lange (USA). pH and conductivity were determined with the pH-Meter GLP 21+ and the conductivity meter EC-Meter GLP 31+, respectively, both supplied by Crison (Spain). High performance liquid chromatography (HPLC) was performed to identify low molecular weight phenolic compounds, such as tyrosol, and high molecular weight phenolic compounds, such as catechin, in the DS samples. For this, 5 mL of sample were mixed with 10 mL of ethyl acetate for 4 minutes in a vortex (Heidolph, Germany). Then it was centrifuged for 5 minutes at 3000 g (model Thermo Heraeus Megafuge 16 R model, Thermo Scientific, USA), then the supernatant was separated with a micropipette. The extraction was

repeated 3 times. Then, with a rotary evaporator (R-114, BUCHI, USA) at 30ºC, the ethyl acetate was separated from the extract. The extract was mixed with 5 mL of NaOH/water (50:50) in a vortex, then filtered at 0.22 μm. Finally, 20 μL of the filtered extracts were injected into the HPLC device (model AS-4150, Jasco, USA). The HPLC system was equipped with a MD-2018 Photodiode Array detector and a Phenomenex Kinetex 5u Biphenyl 100A column (4.6 × 250 mm, 5 μm). The flow rate was 1 $mL \cdot min^{-1}$ with an injection volume of 10 μL and the solvent system was phase A (0.5% acetic acid in water) and phase B (acetonitrile). The applied mobile phase gradient was based on a previous work [26]. Tyrosol and catechin (Sigma Aldrich, Germany) were used as standards.

3. Results and discussion

3.1 Membrane water flux and reverse salt flux

The relationship between permeate flux and reverse solute flux with the DS concentration for both membranes is presented in Fig. 5.41 The experiment was carried out in a recirculation mode with osmotized water as FS. The results showed that, for both membranes, water flux increased gradually as the concentration of salt in the DS increased. In the concentration range of 100 – 150 $g \cdot L^{-1}$, it was observed that, for the FTSHO2 membrane, the increment in water flux was lower than that observed from 50 to 100 $g \cdot L^{-1}$, reaching a more or less stationary state. On the other hand, the HFFO.6 membrane presented an ascendingly tendency. The increase in salt concentration from 150 to 200 $g \cdot L^{-1}$ generated an increase in flux similar to that initially observed. Water flux increased from 7.16 $L \cdot m^{-2} \cdot h^{-1}$ to 18.59 $L \cdot m^{-2} \cdot h^{-1}$, with an increase in reverse salt flux from 2.55 $g \cdot m^{-2} \cdot h^{-1}$ to 7.73 $g \cdot m^{-2} \cdot h^{-1}$, for HFFO.6 membrane. A linear behaviour was expected since an increase in osmotic pressure produces an increase in Jw and an increase in the concentration gradient between the DS and the FS increases diffusive salt transport, Js [27]. On the other hand, the existence of the plateau at high concentrations is due to the fact that the greater the applied osmotic force, the greater the influence of the dilutive external concentration polarization on the permeate side of the membrane, which significantly reduces the osmotic driving force. As a consequence, for high salt concentrations, the permeate flux does not increase proportionally with the applied osmotic pressure difference [28].

The specific reverse salt flux (Js/Jw) has been used as a measure to determine membrane selectivity, with a lower Js/Jw indicating less solute loss per unit of water permeated [29]. The HFFO.6 membrane presented lower Js/Jw than the FTSHO2, with both values corresponding to those given by the manufacturer and the literature [27,30]. For the HFFO.6 membrane, it was measured a specific reverse salt flux of 0.145 $g \cdot L^{-1}$ and a water flux of 11.2 $L \cdot m^{-2} \cdot h^{-1}$, meanwhile for the FTSHO2 the specific reverse salt flux was 0.41 $g \cdot L^{-1}$ and water flux was 6.16 $L \cdot m^{-2} \cdot h^{-1}$ (measured under flow rates of FS and DS of 25$L \cdot h^{-1}$ and 15 $L \cdot h^{-1}$ respectively, using a 0.5M NaCl solution as DS).

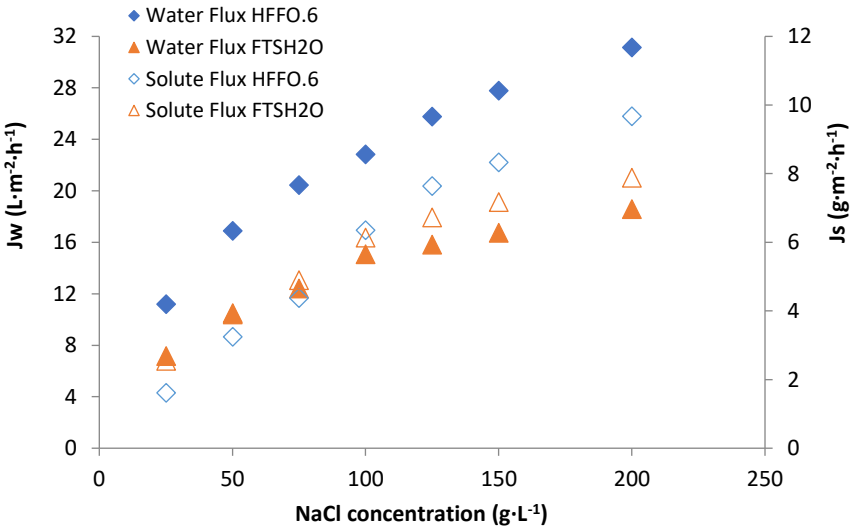

Fig. 5.41 Permeate flux and reverse solute flux for both membranes as a function of NaCl concentration in the draw solution (DS) when the feed solution (FS) was osmotized water: flow rates of 25 $L \cdot h^{-1}$ (FS) and 15 $L \cdot h^{-1}$ (DS)

The higher water permeability of the HFFO.6 membrane compared to the FTSHO2 may be due to the material of the membranes. On the one hand, the active layer made of TFC is more hydrophilic, while the support layer is thinner, more porous and less tortuous. These parameters are directly related to the intrinsic characteristics of the membrane, influencing the solute transport through the support layer, which would decrease with greater porosity and less

tortuosity, which in turn reduces the effect of the internal concentration polarization [31]. The higher fluxes shown by the TFC membrane compared to the CTA one when pure water was used as FS, are consistent with those available in the literature [32].

3.2. Experiments with NaCl solution as DS (E1 and E2)

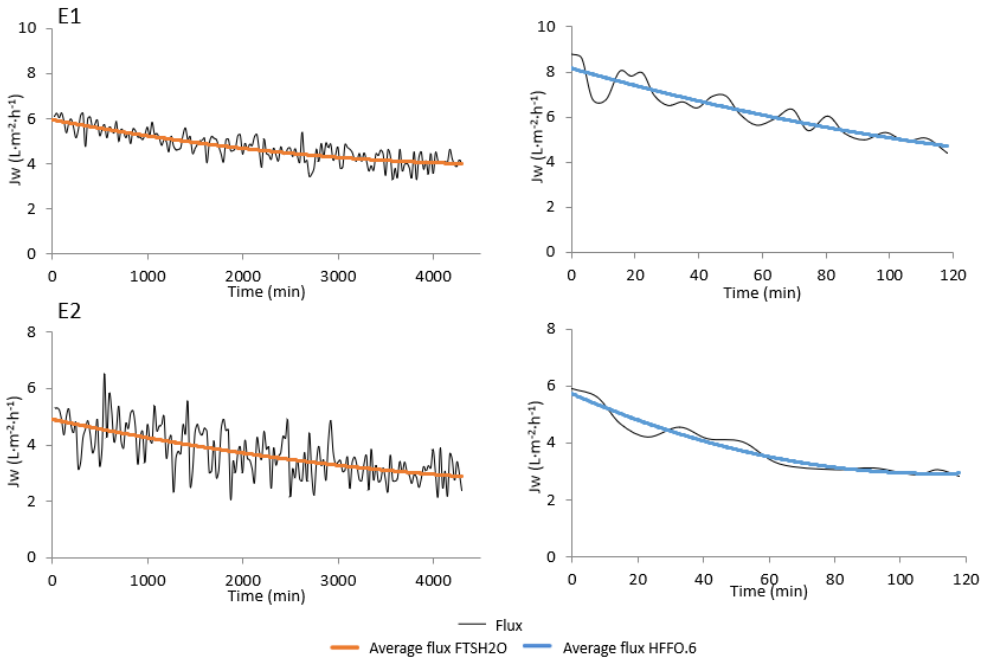

Fig. 5.42 Permeate water flux for the FTSH2O (left) and HFFO.6 (right) membranes for test E1 (1g·L^{-1} tyrosol as FS and 30 g·L^{-1} NaCl as DS) and E2 (Pre-treated OOWW as FS and 30 g·L^{-1} NaCl as DS). FS: feed solution; DS: draw solution; OOWW: olive oil washing wastewater

Permeate flux values obtained in the four tests corresponding to E1 and E2 (Table 5.15) can be seen in Fig. 5.42. It is observed for E1 how Jw for the FTSHO2 membrane was 6.20 L·m^{-2}·h^{-1} at the beginning of the test, reaching 3.98 L·m^{-2}·h^{-1} in 4300 minutes, when a more or less stationary flux was reached. On the other hand, the HFFO.6 membrane presented a more pronounced decrease in Jw, decreasing from 8.81 L·m^{-2}·h^{-1} to 4.42 L·m^{-2}·h^{-1}, in 120 minutes. When the FS was changed, feeding 5F-OOWW, a decrease in the initial Jw was

observed for both membranes, being more pronounced for the HFFO.6 membrane. However, this membrane reached a stationary value of flux in E2, while the FTSHO2 membrane presented a continuous flux decline in E2.

The decrease in flux in E2 when compared to E1 could indicate that fouling has occurred. Moreover, concentration polarization is the limiting factor in the FO process [33], affecting it externally (ECP) at the boundary of FS-membrane and DS-membrane, as well as internally (ICP) inside the substructure of porous support layer [34]. In E1, working only with model solutions, there is little influence of fouling by solute deposition on the membrane surface, so the decrease in Jw is mainly due to the decrease in osmotic pressure over time due to the passage of water from the FS to the DS, forming the dilutive ICP (characteristic of asymmetric FO membranes) [35]. Therefore, this behaviour could be due to the combined effects of the loss of driving force over time, because of the progressive change in the volumes of FS and DS, and the dilutive ICP, discarding while membrane fouling was expected to be negligible [36].

The greater decline in Jw during the E2 test (55 and 52 % for the FTSH2O and HFFO.6 membranes, respectively, when initial al final flux are compared), in addition to dilutive ICP, may be due to two factors, both influenced by the formation of a fouling layer. As can be seen in table 5.16, in E2 salt diffused through the membrane from the DS to the FS. Due to this reverse salt diffusion, there would be a greater accumulation of salt in the FS. This, together with the accumulation of other particles on the membrane surface, which forms a cake layer, suppresses the diffusivity of the salt, resulting in higher osmotic resistance (cake-enhanced osmotic pressure, CEOP) near the membrane surface, which would accelerate FO fouling. In osmosis-driven processes, CEOP causes a decrease in the osmotic driving force (consequently a decrease in water flux) and is promoted by reverse diffusion of salt from the DS [37]. On the other hand, the cake also influences the capillary force resistance (CFR), which manifests itself as a pressure loss. This pressure loss of the feed solution at the membrane interface results in a decrease in the flow of water from the feed solution to the membrane surface. Therefore, the inflow of water from the FS to the membrane surface is reduced by the CFR, while the outflow of water through the membrane is reduced due to the

CEOP effect [38]. It has been reported that phenolic compounds contributed to gel layer fouling formed on the FO membrane surface [24].

Table 5.16 Characteristics of the feed and draw solutions at the beginning and end of the tests carried out with NaCl solution as draw solution (E1 and E2), for both membranes tested.

Test	Parameter	HFFO.6 membrane				FTSH20 membrane			
		FSI[a]	DSI[c]	FSF[b]	DSF[d]	FSI[a]	DSI[c]	FSF[b]	DSF[d]
E1	[e]EC ($mS \cdot cm^{-1}$)	0.08 ± 0.01	45.50 ± 2.00	0.77 ± 0.15	20.10 ± 2.00	0.07 ± 0.01	39.70 ± 5	0.92 ± 0.05	25.50 ± 2.50
	Cl^- ($g \cdot L^{-1}$)	0.00	24.90 ± 4.00	0.014 ± 0.01	10.97 ± 1.83	0.00	26.5 ± 5.5	0.70 ± 0.01	14.10 ± 3.00
	[f]TPhC ($gTyeq \cdot L^{-1}$)	1.00 ± 0.02	0.00	1.92 ± 0.10	0.03± 0.01	1.00 ± 0.01	0.00	1.17 ± 0.50	0.15 ± 0.09
	TPhC increase (%)			91.44 ± 9.39				15.02 ± 3.82	
	[g]VR (%)			66 ± 3.4				43 ± 2.1	
E2	EC ($mS \cdot cm^{-1}$)	3.83 ± 0.20	44.30 ± 1.50	1.48 ± 0.57	24.00 ± 1.00	3.96 ± 0.15	41.50 ± 1.00	4.02 ± 0.50	31.9 ± 0.50
	Cl^- ($g \cdot L^{-1}$)	0.05 ± 0.002	27.90 ± 0.40	0.11 ± 0.03	14.40 ± 1.00	0.06 ± 0.01	27.60 ± 2.00	1.05 ± 0.10	15.0 ± 6.74
	TPhC ($gTyeq \cdot L^{-1}$)	1.02 ± 0.03	0.00	1.81 ± 0.10	0.02 ± 0.01	1.03 ± 0.02	0.00	1.17 ± 0.01	0.10 ± 8.18
	TPhC increase (%)			62.60 ± 4.25				12.72 ± 1.57	
	VR (%)			53 ± 2.7				39 ± 0.9	

[a]FSI: initial feed solution; [b]FSF: final feed solution; [c]DSI: initial draw solution; [d]DSF: final draw solution; [e]EC: electrical conductivity; [f]TPhC: total phenolic compounds; [g]VR: volume reduction

Also, it can be seen in table 5.16 that both membranes managed to concentrate TPhC in the FS stream. However, the FTSH2O membrane allowed a fairly low increment in the concentration of tyrosol in the FS (around 15%), compared to the VR reached (43% regarding

the initial volume). This may be due to the observed passage of tyrosol from FS to DS. This membrane was also the one that presented the greatest reverse passage of salts. On the other hand, the HFFO.6 membrane achieved an increment of 91% in the concentration of TPhC with a VR of 66%. Although tyrosol was observed in the final DS, its concentration was low compared to that measured for the other membrane and low salt concentration was also observed in the FSF. In the second test (E2), both the concentration of TPhC in the final DS and the achieved VR were lower, affecting the HFFO.6 membrane at higher extent. This can be explained due to the presence of organic matter (COD of 15.13 ± 2.86 $g \cdot L^{-1}$), that caused the fouling, affecting the pass of water. In fact, the water flux was also reduced compared to the results of the previous tests (Fig 3). Also, the passage of phenolic compounds was lower to than observed in E1, therefore fouling could also interfere. The influence was greater for the FTSH2O membrane, since the final concentrations in the DS were 150.9 $mgTyeq \cdot L^{-1}$ for E1 and 102.7 $mgTyeq \cdot L^{-1}$ for E2.

Other authors, working with a combination of water produced in a gas field extracted from an offshore reservoir and process water from onshore operations as FS and brine from a desalination plant as DS, reported that hollow fiber membranes had better flux and greater rejection compared to the FTSHO2 membrane with the same effective membrane area [39]. On the other hand, it has also been reported that TFC membranes generally have higher Jw and phenolic compound rejection than CTA membranes under the same operating conditions [40-41]. The lower rejection of phenolic compounds observed for the CTA membrane could be due to the passage of this compounds trough the membrane due to a solution-diffusion mechanism, being adsorbed on the active layer of the FS side of the membrane, diffusing through the membrane and being desorbed to the DS. This is due to the strong solute-membrane affinity as a result of hydrogen bond attraction between phenols and the hydroxyl functional groups of the CTA membranes, generating a higher adsorption capacity and, therefore, a much lower rejection than that of the TFC membranes [42]. On the other hand, the lower TPhC rejection could be also due to the fouling layer. It has been reported that in CTA membranes, fouling facilitated the transport of hydrophobic and hydrophilic organic contaminants across the membranes, resulting in elevated concentrations of target solutes in the permeate [43].

Regarding the permeability recovery of the membrane after cleaning, the HFFO.6 membrane presented better permeability recovery and only one rinsing with osmotized water was necessary. However, the FTSHO2 had to be cleaned with chemicals for the permeability recovery. Other authors working with the same membrane but in a hollow fiber configuration also observed irreversible fouling [44]. They attributed this to pore clogging by humic acid due to the similar size (hydration radius between 2.3 nm and 7.7 nm [45]) when compared to the support layer pore sizes, which resulted in enhanced ICP and thus increased membrane resistance. In this case, the compounds present in the OOWW could also favour the fouling of the membrane. On the other hand, the easy cleaning of the HFFO.6 membrane compared to the FTSHO2 could also be due to its advantages of high packing density, self-supporting structure and uniform flow distribution, which not only facilitates membrane cleaning, but also mass transfer [23].

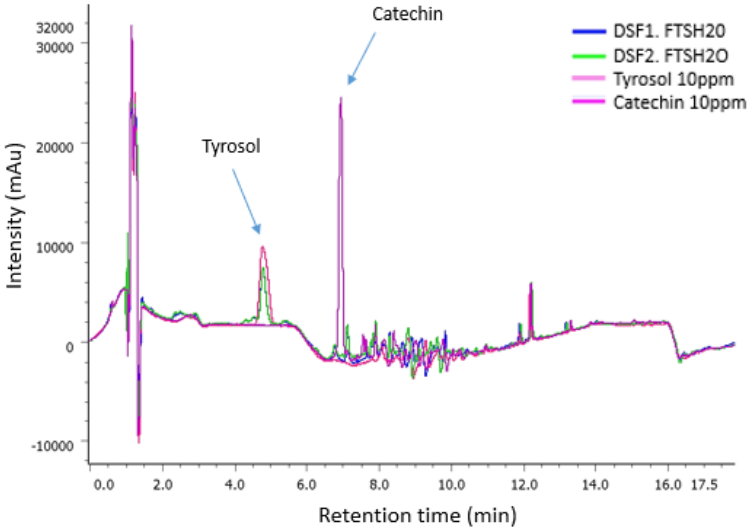

Fig. 5.43. Chromatogram of the HFFO2 membrane draw solution (DSF1 and DSF2, corresponds to final DS of two repeated tests under the same conditions) at the end of the test performed with 1g·L^{-1} tyrosol as feed solution and 30 g·L^{-1} NaCl as draw solution

Due to the high passage of phenolic compounds to the DS with the FTSHO2 membrane, it was decided to analyse the DS at the end of E2. The idea was to identify which compounds crossed the membrane (low or high molecular weight phenolic compounds). For this purpose, the final DS was analysed by HPLC. Two standard solutions, one of tyrosol (MW: 138.164 $g \cdot mol^{-1}$) representing the low molecular weight phenolic compounds and other of catechin (MW: 290.271 $g \cdot mol^{-1}$), representing the high molecular weight ones were used. Tyrosol was quantified in the DS (Fig. 5.43), while catechin was not, so it can be induced that the passage is mainly due to the phenolic compounds with the lowest molecular weights. In previous studies, more than 20 phenolic compounds have been identified in olive oil washing wastewater from two-phase olive oil mills, 12 of them with a molecular weight lower than catechin [46]. Therefore, working with this membrane would imply a considerable loss of phenolic compounds from the sample. For these reasons, it was decided to continue the experiments only with the HFFO.6 membrane.

3.3. Experiments with FTOP as DS (E3 and E4)

The characteristics of the feed and draw solutions used in E3 and E4 tests are shown in Table 5.17. The OOWW is characterized by an intense brown colour and a slightly acid pH. This acid profile is also a characteristic of the FTOP, but as difference, this wastewater has a yellow colour.

Table 5.17. Characterization of the feed and draw solutions used in the tests performed with residual table olive fermentation brine as draw solution

	Feed Solutions		Draw Solution
Parameter	5F-OOWW[a]	UF-OOWW[b]	60F-FTOP[c]
pH	5.03 ±0.04	5.19 ± 0.02	4.70 ± 0.05
[d]EC ($mS \cdot cm^{-1}$)	4.27 ± 0.11	5.15 ± 0.01	55.20 ± 14.1
Turbidity (NTU)	200.8 ± 2.2	0.04 ± 0.00	376.4 ± 25.4
[e]SS (ppm)	287.17 ± 36	< 5	762 ± 107
Colour	1.80 ± 0.14	1.19 ± 0.02	0.41 ± 0.11
[f]COD ($gO_2 \cdot L^{-1}$)	15.13 ± 2.86	10.14 ± 0.01	10.80 ± 4.21
Cl^- ($g \cdot L^{-1}$)	0.03 ± 0.01	0.01 ± 0.01	33.42 ± 1.25
[g]TPhC ($mgTy\ eq \cdot L^{-1}$)	1182.78 ± 284.65	1074.12 ± 114.70	835.19 ± 167.59

[a]5F-OOWW: 5 µm filtered olive oil washing wastewater; [b]UF-OOWW: ultrafiltrated olive oil washing wastewater; [c]60F-FTOP: 60 µm filtered table olive fermentation brine wastewater; [d]EC: electrical conductivity; [e]SS: suspended solids; [f]COD: chemical oxygen demand; [g]TPhC: total phenolic compounds

As shown in Table 5.17, OOWW and FTOP have high levels of suspended solids, being 2.7 times higher the amount in the 60F-FTOP compared to the 5F-OOWW. Accordingly, turbidity, which is related to suspended solids concentration, is also higher in the 60F-FTOP and 5F-OOWW samples (376.4 NTU and 200.8 NTU, respectively, vs 0.04 NTU). The organic matter present in the samples were in the range of 10000 – 15000 $mg \cdot L^{-1}$, being the content of COD in 5F-OOWW 40% higher compared with the 60F-FTOP sample. In all the samples, there was an important presence of phenolic compounds (between 800 and 1200 mg Ty $eq \cdot L^{-1}$), with the lowest concentration value present in 60F-FTOP. Similar acidic profile and phenolic compounds concentrations were reported by Ferrer-Polonio et al. [47], where four samples of FTOP were analysed, presenting a pH between 4 and 4.5 and an average of total phenolic content of 1114.25 ± 396.25 mgTy $eq. \cdot L^{-1}$. Regarding the UF-OOWW sample, the absence of SS and turbidity was due to the UF process, as expected. On the other hand, COD also showed a decrease from 13.13 to 10.14 $gO2 \cdot L^{-1}$, while TPhC were not affected (9% decrease). The results obtained in this work are within the ranges observed in other studies [22].

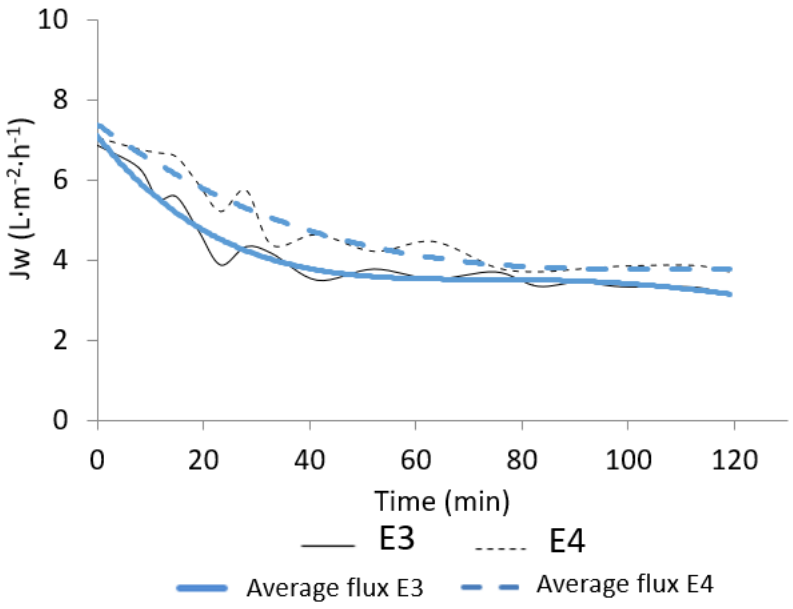

Fig. 5.44 Permeate water flux for the HFFO.6 membrane from tests E3 (pre-treated olive oil washing wastewater (OOWW) as feed solution (FS) and residual table olive fermentation brine (FTOP) as draw solution (DS)) and E4 (Ultrafiltration permeate from OOWW as FS and FTOP as DS)

Fig. 5.44 shows the permeate values obtained in E3 and E4 experiments with the HFFO.6 membrane. It can be seen a more pronounced decrease with respect to E1 and E2 tests, i.e. with the tests using NaCl solution as DS. However, the average flux values were higher than those observed in E2, with flux values from E3 and E4 being 1.2 and 1.3 times higher, respectively. This was due to the higher osmotic pressure difference caused by FTOP (higher salt concentration than in the NaCl solution used in the previous tests). It can also be observed that, when working with the UF-OOWW (E4), flux was higher, more stable and showed a lower drop in the first few minutes. This was due to the higher fouling that occurs when working with the 5F-OOWW compared to the UF-OOWW, since, as mentioned above, this fouling would increase the ICP, reduce the pore size and hinder back diffusion of dissolved substances. However, a greater difference between the Jw of E3 and E4 was expected. Similar water fluxes between E3 and E4 means that filtration of OOWW at 5 microns could be enough for maintaining the membrane without severe fouling during the process. Studies carried out by Volpin et al. [31], pointed out the importance of pre-treating a wastewater with a high organic load before a FO treatment. In their study they used different urban water samples, which were collected from different stages of the treatment process, as FS and wastewater as DS. They observed a large decrease in Jw when working with samples with a high organic matter content (primary effluent), compared to secondary effluents, with less organic matter content. It should not be forgotten that the FTOP used as DS, apart from a large amount of salts, also contained a high concentration of both total suspended solids and phenolic compounds, which can adhere to the membrane surface that faces the DS (support layer), causing fouling and concentration polarization (ECP and ICP), and therefore resistance to the passage of water [48]. Therefore, the reverse solute flux, concentration polarization and fouling on the surface of both sides of the membrane could affect water flux.

In table 5.18 are presented the characterization of FS and DS after and before test E3 and E4. Interestingly, it was observed that the tests carried out with FTOP as DS presented greater percentages of TPhC concentration and higher VR than the tests performed with NaCl solution as DS (E2). This was attributed to the high conductivity (and consequently high osmotic pressure) presented by the FTOP, which has been also used as DS in other studies, obtaining good results in terms of the generation of the osmotic pressure difference necessary

between both sides of the membrane for the permeation of treated water towards the DS side [49]. Salih and Dastgheib [50] observed a similar trend when working with a hypersaline brine extracted from a potential CO_2 sequestration site such as DS, obtaining a higher flux than with $MgSO_4$ (20%) as draw solution.

Table 5.18 Characteristics of the feed and draw solutions at the beginning and end of the E3 (pre-treated olive oil washing wastewater (OOWW) as feed solution (FS) and residual table olive fermentation brine (FTOP) as draw solution (DS)) and E4 (Ultrafiltration permeate from OOWW as FS and FTOP as DS) tests performed with the HFFO.6 membrane.

		HFFO.6 membrane			
Test	Parameter	FSI[a]	DSI[c]	FSF[b]	DSF[d]
E3	[e]EC (mS·cm^{-1})	2.86 ± 0.05	56.20 ± 2.00	4.88 ± 0.15	40.10 ± 1.00
	Cl^- (g·L^{-1})	0.034 ± 0.001	40.10 ± 0.80	0.054 ± 0.003	23.44 ± 2.27
	[f]TPhC (gTyeq·L^{-1})	1.00 ± 0.01	0.83 ± 0.00	1.78 ± 0.00	0.59 ± 0.01
	% [f]TPhC			77.43 ± 0.89	
	% [g]VR			53.0 ± 2.1	
E4	[e]EC (mS·cm^{-1})	2.38 ± 0.49	54.10 ± 1.50	5.21 ± 0.20	42.67 ± 2.14
	Cl^- (g·L^{-1})	0.032 ± 0.002	40.10 ± 0.70	0.074 ± 0.005	18.40 ± 2.00
	[f]TPhC (gTyeq·L^{-1})	0.995 ± 0.003	0.80 ± 0.05	1.63 ± 0.10	0.568 ± 0.01
	% [f]TPhC			74.13 ± 0.46	
	% [g]VR			49 ± 1.01	

[a]FSI: initial feed solution; [b]FSF: final feed solution; [c]DSI: initial draw solution; [d]DSF: final draw solution; [e]EC: electrical conductivity; [f]TPhC: total phenolic compounds; [g]VR: volume reduction

In addition to the higher osmotic pressure difference, the higher concentration of TPhC when FTOP was used as DS was due to the lower difference between TPhC concentration in FS and DS (compared to E2, in which NaCl solution was used). It is important to point out that the mass balance showed that there was no adsorption of TPhC on the membrane, since the concentrations measured at the beginning of the tests were very similar to those measured at

the end of the process (SD 4.7%). These results are important when considering using the FTOP as DS, since, apart from delivering the osmotic force necessary for the concentration of TPhC in the FS, it generates an environment that reduced the passage of TPhC from the FS to the DS.

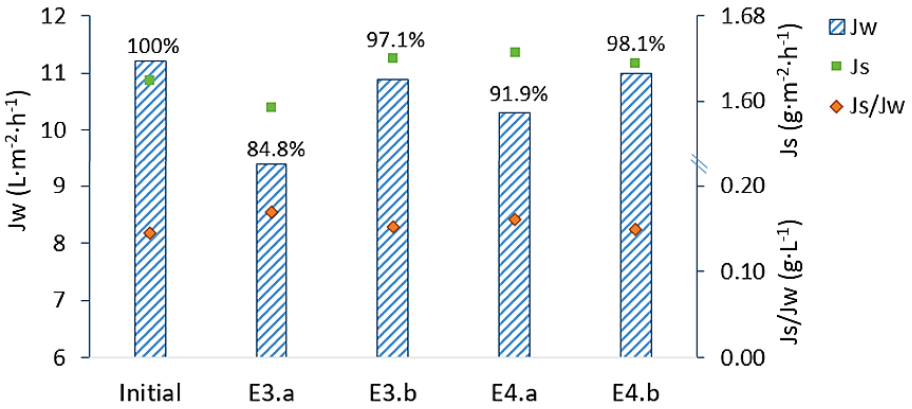

Fig. 5.45 Recovery of the permeability, reverse salt flux (Js) and Js/Jw ratio after cleaning the membrane HFFO.6 after the experiments E3 (5F- OOWW as FS and 60F-FTOP as DS) and E4 (UF-OOWW as FS and 60F-FTOP as DS). Cleaning was performed with water (20°C) in two steps (a) and (b)

It can be seen in Fig. 5.45 that after a cleaning cycle (E3.a and E4.a) the HFFO.6 operated with UF-OOWW as FS achieved a permeability recovery of 91.9%, compared to 84.8% when working with 5F-OOWW. However, in the next cycle (E3.b and E4.b) the global recovery percentages were more or less equal, achieving 98.1 and 97.1%, respectively. This may be due to the fact that the fouling is generated mainly due to cake layer formation, being mainly reversible [24,37,51]. This cake layer formation could also be responsible for the value of Js observed in E3a, being lower than the initial one (1.58 vs 1.63 $g \cdot m^{-2} \cdot h^{-1}$), indicating a lower reverse salt passage. As the calculated Js was after a cleaning cycle, it can be inferred that Js during the test was lower than that measured after E3a (verified by calculating Js with final values of Cl^- in FS and DS, value Js = 1.53 $g \cdot m^{-2} \cdot h^{-1}$). This may be due to the fact that

when working with wastewater on both sides of the membrane, fouling occurs on both sides of the membrane. Although fouling decreases Jw (observed in E3 and E4), it also causes a decrease in Js. This was not observed after E4a (Js of 1.65 $g \cdot m^{-2} \cdot h^{-1}$) because the first rinsing recovered more than 90% of the initial permeability, which means that cake layer has been mostly removed, and because the FS came from a previous ultrafiltration step, and therefore contained smaller particles. This agrees with the higher concentration of chlorides observed in the final FS from E3 (table 5.18). This lower passage of salts in E3 was also verified by mass balance, with the measured value of the concentration of Cl^- in the final FS being slightly higher than that obtained from the theoretical balance. This could explain the slightly higher percentage of TPhC concentration in the final FS and the higher VR. Fouling could enhance the rejection of TPhC. Something similar was observed by Valladares Linares et al. [52], who observed an increase in the rejection of micropollutants in the presence of the fouling layer. They attributed this to a higher hydrophilicity of the fouled than of the clean FO membranes, reduced mass transport capacity, membrane swelling, and higher negative charge of the membrane surface (related to natural organic matter (NOM) acids and polysaccharides).

Although fouling implies a drop in Jw and Js the relationship between the parameters (specific reverse salt flux) was practically constant. With Js/Jw values of 0.17 and 0.16 $mg \cdot L^{-1}$ for E3a and E4a, respectively, and 0.15 $mg \cdot L^{-1}$ for E3b and E4b (pristine membrane value of 0.15 $mg \cdot L^{-1}$).

It is important to point out that in all the tests carried out with the HFFO.6 membrane (i.e. independently of the DS), high permeability recovery values were achieved after two cleaning cycles. However, in E2 (NaCl solution as DS) a Jw recovery higher than 96% was achieved after only one rinsing cycle. This was a result of the higher fouling caused by the FTOP, due to the organic matter divalent salts present. It has been reported that water containing calcium ions would be associated with increased membrane fouling due to the chemical interactions with the organic matter present, forming bridges between other molecules, which gives rise to a cross-linked gel layer that increases adherence to the membrane surface [53,54].

Finally, it has to be commented that though working with UF-OOWW generated lower flux decay, it did not present a greater concentration of phenolic compounds or volume reduction compared to 5F-OOWW. Thus, including the UF step would only generate an increase in process costs.

4. Conclusions

The concentration of olive oil washing wastewater (OOWW), effluent rich in phenolic compounds, was studied by forward osmosis. Two membranes, FTSH2O and HFFO.6, were evaluated for this process in terms of Jw, Js/Jw, TPhC concentration and VR. The HFFO.6 membrane presented higher flux and lower Js/Jw, which was attributed to its material. When working with NaCl as DS, both membranes tested were able to concentrate phenolic compounds without presenting a high decrease in Jw. However, the reverse passage of salts and the passage of phenolic compounds from the FS to the DS was higher using the FTSH2O membrane.

Then, with HFFO.6, for the first time the concentration of OOWW was studied using FTOP as draw solution in a FO process. FTOP results as a suitable wastewater to be used as DS for the proposed FO process. Its two main advantages are the high osmotic pressure and the concentration of TPhC, which implies that the loss of these compounds by passage through the membrane from the FS to the DS is lower, achieving a concentrated OOWW with higher concentration of these compounds in comparison by using NaCl as draw solution. In addition, unlike a NaCl solution, this is not a DS that has to be regenerated, since the diluted FTOP can be managed and fresh FTOP can be used in the process.

The use of UF-OOWW permeate as FS in comparison to 5F-OOWW, generated a lower decrease in flux. However, it did not present a greater concentration of phenolic compounds. The fouling observed was mainly reversible, being mitigated with two cleaning cycles with water. In this way, the process can be performed with 5F-OOWW, since severe fouling was not observed, being not needed an ultrafiltration step.

Summarizing, it was shown that FO is a promising process for both the concentration of phenolic compounds from OOWW and the dilution of FTOP. In addition, the proximity of table olive processing plants with olive oil mills (both near olive tree cultivars) make the process feasible since the cost of the brine transport will be very low. More studies at higher scale need to be done to evaluate long-term fouling and the economic viability of the process.

Acknowledgements

The authors acknowledge the financial support from the Ministry of Economy, Industry and Competitiveness of Spain through the project CTM2017-88645-R and The European Union through the Operational Program of the Social Fund (FSE).

References

[1] European Environment Agency, Industrial waste water treatment - pressures on Europes's environment, 2018.

[2] J.M. Ochando-Pulido, J.R. Corpas-Martínez, J.A. Vellido-Perez, A. Martinez-Ferez, Optimization of polymeric nanofiltration performance for olive-oil-washing wastewater phenols recovery and reclamation, Sep. Purif. Technol. 236 (2020) 116261. https://doi.org/10.1016/j.seppur.2019.116261.

[3] G. Hodaifa, P.A.R. Gallardo, C.A. García, M. Kowalska, M. Seyedsalehi, Chemical oxidation methods for treatment of real industrial olive oil mill wastewater, J. Taiwan Inst. Chem. Eng. 97 (2019) 247–254. https://doi.org/10.1016/j.jtice.2019.02.001.

[4] T. El Moussaoui, Studies on the activated sludge process crucial parameters controlling olive mill wastewater treatment, Sci. Total Environ. 838 (2022) 156455. https://doi.org/10.1016/j.scitotenv.2022.156455.

[5] J.S. Torrecilla, M.L. Mena, P. Yáñez-Sedeño, J. García, Application of artificial neural network to the determination of phenolic compounds in olive oil mill wastewater, J. Food Eng. 81 (2007) 544–552. https://doi.org/10.1016/j.jfoodeng.2006.12.003.

[6] H.K. Obied, M.S. Allen, D.R. Bedgood, P.D. Prenzler, K. Robards, R. Stockmann, Bioactivity and analysis of biophenols recovered from olive mill waste, J. Agric. Food Chem. 53 (2005) 823–837. https://doi.org/10.1021/jf048569x.

[7] J. Rodríguez-Morató, L. Xicota, M. Fitó, M. Farré, M. Dierssen, R. De La Torre, Potential role of olive oil phenolic compounds in the prevention of neurodegenerative diseases, Molecules. 20 (2015) 4655–4680.

https://doi.org/10.3390/molecules20034655.

[8] H. Lee, S.W. Im, C.H. Jung, Y.J. Jang, T.Y. Ha, J. Ahn, Tyrosol, an olive oil polyphenol, inhibits ER stress-induced apoptosis in pancreatic β-cell through JNK signaling, Biochem. Biophys. Res. Commun. 469 (2016) 748–752. https://doi.org/10.1016/j.bbrc.2015.12.036.

[9] R.W. Owen, A. Giacosa, W.E. Hull, R. Haubner, G. Würtele, B. Spiegelhalder, H. Bartsch, Olive-oil consumption and halth: the possible role of antioxidants, Lancet Oncol. 1 (2000) 107–112. https://doi.org/10.1007/978-3-642-37404-3-4.

[10] A.M. Goula, H.N. Lazarides, Integrated processes can turn industrial food waste into valuable food by-products and/or ingredients: The cases of olive mill and pomegranate wastes, J. Food Eng. 167 (2015) 45–50. https://doi.org/10.1016/j.jfoodeng.2015.01.003.

[11] A.M. Gómez-Caravaca, A. Segura-Carretero, A. Martínez-Férez, J.M. Ochando-Pulido, Recovery of Phenolic Compounds From Olive Oil Mill Wastewaters by Physicochemical Methodologies, in: Food Bioconversion, Elsevier Inc., 2017: pp. 467–489. https://doi.org/10.1016/B978-0-12-811413-1.00014-0.

[12] A.Y. Gebreyohannes, E. Curcio, T. Poerio, R. Mazzei, G. Di Profio, E. Drioli, L. Giorno, Treatment of Olive Mill Wastewater by Forward Osmosis, Sep. Purif. Technol. 147 (2015) 292–302. https://doi.org/10.1016/j.seppur.2015.04.021.

[13] A. Cassano, C. Conidi, R. Ruby-Figueroa, R. Castro-Muñoz, Nanofiltration and tight ultrafiltration membranes for the recovery of polyphenols from agro-food by-products, Int. J. Mol. Sci. 19 (2018) 351. https://doi.org/10.3390/ijms19020351.

[14] K. Lutchmiah, A.R.D. Verliefde, K. Roest, L.C. Rietveld, E.R. Cornelissen, Forward osmosis for application in wastewater treatment: A review, Water Res. 58 (2014) 179–197. https://doi.org/10.1016/j.watres.2014.03.045.

[15] G. Blandin, F. Ferrari, G. Lesage, P. Le-Clech, M. Héran, X. Martinez-Lladó, Forward osmosis as concentration process: Review of opportunities and challenges, Membranes (Basel). 10 (2020) 284. https://doi.org/10.3390/membranes10100284.

[16] D.T. Sponza, Y. Biyink, The Performance of a Hybrid Integrated Forward Osmosis (FO) and Contact Membrane Distillation (CMD) Processes to Threat the Olive Mill Effluents and Recovery of Some Polyphenols, J. Membr. Sci. Technol. 10 (2020) 211. https://doi.org/10.35248/2155-9589.20.10.211.Copyright.

[17] A.J. Ansari, F.I. Hai, W.E. Price, J.E. Drewes, L.D. Nghiem, Forward osmosis as a platform for resource recovery from municipal wastewater - A critical assessment of the literature, J. Memb. Sci. 529 (2017) 195–206. https://doi.org/10.1016/j.memsci.2017.01.054.

[18] J.E. Kim, J. Kuntz, A. Jang, I.S. Kim, J.Y. Choi, S. Phuntsho, H.K. Shon, Techno-economic assessment of fertiliser drawn forward osmosis process for greenwall plants from urban wastewater, Process Saf. Environ. Prot. 127 (2019) 180–188. https://doi.org/10.1016/j.psep.2019.05.014.

[19] M. Salamanca, R. López-Serna, L. Palacio, A. Hernandez, P. Prádanos, M. Peña, Ecological Risk Evaluation and Removal of Emerging Pollutants in Urban Wastewater by a Hollow Fiber Forward Osmosis Membrane, Membranes (Basel). 12 (2022). https://doi.org/10.3390/membranes12030293.

[20] R. Valladares Linares, Z. Li, M. Abu-Ghdaib, C.H. Wei, G. Amy, J.S. Vrouwenvelder, Water harvesting from municipal wastewater via osmotic gradient: An evaluation of process performance, J. Memb. Sci. 447 (2013) 50–56. https://doi.org/10.1016/j.memsci.2013.07.018.

[21] E. Ferrer-Polonio, J.A. Mendoza-Roca, A. Iborra-Clar, J.L. Alonso-Molina, L. Pastor-Alcañiz, Comparison of two strategies for the start-up of a biological reactor for the treatment of hypersaline effluents from a table olive packaging industry, Chem. Eng. J. 273 (2015) 595–602. https://doi.org/10.1016/j.cej.2015.03.062.

[22] M. Cifuentes-Cabezas, C. Carbonell-Alcaina, M.C. Vincent-Vela, J.A. Mendoza-Roca, S. Álvarez-Blanco, Comparison of different ultrafiltration membranes as first step for the recovery of phenolic compounds from olive-oil washing wastewater, Process Saf. Environ. Prot. 149 (2021) 724–734. https://doi.org/10.1016/j.psep.2021.03.035.

[23] V. Sanahuja-Embuena, G. Khensir, M. Yusuf, M.F. Andersen, X.T. Nguyen, K. Trzaskus, M. Pinelo, C. Helix-Nielsen, Role of operating conditions in a pilot scale investigation of hollow fiber forward osmosis membrane modules, Membranes (Basel). 9 (2019) 2–7. https://doi.org/10.3390/membranes9060066.

[24] N. Singh, I. Petrinic, C. Hélix-Nielsen, S. Basu, M. Balakrishnan, Influence of Forward Osmosis (FO) membrane properties on dewatering of molasses distillery wastewater, J. Water Process Eng. 32 (2019) 100921. https://doi.org/10.1016/j.jwpe.2019.100921.

[25] V.L. Singleton, R. Orthofer, R.M. Lamuela-Raventós, Analysis of total phenols and other oxidation substrates and antioxidants by means of folin-ciocalteu reagent, Methods Enzymol. 299 (1999) 152–178. https://doi.org/10.1016/S0076-6879(99)99017-1.

[26] C.M. Sánchez-Arévalo, A. Iborra-Clar, M.C. Vincent-Vela, S. Álvarez-Blanco, Exploring the extraction of the bioactive content from the two-phase olive mill waste and further purification by ultrafiltration, LWT - Food Sci. Technol. 165 (2022) 113742. https://doi.org/10.1016/j.lwt.2022.113742.

[27] M. Salamanca, R. López-Serna, L. Palacio, A. Hernández, P. Prádanos, M. Peña, Study of the rejection of contaminants of emerging concern by a biomimetic aquaporin

hollow fiber forward osmosis membrane, J. Water Process Eng. 40 (2021) 101914. https://doi.org/10.1016/j.jwpe.2021.101914.

[28] M.S. Camilleri-Rumbau, J.L. Soler-Cabezas, K.V. Christensen, B. Norddahl, J.A. Mendoza-Roca, M.C. Vincent-Vela, Application of aquaporin-based forward osmosis membranes for processing of digestate liquid fractions, Chem. Eng. J. 371 (2019) 583–592. https://doi.org/10.1016/j.cej.2019.02.029.

[29] J. Ren, J.R. McCutcheon, A new commercial biomimetic hollow fiber membrane for forward osmosis, Desalination. 442 (2018) 44–50. https://doi.org/10.1016/j.desal.2018.04.015.

[30] M. Nikbakht Fini, H.T. Madsen, J.L. Sørensen, J. Muff, Moving from lab to pilot scale in forward osmosis for pesticides rejection using aquaporin membranes, Sep. Purif. Technol. 240 (2020) 116616. https://doi.org/10.1016/j.seppur.2020.116616.

[31] F. Volpin, E. Fons, L. Chekli, J.E. Kim, A. Jang, H.K. Shon, Hybrid forward osmosis-reverse osmosis for wastewater reuse and seawater desalination: Understanding the optimal feed solution to minimise fouling, Process Saf. Environ. Prot. 117 (2018) 523–532. https://doi.org/10.1016/j.psep.2018.05.006.

[32] J.C. Ortega-Bravo, G. Ruiz-Filippi, A. Donoso-Bravo, I.E. Reyes-Caniupán, D. Jeison, Forward osmosis: Evaluation thin-film-composite membrane for municipal sewage concentration, Chem. Eng. J. 306 (2016) 531–537. https://doi.org/10.1016/j.cej.2016.07.085.

[33] S. Loeb, L. Titelman, E. Korngold, J. Freiman, Effect of porous support fabric on osmosis through a Loeb-Sourirajan type asymmetric membrane, J. Memb. Sci. 129 (1997) 243–249. https://doi.org/10.1016/S0376-7388(96)00354-7.

[34] A. Achilli, T.Y. Cath, A.E. Childress, Selection of inorganic-based draw solutions for forward osmosis applications, J. Memb. Sci. 364 (2010) 233–241. https://doi.org/10.1016/j.memsci.2010.08.010.

[35] S.K. Singh, C. Sharma, A. Maiti, A comprehensive review of standalone and hybrid forward osmosis for water treatment: Membranes and recovery strategies of draw solutions, J. Environ. Chem. Eng. 9 (2021) 105473. https://doi.org/10.1016/j.jece.2021.105473.

[36] C.Y. Tang, Q. She, W.C.L. Lay, R. Wang, A.G. Fane, Coupled effects of internal concentration polarization and fouling on flux behavior of forward osmosis membranes during humic acid filtration, J. Memb. Sci. 354 (2010) 123–133. https://doi.org/10.1016/j.memsci.2010.02.059.

[37] C. Boo, S. Lee, M. Elimelech, Z. Meng, S. Hong, Colloidal fouling in forward osmosis: Role of reverse salt diffusion, J. Memb. Sci. 390–391 (2012) 277–284.

https://doi.org/10.1016/j.memsci.2011.12.001.

[38] T. Takahashi, M. Yasukawa, H. Matsuyama, Highly condensed polyvinyl chloride latex production by forward osmosis: Performance and characteristics, J. Memb. Sci. 514 (2016) 547–555. https://doi.org/10.1016/j.memsci.2016.04.012.

[39] J. Minier-Matar, A. Santos, A. Hussain, A. Janson, R. Wang, A.G. Fane, S. Adham, Application of Hollow Fiber Forward Osmosis Membranes for Produced and Process Water Volume Reduction: An Osmotic Concentration Process, Environ. Sci. Technol. 50 (2016) 6044–6052. https://doi.org/10.1021/acs.est.5b04801.

[40] W.Y. Chia, S.R. Chia, K.S. Khoo, K.W. Chew, P.L. Show, Sustainable membrane technology for resource recovery from wastewater: Forward osmosis and pressure retarded osmosis, J. Water Process Eng. 39 (2021) 101758. https://doi.org/10.1016/j.jwpe.2020.101758.

[41] X. Zhang, Q. Li, J. Wang, J. Li, C. Zhao, D. Hou, Effects of feed solution pH and draw solution concentration on the performance of phenolic compounds removal in forward osmosis process, J. Environ. Chem. Eng. 5 (2017) 2508–2514. https://doi.org/10.1016/j.jece.2017.03.030.

[42] T. Xiao, L.D. Nghiem, J. Song, R. Bao, X. Li, T. He, Phenol rejection by cellulose triacetate and thin film composite forward osmosis membranes, Sep. Purif. Technol. 186 (2017) 45–54. https://doi.org/10.1016/j.seppur.2017.05.047.

[43] P. Xu, J.E. Drewes, T.U. Kim, C. Bellona, G. Amy, Effect of membrane fouling on transport of organic contaminants in NF/RO membrane applications, J. Memb. Sci. 279 (2006) 165–175. https://doi.org/10.1016/j.memsci.2005.12.001.

[44] D. Yee, F. Ng, B. Wu, Y. Chen, Z. Dong, R. Wang, A novel thin film composite hollow fiber osmotic membrane with one-step prepared dual-layer substrate for sludge thickening, J. Memb. Sci. 575 (2019) 98–108. https://doi.org/10.1016/j.memsci.2019.01.007.

[45] M. Kawahigashi, H. Sumida, K. Yamamoto, Size and shape of soil humic acids estimated by viscosity and molecular weight, J. Colloid Interface Sci. 284 (2005) 463–469. https://doi.org/10.1016/j.jcis.2004.10.023.

[46] M. Cifuentes-Cabezas, C.M. Sanchez-Arévalo, J.A. Mendoza-Roca, M.C. Vincent-Vela, S. Álvarez-Blanco, Recovery of Phenolic Compounds from Olive Oil Washing Wastewater by Adsorption/Desorption Process, Sep. Purif. Technol. 298 (2022) 121562. https://doi.org/10.1016/j.seppur.2022.121562.

[47] E. Ferrer-Polonio, C. Carbonell-Alcaina, J.A. Mendoza-Roca, A. Iborra-Clar, S. Álvarez-Blanco, A. Bes-Piá, L. Pastor-Alcañiz, Brine recovery from hypersaline wastewaters from table olive processing by combination of biological treatment and

membrane technologies, J. Clean. Prod. 142 (2017) 1377–1386. https://doi.org/10.1016/j.jclepro.2016.11.169.

[48] M.R. Mayko, J. Lora-Garcia, M.F. López-Pérez, Experimental study and modeling of forward osmosis process for activated sludge concentration by using residual brine from a stuffed olive factory as draw solution, J. Water Process Eng. 21 (2018) 143–153. https://doi.org/10.1016/j.jwpe.2017.12.008.

[49] M.J. Luján-Facundo, J.A. Mendoza-Roca, J.L. Soler-Cabezas, A. Bes-Piá, M.C. Vincent-Vela, B. Cuartas-Uribe, L. Pastor-Alcañiz, Management of table olive processing wastewater by an osmotic membrane bioreactor process, Sep. Purif. Technol. 248 (2020) 117075. https://doi.org/10.1016/j.seppur.2020.117075.

[50] H.H. Salih, S.A. Dastgheib, Treatment of a hypersaline brine, extracted from a potential CO2 sequestration site, and an industrial wastewater by membrane distillation and forward osmosis, Chem. Eng. J. 325 (2017) 415–423. https://doi.org/10.1016/j.cej.2017.05.075.

[51] X. Zhang, Z. Ning, D.K. Wang, J.C. Diniz da Costa, Processing municipal wastewaters by forward osmosis using CTA membrane, J. Memb. Sci. 468 (2014) 269–275. https://doi.org/10.1016/j.memsci.2014.06.016.

[52] R. Valladares Linares, V. Yangali-Quintanilla, Z. Li, G. Amy, Rejection of micropollutants by clean and fouled forward osmosis membrane, Water Res. 45 (2011) 6737–6744. https://doi.org/10.1016/j.watres.2011.10.037.

[53] B. Mi, M. Elimelech, Chemical and physical aspects of organic fouling of forward osmosis membranes, J. Memb. Sci. 320 (2008) 292–302. https://doi.org/10.1016/j.memsci.2008.04.036.

[54] Q. She, X. Jin, Q. Li, C.Y. Tang, Relating reverse and forward solute diffusion to membrane fouling in osmotically driven membrane processes, Water Res. 46 (2012) 2478–2486. https://doi.org/10.1016/j.watres.2012.02.024.

V.6 Recovery of phenolic compounds from olive oil washing wastewater by adsorption/desorption process

Separation and Purification Technology
Volume 298, 1 October 2022, 121562

Recovery of phenolic compounds from olive oil washing wastewater by adsorption/desorption process

Magdalena Cifuentes-Cabezas [a], Carmen María Sanchez-Arévalo [a], José Antonio Mendoza-Roca [a, b], María Cinta Vincent-Vela [a, b], Silvia Álvarez-Blanco [a, b]

https://doi.org/10.1016/j.seppur.2022.121562

Abstract

Agroindustry wastewater represents an opportunity to recover high added value antioxidants such as phenolic compounds. An adsorption/desorption process was investigated to recuperate these compounds using Purolite non-ionic resins (MN200, MN202, PAD900 and PAD950). The study was conducted on a model solution containing 1.1 $g{\cdot}L^{-1}$ of tyrosol and 0.2 $g{\cdot}L^{-1}$ of catechin, which are two of the main phenolic compounds found in olive mill wastewaters, and with the olive mill wastewater. The main objective was to determine the optimal concentration of resin and the best desorption solvent for the maximum recovery of phenolic compounds. For it, the process kinetics were determined, and the adsorption mechanisms were characterized by means of isotherm models. Results showed that the pseudo-second order kinetic model fitted to the experimental data, while the Langmuir isotherm correctly modelled the adsorption process for the MN resins, whereas the Freundlich isotherm was the model that best described the adsorption process with PAD resins. A resin

concentration of 40 $g \cdot L^{-1}$ and a 50% v/v ethanol-water solution were selected as the best options for recovering the phenolic compounds. The tests with olive oil washing wastewater showed that, for some of the resins, other compounds present, such as sugars, interfered with the adsorption of phenolic compounds, reducing the effectiveness of their recovery. Finally, the MN200 resin was selected as the best adsorbent. It achieved a recovery of 91% of the phenolic compounds present in the initial wastewater, being only 5% of the initial sugars present in the final stream.

Keywords: adsorption; desorption; non-ionic resins; olive oil washing wastewater; phenolic compounds recovery.

1. Introduction

In recent years, plant-based functional foods are receiving a great attention due to their natural availability and therapeutic potential, paying special attention to the phytochemicals present in edible plants. Among them, phenolic compounds are the most numerous and widely distributed group of bioactive molecules [1]. The high antioxidant capacity of natural phenolic compounds is beneficial for health, since they reduce free radicals through enzymatic regulation, being of great help against cardiovascular diseases, diabetes, osteoporosis and neurodegenerative conditions, among other diseases [2-3]. These antioxidant compounds are also found in agro-food wastes from different sectors, such as olive mill wastewaters (OMW) [4], table olive processing wastewaters [5] and effluents from pickle manufacturing, wine industry and citrus processing [6], among others.

Several studies have been focused on the investigation, design, development and optimization of processes to achieve the concentration and purification of the phenolic compounds from these wastewaters, such as electrocoagulation [7], liquid/liquid extraction [8], cooling crystallization [9], ultrasound treatment [10] and adsorption [11]. Among all the physical methods, adsorption is considered as the most economical, simple and effective one [12].

Adsorption is a separation process where one or more components are attracted to the surface of a solid adsorbent when they are in contact. The nature of the interaction depends on the properties of the compounds involved. This phenomenon is superficial, and it is produced

by the action of forces on the surface of the adsorbent, which cause a net force normal to its surface. The adsorption process is composed of a series of interactions, including: mass transfer from the fluid phase to the external surface of the particle, pore diffusion in the solid phase, solute–solid interaction, hydrophobic and electrostatic attractions and hydrogen bonding [13]. The rate of the overall process can be controlled by one or several of these steps and it is dependent on the physico-chemical characteristics of the solute and adsorbent, particle size and affinities, and operating conditions. Equilibrium and kinetics information, as well as column operation parameters, are essential for practical operation [14].

Different materials have been tested as adsorbents for the selective adsorption of phenolic compounds, with activated carbon being the most used. However, the utilization of this material presents difficulties when the adsorbed compounds must be desorbed, being, the adsorption process very often irreversible [15]. Within synthetic adsorbents, resins are the most studied and used, due to their chemical stability, selectivity, adsorption capacity and low toxicity, which makes them very interesting for recovering compounds [14]. These resins have different characteristics that distinguish them, such as polarity, material, particle size, specific surface area, and pore diameter. In general, they are relatively low cost, easy to pre-process and recover, and suitable for large-scale production [16].

The objective of this work was to evaluate the adsorption and desorption capacity of four non-ionic commercial resins (MN200, MN202, PAD900 and PAD950 distributed by Purolite) in order to find the best one to selectively recover the phenolic compounds present in olive mill wastewater. Firstly, the resins were tested with a model solution with a high concentration of phenolic compounds to find the best dose to recover the antioxidant compounds. Then, with the selected resin dose, the performance of the resins was validated with a real wastewater from olive oil production (olive oil washing wastewater, OOWW) to observe the impact of other substances on the behaviour of the resins. Until now, few studies have been carried out on the recovery of value-added compounds from real OOWW by means of non-ionic resins, considering both (adsorption and desorption). On the other hand, to date only one study has been found using a mixture of ethanol/water at 50% v/v without acidification as a solvent for the desorption of phenolic compounds [17]. However, the objective of that study was to investigate the binary interaction between phenol and tyrosol by

comparing the behaviour of these with the resins separately, as with a binary solution. The study showed high desorption of tyrosol (94%) and phenol (85%), however it was not tested in real OMW. Another novelty of this work is the thorough characterization of the individual phenolic compounds adsorbed and desorbed by the resins.

2. Material and Methods

2.1 Model Solutions

The model solution was prepared with osmotized water and 1.3 $g \cdot L^{-1}$ of phenolic compounds. This concentration was selected to simulate a real olive oil washing wastewater, being within the range characterized in other studies [18-20]. The model solution included 1.1 $g \cdot L^{-1}$ of tyrosol (Maybridge, United Kingdom), representing the simple phenolic compounds of low molecular weight, and 0.2 $g \cdot L^{-1}$ of catechin (Sigma Aldrich, Germany), which represents the class of flavonoids, with higher molecular weight. As the wastewaters from olive oil production have a pH value between 4.5 and 5.5 [21], hydrochloric acid (J.T. Baker, The Netherlands) was added in order to obtain a pH close to 5.

2.2 Adsorption process

The aim of adsorption tests was to evaluate the influence of resin dosage on the adsorption of phenolic compounds. To this purpose, two Macronet^{TM} MN200 and MN202, and two Purosorb^{TM} PAD900 and PAD950 resins, supplied all by Purolite, were evaluated at different concentrations (10, 20, 30, 40, 50 and 60 $g \cdot L^{-1}$). The main physical properties of the resins are reported in Table 5.19. Before use, the resins were conditioned in a sodium hydroxide solution (2% w/v) for 60 minutes at 140 rpm. Then, they were washed twice with osmotized water for 5 min at the same speed.

Table 5.19. Main physical properties of the employed resins (data from supplier).

Resin	Matrix	*Surface area ($m^2 g^{-1}$)	*Pore diameter (Å)	*Pore volume (mL g^{-1})	Specific gravity	Particle size (mm)	Hydrophobicity
MN200	PS/DVB[1]	1100	700/15[#]	0.4	1.04	0.5-0.7	Moderate
MN202	PS/DVB[1]	950	220/15[#]	0.3	1.04	0.3-1.2	Moderate
PAD900	PDVB[2]	850	220	1.9	1.02	0.35-1.2	Moderate
PAD950	Polymethacrylic	450	120	0.6	1.1	0.35-1.2	Low

[1]PS/DVB: polystyrene crosslinked with divinylbenzene
[2]PDVB: Polydivinylbenzene
*measured by nitrogen adsorption
[#] macropores/micropores

The different doses of resin studied, indicated above, were mixed with 200 mL of model solution for 180 min at a constant stirring of 140 rpm at room temperature (21 ± 2°C). After adsorption, the liquid phase, which contains the fraction of non-adsorbed phenolic compounds, was separated from the solid matrix by filtration through a 0.2 μm membrane filter. Then, the concentration of total phenolic compounds (TPhC) was measured with the Folin–Ciocalteu (FC) method [22]. TPhC were expressed as tyrosol equivalents (Tyeq). All the adsorption experiments were carried out in a Flocculator "FLOC-6" jar test apparatus, supplied by RAYPA. The Adsorption efficacy (%Ads) related to total phenolic compounds was calculated as follow:

$$\%Ads = \frac{C_0 - C_e}{C_0} \cdot 100 \quad (1)$$

Being C_0 and C_e the initial and equilibrium concentrations of the TPhC in the solution, respectively. The adsorption capacity (q_t) for every resin concentration (C_r, $g \cdot L^{-1}$), at time *t* (min) was also calculated according to Equation 2:

$$q_t = \frac{C_0 - C_t}{C_r} \quad (2)$$

Where C_t is the concentration of TPhC in the solution at a given time. The equilibrium adsorption time was also calculated and the general models for adsorption kinetics were analysed (pseudo-first order kinetic model and pseudo-second order kinetic model). Data were

also plotted to find out whether they followed the behaviour of the Langmuir or Freundlich isotherms.

2.3 Pseudo-first and Pseudo- second order kinetic models

Kinetic parameters are useful for adsorption rate prediction, providing important information for designing and modelling the processes. For their determination, an assay was carried out following the same protocol described in the adsorption section (2.2). This time, 2 mL of each extract solution were withdrawn at time intervals of 1, 5, 10, 20, 30, 40, 60, 90, 120 and 180 min, to later determine their phenolic content. The tests were carried out for the different concentrations of resins considered. Then, two models were fitted to the experimental data to determine which best represents the process.

The Lagergren equation (Equation 3), better known as the pseudo first order kinetic equation [23], was the first model proposed to describe adsorption in a solid-liquid system, where the adsorption rate is based on the sorption capacity of the solids. The pseudo second order model [24] (Equation 4) indicates that the adsorption rate is proportional to the available sites on the sorbent surface. These two equations have been widely used to study adsorption from liquid solutions. The equations that describe these models are:

$$\ln(q_e - q_t) = \ln q_e - k_1 \cdot t \tag{3}$$

$$\frac{t}{q_t} = \frac{1}{k_2 \cdot q_e^2} + \frac{1}{q_e} \cdot t \tag{4}$$

Where q_e (mg·g^{-1}) is the amount of solute adsorbed per gram of adsorbent at equilibrium; k_1 (min^{-1}) is the pseudo first order rate constant and k_2 (g·mg^{-1}· min^{-1}) is the pseudo second order rate constant. For the determination of the constants, two graphics were plotted, one corresponded to *Ln* (q_e-q_t) versus time (t) and the other to t/q_t versus time (t). Then, performing a linear regression, it was possible to obtain q_e from each model as well as the model parameters.

2.4 Freundlich and Langmuir Isotherms

Adsorption isotherms describe the adsorption equilibrium of an adsorbate (phenolic compounds in this work) against a given dose of resin. The Langmuir model considers a monolayer adsorption with energetically identical sorption sites, where no interaction occurs

between the adsorbed molecules. Equation 5 presents the linear form of the Langmuir isotherm.

$$\frac{C_e}{q_e} = \frac{1}{k_L \cdot q_0} + \frac{1}{q_0} \cdot C_e \quad (5)$$

where q_0 ($mg \cdot g^{-1}$) is the maximum adsorption capacity and k_L is the Langmuir constant, which is obtained by the extrapolation of the analytical data.

On the other hand, the Freundlich model assumes a heterogeneous adsorption surface that is characterized by sorption sites at different energies. The linear form of the equation that represents the Freundlich isotherm corresponds to Equation (6).

$$\log q_e = \log K_f + \frac{1}{n} log C_e \quad (6)$$

where K_f ($(mg \cdot g^{-1})$ $(mg \cdot L^{-1})^{-1/n}$) and n are empirical coefficients. Kf is a measure of the adsorption capacity of the adsorbent and n is related to the adsorption intensity [25].

The isotherms were determined using the different resin concentrations tested. For this, $Ln\ q_e$ versus $Ln\ C_e$ and C_e/q_e versus C_e were plotted. Then, adjusting to a linear regression, it was possible to obtain each coefficient.

2.5 Desorption process

For the best dosage selected from the adsorption experiments, the subsequent recovery of the adsorbed phenols was carried out by a desorption process. Several studies have concluded that ethanol is one of the best solvents for the desorption of phenolic compounds from olive mill wastewater adsorbed onto resins [26-27], however, this carries a high cost. A study performed by Frascari et al. [28] showed that 50% v/v mixture of deionized water and ethanol, acidified with HCl until reaching a concentration of 2 $mol \cdot L^{-1}$ (pH -0.3), was the best option for the desorption of phenolic compounds from an ion exchange resin using OMW microfiltration permeate as feed. This acidification also entails an additional cost and could affect the equipment. No studies were found that used an ethanol/water mixture as a solvent without prior acidification to recover phenolic compounds and using non-ionic resins. In this way, the use of 50% v/v ethanol/water mixture without pH modification could lead to economical savings in comparison with the use of non-diluted ethanol.

After the adsorption tests, the resins were washed 3 times with osmotized water for 5 minutes at 150 rpm, then the resins were dried at 50°C for 3 hours. Then the two solvents, ethanol and a mixture of ethanol-water 50% v/v were tested in order to recover the highest amount of phenolic compounds. Absolute ethanol (H_3CCH_2OH, ≥ 99.5%) was purchased from VWR International. Resins were contacted with 100 mL of each solvent for 180 minutes at a constant rate of 140 rpm and room temperature (21 ± 2°C). After desorption, the resins were washed again under the same protocol mentioned above and were reused for the next test.

Apart from FC method, for the individual determination of each phenolic compound, liquid chromatography coupled to mass spectrometry (LC-MS) was used. To that end, it was employed a 1260 Infinity II LC chromatograph coupled to a 6546 quadrupole-time-of-flight (qTOF) mass analyzer (Agilent Technologies, USA) with an electrospray interface (ESI). A Zorbax Extend C18 column (4.6 x 100 mm, 1.8 μm) was used, operating at 40°C. The initial conditions for the mobile phases were set at the beginning of the analysis: 95% A and 5% B, where A was water and B was acetonitrile. Both mobile phases were acidified with a 0.5% of acetic acid. Afterwards, the following gradient was applied: 65% B at 12 min, 20% B at 14 min, 100% B at 18 min. That percentage was maintained during 3 minutes until 21 min of gradient program and then the initial conditions were reached in 3.5 minutes. A post-time for the re-equilibration of the column was set during 2.5 minutes. Injection volume was 10 μL and the flow rate was fixed at 1 mL/min.

The corresponding mass spectrometry conditions were described in Sánchez-Arévalo et al. (in press). Briefly, it was applied a capillary voltage of 3500V, nebulizer pressure of 30 psi and gas temperature of 200°C. In order to quantify the analytes, an external calibration was applied. To that end, standard solutions of tyrosol and catechin were prepared and diluted in ethanol/water 50:50 (v,v) in the range of 0.2 – 50 $g \cdot mL^{-1}$.

In addition, the concentration of total phenols in the liquid phase was measured to calculate the equilibrium desorption time. The desorption ratio (%Des), that is, desorption percentage of phenolic compounds from the total adsorbed, and adsorption-desorption recovery (%R) of phenolic compounds from the initial feed were calculated according to equation 7 and 8, respectively.

$$\%Des = \frac{C_d \cdot V_d}{(C_o - C_e) \cdot V_o} \cdot 100 \quad (7)$$

$$\%R = \frac{C_d \cdot V_d}{C_0 \cdot V_0} \cdot 100 \quad (8)$$

where, C_d is the concentration of TPhC (mg·L^{-1}) in the desorption solution, and V_d and V_0 are the volume of the desorption solution (solvent) and that of the initial feed (model solution) (mL), respectively.

2.6 Test with olive oil washing wastewater

Once the optimal dose of resin for the adsorption of phenolic compounds and the best solvent for their desorption were determined, the test was replicated with pre-treated olive oil washing wastewater (OOWW) (following the protocol reported in [20]). The samples were provided by an olive oil milling plant located in the Valencian Community (Spain) and were collected during the 2020 olive oil production campaign. The OOWW corresponds to the residual water obtained at the exit of the vertical centrifuge after the olive oil washing step from a continuous two-phase olive mill. The same procedures indicated above were followed for the determination of adsorption and desorption efficiency. The determination of adsorption kinetics of the process was also carried out. Regarding the characterization of the supernatant after the adsorption process, in addition to the phenolic compounds, the sugar content and the chemical oxygen demand (COD) were also determined. For the determination of sugars concentration, the Sucrose/D-Glucose/D-Fructose colorimetric kit from r-biopharm (Germany) was employed, using glucose (Panreac, Spain) as a standard. For COD measurement, commercial kits supplied by Merck (Germany) were used. The phenolic compounds in the raw OOWW and from the desorption tests were determined with the LC-MS procedure described in the previous section. In this case, for the external calibration, standard solutions of citric acid, hydroxytyrosol, tyrosol, caffeic acid, *p*-coumaric acid, oleuropein, oleacein and dihydroxy-octadecanoic acid were prepared and diluted in ethanol/water 50:50 (v/v) in the range of 0.2 – 50 g·mL^{-1}.

For the adsorption and desorption percentage of sugars and COD, equations 1 and 7 were used. In this case, C_0 and C_e were the initial and equilibrium concentrations of sugars or COD in the feed solution, respectively; C_d was the concentration of sugars or COD in the

desorption solution. All tests for both model solution and real wastewater were performed in triplicate.

3. Results and discussion

3.1 Tests with model solution

3.1.1 Adsorption capacity

Table 5.20 shows the adsorption of phenolic compounds for the different resins and dosages. The values correspond to the mean value together with the standard deviation. It can be seen that the highest adsorption percentage was achieved with the highest resin dosage ($60 g \cdot L^{-1}$). As expected, this behaviour was observed for all the resins, which is mainly due to an increase in the number of available adsorption sites by increasing the surface area of the adsorbent [29].

Table 5.20. Adsorption of phenolic compounds for the different resins and dosages after 180 minutes treatment of the model solution.

		Resin			
Dosage ($g \cdot L^{-1}$)	$TPhC._{ads}$	MN200	MN202	PAD900	PAD950
10	% Ads	78.73 ± 1.43	59.88 ± 1.40	55.42 ± 0.42	51.66 ± 2.81
	$mgTyeq \cdot L^{-1}$	1001.35 ± 16.02	761.53 ± 15.26	704.89 ± 4.75	657.01 ± 31.29
20	% Ads	91.79 ± 0.94	70.28 ± 2.84	60.05 ± 0.54	59.23 ± 0.79
	$mgTyeq \cdot L^{-1}$	1167.34 ± 10.37	893.89 ± 29.12	763.71 ± 5.96	758.81 ± 7.93
30	% Ads	94.24 ± 0.48	80.08 ± 2.11	67.61 ± 1.03	59.83 ± 1.08
	$mgTyeq \cdot L^{-1}$	1198.54 ± 5.30	1018.52 ± 23.13	859.88 ± 11.45	760.91 ± 11.59
40	% Ads	95.68 ± 0.60	91.43 ± 1.06	74.23 ± 2.57	63.84 ± 1.43
	$mgTyeq \cdot L^{-1}$	1209.34 ± 7.57	1162.82 ± 13.43	944. 08 ± 33.59	811.98 ± 9.09
50	% Ads	97.52 ± 0.09	91.81 ± 1.38	74.80 ± 0.46	63.57 ± 0.62
	$mgTyeq \cdot L^{-1}$	1240.33 ± 1.09	1167.60 ± 14.23	954.36 ± 3.08	812.27 ± 5.07
60	% Ads	98.28 ± 0.05	93.07 ± 1.50	74.18 ± 1.42	64.71 ± 0.64
	$mgTyeq \cdot L^{-1}$	1249.89 ± 0.54	1183.64 ± 15.07	953.05 ± 8.21	826.42 ± 6.06

TPhC.ads= Total phenolic compounds adsorbed from the initial feed solution
%Ads= adsorption percentage of total phenolic compounds from the initial feed solution
$mgTYeq.L^{-1}$= total phenolic compounds adsorbed in milligram tyrosol equivalents per liter of sample

However, as the resin dose increases, the adsorption percentage showed less variation, with the PAD resin exhibiting practically similar adsorption percentage values at the three highest resin concentrations. Although the four resins achieved good adsorption percentages, the MN resins were able to retain the phenolic compounds almost completely, achieving percentages greater than 90% in some tests. The good performance of MN resins was also observed in studies performed by other authors. De Marco [30] showed that the MN202 resin was capable of retaining 99% of the phenolic compounds present in a vegetation water from the olive oil extraction process. The MN200 resin was tested by Ferrer-Polonio [31] in order to separate phenols from fermentation brines from table olive processing, achieving phenols removal efficiencies higher than 90% with resin concentrations of 20 and 40 $g \cdot L^{-1}$.

The high adsorption percentage of the MN resins can be explained by their higher surface area (1100 – 950 $m^2 \cdot g^{-1}$) compared to the PAD resins (850-450 $m^2 \cdot g^{-1}$). However, the MN202 and PAD900 resins present similar surface area (950 and 850 m2·g−1, respectively), but the former resin material could have a higher affinity with the analysed phenolic compounds, providing greater adsorption ability. The MN202 has a hypercrosslinked polystyrene polymeric matrix with polymeric chains separated by long, homogeneously distributed, rigid bridges. This allows the bridges to remain permanently exposed to the gaseous or liquid medium, generating a greater attraction of organic compounds [32]. In particular, adsorption interaction mechanism depends on intrinsic characteristics of the resin such as surface area, pore volume, pore size and functional groups of the adsorbent surface [33]. Furthermore, the MN resins have two types of pores, micropores (in the range of 10 to 30 Å), which are responsible for the adsorption of small molecules, and macropores which act as “transport channels” that ensure the diffusion of small to large molecules through the resin. This could allow better adsorption of tyrosol and catechin onto MN202 resin than onto PAD900 resin.

The low adsorption capacity of PAD950 resin may be due to its small pore diameter (120 Å). Buran et al. [34] studied the separation of blueberry polyphenols and anthocyanins using different cross-linked aromatic polymeric resins. These authors observed that the resin with the highest surface area had the lowest adsorption capacity, due to its very small pore envelope. It can be also explained considering the ma- trix, since this resin is the only one with

an aliphatic matrix with the lowest hydrophobicity. The MN and PAD900 resins are aromatic ad- sorbents with polystyrene- divinylbenzene (DVB) matrix, while the PAD950 resin is a polymethacrylic adsorbent. Valderrama et al. [35] reported that polystyrene-DVB adsorbents, including hypercrosslinked polystyrene, usually have a very hydrophobic surface, exhibiting a high affinity for solutes such as phenol or aniline with phenyl groups. In addition, the matrix of the PAD950 resin presents greater affinity for aliphatic or semi aliphatic molecules than for aromatic ones. Different results were obtained by Silva et al. [36], who tested different resins for the adsorption of polyphenols from Inga edulis leaves. These authors found that the XAD-7 resin, made of an acrylic polymeric material (similar to the PAD950 used in this study), presented the best results in terms of adsorption capacity compared to the other resins based on styrene–divinylbenzene (similar to MN and PAD900 resins). It is important to note that these authors also pointed out that the use of the same resins for other phenolic extracts could lead to completely different results, concluding that the chemical nature of the adsorbent had more influence than its physical structure (surface area) on phenolic compounds adsorption.

3.1.2 Kinetics of phenol adsorption

Fig. 5.46 shows the amount of total phenolic compounds adsorbed per gram of resin during the adsorption process for all resins and concen- trations tested. It can be seen that during the first minutes the adsorption was very fast, because all the active adsorption sites on the resin were available. Then, adsorption slowed down due to a decrease in the adsorption sites available, achieving finally the equilibrium.

As expected, initial adsorption was faster as resin concentration increased, reaching the equilibrium earlier. Furthermore, the adsorption kinetics showed that, in general terms, the amount TPhC absorbed did not significantly vary after 30 min. For the lowest resin concentration tested, the MN200 resin showed a higher amount of phenolic com- pounds adsorbed per gram of resin compared to the other resins. On the other hand, the PAD950 resin presented the lowest amount of phenolic compounds adsorbed in all the tests carried out, confirming the results of section 3.1.1. Regarding the contact time, the MN200 resin was the one that achieved the equilibrium in the shortest time, followed by the PAD900 resin.

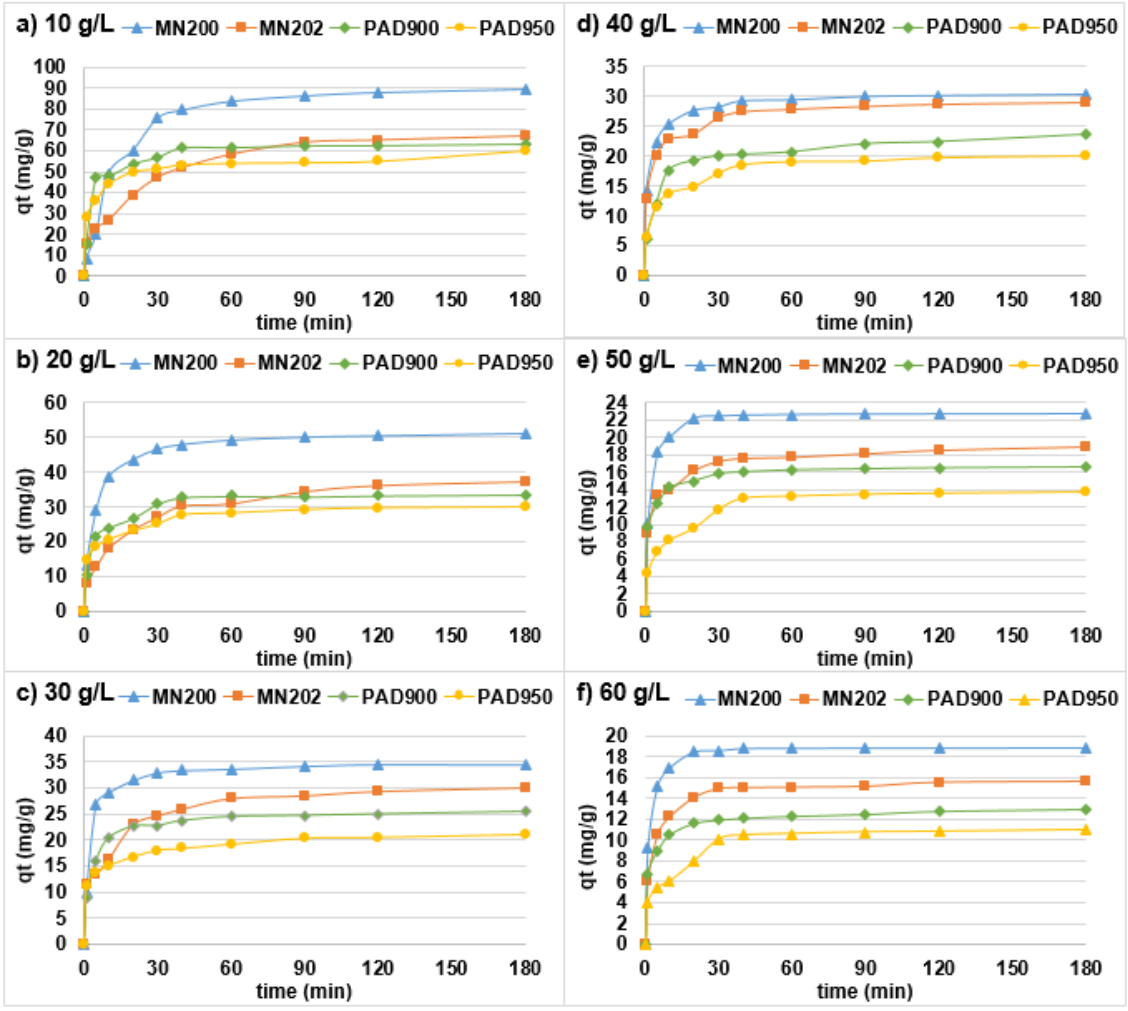

Fig. 5.46 Variation of the amount of phenolic compounds adsorbed with time for all the resins, using the model solution and different resin dosages: a) 10 gL^{-1}, b) 20 gL^{-1}, c) 30 gL^{-1}, d) 40 gL^{-1}, e) 50 gL^{-1} and f) 60 gL^{-1} (results expressed in mg of tyrosol equivalents per gram of resin)

The analysis of the adsorption process based on kinetic models is presented in Table 5.21. It can be seen that the qe values obtained by the pseudo-second order model are very close to the experimental ones (Fig. 5.46), indicating a good approximation of the experimental adsorption data to this model. On the other hand, the pseudo-first order model yielded very low qe values, being in some cases incoherent and far from those obtained experimentally. As can be seen, the pseudo-second-order model pro- vided the best correlation for the phenols

adsorption (obtaining an r^2 close to 1). This infers that the adsorption rate depends on the adsorption capacity and not on adsorbate concentration [37]. This behaviour was also observed by other authors [16,38], which supports the affir- mation that this kinetic model is characteristic of phenolic compounds.

Table 5.21. Kinetic parameters for the adsorption of phenolic compounds on the different resins for the tests carried out with the model solution

		Pseudo-first-order			Pseudo-second-order		
Resin	dosage ($g \cdot L^{-1}$)	qe ($mg \cdot g^{-1}$)	k1(min^{-1})	r^2	qe ($mg \cdot g^{-1}$)	k2($g \cdot mg^{-1} \cdot min^{-1}$)	r^2
MN200	10	64.593	0.0385	0.9676	94.340	0.0012	0.9947
	20	29.973	0.0611	0.9741	51.813	0.0066	0.9997
	30	13.125	0.0513	0.8758	34.843	0.0172	0.9999
	40	13.197	0.0627	0.8805	30.675	0.0195	0.9999
	50	15.749	0.1823	0.9873	22.831	0.0573	0.9999
	60	10.710	0.1575	0.9459	18.939	0.0783	1
MN202	10	63.092	0.0432	0.9867	70.423	0.0014	0.9921
	20	27.268	0.0323	0.9669	38.610	0.0028	0.9943
	30	18.495	0.0392	0.9516	30.581	0.0060	0.9979
	40	12.929	0.0452	0.9122	29.326	0.0138	0.9996
	50	8.429	0.0577	0.9458	19.011	0.0202	0.9994
	60	5.384	0.0476	0.7800	15.748	0.0322	0.9997
PAD900	10	26.486	0.0469	0.9148	64.103	0.0062	0.9996
	20	18.666	0.0636	0.9240	34.130	0.0109	0.9994
	30	11.345	0.0504	0.9178	25.575	0.0157	0.9996
	40	11.127	0.0323	0.9101	23.641	0.0094	0.9978
	50	7.183	0.0774	0.9448	16.639	0.0437	0.9999
	60	4.897	0.0554	0.9280	12.987	0.0360	0.9996
PAD950	10	22.495	0.0539	0.9083	58.824	0.0047	0.9966
	20	16.188	0.0424	0.9528	30.488	0.0090	0.9988
	30	10.205	0.0375	0.9626	21.186	0.0129	0.9986
	40	10.944	0.0457	0.9119	20.325	0.0124	0.9988
	50	10.360	0.0624	0.9829	14.045	0.0158	0.9982
	60	8.685	0.0771	0.9666	11.211	0.0216	0.9982

3.1.3 Adsorption isotherms

Table 5.22 summarizes the parameters and correlation coefficients when data were fitted to the Freundlich and Langmuir isotherms. According to the r^2 values obtained, the Langmuir model was the most appropriate for the MN resins, while the Freundlich model showed the best fit to the data of the PAD resins. It is important to note that the Langmuir model did not provide consistent values for PAD resins. The fact that the experimental data of the MN resins fit best the Langmuir equation indicates a homogeneous nature of the adsorbent surface [39]. On the contrary, the PAD resins presented a heterogeneous surface or surfaces with sites of varied affinities, which is confirmed by the fitting to the Freundlich isotherm [38].

Table 5.22. Isotherm parameters for total phenolic compounds adsorption for all the tests carried out with the model solution

	Langmuir				Freundlich		
Resin	k_L ($L \cdot mg^{-1}$)	q_o ($mg \cdot g^{-1}$)	R_L	r^2	k_f $(mg \cdot g^{-1}) \cdot (mg \cdot L^{-1})^{-1/n}$	1/n	r^2
MN200	0.0043	163.93	0.19	0.9955	1.41	0.75	0.9787
MN202	0.0015	136.99	0.38	0.9971	1.14	0.64	0.9411
PAD900	n.c.	n.c.	n.c.	n.c.	5746.23	2.03	0.9742
PAD950	n.c.	n.c.	n.c.	n.c.	792.27	3.31	0.9634

n.c. = not calculated (since the model did not fit properly the experimental data)

The dimensionless equilibrium parameter R_L was calculated for the MN resins. This parameter is related to the K_L parameter (obtained with Langmuir model) through equation (7):

$$R_L = \frac{1}{1+K_L+C_0} \quad (7)$$

When $R_L = 0$, it is considered that the adsorption is irreversible, when $0 < R_L < 1$ the adsorption is favourable and when $R_L > 1$ it is unfavourable. Both MN resins presented a value of R_L that corresponds to favourable adsorption of phenolic compounds. MN200 resin had the lowest R_L, which means that it presents the best adsorption conditions. This agrees with the results of adsorption percentages, where the MN200 resin showed the highest adsorption of

total phenolic compounds (Table 5.20). On the other hand, in the Freundlich model, the values of 1/n are related to the adsorption intensity, being the adsorption favourable if they are lower than 1 [13]. Although the data of PAD resins fit the Freundlich model, the operating conditions tested were not very appropriate for adsorption, as the 1/n values were greater than 1. On the other hand, the MN resins presented 1/n values between 0.64 - 0.75, indicating a favourable adsorption. The results also indicated that the PAD900 resin presented a significant higher adsorption capacity than the PAD950 resin due to the higher k_f value, which is a parameter related to the adsorption capacity [39].

3.2 Desorption

The adsorption tests showed that the adsorption of phenolic compounds did not present great variation when the resin concentration increased from 40 to 60 $g \cdot L^{-1}$. Therefore, it was decided to select the concentration of 40 $g \cdot L^{-1}$ as the optimal one for the recovery of phenolic compounds, taking into account that the cost of increasing the resin concentration from 40 to 60 $g \cdot L^{-1}$ does not entail a measurable increase in the adsorption efficiency of these compounds. For this reason, it was decided to analyse the desorption of phenolic compounds for the resin dose of 40 $g \cdot L^{-1}$. Fig. 5.47 shows the desorption kinetics for two different eluents.

No significant variations were observed in the desorption process for times greater than 1 hour. It can be seen that the PAD950 resin was the one that presented the highest desorption percentages with both solvents tested, followed by the MN202 resin. On the other hand, the 50% v/v ethanol/water solution presented better desorption performance than pure ethanol, which was observed for all the tested resins, as the desorption equilibrium was reached earlier (at 40 minutes) and higher desorption percentages were obtained.

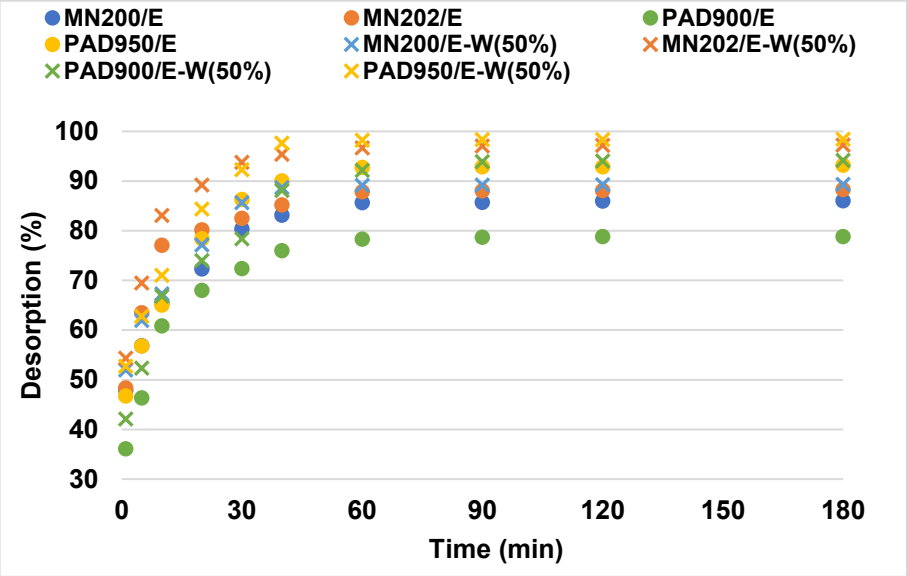

Fig. 5.47 Desorption kinetics from previously saturated resins (dosage of 40 $g \cdot L^{-1}$) using ethanol (/E) and a 50% v/v mixture of ethanol/water (/E-W(50%)) as eluents. (Results for the model solution).

The resins presented high percentages of desorption with both tested solvents, with values greater than 78%, reaching in some cases values larger than 90%. For the pure ethanol solvent, the PAD950 resin was the one that presented the highest desorption value, with 93.18%, while the PAD900 resin presented the lowest percentage (78.85%). For the ethanol-water mixture, all the resins presented desorption values over 90%. Again, the PAD950 resin had the highest desorption value (98.37%), being 5% higher than that with pure ethanol. Although the MN200 resin was the one with the lowest desorption percentage (92.74%) with the ethanol/water mixture, its percentage increased by around 7% in comparison with the results obtained with pure ethanol. The PAD900 resin was the one that presented the greatest increase in desorption, from 78.86% with ethanol to 94.18% with the ethanol/water mixture. Taking into account the results displayed in fig. 2, the ethanol/water 50% v/v mixture appears to be the best eluent for the recovery of phenolic compounds for all the tested resins. In addition, from an economic point of view, it is much more profitable (0.36 euros savings per test).

Within the non-ionic resins, the most often used for the recovery of phenolic compounds from OMW is Amberlite XAD16. Although good adsorption percentages of phenolic compounds with this resin have been published (greater than 80% in some cases), the percentage of desorption approached 50% [40]. Another study for the recovery of phenols from OMW, carried out by Ferri et al. [41], achieved adsorption/desorption percentages of 76% and 96%, respectively. In this case, the ENV+ was the best option for the entire process with acidified ethanol as eluent. A similar desorption percentage was observed by Caetano et al. [42] with the MN200 resin. Although, when they evaluated different resins (MN200, Dowex XZ and AuRIX 100) to remove phenols from an aqueous solution, the MN200 resin did not present the best adsorption percentages, it was the one that showed the highest recovery of phenolic compounds (90%) when using a methanol/water solution as a solvent.

Table 5.23 summarizes the results of the adsorption/desorption process when ethanol/water (50% v/v) solution was used as desorption solvent. Considering the entire process adsorption/desorption, the MN resins presented much higher adsorption percentages than the PAD resins, and globally showed the highest recovery of phenolic compounds from the model wastewater (which was 28 mgTyeq per gram of resin). It is important to emphasize that all the resins were used several times to determine the repeatability of the results. The resins did not lose their properties against the adsorption of phenolic compounds after three adsorption cycles.

Table 5.23 Summary table of adsorption/desorption process using a dosage of 40 gL^{-1} of resin and ethanol/water 50% solution as desorption solvent for the model solution

Resin	% Ads.	% Des	% R	mgTyeq/g resin*
MN200	95.68 ± 0.60	92.74 ± 0.05	88.73 ± 0.04	28.21 ± 0.01
MN202	91.43 ± 1.06	96.99 ± 1.57	88.68 ± 1.43	28.19 ± 0.46
PAD900	74.23 ± 2.57	94.18 ± 4.27	69.90 ± 4.45	22.23 ± 1.42
PAD950	63.84 ± 1.43	98.37 ± 2.09	62.81 ± 1.96	19.97 ± 0.62

%Ads= adsorption percentage of phenolic compounds from the initial feed solution
%Des= desorption percentage of phenolic compounds from the total phenolic compounds adsorbed
%R=recovery percentage of phenolic compounds from the initial feed solution
*mgTyeq/g resin: recovered mg of total phenolic compounds in the final solution after desorption per grams of resin used

To detect the specific concentration of catechin and tyrosol in the desorption solution, liquid chromatography coupled to mass spectrometry analyses were performed on the desorption samples obtained with the 50 % ethanol/water solution. This study was carried out with the objective of analysing the affinity of the resins with the two different compounds present in the model solution.

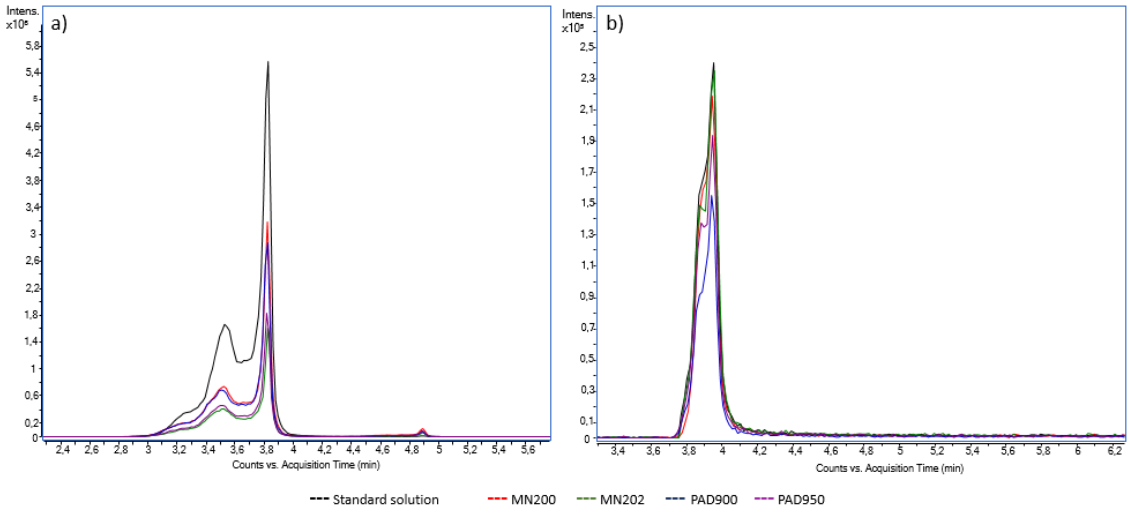

Fig. 5.48. Chromatogram of the desorption solution when 50% v/v ethanol/water mixture was used as eluent for the most efficient adsorption conditions (40 g/L of resin using the model solution). a) catechin b) tyrosol

Fig. 5.48 shows the chromatograms of the samples from the desorption process with ethanol/ water mixtures for the two phenolic compounds. In both cases, the black line represents the standard solution. As expected, all the resins showed desorption of both compounds. Catechin desorption sequence was MN200>PAD900>PAD950>MN202, while for tyrosol the sequence was MN202>MN200>PAD950>PAD900 (from the highest concentration in the sample to the lowest one). The concentration sequence observed for tyrosol followed the trend shown in table 5, where the MN resins provided a higher concentration of desorbed phenolic compounds compared to PAD resins. This result was expected since the model solution had a higher concentration of tyrosol than catechin.

Regarding the desorption of catechin, the MN200 resin showed the largest desorption percentage (99.4% tyrosol and 96.6% catechin). However, greater concentration of this compound was observed in the samples from PAD900 resins in comparison with those from the MN202 resin. After desorption from the MN202 resin, 30% of the catechin present in the initial model solution (59.72 ppm) was recovered, while in the case of the PAD900 resin the amount present in the desorption solution corresponded to 88 % of the catechin in the initial model solution (175.06 ppm). The PAD950 resin presented a similar behaviour to the MN202, desorbing only 35.5% of catechin from the initial total in the model solution. Therefore, these resins could have a higher affinity for catechin (flavonoids, large compounds) compared to tyrosol (simple phenol, smaller compounds), adsorbing it but not allowing desorption.

3.3 Tests with OOWW

3.3.1 Adsorption process

Once it has been shown that the resins were capable of adsorbing phenolic compounds and desorbing them almost entirely, it was studied whether the presence of other compounds could affect the performance of these adsorption resins. It has been reported that the adsorption yields of phenolic compounds can be affected by competitive adsorption and, at the same time, by the interaction among them [43].

Table 5.24. Characterization of pre-treated olive oil washing wastewater (OOWW)

Parameter	Pre-treated OOWW
pH	5.18 ± 0.05
Conductivity ($mS \cdot cm^{-1}$)	4.36 ± 0.03
COD[a] ($mgO_2 \cdot L^{-1}$)	27208.5 ± 341.2
TPhC[b] (mg tyrosol eq.$\cdot L^{-1}$)	1440.01 ± 11.81
Sugars (mg glucose $\cdot L^{-1}$)	1491.20 ± 21.12
%Sug $_{Glu}$[c]	59.64
%Sug $_{Fruc}$[d]	22.31
%Sug $_{Suc}$[e]	18.04

[a] COD: chemical oxygen demand
[b] TPhC: Total phenolic compounds
[c] %SugGlu: percentage of glucose with respect to total sugars
[d] %SugFruc: percentage of fructose with respect to total sugars
[e] %SugSuc: percentage of sucrose with respect to total sugars

Before starting the adsorption tests, pre-treated OOWW was characterized. It can be observed in table 5.24 that, apart from a high concentration of phenolic compounds, OOWW had a high organic load and a significant presence of sugars. These characteristics, together with an acidic profile, are typical of the wastewaters coming from the oil mills [20]. With regards to sugars, glucose and fructose are the ones at the highest concentrations. This was expected since these monosaccharides are the main sugars in most fruits [44]. Another fact to take into account is that the concentration of phenolic compounds is similar to that of the model solution used in the adsorption/desorption study.

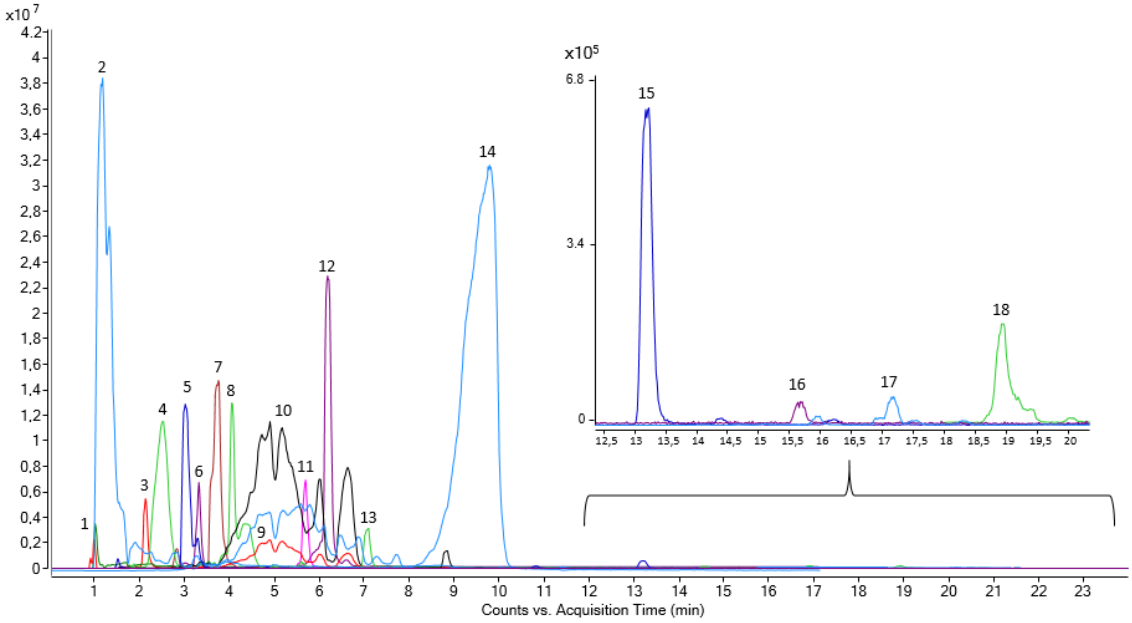

Fig 5.49. Chromatogram of detected compounds in OOWW by LC-ESI-qTOF-MS. The number correspond to the compound presented in table 7

In addition, the identification of the specific phenolic compounds present in the sample was carried out. More than twenty-five phenolic compounds were found, of which 13 could be identified. Fig. 5.49 shows 18 identified compounds, including organic acids, simple phenols, phenolic acids, secoiriodoids, flavonoids and fatty acids derivatives. The aldehydic form of decarboxymethyl elenolic acid, dihydroxy-hexadecanoic acid and dehydroxy-octadecatrienoic acid were also found, although they are not visible in the chromatogram due to the scale.

Table 5.25 contains the concentrations of all identified compounds. The concentration of the phenolic compounds in the sample may be influenced by several factors [45], such as the olives cultivar area, the technological details of the olive processing, and the climate conditions, among others. Additionally, the analytical procedure and quantification methodology should be considered when exploring this quantitative data.

Table 5.25. Concentration of the detected compounds in OOWW by LC-ESI-qTOF-MS

	Detected Compound	Rt (min)	ppm	SD
1	Malic acid	1.02	7.96	0.015
2	Citric acid	1.19	353.47	0.491
3	Quinic acid	1.01	149.25	0.153
4,8	hydroxy-decarboxymethyl elenolic acid (isomer 1+2)	3.95	40.44	0.007
5	hydroxytyrosol glucoside	3.02	1.70	0.004
6	hydroxytyrosol	3.30	1.15	0.000
7	acyclodihydroelenolic acid hexoside	3.95	86.84	0.010
9	tyrosol	5.90	529.62	0.927
10	hydroxy-elenolic acid	5.91	18.64	0.050
11	gallocatechin	5.70	2.52	0.001
12	decarboxymethyl elenolic acid	6.21	174.56	0.159
13	p-coumaric acid	7.08	0.91	0.000
14	elenolic acid	9.79	17.52	0.310
15	luteolin	13.23	0.07	0.017
16	apigenin	15.70	0.30	0.075
17	trihydroxy-octadecadienoic acid	17.20	1.05	0.001
18	trihydroxy-octadecenoic acid	18.82	0.49	0.071
19	Aldehydic form of decarboxymethyl elenolic acid	7.10	1.35	0.005
20	dihydroxy-hexadecanoic acid	19.83	0.25	0.000
21	dehydroxy-octadecatrienoic acid	22.95	0.15	0.001

It can be seen that the measured phenolic compounds encompass different classes of compounds, being secoiridoids the most abundant family. This chemical class includes biomolecules with relevant antibacterial properties [46]. Simple phenols were the compounds at the highest concentrations (61%), being tyrosol and hydroxytyrosol among them. These compounds have been recognized as antioxidant, anti- inflammatory and antimicrobial, with promising applications in cos- metics, food, and medical areas [47,48]. Phenolic acids and

flavonoids, whose antioxidant properties are also of interest, were found in the OOWW as well [49].

Fig. 5.50 shows the adsorption of phenolic compounds from OOWW by the selected resins. It can be seen that, as for the model solution, during the first minutes the adsorption is faster. After ten minutes of testing, a high adsorption is already observed. Then, the increase becomes less abrupt. However, comparing with the model solution, it takes more time to reach an equilibrium, i.e. after 90 minutes. Regarding the behaviour of the resins, a similar but more pronounced trend was observed. Clearly, the results were better for the MN200 resin in comparison with those yielded by the other resins, while the PAD900 had the worst performance. Regarding the mass of phenolic compounds adsorbed by the resin, MN202 and PAD900 resins decreased their yield compared to that obtained with the model solution. Therefore, it can be inferred that, for these resins, there were compounds in the wastewater that interfered with the adsorption of phenolic compounds. This was expected since the presence of various adsorbates in solution can generate competition for active site effects, which lead to a worse adsorption of the target compounds [50].

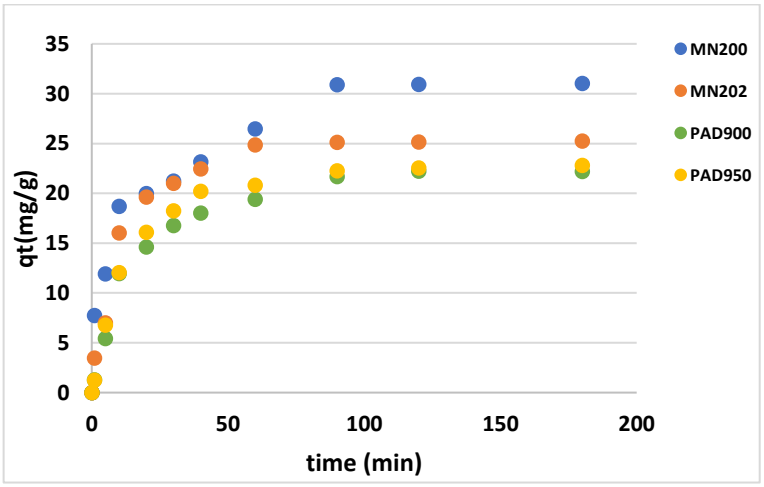

Fig. 5.50 Mass (mg) of total phenolic compounds from olive oil washing wastewater absorbed per gram of resin over time for all resins tested at a dose of 40 g/L

The use of OOWW produced a delay in the adsorption process, multiplying by three the equilibrium time compared to that measured with the model solution, where equilibrium was reached after half an hour of contact time.

Another aspect to highlight is that the pH of the OOWW was not modified for the tests. This is a factor to be taken into account since the pH has an important effect on the adsorption of phenolic compounds [51]. Frascari et al. [28] compared five resins (four neutral and one ion exchange resin, three of them with the same matrix (microporous styrene-divinylbenzene) as the resins used in this work), for the recovery of phenolic compounds from OMW. For the neutral resins, they reported a decrease in the absorbed percentage when pH increased, so they decided to work at the natural pH of the OMW (pH=4.2). Caetano et al. [42] also tested different resins for the recovery of phenolic compounds from aqueous solution. They reported that, in the case of the non-functionalized resin, under acidic conditions (pH = 3), greater adsorption capacities were measured than under alkaline conditions (pH = 11). This indicates a preference for the molecular form of phenol over phenolate, which involves an increase in electrostatic repulsion. Therefore, it should be emphasized that the analysed resins presented a good performance of adsorption of phenolic compounds without varying the feed pH.

Table 5.26. Kinetic parameters of adsorption of phenolic compounds from olive oil washing wastewater

Resin	dosage ($g \cdot L^{-1}$)	q_e (exp.) ($mg \cdot g^{-1}$)	Pseudo-first-order			Pseudo-second-order		
			q_e ($mg \cdot g^{-1}$)	$k_1 \cdot 10^{-2}$ (min^{-1})	r^2	q_e ($mg \cdot g^{-1}$)	$k_2 \cdot 10^{-3}$ ($g \cdot mg^{-1} min^{-1}$)	r^2
MN200	40	30.946	34.726	5.70	0.831	30.362	3.595	0.9918
MN202	40	25.163	15.331	7.95	0.926	26.316	6.055	0.9966
PAD900	40	22.035	19.939	4.17	0.968	23.866	3.600	0.9932
PAD950	40	22.540	20.206	4.65	0.981	23.213	4.234	0.9944

Regarding the adsorption kinetics of phenolic compounds, it can be seen in Table 5.26 that again, the pseudo-first order model did not provide consistent data on the solute adsorbed per gram of sorbent at equilibrium, with values below those experimentally obtained. As in

the model solution, the pseudo second order model was the one that most accurately fitted to the experimental data of adsorption of phenolic compounds. Pseudo-second order kinetics indicates that the process is dominated by adsorption on active sites, so it is the best fitting model when the adsorbent has many active sites [52]. Previously, it was commented that the amount of adsorbed phenolic compounds for some of the resins was smaller than in the case of the model solution. It can also be observed that the experimental q_e value was approximately 12% lower for the MN202 resin and 6% lower for the PAD900 resin than the values experimentally obtained with simulated water (28.74mg·g^{-1} vs 25.16 mg·g^{-1} and 22.68 vs 22.03 mg·g^{-1}, respectively). This shows the existence of other compounds that occupy adsorption sites on the resins, thus reducing the separation efficiency of phenolic compounds. The MN200 resin, however, did not present significant variation (+2%) in the experimental q_e compared to that obtained with the simulated wastewater; the PAD950 resin showed an improvement in the performance, with a q_e 10% higher than that obtained with the simulated solution. This may be due to the compounds present in each sample. The model solution only presents one type of flavonoid and simple phenol, while the OOWW presents a variety of phenolic compounds, which can have more affinity with the PAD950 resin. Thus, it has been reported in the bibliography that PAD950 resin presents high adsorption capacity for phlorotannins [38], a type of tannin present in seaweed Sargassum muticum. It has been reported the presence of tannins in OOWW [53], which could explain the higher PAD950 adsorption

In order to find out whether sugars and COD (which includes the rest of organic compounds in OOWW in addition to sugars and TPhC) interfered the phenolic compounds adsorption, the theoretical COD of the adsorbed phenols ($COD_{PhC.ads}$) and sugars ($COD_{Sug.ads}$) was calculated. This parameter was calculated following the correlation proposed by [31]. As total phenols are expressed in mgTYL^{-1} and 1 mol of tyrosol requires 9.5 mol of O_2 for its oxidation, 2.2mg O_2 per mg of tyrosol are needed. In the case of glucose, 1 mole of glucose needs 6 mol of O_2 for its oxidation, i.e. 1.1mg O_2 per mg of glucose. Thus, the equations used for the calculation were the following:

$$COD_{PhC.ads} = (C_{0.PhC} - C_{e.PhC}) \cdot 2.2 = C_{PhC.ads} \cdot 2.2 \quad (8)$$

$$COD_{Sug.ads} = \left(C_{0.Sug} - C_{e.Sug}\right) \cdot 1.1 = C_{Sug.ads} \cdot 1.1 \quad (9)$$

Being $C_{0.PhC}$ and $C_{0.Sug}$ the initial concentration of total phenols and sugars, respectively, and $C_{e.PhC}$ and C_{eSug} the concentration of total phenols and sugars, respectively, in the liquid phase when adsorption equilibrium was achieved. Finally, $C_{PhC.ads}$ and $C_{Sug.ads}$ are the concentrations of total phenols and sugars adsorbed on the resins expressed in ($mgTyeqL^{-1}$) and (mg glucose $\cdot L^{-1}$), respectively. These results can be expressed in percentages (Eq. 10 and 11):

$$COD_{PhC.ads}(\%) = \frac{COD_{PhC.ads}}{COD_{ads}} \cdot 100 \quad (10)$$

$$COD_{Sug.ads}(\%) = \frac{COD_{Sug.ads}}{COD_{ads}} \cdot 100 \quad (11)$$

Being COD_{ads} the difference between initial COD in the samples (COD_0) and COD in the liquid phase when the adsorption equilibrium was reached (COD_e). The results of the adsorption of phenolic compounds, sugars and COD are presented in Table 5.27. The theoretical percentage of COD that corresponded to the total phenolic compounds and sugars adsorbed is also shown in the table. The results followed the same trend that was observed with the model solution. The MN200 resin presented the largest adsorption of phenolic compounds, while the PAD950 showed the smallest one. The low TPhC adsorption of PAD950 resin is again attributed to its small pore size. According to the literature, the smallest the diameter of the pores of the resin, the lowest the diffusion of the adsorbate molecules from the aqueous phase to the pores of the adsorbent [54]. Interestingly, this resin was the only one that did not exhibit a decrease in the adsorption of phenolic compounds in comparison with the model solution. The MN202 resin was the one that presented the greatest decrease in TPhC adsorption (19% lower). However, this resin showed a high adsorption of phenolic compounds, again being the MN resins the ones that exhibited the best performances. This is directly related to the material of the resins. Studies carried out by Kammerer et al. [55] observed that resins with a polystyrene-based matrix (the same matrix as MN resins) exerted a significantly greater polyphenol binding than polyacrylamide-based resins as a result of stronger hydrophobic interactions and hydrogen bonding due to their higher hydrophobicity. In that study, the authors also reported the impact of saccharides and amino acids on apple polyphenols adsorption on resins. They concluded that the presence of glucose, fructose and sucrose could affect the adsorption of some phenolic compounds on both neutral and ion

exchange resins. They observed that the adsorption of catechin in a non-ionic resin was less effective when glucose and sucrose were present. On the contrary, the adsorption of caffeic acid was better in the presence of all the sugars together or separately. They attributed it to the possibility of a multilayer adsorption on the resin surface, which might be enhanced in the presence of sugars through hydrogen bridges. Carbohydrates might enhance the formation of several layers of some compounds that do not normally interact directly with the resin; significantly improving the recovery rates. This might also explain the slightly higher adsorption (+5%) exhibited by the PAD950 resin compared to the model solution.

Table 5.27. Removal percentages for each resin after reaching the equilibrium and study of adsorption of COD for all the resins tested when the olive oil washing wastewater was treated

Removal percentage (%)	MN200	MN202	PAD900	PAD950
[a]$TPhC._{ads}$	91.89 ± 0.97	74.31 ± 0.18	69.99 ± 0.92	66.95 ± 0.79
[b]$Sug._{ads}$	23.60 ± 0.28	29.47 ± 0.60	54.38 ± 0.84	41.71 ± 1.73
[c]$COD_{total.ads}$	19.11 ± 0.06	20.89 ± 0.25	25.96 ± 1.20	22.99 ± 0.86
[d]$COD_{PhC.ads}$	52.37 ± 0.62	39.01 ± 0.40	27.37 ± 1.06	31.95 ± 0.85
[e]$COD_{Sug.ads}$	12.86 ± 0.13	15.72 ± 0.19	35.32 ± 0.75	19.28 ± 0.43

[a]TPhC.ads.: Percentage of total phenolic compounds adsorbed from the initial feed solution
[b]Sug.ads: Percentage of sugars adsorbed from the initial feed solution
[c]COD.Total.ads: Percentage of total COD adsorbed from the initial feed solution
[d]COD.PhC.ads : COD percentage corresponding to the adsorbed phenolic compounds
[d]COD.Sug.ads: COD percentage corresponding to the adsorbed sugars

To know how selective the resins are for these compounds and how many other organic substances they can remove, the adsorbed COD corresponding to phenolic compounds and sugars was determined. The MN200 resin showed the highest percentage of adsorbed COD linked to phenolic compounds (52.4%). This means that this resin is more selective than the others towards phenolic compounds, since more than 50% of the adsorbed COD corresponds to these antioxidant compounds. This resins also yielded the lowest COD removal related to sugar adsorption (12.86%). The MN202 and PAD950 resins also presented a low percentage of COD removal corresponding to adsorbed sugars. This implies a small competition between phenolic compounds and sugars on the adsorption sites of these resins.

On the other hand, MN202 also had a removal of COD linked to phenolic compounds similar to that of PAD950 resin (between 32-39%).

With respect to the PAD900 resin, it showed a greater adsorption of COD linked to sugars than to phenolic compounds (1.3 times higher). Therefore, in this case, the sugars competed for the resin sites, thus interfering with the adsorption of the phenolic compounds. The adsorbed COD represented by sugars together with that represented by phenolic compounds gives percentage values between 51 and 65%. Frascari et al. [56] reported that in addition to carbohydrates, the presence of proteins was detected in non-phenolic COD desorbed after an adsorption process performed in a continuous flow column for OMW valorisation. This implies that the resins adsorbed organic compounds other than sugars and phenols. With these results, it can be inferred that the phenolic compounds adsorbed by the MN200 resin contained fewer impurities than those adsorbed by the other resins. In this way, it can be commented that, although the resins are specific for phenolic compounds, they also adsorb other compounds, which interferes with the performance of the resins for the adsorption of phenolic compounds. However, all the resins presented adsorption percentages of phenolic compounds higher than 66%, with the MN200 resin presenting values higher than 91%. Chaari et al. [57] achieved adsorption percentages of phenolic compounds from OMW between 77.61% and 84.21% using calcined clay as adsorbent at acidic pH. In this work, by means of the MN resins, greater percentages can be achieved without acidifying the medium and with easily recoverable adsorbents. Ochando-Pulido et al. [58] tested different resins for the recovery of phenolic compounds from OOWW. They achieved the highest rejection percentage with an ionic resin (95.3%). However, with the non-ionic resins tested only 70.5% adsorption of phenolic compounds was reached with a resin dose of 60 $g \cdot L^{-1}$. In this case, the MN resins presented better performance, while the PAD resins presented similar adsorption to the one reported by those authors. Moreover, in our work a lower resin concentration was used. This demonstrates the high affinity of these resins against phenolic compounds. The studies carried out by Zagklis et al. [59], using an reverse osmosis OMW concentrate as feed, showed similar percentages of adsorption of sugars and phenolic compounds using non-ionic resins (XAD4, XAD7 and XAD16). The best result was obtained with the XAD4 resin, with 35.8% and 93.1% adsorption of sugars and phenolic compounds, respectively. Although the MN200

resin has a slightly lower adsorption of phenolic compounds (-1.21%), it has 12.2% less adsorption of sugars.

3.3.2 Desorption process

As in the desorption tests with the model solution a 50% v/v ethanol/water solution was the one that reached the highest percentages of desorption, this eluent was the one selected for the tests with OOWW. Desorption percentages of phenolic compounds and sugars are shown in fig. 5.51. It is important to highlight that the percentage of desorption is calculated based on the amount adsorbed by each resin, not on the total amount in the initial sample. The results obtained for phenolic compounds were completely different from those observed for the model solution.

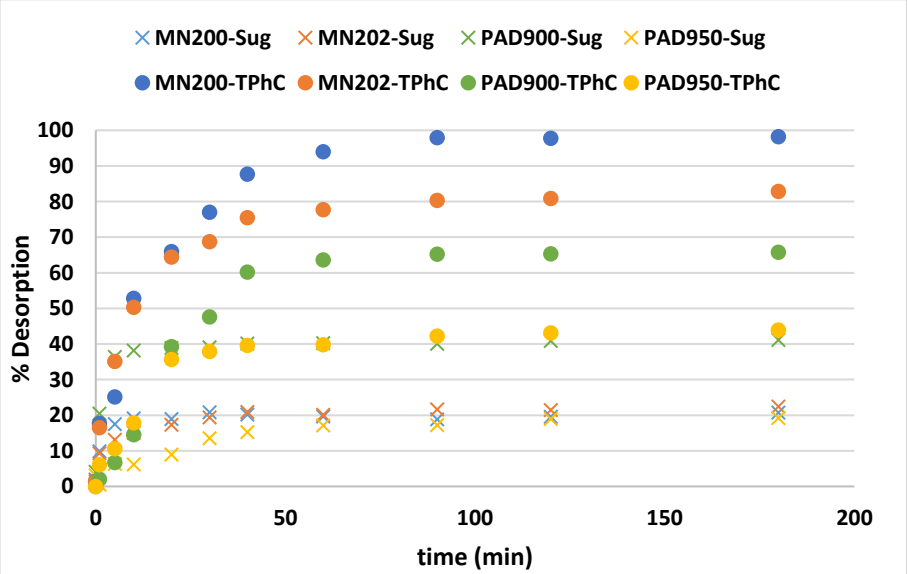

Fig. 5.51 Desorption of Phenolic compounds (TPhC) and sugars (Sug.) using a 50% v/v ethanol/water mixture as solvent for 40 g/L resin dose when the olive oil washing wastewater was treated.

The obtained sequence (from the highest to the lowest desorption percentage) was MN200>MN202>PAD900>PAD950, while the sequence with the model solution was

PAD950>MN202>PAD900>MN200. The MN200 resin improved the desorption percentage, exceeding 98% (92% with model solution). However, the rest of the resins presented lower desorption percentages than those obtained with the simulated solution. The lowest percentage was observed for the PAD950 resin (45%), desorbing less than half of the adsorbed phenolic compounds. In this case, it is possible that the affinity between the resin and the adsorbed compounds is so strong that their desorption is not enhanced. This was also commented in the section 3.2 for the model solution. This was also observed by Buran et al. [34] in their adsorption/desorption studies of blueberry phenolic compounds. They attributed it to the great affinity of the resinous material towards phenolic compounds (mainly anthocyanins and flavonols). The resin was made of a polar phenol formaldehyde polymer (dipole moment = 1.80), while the other adsorbents were made of styrene-divinylbenzene co-polymer (dipole moment = 0.30). In our case, the PAD950 resin is made of an acrylic material, which has a similar dipole moment to phenolic compounds [36]. Thus, it could explain that a significant amount of phenolic compounds were irreversibly adsorbed.

Regarding the percentages of desorbed sugars, it can be clearly seen that they are significantly lower than the desorption percentages of phenolic compounds. PAD900 resin offered the highest and PAD950 resin the lowest sugar desorption ratio. Although in the previous section high COD linked to adsorbed sugars was obtained for the PAD900 resin, these were not completely desorbed. These are valuable results for the objective of recovering phenolic compounds, since, regardless of whether the resins can adsorb sugars, they were not completely desorbed, so a concentrated stream of relatively pure phenolic compounds can be obtained. Nevertheless, sugars adsorption can affect the durability of the resin, since extra cleaning would be needed to remove the not desorbed sugars (and other compounds), affecting its useful life.

Table 5.28. Summary of adsorption/desorption of phenolic compounds and sugars from OOWW, using a resin dosage of 40 gL^{-1} and a 50% v/v ethanol/water mixture as eluent

	Resins			
	MN200	MN202	PAD900	PAD950
[a]$TPhC._{ads}$ (%)	91.89 ± 0.97	74.31 ± 0.18	69.99 ± 0.92	66.95 ± 0.79
[b]$TPhC._{des}$ (%)	99.07 ± 0.25	69.22 ± 1.32	50.94 ± 0.25	44.52 ± 0.88
[b]$TPhC._{des}$ (ppm)	1310.97 ± 1.22	915.92 ± 5.32	674.12 ± 0.88	589.12 ± 3.22
[c]$Sug._{ads}$ (%)	23.60 ± 0.28	29.47 ± 0.60	54.38 ± 0.84	41.71 ± 1.73
[d]$Sug._{des}$ (%)	20.04 ± 0.94	22.48 ± 0.54	41.18 ± 0.56	19.23 ± 1.06
[d]$Sug._{des}$ (ppm)	73.00 ± 6.28	98.80 ± 4.82	255.80 ± 6.06	119.60 ± 13.09
[e]$TPhC._{rec}$ (%R)	90.90 ± 0.56	76.11 ± 1.14	60.01 ± 1.37	40.91 ± 0.37

[a]TPhC.ads= total phenolic compounds adsorbed from the initial feed solution
[b]TPhC.des= total phenolic compounds desorbed from the total adsorbed
[c]Sug.ads =total of sugars adsorbed from the initial feed solution
[d]Sug.des =total of sugars desorbed from the total adsorbed
[e]TPhC.rec.= total phenolic compounds recovery from the initial feed solution

Table 5.28 shows a summary of the adsorption/desorption process for the recovery of phenolic compounds from OOWW. It can be seen that the MN resins presented the best results in terms of recovery of phenolic compounds from the initial sample (table 5.24), obtaining a recovery of 90% with the MN200 resin. On the other hand, the solution obtained after the desorption step showed a 18 times lower concentration of sugars (73ppm) compared to the concentration of phenolic compounds (1310.97ppm). That means that the obtained extract contained only 5% of the initial sugar content of the OOWW. This implies a great purity of the phenolic compounds. Similar results were obtained with the MN202 resin, where the concentration of sugars in the final solution was 11 times lower than that of the phenolic compounds present. The purity of the final stream followed the following sequence MN200>MN202>PAD950>PAD900.

The study carried out by Ochando-Pulido et al. [60] achieved a slightly higher recovery of phenolic compounds (92.5%) from OOWW. However, they used an ion exchange resin, and they worked under certain operational conditions (effluent at 20.3 °C, pH 6.7 and resin dose of 114 $g \cdot L^{-1}$) that implied changes in the system. In our case, we worked without modifying the pH of the effluent and the resin dose was much smaller (40 $g \cdot L^{-1}$). All this makes the recovery

process of phenolic compounds proposed in this work more profitable from an economic point of view.

One of the latest studies on the valorisation of phenolic compounds from solid oil mill residues by means of adsorption/desorption [61] showed recovery percentages of total phenols between 74.6% - 70.31%, using contents of resin of 100 and 50 $g \cdot L^{-1}$, respectively. In addition, these authors worked under acid conditions. In our case, we could obtain higher recovery percentages without acidifying the feed solution. It is important to note that this study was conducted using the solid residue from olive oil production, which was submitted to an extraction process with hydroalcoholic solutions. The feed solution for the adsorption process was the dealcoholized extract acidified to pH 2.8.

Table 5.29 shows the final concentration of individual phenols, organic acids, fatty acid derivatives and sugars in the eluent of each resin. The final recovery of phenolic compounds and sugars through the adsorption/desorption process is also presented. It is important to highlight that sugar concentrations were not obtained by LC-MS, but by colorimetric kits as explained in section 2.6. A difference in the total concentration of phenolic compounds is observed when the desorption results obtained with FC and LC-MS are compared. This may be due to different reasons, such as interference with other compounds or that there are phenolic compounds not detected with LC-MS methodology, but quantified with FC. Some studies have concluded that fructose and sucrose could react with the FC reagent and be measured as phenolic compounds, affecting the final total phenolic compounds values [62]. Nevertheless, the FC method is the prevailing method for the determination of the total concentration of these compounds in food samples and, according to Olmo-García et al. [63], it can be considered a valid and reliable method when global concentration is pursued. These authors mentioned that, although all the published options for the quantification of phenolic compounds are valid, the main limitation is the disparity of criteria regarding the expression of the results on the quantification of phenolic compounds. Thus, the results are not comparable. From table 5.29 the chemical classes that are predominant in the final solution of each resin can be inferred. In addition, recovery percentages of the main individual phenolic compounds and sugars are shown.

In can be seen from table 5.29, that the highest concentration of phenolic compounds was found in the final elution solution obtained with the MN200 resin, being 3.6 times greater than that from the PAD950 resin. In general, all the resins presented a high concentration of tyrosol in the final stream. The MN200 resin was able to recover all the phenolic compounds present in the initial OOWW sample. This resin was the one that, considering all the simple phenols together, achieved the highest recovery. However, this resin did not present the highest recovery of hydroxytyrosol, having a similar performance to the PAD900 resin (recovery of 42-43%). The highest recovery of hydroxytyrosol was achieved with the MN202 resin and was 87%. On the other hand, this compound was not found in the desorption solution obtained with the PAD950 resin. Therefore, it can be concluded that the recovery of small phenolic compounds, such as simple phenols, by the MN resins is possible.

Regarding the phenolic acid, the MN202 resin presented by far the largest recovery, with the MN200 resin only recovering a 12%, while in the eluent from the PAD resins this compound was not detected. Once again, the MN202 resin was the one that presented the greatest recovery of secoiriodoids (90%), followed by the MN200 resin with 68.72%. The same trend was observed with the flavonoids, obtaining largest recovery percentages with the MN resins. Similar results were presented by Yangui et al. [64] when studying the recovering phenolic compounds from OMW with MN202 and FPX66 resin, at a resin concentration close to that presented in this study (50 gL^{-1}). Obtaining the greatest phenolic acid (100% p-coumaric acid and caffeic acid) and flavonoids (91.3% catechin) recovery with the MN202 resin.

Depending on which compounds are to be recovered, one MN resin is more suitable than the another one. Thus, to recover simple phenolic compounds, the MN200 resin is more suitable, while MN202 would be the one selected to recover phenolic acids, secoirioldoids and flavonoids.

Taking into account the concentration of total phenolic compounds, as with the FC method (table 10), the MN200 resin was the one that presented the best performance, obtaining a total recovery of 89.75%.

Regarding sugars, the solution obtained with the PAD900 resin was the one that presented the greatest concentration of sugars, being almost similar to the concentration of total phenolic compounds (equivalent to almost 40% of the concentration of total phenolic compounds in the extract). In general, glucose showed the highest concentration in the samples in comparison with the rest of the sugars. The MN resins were the ones that obtained desorption solutions with the lowest concentration of sugars, thus being the purest ones.

Table 5.29. Specific concentration of phenolic compounds, organic acids, fatty acids and sugars in the eluent for each resin and recovery percentage of the phenolic compounds and sugars.

		MN200		MN202		PAD900		PAD950	
Chemical class	Detected Compound	[a]ppm	[b]%Recovery	[a]ppm	[b]%Recovery	[a]ppm	[b]%Recovery	[a]ppm	[b]%Recovery
Simple phenols	Hydroxytyrosol	0.49 ± 0.01	42.61	1.00 ± 0.05	86.96	0.48 ± 0.07	41.74	0.00 ± 0.00	0.00
	Tyrosol	548.17 ± 18.55	100.00	166.76 ± 0.09	31.49	213.92 ± 14.55	40.39	156.34 ± 6.25	29.52
	Hydroxytyrosol glucoside	1.58 ± 0.08	92.94	1.08 ± 0.01	63.53	1.07 ± 0.06	62.94	0.73 ± 0.11	42.94
Phenolic acid	p-coumaric acid	0.11 ± 0.00	12.09	0.99 ± 0.13	100.00	0.00 ± 0.00	0.00	0.00 ± 0.00	0.00
Secoiriodoids	Hydroxy decarboxymethyl elenolic acid 1+2	8.81 ± 0.14	21.79	38.50 ± 0.37	95.20	1.94 ± 15.18	4.80	1.00 ± 0.14	2.47
	Elenolic acid glucoside	0.71 ± 0.04	34.66	1.73 ± 0.02	84.46	0.00 ± 0.03	0.00	0.00 ± 0.00	0.00
	Hydroxy elenolic acid	18.06 ± 1.00	96.89	5.55 ± 0.56	29.77	8.49 ± 0.43	45.55	4.03 ± 0.24	21.62
	Decarboxymethyl elenolic acid	104.85 ± 3.19	60.07	170.67 ± 0.14	97.77	49.83 ± 6.53	28.55	22.72 ± 0.90	13.02
	Acyclodihydroelenolic acid hexoside	83.80 ± 0.20	96.50	83.97 ±0.01	96.70	39.59 ± 0.11	45.59	31.04 ± 0.33	35.74
	Elenolic acid	17.46 ± 0.62	99.66	5.08 ± 0.24	29.00	7.44 ± 0.70	42.47	2.73 ± 0.19	15.58
Flavonoids	Apigenin	0.26 ± 0.00	86.67	0.10 ± 0.01	33.33	0.11 ± 0.01	36.67	0.05 ± 0.00	16.67
	Luteolin	0.04 ± 0.00	57.14	0.06 ± 0.00	85.71	0.00 ± 0.00	0.00	0.00 ± 0.00	0.00
	Gallocatechin	2.19 ± 0.02	86.90	2.54 ± 0.05	100.00	1.73 ± 0.11	68.65	1.62 ± 0.14	64.29
Organic acids	Quinic acid	143.92 ± 3.06	96.42	118.45 ± 0.05	79.36	98.91 ± 0.13	66.27	105.93 ± 14.59	70.97
	Malic acid	8.54 ± 0.30	100.00	4.34 ± 0.00	54.48	5.36 ± 0.13	67.37	6.10 ± 0.91	76.57
	Citric acid	368.28 ± 9.82	100.00	256.82 ± 0.03	72.66	230.67 ± 0.22	65.26	249.74 ± 24.28	70.65
Fatty acids derivatives	Trihydroxy-octadecadienoic acid	0.37 ± 0.03	34.87	0.93 ± 0.01	88.10	0.19 ± 0.02	17.72	0.05 ± 0.00	4.29
	Dihydroxy-hexadecanoic acid	0.11 ± 0.02	42.14	0.34 ± 0.05	100.00	0.02 ± 0.00	9.23	0.05 ± 0.00	18.01
	Trihydroxy-octadecenoic acid	0.00 ± 0.00	0.00	0.00 ± 0.00	0.00	0.00 ± 0.00	0.00	0.49 ± 0.02	99.47
	Dehydroxy-octadecatrienoic acid	0.14 ± 0.01	95.68	0.11 ± 0.01	73.09	0.11 ± 0.01	74.33	0.13 ± 0.01	89.86
Sugars	Glucose	64.00 ± 3.00	7.20	72.00 ± 4.50	8.10	115.20 ± 12.00	12.95	87.50 ± 6.00	9.84
	Fructose	6.00 ± 0.10	1.80	20.80 ± 1.00	6.25	86.60 ± 6.40	26.03	25.50 ± 1.20	7.67
	Sucrose	3.00 ± 0.00	1.12	6.00 ± 0.00	2.23	54.00 ± 7.00	20.08	6.60 ± 0.00	2.45

[a]ppm= from in the desorption eluent [b]%Recovery= from the initial concentration in the OOWW sample

3. Conclusions

The adsorption/desorption capacity of four resins was studied in order to find the best resin dose and eluent to recover phenolic compounds, firstly from a simulated solution that contained catechin and tyrosol and, secondly, from olive oil washing wastewater.

All the resins tested with the model solution showed high adsorption towards phenolic compounds. The adsorption capacity of the resins increased with increasing their dose in solution. The greatest increase in adsorption efficiency occurred when the dose was augmented from 10 to 40 gL^{-1}; then the change from 40 to 60 gL^{-1} did not generate a significant variation in adsorption.

With the model solution, the MN resins achieved adsorption percentages greater than 90%, being the MN200 the resin that presented the highest total phenolic compounds adsorption (97.41 ± 0.07 %, for a resin dosage of 60 $g \cdot L^{-1}$). The pseudo-second order kinetic model provided the best fitting of the experimental data for all the resins. For the MN resins, the adsorption process was properly described by the Langmuir isotherm model, while the adsorption onto the PAD resins was better fitted by the Freundlich isotherm model.

From the tests performed with the model solution, a 50%v/v ethanol/water mixture was observed to be the best eluent to recover the phenolic compounds, being the MN202 the resin that yielded the highest desorption efficiency of phenolic compounds.

The adsorption-desorption of phenolic compounds from olive oil washing wastewater yielded a similar behaviour as that observed with the model solution, with the MN resins presenting the best performance. The adsorption of phenolic compounds onto PAD resins was worse than onto MN resins due to interferences with sugars that competed for the active sites of the resins.

The resins tested showed good affinity for the phenolic compounds, presenting high percentages of adsorption/desorption. In this way, an extract rich in phenolic compounds of high purity could be obtained. The MN200 resin showed the best performance, being almost 90% of the initial phenolic compounds recovered, with low presence of sugars (about 5%).

In summary, this work has shown that it is possible to revalue mill waste using adsorption/desorption technology, since bioactive compounds with promising health benefits can be recovered with high purity.

Acknowledgements

The authors acknowledge the financial support from the Spanish Ministry of Economy, Industry and Competitiveness through the project CTM2017-88645-R and The European Union through the Operational Program of the Social Fund (FSE). In addition, we thank the Purolite® Company for kindly providing resin samples for testing.

References

[1] M. Abbas, F. Saeed, F.M. Anjum, M. Afzaal, T. Tufail, M.S. Bashir, A. Ishtiaq, S. Hussain, H.A.R. Suleria, Natural polyphenols: an overview, Int. J. Food Prop. 20 (8) (2017) 1689–1699, https://doi.org/10.1080/10942912.2016.1220393.

[2] R. Chandramohan, L. Pari, Anti-inflammatory effects of tyrosol in streptozotocin-induced diabetic Wistar rats, J. Funct. Foods. 27 (2016) 17–28, https://doi.org/ 10.1016/j.jff.2016.08.043.

[3] A.M. Pisoschi, A. Pop, F. Iordache, L. Stanca, G. Predoi, A.I. Serban, Oxidative stress mitigation by antioxidants - An overview on their chemistry and influences on health status, Eur. J. Med. Chem. 209 (2021) 112891, https://doi.org/10.1016/ j.ejmech.2020.112891.

[4] R. Castro-Mu˜noz, C. Conidi, A. Cassano, Recovery of phenolic-based compounds from agro-food wastewaters through pressure-driven membrane technologies, 2019. https://doi.org/10.1016/b978-0-12-815056-6.00006-1.

[5] B.d.L. Santos, E. Medina, M. Brenes, A. Aguado, P. García, C. Romero, Chemical composition of table olive wastewater and its relationship with the bio-fortifying capacity of tomato (Solanum lycopersicum L.) plants, Agric. Water Manag. 227 (2020) 105833, https://doi.org/10.1016/j.agwat.2019.105833.

[6] A. Di Mauro, B. Fallico, A. Passerini, P. Rapisarda, E. Maccarone, Recovery of Hespiridin from Orange Peel by Cocentration of Extracts on Styrene- Divinylbenzene Resin, J. Agric. Food Chem. 47 (1999) 4391–4397. http://pubs. acs.org/doi/pdf/10.1021/ac0351769.

[7] E. Hern´andez-Francisco, J. Peral, L.M. Blanco-Jerez, Removal of phenolic compounds from oil refinery wastewater by electrocoagulation and Fenton/photo- Fenton processes, J. Water Process Eng. 19 (2017) 96–100, https://doi.org/ 10.1016/j.jwpe.2017.07.010.

[8] M.O.J. Azzam, S.A. Hazaimeh, Olive mill wastewater treatment and valorization by extraction/concentration of hydroxytyrosol and other natural phenols, Process Saf. Environ. Prot. 148 (2021) 495–523, https://doi.org/10.1016/j.psep.2020.10.030.

[9] S.S. Kontos, P.G. Koutsoukos, C.A. Paraskeva, Removal and recovery of phenolic compounds from olive mill wastewater by cooling crystallization, Chem. Eng. J. 251 (2014) 319–328, https://doi.org/10.1016/j.cej.2014.04.047.

[10] T. Jerman Klen, B. Mozeti˘c Vodopivec, Ultrasonic extraction of phenols from olive mill wastewater: comparison with conventional methods, J. Agric. Food Chem. 59 (2011) 12725–12731, https://doi.org/10.1021/jf202800n.

[11] A. Al Bsoul, M. Hailat, A. Abdelhay, M. Tawalbeh, A. Al-Othman, I.N. Al-kharabsheh, A.A. Al-Taani, Efficient removal of phenol compounds from water environment using Ziziphus leaves adsorbent, Sci. Total Environ. 761 (2021) 143229, https://doi.org/10.1016/j.scitotenv.2020.143229.

[12] N. Solomakou, A. Goula, A novel low cost biosorbent of phenolic compounds from olive mill wastewaters, in: 1st Int. Electron. Conf. Appl. Sci., 2020: p. 7544. https://doi.org/10.3390/ASEC2020-07544.

[13] P. Barkakati, A. Begum, M.L. Das, P.G. Rao, Adsorptive separation of Ginsenoside from aqueous solution by polymeric resins: Equilibrium, kinetic and thermodynamic studies, Chem. Eng. J. 161 (1-2) (2010) 34–45, https://doi.org/ 10.1016/j.cej.2010.04.018.

[14] P. P´erez-Larr´an, B. Díaz-Reinoso, A. Moure, J.L. Alonso, H. Domínguez, Adsorption technologies to recover and concentrate food polyphenols, Curr. Opin. Food Sci. 23 (2018) 165–172, https://doi.org/10.1016/j.cofs.2017.10.005.

[15] F. Elayadi, W. Boumya, M. Achak, Y. Chhiti, F.E.M. Alaoui, N. Barka, C.E. Adlouni, Experimental and modeling studies of the removal of phenolic compounds from olive mill wastewater by adsorption on sugarcane bagasse, Environ. Challenges 4 (2021) 100184, https://doi.org/10.1016/j.envc.2021.100184.

[16] Q. Yang, M. Zhao, L. Lin, Adsorption and desorption characteristics of adlay bran free phenolics on macroporous resins, Food Chem. 194 (2016) 900–907, https:// doi.org/10.1016/j.foodchem.2015.08.070.

[17] J.R. Njimou, M. Stoller, A. Cicci, A. Chianese, C.P. Nanseu-Njiki, E. Ngameni, M. Bravi, Adsorption of phenol/tyrosol from aqueous solutions on macro-reticular aromatic and macro-porous polystyrene cross-linked with divinylbenzene polymeric resins, Chem. Eng. Trans. 57 (2017) 757–762, https://doi.org/10.3303/ CET1757127.

[18] M.A.N. Camacho, A.I.G. L´opez, A. Martinez-Ferez, J.M. Ochando-Pulido, Increasing large-scale feasibility of two-phase olive-oil washing wastewater treatment and phenolic fraction recovery with novel ion exchange resins, Chem. Eng. Process. - Process Intensif. 164 (2021) 108416, https://doi.org/10.1016/j. cep.2021.108416.

[19] G.S.L. Lozada, A.I.G. L´opez, A. Martínez-F´erez, J.M. Ochando-Pulido, Boundary flux modelling of ceramic tubular microfiltration towards fouling control and performance maximization for olive-oil washing wastewater treatment and revalorization, J. Environ Chem. Eng. 10 (2) (2022) 107323.

[20] M. Cifuentes-Cabezas, C. Carbonell-Alcaina, M.C. Vincent-Vela, J.A. Mendoza-Roca, S. ´Alvarez-Blanco, Comparison of different ultrafiltration membranes as first step for the recovery of phenolic compounds from olive-oil washing wastewater, Process Saf. Environ. Prot. 149 (2021) 724–734, https://doi.org/10.1016/j. psep.2021.03.035.

[21] D.O. Aderibigbe, A.A. Giwa, I.A. Bello, Characterization and treatment of wastewater from food processing industry: a review, Imam, J. Appl. Sci. 2 (2017) 27–36, https://doi.org/10.4103/ijas.ijas_11_17.

[22] V.L. Singleton, R. Orthofer, R.M. Lamuela-Ravent´os, Analysis of total phenols and other oxidation substrates and antioxidants by means of folin-ciocalteu reagent, Methods Enzymol. 299 (1999) 152–178, https://doi.org/10.1016/S0076-6879(99) 99017-1.

[23] S. Lagergreen, About the theory of so called adsorption of solute substances, Ksver Veterskapsakad Handl. 24 (1898) 1–6.

[24] Y.S. Ho, G. McKay, Pseudo-second order model for sorption processes, Process Biochem. 34 (5) (1999) 451–465, https://doi.org/10.1016/S0032-9592(98) 00112-5.

[25] D.R. Kammerer, Z.S. Saleh, R. Carle, R.A. Stanley, Adsorptive recovery of phenolic compounds from apple juice, Eur. Food Res. Technol. 224 (5) (2007) 605–613, https://doi.org/10.1007/s00217-006-0346-5.

[26] L. Bertin, F. Ferri, A. Scoma, L. Marchetti, F. Fava, Recovery of high added value natural polyphenols from actual olive mill wastewater through solid phase extraction, Chem. Eng. J. 171 (3) (2011) 1287–1293, https://doi.org/10.1016/j. cej.2011.05.056.

[27] M. Savarese, E. De Marco, S. Falco, I. D'Antuoni, R. Sacchi, Biophenol extracts from olive oil mill wastewaters by membrane separation and adsorption resin, Int. J. Food Sci. Technol. 51 (11) (2016) 2386–2395, https://doi.org/10.1111/ijfs.13219.

[28] D. Frascari, G. Rubertelli, F. Arous, A. Ragini, L. Bresciani, A. Arzu, D. Pinelli, Valorisation of olive mill wastewater by phenolic compounds adsorption: development and application of a procedure for adsorbent selection, Chem. Eng. J. 360 (2019) 124–138, https://doi.org/10.1016/j.cej.2018.11.188.

[29] I. Hamadneh, R.A. Abu-Zurayk, A.H. Al-Dujaili, Removal of phenolic compounds from aqueous solution using MgCl2 -impregnated activated carbons derived from olive husk: the effect of chemical structures, Water Sci. Technol. 81 (2020) 2351–2367, https://doi.org/10.2166/wst.2020.297.

[30] E. De Marco, M. Savarese, C. Parisini, S. Falco, A. Paduano, R. Sacchi, Ingredienti fenolici da sottoprodotti oleari, Ingredienti Aliment. 48 (2010) 16–22.

[31] E. Ferrer-Polonio, J.A. Mendoza-Roca, A. Iborra-Clar, L. Pastor-Alca˜niz, Adsorption of raw and treated by membranes fermentation brines from table olives processing for phenolic compounds separation and recovery, J. Chem. Technol. Biotechnol. 91 (7) (2016) 2094–2102, https://doi.org/10.1002/jctb.4807

[32] V. Davankov, M. Tsyurupa, Hypercrosslinked polymers - A novel class of polymeric materials, Compr. Anal. Chem. 56 (2011) 315–358, https://doi.org/10.1016/ S0166-526X(11)56009-X.

[33] J. Huang, X. Wu, H. Zha, B. Yuan, S. Deng, A hypercrosslinked poly(styrene-co-divinylbenzene) PS resin as a specific polymeric adsorbent for adsorption of 2- naphthol from aqueous solutions, Chem. Eng. J. 218 (2013) 267–275, https://doi. org/10.1016/j.cej.2012.12.032.

[34] T.J. Buran, A.K. Sandhu, Z. Li, C.R. Rock, W.W. Yang, L. Gu, Adsorption/desorption characteristics and separation of anthocyanins and polyphenols from blueberries using macroporous adsorbent resins, J. Food Eng. 128 (2014) 167–173, https:// doi.org/10.1016/j.jfoodeng.2013.12.029.

[35] C. Valderrama, J. Poch, J.I. Barios, A. Farran, J.L. Cortina, Binary fixed bed modeling of phenol/aniline removal from aqueous solutions onto hyper-cross- linked resin (Macronet MN200), J. Chem. Eng. Data. 57 (5) (2012) 1502–1508, https://doi.org/10.1021/je3001415.

[36] E. Silva, D. Pompeu, Y. Larondelle, H. Rogez, Optimisation of the adsorption of polyphenols from Inga edulis leaves on macroporous resins using an experimental design methodology, Sep. Purif. Technol. 53 (3) (2007) 274–280, https://doi.org/ 10.1016/j.seppur.2006.07.012.

[37] T.R. Sahoo, B. Prelot, Adsorption processes for the removal of contaminants from wastewater, Elsevier Inc., 2020. https://doi.org/10.1016/b978-0-12-818489- 9.00007-4.

[38] M.P. Casas, V. Rodríguez-Hermida, P. P´erez-Larr´an, E. Conde, M.T. Liveri, D. Ribeiro, E. Fernandes, H. Domínguez, In vitro bioactive properties of phlorotannins recovered from hydrothermal treatment of Sargassum muticum, Sep. Purif. Technol. 167 (2016) 117–126, https://doi.org/10.1016/j. seppur.2016.05.003.

[39] F. Zhenghao, C. Jinlong, C. Jianguo, G. Guandao, L.i. Aimin, Z. Quanxing, Adsorption characteristics of phenolic compounds onto a new hypercrosslinked polymeric resin containing the 2-carbonylbenzoyl group (ZH-01), Adsorpt. Sci. Technol. 22 (5) (2004) 439–449, https://doi.org/10.1260/0263617042863048.

[40] A. Scoma, C. Pintucci, L. Bertin, P. Carlozzi, F. Fava, Increasing the large scale feasibility of a solid phase extraction procedure for the recovery of natural antioxidants from olive mill wastewaters, Chem. Eng. J. 198–199 (2012) 103–109, https://doi.org/10.1016/j.cej.2012.05.079.

[41] F. Ferri, L. Bertin, A. Scoma, L. Marchetti, F. Fava, Recovery of low molecular weight phenols through solid-phase extraction, Chem. Eng. J. 166 (3) (2011) 994–1001, https://doi.org/10.1016/j.cej.2010.11.090.

[42] M. Caetano, C. Valderrama, A. Farran, J.L. Cortina, Phenol removal from aqueous solution by adsorption and ion exchange mechanisms onto polymeric resins, J. Colloid Interface Sci. 338 (2) (2009) 402–409, https://doi.org/10.1016/j. jcis.2009.06.062.

[43] J. Kammerer, D.R. Kammerer, U. Jensen, R. Carle, Interaction of apple polyphenols in a multi-compound system upon adsorption onto a food-grade resin, J. Food Eng. 96 (4) (2010) 544–554, https://doi.org/10.1016/j.jfoodeng.2009.08.038.

[44] F.A. Ayaz, E. Bertoft, Sugar and phenolic acid composition of stored commercial oleaster fruits, J. Food Compos. Anal. 14 (5) (2001) 505–511, https://doi.org/ 10.1006/jfca.2001.1004.

[45] C.I.L. Justino, R. Pereira, A.C. Freitas, T.A.P. Rocha-Santos, T.S.L. Panteleitchouk, A.C. Duarte, Olive oil mill wastewaters before and after treatment: a critical review from the ecotoxicological point of view, Ecotoxicology 21 (2) (2012) 615–629, https://doi.org/10.1007/s10646-011-0806-y.

[46] E. Medina, M. Brenes, A. Garcia, C. Romero, A. De Castro, Bactericidal activity of glutaraldehyde-like compounds from olive products, J. Food Prot. 72 (2009) 2611–2614, https://doi.org/10.4315/0362-028X-72.12.2611.

[47] A. Debo, T. Yangui, A. Dhouib, M. Ksantini, S. Sayadi, Efficacy of a hydroxytyrosol- rich preparation from olive mill wastewater for control of olive psyllid, Euphyllura olivina, infestations, Crop Prot. 30 (12) (2011) 1529–1534, https://doi.org/ 10.1016/j.cropro.2011.08.006.

[48] T.B. Ribeiro, A.L. Oliveira, C. Costa, J. Nunes, A.A. Vicente, M. Pintado, Total and sustainable valorisation of olive pomace using a fractionation approach, Appl. Sci. 10 (19) (2020) 6785, https://doi.org/10.3390/app10196785

[49] M. Bullo, L.-R. Rosa, J. Salas-Salvado, Mediterranean diet and oxidation: nuts and olive oil as important sources of fat and antioxidants, 2011. https://dx.doi.org/ 10.2174/156802611796235062.

[50] B.M. Esteves, S. Morales-Torres, L.M. Madeira, F.J. Maldonado-H´odar, Specific adsorbents for the treatment of OMW phenolic compounds by activation of bio-residues from the olive oil industry, J. Environ. Manage. 306 (2022) 114490, https://doi.org/10.1016/j.jenvman.2022.114490.

[51] D. Pinelli, A. Esther, M. Bacca, A. Kaushik, S. Basu, M. Nocentini, L. Bertin, D. Frascari, Batch and continuous flow adsorption of phenolic compounds from olive mill wastewater: a comparison between nonionic and ion exchange resins, Int. J. Chem. Eng. 2016 (2016) 1–13, https://doi.org/10.1155/2016/9349627.

[52] J. Wang, X. Guo, Adsorption kinetic models: physical meanings, applications, and solving methods, J. Hazard. Mater. 390 (2020) 122156, https://doi.org/10.1016/j. jhazmat.2020.122156.

[53] G.S. Live Lozada, A.I. García L´opez, A. Martínez-F´erez, J.M. Ochando-Pulido, On the modeling and optimization of two-phase olive-oil washing wastewater treatment and polyphenols recovery by ceramic tubular microfiltration membranes, J. Environ. Manage. 316 (2022) 115227, https://doi.org/10.1016/j. jenvman.2022.115227.

[54] J.J. Park, W.Y. Lee, Adsorption and desorption characteristics of a phenolic compound from Ecklonia cava on macroporous resin, Food Chem. 338 (2021) 128150, https://doi.org/10.1016/j.foodchem.2020.128150.

[55] J. Kammerer, D.R. Kammerer, R. Carle, Impact of saccharides and amino acids on the interaction of apple polyphenols with ion exchange and adsorbent resins, J. Food Eng. 98 (2) (2010) 230–239, https://doi.org/10.1016/j. jfoodeng.2010.01.001.

[56] D. Frascari, A.E.M. Bacca, F. Zama, L. Bertin, F. Fava, D. Pinelli, Olive mill wastewater valorisation through phenolic compounds adsorption in a continuous flow column, Chem. Eng. J. 283 (2016) 293–303, https://doi.org/10.1016/j. cej.2015.07.048.

[57] I. Chaari, A. Touil, M. Medhioub, Adsorption-desorption of phenolic compounds from olive mills wastewater using Tunisian natural clay, Chin. J Chem. Eng. 40 (2021) 287–292, https://doi.org/10.1016/j.cjche.2020.12.020.

[58] J.M. Ochando-Pulido, R. Gonz´alez-Hern´andez, A. Martinez-Ferez, On the effect of the operating parameters for two-phase olive-oil washing wastewater combined phenolic compounds recovery and reclamation by novel ion exchange resins, Sep. Purif. Technol. 195 (2018) 50–59, https://doi.org/10.1016/j.seppur.2017.11.075.

[59] D.P. Zagklis, A.I. Vavouraki, M.E. Kornaros, C.A. Paraskeva, Purification of olive mill wastewater phenols through membrane filtration and resin adsorption/ desorption, J. Hazard. Mater. 285 (2015) 69–76, https://doi.org/10.1016/j. jhazmat.2014.11.038.

[60] J.M. Ochando-Pulido, J.A. Vellido-P´erez, R. Gonz´alez-Hern´andez, A. Martínez- F´erez, Optimization and modeling of two-phase olive-oil washing wastewater integral treatment and phenolic compounds recovery by novel weak-base ion exchange resins, Sep. Purif. Technol. 249 (2020) 117084, https://doi.org/ 10.1016/j.seppur.2020.117084.

[61] S.M. Niknam, M. Kashaninejad, I. Escudero, M.T. Sanz, S. Beltr´an, J.M. Benito, Valorization of olive mill solid residue through ultrasound-assisted extraction and phenolics recovery by adsorption process, J. Clean. Prod. 316 (2021) 128340, https://doi.org/10.1016/j.jclepro.2021.128340.

[62] J.C. S´anchez-Rangel, J. Benavides, J.B. Heredia, L. Cisneros-Zevallos, D.A. Jacobo- Vel´azquez, The Folin-Ciocalteu assay revisited: Improvement of its specificity for total phenolic content determination, Anal. Methods. 5 (2013) 5990–5999, https://doi.org/10.1039/c3ay41125g.

[63] L. Olmo-García, C. Fernández-Fernández, A. Hidalgo, P. Vílchez, A. Fern´andez-Guti´errez, R. Marchal, A. Carrasco-Pancorbo, Evaluating the reliability of specific and global methods to assess the phenolic content of virgin olive oil: do they drive to equivalent results? J. Chromatogr. A. 1585 (2019) 56–69, https://doi.org/ 10.1016/j.chroma.2018.11.031.

[64] A. Yangui, J.R. Njimou, A. Cicci, M. Bravi, M. Abderrabba, A. Chianese, Competitive adsorption, selectivity and separation of valuable hydroxytyrosol and toxic phenol from olive mill wastewater, J. Environ. Chem. Eng. 5 (4) (2017) 3581–3589.

V.7 Management of reject streams from hybrid membrane processes applied to phenolic compounds removal from olive mill wastewater by adsorption/desorption and biological processes

ELSEVIER

Journal of Water Process Engineering

Volume 50, December 2022, 103208

Management of reject streams from hybrid membrane processes applied to phenolic compounds removal from olive mill wastewater by adsorption/desorption and biological processes

Magdalena Cifuentes-Cabezas [a], José Antonio Mendoza-Roca [a, b], María Cinta Vincent-Vela [a, b], Silvia Álvarez-Blanco [a, b]

Show more

+ Add to Mendeley Share Cite

https://doi.org/10.1016/j.jwpe.2022.103208

Abstract

This work studies the valorisation of the concentrates obtained through membrane processes for the purification of olive oil washing wastewater (OOWW). The adsorption with resins/desorption process, followed by a biological treatment with sequencing batch reactor SBRs. Three different wastewater samples were treated: an ultrafiltration reject stream (UF-R), with a high organic load and low content of phenolic compounds; a nanofiltration reject stream (NF-R), which rich in phenolic compounds and with medium organic load; a stream concentrated by forward osmosis (FO-C) with high organic content and concentration of phenolic compounds. Through the adsorption/desorption process, it was possible to recover

90% and 73%, which corresponds to 1.69 and 1.66 $g \cdot L^{-1}$ of the total phenolic compounds reject streams of NF-R and FO-C, respectively. With the SBRs, it was possible to eliminate around 80% of the organic matter present in the effluent of adsorption, and also 90% of the remaining phenolic compounds in the case of UF-R. The results obtained are promising since, on the one hand, a high recovery of phenolic compounds was achieved and, on the other hand, a large part of the organic matter of the remaining streams after adsorption was eliminated. In this way, a solution for the management of the membrane reject streams is proposed, allowing a circular economy in the wastewater treatment of olive oil processing.

Keywords: Adsorption/desorption; Olive mill wastewater; phenolic compounds recovery; Sequencing batch reactor

1. Introduction

The world production of virgin olive oil has tripled in the last years. The member countries of the International Olive Council (IOC) produced 93.3% of the world total olive oil production in the 2020/21 campaign, with Spain (49%) being the main producer, followed by Greece (9.8%), Italy (9.7%) and Portugal (4.9%) [1]. This production generates large quantities of liquid effluents called oil mill wastewaters (OMW), whose production in the Mediterranean countries fluctuates between 7×106 and 30×106 m3 [2]. A high organic load, a slightly acidic pH, low alkalinity, low nitrogen content and the presence of lipid fractions and phytotoxic compounds generally characterize these wastewaters. These characteristics generate a toxic effect for microorganisms, making their treatment difficult [3].

Over the last few years, this wastewater has gone from a waste to a co-product of the olive industry. All this because it is an outstanding source of antioxidant components (phenolic compounds) [4]. Various processes have been proposed for the recovery of phenolic compounds from these sources such as adsorption [5], liquid–liquid extraction [6], cloud point extraction [7], cooling crystallization [8], solar distillation [9] and hybrid processes [10]. In addition, many studies have been reported in which phenolic solutes were successfully recovered using integrated membrane systems. In some studies [11], the phenolic fraction is concentrated in the reject streams, by means of forward osmosis (FO), to later fractionate it

with ultrafiltration (UF) and nanofiltration (NF). Other studies [12] used a sequence of microfiltration (MF) followed by NF membranes and by osmotic distillation (OD) or vacuum membrane distillation (VMD).

Although, these hybrid membrane processes have been extensively studied for the recovery of phenolic compounds, all of them produce a reject stream, which is mainly formed by organic matter, though phenolic compounds are also present. The idea of working with sequential membrane processes is to obtain permeates and/or concentrated streams that contain high phenolic compounds concentrations for their further valorisation. However, there is few information about the management of the streams that are not of interest, generally the reject currents, considering them as waste. In some studies, it has been suggested that that they could be used as fertilizers or for biogas production [13,14]. Nonetheless, these currents were not the focus of attention, concentrating most of the research only on the recovery of phenolic compounds.

The adsorption/desorption process has been widely studied and used. The study of different materials for the adsorption of pollutants is a strong point. Some of the materials considered are rice husk nanosilica [15,16], activated carbon [17], crude olives stone [18] and polymeric resins [19]. Although the utilization of bio-sorbents from agricultural by-products presents some advantages, their utilization in the adsorption of phenolic compounds from OMW has not offered good results until now [20]. Among the most used materials currently applied for phenolic compounds, resins occupy an important position. Various studies have shown the great affinity between some resins and phenolic compounds, producing effluent from the treatment having a great purity. On the other hand, their easy recovery and reuse, together with low cost and low for the environment, make them appropriate technologies for the recovery of these antioxidant compounds On the other hand, their easy recovery and reuse, together with low cost and low environmental impact, make them appropriate technologies for the recovery of these antioxidant compounds [21,22].

After the recovery of these compounds, the remaining streams, which are concentrated in other organic compounds, become residues that have to be treated to reduce their organic load [23]. In membrane processes there is always a reject current, which is mainly formed by

organic matter like suspended or colloidal matter. Biological treatment is an option that offers several advantages, such as allowing the removal of organic compounds in an economical, space-saving and environmentally friendly way without the addition of any chemical reagent [24].

An interesting study was carried out by Conidi et al. [25], where OMW was treated with a hybrid membrane process that contemplated first stages of MF and UF, followed by two biocatalytic membrane reactors (MBMR) for the conversion of oleuropein into the isomer of the oleuropein aglycone. In this study, both the MF and UF rejection currents were recycled to the process feed and no data about the management of the withdrawals from the systems were reported. To date no work has been found that presents the recover of all the currents generated in the hybrid membrane processes. To sum up, through some membrane processes concentrated streams with high purity of phenolic compounds and permeates with characteristics to be reincorporated into the process are obtained [26]. However, after other treatments proposed in the literature, there are residual streams with a high contaminant load, either after recovering/extracting the phenolic compounds or simply discarded streams during the process

In this work, the recovery by adsorption of phenolic compounds from reject streams of membrane processes of OMW treatment was studied, as well as the management of the remaining streams. The water samples corresponded to the rejections obtained from UF and NF processes and to the concentrated stream coming from a FO process. These streams were further treated by a SBR and the effects of the different pre-treatments on the biodegradation were investigated.

2. Materials and Methods

2.1 Feed samples characterization

The samples corresponded to reject/concentrated streams from different membrane processes (UF, NF and FO). Fig. 5.52 shows a diagram in which the origin of the different waters to be treated can be seen adsorption is highlighted in pink whereas SBR in green color. The figure presents two different hybrid processes proposed for the recovery of phenolic

compounds. The initial raw samples corresponded to olive oil washing wastewaters (OOWW) and were provided by an olive oil milling plant located in the Valencian Community (Spain). The raw water was subjected to pre-treatment following the protocol presented in previous studies [23], including flotation, sedimentation and cartridge filtration.

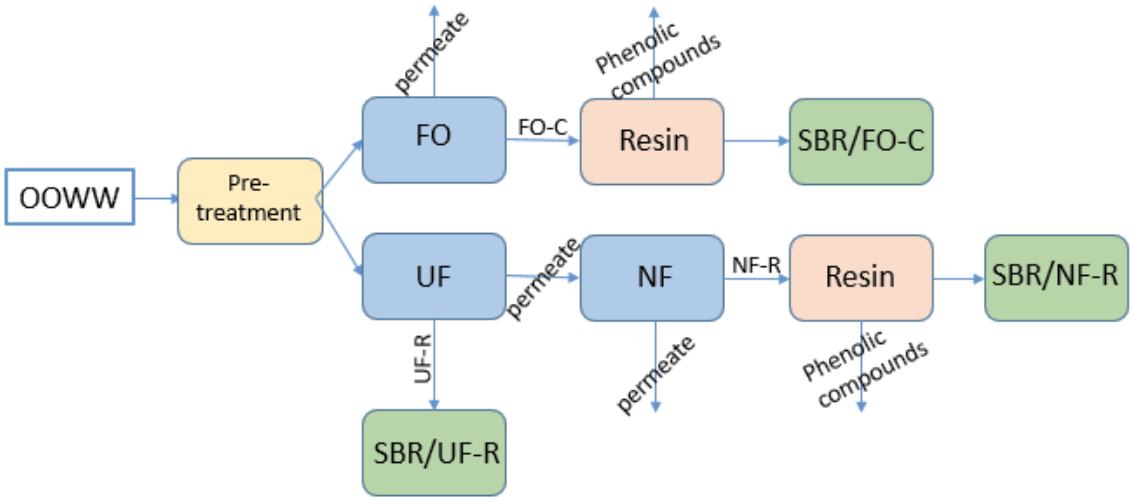

Fig 5.52. Diagram of olive oil washing wastewater (OOWW) treatment

The concentrate obtained in the FO process (FO-C) and the reject stream from the NF process (NF-R) were subjected to the adsorption process with resins prior to biological treatment to recover the phenolic compounds. In addition, the reject stream from the UF process (UF-R) was treated directly with the SBR due to the lower concentration of phenolic compounds. Table 5.30 shows the average values of the main parameters measured in the different wastewater samples before the proposed treatment.

Table 5.30. Main characteristics of the different samples used in the study

Parameters	UF- R	NF-R	FO-C
pH	5.3 ± 0.10	5.1 ± 0.00	5.0 ± 0.00
Conductivity ($mScm^{-1}$)	4.7 ± 0.2	5.18 ± 0.3	4.73 ± 0.2
TSS (gL^{-1})	2.7 ± 0.5	< 5 ppm	2.5 ± 0.1
COD (gL^{-1})	33.16 ± 3.29	18.54 ± 1.36	28.05 ± 1.87
TPhC ($mgTyeq.L^{-1}$)	372.15 ± 4.13	1874 ± 12.01	2342 ± 19.16
SUG ($mgGlu.L^{-1}$)	960 ± 3.14	3703 ± 7.15	4977 ± 10.03

TSS: total suspended solids; COD: TPhC: total phenolic compounds SUG: sugars

2.2 Adsorption/Desorption process

The resin used was Macronet's MN200 (supplied by Purolite), which was selected based on a previous study where the adsorption/desorption process was optimized [27]. The resin is moderately hydrophobic, whit a polystyrene crosslinked with divinylbenzene matrix, with a surface area of 1100 m2/g and a pore diameter of 700/15 Å (macropores/micropores). The resin was conditioned for 60 minutes at 140 rpm in a 2% w/v solution of sodium hydroxide before being used. Then, the NF-R and FO-C samples were mixed with a dosage of 40 g/L of resin for 180 min at a constant speed of 140 rpm. After the working time, the liquid fraction was separated by means of a 0.2 μm filter to analyse removal efficiency. The resins were washed three times with osmotized water and then subjected to desorption with a 50% v/v ethanol/water solution under the same conditions used for adsorption (180 min at a constant speed of 140 rpm). The supernatant was analysed to measure concentration of COD, TPhC and SUG and calculate the recovery rates. The adsorption (removal) and desorption (recovery) were calculated with the following equations:

$$\%Removal = \frac{C_0 - C_e}{C_0} \cdot 100 \quad (1)$$

$$\%Recovery = \frac{C_d \cdot V_d}{(C_0 - C_e) \cdot V_0} \cdot 100 \quad (2)$$

Where C_0 and C_e are the initial and equilibrium concentrations, respectively (in terms of COD, TPhC and SUG); C_d is the concentration in the desorption solution. V_d and V_0 correspond to the volume (in mL) of the desorption solution (ethanol/water 50%) and of the initial sample volume, respectively.

Adsorption kinetics were studied through two models, the pseudo first [28] and pseudo second [29] order reaction which were used to fit the experimental data under the following equations, respectively:

$$\ln(q_e - q_t) = \ln q_e - k_1 \cdot t \quad (3)$$

$$\frac{t}{q_t} = \frac{1}{k_2 \cdot q_e^2} + \frac{1}{q_e} \cdot t \quad (4)$$

Where the amount of solute adsorbed per gram of adsorbent at equilibrium is represented by *qe* ($mg \cdot g^{-1}$), whereas *qt* ($mg \cdot g^{-1}$) is the concentration of adsorbate in solid phase at time *t* (min), *k1* (min^{-1}) and *k2* ($g \cdot mg^{-1} \cdot min^{-1}$) represent the pseudo first order and the pseudo second order rate constant, respectively. These constants were determined by linear regression of two plotted graphs, *Ln (qe-qt)* versus time (t) for the pseudo first order and *t/qt* versus time (t) for the pseudo second order.

The intra particle diffusion model, also known as Weber's diffusion model, was used for the identification of the mechanism involved in the adsorption process. The adsorption of phenolic compounds is controlled by different steps, which can be related to film or external surface diffusion, pore diffusion, surface diffusion and adsorption on the pore surface, or a combination of them [30]. The followed equation (5) represents the Weber's diffusion model,

$$q_t = k_d^{1/2} + I \quad (5)$$

Where k_d ($mg \cdot g^{-1}\ min^{-½}$) is the intra-particle diffusion rate constant and *I* represents the thickness of the boundary layer on the adsorbent surface. Both parameters were obtained by a linear plot of *qt* versus $t^{½}$.

2.3 Biological treatment

After the removal of phenolic compounds, UF-R and NF-R and FO-C samples were subjected to biological treatment, using the following protocol.

2.3.1 Experiment 1

Due to the high organic load present in the wastewater samples, a preliminary study in batch mode was carried out. The main objective was to find a concentration at which the bacteria were not affected. Different concentrations of each sample in tap water (5%, 10%, 15%, 20% and 30% v/v) were mixed with biomass taken from an activated sludge reactor of a municipal wastewater treatment plant in beakers. The operation time was 24 h and agitation and aeration were continuous. The operating conditions were the same for all the tests, maintaining mixed liquor suspended solids (MLSS) of 3.5 $g \cdot L^{-1}$, a feed volume of 0.25 L and a food-to-microorganism ratio (F/M) of 0.15 $gCOD \cdot gMLSS^{-1} \cdot d^{-1}$. The required sludge volume was calculated based on the percentage (COD concentration) of wastewater in the feed. As mentioned above, the purpose of this study was to determine the concentration of each type of wastewater (in percentage) that would be appropriate as the initial feed to a biological reactor. Then once the bacteria have adapted, the concentration of wastewater in the feed (diluted with tap water), was progressively increased to reach the maximum concentrations as possible. In addition, a biodegradability analysis by a respirometric test was carried out to determinate the toxicity of each sample. The test was performed following the protocol presented by Zuriaga-Agustí et al. [31]. It was carried out by adding different doses (10 mL as first dose and 5 mL for the rest of the doses) of wastewater to a 500 mL of mixed liquor sample in order to measure the influence of the sample addition on the standard oxygen uptake rate.

2.3.2 Experiment 2

Once the starting concentration was selected, three laboratory reactors, named as SBR/UF-R, SBR/NF-R and SBR/FO-C (Volume of reaction = 6L in each reactor), were operated as sequencing batch reactors (SBR) for 65 days. The reactors were seeded with activated sludge from a municipal wastewater treatment plant (Valencia, Spain) and fed with the above-mentioned samples. Dipotassium phosphate and urea (both reagents supplied by Panreac, Spain) were added to each feed solution to adjust the phosphorous and nitrogen concentrations to obtain a COD:N:P relationship of 100:5:1 [32]. The SBRs were operated setting 1 cycle per day, with five phases per cycle, filling (10 min), reaction (1h/21h anaerobic/aerobic), sedimentation (1.5 h), draw (10 min) and idle (10 min). The initial feeding

volume (ml/day) was 900 for the SBR fed with FO-C and NF-R samples and 600 for the SBR/UF-R. The feed volume (and consequently the withdrawn volume of treated wastewater) was increased gradually during the experiment. In fact, the feed volume increased a 5% every 10 or 15 days (depending on the reactor). Therefore, the hydraulic retention times (HRT) and the volume exchange ratio (VER), which is the quotient between the feed volume and the reaction volume, were variable during the operation of the reactors, being also different for each reactor.

2.3.3 Analytical methodology of the mixed liquor

In both experiments, COD, MLSS, total nitrogen (TN), total phosphorous (TP), and Total Phenolic Compounds (TPhC) (for SBR/UF-R) were measured. The cell lysis was studied through DNA analysis, and the dissolved oxygen concentration (DO) was monitored throughout the process by using standard probes. In experiment 1, the parameters were measured at 3 hour, 6 hour and at the end of the test (24 h). In Experiment 2, these parameters were analysed every two days in each reactor. In both tests the removal efficiency (*%R*) of COD (and TPhC for SBR/UF-R) was calculated for each reactor by the following equation,

$$\%R = \frac{C_{IN} - C_{EF}}{C_{IN}} \cdot 100 \quad (6)$$

Where C_{IN} and C_{EF} correspond to the concentration ($mg \cdot L^{-1}$) of COD or TPhC measured in the feed and the SBR effluent (experiment 2) or dissolved in the beaker (experiment 1), respectively. The COD, TP, TN and the other nitrogen forms, were measured by kits (Merck) using a DR600 Spectrophotometer (Hach Lange); MLSS concentrations were measured according to APHA [33]. TPhC (mgTYeq·L-1) was measured according to Singleton et al. [34] following the Folin–Ciocalteau method whereas sugars were analysed with Sucrose/D-Glucose/D-Fructose colorimetric kit from r-biopharm (Germany), using glucose (Panreac, Spain) as a standard. DNA was determined by FastDNA® SPIN kit (MP Biomedicals, USAATPc) following the protocol presented in Ferrer-Polonio et al. [35].

In experiment 2, ATPc (Adenosine triphosphate from living cells), AVSS (Active Viable Solids) and BSI% (Bacterial Stress Index) were determined at the end of each stage

following the protocol also presented in the above mentioned paper [273]. The results of total and dissolved ATP were obtained from PhotonMaster™ Luminometer (Luminultra®) in RLU (Related Luminescence Units), for then being converted to ngATP/mL using a Standard ATP solution UltraCheck™ and LumiCapture™ Lite software.

3. Results

3.1 Adsorption/Desorption

Table 5.31 shows the results obtained in the adsorption/desorption of phenolic compounds from NF-R and FO-C samples with the MN200 resin. The great affinity of the resin with phenolic compounds can be clearly seen, which is reflected in high adsorption percentages (>90%). This is mainly due to the properties of the resin, since the hypercrosslinked polystyrene material gives the surface of the resin the characteristic of being very hydrophobic, thus having a great affinity for adsorbates with phenyl groups [36,37]. Since it has been reported that the presence of other substances present in OMW can interfere with the adsorption of phenolic compounds [38]. As these substances are able to cause inhibitory effects and reduce the elimination of contaminants, the adsorption of COD and sugars has been studied. The low adsorption of sugars was also expected. Since it was observed in a previous study performed by the authors [27], where the low affinity of the MN200 resin for sugars was demostrated. The high selectivity for phenolic compounds was one of the reasons considered to selected this resin. This behaviour is explained because polymeric styrene-based adsorbents have a high specificity for hydrophobic substances (such as phenolic compounds), showing little interaction with sugars [39,40]. This is due to the more favorable interactions between a polymer (styrene-DVB) with aromatic adsorbent species and a hydrophobic substance in comparison with sugars. This causes the inhibition of sugars adsorption due to the competitiveness with phenolic compounds adsorption [41]. Phenolic compounds-resin interactions could be of the pi-pi type and/or hydrogen bonds, and occur between the benzene rings in the polymer and the adsorbent aromatic species [42].

The highest removal of TPhC and the lowest removal of sugars occurred in the NF-R sample. This may be due to the fact that, compared to the FO-C sample, the NF feed was preceded by an UF process, which removed a considerable concentration of organic matter.

Organic matter could compete with the phenolic compounds for the adsorption sites in addition to generate a rapid clogging of the resin, reducing the adsorption of specific species [43].

Table 5.31. Removal efficiency of the adsorption with MN200 (40 $g \cdot L^{-1}$) and recovery of the desorption (ethanol/water 50%) for the NF-R and FO-C samples

		NF-R		FO-C	
		mgL^{-1}	%	mgL^{-1}	%
Removal	TPhC[a]	1811.43 ± 1.21	96.42 ± 0.76	2173.42 ± 6.07	92.78 ± 0.26
	SUG[b]	668.97 ± 16.38	17.13 ± 0.44	1276.17 ± 49.5	25.73 ± 4.16
	COD[c]	5676.00 ± 66.40	24.49 ± 1.78	8344.00 ± 72.00	21.28 ± 0.18
	COD_{TPhC}[d]	3985.16 ± 2.64	71.79 ± 0.37	4781.53 ± 13.36	57.31 ± 0.65
	COD_{SUG}[e]	715.79 ± 17.53	12.61 ± 0.75	1492.02 ± 37.45	17.96 ± 2.55
Recovery*	TPhC[a]	1689.18 ± 15.67	93.23 ± 0.87	1716.33 ± 54.42	76.55 ± 2.51
	SUG[b]	278.13 ± 7.76	38.86 ± 1.08	678.80 ± 43.87	43.86 ± 2.94
	COD[c]	4733.00 ± 93.86	85.27 ± 1.66	5540.00 ± 22.00	66.40 ± 1.08
	COD_{TPhC}[d]	3716.88 ± 34.48	82.26 ± 1.28	3649.70 ± 62.76	65.88 ± 1.10
	COD_{SUG}[e]	296.42 ± 8.54	6.26 ± 0.12	696.48 ± 48.26	12.57 ± 0.67

[a]TPhC: total phenolic compounds; [b]SUG: sugars; [c]COD: chemical oxygen demand; [d]COD_{TPhC}: COD concentration of total phenolic compounds adsorbed or desorbed; [e]COD_{SUG}: COD concentration of total sugar adsorbed or desorbed; *Recovery based on the adsorbed amount

Another way to justify the better performance of the process for NF-R is by calculating the COD related to the total phenolic compounds. Through the analysis presented by Ferrer-Polonio et al. [44] it is possible to calculate theoretically the COD associated to the TPhC (in mgTy·L-1) using Eq (6).

$$COD_{TPhC.ads} = (C_{0.TPhC} - C_{e.TPhC}) \cdot 2.2 \quad (6)$$

Where 2.2 corresponds to the mg of O_2 needed to oxidate one mg of tyrosol. Following the same analysis, the COD associated to the sugars has been calculated using Eq (7), considering that 1 g of glucose is equivalent to 1.1 g of COD.

$$COD_{SUG.ads} = (C_{0.SUG} - C_{e.SUG}) \cdot 1.1 \quad (7)$$

The difference between the initial concentration (*C0*) and the equilibrium concentration (*Ce*) corresponds to the total of TPhC or SUG adsorbed. It can be seen that the percentage of COD that represents the adsorbed phenolic compounds is higher for the NF-R sample. This trend was also observed for recovery, as the solution obtained after desorption presented a higher CODTPhC/COD ratio in the case of the NF-R sample. This is due to the presence of a large amount of high and low molecular weight compounds, such as saccharides, amino acids and macromolecules in the FO-C sample, which could affect the sorption of phenolic compounds [45]. However, as a result of the ultrafiltration pretreatment (see Fig. 5.52), the NF-R had lower organic content than the FO-C. These results can relate the pre-treatment of the OOWW to the phenolic compopunds purity in the final concentrated sample obtained.

Table 5.32. Kinetic parameters of pseudo first and pseudo second order for the adsorption process

Sample	q_e (ex) ($mg \cdot g^{-1}$)	Pseudo-first order			Pseudo second order		
		q_e ($mg \cdot g^{-1}$)	k_1 (min^{-1})	r^2	q_e ($mg \cdot g^{-1}$)	k_2 ($g \cdot mg^{-1} \cdot min^{-1}$)	r^2
NF-R	54.46	28.81	0.0733	0.9464	55.25	0.008465	0.9953
FO-C	45.25	35.21	0.0910	0.8795	46.30	0.004265	0.9988

Regarding the kinetics of the adsorption process, the values obtained after fitting the data to pseudo first and pseudo second order reactions are presented in table 5.32. It can be seen that the qe obtained with the pseudo first order model gives a very low value compared to the experimental one (qe ex). On the other hand, the pseudo second order model gives an r^2 closer to one, which better fitting of the experimental data. This implies that the adsorption rate depends more on the adsorption capacity of the resin and not on the adsorbate concentration [46].

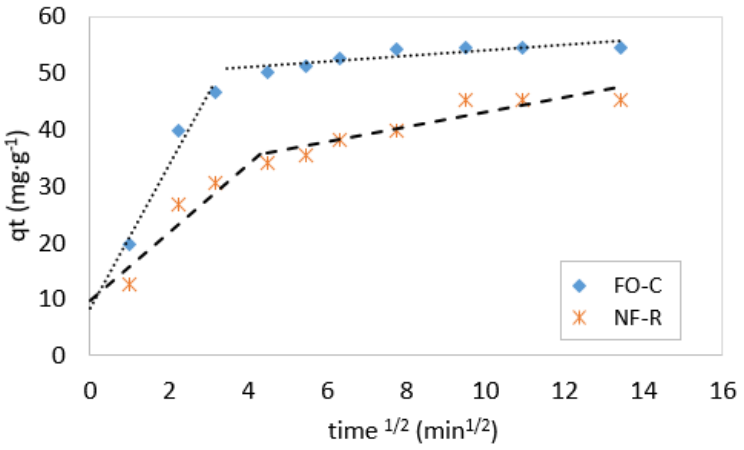

Fig. 5.53 Intra particle diffusion model for the adsorption process

In fig. 5.53, the representation of the intra-particle diffusion model is presented. A non-linearity of the data is observed, in fact two trends are clearly seen for both adsorption processes. This implies that not only intra particle diffusion controls the process, but more than one process affected adsorption [46]. The first adsorption step controls up to 4 $min^{1/2}$. A positive value of the intercept of this first stage can be interpreted as a very fast kinetic process, which is responsible for a fast (inter-particle) adsorption of the phenolic compounds on the resin in the initial stage of the kinetic isotherm. Then, the passage from one trend to the other is generally attributed to boundary layer diffusion effects or external mass transfer effects. Finally, the second stage is governed by intra-particle diffusion [30,44,47]. Similar results were obtained by other authors studying the phenolic compounds adsorption with MN200 resin. Such is the case of the study carried out by Valderrama et al. [48], who attributed this trend to the sorption stages of the external (inter-particle diffusion, fist stage) and internal (intra-particle diffusion, fist stage) surfaces and to the equilibrium approach, respectively. These authors explained that the fast adsorption speed of the first section is due to the sorption in the macroporous structure. Then the molecules diffuse towards the microporous structure, to finally be adsorbed by the surface of the adsorbent particles. In the present work, the resistance to diffusion increased from the first to the second stage. This could explain the

decrease observed in the value of K_d, which changed from 12.61 to 0.48 $mg \cdot g^{-1} \cdot min^{-1/2}$ for the NF-R and from 6.03 to 1.32 $mg \cdot g^{-1} \cdot min^{-1/2}$ for the FO-C.

It has to be highlighted that it was possible to remove almost all the phenolic compounds presented in the water samples (96.42% and 92.78% from the NF-R and FO-C samples respectively). This is important to ensure a better treatment in the following biological step, since microbial bioconversion can be inhibited due to the toxic and biostatic effects of phenolic compounds [49]. In addition, a concentrated solution rich in phenolic compounds of the order of 1.7 $g \cdot L^{-1}$ was achieved, corresponding to 90% and 73% of the initial total phenolic compounds present in the NF-R and FO-C water samples, respectively.

An issue to consider in adsorption/desorption processes is both the recovery and reuse of the adsorbents. In this case, it was possible to recover the resin by means of 3 washes with water (5 min at 150 rpm) followed by drying in an oven for 3 h at 50 ℃. Regarding their reuse, it was possible to use the same resins in 4 adsorption/desorption cycles without losing their efficiency. Other studies [44] have reported that after 10 cycles of reuse these resins begin to be affected in terms of their efficiency. These authors observed a decrease of 0.9% in the adsorption capacity of phenolic compounds and 8.5% in the desorption percentage when working with ultrafiltered fermentation brines from table olive processing (FTOP). It is important to note that these results were obtained with the permeate from an ultrafiltration process. Thus the stream is comparable to NF-R. These authors observed greater decrease in the efficiency (7.9% and 12.1% for the adsorption and desorption capacities, respectively) when the FTOP filtered at 60 μm was directly submitted to an adsorption/desorption process. Therefore, both the pretreatment and the characteristics of the wastewater to be treated are key points for resin reuse.

In summary, through the adsorption process, the removal of phenolic compounds from NF-R and FO-C was achieved. This implies, the recovery of valuable compounds, on the one hand, as well as the removal of phytotoxic compounds prior to a biological treatment, on the other hand.

3.2 Biological treatment: Preliminary study

The preliminary study was performed in order to obtain information about the biodegradability of the samples and to select the initial feed volume of each SBR operated in the experiment 2.

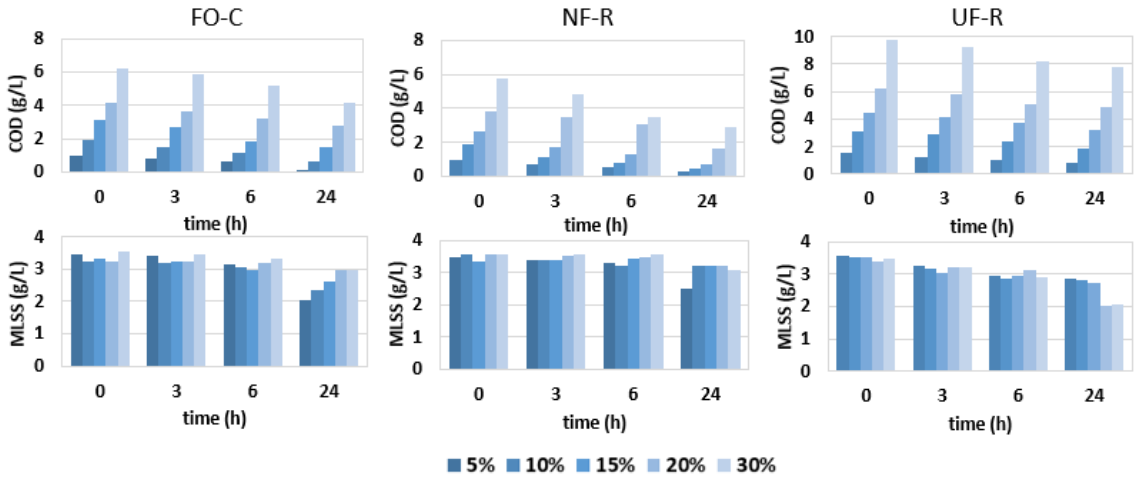

Fig. 5.54 Variation of COD and MLSS over time for the different concentrations of samples analysed

It can be seen in Fig 5.54. that the water samples without phenolic compounds (FO-C and NF-R) are more easily degradable by microorganisms, as the organic matter was consumed in less time (greater decrease in COD). Thus, more than 50% of the organic matter for the concentrations of 5%, 10% and 15% for the FO-C sample was eliminated in 24 h. At concentrations of 20% and 30% the elimination after 24 h droped to 33% approximately. For the NF-R sample, the organic matter removal increased up to 75% for concentrations less than 15%. Above this concentration, organic matter removal decreased to an average value of 53%. The soluble COD values did not present a great variation from 6 to 24 hours, which was more noticeable for the concentrations of 5% and 10% in both samples. This implies that there is no more readily biodegradable organic matter that could be consumed by organisms. This is also evidenced by the MLSS values. Once microorganisms have consumed all the readily

biodegradable organic compounds they pass to an endogenous respiration phase, in which cell lysis is generated. This produced a decrease of the MLSS concentration from 3.37 ± 0.14 $g \cdot L^{-1}$ to 2.58 ± 0.40 $g \cdot L^{-1}$ for FO-C and from 3.51 ± 0.10 $g \cdot L^{-1}$ to 3.06 ± 0.30 $g \cdot L^{-1}$ for NF-R (mean value). In addition, an increase of the dissolved oxygen at 24 hours was detected, reflecting that organic matter degradation has slowed down.

A different behaviour was observed for the UF-R sample. The COD decreased only 43 ± 5% (average value for 5 and 10% concentrations, respectively). Then, the increase in the concentration of the sample caused the COD removal to be reduced to 24 ± 4%. The high concentration of TPhC and their antimicrobial characteristics explains the slower degradation and possible cell lysis. In other words, inhibition of biomass occured. Other authors also reported the antimicrobial characteristics of phenolic compounds [50–53]. This can be observed by the decrease in MLSS concentration (more pronounced when the percentage of wastewater in the feed was higher). To confirm the cell lysis, a DNA test (Fig. 5.55) was performed. It was observed how the DNA in the UF-R samples increased considerably compared to the other samples.

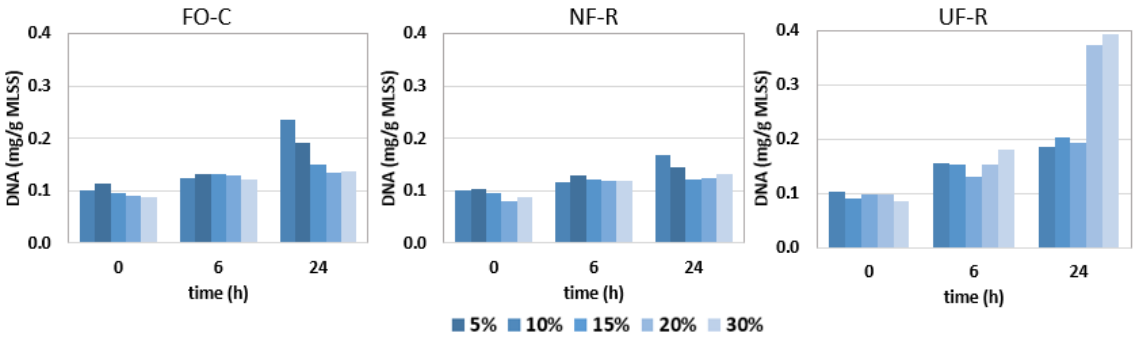

Fig. 5.55 Variation of DNA with time for the different water samples

Table 5.33. Percentage of total phenolic compounds removal during the tests for the different concentrations of UF-R

	TPhC[a] removal (%)		
Concentration of UF-R[b]	3 (h)	6 (h)	24 (h)
5%	13.3 ± 3.4	26.7 ± 2.8	41.3 ± 8.0
10%	18.0 ± 4.6	25.6 ± 3.8	40.0 ± 6.1
15%	16.0 ± 6.5	19.0 ± 1.2	36.8 ± 2.3
20%	6.0 ± 2.3	21.3 ± 5.3	34.7 ±
30%	5.4 ± 0.7	12.3 ± 3.2	20.5 ± 5.7

[a] TPhC: total phenolic compounds
[b] UF-R: rejection of the ultrafiltration process performed with olive oil washing wastewater

Likewise, the elimination of TPhC in the sample was assessed in the UF-R sample. In table 5.33, it can be seen that the removal percentages at 24 hours were around 21 - 41%. These values are high taking into account the toxicity of these compounds and the conditions of the batch tests (section 2.3.1). However, the possible elimination of phenolic compounds from the sample by adsorption in the biomass must also be taken into account. The highest reduction percentages were observed for sample concentrations of 5 and 10%. Similar results were seen in a study with Pleurotus ostreatus grown in SBR with an OMW model solution [54]. These authors observed that the removal of phenolic compounds from the fermentation medium was higher in the OMW with low phenolic content compared to those with high phenolic content.

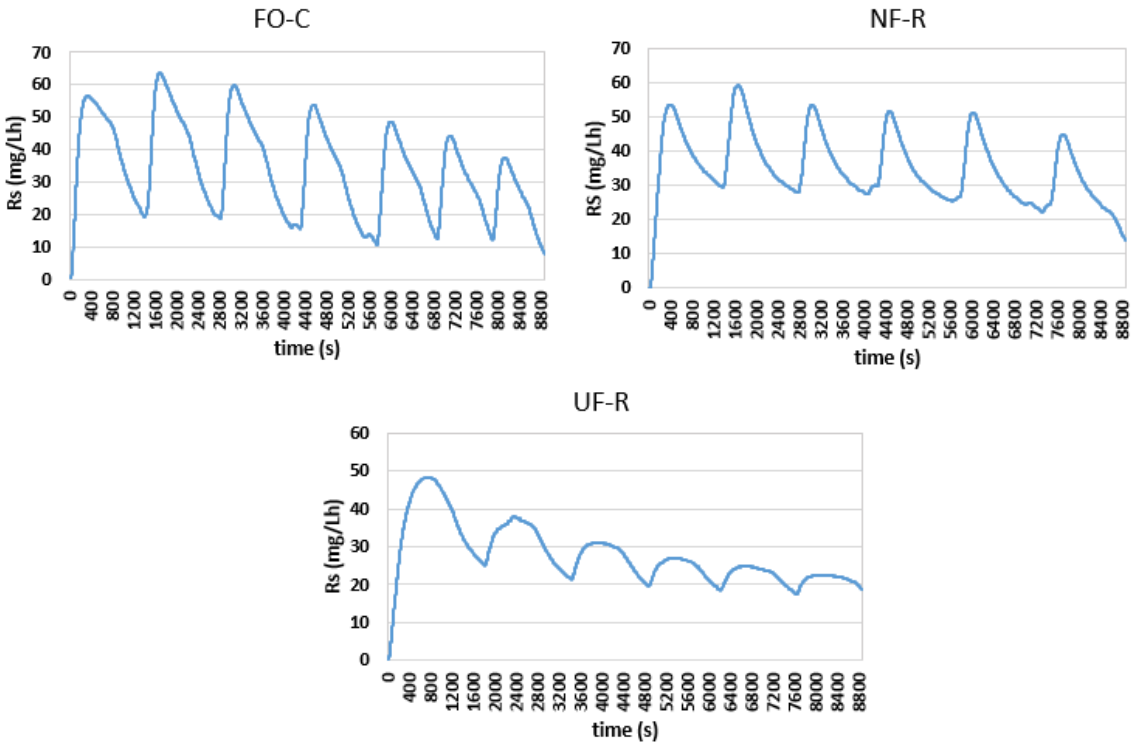

Fig. 5.56 Water samples toxicity test

Respirometry tests (Fig. 5.56) confirmed what was expected after batch tests. This assay is based on the measurement of the rate of oxygen consumption by the bacteria when they degrade the different samples. It can be seen how the FO-C and NF-R samples show a similar trend, slowly decreasing the respiration rate. The tests show that there was negligible toxic impact on the activated sludge, as almost the same maximum respiration rate (Rs) was achieved after the addition of each sample dose. On the other hand, a completely different behavior can be observed for the UF-R sample, compared to the other two wastewaters analyzed. The symptoms of toxicity are evident, observing a drastic decrease in Rs, which implies that this sample was more toxic for the microorganisms. The results were consistent with those obtained in experiment 1. Although several compounds present in OMW contribute to its toxicity [55], this was attributed to the presence of phenolic compounds, since the samples have similar characteristics, only differing in the concentration of these compounds.

As previusly commented and reported by other authors, it is known that phenolic compounds are characterized by having intense phytotoxic and antimicrobial properties [56]. Therefore, their presence would limit the biodegradation of the different wastewater samples studied.

Considering the results explained above, it was decided to start the tests of the experiment 2 with a concentration of 15% of NF-R (COD of 2.71 $g \cdot L^{-1}$) and FO-C (COD of 4.21 $g \cdot L^{-1}$) in the feeds to SBR/NF-R and SBR/FO-C and with a concentration of 10% of the UF-R (COD of 3.30 $g \cdot L^{-1}$) in the feed to SBR/UF-R.

3.3 Biological treatment: SBR-performance

3.3.1 COD, MLSS and TPhC removal

Fig. .57 shows the MLSS growth rates together with the COD removal efficiencies for the SBRs. The dashed lines indicate the increments of the feed (wastewater sample) volume, delimiting different operation stages. It can be observed that microorganisms better adapted to the water samples without phenolic compounds (SBR/FO-C and SBR/NF-R), since in these reactors COD removal efficiencies reached values above 80%. It led to increase the feed volume sample by 5% every 10 days, which determined an increase of VER up to 0.01 at each stage. In the first ten days, the SBR/FO-C and the SBR/NF-R reactors reached an average COD removal efficiency of 84 ± 0.3% and 86 ± 0.7%, corresponding to a COD concentration in the effluent of 440 ± 9 $mg \cdot L^{-1}$ and 280 ± 15.8 $mg \cdot L^{-1}$, respectively. In stage 2, SBR/FO-C showed an increase in the removal of organic matter above to 92%. This behaviour remained stable until the fourth stage, achieving an average removal rate of 89 ± 4%. Similar results were presented by Farabegoli et al. [57] treating diluted OMW with SBR. They observed that from the first stage (dilution 1:50, COD close to 1.3 $g \cdot L^{-1}$) to the second one (dilution 1:25, COD close to 2.4 $g \cdot L^{-1}$), the COD removal increased from 75% to 90% (average values). They attributed it to the fact that in the first stage the elimination kinetics were slower, depending strictly on the concentration of the substrate. On the other hand, by having less substrate availability, the biomass could pass into a state of endogenous respiration, producing a partial mineralization. In the second stage, once biomass has been acclimated, the rate of organic matter removal increases. After this period, the COD removal efficiency fell to 85 ± 2% in the

fifth stage. This could be due to the fact that the microorganisms would be affected by the increase in food, which leads to an increase of the food to microorganisms ratio. A high F/M ratio can result in an excess of substrate in the effluent if biodegradable organic matter exceeds biomass consumption capacity [58]. Therefore, the COD level in the effluent would increase. On the other hand, analyzing the results, it can be observed that in the fifth stage, there was a low growth of MLSS, which therefore means that there was not enough bacteria in the systems to dispose of the organic matter. It has been reported that maintaining an adequate concentration of MLVSS and MLSS is necessary to prevent overloading the process and make sure that the biomass (bacterial population) is sufficient for the biological reaction to take place during aerobic degradation [59].

Regarding the SBR/NF-R, the COD elimination was stable until the fifth stage with an average value of 92 ± 2%. Then, it decreased to 84%, and finally, in the last stage it managed to achieve an elimination of 89 ± 3%. In this reactor, the increase in feed volume did not corresponded to a significant decrease in COD removal efficiency.

Finally, it should be noted that the low fluctuation in the COD removal efficiencies presented by SBR/FO-C and SBR/NF-R was due to the adaptation of the microorganisms to the medium. The high values observed for COD removal percentages, which remained relatively stable, implied that the sludge microbial community was well adapted to the new environment. Other studies also indicated that the good performance of the SBR in terms of high COD elimination could be related to an adaptability of the biomass to the environment [51,59,60].

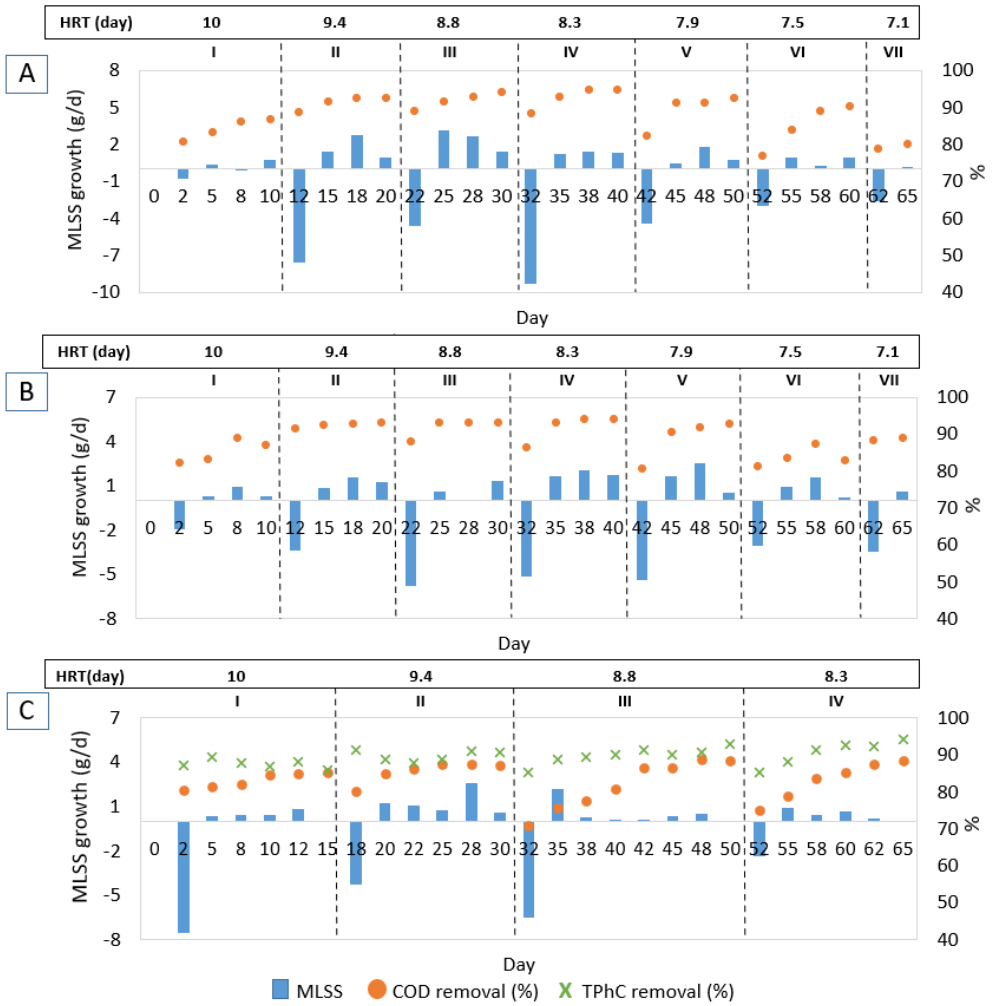

Fig. 5.57 COD removal and MLSS variation during all the tests for the three SBRs. A: SBR/FO-C; B: SBR/NF-R; C: SBR/UF-R. For SBR/UF-R the total phenolic compounds (TPhC) removal efficiency is also presented. (Dashed lines indicate the days on which the feed was increased in each reactor)

The behaviour presented by the SBR/UF-R was very different from the other two SBRs. After a first stage of 15 days for acclimation to the initial wastewater feed volume, it was possible to increase the feed volume three times, achieving 4 stages in the experimental period. The COD removal efficiency in the first stage was 83 ± 0.7% for the COD and 88 ± 0.9% for the TPhC. Like the other SBRs, COD removal increased in the second stage, reaching

up to 85 ± 3%. Then, it decreased to 83 ± 7% in the third stages. Regarding the elimination of TPhC, it increased in the second stage reaching 90% at the end of the second and third stages. In the last 15 days, the COD removal efficiencies tended to a stationary value close to 80%, meanwhile TPhC elimination reached values above 90%.

Although the SBR/UF-R reactor presented a high TPhCs removal, it was not possible to remove them completely, leaving a constant content of phenols in the system. This may be due to the fact that a phenolic fraction is highly resistant to oxidation [54,61]. This fraction mainly consists of phenolic compounds of higher molecular weight (>5kDa), since the wastewater was obtained by the rejection of a 5kDa UF membrane, which is more difficult to be biodegraded [57]. Finally, it was possible to feed the SBR/UF-R reactor with 720 mL of sample (concentration of about 3.3 $g \cdot L^{-1}$ COD and 210 $mg \cdot L^{-1}$ of TPhC), keeping the removal of COD (close to 80%) and TPhC (between 88-90%) constant. Acoording to other authors, in addition to biodegradation, the elimination of phenolic compounds could also be related to other mechanisms, such as chemical oxidation, evaporation or adsorption onto activated sludge [62]. However, this was not studied in this work.

It has to be highlighted that COD removal percentages obtained in the three SBRs were higher than those reported in other studies [63,64], which may be mainly due to the pre-treatment and the low concentration of phenolic compounds.

Although the removal percentages of COD and TPhC remained constant, the concentration of both parameters in the effluent increased. Chiavola et al. [65] in their study of the treatment of raw OMW and OMW-UF permeate with a bioreactor, also observed that the concentration of residual polyphenols and total organic matter scaled linearly with the concentration of the influent (these authors also mixed OMW with dilution water). These authors indicated that the increase in the concentration of the effluent corresponded approximately to the inert soluble fraction of the influent, which was about 10%. Also in the mentioned study [65], it was reported a constant removal of around 90% of the COD, which implied meeting the required COD value by the legislation. However, the concentration of phenols was higher than the legal standards required for discharge. In the present case, by

removing previously TPhC using resins in the case of FO-C and NF-R, the effluents met the limits for both discharge and reuse as machinery cleaning water.

The decrease of the removal that occurred in the final stages of the tests could be related to the concentration of microorganisms. It can be seen that after each increase in the feed concentration, the MLSS concentration showed a significant decrease. This is due the fact that not all microorganisms could be able to adapt to changes in the medium. Then, a period of acclimation to the new food to microorganisms ratio is needed. It can be observed how the MLSS from SBR/FO-C shows the greatest decrease on day 32, which implies that the increase in the feed volume caused a great impact on the organisms. On the other hand, the MLSS concentrations from the SBR/UF-R reactor were the ones that showed the greatest decrease at the beginning of the test. This may be due to the fact that these organisms must deal with both a high organic load and the presence of phenolic compounds, which may inhibit the biomass. On the other hand, although in the later stages the decrease in MLSS was less than in the first ones, the growth rate of microorganisms was also lower. The most affected SBR was the one fed with FO-C, which started with a MLSS concentration of 3.476 ($g \cdot L^{-1}$) and ended (last stage) with only 0.6 ($g \cdot L^{-1}$). SBR/NF-R and SBR/UF-R began with 3.452 ($g \cdot L^{-1}$) and 3.488 ($g \cdot L^{-1}$) and ended with 1.2 ($g \cdot L^{-1}$) and 1.42 ($g \cdot L^{-1}$), respectively.

3.3.2 ATP, DNA and BSI

The decrease in the MLSS is related to cell lysis. This can be confirmed with the data presented in Fig. 5.58. It is important to point out that on day 11 no sample was taken from the SBR/UF-R reactor because its first stage, which is biomass conditioning, lasted 15 days.

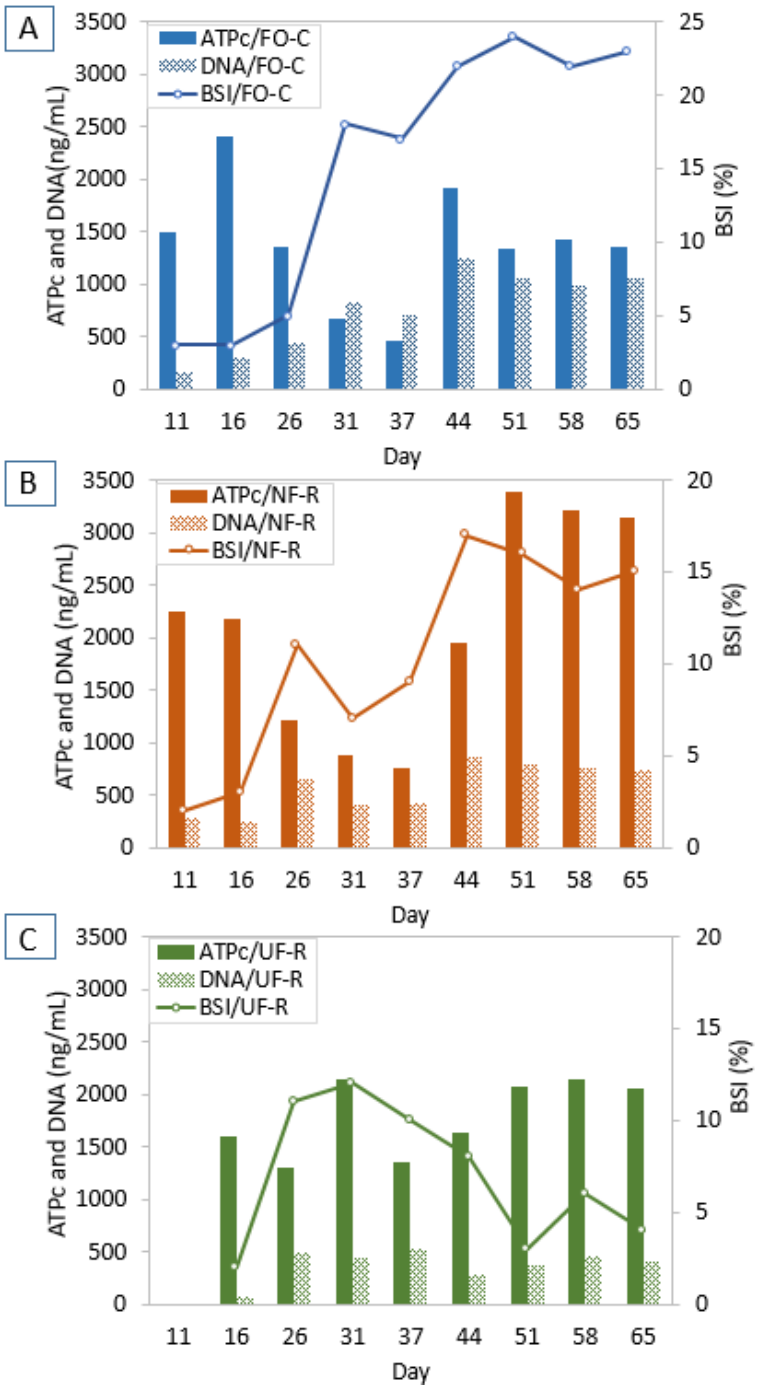

Fig. 5.58 ATPc, DNA concentrations and BSI index evolution for the three different effluents.

A: SBR/FO-C; B: SBR/NF-R; C: SBR/UF-R.

DNA values increased in the three SBRs until day 26. Specifically, DNA in SBR/FO-C increased from 163 to 443 ng/mL, DNA in SBR/NF-R increased from 265 to 645 ng/mL and DNA in SBR/UF-R rose from 69 to 488 ng/mL. From that day on, the behaviour was different in SBR/UF-R in comparison with the other two SBRs. In SBR/UF-R, i.e. in the SBR treating the sample with the presence of phenolic compounds, the lowest values of DNA were measured (397 ng/mL in the sample taken at the end of the experiment), which may be due to the longer time between feeding changes, which allows a better adaptation of the microorganisms to the increase in COD and TPhC. The highest values of DNA were measured in the SBR/FO-C (to around 1000 ng/mL). These high concentrations are in concordance with the decrease of MLSS and COD elimination. Lower ATPc values and higher BSI values than in the other two SBRs confirm the gradual deterioration of the biological process, as well as low metanabolic activity [66]. The highest BSI for the samples from SBR/FO-C implies that the stress not only depend on the presence of phenolic compounds but would be also related to the content of organic matter, since the wastewater feeding this SBR was the one with the highest concentration of COD [51]. In addition, it should be noted that this wastewater sample came from a FO process. Therefore, this behaviour could also be related to the increase in conductivity caused by reverse salt diffusion in the FO process. It has been reported that an increase in salinity in wastewater samples could increase cell stress and therefore cell lysis in SBR [66,67].

4. Conclusions

In this study, the recovery of valuable antioxidant compounds by adsorption/desorption with resins and the management by biological treatment of reject/concentrate streams from different membrane processes was evaluated.

By means of adsorption/desorption with the MN200 resin, percentages of elimination of phenolic compounds greater than 90% were achieved. The eluent had a high purity and antioxidant concentrations around 1.7 $g \cdot L^{-1}$.

Regarding the biological treatment, the optimal initial feed concentration was obtained for the three water samples by means of the preliminary biological tests. The biological treatment by SBR achieved a high removal of organic matter (around 80%) and elimination of phenolic compounds (around 90% for the UF-R).

Finally, it should be noted that the effluents meet the limits for both discharge and reuse as machinery cleaning water. In this way, the combination of the processes evaluated in this work can become a solution for the management of retentate streams from the treatment of OMW by membrane processes.

Acknowledgements

The authors acknowledge the financial support from the Spanish Ministry of Economy, Industry and Competitiveness through the project CTM2017-88645-R and The European Union through the Operational Program of the Social Fund (FSE).

References

[1] International Olive Council, The world of olive oil, (2022). https://www.internationaloliveoil.org/the-world-of-olive-oil/ (accessed May 15, 2022).

[2] T. Chatzistathis, T. Koutsos, Olive mill wastewater as a source of organic matter, water and nutrients for restoration of degraded soils and for crops managed with sustainable systems, Agric. Water Manag. 190 (2017) 55–64. https://doi.org/10.1016/j.agwat.2017.05.008.

[3] M.C. Morón, L. Pozo-Morales, D. Garvi, A.J. Alonso-Contreras, J. Lebrato, Bioparticles consisting of olive mill wastewater (OMW)-adapted bacteria and OMW-polluted soil as carrier– An application in an anaerobic fluidized bed bioreactor, J. Water Process Eng. 32 (2019) 100976. https://doi.org/10.1016/j.jwpe.2019.100976.

[4] A. Romani, F. Ieri, S. Urciuoli, A. Noce, G. Marrone, C. Nediani, R. Bernini, Health effects of phenolic compounds found in extra-virgin olive oil, by-products, and leaf of olea europaea L., Nutrients. 11 (2019). https://doi.org/10.3390/nu11081776.

[5] A. Turco, C. Malitesta, Removal of phenolic compounds from olive mill wastewater by a polydimethylsiloxane/oxmwcnts porous nanocomposite, Water. 12 (2020) 1–13. https://doi.org/10.3390/w12123471.

[6] E. De Marco, M. Savarese, A. Paduano, R. Sacchi, Characterization and fractionation of phenolic compounds extracted from olive oil mill wastewaters, Food Chem. 104 (2007) 858–867. https://doi.org/10.1016/j.foodchem.2006.10.005.

[7] H. Kiai, J. Raiti, A. El-Abbassi, A. Hafidi, Recovery of phenolic compounds from table olive processing wastewaters using cloud point extraction method, J. Environ. Chem. Eng. 6 (2018) 1569–1575. https://doi.org/10.1016/j.jece.2018.05.007.

[8] S.S. Kontos, P.G. Koutsoukos, C.A. Paraskeva, Removal and recovery of phenolic compounds from olive mill wastewater by cooling crystallization, Chem. Eng. J. 251 (2014) 319–328. https://doi.org/10.1016/j.cej.2014.04.047.

[9] S. Sklavos, G. Gatidou, A.S. Stasinakis, D. Haralambopoulos, Use of solar distillation for olive mill wastewater drying and recovery of polyphenolic compounds, J. Environ. Manage. 162 (2015) 46–52. https://doi.org/10.1016/j.jenvman.2015.07.034.

[10] J.M. Ochando-Pulido, S. Pimentel-Moral, V. Verardo, A. Martinez-Ferez, A focus on advanced physico-chemical processes for olive mill wastewater treatment, Sep. Purif. Technol. 179 (2017) 161–174. https://doi.org/10.1016/j.seppur.2017.02.004.

[11] A.Y. Gebreyohannes, E. Curcio, T. Poerio, R. Mazzei, G. Di Profio, E. Drioli, L. Giorno, Treatment of Olive Mill Wastewater by Forward Osmosis, Sep. Purif. Technol. 147 (2015) 292–302. https://doi.org/10.1016/j.seppur.2015.04.021.

[12] E. Garcia-Castello, A. Cassano, A. Criscuoli, C. Conidi, E. Drioli, Recovery and concentration of polyphenols from olive mill wastewaters by integrated membrane system., Water Res. (2010). https://doi.org/10.1016/j.watres.2010.05.005.

[13] A. Cassano, C. Conidi, E. Drioli, Comparison of the performance of UF membranes in olive mill wastewaters treatment, Water Res. 45 (2011) 3197–3204.

https://doi.org/10.1016/j.watres.2011.03.041.

[14] A. Cassano, C. Conidi, L. Giorno, E. Drioli, Fractionation of olive mill wastewaters by membrane separation techniques, J. Hazard. Mater. 248–249 (2013) 185–193. https://doi.org/10.1016/j.jhazmat.2013.01.006.

[15] T. Ngan, P. Hai, P. Le, D. Nam, P. Pham, T. Ha, A. Kumar, T. Son, T. Duc, Chemosphere Highly adsorptive protein inorganic nanohybrid of Moringa seeds protein and rice husk nanosilica for effective adsorption of pharmaceutical contaminants, Chemosphere. 307 (2022) 135856. https://doi.org/10.1016/j.chemosphere.2022.135856.

[16] T.D. Dinh, M.N. Phan, D.T. Nguyen, T.M.D. Le, A.K. Nadda, A.L. Srivastav, T.N.M. Pham, T.D. Pham, Removal of beta-lactam antibiotic in water environment by adsorption technique using cationic surfactant functionalized nanosilica rice husk, Environ. Res. 210 (2022) 112943. https://doi.org/10.1016/j.envres.2022.112943.

[17] L. Li, P.A. Quinlivan, D.R.U. Knappe, Effects of activated carbon surface chemistry and pore structure on the adsorption of MTBE from natural water, ACS Div. Environ. Chem. Prepr. 41 (2001) 448–453.

[18] S. Allaoui, M.N. Bennani, H. Ziyat, O. Qabaqous, N. Tijani, N. Ittobane, G. Hodaifa, Valorization of crude olive stone in the removing of polyphenols from crude olive mill wastewater: kinetic, isotherm and mechanism study, Heliyon. 7 (2021) e07525. https://doi.org/10.1016/j.heliyon.2021.e07525.

[19] Q. Yang, M. Zhao, L. Lin, Adsorption and desorption characteristics of adlay bran free phenolics on macroporous resins, Food Chem. 194 (2016) 900–907. https://doi.org/10.1016/j.foodchem.2015.08.070.

[20] F. Elayadi, W. Boumya, M. Achak, Y. Chhiti, F.E.M. Alaoui, N. Barka, C. El Adlouni, Experimental and modeling studies of the removal of phenolic compounds from olive mill wastewater by adsorption on sugarcane bagasse, Environ. Challenges. 4 (2021) 100184. https://doi.org/10.1016/j.envc.2021.100184.

[21] J.J. Park, W.Y. Lee, Adsorption and desorption characteristics of a phenolic compound from Ecklonia cava on macroporous resin, Food Chem. 338 (2021) 128150. https://doi.org/10.1016/j.foodchem.2020.128150.

[22] P. Pérez-Larrán, B. Díaz-Reinoso, A. Moure, J.L. Alonso, H. Domínguez, Adsorption technologies to recover and concentrate food polyphenols, Curr. Opin. Food Sci. 23 (2018) 165–172. https://doi.org/10.1016/j.cofs.2017.10.005.

[23] M. Cifuentes-Cabezas, C. Carbonell-Alcaina, M.C. Vincent-Vela, J.A. Mendoza-Roca, S. Álvarez-Blanco, Comparison of different ultrafiltration membranes as first step for the recovery of phenolic compounds from olive-oil washing wastewater, Process Saf. Environ. Prot. 149 (2021) 724–734. https://doi.org/10.1016/j.psep.2021.03.035.

[24] T.E. Elmansour, L. Mandi, A. Hejjaj, N. Ouazzani, Nutrients' behavior and removal in an activated sludge system receiving Olive Mill Wastewater, J. Environ. Manage. 305 (2022) 114254. https://doi.org/10.1016/j.jenvman.2021.114254.

[25] C. Conidi, R. Mazzei, A. Cassano, L. Giorno, Integrated membrane system for the production of phytotherapics from olive mill wastewaters, J. Memb. Sci. 454 (2014) 322–329. https://doi.org/10.1016/j.memsci.2013.12.021.

[26] R. Castro-Muñoz, J. Yáñez-Fernández, V. Fíla, Phenolic compounds recovered from agro-food by-products using membrane technologies: An overview, Food Chem. 213 (2016) 753–762. https://doi.org/10.1016/j.foodchem.2016.07.030.

[27] M. Cifuentes-Cabezas, C.M. Sanchez-Arévalo, J.A. Mendoza-Roca, M.C. Vincent-Vela, S. Álvarez-Blanco, Recovery of Phenolic Compounds from Olive Oil Washing Wastewater by Adsorption/Desorption Process, Sep. Purif. Technol. 298 (2022) 121562. https://doi.org/10.1016/j.seppur.2022.121562.

[28] S. Lagergren, Lagergren, S., About the Theory of so Called Adsorption of Soluble Substances, Kungliga Svenska Vetenskapsakademiens Handlingar, 24, 1-39, 1898., K. Sven. Vetenskapsakademiens Handl. (1898) 1–39.

http://www.sciepub.com/reference/163936.

[29] Y.S. Ho, G. McKay, Pseudo-second order model for sorption processes, Process Biochem. 34 (1999) 451–465. https://doi.org/10.1016/S0032-9592(98)00112-5.

[30] P. Barkakati, A. Begum, M.L. Das, P.G. Rao, Adsorptive separation of Ginsenoside from aqueous solution by polymeric resins: Equilibrium, kinetic and thermodynamic studies, Chem. Eng. J. 161 (2010) 34–45. https://doi.org/10.1016/j.cej.2010.04.018.

[31] E. Zuriaga-Agustí, J.A. Mendoza-Roca, A. Bes-Piá, J.L. Alonso-Molina, I. Amorós-Muñoz, Sludge reduction by uncoupling metabolism: SBR tests with para-nitrophenol and a commercial uncoupler, J. Environ. Manage. 182 (2016) 406–411. https://doi.org/10.1016/j.jenvman.2016.07.100.

[32] M.J. Luján-Facundo, J.A. Mendoza-Roca, J.L. Soler-Cabezas, A. Bes-Piá, M.C. Vincent-Vela, B. Cuartas-Uribe, L. Pastor-Alcañiz, Management of table olive processing wastewater by an osmotic membrane bioreactor process, Sep. Purif. Technol. 248 (2020) 117075. https://doi.org/10.1016/j.seppur.2020.117075.

[33] APHA, Standard Methods for the Examination of Water and Wastewater, in: Am. Public Heal. Assoc. Washington, DC, 2005: p. 21 st. ed.

[34] V.L. Singleton, R. Orthofer, R.M. Lamuela-Raventós, Analysis of total phenols and other oxidation substrates and antioxidants by means of folin-ciocalteu reagent, Methods Enzymol. 299 (1999) 152–178. https://doi.org/10.1016/S0076-6879(99)99017-1.

[35] E. Ferrer-Polonio, J. Fernández-Navarro, J.L. Alonso-Molina, J.A. Mendoza-Roca, A. Bes-Piá, I. Amorós, Towards a cleaner wastewater treatment: Influence of folic acid addition on sludge reduction and biomass characteristics, J. Clean. Prod. 232 (2019) 858–866. https://doi.org/10.1016/j.jclepro.2019.06.021.

[36] C. Valderrama, J.L. Cortina, A. Farran, X. Gamisans, F.X. de las Heras, Evaluation of hyper-cross-linked polymeric sorbents (Macronet MN200 and MN300) on dye (Acid

red 14) removal process, React. Funct. Polym. 68 (2008) 679–691. https://doi.org/10.1016/j.reactfunctpolym.2007.11.005.

[37] J. Kammerer, R. Carle, D.R. Kammerer, Adsorption and ion exchange: Basic principles and their application in food processing, J. Agric. Food Chem. 59 (2011) 22–42. https://doi.org/10.1021/jf1032203.

[38] B.M. Esteves, S. Morales-Torres, L.M. Madeira, F.J. Maldonado-Hódar, Specific adsorbents for the treatment of OMW phenolic compounds by activation of bio-residues from the olive oil industry, J. Environ. Manage. 306 (2022). https://doi.org/10.1016/j.jenvman.2022.114490.

[39] M.H.L. Ribeiro, D. Silveira, S. Ferreira-Dias, Selective adsorption of limonin and naringin from orange juice to natural and synthetic adsorbents, Eur. Food Res. Technol. 215 (2002) 462–471. https://doi.org/10.1007/s00217-002-0592-0.

[40] M.L. Soto, A. Moure, H. Domínguez, J.C. Parajó, Recovery, concentration and purification of phenolic compounds by adsorption: A review, J. Food Eng. 105 (2011) 1–27. https://doi.org/10.1016/j.jfoodeng.2011.02.010.

[41] J.P. Stanford, P.H. Hall, M.R. Rover, R.G. Smith, R.C. Brown, Separation of sugars and phenolics from the heavy fraction of bio-oil using polymeric resin adsorbents, Sep. Purif. Technol. 194 (2018) 170–180. https://doi.org/10.1016/j.seppur.2017.11.040.

[42] T.T. Le, X. Framboisier, A. Aymes, A. Ropars, J.P. Frippiat, R. Kapel, dentification and Capture of Phenolic Compounds from aRapeseed Meal Protein Isolate Production Process By-Productby Macroporous Resin and Valorization TheirAntioxidant Properties, Molecules. 26 (2021). https://doi.org/10.3390/molecules26195853.

[43] M.A. Núñez Camacho, A.I. García López, A. Martinez-ferez, J.M. Ochando-Pulido, Increasing large-scale feasibility of two-phase olive-oil washing wastewater treatment and phenolic fraction recovery with novel ion exchange resins, Chem. Eng. Process. - Process Intensif. 164 (2021) 108416. https://doi.org/10.1016/j.cep.2021.108416.

[44] E. Ferrer-Polonio, J.A. Mendoza-Roca, A. Iborra-Clar, L. Pastor-Alcañiz, Adsorption of raw and treated by membranes fermentation brines from table olives processing for phenolic compounds separation and recovery, J. Chem. Technol. Biotechnol. 91 (2016) 2094–2102. https://doi.org/10.1002/jctb.4807.

[45] J. Kammerer, J. Boschet, D.R. Kammerer, R. Carle, Enrichment and fractionation of major apple flavonoids, phenolic acids and dihydrochalcones using anion exchange resins, LWT - Food Sci. Technol. 44 (2011) 1079–1087. https://doi.org/10.1016/j.lwt.2010.10.008.

[46] T.R. Sahoo, B. Prelot, Adsorption processes for the removal of contaminants from wastewater, Elsevier Inc., 2020. https://doi.org/10.1016/b978-0-12-818489-9.00007-4.

[47] J. Kammerer, D.R. Kammerer, U. Jensen, R. Carle, Interaction of apple polyphenols in a multi-compound system upon adsorption onto a food-grade resin, J. Food Eng. 96 (2010) 544–554. https://doi.org/10.1016/j.jfoodeng.2009.08.038.

[48] C. Valderrama, J.I. Barios, M. Caetano, A. Farran, J.L. Cortina, Kinetic evaluation of phenol/aniline mixtures adsorption from aqueous solutions onto activated carbon and hypercrosslinked polymeric resin (MN200), React. Funct. Polym. 70 (2010) 142–150. https://doi.org/10.1016/j.reactfunctpolym.2009.11.003.

[49] A.S. Ciggin, A. Iravanian, S. Doğruel, D. Orhon, Co-metabolism of olive mill wastewater in sequencing batch reactor under aerobic conditions after Fenton-based oxidation, J. Water Process Eng. 43 (2021). https://doi.org/10.1016/j.jwpe.2021.102277.

[50] C. Ehaliotis, K. Papadopoulou, M. Kotsou, I. Mari, C. Balis, Adaptation and population dynamics of Azotobacter vinelandii during aerobic biological treatment of olive-mill wastewater, FEMS Microbiol. Ecol. 30 (1999) 301–311. https://doi.org/10.1016/S0168-6496(99)00066-5.

[51] Y. Jaouad, M. Villain, N. Ouazzani, L. Mandi, B. Marrot, Biodegradation of olive mill

wastewater in a membrane bioreactor: acclimation of the biomass and constraints, Desalin. Water Treat. 57 (2016) 8109–8118. https://doi.org/10.1080/19443994.2015.1025435.

[52] N.A. Yusoff, S.A. Ong, L.N. Ho, Y.S. Wong, F.N. Mohd Saad, W.F. Khalik, S.L. Lee, Evaluation of biodegradation process: Comparative study between suspended and hybrid microorganism growth system in sequencing batch reactor (SBR) for removal of phenol, Biochem. Eng. J. 115 (2016) 14–22. https://doi.org/10.1016/j.bej.2016.07.018.

[53] F. Di Caprio, L. Tayou Nguemna, M. Stoller, M. Giona, F. Pagnanelli, Microalgae cultivation by uncoupled nutrient supply in sequencing batch reactor (SBR) integrated with olive mill wastewater treatment, Chem. Eng. J. 410 (2021) 128417. https://doi.org/10.1016/j.cej.2021.128417.

[54] G. Aggelis, D. Iconomou, M. Christou, D. Bokas, S. Kotzailias, G. Christou, V. Tsagou, S. Papanikolaou, Phenolic removal in a model olive oil mill wastewater using Pleurotus ostreatus in bioreactor cultures and biological evaluation of the process, Water Res. 37 (2003) 3897–3904. https://doi.org/10.1016/S0043-1354(03)00313-0.

[55] S. Ntougias, K. Bourtzis, G. Tsiamis, The Microbiology of Olive Mill Wastes, Biomed Res. Int. 2013 (2013) 1–16. https://doi.org/10.1155/2013/784591.

[56] A. Fiorentino, A. Gentili, M. Isidori, P. Monaco, A. Nardelli, A. Parrella, F. Temussi, Environmental Effects Caused by Olive Mill Wastewaters: Toxicity Comparison of Low-Molecular-Weight Phenol Components, J. Agric. Food Chem. 51 (2003) 1005–1009. https://doi.org/10.1021/jf020887d.

[57] G. Farabegoli, A. Chiavola, E. Rolle, SBR treatment of olive mill wastewaters: Dilution or pre-treatment?, Water Sci. Technol. 65 (2012) 1684–1691. https://doi.org/10.2166/wst.2012.068.

[58] R.A. Hamza, Z. Sheng, O.T. Iorhemen, M.S. Zaghloul, J.H. Tay, Impact of food-to-microorganisms ratio on the stability of aerobic granular sludge treating high-strength

organic wastewater, Water Res. 147 (2018) 287–298. https://doi.org/10.1016/j.watres.2018.09.061.

[59] Y.J. Chan, M.F. Chong, C.L. Law, Biological treatment of anaerobically digested palm oil mill effluent (POME) using a Lab-Scale Sequencing Batch Reactor (SBR), J. Environ. Manage. 91 (2010) 1738–1746. https://doi.org/10.1016/j.jenvman.2010.03.021.

[60] X.C. Feng, W.Q. Guo, S.S. Yang, H.S. Zheng, J.S. Du, Q.L. Wu, N.Q. Ren, Possible causes of excess sludge reduction adding metabolic uncoupler, 3,3',4',5-tetrachlorosalicylanilide (TCS), in sequence batch reactors, Bioresour. Technol. 173 (2014) 96–103. https://doi.org/10.1016/j.biortech.2014.09.085.

[61] L. Ayed, N. Asses, N. Chamme, N. Ben Othman, M. Hamdi, Advanced oxidation process and biological treatmentsfor table olive processing wastewaters: constraintsand a novel approach to integrated recycling process:a review, Biodegradation. 28 (2017) 125–138.

[62] C.A. Papadimitriou, P. Samaras, G.P. Sakellaropoulos, Comparative study of phenol and cyanide containing wastewater in CSTR and SBR activated sludge reactors, Bioresour. Technol. 100 (2009) 31–37. https://doi.org/10.1016/j.biortech.2008.06.004.

[63] A. Chiavola, G. Farabegoli, E. Rolle, Combined biological and chemical-physical process for olive mill wastewater treatment, Desalin. Water Treat. 23 (2010) 135–140. https://doi.org/10.5004/dwt.2010.1987.

[64] S.K. Rifi, L.E. Fels, A. Driouich, M. Hafidi, Z. Ettaloui, S. Souabi, Sequencing batch reactor efficiency to reduce pollutant in olive oil mill wastewater mixed with urban wastewater, Int. J. Environ. Sci. Technol. (2022). https://doi.org/10.1007/s13762-021-03866-2.

[65] A. Chiavola, G. Farabegoli, F. Antonetti, Biological treatment of olive mill wastewater in a sequencing batch reactor, Biochem. Eng. J. 85 (2014) 71–78.

https://doi.org/10.1016/j.bej.2014.02.004.

[66] M.J. Luján-Facundo, J. Fernández-Navarro, J.L. Alonso-Molina, I. Amorós-Muñoz, Y. Moreno, J.A. Mendoza-Roca, L. Pastor-Alcañiz, The role of salinity on the changes of the biomass characteristics and on the performance of an OMBR treating tannery wastewater, Water Res. 142 (2018) 129–137. https://doi.org/10.1016/j.watres.2018.05.046.

[67] H. Li, F. Meng, W. Duan, Y. Lin, Y. Zheng, Biodegradation of phenol in saline or hypersaline environments by bacteria: A review, Ecotoxicol. Environ. Saf. 184 (2019) 109658. https://doi.org/10.1016/j.ecoenv.2019.109658.

CAPÍTULO VI
CONCLUSIONES

VI.1 CONCLUSIONES

A continuación, se presentan conclusiones de esta Tesis Doctoral.

La presente tesis doctoral pretende lidiar con el problema de contaminación debida a las aguas residuales provenientes del proceso de elaboración de aceite de oliva por centrifugación en dos fases. Para ello diversos objetivos fueron propuestos. A continuación, se responde a ellos mediante conclusiones:

- Se caracterizó un agua residual de almazara proveniente de un proceso de centrifugación de dos fases, denominada OOWW. Se determinó que posee un color amarillento con un olor fuerte a oliva, de perfil ácido y con una elevada concentración de DQO (23775.3 ± 238.2 $mg \cdot L^{-1}$) y compuestos fenólicos (1161.80 ± 13.43 $mgTyeq \cdot L^{-1}$).
- Mediante el pretratamiento implementado, que contempla flotación, sedimentación y filtración, se logró eliminar en casi un 90% las grasas y aceites de la muestra. Por otra parte, se logró reducir en gran cantidad (entre 40 y 41%) los sólidos en suspensión, turbidez y color.
- En el estudio de ultrafiltración con membranas orgánicas e inorgánicas se observó que, independientemente del material, las membranas con mayor MWCO presentaban la mayor disminución de densidad de flujo de permeado con el tiempo (60%-65%), debido al mayor tamaño de poro. Todas las membranas fueron capaces de eliminar eficazmente los sólidos en suspensión, el color y la DQO, mientras que el rechazo de compuestos fenólicos fue bajo, con las membranas orgánicas presentando los mayores porcentajes de rechazo a la DQO. Por consiguiente, todas las membranas lograron enriquecer el permeado en compuestos fenólicos; obteniendo relaciones compuestos fenólicos/DQO entre 1,2 a 2,1 veces mayor que la relación en la alimentación. Las membranas UP005 e Inside céram 15 fueron las que presentaron mejor eliminación de DQO, sin afectar en gran medida a la concentración de compuestos fenólicos.
- En cuanto a la limpieza, la membrana UH050 y las tres membranas cerámicas requirieron el protocolo de limpieza más extremo (limpieza química con P3 Ultrasil 115 (1% v/v) a 30ºC) para restaurar la permeabilidad inicial al agua, mientras que el

resto de las membranas fueron limpiadas con un simple enjuague con agua. La membrana UP005 fue la que logró la mayor recuperación de su permeabilidad inicial (más del 95%) con solo limpiarla con agua a 25 °C.

- El objetivo de la etapa de UF era seleccionar la membrana que presentara mayor eliminación de materia orgánica sin afectar a la concentración de compuestos fenólicos (mínimo rechazo de compuestos fenólicos) con alto valor de densidad de flujo de permeado y fácil limpieza. La membrana UP005 fue seleccionada como la mejor opción de acuerdo con estos criterios.
- Con respecto a los modelos analizados para predecir la variación de la densidad de flujo de permeado con el tiempo en la ultrafiltración, empleando los modelos de Hermia, el bloqueo completo de poros proporcionó la mejor precisión de ajuste para las membranas orgánicas con el MWCO más bajo, independientemente de las condiciones de operación y el material. En el caso de las membranas inorgánicas, solo la formación de la capa de torta proporcionó buenas medidas de ajuste. El modelo estándar de bloqueo de poros no proporcionó datos consistentes tanto para las membranas orgánicas como para las inorgánicas. A pesar del buen ajuste que brindan estos modelos, el principal inconveniente es que no consideran la posibilidad de que estos mecanismos ocurran simultáneamente en un mismo proceso. Se comprobaron experimentalmente los resultados predichos por los modelos, mostrando las membranas inorgánicas una mayor tendencia al ensuciamiento irreversible, con mayores valores de relación Ra/RT (resistencia adsorción/resistencia total de la memrbana). De acuerdo con la precisión del ajuste de los modelos, en cuanto a R^2 y SD, tanto el modelo de resistencias en serie como el modelo combinado lograron representar bien los datos experimentales. Esto indica que tanto la formación de la capa de torta como el bloqueo de los poros contribuyeron al ensuciamiento de las membranas. Esto confirma la necesidad de un pretratamiento antes del proceso de ultrafiltración.
- El ANOVA realizado al ajustar los modelos de superficie de respuesta muestra que tanto la CFV como la TMP son variables significativas respecto a la densidad de flujo de permeado para todas las membranas estudiadas, con la única diferencia de que, dependiendo de la membrana estudiada, el efecto que generan sobre la variable de

salida es de un primer grado, un segundo grado o un efecto acoplado. Mediante RSM se logó obtener las mejores condiciones de operación para los procesos de membrana. Sin embargo, no se pudo obtener un buen ajuste para la velocidad de flujo tangencial de 4 $m \cdot s^{-1}$ para las membranas inorgánicas.

- Mediante ANN, se logró estimar todos los datos experimentales de variación de densidad de flujo de permeado con el tiempo con altos coeficientes de regresión (R^2 de 0,96 a 0,99). Dependiendo de la membrana considerada, el modelo que proporcionó un mejor ajuste a los datos experimentales no fue siempre el mismo. Sin embargo, el modelo ANN es el que mejor ajuste a los datos experimentales proporcionó contemplando todas las membranas de ultrafiltración en conjunto.
- Se seleccionó la nanofiltración como segunda etapa para el tratamiento de aguas residuales de una almazara con el objetivo de encontrar una membrana que consiga el mayor rechazo de compuestos fenólicos para poder concentrarlos. Dentro de las condiciones de operación probadas, se encontró que la densidad de flujo de permeado se vio más afectado por la TMP ue por la CFV. Todas las membranas fueron capaces de concentrar compuestos fenólicos con un rechazo superior al 70%. Tras el análisis de diferentes membranas y condiciones de operación, se demostró la eficacia de la nanofiltración para concentrar polifenoles procedentes de OOWW, así como para obtener un permeado apto para su reutilización.
- El estudio del ensuciamiento de membranas mediante espectroscopía de fluorescencia 2D y FTIR permitió obtener información valiosa sobre el ensuciamiento de las membranas. El análisis de espectroscopía de fluorescencia mostró una respuesta más pronunciada a los compuestos coloreados, mientras que por medio de FTIR fue posible ver más claramente el efecto de los demás compuestos susceptibles de producir ensuciamiento presentes en las disoluciones. Estas técnicas juntas representan un enfoque prometedor para analizar la eficiencia de los protocolos de limpieza. Finalmente, a la vista de los resultados obtenidos, se consideró como la más adecuada la membrana NF270 bajo una CFV de 1 $m \cdot s^{-1}$ y una TMP de 10 bar.
- Paralelamente, se estudió el proceso de ósmosis directa para la concentración de los compuestos fenólicos del OOWW. De las dos membranas evaluadas, la HFFO.6

presentó mayor densidad de flujo de permeado y menor paso inverso de sales. Con esta membrana se estudió la concentración de OOWW utilizando FTOP como disolución de extracción. La FTOP resultó ser un agua residual adecuada para ser utilizada como DS para el proceso de FO propuesto. Sus dos principales ventajas son la alta presión osmótica y la concentración de fenoles totales, lo que implica que la pérdida de estos compuestos por el paso a través de la membrana desde la FS a la DS es menor, consiguiendo un OOWW concentrado con mayor concentración de estos compuestos en comparación con la conseguida utilizando NaCl como disolución de extracción. Además, a diferencia de una disolución de NaCl, no se trata de una DS que deba regenerarse, ya que se puede gestionar el FTOP diluido y utilizar FTOP fresco en el proceso. Finalmente, con esta membrana, aparte de lograr concentrar con éxito los compuestos fenólicos presentes en la OOWW, se demostró que la FO es un proceso prometedor tanto para la concentración de compuestos fenólicos de OOWW como para la dilución de la FTOP, que es un paso necesario antes de su tratamiento.

- Concentrados los compuestos fenólicos en la corriente de rechazo de la NF y en el concentrado de la FO, se evaluó su recuperación mediante adsorción con resinas, para luego gestionar por tratamiento biológico los efluentes resultantes. Para ello, primero se realizó un estudio de adsorción/desorción tanto con agua modelo como con disolución real de OOWW (pretratada), para encontrar la mejor resina, dosis y disolución extractante para la recuperación de estos compuestos. En cuando a la dosis de resina, se observó un mayor aumento en la eficiencia de adsorción incrementando de 10 a 40 $g \cdot L^{-1}$ la concentración de resina en la disolución. El incremento de 40 a 60 $g \cdot L^{-1}$ no generó una variación significativa en la adsorción, por lo que se seleccionó la dosis de 40 $g \cdot L^{-1}$ como óptima. El modelo cinético de pseudo-segundo orden proporcionó el mejor ajuste de los datos experimentales para todas las resinas. Mediante este estudio se demostró que, si bien los adsorbentes eran específicos para compuestos fenólicos, de igual manera existe interferencia y adsorción de otros compuestos orgánicos, como los azúcares. En cuanto a la desorción, la mezcla de etanol/agua al 50 %v/v fue el mejor eluyente para recuperar los compuestos fenólicos. De las cuatro resinas evaluadas, la MN200 fue la que presentó mayor capacidad de adsorción tanto en la disolución modelo como en agua real, recuperando casi el 90%

de los compuestos fenólicos iniciales, con baja presencia de azúcares (alrededor del 5%).

- Utilizando las condiciones óptimas del proceso de adsorción/desorción, se logró eliminar casi en su totalidad a los compuestos fenólicos presentes en las muestras de NF-R y FO-C, alcanzándose porcentajes de eliminación del 96,42% y 92,78%, respectivamente. A continuación, mediante la desorción con la disolución etanol/agua al 50 %v/v, se recuperaron, lográndose disoluciones con concentraciones de antioxidantes de alta pureza (entre 87 y 95%) de 1,69 y 1,66 $g \cdot L^{-1}$.
- Finalmente, se trataron los rechazos y concentrados obtenidos en los tres procesos de membrana estudiados mediante el tratamiento biológico por SBR. Se logró una alta eliminación de materia orgánica (alrededor del 80%) y de los compuestos fenólicos (alrededor del 90%) remanentes en UF-R. Aunque la adaptación de la biomasa a UF-R fue más lenta que en los otros SBR, debido a la presencia de compuestos fenólicos, los valores de lisis celular y BSI fueron los más bajos en SBR/UF-R, consiguiendo un proceso biológico estable.
- La muestra con mayor concentración de materia orgánica (concentrado de la FO) fue la corriente que presentó la menor eficiencia de eliminación de DQO al final del ensayo, coincidiendo con valores bajos de ATPc y valores altos de ADN y BSI. Los efluentes obtenidos de los tres procesos biológicos pasados los 65 días cumplieron los límites tanto de vertido como de reutilización como agua de limpieza de maquinaria.

De esta forma, la combinación de procesos evaluados en este trabajo puede convertirse en una solución para la gestión de las corrientes residuales provenientes de almazaras, logrando extraer compuestos valiosos con alta pureza y recuperando cursos de agua para ser incorporados en el proceso productivo.

VI.2 CONCLUSIONS

The conclusions of this Doctoral Thesis are presented below.

This doctoral thesis aims to deal with the problem of contamination due to wastewater from the olive oil production process by centrifugation in two phases. To this end, various objectives were proposed. Next, they are answered by conclusions:

- An oil mill wastewater from a two-phase centrifugation process, called OOWW, was characterized. It was determined that it has a yellowish color with a strong olive odor, acid profile and a high concentration of COD (23775.3 ± 238.2 $mg \cdot L^{-1}$) and phenolic compounds (1161.80 ± 13.43 $mgTyeq \cdot L^{-1}$).
- Through the implemented pretreatment, which includes flotation, sedimentation and filtration, it was possible to eliminate almost 90% of the fats and oils in the sample. On the other hand, it was possible to reduce in great quantity (between 40 and 41%) the solids in suspension, turbidity and color.
- In the ultrafiltration study with organic and inorganic membranes, it was observed that, regardless of the material, the membranes with the highest MWCO presented the greatest decrease in permeate flux density over time (60%-65%), due to to the larger pore size of the membranes. All the membranes were able to effectively remove suspended solids, color and COD, while the rejection of phenolic compounds was low, with the organic membranes presenting the highest percentages of COD rejection. Consequently, all the membranes managed to enrich the permeate in phenolic compounds; obtaining ratios of phenolic compounds/COD between 1.2 to 2.1 times higher than the ratio in food. The UP005 and Inside céram 15 membranes were the ones that presented the best COD removal, without greatly affecting the concentration of phenolic compounds.
- In terms of cleaning, the UH050 membrane and the three ceramic membranes required the most extreme cleaning protocol (chemical cleaning with P3 Ultrasil 115 (1% v/v) at 30ºC) to restore initial water permeability, while the rest of the membranes were cleaned with a simple rinse with water. The UP005 membrane was the one that

achieved the highest recovery of its initial permeability (more than 95%) just by cleaning it with water at 25 °C.

- The objective of the UF stage was to select the membrane that presented the greatest removal of organic matter without affecting the concentration of phenolic compounds (minimum rejection of phenolic compounds) with a high value of permeate flux density and easy cleaning. The UP005 membrane was selected as the best option according to these criteria.
- Regarding the models analyzed to predict the variation of the permeate flux density with time in ultrafiltration, using the Hermia models, complete pore blocking provided the best accuracy of fit for organic membranes with the lowest MWCO, regardless of operating conditions and material. In the case of inorganic membranes, only the formation of the cake layer provided good fit measurements. The standard pore blocking model did not provide consistent data for both organic and inorganic membranes. Despite the good adjustment provided by these models, the main drawback is that they do not consider the possibility that these mechanisms occur simultaneously in the same process. The results predicted by the models were verified experimentally, showing the inorganic membranes a greater tendency to irreversible fouling, with higher values of the Ra/RT ratio (adsorption resistance/total resistance of the membrane). According to the precision of the fit of the models, in terms of R^2 and SD, both the resistance in series model and the combined model were able to represent the experimental data. This indicates that both cake layer formation and pore blockage contributed to membrane fouling. This confirms the need for a pretreatment before the ultrafiltration process.
- The ANOVA carried out by fitting the response surface models shows that both the CFV and the TMP are significant variables with respect to the permeate flux density for all the membranes studied, with the only difference that, depending on the membrane studied, the effect they generate on the output variable is of a first degree, a second degree or a coupled effect. Using RSM, it was possible to obtain the best operating conditions for membrane processes. However, a good fit for the tangential flow velocity of 4 $m \cdot s^{-1}$ could not be obtained for inorganic membranes.

- Through ANN, it was possible to estimate all the experimental data of permeate flux density variation over time with high regression coefficients (R^2 from 0.96 to 0.99). Depending on the membrane considered, the model that provided a better fit to the experimental data was not always the same. However, the ANN model is the one that best fits the experimental data provided considering all the ultrafiltration membranes together.
- Nanofiltration was selected as the second stage for the treatment of wastewater from an oil mill with the aim of finding a membrane that achieves the greatest rejection of phenolic compounds in order to concentrate them. Within the operating conditions tested, it was found that the permeate flux density was more affected by TMP than by CFV. All the membranes were capable of concentrating phenolic compounds with a rejection higher than 70%. After the analysis of different membranes and operating conditions, the efficiency of nanofiltration to concentrate polyphenols from OOWW was demonstrated, as well as to obtain a permeate suitable for reuse.
- The study of membrane fouling using 2D fluorescence spectroscopy and FTIR provided valuable information on membrane fouling. The fluorescence spectroscopy analysis showed a more pronounced response to the colored compounds, while by means of FTIR it was possible to see more clearly the effect of the other compounds capable of producing fouling present in the solutions. These techniques together represent a promising approach to analyze the efficiency of cleaning protocols. Finally, in view of the results obtained, the NF270 membrane was considered the most suitable under a CFV of 1 $m \cdot s^{-1}$ and a TMP of 10 bar.
- At the same time, the forward osmosis process for the concentration of the phenolic compounds of the OOWW was studied. Of the two membranes evaluated, the HFFO.6 presented higher permeate flux density and lower reverse passage of salts. With this membrane, the concentration of OOWW was studied using FTOP as extraction solution. The FTOP turned out to be a suitable wastewater to be used as DS for the proposed FO process. Its two main advantages are the high osmotic pressure and the concentration of total phenols, which implies that the loss of these compounds by passing through the membrane from the SF to the DS is lower, achieving a

concentrated OOWW with a higher concentration of these compounds compared to that achieved using NaCl as extraction solution. Also, unlike a NaCl solution, it is not a DS that needs to be regenerated, as the diluted FTOP can be managed and fresh FTOP used in the process. Finally, with this membrane, apart from successfully concentrating the phenolic compounds present in the OOWW, it was shown that FO is a promising process both for the concentration of OOWW phenolic compounds and for the dilution of FTOP, which is a step necessary before your treatment.

- Once the phenolic compounds were concentrated in the NF reject current and in the FO concentrate, their recovery was evaluated by adsorption with resins, to then manage the resulting effluents by biological treatment. To do this, first an adsorption/desorption study was carried out with both model water and real OOWW solution (pretreated), to find the best resin, dose and extractant solution for the recovery of these compounds. Regarding the resin dose, a greater increase in the adsorption efficiency was observed by increasing the resin concentration in the solution from 10 to 40 $g \cdot L^{-1}$. The increase from 40 to 60 $g \cdot L^{-1}$ did not generate a significant variation in the adsorption, so the dose of 40 $g \cdot L^{-1}$ was selected as optimal. The pseudo-second order kinetic model provided the best fit to the experimental data for all resins. Through this study it was shown that, although the adsorbents were specific for phenolic compounds, there is also interference and adsorption of other organic compounds, such as sugars. Regarding desorption, the 50% v/v ethanol/water mixture was the best eluent to recover the phenolic compounds. Of the four resins evaluated, MN200 was the one with the highest adsorption capacity both in the model solution and in real water, recovering almost 90% of the initial phenolic compounds, with a low presence of sugars (around 5%).
- Using the optimal conditions of the adsorption/desorption process, it was possible to almost completely eliminate the phenolic compounds present in the NF-R and FO-C samples, reaching elimination percentages of 96.42% and 92.78%, respectively. Then, by desorption with the 50% v/v ethanol/water solution, they were recovered, achieving solutions with high purity antioxidant concentrations (between 87 and 95%) of 1.69 and 1.66 $g \cdot L^{-1}$.

- Finally, the rejects and concentrates obtained in the three membrane processes studied were treated through biological treatment by SBR. A high removal of organic matter (around 80%) and phenolic compounds (around 90%) remaining in UF-R was achieved. Although the biomass adaptation to UF-R was slower than in the other SBRs, due to the presence of phenolic compounds, the cell lysis and BSI values were the lowest in SBR/UF-R, achieving a stable biological process.
- The sample with the highest concentration of organic matter (FO concentrate) was the stream that presented the lowest COD removal efficiency at the end of the test, coinciding with low ATPc values and high ADN and BSI values. The effluents obtained from the three biological processes after 65 days met the limits for both discharge and reuse as machinery cleaning water.

In this way, the combination of processes evaluated in this work can become a solution for the management of wastewater from oil mills, managing to extract valuable compounds with high purity and recovering water courses to be incorporated into the production process.